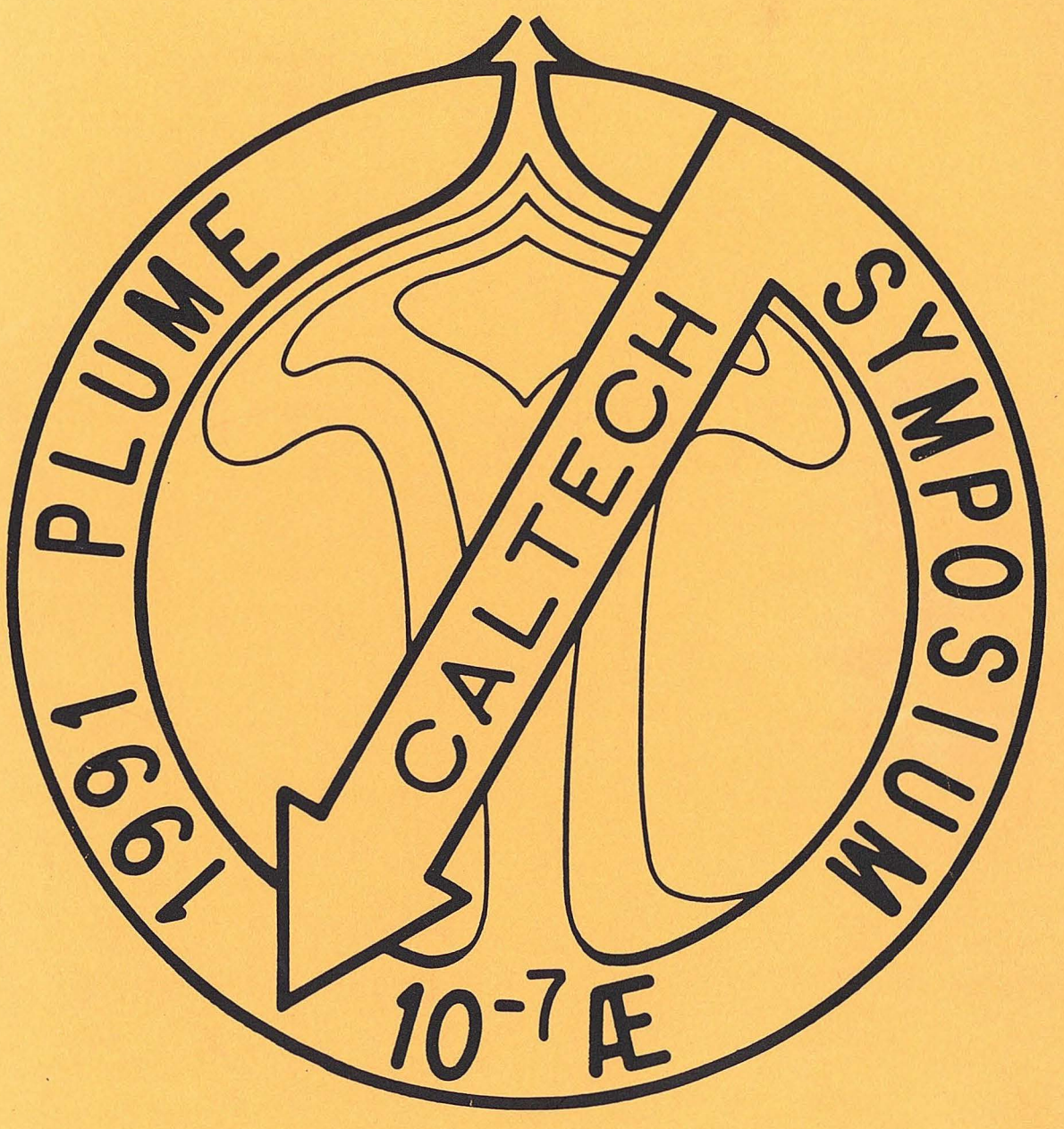
1991 PLUME
CALTECH
SYMPOSIUM
10-7 Æ

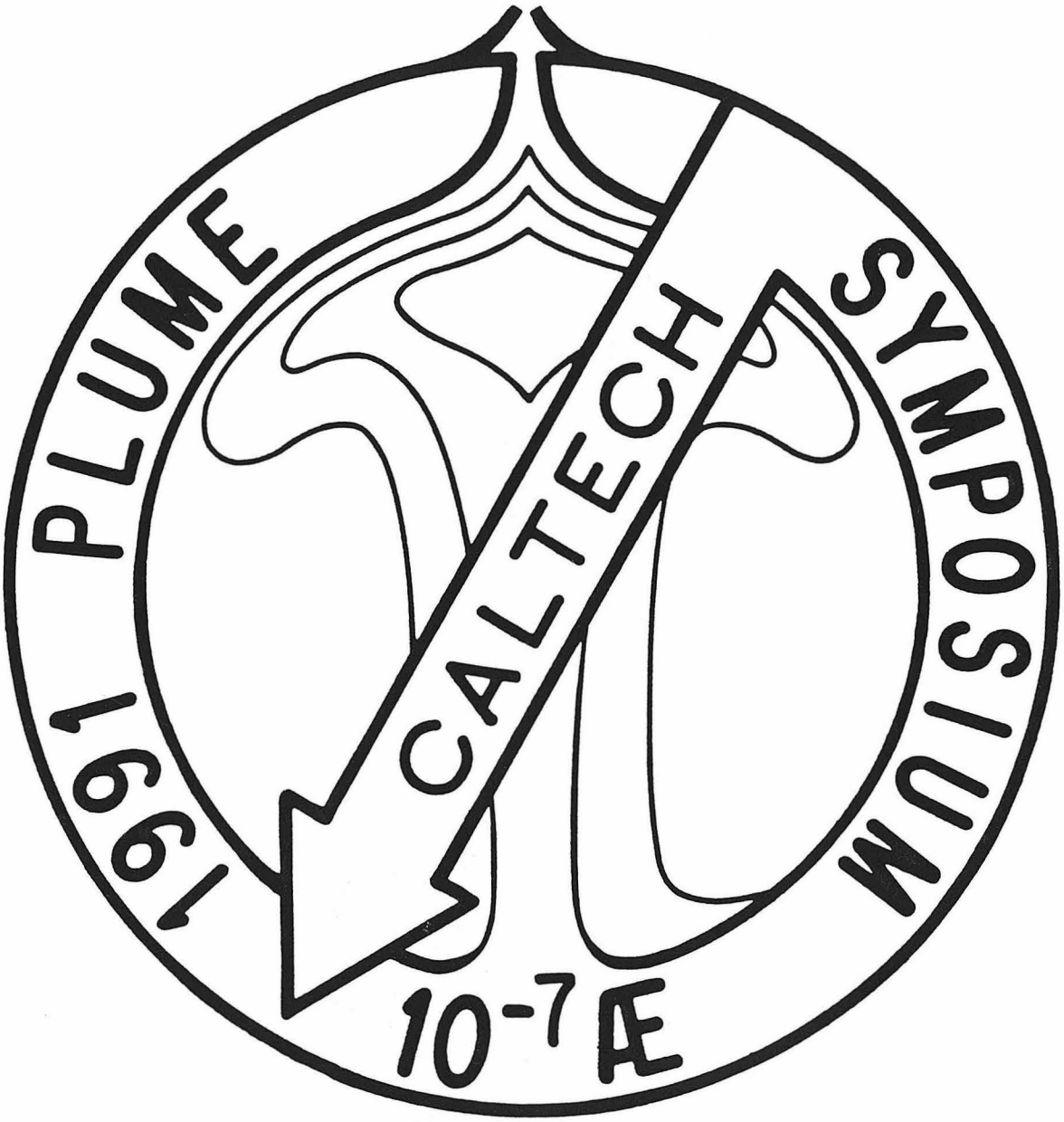
1991 PLUME
CALTECH
SYMPOSIUM
10-7 Æ

THE GREAT SEAL OF PLUMACY

A plunging slab piercing rising plumage, with encircling plates, crested by basaltic edifice; recycle ad nauseam. Upper quadrant, the backarch option. To be placed on mantle and stationary.

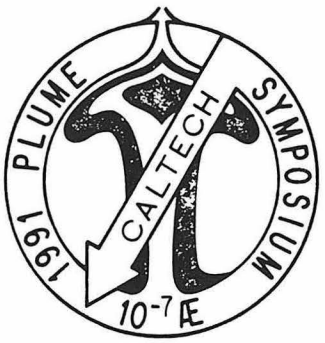

1891-1991

HOTSPOT HANDBOOK

Plume Program
Experts
Onamasticon
Hotspot Time Line
Where are they?
Where aren't they?
Where shouldn't they be?
Plateaus
Sperical Harmonic Expansions
Correlations
Hotspot Chemistry
Plume Plans
Profiles
Swell (and not so swell) Parameters
Eruption rates
Questionable Hotspots
Plume Problems
Cosmic Coincidences
Daffy Definitions
Plume Prophecies
Geophysicists, Geochemists, Geologists and the Earth
Discussion Topics
Abstracts and Essays

PRELIMINARY
PLUME SYMPOSIUM SCHEDULE

Wednesday evening 6:30 PM DABNEY
Reception and Poster Putting Up

Thursday morning BAXTER

8:45-9:00	Introduction and ground rules
9:00-9:15	Turcotte- Intraplate volcanism: Associations with plumes and other sources
9:15-9:25	Buck- A non-Rayleigh Taylor instability in upwelling below mid-ocean ridges
9:25-9:40	Halliday- Plumes, fossil, pseudo-plumes and the Cameroon line
9:40-9:55	Stern- Where is OIB source? Further constraints from arcs
9:55-10:15	Discussion (Leaders- Loper, Olson, Stevenson)
10:15-10:45	Coffee/Posters DABNEY
10:45-11:00	Hart- Mantle plumes: Interpreting the isotopic record (and other arcane pursuits)
11:00-11:10	Hoernle- Enriched shallow mantle beneath ocean basins-evidence from evolved ocean island volcanics
11:10-11:25	Gill- An OIB-BABB-subcontinental lithosphere connection
11:25-11:35	TBS
11:35-11:45	Hofmann- The origin of the species
11:45-12:15	Discussion (Leaders- Oxburgh, Stolper)
12:15-1:30	Lunch; Posters DABNEY

Thursday afternoon BAXTER

1:30-2:00	Anderson- The overview, the standard model and the strawman
2:00-2:10	Humphreys- Western US-interior structure tectonism and volcanism: Hot or wet?
2:10-2:25	Tanimoto- Long wavelength characteristics of Earth structure
2:25-2:40	Lay- The slab penetration controversy
2:40-2:50	Wyllie- Does ocean water reach mantle plume sources? If so what are the consequences?
2:50-3:00	McNutt- Plume observations: How much are they contaminated by lithospheric effects?
3:00-3:15	TBS
3:15-3:35	Debate (Leaders- Kanamori, Solomon)
3:35-4:05	Coffee/Posters
4:05-4:15	Albarede- The T, P, path of OIB generation
4:15-4:25	Menzies- Continental lower lithosphere- An insignificant reservoir for flood volcanism
4:25-4:40	TBS
4:40-4:50	Michael- Large scale mantle heterogeneity revealed by trace elements in MORB
4:50-5:00	Schilling- Mantle plume-Migrating ridge dynamics
5:00-5:15	Houseman- The geometry of thermal mantle plumes
5:15-5:30	Debate (Leaders- Gill, Wyllie)
6:00-7:45	Dinner- ATHENEAUM and local restaurants

Thursday evening MODELLING DEBATE BAXTER

8:00-9:45
Loper- Models of mantle plumes
Olson- The coupling between plume activity and geomagnetic reversal frequency
Richards- A mantle plume initiation model for the formation of Wrangellia and other oceanic flood basalt plateaus
Travis- High resolution calculation of compositional mixing in a plume
Kellogg- Mantle plumes and the 670 km discontinuity
Campbell- Stirring and structure in mantle plumes
Yuen- Various mechanisms for generating diapiric structures in the mantle
King- Plate velocity and subduction rate: A key to mantle differentiation?
(Leaders- Turcotte, Stevenson)

Friday morning BAXTER

8:30-8:40 Coffin- Crustal structure and emplacement rates of the Kerguelen and Ontong Java plateaus
8:40-8:50 Frey- Compositional differences between Hawaiian shields: Source or process related
8:50-9:00 Garcia- Geochemical evolution of a plume volcano: Lessons from Hawaii
9:00-9:10 Graham-Helium isotope variations along mid-ocean ridges: Implications for mantle heterogeneity
9:10-9:25 Craig- ^{3}He hotspots and the elusive primitive mantle component: or, Plume hunting along the Tonga Trail
9:25-9:40 White- Plume- asthenosphere interaction
9:40-10:00 Debate (Leaders- Clague, Klein)
10:00-10:30 Coffee/Posters

Friday morning

10:30-10:45 Black- The African lithosphere and alkaline intraplate magmatism
10:45-10:55 Basu- Primitive mantle plume origin for the Siberian flood basalts at the Permo-Triassic boundary and implications for the origin of continental flood basalt provinces
10:55-11:05 Hansen- Plumes in strongly time dependent convection: Effects from depth-dependent properties and thermal-chemical buoyancy
11:05-11:15 Hooper- The Columbia River basalt: A mantle plume or back arc extension? Chemical, isotopic and tectonic evidence
11:15-11:25 LeMasurier- Possibilities for mantle plume activity on Antarctica: Geochemical and structural characteristics of Cenozoic volcanism
11:25-11:35 Sleep- Time dependance of mantle plumes
11:35-11:45 Zindler- Isotopic evidence for plume-upper mantle mixing
11:45-12:15 Debate (Leaders- Silver, Spera)

Friday afternoon VENUS RAMO

1:30-2:50
Saunders- Geologic constraints on Venus Highland structure and evolution
Solomon- Venus: Global and regional tectonics
Phillips- Venusian hot spots and plumes

1:30-2:50	Schubert- Three dimensional models of Venusian interior dynamics
(cont'd.)	Bindschadler- Coronae: Plumes on Venus*
	Head- Centers of volcanism and volcanic sequence: Relation to tectonics in Highlands of Venus
	Kaula- Volatiles, plumes and Venus
2:50-3:15	Debate (Leaders- Burke, Sandwill)
3:15-3:45	Coffee/Posters
3:45-4:00	Wilson, Morgan, Vogt- Words of wisdom from Olympus

*in collaboration with G. Schubert, E. Stofan and other members of the Magellan Corona Sceince Analysis Team

Saturday morning ARMS

9:00-9:10	Okal- A surface -wave test of the lithosphere reheating model for hotspot swell formation
9:10-9:20	Pringle- Early Cretaceous plateau basalts, EM1 from the lower mantle, and the origin of the Dupal anomaly
9:20-9:30	Clague- An estimate of primary magma composition of tholeiitic basalt from Kilauea Volcano, Hawaii
9:30-9:40	Larson- Super plumes stop magnetic field reversals
9:40-9:50	Tarduno- Mantle plume volcanism and the formation of Ontong Java Plateau
9:50-10:00	Sandwell/Hill- Plume tectonics
10:00-10:10	Stolper- Mariannas BABB and the heterogeneity of the mantle
10:10-10:20	Tatsumoto- DUPAL anomaly in the Sea of Japan: A plate recycling model for OIB sources
10:20-10:35	Debate (Leaders- Davies, Langmuir)
10:35-11:00	Coffee/Posters
11:00-11:10	Acton- Global plate circuits and motion between hotspots: Paleomagnetic tests
11:10-11:20	Jurdy- Hotspots: Inferences from their distribution, and plate kinematics
11:20-11:30	Dalziel- Supercontinental fragmentation, Cambrian and Mesozoic-plume related?
11:30-11:40	Davies, G.- Mantle convection and the role of plumes
11:40-11:50	Evans- A general hotspot model accounting for known lithospheric structure
11:50-12:00	Yuen- Various mechanisms for generating diapiric plumes in the mantle
12:00-12:10	Froidevaux- Mantle plumes: What sizes, from what depths
12:10-12:20	King- Plate velocity and subduction rate: The key to mantle differentiation
12:20-12:35	Debate (Leaders- McNutt, Olson, Phillips)
Lunch	On your own
1:45	Additional talks
2:00	

Saturday afternoon MASSIVE OCEANIC AND CONTINENTAL MAGMATISM WORKSHOP; TOWARDS AN UNDERSTANDING
LEADER - Dave Stevenson

Discussion Topics:

1. Plumes- main flow or secondary?
2. - Rayleigh-Taylor or plate controlled?
3. - Enriched, depleted or recycled?
4. Depleted mantle- shallowest?
   - plume source?
5. Source of energy- lower mantle?
   - within?
   - core?
6. Plume heads or pervasive shallow EM?
7. CFB≡OIB≡IAB≡BABB≡MORB+? (?)
8. Whole mantle vs non-whole mantle?

Talks to be scheduled or possibly rescheduled (TBS):

Black- The African lithosphere and alkaline intraplate magmatism
Bonatti- MAR temperatures
Burke- The mantle role in mountain building: Implications for crust and mantle evolution as well as hot-spot distribution
Hanan- Pb isotopic constraints on mantle geodynamics: Observations from the Iceland hotspot and zero age MORBs
Hill- Plume tectonics
Jeanloz- Composition of the deep mantle
Kirschvink- A case for catastrophic true polar wander in the Cambrian
Kurz- Helium isotoes in ocean island volcanoes: Variability in time and space and some inferences about mantle plumes
Oxburgh- Helium, plumes and mantle reservoirs

4/8/91

Caltech Plume Symposium

TITLES OF PAPERS

*Acton, Gary (with Gordon)	Global plate circuits and motion between hotspots: Paleomagnetic tests
*Albarède, Francis	The T, P, path of OIB generation
*Anderson, Don L.	The overview, the standard model and the strawman
*Basu, Asish R.	Primitive mantle plume origin for the Siberian flood basalts at the Permo-Triassic boundary and implications for the origin of continental flood basalt provinces
Black, Russell	The African lithosphere and alkaline intraplate magmatism
*Bonatti, Enrico	Upper mantle temperature beneath the Mid-Atlantic Ridge
*Buck, Roger	A non-Rayleigh-Taylor instability in upwelling below mid-ocean ridges
*Burke, Kevin	The mantle role in mountain building: Implications for crust and mantle evolution as well as hot-spot distribution
*Campbell, Ian (with Griffiths)	Stirring and structure in mantle plumes
*Clague, David (with Weber)	An estimate of primary magma composition of tholeiitic basalt from Kilauea Volcano, Hawaii
*Coffin, Millard	Crustal structure and emplacement rates of the Kerguelen and Ontong Java plateaus
*Craig, Harmon	^{3}He in MORB, BABB hotspots and primitive mantle
*Dalziel, Ian W. D.	Supercontinental fragmentation, Cambrian and Mesozoic - plume related?
*Davies, Geoffrey	Mantle convection and the role of plumes
*Evans, John R. (with Iyer)	A general hotspot model accounting for known lithospheric structure
*Frey, Fred	Compositional differences between Hawaiian shields: Source or process related?
*Froidevaux, Claude	Mantle plumes: What sizes, from what depths?
*Garcia, Michael O.	Geochemical evolution of a plume volcano: Lessons from Hawaii

*Gill, James (with others)	An OIB-BABB-subcontinental lithosphere connection
*Graham, David (with others)	Helium isotopes in submarine tholeiitic basalts from the island of Hawaii
*Graham, David	Helium isotope variations along mid-ocean ridges: Implications for mantle heterogeneity
*Halliday, Alex (with others)	Plumes, fossil plumes, pseudo-plumes and the Cameroon line
*Hanan, Barry B.	Pb isotopic constraints on mantle geodynamics: Observations from the Iceland hotspot and zero age MORBs
*Hansen, Ulrich (with Yuen)	Plumes in strongly time dependent convection: Effects from depth-dependent properties and thermal-chemical buoyancy
*Hart, Stanley R.	Mantle plumes: Interpreting the isotopic record (and other arcane pursuits)
Head, J. W.	Centers of volcanism and volcanic sequence: Relation to tectonics in Highlands of Venus
*Hill, Robert I.	Plume tectonics
*Hoernle, Kaj	Enriched shallow mantle beneath ocean basins - evidence from evolved ocean island volcanics
*Hofmann, A. W.	The origin of the species
*Hooper, Peter R. (with Hawkesworth)	The Columbia River basalt: A mantle plume or back arc extension? Chemical, isotopic and tectonic evidence.
*Houseman, Gregory	The geometry of thermal mantle plumes
*Humphreys, Gene	Young western U.S.-interior tectonism and volcanism: Hot or wet?
*Iyer, H. M. (with others)	Imaging deep seismic structures beneath Yellowstone, Hawaii and Iceland, present hot spot locations in three global tectonic environments
Jeanloz, Raymond	Composition of the deep mantle
*Jurdy, Donna M.	Hotspots: Inferences from their distribution, and plate kinematics
*Kaula, William	The implications of volatiles at depth for plumes on Venus
*Kedar, Sharon (with others)	Relationship between hotspots and mantle structure: Correlation with whole mantle seismic tomography
*Kellogg, Louise	Mantle plumes and the 670 km discontinuity

*King, Scott (with Staudigel)	Plate velocity and subduction rate: A key to mantle differentiation?
*Kirschvink, Joseph	A case for catastrophic true polar wander in the Cambrian
*Kurz, Mark D.	Helium isotopes in ocean island volcanoes: variability in time and space and some inferences about mantle plumes
Langmuir, Charles H.	Major element systematics of ocean island basalts
*Larson, Roger L.	Super plumes stop magnetic field reversals
*Lay, Thorne	The slab penetration controversy
*LeMasurier, Wesley	Possibilities for mantle plume activity on Antarctica: Geochemical and structural characteristics of Cenozoic volcanism
Leitch, A. M. (with others)	The stabilization of hot plumes by variable mantle properties
*Loper, David S.	Models of mantle plumes
*McNutt, Marcia	Plume observations: How much are they contaminated by lithospheric effects?
*Menzies, Martin	Continental lower lithosphere - An insignificant reservoir for flood volcanism
*Michael, Peter J.	Large-scale mantle heterogeneity revealed by H_2O and trace elements in MORB
*Olson, Peter	The coupling between plume activity and geomagnetic reversal frequency
*Oxburgh, E. R.	Helium, plumes, and mantle reservoirs
*Phillips, Roger	Venusian hot spots and plumes
*Phipps, Stephen P.	Hot spots, hot lines, and magmatism from plume-modified lithosphere
*Pringle, Malcolm	Early Cretaceous plateau basalts, EM1 from the lower mantle, and the origin of the Dupal anomaly
*Ray, Terrill (with Anderson)	Correlation of hotspot isotopic data with mantle tomography
*Richards, Mark (with others)	A mantle plume initiation model for the formation of Wrangellia and other oceanic flood basalt plateaus
*Saunders, R. Steven (with others)	Geologic constraints on Venus Highland structure and evolution

*Schilling, Jean-Guy	Mantle plume - Migrating ridge dynamics
*Schubert, Gerald	Three dimensional models of Venusian interior dynamics
*Scrivner, Craig (with Anderson)	Correlation of Pangea and subducted slab with global seismic tomography
*Sleep, Norman H.	Time dependance of mantle plumes.
*Solomon, S. C.	Venus: Global and regional tectonics
*Stern, Robert J.	Where is the OIB source? Further constraints from arcs
*Stofan, E. R. (with others)	Coronae: Plumes on Venus* (*in collaboration with G. Schubert, Ellen Stofan & other members of the Magellan Corona Science Analysis Team)
Stolper, Edward	Marianas BABB and heterogeneity of the mantle
*Takata, Toshiko (with Anderson)	Correlation between plate motion and tomography
*Tanimoto, Toshiro (with Inoue)	Long wavelength characteristics of Earth structure
*Tarduno, John A. (with others)	Mantle plume volcanism and the formation of Ontong Java Plateau
*Tatsumoto, M.	DUPAL anomaly in the Sea of Japan: A plate recycling model for OIB sources
*Todesco, M) (with Spera)	Convective evolution of a chemically-stratified fluid heat from below: Application to mixing within the upper mantle
Travis, Bryan	High resolution calculation of compositional mixing in a plume
*Turcotte, Donald L.	Intraplate volcanism: Associations with plumes and other sources
White, William	Plume-asthenosphere interaction
*Wilson, J. Tuzo	On moving mountains
*Woods, M. T. (with Okal)	A surface-wave test of the lithosphere reheating model for hotspot swell formations
*Wyllie, Peter	Does ocean water reach mantle plume sources? If so what are the consequences?
*Yuen, David A. (with others)	Various mechanisms for generating diapiric structures in the mantle
*Yuen, David A.	The stabilization of hot plumes by variable mantle properties

*Zhang, Yu Shen (with Tanimoto)	Ridges and hotspots: perspectives from global tomography
*Zhang, Yu Shen (with Tanimoto)	Oceanic lithosphere: perspectives from Love wave phase velocity
Zindler, Alan	Isotopic evidence for plume-upper mantle mixing

*Abstracts received as of 5 April 1991

ONAMASTICON

asthenosphere- Literally the "weak layer". Various physical arguments suggest an upper mantle low-viscosity region of several hundred kilometers thickness. Unfortunately, some geochemists have redefined it as the "depleted low viscosity zone", the "depleted asthenosphere" or the MORB-reservoir. Others have used the term "asthenosphere" for the whole upper mantle. In current literature, "asthenosphere", "MORB reservoir", "depleted mantle" and "upper mantle" are synonyms. This makes it semantically impossible to imagine enriched basalts such as CFB and OIB as originating in the "upper mantle". Hence, CL and lower mantle and D" are often treated as "the only remaining possibilities" for "enriched" or "primitive" mantle. Recent discussions of asthenospheric pollution, enriched streaks, tongues, and giant plume heads displacing the asthenosphere, and contamination by continental lithosphere (CL) highlight the sterility of the "depleted asthenosphere" concept and the need for a widespread, shallow enriched layer (see "perisphere").

continental lithosphere- Usually defined as the "mantle underneath the continent at the time of some event". Generally assumed to be a permanent part of the continent. Can soak up melts and LIL and is, in part, composed of accreted island arcs and mantle wedges. LIL and HFSE studies, however, show that it is not primarily made at convergent zones and requires it is not fertile nor a potential source of magmas. However, it has been proposed as a source of both CFB and OIB, primarily because it is assumed that the "asthenosphere" is depleted and only MORB comes out of "normal" mantle. In some theories a plume is required to reactivate, mobilize or delaminate the CL so that it can provide enriched magmas. Being embedded in the cold thermal boundary layer and, probably infertile (even if enriched) it is not a stand-alone plume source-it requires a plume to make it work. The arguments used to enrich the CL enrichment by trapped melts and subduction products apply to the shallow mantle in general. In fact, the lithosphere can act as both a buoyancy and strength filter, making the sublithospheric mantle a sink for LIL, i.e. an enriched asthenosphere is a natural result of mantle differentation and intramantle fluid transfer processes. The lithosphere is an effective lid to mantle melts unless it is under tension or broken. The maximum thickness of CL occurs under ancient "stable" shields, ~180 km. The 600°C isothermal defines the "plate thickness" or boundary between rigid and viscous behavior. In high heat flow areas, with thermal gradients of 10 to 20°/km, the "permanent" lithosphere is only 60 to 30 km thick. Clearly, the continental lithosphere is not a significant reservoir although it serves as a mantle "cold-finger", affecting trace elements of traversing magmas. CL is probably more easily moved away from hot upwellings, than penetrated by them. CFB outpourings are rare but tend to be voluminous since melts collect under the lithosphere until plate reorganizations put it into tension.

D" - The highly irregular, inhomogeneous layer at the base of the mantle which is embedded in a TBL. In a homogeneous mantle this is the only plausible region in which buoyant instabilities can originate (ignoring phase changes, partial melting and near-surface induced instabilities). Since the CMB is the largest density contrast in the Earth it represents the sink for dense material from the mantle and light material from the core. D" may be chemically distinct (intrinsically dense) compared to the bulk of the lower mantle. High temperatures can overwhelm the

chemical effects and plumes may rise into the lower mantle. A "chemical" plume is likely to cool off and sink back to D". Theoretical calculations suggest high thermal gradients and large viscosity contrasts cannot be built up in D" in a convecting mantle, limiting the possibility of strong plumes. The effects of pressure on thermal expansion and conductivity also serve to suppress plume-like instabilities in D". Plumes require a high ratio of bottom heating to internal heating, a condition appropriate for the mesosphere but not for D".

hotspot- A volcano, or the inferred location of a volcano, except at island arcs or midocean ridges, unless exceptionally large. Sometimes referred to as "coldspot", "wetspot" or "melting anomaly". Often, but not always (St. Peters-Pauls), volcanic. Often, but not always (Azores), hot. Often found at triple junctions, in continental rifts, along reactivated sutures, at sites of plate reorganizations, propagating rifts, at new and old sites of jumped rifts. Hotspots may or may not be fixed relative to one another but they certainly drift relative to the rotation and magnetic poles. Hotspot influences have been reported as far away as 1000 km from conjectured "point sources" (a concept needed in "fixed hotspot" discussions). "Hotlines" and "hot regions" are generalizations of "hotspot" and are needed, along with the concepts of enriched "tongues", "streaks", "lamina", "channels" etc. to protect the "Depleted Asthenosphere" paradigm from replacement by the "Enriched Shallow Mantle" alternative. Many "hotspots" are short lived, leave no tracks, erupt simultaneously over large areas, erupt MORB-like basalts, have low $^{3}He/^{4}He$, erupt continuously under continents that have moved thousands of kilometers, erupt for tens of millions of years from a single ediface on a moving plate, are close to ridges, are close to continental boundaries or are apparently triggered by changes in plate stresses or configurations. There are somewhere between 20 and 120 "hotspots" but no general definition applies to more than a few except that none of them are spots.

lithosphere- Often defined as the "thermal boundary layer" (TBL) or the "mantle above the horizontal isotherm". With these definitions its thickness is generally 100 to 200 km and this depends on age and thermal properties, such as lattice conductivity, but not on strength. More logically the "lithosphere" is that part of the mantle which is strong enough to behave coherently over long periods of time and to have a long-term attachment to the overlying crust. The 600°C isotherm defines the base of the "elastic plate", the maximum temperature of mantle earthquakes, the onset of viscous flow at mantle stress in silicates, and the depth of the seismic high-velocity layer. This temperature is much less than the melting temperature and the equilibration temperatures of mantle xenoliths which are often associated with the "continental lithosphere." These nodules may come from "the convecting mantle" and not from mantle that is rigidly attached to the overlying mantle. In principle, this enriched mantle, which flows readily can be found anywhere, not just below continents. However, because it flows readily it can easily be pushed aside by deep, hot, buoyant upwellings from, for example, a depleted reservoir. A shallow enriched reservoir (called here the "perisphere") would be complementary to both the continental crust and the depleted (MORB) reservoir and, hence, would exhibit crude "mantle geochrons". A shallow layer can be constantly re-enriched by trapped melts and subduction products and is probably hydrated and buoyant. The lower mantle may have a high viscosity. A slowly convecting lower mantle may provide relatively stationary "hotspots" which can stabilize the locations of upper mantle upwellings. If the lower mantle is chemically distinct from the upper mantle it will slow down the cooling of the earth and may preclude transfer of material between the upper and lower mantles. the density of the lower mantle cannot distinguish

between a chemically stratified mantle. This fact has been used as proof that the mantle is homogeneous and, therefore, that whole mantle convection prevails. If buoyant upwellings originate in the upper mantle they may be the result of "differential heating from below", a boundary condition yet to be treated theoretically or experimentally. In contrast to the lower mantle the core is almost isothermal and this is an appropriate boundary condition for D" plumes (plus a stress-free condition) making D"-based plumes highly non-stationary).because of its buoyancy and ability to flow, rather than by its strength. It is also not a stand-alone plume reservoir but it can interact with hot upwellings rising through it. Its chemical characteristics are implanted into "initial" magmas, before it is pushed aside or depleted, and the "final" magmas, as the weak perisphere flows laterally back into the region being vacated by a waning upwelling.

lower mantle- Variously described as 1. primitive, unfractionated, undifferentiated material, differing from the "depleted" upper mantle by not having lost its continental crust component 2. identical in composition to the upper mantel 3. "enriched" in SiO_2 and FeO compared to the upper mantle 4. the refractory, depleted, infertile, dense product of mantle differentiation, complementary to the continental crust and upper mantle depleted and enriched reservoirs. In many scenarios the lower mantle is the source of plumes and "enriched" (or "primitive") magmas, mainly by a process of elimination, since, semantically, the "upper mantle" is depleted. The lower mantle may have a high viscosity. A slowly convecting lower mantle may provide relatively stationary "hotspots" which can stabilize the locations of upper mantle upwellings. If the lower mantle is chemically distinct from the upper mantle it will slow down the cooling of the Earth and may preclude transfer of material between the upper and lower mantles. The density of the lower mantle cannot distinguish between a chemically stratified mantle. This fact has been used as proof that the mantle is homogeneous and, therefore, that whole mantle convection prevails. If buoyant upwellings originate in the upper mantle they may be the result of "differential heating from below", a boundary condition yet to be treated theoretically or experimentally. In contrast to the lower mantle the core is almost isothermal and this is an appropriate boundary condition for D" plumes (plus a stress-free condition) making D"-based plumes highly non-stationary).

mesosphere- Transition region. The main minerals are the "spinel" forms of olivine, garnet, majorite and the garnet forms of clinopyroxene. The "ilmenite" form of pyroxene may exist in colder regions. May or may not differ in chemistry from shallow mantle (perisphere) and lower mantle. In some models it is the fertile, depleted MORB-reservoir and the sink of subducted, de-metasomatized, de-watered slabs. In others it is the source and sink of enriched basalts and the continental lithosphere. In the less imaginative scenarios it is identical to the rest of the mantle.

onomastic- Of or pertaining to a name or names. Onomatopoiein - to coin names.

onomastican- Neither a wooley mammoth nor a one-toothed dinosaur. A thesaurus (which is also not a dinosaur).

perisphere- An "all around" or global shallow layer. Probably weak, hydrous and enriched. Interacts strongly with the initial and final melts from depleted upwellings. Can be sampled passively, from above, by plate reorganizations and lithospheric extension, or actively, from below, by upwellings. Easily (eventually) displayed, replaced or depleted by hot upwellings. Prevents initial (and final) melts at new (or dying) rifts from being N-MORB-like. Constantly re-enriched by

trapped small-volume melts and subduction. Has the physical properties usually attributed to "asthenosphere" and "plume heads" [readily flows laterally] and chemical properties often attributed to CL. The neutral word is needed to avoid mixing chemical and physical concepts (e.g. the "asthenosphere" is not, by definition, depleted.

plume- A large ornamental feather, a token of honor or achievement, to pride or congratulate oneself, to scribble, to dung; to puff, crow, boast, flourish, gloat, bray, vaunt or revel.

thesaurus- A late Pasadenean creature found encased in mudd, having choked on its words.

vulcanodon- "Volcano tooth" sauropod. Found in Zimbabwe in early Jurassic rocks sandwiched by lava flows (Karoo?), proving that continental flood basalts can extinct dinosaurs. The rest of the dinosaurs did not survive the late Cretaceous Deccan Trapps. Dinosaurs originated at 225 Ma, about the time of the Siberian Trapps, showing that these things work both ways.

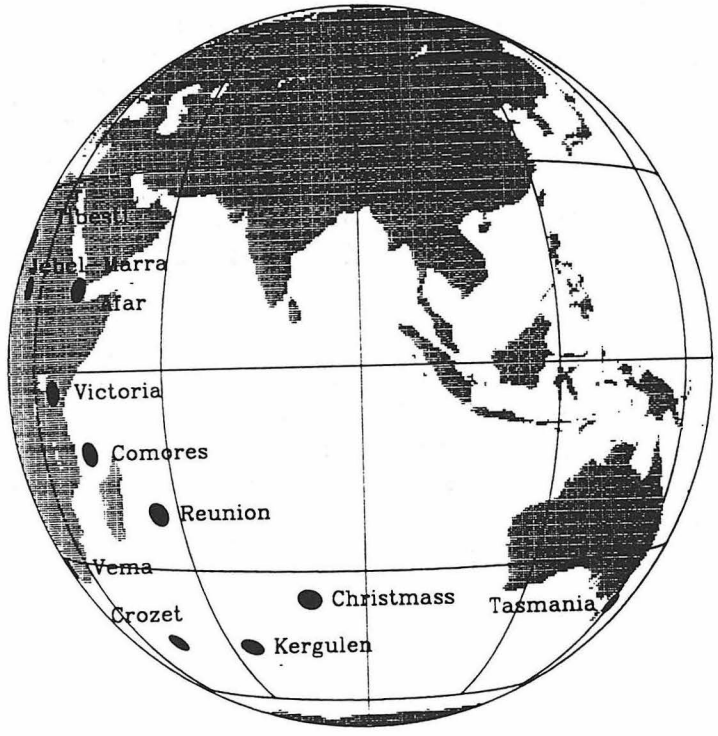

HOTSPOT TIME LINE

Archean	Komatiites
1200 Ma	Coppermine River
1120-1140 Ma	Keweenawan
500-570 Ma	N. Australia
220-250 Ma	Siberia
180 Ma	Karoo Africa- N. America separate
170 Ma	African rift activity (180-130 Ma)
160 Ma	Fast Continental Velocities India-Antarctica Separate
150 Ma	Shatsky Rise Mozambique Plateau
140 Ma	Appalachian-Labrador Rise E. Indian Ocean opens
130 Ma	Mid Pacific Mts. Wallaby Plateau S. China Sea
120 Ma	Africa-S. America separate High subduction rates Falkland Plateau Etendeka

---

120 Ma	Fast Pacific spreading Ontong-Java; Parana Kerguelen Kimberlites Manikiki Plateau
110 Ma	TPW Wallaby Plateau Broken Ridge Marcus Wake Seamounts Rapid Kula subduction
100 Ma	Labrador Rise; Tethys Ridge lost Pacific plate direction change Kerguelen Plateau Marshalls; Hess Rise Australia

100 Ma	Antarctic
90 Ma	Hairpin, kimberlites, 90°E Ridge Rapid spreading Gorgona komatiite India fast moving Rio Grande Rise Caribbean
80 Ma	Reunion; Greenland Canada St. Helena fades; Tasman Sea opens Corner Seamounts; Cruiser Plateau Line Islands Hawaii bend Mid Pacific Mountains
70 Ma	Cape Verde Louisville Ridge Reunion; Chagus Laccadive Ridge Greenland-Europe Ridge Bermuda uplift; Deccan Walvis Ridge Madagascar Ridge
60 Ma	Afar; Greenland-Br. Tertiary Aleutians Line Islands; Iceland SWIR direction change Emperor Seamounts Crozet Plateau
50 Ma	Global Reorganization Bermuda TPW slows

---

40 Ma	Hawaii peak; Cape Verde; Eiffel; Sea of Japan; Kerguelen; Tristan off; Andes; Bermuda -Labrador Rise; Nazca Ridge Pacific Direction change Caroline Basin Canary; Hawaii wanes Bermuda wanes S. Fiji Basin PareceVela Basin; Red Sea S. China Sea; Azores
30 Ma	Bermuda wanes; Ethiopia; Iceland wanes Arizona; Aden; Yeman; Scotia Sea Marie Byrd Land rifts Midway; Kerguelen Shikoku Basin

30 Ma	Ethiopia Peak; Spreading direction change, S. Pac. Cape Verde 12 volcanic chains on Pacific Plate (26-0 Ma) Hawaii Azores on; Fernando on; Iceland Large change in Sea Level
20 Ma	Cape Verde; Louisville off; S. Shetlands; Cordillera wanes Mangaia; E. China; Snake River; Hawaii peak (15-17) Canary - high activity; Azores (16-20 Ma) Reykjanes Ridge, scarps; Parece Vela off; Bouvet Columbia River; St. Helena; Hawaii wanes; Mangaia off Yellowstone on; Gulf of Alaska Canary, C. Europe, Afar, Galapagos; Cape Verde Bouvet; Erebus; Easter E. Pacific hotspots, Canaries wane; Fiji Great Meteor, Cook-Austral Fernando de Noronha; Columbia River wanes Fiji
10 Ma	Cape Verde, Necker; Fiji off; Canaries off Plates speed up; Caroline Seamounts St. Helena wanes; Ascension Canary, high activity; E. China off Lau Basin; Ross

Global Distribution of Hotspots

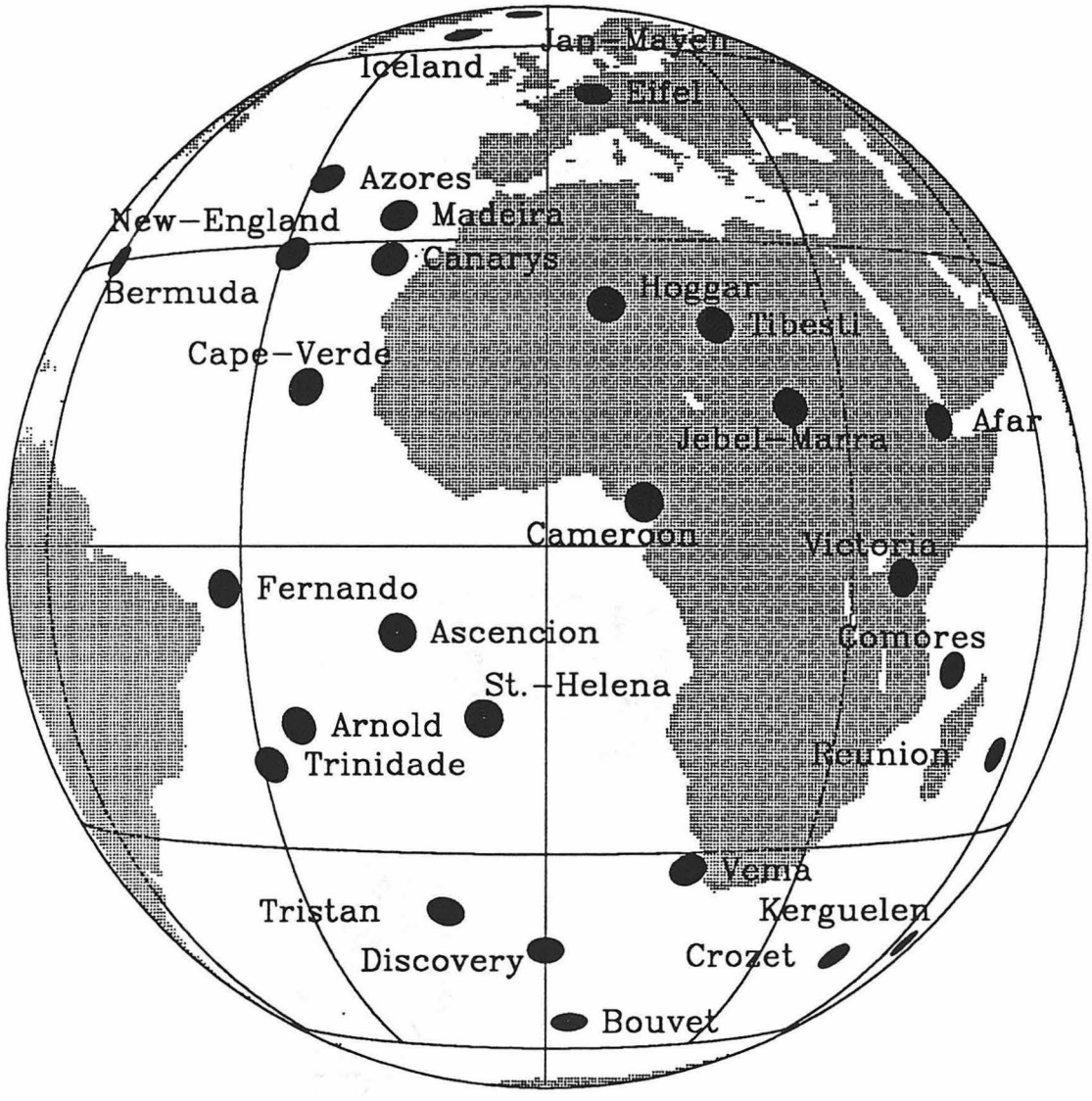

Global Distribution of Hotspots

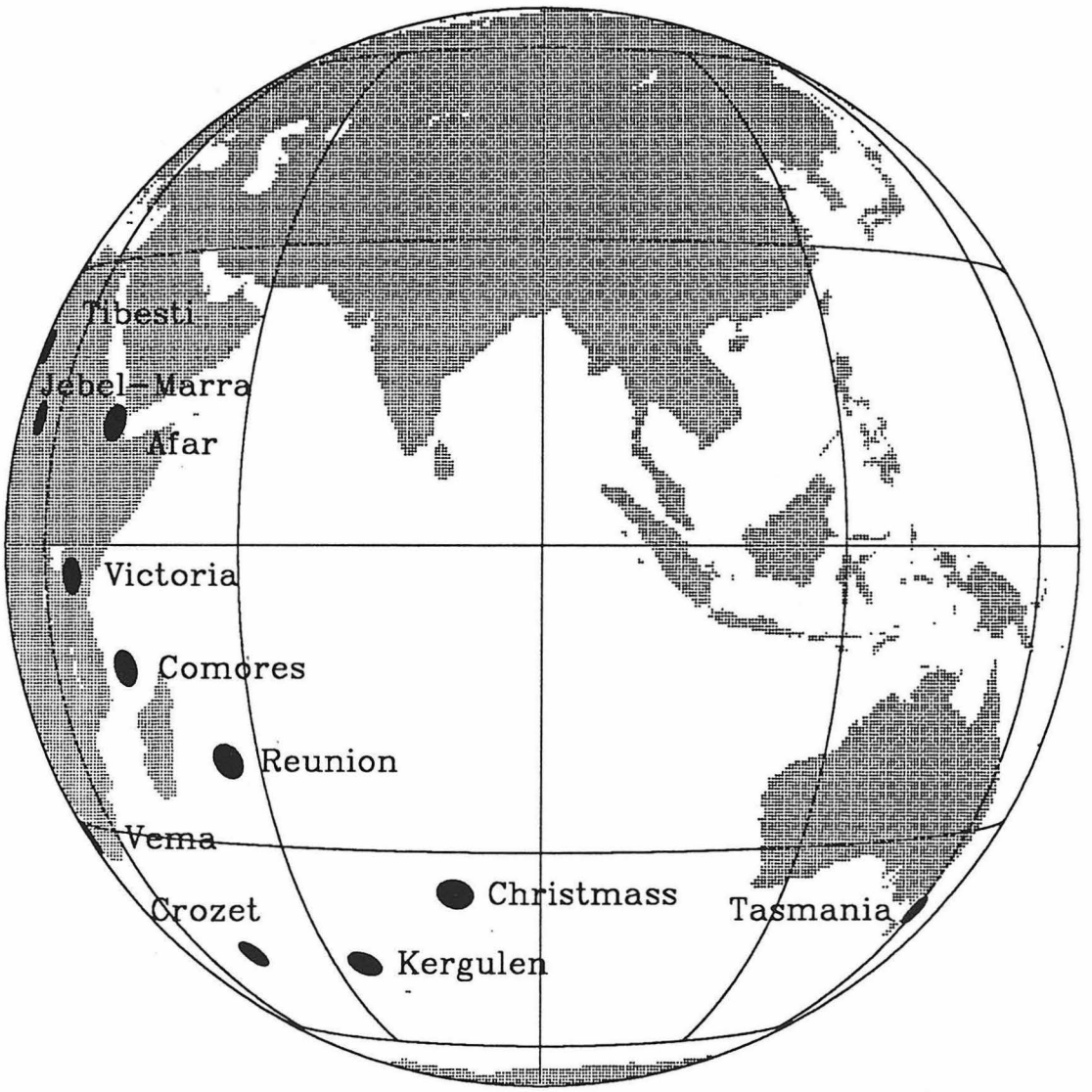

Global Distribution of Hotspots

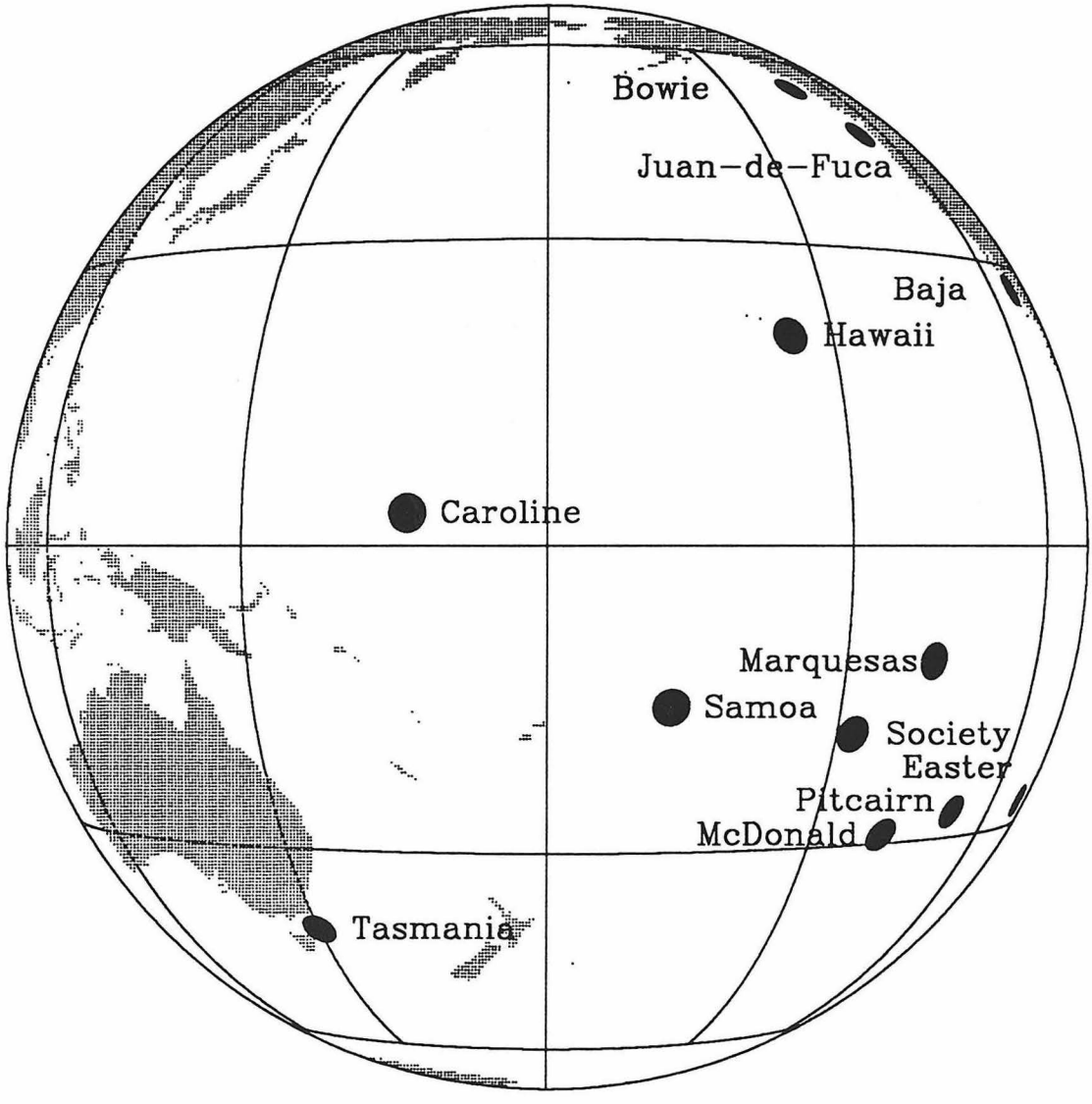

Global Distribution of Hotspots

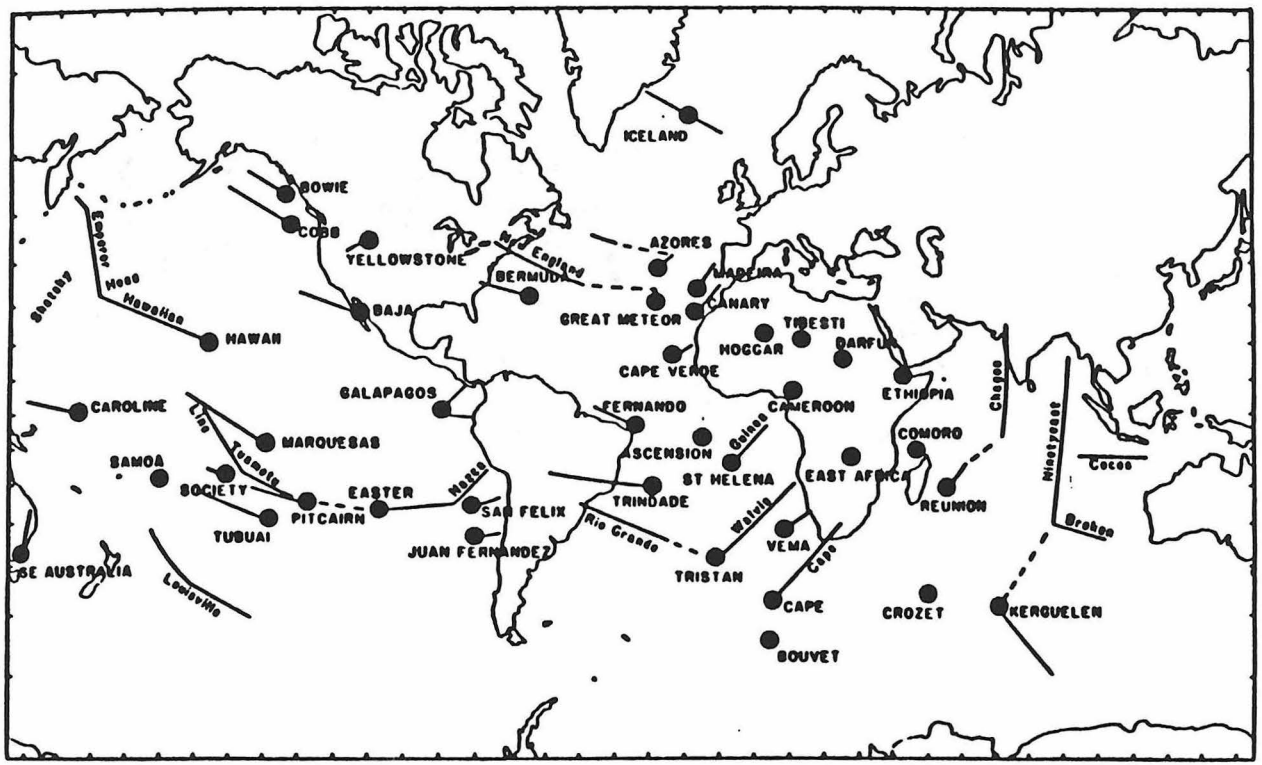

FIGURE 8-4
Global distribution of hotspots and hotspot tracks (after Crough, 1983).

Global Distribution of Hotspots (after Morgan)

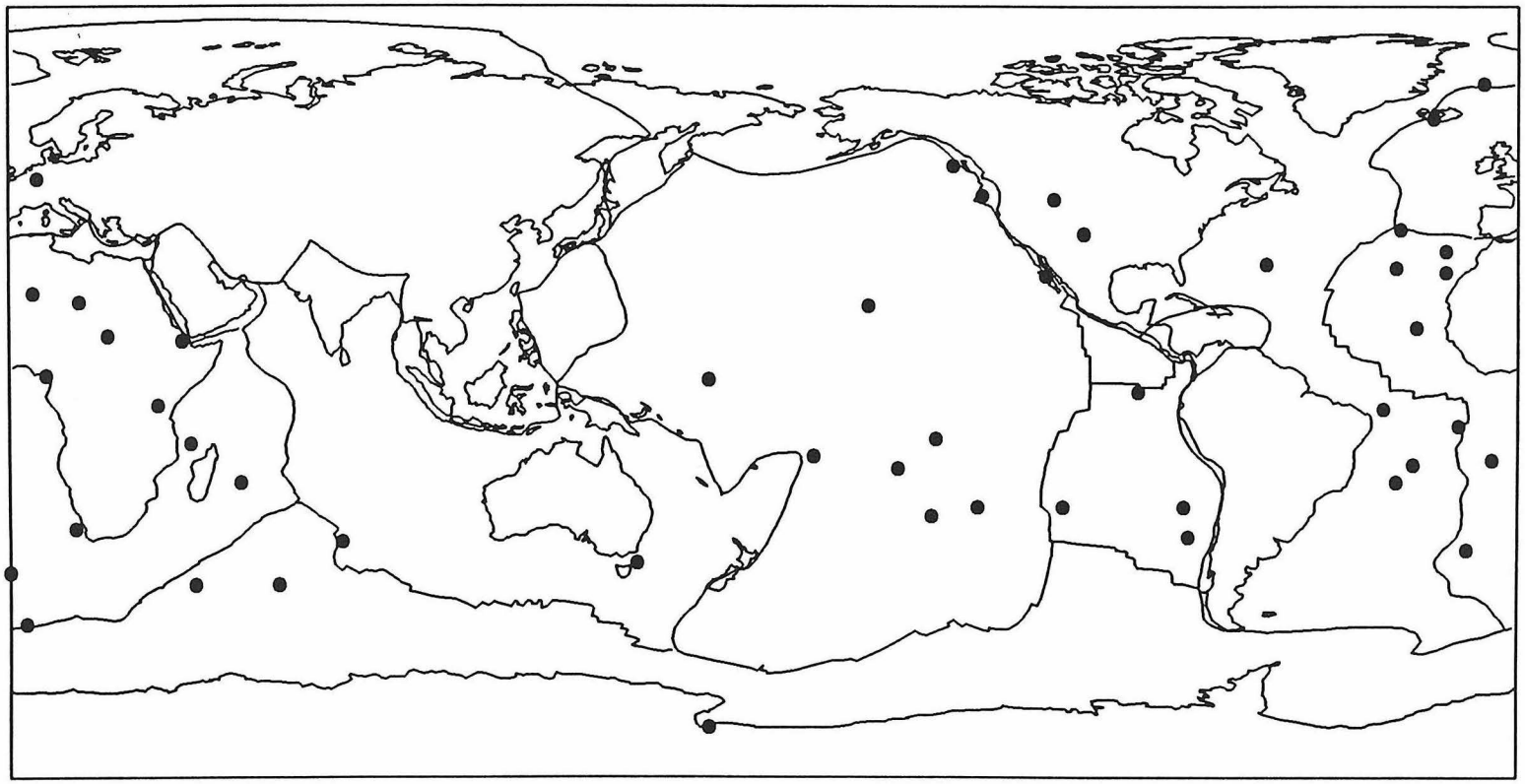

Global Distribution of Hotspots (after Vogt)

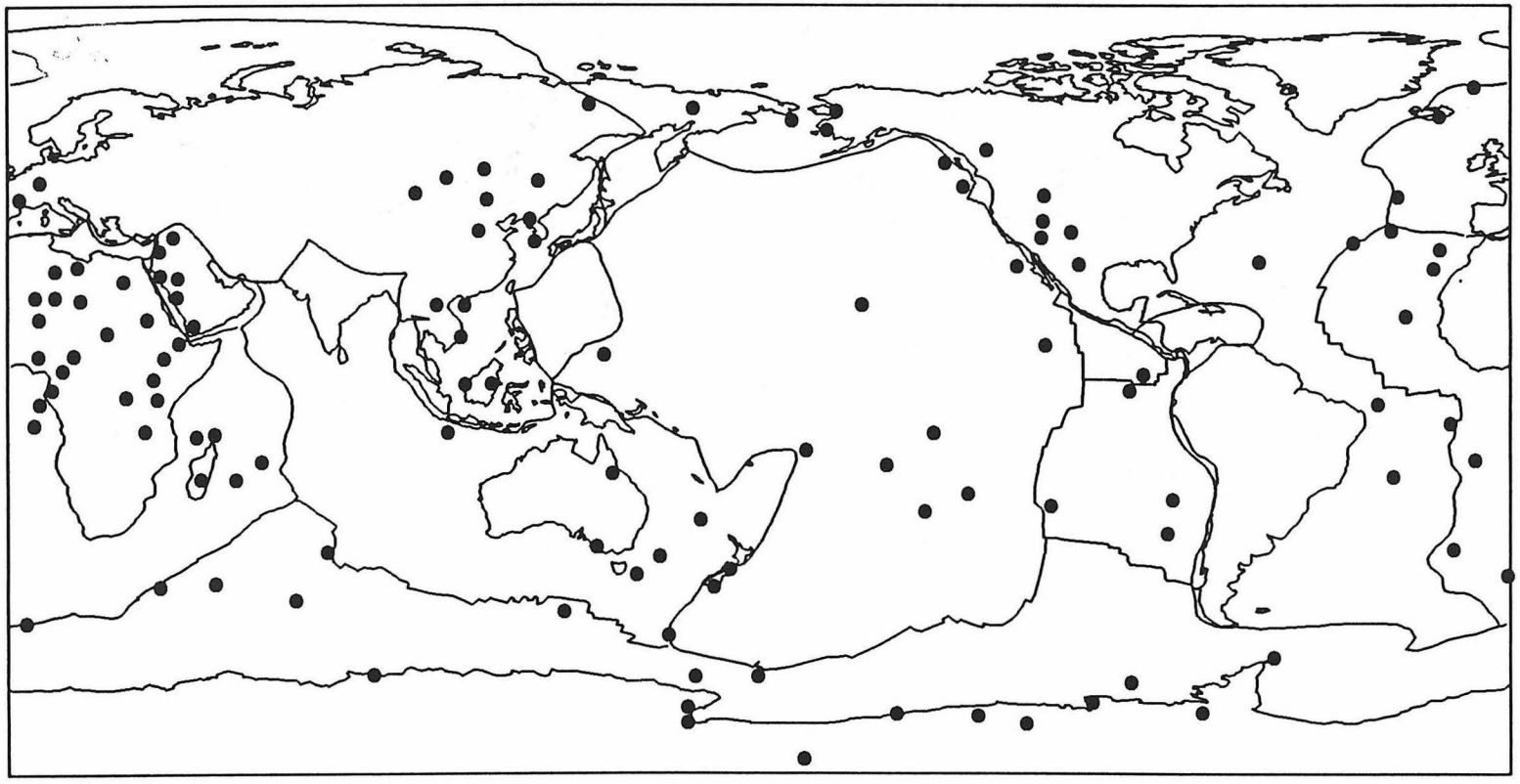

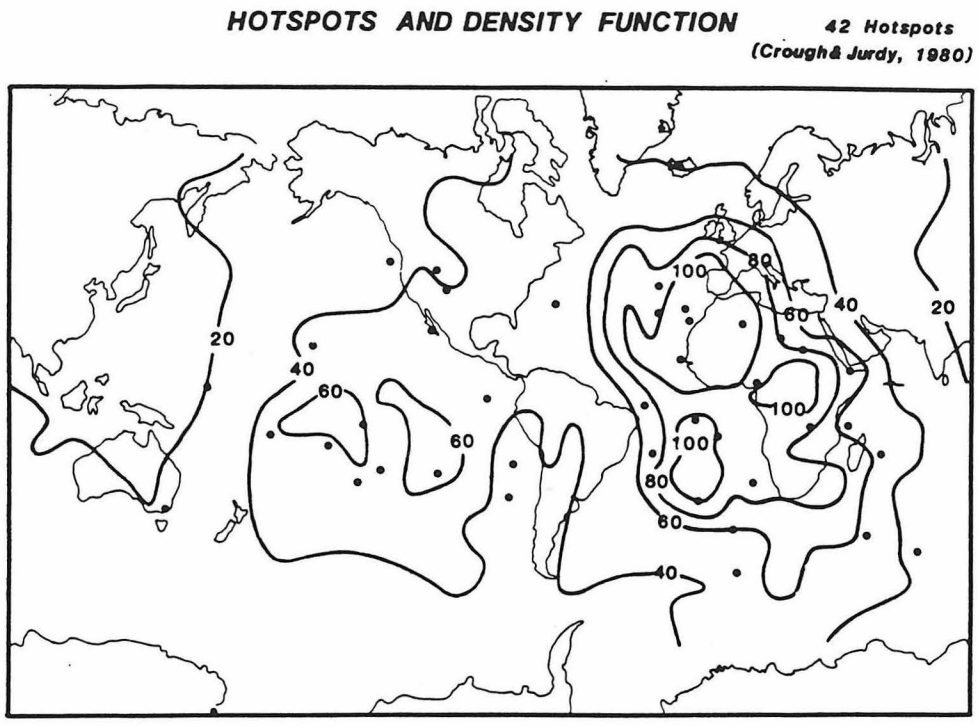

Fig. 3. Distribution of 42 hot spots [*Crough and Jurdy*, 1980]. Hot spot density function contoured in units of hot spots per earth area as extrapolated from local density.

served density ($\simeq 180$) and $n = 6$ gives $A = 6/180 = 1/30$, a relatively small area (about one half of the box area used in the chi-square analysis). This density, when it is integrated over the earth's surface, gives 46 hot spots rather than 42. (This error is about what could be expected for the sample size.) Similarly, a density function for the larger hot spot data set is computed and shown in Figure 4. As no normalization is used, the densities are higher than those in Figure 3 simply because of the greater number of hot spots. The main difference between this density function and the one in Figure 3 is the highs over Asia and North America. As noted previously [*Anderson*, 1982; *Chase and Sprowl*, 1983; *LePichon and*

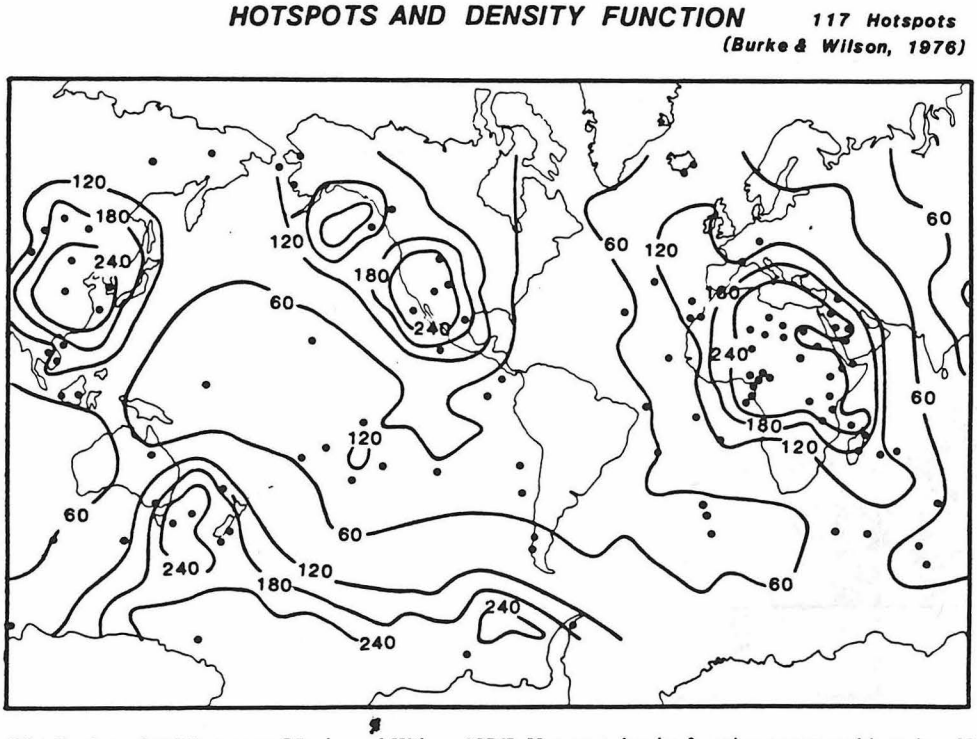

Fig. 4. Distribution of 117 hot spots [*Burke and Wilson*, 1976]. Hot spot density function contoured in units of hot spots per earth area as extrapolated from local density.

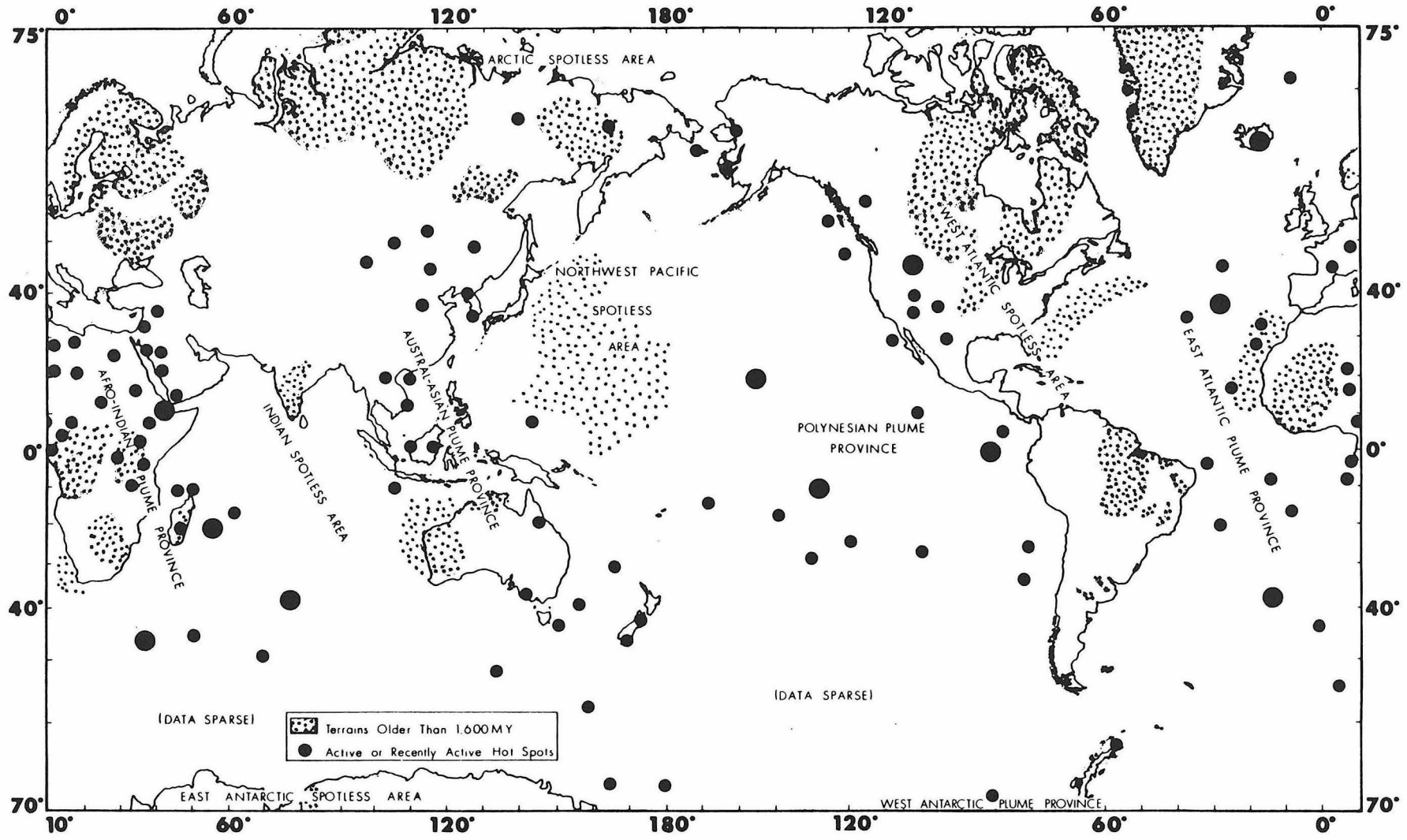

Fig. 5. Hot spots (Figure 1) in relation to shield areas older than ~1600 m.y. (stippled; based on *Hurley and Rand* [1969] and other sources). The actual area of pre-1600-m.y. crust may be larger than shown. In ocean basins, stippling shows lithosphere 110 to perhaps 180 m.y. B.P. in age. Note that 'continental' hot spots seem to occur preferentially on crust younger than 1600 m.y.

P. VOGT

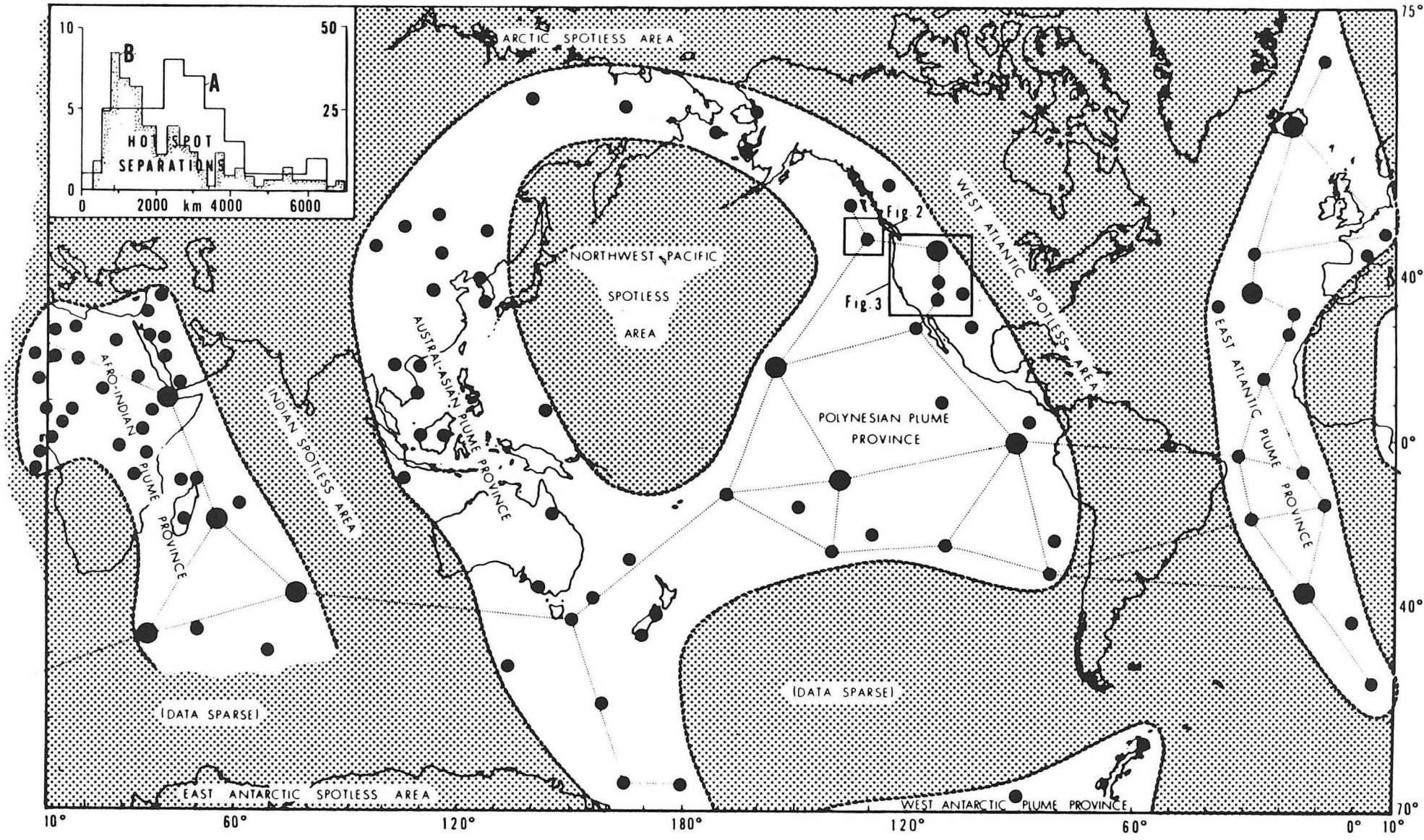

Fig. 1. Locations of world's hot spots, modified slightly from *Burke and Wilson* [1976]. Stippled spotless areas are generally devoid of hot spots. Plume provinces are regions of relatively closely spaced hot spots, subjectively interpreted. Large solid circles denote relatively more productive hot spots. Distances between the most well-defined hot spots (dashed straight lines approximate actual great circle arcs) are shown in histogram A. If all distances between adjacent hot spots (including polar areas not shown here) are measured, histogram B results. Boxes show two complex areas—examples of regions where hot spot definition is uncertain (Figures 2 and 3).

P. Vogt

SEISMIC VELOCITIES IN TRANSITION REGION COMPARED WITH EXPECTED LOCATIONS OF SLABS TRAPPED IN UPPER MANTLE (MESOSPHERE)

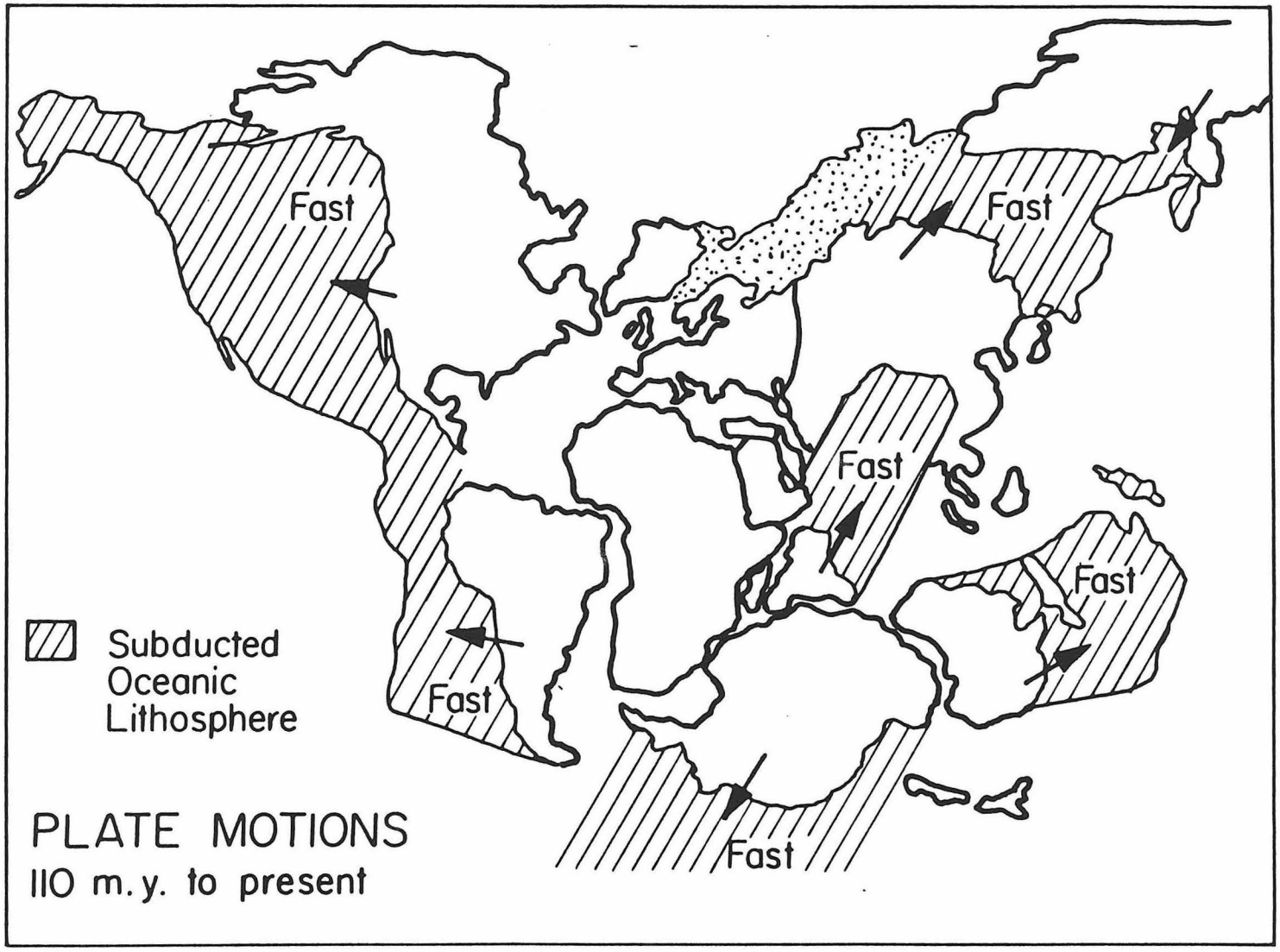

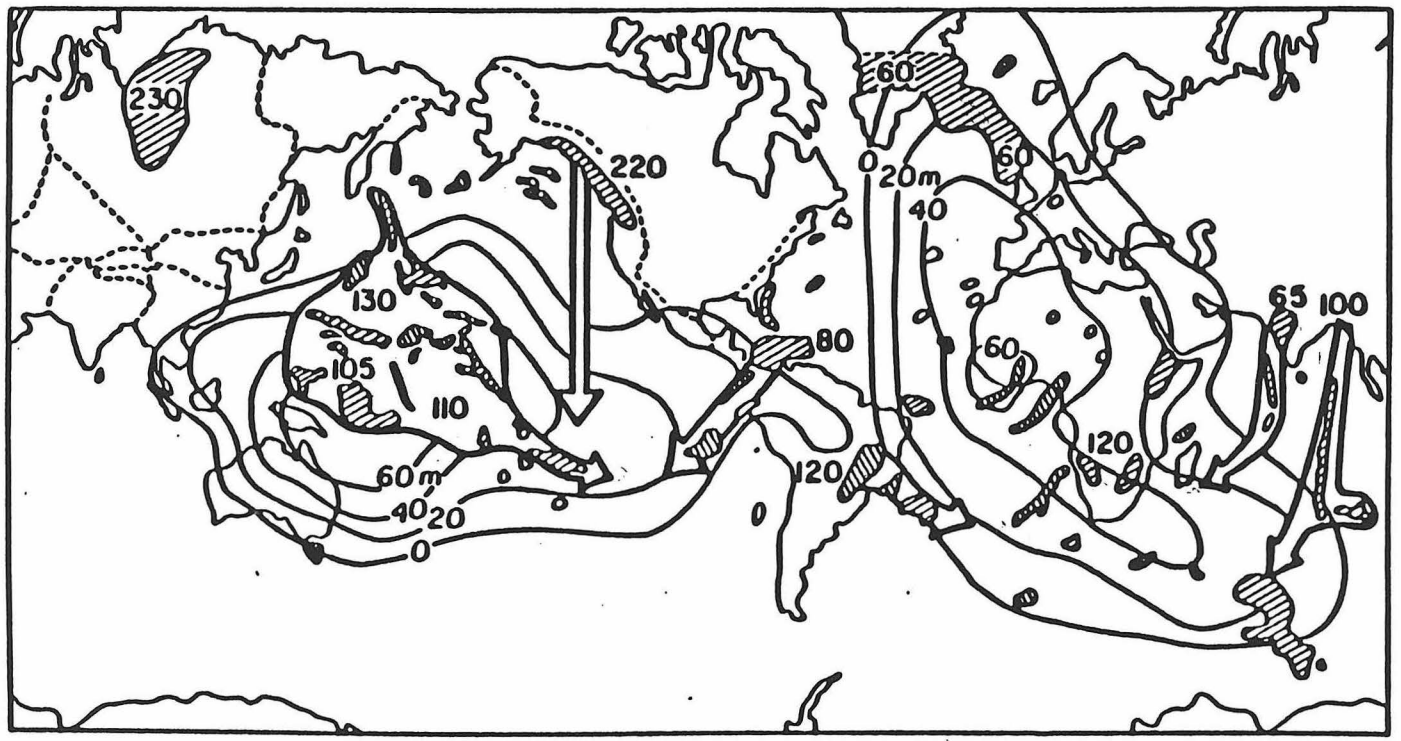

Map of continental flood basalts, hotspots, and oceanic plateaus, with age in millions of years. The period between 65 and 130 My ago was one of extensive volcanism and most of this occurred inside geoid highs (contours) which, in general, are areas of high elevation. Some of the basalt areas have drifted away from their point of origin (arrows). Geoid highs seem to represent hotter than normal mantle.

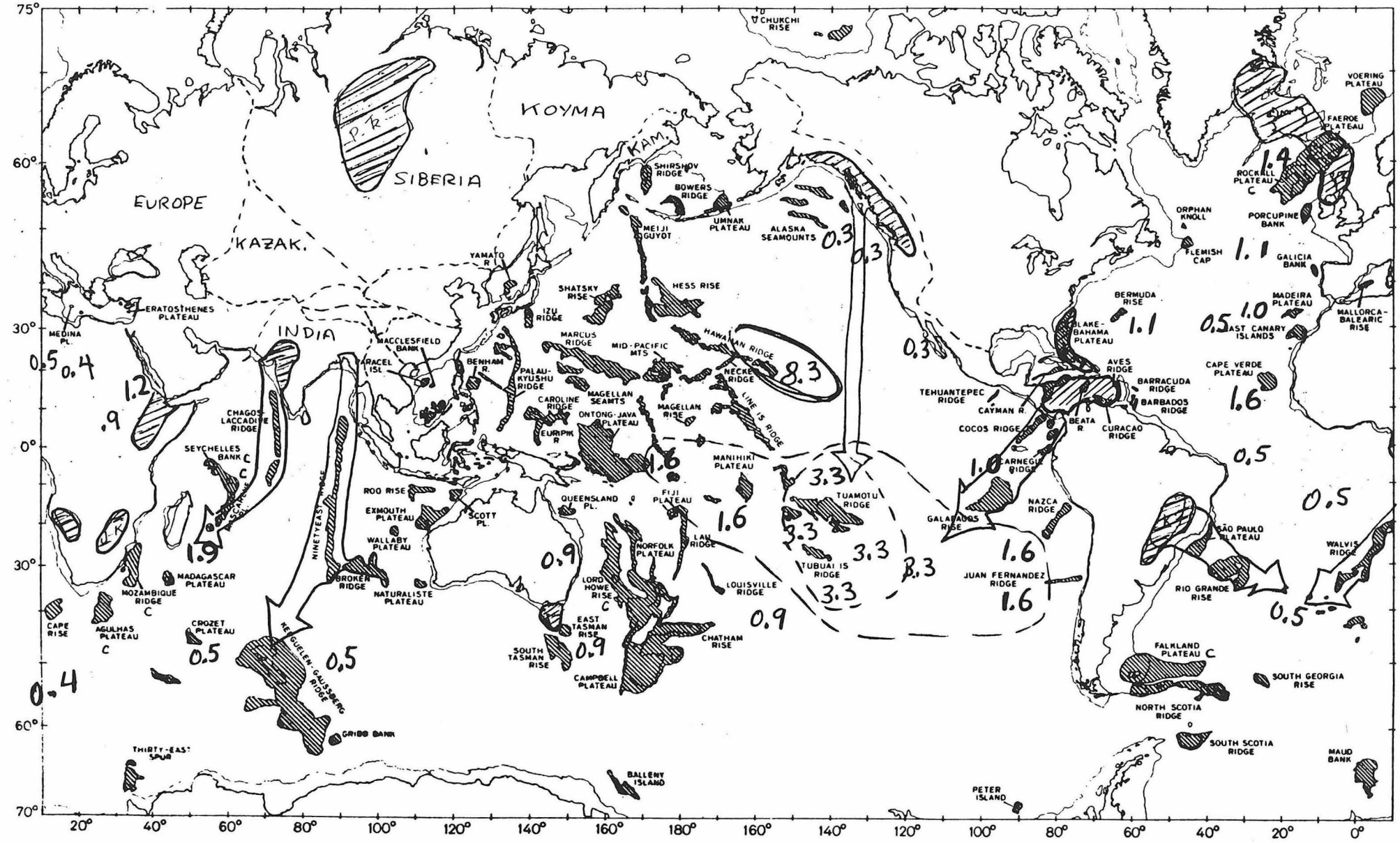

Fig. 1. Distribution of oceanic plateaus (shaded areas) in the world's oceans.

Flux (sleep)

SPHERICAL HARMONIC EXPANSIONS

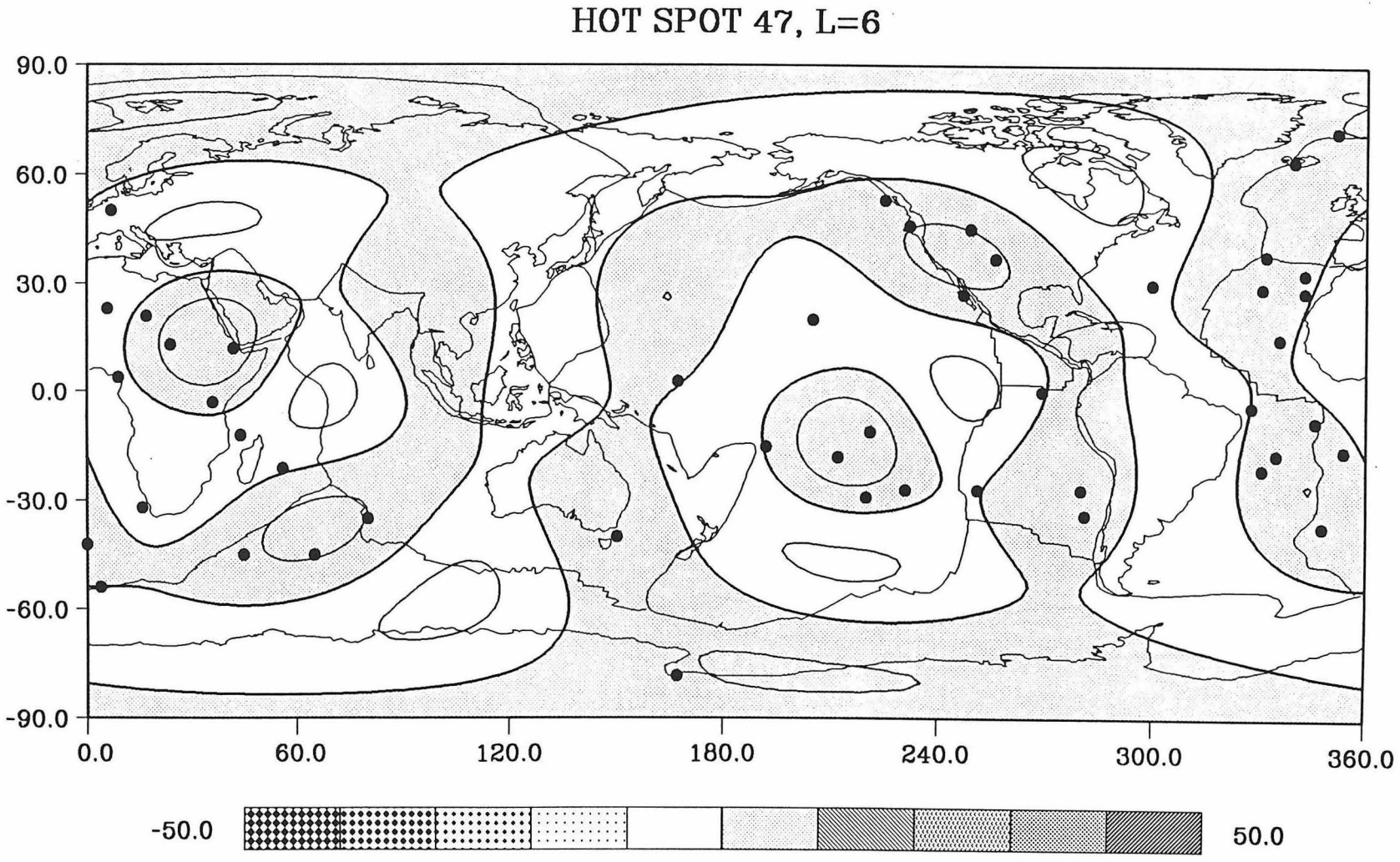

HOT SPOT 117

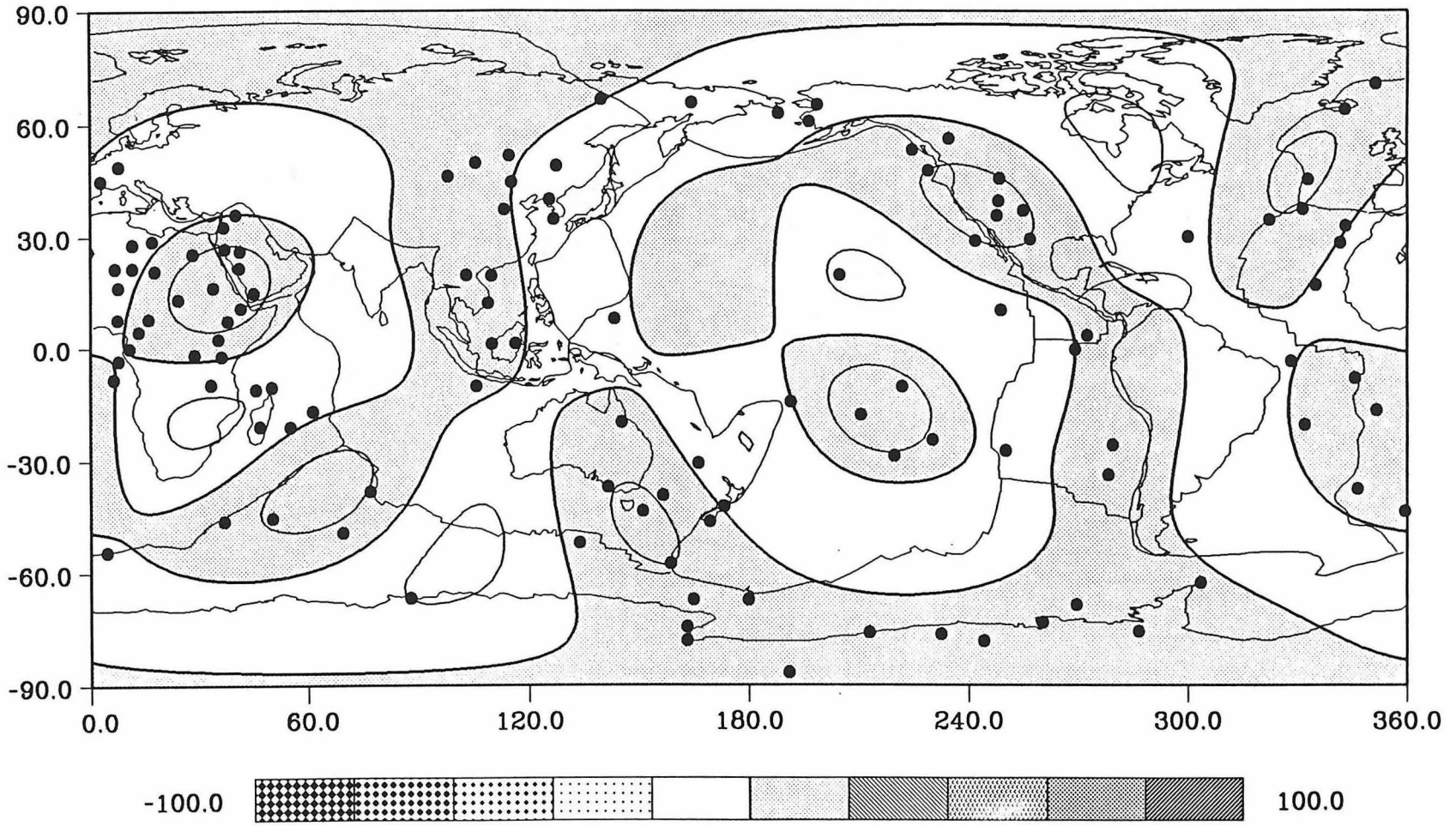
90.0
60.0
30.0
0.0
-30.0
-60.0
-90.0
0.0
60.0
120.0
180.0
240.0
300.0
360.0
-100.0
100.0

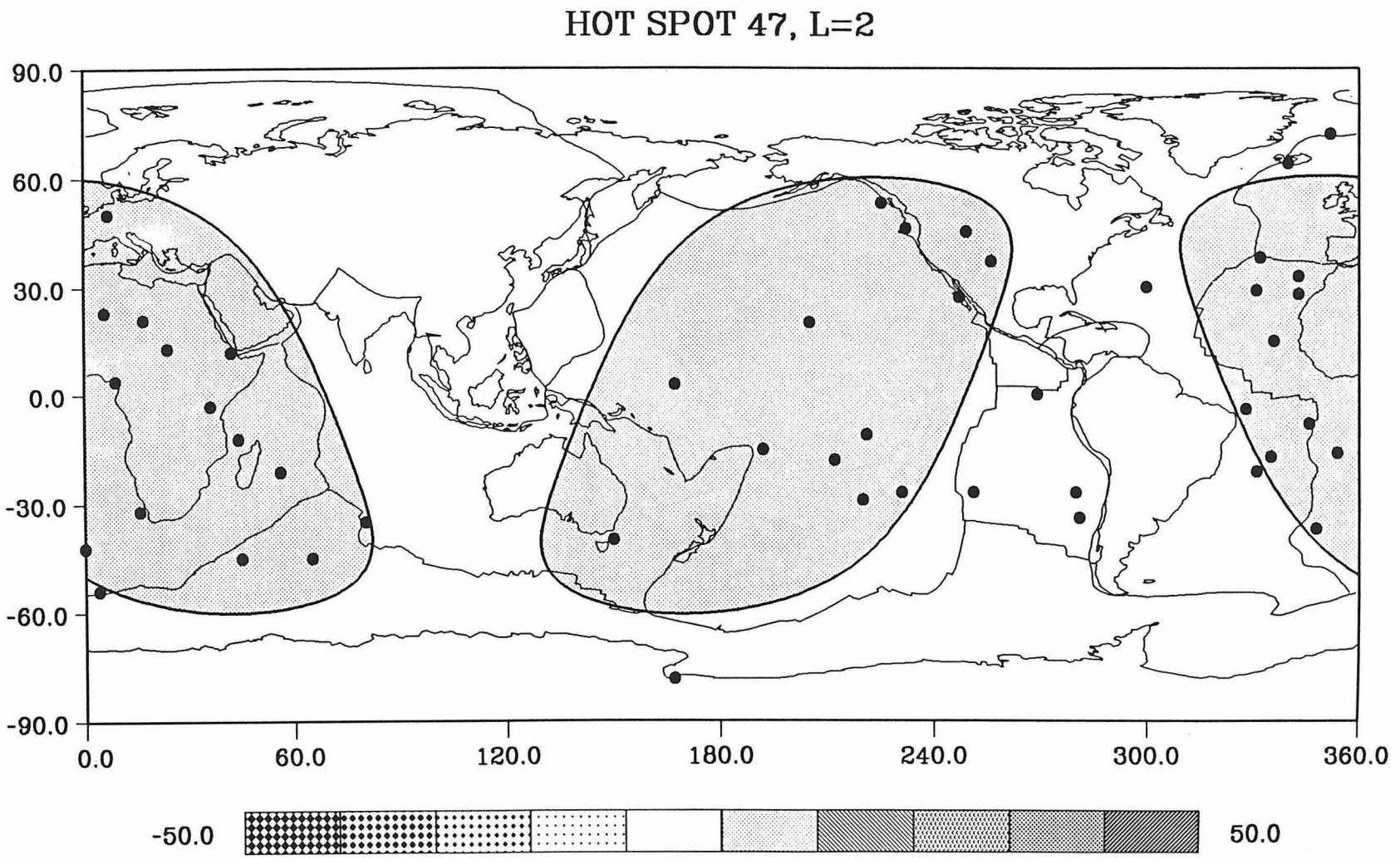
HOT SPOT 47, L=2
90.0
60.0
30.0
0.0
-30.0
-60.0
-90.0
0.0
60.0
120.0
180.0
240.0
300.0
360.0
-50.0
50.0

HOT SPOT 117

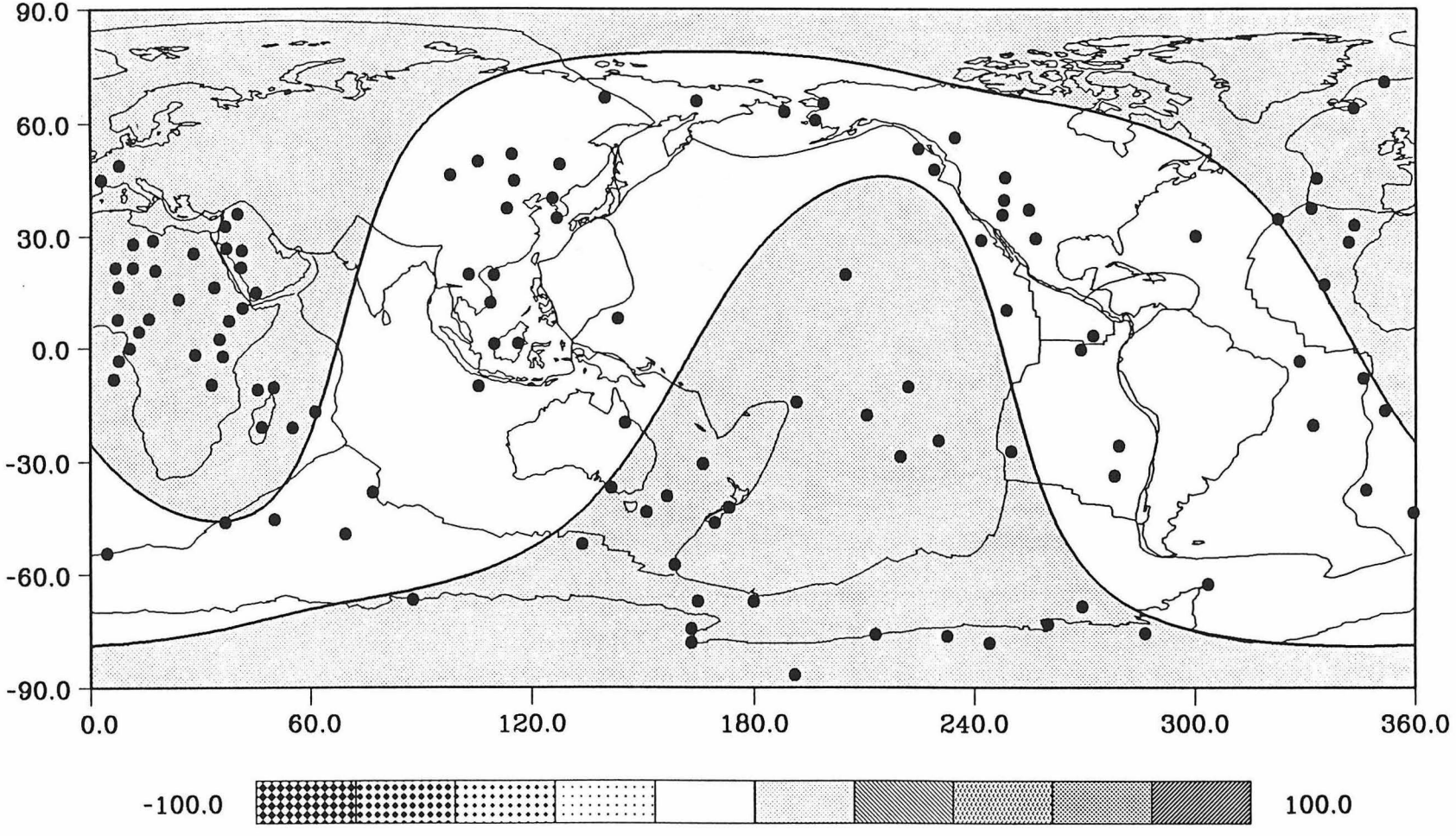
90.0
60.0
30.0
0.0
-30.0
-60.0
-90.0
0.0
60.0
120.0
180.0
240.0
300.0
360.0
-100.0
100.0

SPECTRUM AMPLITUDE, HOTSPOT 47 & 117

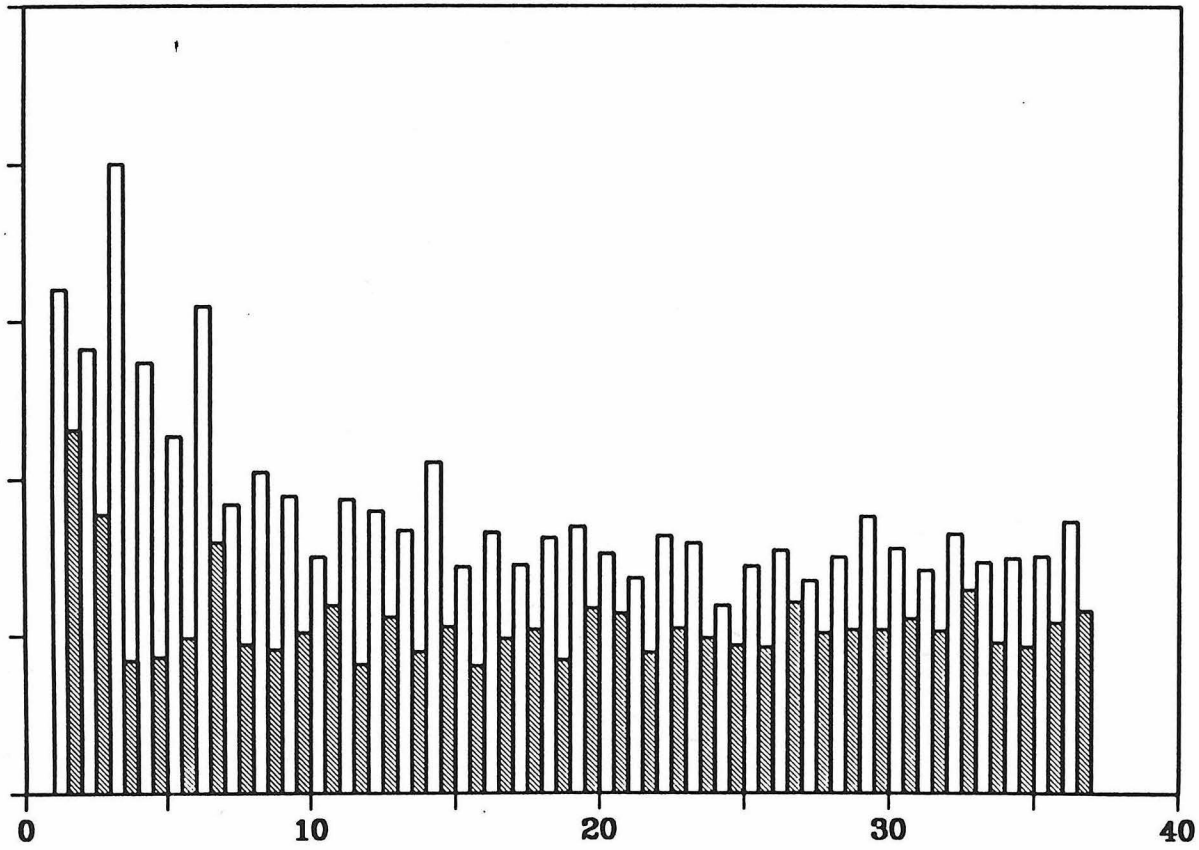

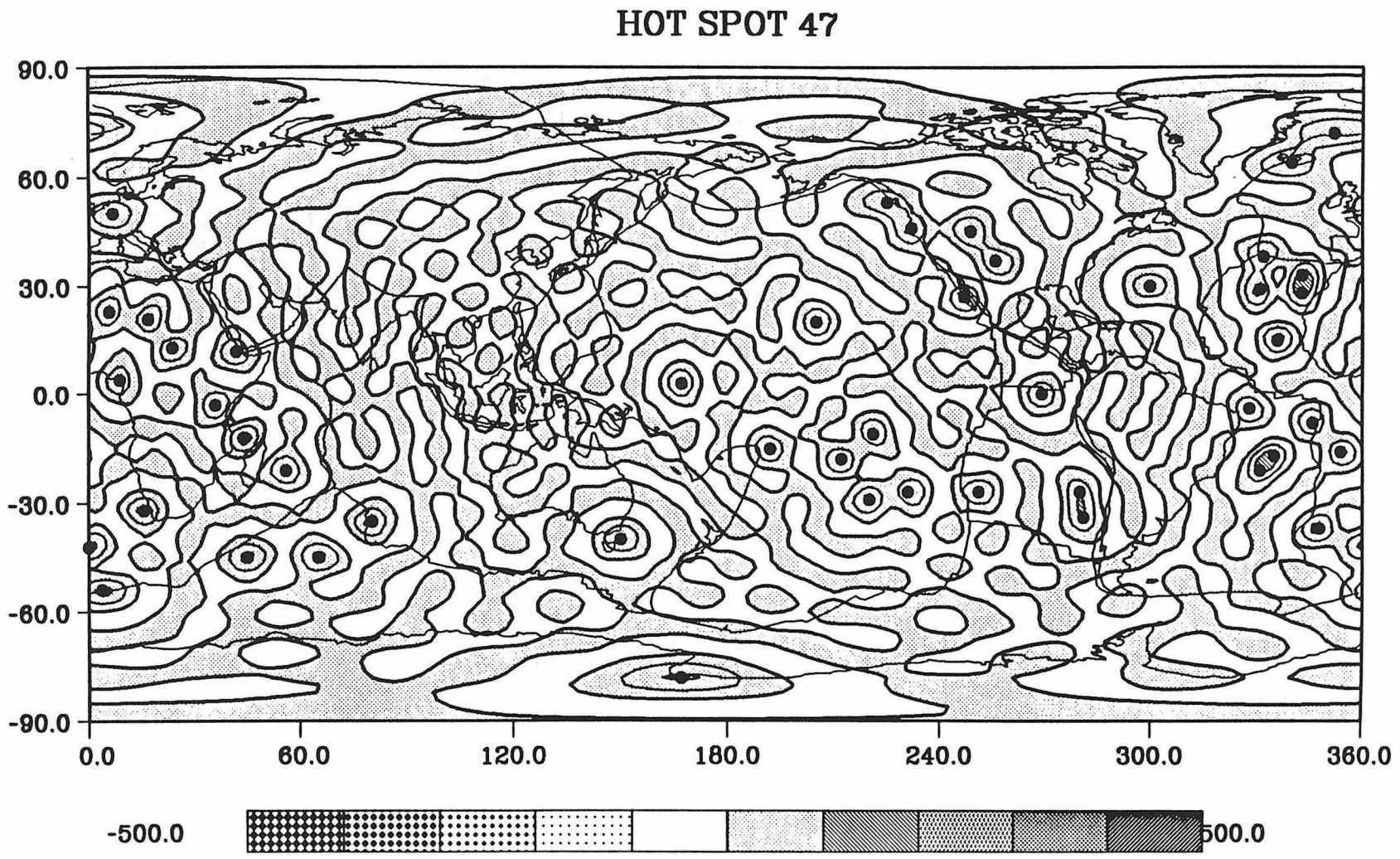
HOT SPOT 47
90.0
60.0
30.0
0.0
-30.0
-60.0
-90.0
0.0
60.0
120.0
180.0
240.0
300.0
360.0
-500.0
500.0

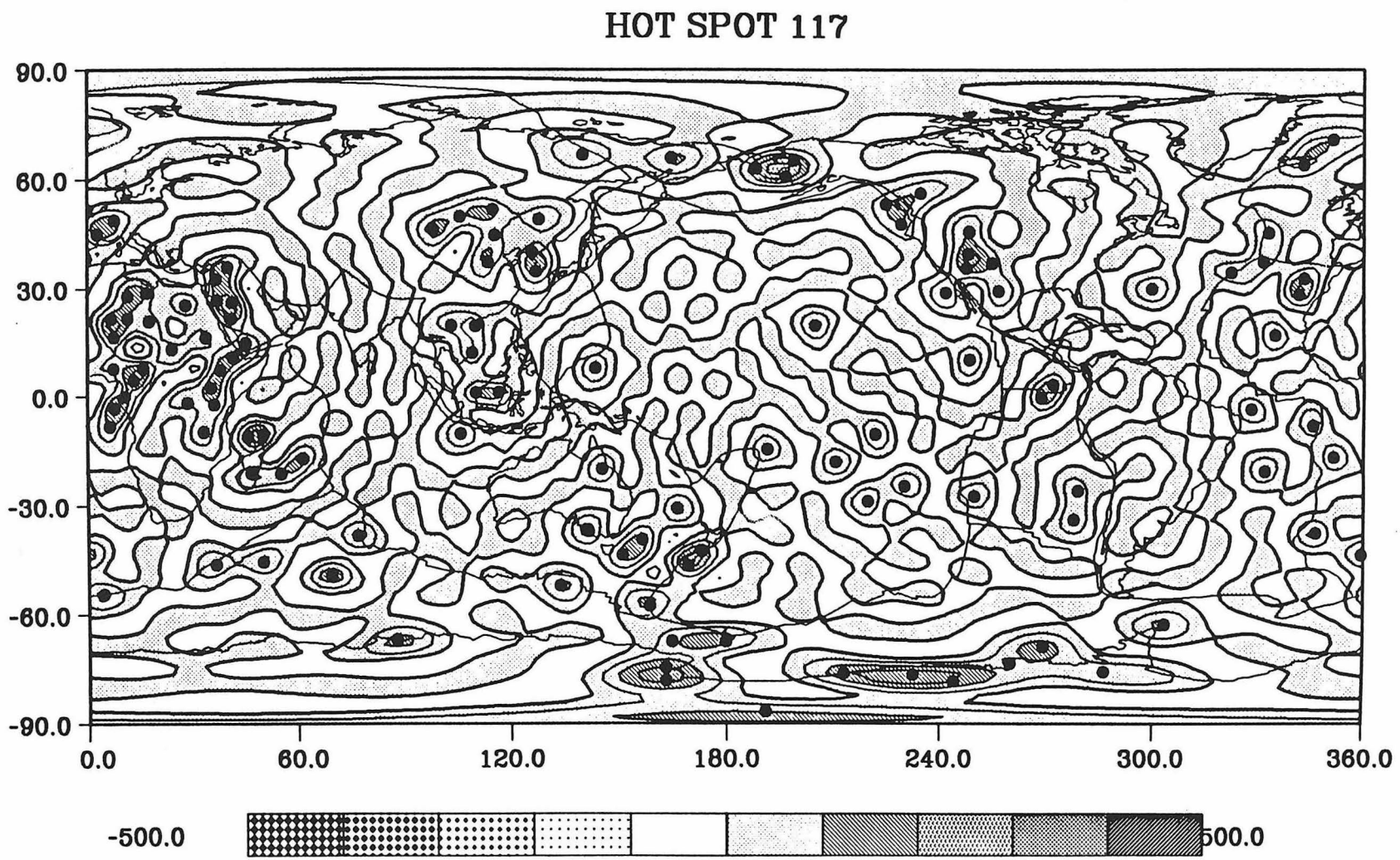
HOT SPOT 117
90.0
60.0
30.0
0.0
-30.0
-60.0
-90.0
0.0
60.0
120.0
180.0
240.0
300.0
360.0
-500.0
500.0

GEOID: DEGREE 6 - 6

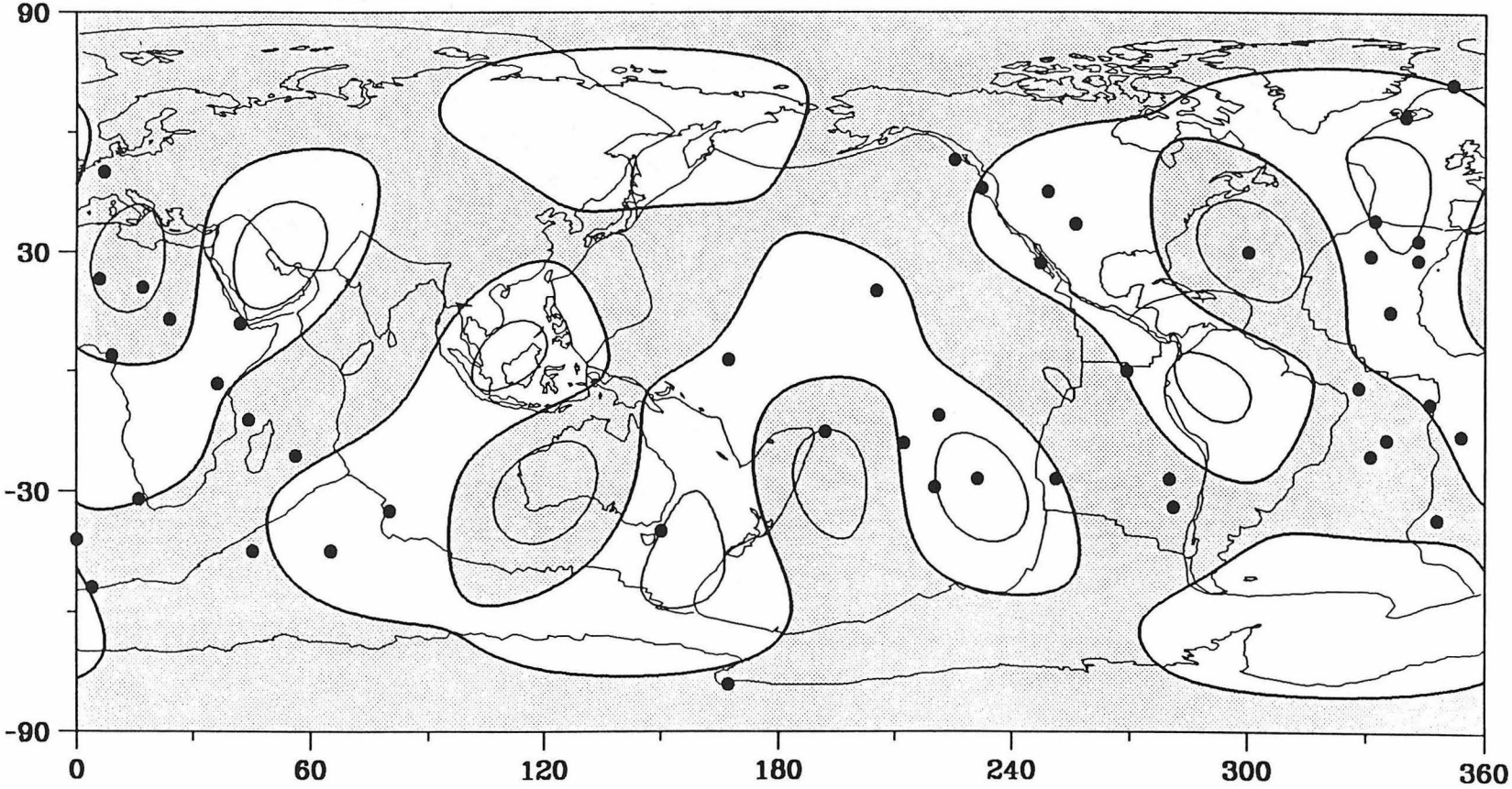

Contour interval: 10

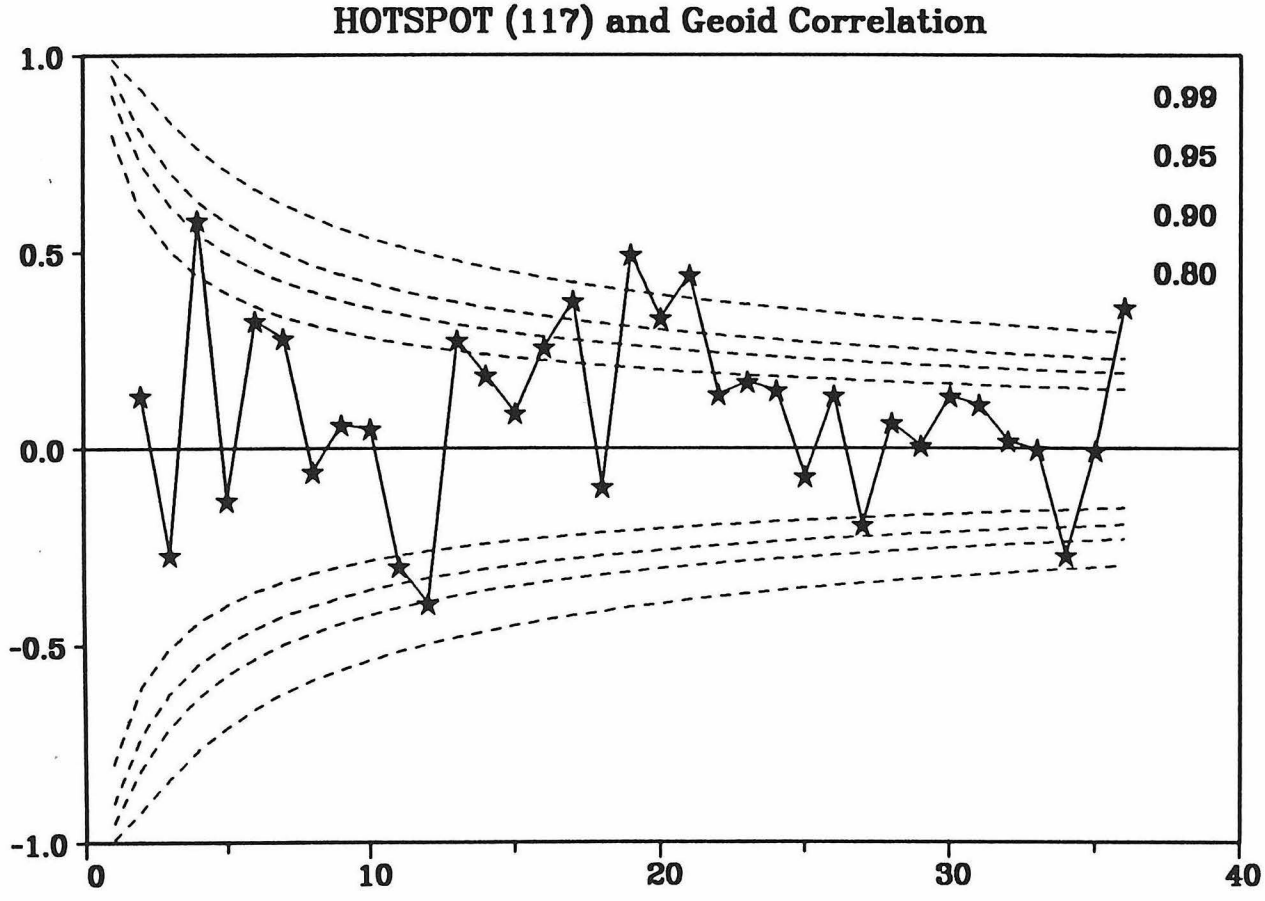
HOTSPOT (117) and Geoid Correlation
1.0
0.5
0.0
-0.5
-1.0
0
10
20
30
40
0.99
0.95
0.90
0.80

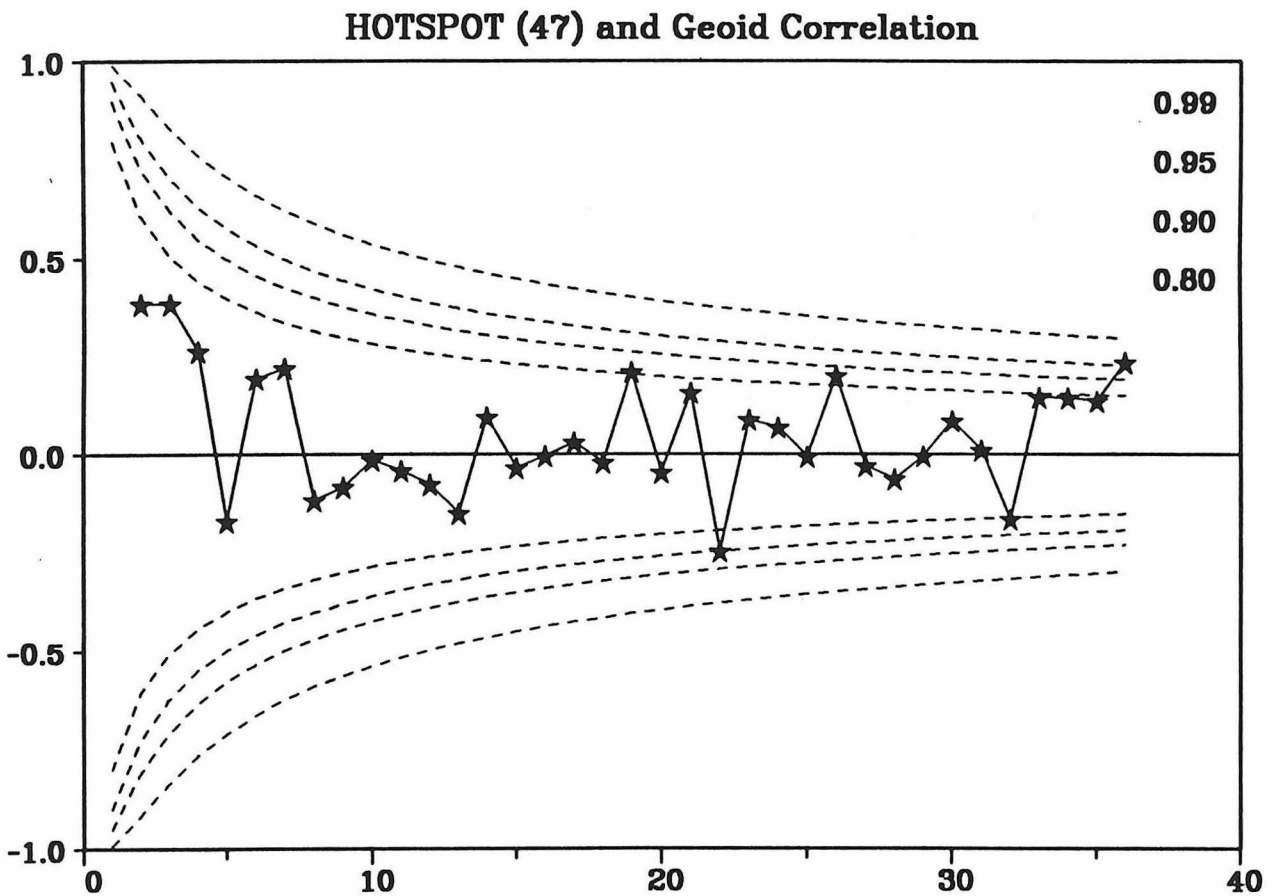
HOTSPOT (47) and Geoid Correlation
1.0
0.5
0.0
-0.5
-1.0
0
10
20
30
40
0.99
0.95
0.90
0.80

HOTSPOT GEOCHEMISTRY

Table 1. The data for hotspot size and geochemistry.

Hotspot	Swell Magnitude	Buoyancy flux	Geoid Anomaly	Eruption Rate	$\frac{^{206}Pb}{^{204}Pb}$	$\frac{^{207}Pb}{^{204}Pb}$	$\frac{^{208}Pb}{^{204}Pb}$	$\frac{^{87}Sr}{^{86}Sr}$	$\frac{^{143}Nd}{^{144}Nd}$
Amsterdam			0		19.170	15.708	39.810	.70400	
Ascension	0.38		0.89	6±3E-5	19.568	15.625	39.112	.70282	.513010
Azores		1.1	2.5		19.731	15.626	39.341	.70379	.512891
Bouvet		0.4	0	4±1E-5	19.445	15.652	39.065	.70369	.512840
Canaries		1.0	4.53	7.5E-3	19.600	15.613	39.419	.70307	512980
Cape Verdes	0.20	1.6	3.81	4±3E-5	19.080	15.560	38.900		
Crozet		0.5	3.82		18.913	15.679	39.290	.70411	
Discovery	0.19	0.5			18.246	15.609	38.723		
Easter		3.3	0		19.200	15.600	38.985	.70320	.513022
Fernando	0.38	0.5	4.29	5±2E-6	19.501	15.631	39.429		
Galapagos		1.0	0.67		18.953	15.547	38.586	.70317	512992
Gough	0.22			1.1±.4E-4	18.435	15.599	38.917	.70532	.512574
Hawaiian	2.7	8.3	4.17	1.8E-2	18.282	15.472	37.953	.70355	512993
Iceland	1.4			3.0E-2	18.752	15.502	38.382	.70317	.513045
Juan Fernandez	0.77	1.6		7.2±3E-5	19.100			.70358	
Kerguelen	0.09	0.5		2.2±.1E-4	18.188	15.503	38.573	.70492	.512592
Mangaia				10^{-4}-10^{-5}				.70276	
Marguesas	2.0	3.3	2.37		19.107	15.597	39.077	.70451	
Marion-P				2.0E-2	18.570	15.548	38.412	.70320	
Edward NE Pacific Seamounts				10^{-2}-10^{-3}	18.575	15.492	37.966		
Rarotonga				10^{-4}-10^{-5}	18.388	15.536	38.973	.70420	
Reunion	0.39	1.9	2.37	2.4±.4E-3	18.800	15.585	38.850	.70410	
Rio Grande			3.47		17.619	15.490	38.073	.70476	
Ross				1.2±.2E-3	19.870	15.634	39.450	.70323	
San Felix	1.0	1.6			19.312	15.602	39.349	.70409	
St Helena	0.12	0.5	1.67	2.4±1.2E-5	20.804	15.789	40.091	.70293	
Tahiti	2.5	3.3	2.67		19.006	15.547	38.624	.70411	
Trindade	0.36				19.069	15.559	38.945		
Tristan da Cunha			1.67	3.0E-2	18.551	15.527	39.013	.70507	.512535
Tubuai	1.7	3.3	2.77		21.104	15.770	40.354	.70277	
Bowie	0.36	0.3							
Bermuda	0.64	1.1							
Great Meteor	0.15	0.5	2.73						
Louisville	1.3	0.9							
Pitcairn	0.73	3.3	1.0						
Somoa		1.6	4.32						
Ahaggar					19.915	15.653	39.525	.70328	
Chrismas					18.896	15.616	38.972	.70366	
Comores					19.300	15.549	39.300	.70368	
Fiji					18.688	15.572	38.442	.70369	
Guadalupe					20.151	15.620	40.134	.70326	
NE Seamounts					20.458	15.672	40.406	.70329	
Nunivak					18.628	15.457	38.112	.70297	
Potrillo					18.541	15.530	38.223	.70320	
Pribilofs					18.912	15.484	38.364	.70284	
Rapa					19.051	15.578	38.892	.70370	
San Carlos					18.591	15.508	37.981	.70298	
St. Paul					18.684	15.653	39.050	.70383	
St. Paul's rocks					19.773	15.638	39.360	.70341	
Walvis Ridge					17.914	15.492	38.472	.70457	
W. Victoria					18.444	15.567	38.540	.70425	

Key	Lat	Long	Δ7/4	Δ8/4	ΔSr	ΔNd
AHAG	22.00	7.00	0.3	-17.9	-4.0	0.07
AMST	-37.00	77.00	13.9	100.6	3.2	
ASCE	-8.08	-14.12	1.3	-17.3	-8.6	1.03
AZOR	37.33	-28.42	-0.4	-14.1	0.9	-0.16
BOUV	-54.36	4.58	5.3	-7.1	0.1	-0.67
CANA	28.27	-18.17	-0.3	9.6	-6.1	0.73
CVER	16.97	-24.96	0.1	20.5		
XMAS	-35.00	80.00	7.7	50.0		
COMO	-10.94	45.75	-3.4	33.9	0.0	
CROZ	-45.00	45.00	13.8	79.7	4.3	
DISC	-42.00	0.00	14.0	103.6		
EAST	-27.31	-110.12	2.8	14.5	-4.8	1.15
FERN	-3.54	-31.67	2.6	22.5		
FIJI	-18.00	-179.00	5.5	22.1	0.1	0.81
GALA	-0.38	-91.21	0.1	4.5	-5.1	0.85
GOUG	-40.00	-10.00	11.0	100.2	16.4	-3.33
GUAD	30.00	-120.00	-5.5	14.4	-4.2	
HAWA	19.71	-155.33	0.0	21.8	-3.0	0.78
ICEL	64.03	-16.83	-2.2	8.4	-5.1	1.38
KERG	-45.00	65.00	4.0	95.7	12.4	-3.15
MAPE	-47.00	38.00	4.4	33.4	-4.8	
MARQ	-10.19	-138.21	3.5	35.0	8.3	-1.03
NESM	29.00	-29.00	-3.7	4.5	-3.9	
NEPS	46.00	-131.00	-1.3	-11.8		
NUNI	60.00	-167.00	-5.3	-3.6	-7.1	
POTR	37.00	-105.00	2.9	18.0	-4.8	
PRIB	67.00	-170.00	-5.6	-12.8	-8.4	
RAPA	-30.00	-145.00	2.2	23.3	0.2	
RARA	-21.00	-160.00	5.7	117.5	5.2	
REUN	-21.08	55.17	5.6	49.4	4.2	
RGRR	-31.00	-35.00	8.9	114.5	10.8	
ROSS	-77.30	168.50	-1.1	-20.0	-4.5	
SCAR	35.00	-109.00	0.2	-12.3	-7.0	
SFEL	-25.85	-80.83	1.8	37.4	4.1	
SHEL	-16.60	-8.37	4.3	-68.8	-7.5	0.00
SPAU	-39.00	79.00	13.7	83.4	1.5	
SPAR	1.00	-29.00	0.4	-17.3	-2.7	-0.13
TAHI	-17.79	-149.52	-0.4	1.9	4.3	
TRIN	-20.39	-28.00	0.1	26.4		
TRIS	-37.60	-13.46	2.5	95.8	13.9	-3.72
TUBU	-24.00	-149.00	-0.9	-78.8	-9.1	-0.20
VICT	-3.21	7.92	7.7	61.4	5.7	
WALV	-28.00	3.00	5.9	118.7	8.9	-3.74

All lead and strontium data from Hart (1984). Neodymium data from Zindler et al (1982) except as follows:
AHAG from Allegre et al (1981), FIJI from Gill (1984), MARQ from Vidal et al (1984), SPAR from Roden et al (1984), TUBU from Vidal et al (1984), and WALV from Richardson et al (1982).

PLUME PLANS, PROFILES and PARAMETERS

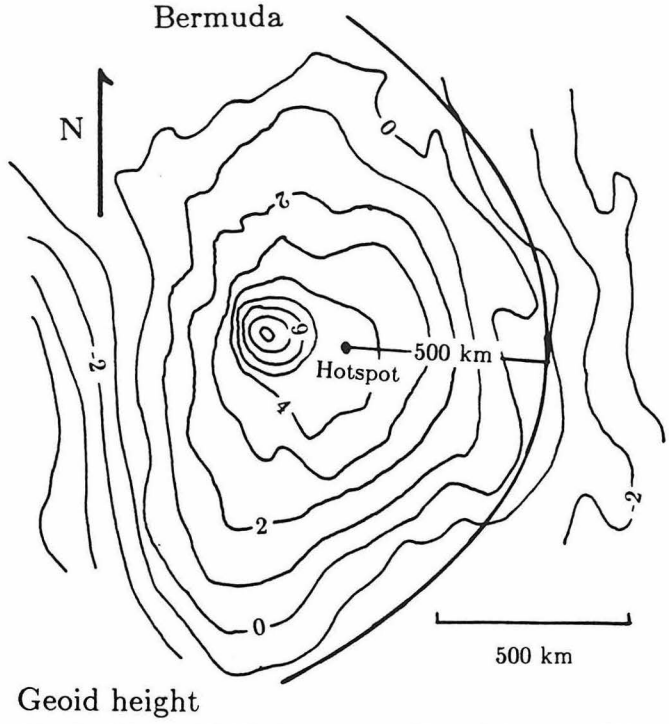

Fig. 11. The geoid height in meters near Bermuda is contoured in meters [*Detrick et al.*, 1986]. A 500-km stagnation curve is fit by eye to the anomaly. The model hotspot is at the dot. The single volcanic edifice is represented by the 6-m contour.

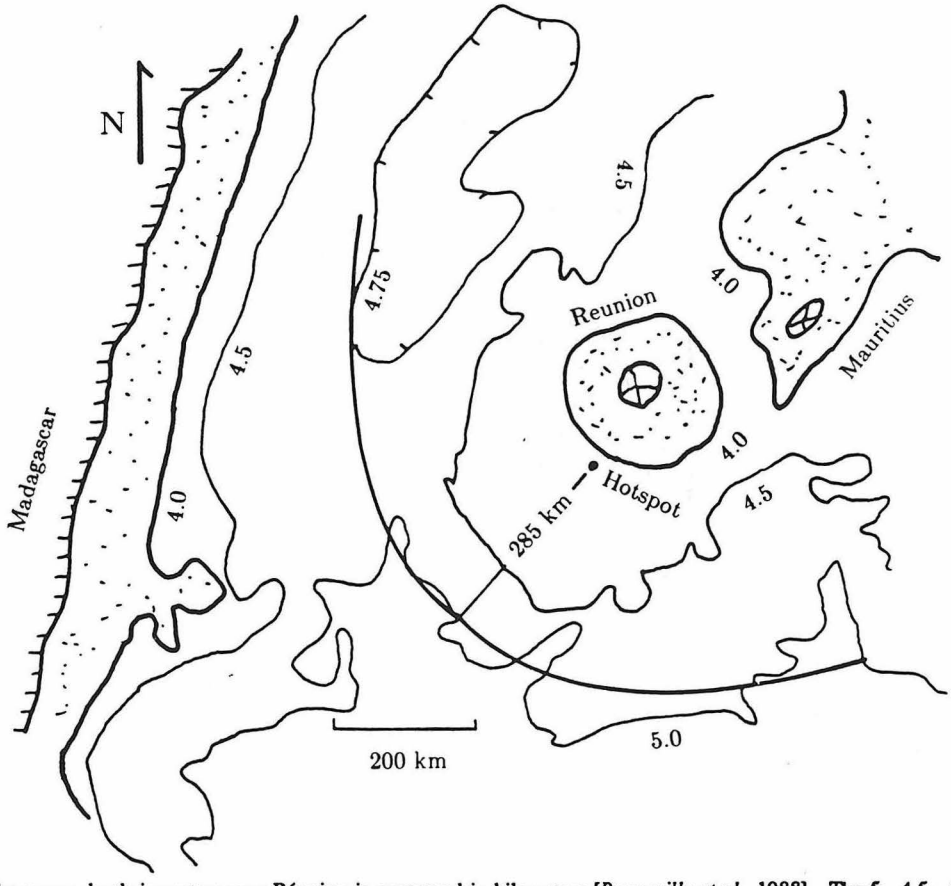

Fig. 13. The ocean depth in meters near Réunion is contoured in kilometers [*Bonneville et al.*, 1988]. The 5-, 4.5-, 4-, and 0-km contours are plotted. The 4.75-km contour is plotted in the basin between Madagascar and Réunion. The interval between 4- and 0-km depth is shaded. A 285-km stagnation curve is fit by eye to the 5-km contour. The model hotspot is indicated by the dot.

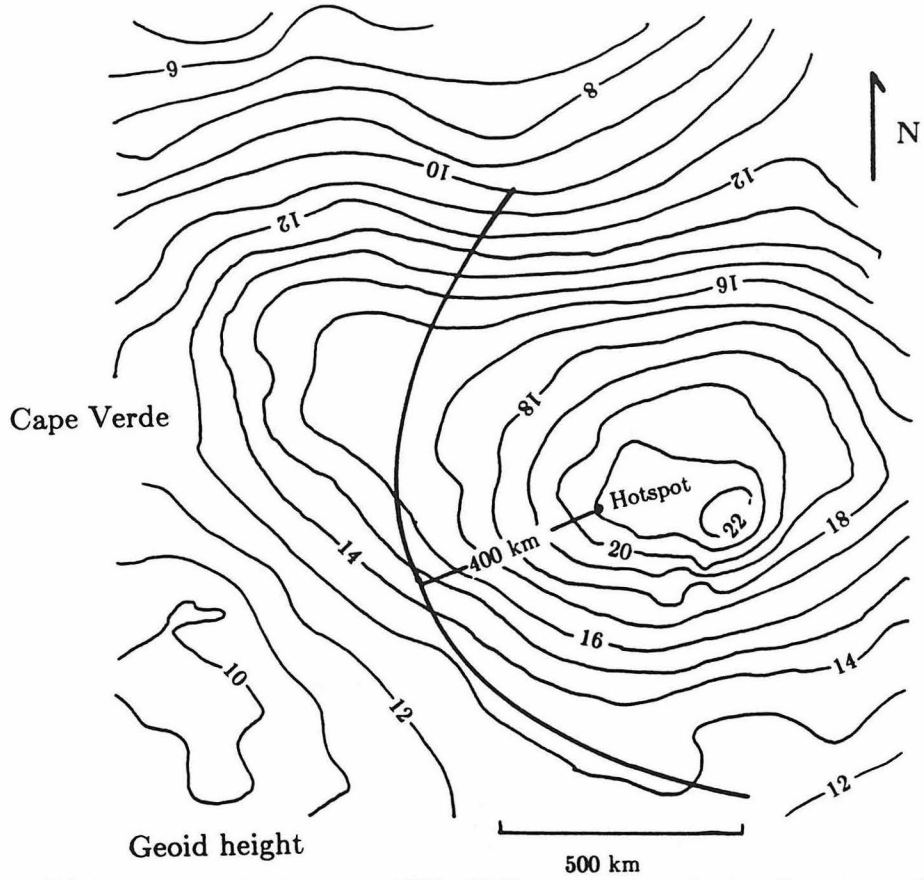

Fig. 10. The geoid height in meters [after *Courtney and White*, 1986] is contoured near the Cape Verde hotspot. The stagnation curve is fit by eye and is defined by the break in slope to the northeast and the 13-m contour to the southwest. The assumed position of the hotspot is indicated by a dot.

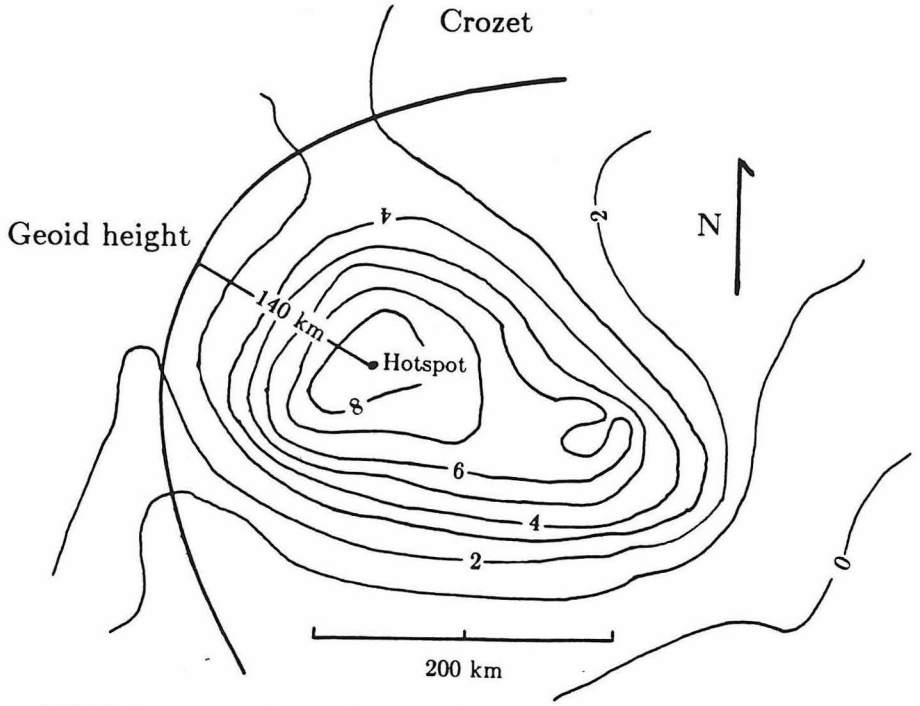

Fig. 12. The geoid height in meters near Crozet is contoured in meters [*Courtney and Recq*, 1986]. A 140-km stagnation curve is fit by eye to the anomaly. The model hotspot is at the dot.

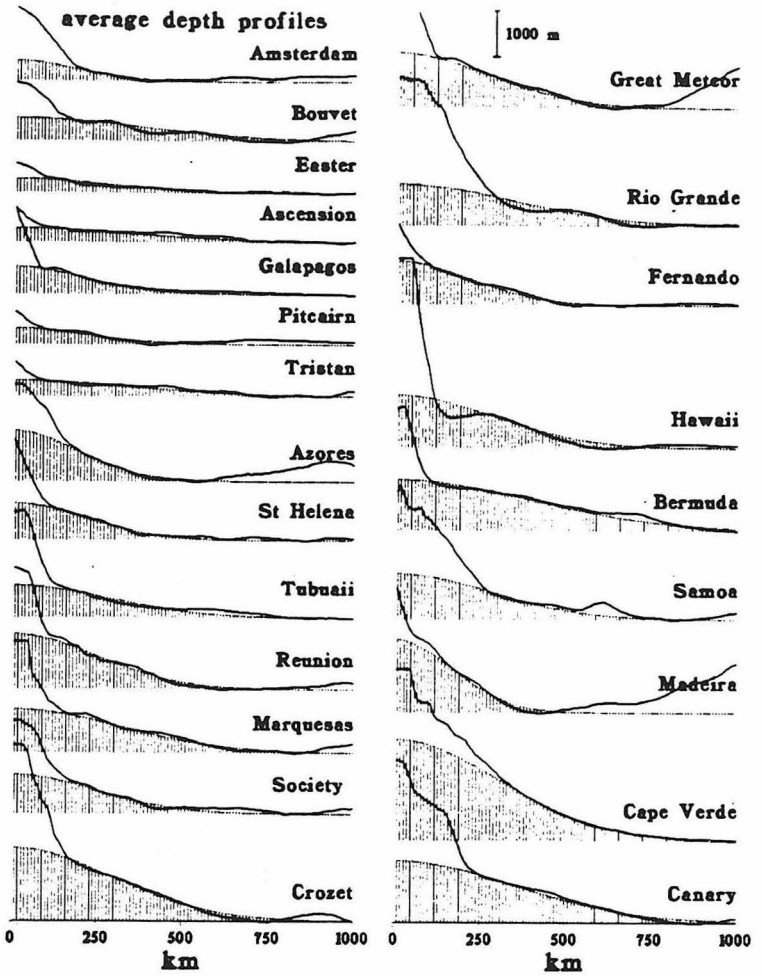

Fig. 3a. Topography anomaly in profile form (average profile) for each of the 23 hotspot swells considered in this study.

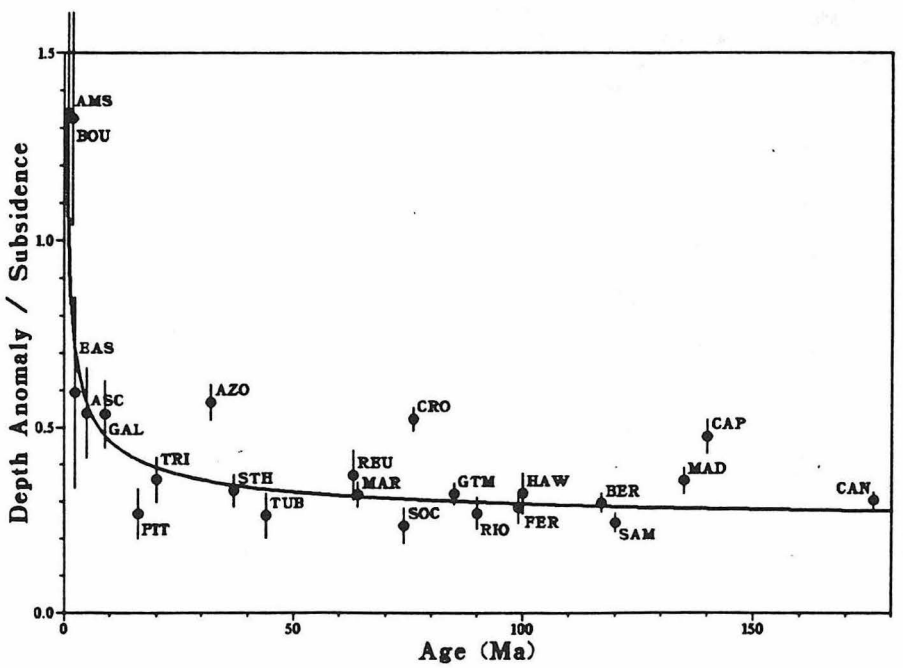

Fig. 8 : Swell height to subsidence ratio as a function of age. (See Table 1 for symbols).

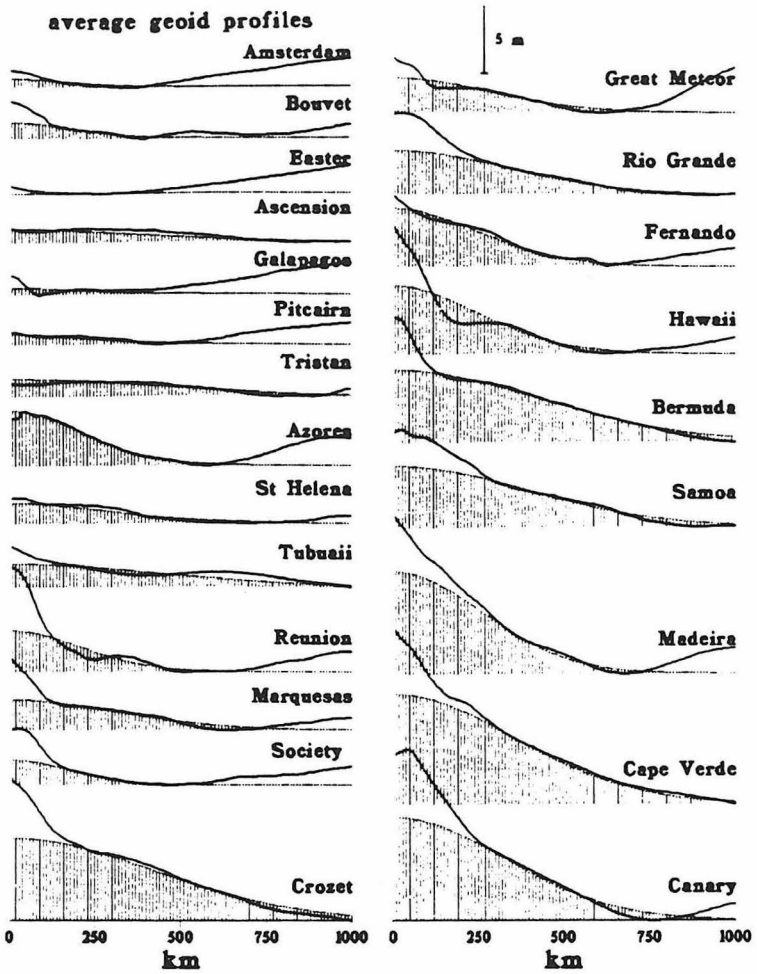

Fig. 3b. Same as Figure 3a, but for the geoid anomaly. Hatched areas represent the best fitting Gaussian function.

TABLE 1. Hotspot Swell Identification, Age of Plate, Swell Height, Geoid Anomaly Amplitude, and Swell Extent

Hotspot Swell Identification		Age of Crust at the Hotspot, Ma	Swell Height, m			Geoid Anomaly, m			Swell Extent, km	
			Mean Value a		Estimate b	Mean Value a		Estimate b		
Amsterdam	(AMS)	<2	500	±100	450	0.0	±0.5	0.6	1200	±200
Bouvet	(BOU)	<2	700	±150	500	0.0	±0.5	1.2	900	±100
Easter	(EAS)	3	350	±150	300	0.0	±0.5	0.0	1000	±200
Ascension	(ASC)	5	450	±150	300	0.40	±0.4	1.0	1500	±200
Galapagos	(GAL)	9	600	±100	600	0.40	±0.4	0.5	1200	±200
Pitcairn	(PIT)	16	400	±100	350	0.40	±0.4	0.8	1300	±100
Tristan	(TRI)	20	600	±100	350	1.00	±0.3	1.3	1000	±100
Azoes	(AZO)	32	1200	±100	1100	3.00	±1.0	4.0	1100	±100
StHelena	(STH)	37	750	±100	800	1.25	±0.3	1.5	1100	±100
Tubuai	(TUB)	44	650	±150	700	1.80	±0.2	1.7	1000	±100
Reunion	(REU)	63	1100	±200	1200	2.60	±0.6	3.0	1000	±100
Marquesas	(MAR)	64	950	±100	950	2.25	±0.8	2.2	1300	±100
Society	(SOC)	74	750	±150	850	2.00	±0.5	1.8	900	±100
Crozet	(CRO)	76	1700	±100	1600	6.50	±1.0	6.0	1600	±100
GreatMeteor	(GTM)	85	1100	±100	1200	3.00	±0.5	2.5	1100	±100
RioGrande	(RIO)	90	950	±150	900	3.30	±0.5	3.2	1400	±200
Fernando	(FER)	99	1050	±150	950	4.50	±0.5	4.2	1000	±100
Hawaii	(HAW)	100	1200	±200	1150	5.00	±1.0	5.0	1450	±150
Bermuda	(BER)	117	1200	±100	1100	5.50	±0.5	5.3	1800	±100
Samoa	(SAM)	120	100	±100	1000	4.75	±1.3	4.5	900	±100
Madeira	(MAD)	135	1550	±150	1600	6.50	±0.7	7.5	1000	±200
CapeVerde	(CAP)	140	2100	±200	2200	8.00	±0.5	8.0	1750	±150
Canary	(CAN)	176	1500	±100	1350	6.80	±1.2	7.5	1500	±150

a Mean value of the individual profiles estimates.
b Estimated on the average profile.

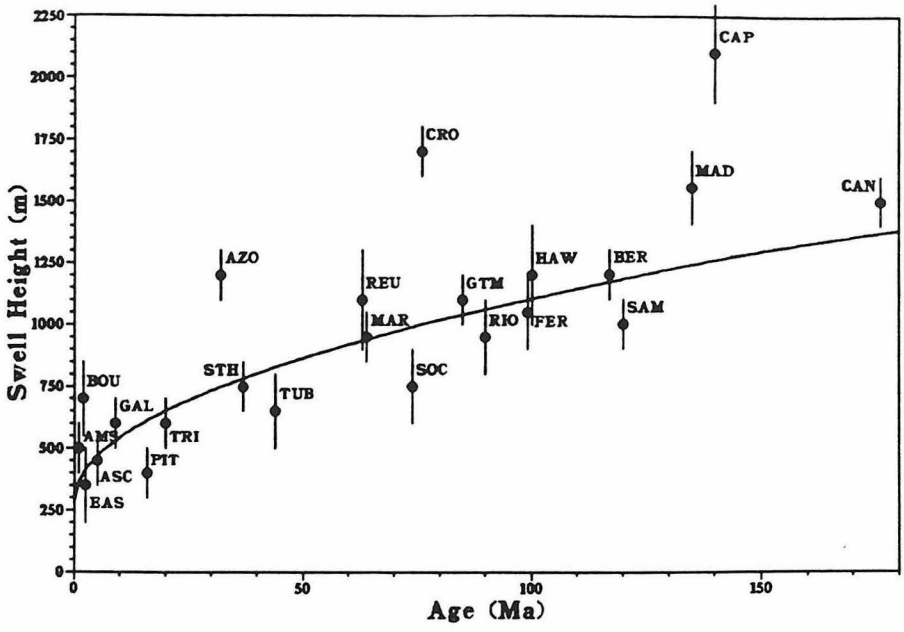

Fig. 4. Swell height estimated at the 23 hotspot as a function of age (see Table 1 for symbols). The solid line is the best fitting square root of age function.

Because swells are two-dimensional features of irregular shape, the lateral extent we measure from the profiles represents a mean value of the actual dimensions of the swell. It would correspond to the diameter of a swell having axial symmetry. As when estimating swell height and geoid anomaly, we have excluded some radial profiles perturbed by unrelated geological features (e.g. the continental margin east of Canary and Cape Verde). In the case of Hawaii, the swell extent is measured using profiles transverse to the island chain direction.

Estimates of the swell extent are reported in Table 1. All swells appear to be at least 1000 km. Bermuda, Crozet, Cape Verde, and Hawaii are the largest. We have plotted the swell extent as a function of age (Figure 6). No trend is emerging, the width of the swell appearing essentially independent on age. On the other hand, plates of similar age can support swells showing 50% variation in width: see, for example, Crozet and Society or Bermuda and Fernando. Bermuda is one of the largest swells while Fernando is one of the smallest. The narrow extent of the

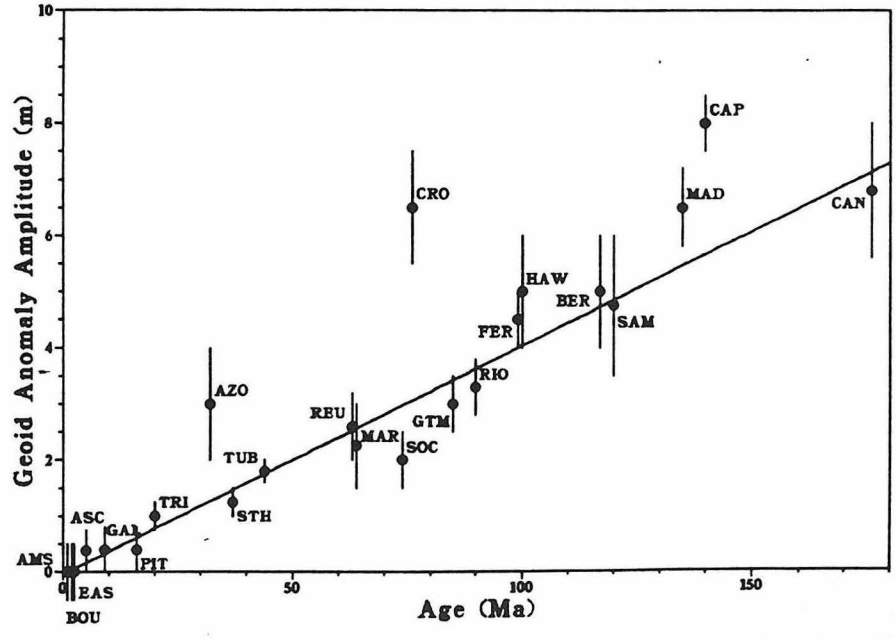

Fig. 5. Geoid anomaly amplitude estimated at the 23 hotspots as un function of age (see Table 1 for symbols). The solid line is the best fitting regression line.

Table 1: Hotspot Swell Parameters

Hotspot	Magnitude $m^3/s^\dagger$	Plate Speed mm/yr	Intrusion Number $(\text{x}10^{21}/\eta_p)^\ddagger$	Length Scale (km)
Hawaii	2.7	96	0.03	117
St Helena	0.12	10	0.12	77
Bermuda	0.64	27	0.09	108
Cape Verde	0.20	5	0.8	140
Louisville	1.3	90	0.016	84
McDonald	1.7	105	0.015	89
Marquesas	2.0	105	0.018	97
Society	2.5	105	0.022	108
Reunion	0.39	15	0.17	113
Juan Fernandez	0.77	65	0.018	76
Ethiopia	0.42	7	0.86	172
Asencion	0.38	40	0.024	68
Bowie	0.36	50	0.014	59
Darfur	0.19	10	0.19	96
Discovery	0.19	13	0.11	85
East Africa	0.26	12	0.18	103
Fernando	0.38	32	0.037	76
Great Meteor	0.15	4	0.94	136
Hoggar	0.12	5	0.48	108
Kerguelen	0.09	6	0.25	86
Pitcairn	0.73	100	0.007	60
San Felix	1.0	60	0.028	90
Tibesti	0.14	5	0.56	117
Trinadade	0.36	30	0.04	77
Tristan-Gough	0.22	12	0.15	95
Vema	0.17	12	0.1	83

† Swell magnitude as defined by Davies [1988].

‡η_p in Pa s.

(from Olson)

TABLE 1. Oceanic Swells

Swell	Crustal Age, Ma	Residual Depth Anomaly at Center,* m	Width of Swell, km	Source
Bermuda	110	1000	800	*Detrick et al.* [1986]
Cape Verde	125	1900	1550	*Courtney and White* [1986]
Cook-Austral	46	650	1250	*Crough* [1978]
Crozet	67	~ 800	> 1000	*Courtney and Recq* [1986]
Hawaii	90	1200	1200	*von Herzen et al.* [1982]
Iceland	0	~ 2000	2000	this study
Marquesas	45	~ 800	~ 1500	*Crough and Jarrard* [1981]
Reunion	67	1050		*Crough* [1978]
Society	70	1100		*Crough* [1978]

*Residual depth anomaly with respect to normal oceanic depth [from *Parsons and Sclater*, 1977] attributed to thermal uplift.

TABLE 1. Hotspot Buoyancy Flux

Hotspot	Flux* Mg s^{-1}	Reliability	Flux† Mg s^{-1}
Afar	1.2	good	
Australia, East	0.9	fair	
Azores	1.1	fair	
Baja	0.3	poor	
Bermuda	1.1	good	1.5
Bouvet	0.4	fair	
Bowie	0.3	poor	0.8
Canary	1.0	fair	
Cape Verde	1.6	good	0.5
Caroline	1.6	poor	
Crozet	0.5	good	
Discovery	0.5	poor	0.4
Easter	3.3	fair	
Fernando	0.5	poor	0.9
Galapagos	1.0	fair	
Great Meteor	0.5	poor	0.4
Hawaii	8.3	good	6.2
Iceland	1.4	good	
Juan de Fuca	0.3	fair	
Juan Fernandez	1.6	poor	1.7
Kerguelen	0.5	poor	0.2
Louisville	0.9	poor	3.0
Macdonald	3.3	fair	3.9
Marqueses	3.3	fair	4.6
Martin	0.5	poor	0.8
Meteor	0.5	poor	0.4
Pitcarn	3.3	fair	1.7
Reunion	1.9	good	0.9
St. Helena	0.5	poor	0.3
Samoa	1.6	poor	
San Felix	1.6	poor	2.3
Tahiti	3.3	fair	5.8
Tasman, Central	0.9	poor	
Tasman, East	0.9	poor	
Tristan	0.5	poor	0.5

*This paper [N. Sleep]
†[Davies, 1988]

Table 2. Volcanoes presented in this study with the value of elastic thickness (T_e), age of plate (t_p) and age of volcano (t_v) used—south-central Pacific excepted—to determine (6).

	Location		Age of plate (Ma)	Age of volcano (Ma)	Elastic thickness T_e (km)
Atlantic Ocean					
Atlantis	38 °N	63.9°W	170	95	22.5±2
Azores	37.8°N	25.5°W	32	30	< 6
Corner	36.5°N	51.5°W	98	73	6 ±1
Madeira	33 °N	17 °W	129	1	32.5±4
Bermuda	32.4°N	64.8°W	117	30	32.5±8
Cruiser	32 °N	28.2°W	70	60	7 ±1
Great Meteor	30 °N	28.5°W	80	14	19 ±2
Cape Verde	17.1°N	25.2°W	116	10	21 ±2
Cape Verde	16.1°N	22.7°W	140	10	30 ±5
Ascencion	7.9°N	14.4°W	7	2	7 ±1
St Helena	16 °S	5.7°W	41	16	9.5±3
Indian Ocean					
Mayotte	12.9°S	45.2°E	150	5	40.5±4
Rodriguez	19.6°S	63.5°E	10.6	1.5	< 6
Mauritius	20 °S	57.7°E	59	8	16.5±1.5
Réunion	21.2°S	55.5°E	64	2	32 ±5
Crozet +	46 °S	51 °E	80	5	22.5±2
P. Edward	47 °S	38 °E	39	0	16.5±3
Pacific Ocean +++					
Hawaiian chain					
Kauai	22 °N	159.5°W	93.5	5	32.5±1.5
Niihau	22.8°N	161 °W	94.5	6.5	28 ±2.5
Nihoa	23 °N	162 °W	97	7.5	21.5±1.5
Necker	23.5°N	164.5°W	100	10.5	26 ±2.5
Raita Bank	25.5°N	159.5°W	108	17	21.5±1.5
Gardner pin.	25.5°N	168 °W	106	15	25.5±1.5
	25.5°N	172 °W	110.5	19.5	22.5±1.5
	25.5°N	170.7°W	112	18	28 ±1
	26.5°N	174.5°W	114.5	22.5	26.5±2
Lisianski	26 °N	174 °W	114	22	25.5±3
Pearl Hermes	28 °N	176 °W	116.5	20.5	27 ±2.5
Midway	29 °N	179 °W	119	27	26.5±2.5
	31 °N	176 °S	127	35	20 ±2
Kanmu	32 °N	173 °E	121	40	24.5±1.5
Emperor chain					
Diadakuji	32 °N	172.3EW	123	41.5	25.5± 6
Koko	35 °N	171.5°E	118	46.5	19 ± 1
Ojin	35.5°N	171.5°E	118	55	19 ± 2
Nintoku	41 °N	170.5°E	110	56	22.5±3.5
Suiko	45 °N	170°E	117	64.5	18 ±1.5
Jimmu	46.5°N	169.5°E	113	65	20 ± 2
Pitcairn chain					
Pitcairn	23.9°S	130.8°W	23	1	< 6
Gambier	23.2°S	135 °W	29.5	6	6 ± 1
Mururoa	22 °S	139 °W	35	7	6 ± 2
Easter chain					
Easter	27 °S	109 °W	4.5	0.3	< 6
Sala y Gomez	26.5°S	107.3°W	6	1.7	< 6
Cook Austral chain					
Mac Donald	29 °S	140.2°W	43	0	< 6
Rapa	27.5°S	144.5°W	52	5	< 6
Raivavae	24 °S	147.5°W	65	6.5	11 ± 2
Tubuai	13.3°S	149.5°W	70	9.5	8 ± .5
Rimatora	22.7°S	153.7°W	78	13.5	12.5± 2
Maria	22 °S	154.7°W	80	15	10.5± .5
Atiu	20 °S	158.2°W	87	4	10 ±1.5
Mauke	20.1°S	157.3°W	85	5	12 ±1.5
Aitutaki	18.7°S	159.8°W	87	7	10.5±1.5
Rarotonga	21.2°S	159.8°W	87	1.5	15 ±1.5
Mangaia	21.9°S	157.9°W	85	17.7	7 ± .5
Society chain					
Tahiti	17.6°S	149.5°W	71	1	20 ± 2
Bora Bora	16.6°S	151.3°W	75	3	15 ±1.5
Maupiti	16.4°S	152.3°W	76.5	4	14 ± 1
Marquesas					
Central group	9.4°S	139.5°W	63	3	14 ± 2
Samoa					
Manuae	14.2°S	169.5°W	100	0	24 ±2.5
Louisville Ridge ++					
Valerie Guyot	41.5°S	164.3°W	85	35	18 ±1.5

+ Cazenave et al., 1980.
++ cazenave and Dominh, 1984
+++ Calmant, 1987; Calmant and Cazenave, 1986

TABLE 1. Data for Hotspot Volcanoes

No.	Hotspot	Volcano/Island	Volcano Age, Ma	Lithosphere Age, Ma	t, Ma	h_w, m	Elevation, m	h_p, m	H^*, m
1	Hawaii	Mauna Loa	0.00	92	92.0	−4023	4169	150	6870
2		Mauna Kea	0.38	92	91.6	−4023	4201	150	6902
3		Haleakala	0.86	93	92.1	−1829	3055	150	4308
4		West Maui	1.32	94	92.7	−1829	1764	150	3017
5		E. Molokai	1.52	94	92.5	−1829	1514	150	2767
6	Society	Mehetia Is.	0.00	65	65.0	−3292	435	100	2638
7		Tahiti-iti	0.61	66	64.9	−2926	1332	100	3294
8		Tahiti	1.00	66	65.0	−2926	2066	100	4028
9		Moorea	2.10	67	64.4	−2926	1207	100	3169
10	Pitcairn	Pitcairn	0.95	23	22.0	−3292	305	100	2508
11	Caroline	Kusaie	1.30	153	151.7	−4389	192	300	3181
12		Ponape	5.40	165	159.6	−3658	786	100	3231
13	Kodiak	Bowie	0.02	18	18.0	−2195	−44	600	1590
14		Dickens	4.07	20	15.9	−2560	−474	680	1426
15	Cobb	Cobb	1.60	4	2.4	−2195	−27	170	1474
16	Marquesas	Fatu Hiva	1.43	60	58.6	−2926	960	100	2922
17		Mohotaui	1.90	60	58.1	−2195	500	100	1979
18		Tahuatu	2.09	60	57.9	−2195	1000	100	2479
19		Hiva Oa	2.55	60	57.5	−2195	1190	100	2669
20		Ua Huka	2.78	61	58.2	−2926	855	100	2817
21		Nuku Hiva	4.34	62	57.7	−2926	1186	100	3148
22	Easter	Easter	2.50	3	0.5	−2200	510	50	1977
23		Sala-y-Gomez	1.90	9	7.1	−2520	210	50	1888
24	Galapagos	Isabela	0.00	10	10.0	−1000	1689	750	2581
25		Santa Cruz	1.03	8	7.0	−1000	864	750	1756
26		San Cristobal	0.66	8	7.3	−1000	759	750	1651
27		Espanola	3.31	12	8.7	−1000	198	750	1090
28		Wolf	0.72	4	3.3	−1000	253	750	1145
29	P. Edward	Prince Edward	0.00	75	75.0	−2500	722	400	2496
30		Marion	0.00	75	75.0	−2500	1185	400	2959
31	Kerguelen	Heard Is.	0.00	34	34.0	−2500	2745	600	4581
32		Kerguelen	0.00	34	34.0	−2500	1850	600	3686
33	St. Paul	St. Paul Is.	0.00	4	4.0	−900	279	51	888
34	Amsterdam	Amsterdam Is.	0.00	4	4.0	−1200	911	49	1718
35	Reunion	Reunion Is.	2.00	63	61.0	−4000	3069	150	5755
36		Mauritius Is.	7.80	57	69.2	−3500	826	150	3182
37		Rodrigues Is.	1.60	5	3.4	−2500	395	55	2062
38	Comores	Grande Comore	0.00	128	128.0	−3000	2560	650	4741
39		Moheli Is.	1.90	128	126.1	−3000	810	400	2914
40		Anjouan Is.	1.20	128	126.8	−3000	1578	450	3697
41		Mayotte Is.	5.40	128	122.6	−3000	660	400	2764
42	Tristan	Gough	2.60	30	26.0	−3000	910	200	2952
43		Tristan	0.10	30	29.9	−3000	2060	250	4117
44		Inaccessible	2.90	30	27.1	−3000	560	200	2602
45	St. Helena	St. Helena	13.00	42	29.0	−4000	818	100	3489
46	Ascension	Ascension	1.50	7	5.5	−2500	874	50	2539
47	Bouvet	Bouvet	0.00	2	2.0	−500	935	100	1296
48	Trindade	Trindade	1.50	90	88.5	−4900	590	500	3979
49	C. Verde	Fogo (Pico)	0.00	118	118.0	−3000	2829	1000	5119
50	Canary	La Palma	1.60	155	153.4	−3000	2423	1150	4759
51		Tenerife	15.70	168	152.3	−2500	3718	1100	5709
52		Gran Canaria	13.70	180	166.3	−2000	1949	1100	3610
53	Azores	Sao Miguel	0.00	45	45.0	−1500	1105	300	2188
54		Terceira	0.00	26	26.0	−1000	1023	300	1776
55		Ilha do Pico	0.00	10	10.0	−500	2321	300	2744
56	Iceland	Oraefajokull	0.00	10	10.0	−1500	2119	100	3140
57	N. England	Nashville	85.00	95	10.0	−4600	−1925	1300	1514
58		Vogel	92.00	120	28.0	−5000	−2212	1600	1584
59	Bermuda	Bermuda	45.00	110	65.0	−4000	79	500	2874

Table 2. Plate speed (Davies), long wavelength geoid, relative distance to continent, and to ridge.

Hotspot	Locality	Latitude	Long Wave-length Geoid	Plate Speed	Relative Distance to Continent	ridge
Ascension	SA	-8	38	40	1.3	0
Azores	NA	38	44		1.2	0
Bouvet	IN	-54	-9		2.2	0
Canaries	NA	28	51		0.2	4
Cape Verdes	SA	15	40	5	0.4	0.3
Crozet	IN	-45	33		1.85	0.1
Discovery	SA	-42		13		
Easter	PA	-27	14		2.3	0.1
Fernando	SA	-4	17	32	0.2	0.1
Galapagos	PA	0	7		0.65	0
Gough	SA			12		
Hawaiian	PA	20	44	96	2.6	0.95
Iceland	NA	64	27		1.0	0
Juan Fernandez	PA	-34	-20	65	0.5	0.15
Kerguelen	IN	-45	23	6	3.	0.3
Marguesas	PA	-11	40	105	2.9	0.5
Reunion	IN	-21	24	15	0.55	0.2
San Felix	PA	-27	-20	60	0.7	0.3
St Helena	SA	-16	35	10	1.2	0.15
Tahiti	PA	-18	40	105	3.8	0.65
Trindade	SA	-21	5	30	0.7	0.3
Tristan da Cunha	SA	-37	12		2.0	0.15
Tubuai	PA	-29	19	105	4.3	0.5
Bowie	PA	53	-17	50	0.3	
Bermuda	NA	30	-40	27	0.8	0.45
Great Meteor	NA	29	43	4	0.9	0.2
Louisville	PA			90		
Pitcairn	PA	-27	21	100	3.4	0.3
Somoa	PA	-15	40		2.55	0.95
Chrismas	SA	-35				
Comores	IN	-12	14		0.4	0.45

* Abbreviation: PA-Pacific, NA-North Atlantic, SA-South Atlantic, and IN-Indian Ocean.

TABLE 1

Estimated eruption rates for selected volcanic ocean islands

Locality	Approximate duration of volcanism (Ma)	Estimated eruption rate (km^3/yr)	References *
St. Helena	15–7	$2.4 \pm 1.2 \times 10^{-5}$	Baker et al. (1967); Grant et al. (1976); Chaffey et al. (1989)
Cape Verdes	40(?)–0	$4 \pm 3 \times 10^{-5}$	Bebiano (1932); Mitchell et al. (1983); Robertson (1984); Stillman et al. (1982)
Ascension	1.5–0	$6.0 \pm 3 \times 10^{-5}$	Daly (1925); Atkins et al. (1964); Bell et al. (1972); Harris (1983)
Gough	1.0–0.1	$1.1 \pm 0.4 \times 10^{-4}$	LeMaitre (1960, 1962); LeRoex (1985);
Iceland		3×10^{-2}	Chevallier (1987)
Bouvet	0.7–0	$4.0 \pm 1 \times 10^{-5}$	Verwoerd et al. (1974); Imsland et al. (1977)
Reunion	2.0–0	$2.4 \pm 0.4 \times 10^{-3}$	Upton and Wadsworth (1969, 1972); McDougall (1971);
Canaries		7.5×10^{-3}	Oversby (1972)
Ross, San Miguel	4–0	$1.2 \pm 0.2 \times 10^{-3}$	Hamilton (1972); Sun and Hanson (1975); Goldich et al. (1975)
Kerguelen	27–1	$2.2 \pm 0.1 \times 10^{-4}$	Nougier (1969); Watkins et al. (1974)
Juan Fernandez	4–3	$7.2 \pm 3 \times 10^{-5}$	Baker (1967); Gerlach et al. (1986);
Hawaiian Chain		18.0×10^{-3}	Baker et al. (1987)
Fernando de Noronha	14–2	$5.0 \pm 2 \times 10^{-6}$	Cordani (1967); De Almeida (1958); Gerlach et al. (1987)
Rarotonga	2.8–2	10^{-5}–10^{-4}	Wood (1967); Wood and Hay (1970);
Mangaia	19–16	10^{-5}–10^{-4}	Dalrymple et al. (1975)

* Representative references cited containing age data and geologic information; sources of isotopic data are listed in caption of Fig. 1.

Hawaii, Shield $.4 \times 10^6$ 10^{-1} km^3/yr

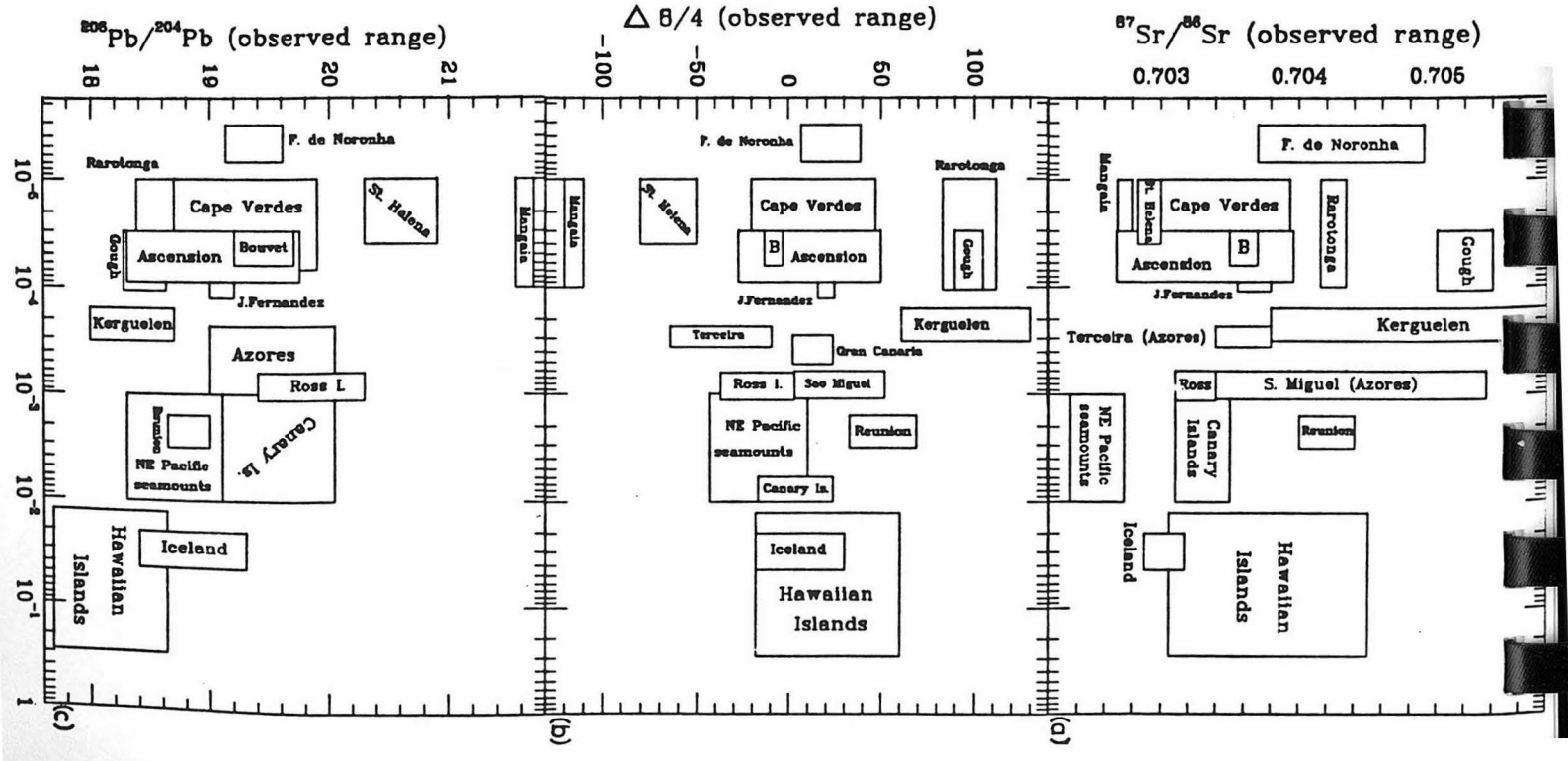

QUESTIONABLE HOTSPOTS

Bermuda- no track; single pulse; swell in wrong direction; strange geoid/topo ratio; not a hotspot (Vogt)
Cape Verde- no track; strange geoid/topo
Canaries - no track; strange geoid/topo
Fernando- no track; strange geoid/topo
Nasca Plate (2)- no track; strange geoid/topo
    Juan Fernandez
    San Felix
Crozet- Non-plume-like geoid/topo
Ascension- Not a hotspot (Schilling); no swell
Comores- No track

Triple junctions
    Azores- anomalous depth; wetspot
    Easter- hot line; no swell
    Galapagos- no geoid anomaly
    Bouvet- no enrichment; no geochm. gradient
    Afar
    Baja
Age Progression problems
    Antarctica- Victorialand
    Cook-Australes
    Easter
    S. E. Australia
    Erebus- single pulse, along rift
    Yellowstone- backarc; conflicting tracks
    Trinidade
    Samoa
Not Enriched
    Bowie, Kodiak
    Echleberger
(Many others very close to MORB in geochemistry)

Pitcairn- no swell; no geoid
Amsterdam- no swell; no geoid
Samao- crackings due to subduction
Baja- no track; ridge-trench collision
Marquesas- trend wrong
African- no tracks
Cameroon- hot line

The following probably should be included in hotspot list:

China, better candidates than some others,
Nunivak- based on geochemistry
Antarctica- based on geochemistry

PLUME PROBLEMS

Cape Verde- heat flow and stagnation "nose" not obviously plume-like

Jan Mayan- little topograhic expression

Bowie, Kodiak etc.- depleted

Plume heads, lateral flow, plate entrainment- imply widespread shallow enriched layer

North Central Atlantic- continuous volcanism at hotspot islands for ~10^7 years

Many hot spots related to tension in plate

Amsterdam, Rodriguez- related to ridge entrained flow

Comores- stress feature; continuation of EAR

Erebus- geoid low

Bermuda, Shimada- single pulse

No geoid anomaly-Great Meteor, Fernando, Martin, Discovery, Meteor, Helena, Madeira, Erebus, Bermuda

Azores, Bouvet, Tristan- near ridge but no Iceland-like islands

Tasmans- continental margin; extinct spreading axis

Caroline, Samoa, Juan Fernandez, San Felix- no swells; intraplate stress related

Pratt-Welker-Cobb-Kodiak-Bowie- alignment fortuitous; dates wrong, (DBD et al.)

Louisville ridge hotspot - (no bathymetry, geoid signal)

Galapagos- ridge reorganizations

Juan de Fuca, Bowie- ill defined chains; plate reorganizations

Crozet- inconsistent stagnation profile

Ridges cross hotspots, hotspots cross ridges- which are deeper?

Archaean plumes; inconsistent with plume theories

D" viscosity cannot drop low enough to generate plumes in a convecting mantle

Why do Morgan, Schilling- strength plumes not close up ridges?

Where are the picrites in plume tails? They occur in the colder, conjectured plume heads.

The picrites of Karoo and Deccan are LIL-rich, consistent with OIB, not entrained MORB.

COSMIC COINCIDENCES

1. Alkali sources always metasomatized just before eruption.

2. Alkalics always seek out ancient fractures.

3. "Plumes" are almost always near major structural boundaries; fracture zones, continent-ocean boundary; ridges.

4. "Plumes" start (and stop) at times of major plate reorganizations.

5. Basalts become more depleted with time, until waning stages.

6. Volcanism at hotspot initiated center can last for tens of millions of years and thousands of kilometers of travel over the mantle.

7. OIB, CFB and BABB are similar.

8. N-MORB is never the first magma up.

9. Half the measured hotspots have $^{3}He/^{4}He$ lower than MORB.

DEFINITIONS IN CURRENT USE
(mainly not recommended)

Asthenosphere- a weak, low viscosity layer in the upper mantle, probably about 200 km thick and, perhaps, partially molten, at least in high heatflow areas. It is commonly assumed to be "depleted" and the source of MORB and/or OIB but this is mixing mechanical and chemical concepts. Often used loosely to refer to whole upper mantle or as a substitute for "depleted mantle".

BSE- bulk silicate Earth=primitive mantle=present mantle + crust.

Continental lithosphere (CL)- in most papers it means "shallow mantle", sometimes "the mantle under the continent at the time". Very seldom is it demonstrated that the samples in question come from mantle that satisfies the definition of lithosphere. It usually means "non-MORB mantle" under the supposition that if basalts were not from the CL they would be depleted. If a basalt or xenolith is "depleted" it is usually, by definition, from the "asthenosphere".

Convecting mantle- (not recommended) used for upper mantle, asthenosphere or depleted mantle. Non-MORB basalts are, by definition, not from the convecting mantle.

D"- the 200-300 km thick layer at the base of the mantle; highly irregular and inhomogeneous. Possibly differs in chemistry from rest of lower mantle. A thermal boundary layer. Probably reacts with both the core and perovskite-magnesiowustite lower mantle to give unusual chemistry (depleted in siderophiles or an iron sponge).

Depleted- poor in incompatible elements and has the isotopic indicators of LIL-depletion (the MORB-source is fertile and depleted). Sometimes "depleted" is erroneously used for "infertile".

E-rich- enriched relative to BSE, in LIL, Rb/Sr, $^{87}Sr/^{86}Sr$...etc.

Enriched- higher in LIL, LREE/HREE, Rb/Sr, $^{87}Sr/^{86}Sr$ etc. than MORB; sometimes used for higher than bulk silicate Earth (BSE) or primitive mantle. N-rich and E-rich, respectively, can be used for these two cases.

Fertile- rich in basaltic components (CaO, Al_2O_3, Na_2O, clinopyroxene, garnet, plagioclase). Not the same as "enriched".

Lithosphere- the strong, rigid outer shell of the Earth, reaching thicknesses of 40 km in the oceans and 180 km in cratons, as defined by flexural studies. The base of the lithosphere seems to be defined by the roughly 400-600°C isotherm, hotter material being able to flow easily. Sometimes, erroneously used for the thermal boundary layer (TBL), a thicker conductively cooled layer with no long term strength in its lower portions. Lithosphere has a connotation of coldness, strength, stability and permanence, not shared by the TBL. The thickness of the plate is probably the same as the thickness of the lithosphere, as defined by elastic thickness. The plate can drag extra material along at its base but this is not a permanent part of the plate. Isotopic anomalies can only build up in the mechanical strong (T<600°C) part of the TBL. Buoyant mantle can also be isolated from deeper mantle, even if weak.

Mesosphere- middle mantle, the transition zone of the upper mantle (400-650 km). The home of dead depleted slabs in some models and dead enriched slabs or delaminated CL in others. Also, a thermal boundary layer if convection is obstructed at 650 km. A region of high seismic gradient. May be primarily garnet plus majorite and β - spinel; garnetite.

Perisphere- a neutral word meaning the shallow mantle. The new word is necessary because asthenosphere, lithosphere, continental lithosphere and upper mantle all have ambiguous implications.

Plumes- all things to all people. We have cavity plumes, diapiric plumes, starting plumes, chemical plumes, thermal plumes, active plumes, passive plumes, secondary instability plumes, enriched plumes, depleted plumes, plume heads, steady-state plumes, transient plumes, jets and non-plumes.

Plume heads- those things that fill up the "asthenosphere" making it no longer depleted thereby confounding those that invented deep plumes because the "asthenosphere" was depleted and could not be the plume source.

Primitive mantle (not recommended)- used as synonym for lower mantle, OIB source, CFB source, chondritic mantle. Used to refer to mantle source of magmas which have chondritic ratios of two elements or isotopes. Unfractionated, undifferentiated, undepleted, undegassed mantle. Also, crust plus mantle.

Undegassed mantle (not recommended)- Used to refer to the source region of magmas which contain higher fractions of some rare gases than MORB; "primitive" mantle (ignores intramantle transport of gases).

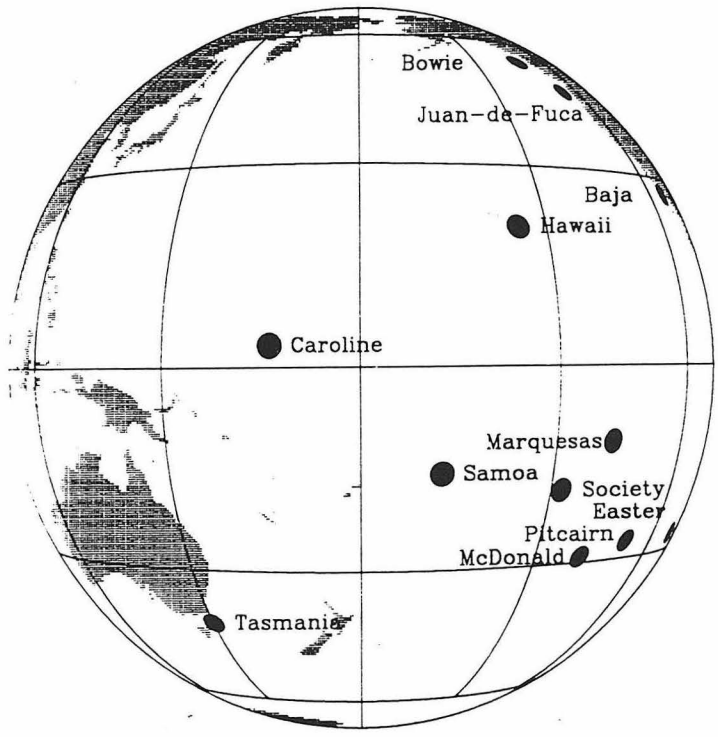

PLUME PROPHECIES

"...hotspots are surface expressions of deep mantle plumes, 150 km diameter, 2 m/yr... rising material spreads horizontally in asthenosphere, stressing plate bottoms, appreciably influencing plate motions; 400 km^3/yr, 50% of mantle heat flow, 80% of mass flux (20 Hawaiis)."

"hotspots are in the open ocean because they have pushed the continents away."
WJM, 72

"The hotspot and hotline models...do not explain E. Australia. (which is) rather the result of extensional stress regime."

"Thus, no hotspots or hotlines are required, volcanism originated from changing intraplate conditions."

"If hotspots originate randomly in the deep mantle, why should the hotspot activity be confined to the terrain immediately adjacent to a margin so recently subject to a major continental extension event?"
RWJ, 89

"Lithospheric extension can trigger the rise of mantle diapirs.
Karro- the similarity to subduction-related magmas should not be ignored".
KG

"The stability of a rising cavity plume is readily upset by even slight relative motion between the plume source and the ambient fluid."
PO & HS, 85

"Jemez Lineament- not a deep mantle source."
WS & RG, 90

"Some 'hotspots' are actually as depleted as MORB and more depleted than nearby ridge segments."
A

"All propagating rifts move away from topographic highs."

"Our extrapolations show that there will be 1,000,000 hotspots by the year 2000. We hope someone proves that hotspots do not exist before it is too late."
H & V, 1977

"(Southern Italy basalts) inherit their enriched signature from a laterally extensive relatively shallow (non-MORB) source rather than from a deep-rooted mantle plume."
RME, 89

"The lack of evidence of a thickened lithosphere (and similarity of BABB and Afar basalts) and presence of slab conflict with deep mantle plume hypothesis."
TA & BCS, 90

"Mantle isochron" idea has great difficulties..different isotopes give different isochrons.
M & T, 80

"All three original proponents of...reactivated lithosphere...have already defected...."

T et. al.

"There is no geochemical gradient away from...Bouvet mantle plume."

APLeR et al.

"There is no doubt that the lower mantle is the OIB source and the upper mantle...the MORB-source.."

DW et al., 90

"Cameroon...only possible source is 'convecting upper mantle'. This poses a problem since 'convecting upper mantle' must also be source of MORB--(but) convection stirs, homogenizes."

F & D, 85

"Seamount chains in NW Atlantic appear to be related to leaky transform faults or extensional fractures rather than hotspots."

JM.H & JB, 84

"Because it is sampled...passively by the world wide spreading ridge system the depleted MORB mantle must reside in the uppermost mantle; there is little or no argument on this point."

"MORB mantle is depleted in LIL and most would agree that the missing budget of these elements is now in--continental crust. The DMM issues are not crippling our forward progress."

SH, 88

"IAB are mix of OIB-type mantle (or melts) and metasomatized MORB-type mantle (or melts). A sediment may be superposed."

PNL, RJS et al, 90

"Whatever the source of the enriched mantle, it must be above the slab, in the top 150 km of mantle."

"Obviously, there is a world wide source for alkalics--tapped in oceanic and continental settings."

"We conclude that trends in [China] lavas can be explained by eclogite fractionation."

XZ, YS, FF, JF, MZ, 88

"Mantle plumes must originate from a hot boundary layer deep within the mantle, possibly the TBL above the CMB where the required heat flux can be drawn from the core."

IHC & RWG, 90

"The enormous size of plume heads also implies that the upper mantle will be displaced by but not wrapped into the head."

IHC & RWG, 90

"Only lower mantle and source material will be stirred into the plume."

"It is unlikely that the CL contributes significantly to CFBs. It certainly cannot attain the high temperatures required to produce picrites."

"Iceland plume has produced picrites with MORB-like geochemical characteristics."
C & G, 91

"Komatiites have depleted geochemical characteristics, implying Archaean plumes originate from MORB-type mantle."

"Of the 17 or so 'generally accepted' plumes many are now questioned or rationalized as having a major plate control (Line, MacDonald, Cobb, Yellowstone, Galapagos, Bermuda, Canary, St. Helena, E. Australia, Erebus, Easter)."

"Unlike the Emperor-Hawaiian chain, other linear chains in Pacific may not have originated from single stationary hotspots."
ASD et al., 89

"AOB identical to those on ocean islands are also erupted on the continental crust and therefore cannot inherit significant chemical traits from either continental crust or subcontinental lithosphere".
MJN, 83

"Thus, the available data seem to rule out OIB-chemistry for subcontinental lithosphere."
S et al, 88

"Karoo may be backarc basin, related to circum Pangeatic subduction."
KG, 83

"Some komatiites may have been flood basalts."
T et al., 83

"Inevitably, the suggestion was made that CFB came from 'undepleted, chondritic, primordial' mantle..subsequently, as mixing lines...Unfortunately, these shifts in geochemical opinion have been too rapid for other geologists to follow."

"...(if other evidence had been considered) it is unlikely that the chondritic mantle source would ever have seen the light of day."
T et al., 83

"Entire ocean subducts in 10^9 years...the system is almost balanced if sediments are subducted--the mantle is recharged as fast as it is depleted."
WSF, 83

"Three major CFB provinces, parallel to margin of Gondwanaland (S. Karoo, Parana, Kirkpatrick), have CA affinitives (as does CRB)."

"Enriched upper mantle supplies early basalts and with continued extension, a more depleted layer is tapped."
B et al., 80

"Indeed, if the upwelling plumes were to stop, the plates would grind to a halt."

GV, WJM, PRV, 85

"The deep mantle feeds the plumes- they in turn empty matter---into the asthenosphere."

"The asthenosphere is the source of normal ocean ridge volcanic activity. There are regions along MAR with OIB character-45°N, 35°N.."

S & S, 78

"Let's hope that no additional isotopic techniques are used---or we might have to think in terms of four, five or more components."

PH, 89

"The continental lithosphere does not have characteristics for source of flood basalts."

RWC, 84

"Most of the observations from swells are well explained by thermal anomalies within the lithosphere alone."

McN, 87

"The remarkable result is that there is no evidence in the depth or geoid data for any swell, any lithospheric heating or any mantle plume (Canaries)."

F & McN, 89

"There is some doubt as to whether the Canaries are indeed due to hotspot processes."

"The geophysical observations of swells can often be solely explained by conductive heating and cooling of---lithosphere."

S & McN, 89

"Taken together--internal heating and compressibility suppress deep mantle plumes."

DY, AL, GS, 89

"Geoid anomalies suggest that upwelling regions in the mantle occur with a spacing of 2500-4000 km."

RW & DMcK, 89

"There is no evidence--for plum pudding type model with preferential melting of enriched veins of plums."

BBN & JGS

"Afar basalts...isotopically similar to Hawaii, Galapagos, Easter---alternative to plume model---compositionally layered mantle...EM on top, DM (MORB) deeper. During early stages of rifting the upper layer contributes."

PJB & LC, 84

"Mantle isochrons now tend to be attributed to mixing rather than discrete mantle events and metasomatism...has emerged from conceptual doghouse to regain position as distinctive albeit shallow-level mantle process."

H et al., 89

"Many continental basalts are derived from mantle source regions that are distinct from 'asthenosphere'."

R, H, O et al., 89

"A viscosity reduction of $2x10^4$ (required) to obtain plume flux from CMB..." EP et al., 75..."Impossible..." HCN, 90

"There is some evidence for activities of widely space hotspots (and subduction zones) to wax and wane in global chorus."

PRV, 81

"Midplate plumes cannot be stable."

LC & VC, 90

"Exactly what different authors mean by the word 'lithosphere' is of central importance to igneous petrology. At present the most commonly used definitions is---the depth to the horizontal isotherm (~125 km, ~1333°C)...delamination is proposed to maintain this (fiction)."

DMcK & MJB, 88

"Depth to base of mechanically strong lithosphere is ~700°C."

G & E, 79

"Passive rifting is caused by stresses which originate from main plate driving forces, e. g. slab pull, transmitted through lithosphere for large distances...difficult to break lithosphere with stresses associated with upwellings...difficult to break plate or get much extension from initial plume."

URC, 90

"There is no doubt that the lower mantle (OIB source) and upper mantle (MORB) are two of the three mantle reservoirs."

DW,DD,SC & MV,87

"The initial stages of submarine arc volcanism are OIB rather than depleted tholeiites. OIB are associated with the tips of propagating rifts."

PNL, RJS

"Marianas lavas (are) indistinguishable from hot-spot basalts."

EI & RJS

"Marianas and Kilauea lavas are similar."

RS & LB

"The essential difference (between BABB, Hawaii, Afar) is not presence or absence of deep mantle plumes but---thick lithosphere and deeper segregation..."

HD, 82

"Early arc melts tap a relatively undepleted OIB-type mantle."

PNL, RJS & SB, 89

"The Marie Byrd Land volcanic province contains three age progressive volcanic chains which have nothing to do with each other or plate motions."

WLeM, DR, 89

"As rifting proceeds depleted material becomes an important component."
WKH, 89

"By definition the plume is assumed to be enriched and the lithosphere is assumed to be the source of MORB."
RD, WMcC, HB & DRN, 86

"Schlanger et al (84) have documented Late Cretaceous volcanism simultaneously over distances of 2500 km--Easter hotline, 2700 km--similar in Australia."
O & B, 72

"The hotspot signatures are there because the lithosphere is already thin."
McN & KF, 90

"Relatively narrow plumes are possible flow solutions if convection is confined to the upper mantle and if heat is primarily provided from below."
MP et al., 75

"The only obvious remaining possibility (for 'less depleted reservoir') is the continental lithosphere (CL)."
McK & O'N, 83

"CL detaches, falls to base of upper mantle, heats up,... unstable, ...hot rising jets, OIB; ^{3}He leaks from lower mantle...."
McK & O'N, 83

"A ubiquitous enriched shallow layer is indicated."
PC & RB, 89

"The shallowest mantle is sampled near lateral edges of slabs, initial stages of BAB...and give OIB signature."

"It is likely the shallow mantle was already enriched in LIL prior to subduction."
JAP, 82

"Distribution of (Yellowstone) volcanism is fracture controlled--not expression of some kind of mantle plume..."
RNT, 1978

"Absence of Pre-Mesozoic hotspot tracks on Canadian shield cannot be chance."
NS, MR, BH, 1988

"The temperature dependance of viscosity prevents plume formation."
HCN, 90

"We propose that a mechanism exists that would allow the surface expression of coeval volcanoes over wider areas than have been allowed for in restricted hotspot models."
SOS et al, 84

"Some hotspot areas represent stagnation points in the mantle return flow."

EMP, UEO, 79; CC, 79

"The fixitity and longevity of hotspots is actually an argument against a deep plume origin."

PO, 87

"Seismic evidence would seem to favor the plume hypotheses since hotspots such as Yellowstone and Iceland are underlain by slow velocity material to a "considerable" depth" (200 km!)

MR, BH, N.S., 88

"Sudden tapping of 2.6 Ga enriched mantle continental lithosphere during waning stages of CRB is problematic...EM exists further east...may physically have moved westward..."

WH & RC, 87

"...recycled material, perhaps slabs, may penetrate into lower mantle...acquire enriched Sr and Pb....recycled plus primitive..."

DG et al, 90

"...because Africa has moved...during past 65 Ma it is clear that magmatic activity cannot be explained by conventional plume models..."

ANH et al, 90

"During 50-300 Ma between rifting and magmatism, continent moved 1000-10,000 km away from rift age plumes...it seems impossible coincidence that tracks of much younger plumes should follow old rifts so closely...times of magmatism do not progress in any regular manner. In other centers, magmatism lasted 30,170, 100 Ma...therefore, not a simple plume track."

SPP, 88

"Igneous centers are related to long-lived sub-rift features that are drifting with North America..."

"---(Antarctic Peninsula)--activity cannot be related to passage of Pacific-Antarctic plate over stationary hotspots---required extension is prerequisite"

JLS, 87

"---OIB cannot be derived from primitive mantle, mixes of primitive and depleted, or recycled C.C."

SUGG, SLG, RKO'N, 89

"---continental lithosphere---is not source or residue from convergent boundary...or primitive...or complementary to CC."

KPU, WFMcD, HP & BS, 89

MORB is not complementary to the continental crust (CC)

A

"In OIB...composition changes with time from tholeiitic to alkaline--in CRB---AOB is followed by tholeiites...related to variations in lithospheric thickness---within-plate magmatism is thus the result of lithospheric dynamics rather than rising asthenospheric plumes."

G & L, 85

"The source of the (Siberian) trapp magmas...was located at a depth of 180-200 km ---(and involved) complete melting of large eclogitic lenses beneath the ancient craton...eclogite nodules from Siberian kimberlites are similar to Siberian tholeiites---"

Y.A.Z. & BMV, 89

"The (hotspot) deficit on 5-23 Ma lithosphere probably means plume flux is concentrated toward ridges...lithosphere of low vulnerability by virtue of rapid motion rather than old age is, ironically, the site for most of the global flux of hotspot volcanism..."

MM, 90

"Hf, Nd isotopes...and trace elements of MORB unquestionably require garnet as a residual phase...melting probably starts below 90 km---require deep garnet-rich source and---large degrees of melting---McKenzie and Bickle (88) and Prinzhofer and Allégre (85) cannot be right..."

VS & SRH, 89

"Hence, there is no reason to assume any longer that enriched volumes in the mantle are deep-seated and it is no longer necessary to relate basalts with "enriched signatures" with plume or hotspot activity by which enriched material becomes part of the asthenosphere and then enters basaltic melts."

RA et al, 88

"...kimberlites are derived from a relatively undifferentiated chondritic mantle..."

B & T, 80

"Nd and Sr isotopic ratios in ---nephelinites are...close to bulk Earth---but they are not primitive and undifferentiated by experienced LIL depletion and enrichment..."

V & N, 83

"The recognition of ancient enriched upper mantle rocks...does not accord with--- two reservoir models..."

S, 83

"...deep mantle (as asthenosphere)...(is same) under oceans and continents...precluding primary, undifferentiated mantle...for these kimberlites."

W & D, 85

"The data...which were taken to justify the notion of primitive undifferentiated mantle would always have been equally well or better explained by mixing---MORB..and enriched component."

Hazi, 89

"...arguments for an undifferentiated mantle reservoir have diminished...with the exception of a few diehards the notion of a primitive source for continental basalts has been laid to rest."

Hazi, 89

"Within-plate magmatism is thus considered to be the result of lithospheric dynamics rather than rising asthenospheric plumes."

G & L, 85

"As rifting proceeds into continental breakup, depleted asthenospheric mantle becomes an important component."

WH et al, 89

"---melts of asthenosphere, i.e. OIB..."

Many

"---the MORB-Source, i.e. the asthenosphere--."

M. More

"---the CFB reservoir, i.e. the continental lithosphere."

M.

"Basalts from B & R extension---are derived initially from enriched lithospheric mantle, then, eventually from upwellings depleted asthenosphere."

CCLL et al, 89

"Oceanic basalts can be used as asthenospheric reference---xenoliths as lithospheric reference..."

MM, 89

"Relative velocities (between Hawaii and Iceland) can reach as high as 15 ± 12 mm/yr ...hotspots can be mislocated by 1500 km is assumed fixed."

PM & US, 87

"Trench migration rates are high, 1-2 cm/yr."

ZG, 86

"CFB, OIB originate in primitive lower mantle. OIB...contaminated by depleted oceanic mantle---CFB shielded by tectosphere from contamination.,"

W & DeP, 79

"Mesosphere is a complex mixture of delaminated continental lithosphere, crust, sediments, depleted mantle and pristine mantle."

CA & DLT, 85

" The only remaining possibility for the "less-depleted" reservoir is continental lithosphere. "

McK & O'N, 83

"The continental lithosphere is cooler and therefore denser than the asthenosphere."

McK & O'N, 83

"Remarkable uniformity is exhibited by Mariana Arc lava (87/86 = .70342±14; 0.09% variation over 500 km) -rules out melting of---sediments; a more uniform mantle than under Hawaii."

"Some IAB are OIB; within top 150 km of mantle."

RS & LB, 84

"An enriched mantle, typical of OIB, must exist beneath the Lau Basin."

"Hypotheses for the origin of BABBs that invoke special, subduction related processes affecting the mantle beneath the basin are questionable."

RCP et al, 90

"We see no logic in attributing major magma-source properties to lithospheric mantle which is rigid, subsolidus and relatively cold---all magmas originate by decompression melting of convecting sub-lithospheric mantle."

RNT et al, 84

"Subduction related magmas are simply MORB-OIB from mantle wedge-with slab introduced complexities..."

"Circumstantial evidence favors a laterally extensive shallow (enriched) source rather than a diametrically restricted plume source originating in lower mantle."

R et al, 82

"CFB sources isolated from convecting, rapidly homogenized asthenosphere from which MORB are derived--therefore, from non-convecting subcontinental lithosphere."

RE & KC, 89

"The transition region (mesosphere) is fertile and depleted; shallow mantle is refractory but LIL-enriched...in general, upper layers of mantle should be enriched in volatiles...continental crust is not only repository for LIL...uppermost mantle (everywhere) is enriched in LIL by metasumatic process that depleted (deeper) source region of MORB. Hotspots are triggered by...insulation and rearranging surface plates."

DLA, 81

"The lower mantle is residue after extraction of basalt, picrite, komatiite and should therefore be barren."

DLA, 80

"The lower mantle has an order of magnitude lower concentration of LIL (including K, U, Th)."

DLA, 83

"Curiously, despite being erupted onto an Archean craton, magmas do not have continental lithosphere contribution...Deccan originates in asthenosphere...the Indian continental lithosphere is mixed into Indian ocean asthenosphere contaminated Tristan, Gough---"

M et al, 89

The asthenosphere is readily contaminated by continental lithosphere, plume heads, starting plumes, slabs, sediments, altered oceanic crust, trapped melts...yet it is assumed always to remain an ancient depleted reservoir with EM confined to much greater depths...

A

The continental lithosphere is often viewed as a plume source yet it needs to be actuated by plumes.

A

"...Etna source is separated from Aeolian and Roman mantle wedge by subducted plate, making it difficult to envisage how a mantle plume could also be tapped by other Italian volcanoes...all the magmas are OIB-type...perhaps the Etna lavas inherit this characteristic from a laterally extensive, relatively shallow level mantle source rather than from a deep rooted plume."

RME, CUH, MAM, NW, 89

"...no hotspot tracks older than Mesozoic are well established...a late onset of plumes is implied. Before the onset of plumes broad upwellings...no hotspot tracks..."

NS, MR, BH, 88

"...Archean hotspots were at least as abundant as at present..."

DA, LB, WS, UL & DW, 91

"Pyrolite - a component of mud used in female mud wrestling contests. The mud is made with equal parts water and pyrolite, a brown, very fine, mortar-like compound. Then, small chunks of cheap foam rubber are thrown in for texture."

L. A. Times, Oct. 26, 1990

"Cobb hotspot has temporal but not isotopic characteristic usually attributed to mantle plume---MORB affinity "

DLD & RAD, 90

"Paraná CFB migrated 750 km north during event---difficult to ascribe to motion of Brazil lithosphere over Tristan plume...plumes do not necessarily initiate flood basalts---need lithospheric extension and rifting.."

DWP, CVH, MM, WS, 90

"The direction of motion of the Tristan hotspot was to the So., yet Paraná lavas migrate North...no simple link with "pure plume" model"

DWP et al, 90

"It is the position of the rift rather than the plume that controls magma site"

"...the superswell is not a superplume---it is located over a region of asthenosphere which has higher content of recycled debris---EM"

D et al, 90

THE BLIND MEN AND THE ELEPHANT

It was six men of Indostan
To learning much inclined,
Who went to see the elephant
(Though all of them were blind),
That each by observation
Might satisfy his mind.

The first approached the elephant
And, happening to fall
Against his broad and sturdy side,
At once began to bawl,
"God bless me! but the elephant
Is very like a wall!"

The second feeling of the tusk
Cried: "Ho! What have we here
So very round and smooth and sharp?
To me 'tis mighty clear
This wonder of an elephant
Is very like a spear!"

The third approached the animal,
And, happening to take
The squirming trunk within his hands,
Thus boldly up and spake:
"I see," quoth he, "the elephant,
Is very like a snake!"

The fourth reached out his eager hand,
And felt around the knee;
"What most this wondrous beast is like
Is mighty plain," quoth he;
"Tis clear enough the elephant
is very like a tree."

The fifth, who chanced to touch the ear
Said:"E'en the blindest man
Can tell what this resembles most,
Deny the fact who can,
This marvel of an elephant
Is very like a fan!"

The sixth no sooner had begun
About the beast to grope
Than, seizing on the swinging tail
That fell within his scope,
"I see," quoth he, "the elephant
Is very like a rope!"

And so these men of Indostan
Disputed loud and long,
Each in his own opinion
Exceeding stiff and strong,
Though each was partly in the right,
And all were in the wrong!

So, oft in theologic wars
The disputants, I ween,
Rail on in utter ignorance
Of what each other mean,
And prate about an elephant
Not one of them has seen!

-John G. Saxe

MANTLE PLUME SYMPOSIUM

DISCUSSION TOPICS

1. Plumes cannot arise spontaneously in a convecting mantle. They exist only in the world of static corn syrup tanks and hypodermic needles.
2. Volatiles and LIL get stripped out of subducted slabs upon dehydration and do not make it to the deep mantle.
3. Backarc basin basalts and ocean islands share the same source.
4. The shallowest mantle is enriched as shown by the sequence of basalts in rifting, ridge jumps, arc volcanism, backarcs and plate reorganizations. The depleted source must be deeper, below some 200 to 400 km.
5. The newly popular giant plumes heads fill up the asthenosphere every 10^8-10^9 years. In this model, therefore, the asthenosphere is enriched.
6. "Plumes" are actually passive upwellings associated with plate reorganizations, or plate edges.
7. Plumes are the upwellings associated with normal mantle convection; they are part of the main flow.
8. Plumes are actually depleted; they become enriched by interacting with the shallow mantle.
9. The location of plumes are stabilized by the locations of hot areas and bumps at the top of the high viscosity lower mantle or by cold slabs at the bottom of the mesosphere.
10. The sources of heat, basalt and trace elements are all different.
11. The shallow mantle is infertile (peridotite) but enriched.
12. The thickness of the elastic plate, the strong lithosphere and the seismic lid coincide; the thermal boundary layer is much thicker but the lower part is weak, hot and temporary. The lithosphere does not contribute to hotspot magmatism.
13. If the "asthenosphere" is depleted why does it take so long to make an appearance when a continent is rifted, a ridge jumps or propagates or subduction or backarc spreading begins?
14. The continental lithosphere is not a good place to obtain continental flood basalts because it is strong, cold and infertile. The lower part of the continental thermal boundary layer is defined as "lithosphere" by Oxbridge but this is "asthenosphere" based on its physical properties and temperature.
15. Enriched basalts, or non-MORB, by definition in current usage, cannot come from the upper mantle or "asthenosphere". They therefore must from the "continental lithosphere" or the lower mantle.
16. The term "continental mantle" as used by petrologists means "the mantle beneath the continent at the time".
17. Mantle hotter than 600°C has no long term strength and cannot become attached to the overlying plate. The depth of this isotherm is much shallower than the thickness of the "lithosphere" in common use by petrologists.
18. The "continental lithosphere" is easily replaced, displaced, delaminated, reactivated or mobilized in current theories. All of this is required because the "asthenosphere" by definition is depleted.
19. Depleted MORB, although from a global depleted layer, only appears at mature spreading centers or where the crust and lithosphere are thin and under extension.
20. The characteristics of backarc basin basalts show that the enriched OIB-like reservoir is shallower than 200-300 km, probably in the depth range of dehydration of subducted material.
21. The uppermost mantle is buoyant relative to the mesosphere because of enrichment in olivine, depletion in FeO and Al_2O_3 and hydration. It is easily pushed aside or displaced by rising plumes and is effectively isolated from the main mantle flow, even if it is weak.
22. The shallow mantle is made up of enriched mantle wedges.
23. The processes devised to enrich the continental lithosphere cannot help but enriching the shallow mantle everywhere.

24. Slabs cannot sink into the lower mantle.
25. Plumes form at the intersections of sheet-like upwellings and are part of the main flow.
26. Plumes are nothing but contaminated MORB.
27. ^{3}He is a mobile trace element that can exist in mantle which is not primitive, primordial or undegassed. ^{3}He, U and Th are stored, transported and removed differently. High $^{3}He/(U,Th)$ regions can exist in processed mantle, including shallow mantle.
28. If asthenosphere is defined as "depleted" then there is no free choice left for plumologists.
29. Most of the controversies among mantle geodynamicists revolve around definitions of lithosphere, asthenosphere, depleted, enriched, fertile, active, passive and deep.
30. Alkalics do not have to come from deeper than tholeiites.
31. The existance of ancient plumes rules out the core-mantle boundary as a source of plumes.
32. The geoid requires a large viscosity increase with depth and a chemically inhomogeneous mantle.
33. Can phase changes be safely ignored in modelling plumes, mantle convection and the geoid?
34. If the mantle is chemically layered models involving pure shear coupling between upper and lower mantles or primitive or enriched lower mantles can be ruled out.
35. The Dupal anomaly does not correlate with lower mantle tomography.
36. Seismic velocity in parts of the lower mantle correlate with hotspots but only at degrees 2 and 3, not at degree 1 or >3.
37. Small degrees of melt are rapidly and efficiently removed from the mantle.
38. Enriched mantle material is carried through the MORB source region on its way both to its long term storage site and to eruption, without contaminating it.
39. The major element chemistry of the hotspot and MORB reservoirs may be identical; the resulting basalts differ because of overlying lithosphere and crust and depth of cooling, fractionation and contamination prior to eruption.
40. Internal heating, convection, plate motions and phase changes all suppress the formation of plumes.
41. There are global synchronisms of hotspot and backarc activity which correlate with changes in plate motions. This seems to rule out lower thermal boundary layer instabilities.

Global Plate Circuits and Motion Between Hotspots: Paleomagnetic Tests

GARY D. ACTON
Woods Hole Oceanographic Institution, Woods Hole, MA 02543

RICHARD G. GORDON
Department of Geological Sciences, Northwestern University, Evanston, IL 60208

The accuracy of plate reconstructions can be independently tested with paleomagnetic data. Previous tests have noted discrepancies and have suggested that they probably result from large systematic errors in the plate reconstructions, missing plate boundaries in the plate circuit, or systematic errors in the paleomagnetic data. The most notable discrepancy, associated with pre-Miocene reconstructions of the Pacific plate with non-Pacific basin plates, has prevented accurate estimates of the motion between the Pacific basin hotspots and other hotspots. Recent improvements in the plate reconstructions, which include the addition of new magnetic and bathymetric data and the incorporation of two previously undetected plate boundaries, have been hypothesized to remove this discrepancy. Hotspot studies, which assume the new reconstructions are accurate and that the Hawaiian hotspot is stationary relative to Atlantic hotspots, predict a Hawaiian hotspot track ~400-1000 km south of the observed Hawaiian-Emperor chain, which corresponds to the Hawaiian hotspot moving 10–20 mm/yr relative to the other hotspots. Other studies, which estimate the motions between hotspots only in the Pacific Ocean or between hotspots in the Atlantic and Indian oceans, find rates less than about 7 mm/yr, indicating that the higher rates may still be an artifact of the reconstructions (most likely related to the plate circuit link between the north Pacific and East Antarctica). Here we test the accuracy of the new reconstructions using global paleomagnetic data from rocks of Late Cretaceous to Miocene age. When reconstructed into a common Pacific reference frame, the data from the other plates indicate ~400-900 km less northward motion than do the Pacific plate data. Neither the reconstruction uncertainties nor a quadrupole field as large as 10% of the dipole paleomagnetic field resolves the discrepancy. With both hotspot and paleomagnetic data recording discrepancies of similar size and direction, an explanation that requires a combination of motion between the hotspots and systematic errors in the paleomagnetic data is unlikely. Systematic plate reconstruction errors, neglected plate boundaries, such as that between East and West Antarctica, intraplate deformation, or some combination of these, likely cause the discrepancies. We conclude that the motion between hotspots, rather than being 10–20 mm/yr, is instead less than about 7 mm/yr and is too small to resolve much further by global plate reconstructions.

INTRODUCTION

A central question about the evolution of hotspots over geologic time is how much they move relative to one another. Several previous studies have addressed this question, though the resulting estimates of interhotspot motions have continually been a point of contention (Figure 1). The estimates vary owing to different hotspot models used, the manner in which hotspot tracks were defined, the different plate reconstructions used, the different lengths of hotspot tracks analyzed, and the different hotspots compared.

Because the surface traces of hotspots are approximately 100 km wide and in some places may be deflected by pre-existing structures in the lithosphere, motions between hotspots cannot be estimated reliably from short hotspot tracks. Because the best defined hotspot tracks, i.e., those for which the bathymetric traces are well mapped and ages well constrained, are located on different plates, estimates of motions between the hotspots responsible for the creation of these tracks must rely on plate reconstruction circuits.

As the Hawaiian hotspot track is much better defined than other tracks, comparing its motion relative to other hotspots is desirable. Previous attempts to estimate the motion between the Hawaiian hotspot and other hotspots in the Atlantic and Indian Oceans have failed, however, owing to problems in the plate reconstruction circuit.

Gordon & Cox [1980] and Suarez & Molnar [1980] found that Late Cretaceous and early Tertiary paleomagnetic data and equatorial sediment facies data from the Pacific plate, both of which give estimates of the position of the paleo-spin axis, were discordant with paleomagnetic data from other plates, when all data were rotated into the Pacific reference frame. Accordingly they concluded that the discrepancy arose from problems in the early Tertiary reconstruction of the Pacific plate to the other major plates. Because the Pacific plate can only be reconstructed to non-Pacific basin plates at the Pacific-Antarctic plate boundary for times earlier than late Miocene, they concluded that a missing plate boundary probably existed between East and West Antarctica or between the North and

South Pacific.

Later work has shown that there were at least two undetected plate boundaries, one between the Antarctic and Bellingshausen plates in the southern Pacific [Stock & Molnar, 1987] and another between the Indian and Australian plates in the equatorial Indian Ocean [Wiens et al., 1985; DeMets et al., 1990; Gordon et al., 1991; Royer & Chang, 1991]. Additionally, Patriat et al. [1985] recognized a large systematic error in the old reconstructions of Africa to Antarctica. Other studies of Pacific magnetic lineations and fracture zone orientations have excluded a possible missing plate boundary within the present Pacific plate along or north of the Eltanin fracture zone [Engebretson et al., 1984; Rosa & Molnar, 1988] or in the southeastern Pacific [Cande et al., 1982].

Here we examine the integrity of the revised global plate circuit by applying paleomagnetic tests to the plate reconstructions of Cenozoic age. We are mainly interested in whether the new reconstructions account for the previously inferred missing plate boundary as has been suggested by Stock & Molnar [1987] and Molnar & Stock [1987]. The absence of a discrepancy between paleomagnetic data from the Pacific plate and data rotated from other plates would support their conclusion. Such a finding would also support Molnar & Stock's [1987] conclusion that the Hawaiian hotspot has moved relative to hotspots beneath Iceland, Tristan da Cunha, Reunion, Kerguelen and St Paul's Island at rates of 10–20 mm/yr. Alternatively, the presence of a paleomagnetic discrepancy of similar size and sense to that seen for the hotspots would indicate that these rates are likely an artifact of the reconstructions.

Besides testing newer reconstructions, our study differs from the prior studies because we explicitly include the plate reconstruction uncertainties, we use a larger paleomagnetic data set, which has a much wider geographical distribution, and we investigate how systematic errors in the paleomagnetic data, including those arising from non-dipole fields, affect the results. We will show, however, that even with these improvements, the paleomagnetic tests still indicate that a significant discrepancy exists within the reconstruction circuit through Antarctica.

The Pacific Discrepancy from the Hotspots

Molnar & Stock [1987] showed that the observed Hawaiian-Emperor hotspot track differs significantly from a track calculated from the motion history of the African plate over the Tristan de Cunha hotspot (Figure 2). In addition they showed that proposed hotspot tracks created by hotspots beneath Iceland, Tristan da Cunha, Reunion, St. Paul's Island, and Kerguelen differ significantly from tracks calculated from the motion history of the Pacific plate over the Hawaiian hotspot. They interpreted these differences as indicating that the hotspots moved relative to one another at rates of 10–20 mm/yr, suggesting that the stationary hotspot assumption is invalid. They noted, however, that their interpretation was dependent on the assumption that the Pacific plate could be accurately reconstructed to the other plates. We will refer to these differences as the Pacific discrepancy.

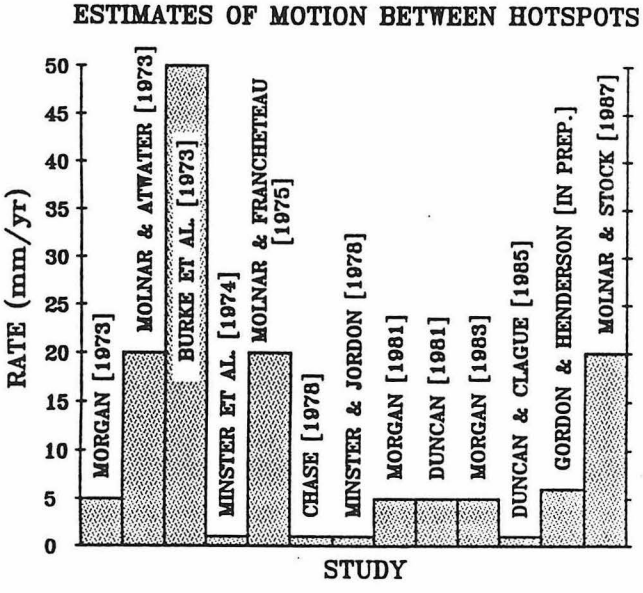

Figure 1.

The Pacific Discrepancy from Paleomagnetic Data

Examination of the Late Cretaceous to Miocene age paleomagnetic poles (Tables to be distributed at the symposium) in any common reference frame reveals a discrepancy between the Pacific poles and poles from other plates. In the Pacific reference frame, we find that mean poles computed from the non-Pacific paleomagnetic data differ significantly at the 95% and 99% confidence levels from similar age Pacific poles (Figure 3). The 6°–12° (700–1300 km) discrepancy between Pacific poles and poles from other plates appears to be systematic and approximately consistent through time.

Repeating the test for the case where the paleomagnetic field consist of a dipole plus a quadrupole component, which is 5% the size and has the same sign as the dipole component, decreases the discrepancy. As above, all Pacific poles differ from similar age non-Pacific mean poles at the 95% confidence level. In all but two of nine pole comparisons, the difference was significant at the 99% confidence level. The overall size of the discrepancy decreases to 5°–10° (600–1100 km).

Attempts to explain the discrepancy by yet larger quadrupole fields are not warranted. Quadrupole components 10% and larger produce unacceptably large dispersion in the non-Pacific paleomagnetic data and can be rejected. Introducing a 10% quadrupole component does, however, reduce the size of the discrepancy relative to the 5% quadrupole model by another ~2° to 3–8°, but the discrepancy remains significant at the 95% confidence level.

Northward Motion Estimates

The difference in the northward motion predicted by the observed Pacific hotspot data relative to that predicted by the calculated hotspot data is ~400–1000 km (Figure 2). Similarly, the difference in the northward motion predicted by the Pacific paleomagnetic poles relative to that predicted by paleomagnetic poles from other plates is ~400–900 km for a dipole field (Figure 3), and ~100–700 km for a dipole plus 5% quadrupole field. Thus the discrepancy estimated from the paleomagnetic data is of similar size and sense to that from the hotspot data, suggesting a common underlying cause that is likely related to the plate reconstructions.

Motion Between East and West Antarctica

Geologic and geophysical evidence support the existence of at least one missing plate boundary for reconstructions through Antarctica in the region between East and West Antarctica. We have found that rotation poles that produce extension and left-lateral translation between East and West Antarctica can explain most of the discrepancy observed in the paleomagnetic and hotspots data, but give rise to a large component of compression on the Alpine Fault in the Tertiary that is inconsistent with geologic observations in New Zealand [e.g., Kamp and Fitzgerald, 1987]. Thus, while it is clear that some motion has occurred between East and West Antarctica during the Cenozoic Era, we can not be certain that this is the only missing plate boundary. The underlying cause of the Pacific discrepancy may yet lie elsewhere.

Conclusions

Through paleomagnetic tests of the global, Cenozoic plate circuit, we have found that the Pacific plate cannot be accurately reconstructed to other plates using reconstructions through Antarctica. Pacific paleomagnetic poles predict motion for the Pacific plate that was shown to be significantly different from that predicted by non-Pacific paleomagnetic poles rotated into the Pacific reference frame. Similarly, Pacific hotspot tracks predict motion for the Pacific that is significantly different from that predicted from non-Pacific hotspot data. The discrepancy between the Pacific and non-Pacific paleomagnetic data was shown to be of similar size and direction to that found between the Pacific and non-Pacific hotspot data.

With both hotspot and paleomagnetic data recording discrepancies of similar size and direction, an explanation that requires a combination of motion between the hotspots and systematic errors in the paleomagnetic data is unlikely. Systematic plate reconstruction errors, neglected plate boundaries, such as that between East and West Antarctica, intraplate deformation, or some combination of these, likely cause the discrepancies.

We conclude that the motion between hotspots can be better estimated by examining hotspot tracks that lie on a common plate or hotspot tracks that lie on different plates that can be accurately reconstructed to one another. The most recent studies giving such estimates find that the hotspots move relative to one another at rates less than about 7 mm/yr [Morgan, 1981, 1983; Duncan, 1981; Duncan and Clague, 1985; R. G. Gordon and L. J. Henderson, unpublished manuscript].

References

Burke et al., *Nature, 245,* 133–137, 1973.
Cande et al., *EPSL, 57,* 63–74, 1982.
DeMets et al., *Geophys. J. Int., 101,* 425–478, 1990.
Duncan, R. A., *Tectonophysics, 74,* 29–42, 1981.
Duncan, R. A. & D. A. Clague, in *The Ocean Basins and Margins, 7A,* 89–121, 1985.
Engebretson et al., *JGR, 89,* 10,291–10,310, 1984.
Gordon, R. G. & A. Cox, *JGR, 85,* 6534–6546, 1980.
Kamp, P. J. J. & P. G. Fitzgerald, *Geology, 15,* 694–697, 1987.
Molnar, P. & T. Atwater, *Nature, 246,* 288–291, 1973.
Molnar, P. & J. Francheteau, *GJRAS, 43,* 763–774, 1975.
Molnar, P. & J. Stock, *Nature, 327,* 587–591, 1987.
Morgan, W. J., in *The Sea, vol. 7,* 443–487, 1981.
Morgan, W. J., *Tectonophysics, 94,* 123–139, 1983.
Patriat et al. *EPSL, 75,* 204–214, 1985.
Rosa, J. C. C. & P. Molnar, *JGR, 93,* 2997–3008, 1988.
Royer, J.-Y. & T. Chang, *JGR,* in press, 1991.
Stock, S. & P. Molnar, *Nature, 325,* 495–499, 1987.
Suarez, G. & P. Molnar, *JGR, 85,* 5257–5280, 1980.
Wiens et al., *GRL, 12,* 429–432, 1985.

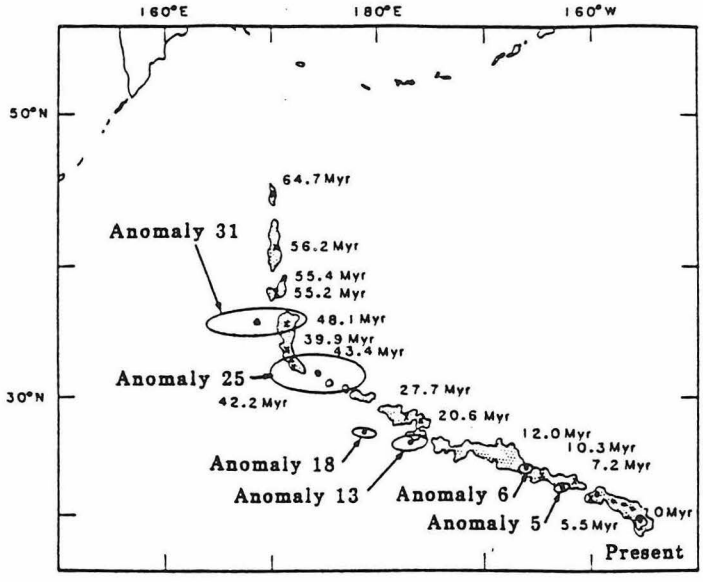

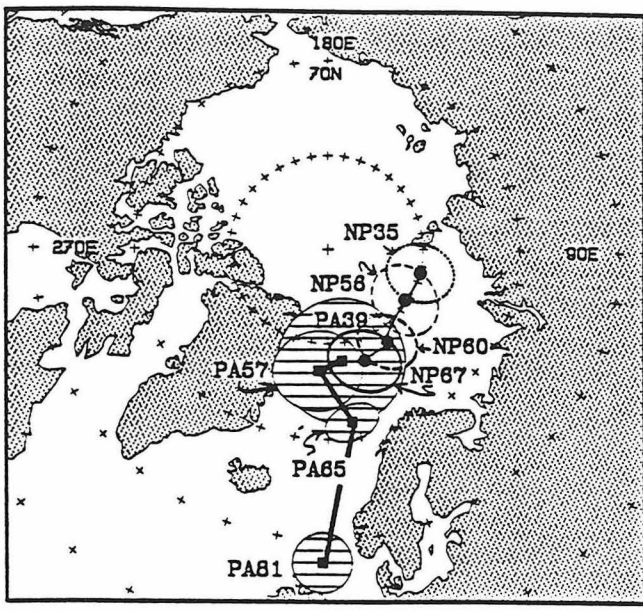

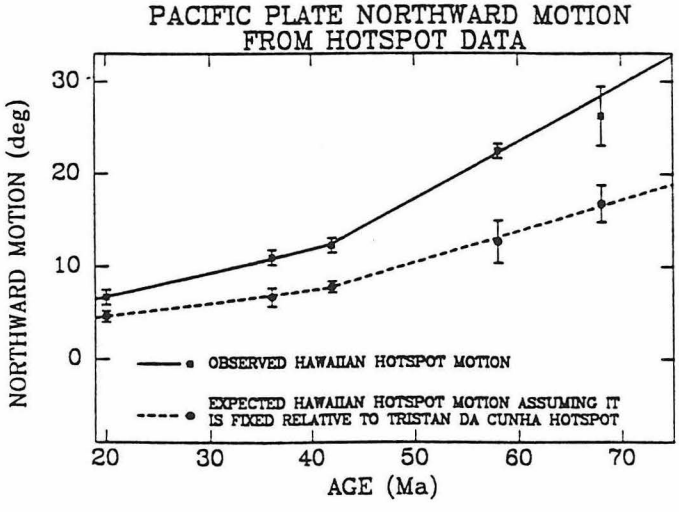

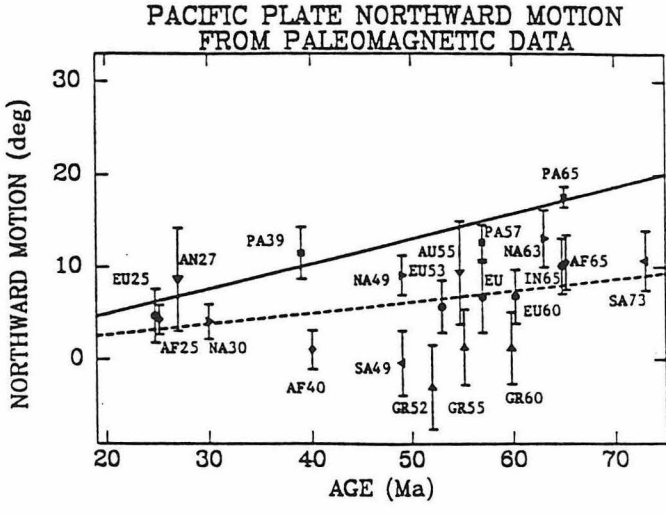

Figure 2. *Top* Comparison of the observed Hawaiian-Emperor hotspot track with a calculated track (ellipses), which was derived by assuming the Hawaiian hotspot is fixed with respect to the Tristan da Cunha hotspot (after Figure 1 of Molnar & Stock [1987]). *Bottom* Northward motion computed from top figure. The solid line is the northward motion of the Pacific plate relative to the Hawaiian hotspot and the dotted line is the northward motion relative to the Tristan da Cunha hotspot in the Atlantic Ocean assuming it is fixed to the Hawaiian hotspot.

Figure 3. *Top* Comparison of Pacific paleomagnetic poles PA39 (PA refers to the Pacific plate and 39 refers to the mean age of 39 Ma), PA57, PA65, and PA81 (ellipses with ruled-pattern) with mean poles computed from paleomagnetic data from other plates. The mean poles are referred to as non-Pacific (NP) poles and have mean ages of 67 Ma (thick solid ellipse), 60 Ma (thick dashed ellipse), 56 Ma (thin dashed ellipse), and 35 Ma (dotted ellipse). The thick line is the Pacific apparent polar wander path from Pacific data and the thin line is that from non-Pacific data. *Bottom* Northward motion computed from Pacific (solid line) and non-Pacific (dashed line) paleomagnetic data. The points PA65, PA57, and PA39 constrain the solid line, whereas all other data constrain the dashed line. Data are from the North American (NA), South American (SA), Greenland (GR), European (EU), African (AF), Australian (AU), Indian (IN), Antarctic (AN), and Pacific (PA) plates. Note that the offset between the solid and dashed lines is similar to that found from the hotspot data (Figure 2).

The T,P Path of OIB generation

Francis Albarède, *CRPG-CNRS, BP 20, 54501 Vanddoeuvre Cedex, France*

Attempts to relate the degree of melting with temperature (T) and pressure (P) (Francis et al., 1983; McKenzie, 1984; Klein and Langmuir, 1987; McKenzie and Bickle, 1988) were unlikely to produce geologically significant results because, for given temperature and pressure conditions of melting, the degree of melting depends strongly on the fertility of the source (basically its content in SiO_2, Al_2O_3, FeO, CaO, and alkalies) which may vary significantly in natural peridotites. In addition, sandwich-type experiments for which the melt fraction is unknown (Takahashi and Kushiro, 1983; Falloon et al., 1987, 1988a, b), could not be included in the analysis whereas runs with known melt fractions (Jaques and Green, 1980) represent fairly extensive degrees of melting not simply applicable to natural melts. I have therefore attempted to relate the chemical composition of basalts to the temperature and pressure of melting without relying specifically on the melted fraction which is clearly a poorly known parameter.

Visual examination of all the existing available data in a rotating three dimensional frame hinted to surprisingly good linear relationships for various T-P-oxide content triplets with, for some elements, a very small number of outliers. These observations being suggestive of a rather limited number of degrees of freedom in the experimental data, principal component analysis of the correlation matrix has been carried out for the following variables: T, P, SiO_2, TiO_2, Al_2O_3, FeOt, MgO, CaO, Na_2O, K_2O. The total variance of the experimental data is accounted for at 80 percent by 3 variables and 92 percent by 4 variables. This variance distribution indicates that, in spite of different starting compositions of the melted peridotites, the chemistry of the melts has barely more than three degrees of freedom. Magma composition is therefore controlled by three statistically independent factors (i) pressure (ii) temperature (iii) the fertility of the source.

P and T were regressed against the 8 independent chemical variables SiO_2, TiO_2, Al_2O_3, FeOt, MgO, CaO, Na_2O, K_2O and whichever variable did not improve significantly (i.e. by more than a few percent) the fit as measured by the standard error of estimate was recursively dropped. Substantial misfit due to non-linearity led to use quadratic regression models taking variables such as $(SiO_2)^2$ or $SiO_2*Al_2O_3$ into account.

Mineral fractionation represents a large potential uncertainty in these calculations. Clinopyroxene fractionation is not expected to bias temperature and pressure estimates very significantly. Since the CaO/Al_2O_3 ratio of oceanic basalts is rather well constrained, about 0.2 unit if nephelinites

are not considered, clinopyroxene removal is not to exceed ~10 percent, which results in maximum pressure underestimates of about 5 kb. Pressure and temperature shifts by clinopyroxene removal are in general positively correlated except at high pressure. Olivine is a mineral somewhat more difficult to trace: low FeO/MgO magmas may either be primitive or result from olivine accumulation. Using novel exact equations suggests a procedure applicable to the many cases where olivine is the only mineral on the liquidus: linear relationships, i.e. "olivine control lines", in a FeO vs MgO diagram are expected from olivine accumulation for a given degree of fractionation, whereas olivine liquid lines of descent have a much pronounced curvature. Applying a K_D value of 0.3 indicates that the non-cumulated liquid had a FeO/MgO value of ~0.9, which makes it possible to correct the concentration data for olivine accumulation. Then, olivine is added to this fractionated melt and its concentrations calculated until it is in equilibrium with the olivine which is thought to represent the range of source peridotites (Figure 1). A very large fraction of mantle peridotites would have a forsterite content in the range 90-92 percent, which is the range for which pressure and temperature of melt segregation have been estimated. Olivine addition or removal move the apparent temperature and pressure of segregation nearly parallel to the solidus.

Temperature and pressure have been calculated for the volatile-free compositions of the more primitive basalts from the few ocean islands investigated well enough to provide well-documented fractionation trends (Figure 2). Hawaii offers the best variety of well-studied volcanic series with the Kilauea (Murata and Richter, 1966; Wright et al., 1975), Loihi (Frey and Clague, 1983), and the Mauna Kea (Frey et al., submitted). The compositions of parent magmas obtained by "redissolving" olivine until they are in equilibrium with olivine Fo_{90-92} are somewhat variable with MgO contents in the range 18 to 22 percent. Shield-stage Hawaiian tholeiites seem to have segregated at a pressure of 20 to 35 kb, in good agreement with the depth of the deepest volcanic earthquakes (Klein et al., 1987) and the compensation depth calculated from the geoid and bathymetric anomalies (Monnereau and Cazenave, 1988). This agreement suggests that solid-liquid segregation took place at the base of the lithosphere where a large volume mantle diapir associated with the most abundant volcanic eruptions has stalled. As discussed by Falloon et al. (1988b), this pressure range is not incompatible with garnet remaining in the residue as required by trace element modelling (Budahn and Schmitt, 1985; Frey et al., submitted). Gough (LeRoex, 1985) and Réunion (Albarède and Tamagnan, 1988) island basalts seem to have formed in similar conditions. Postshield lavas from Mauna Kea record much higher pressure which may indicate that small fluxes of magmas associated with waning volcanic activity stall at significantly greater depth (~45 kb) than the source of major tholeiitic emissions. Tahiti basalts analyzed by McBirney and Aoki (1968) and Brousse et al. (1987) suggest that magmas from the rather weak plume of the Society detach very deep from their source. As the apparent pressure (60 - 70 kb) is much beyond the range used to calibrate the pre-

sent barometer (0 - 35 kb), the particular chemistry of Tahiti rocks may also reflect some unaccounted source heterogeneities or metasomatism in addition to pressure effects.

The temperature gradient recorded by the change in apparent segregation temperature with depth (~5 °K/ kb) is much larger than the adiabatic gradient of solid peridotite (~1.5 °K/ kb) but much smaller than the slope of the solidus (~12 °K/ kb, e.g. Takahashi and Kushiro, 1983). However, in a melting range where latent heat (L) is to be taken into account, the adiabat takes a slightly different form. For low degrees of melting, entropy (S) balance in a medium with thermal expansion coefficient α, isobaric heat capacity C_P, and specific volume V depends on the degree of melting f in such a way as:

$$\left(\frac{\partial T}{\partial P}\right)_S^{\text{molten}} \# \left(\frac{\partial T}{\partial P}\right)_S^{\text{solid}} + \frac{\frac{L}{C_P}\left(\frac{\partial f}{\partial T}\right)_P}{1+\frac{L}{C_P}\left(\frac{\partial f}{\partial T}\right)_P}\left[\frac{dT_{\text{solidus}}}{dP} - \left(\frac{\partial T}{\partial P}\right)_S^{\text{solid}}\right] \qquad (11)$$

For a reasonable L/C_p ratio of 400°K, a derivative $(\partial f/\partial T)_P$ of ~ 0.0025 (Jaques and Green, 1980), a solidus slope of 12°K/ kb, the adiabat in the melting range increases to ~6°K/ kb, i.e. is ~4 times steeper than the solid adiabat. Position of solidus and liquidus in the P, T space may vary with the fertility of the source (e.g. Takahashi and Kushiro, 1983, for the effect of K_2O), hence T, P variations cannot be uniquely translated into melted fractions. Nevertheless, the slope dT/dP which seems to characterize the estimated T, P conditions at which Ocean Island Basalts segregate from their source seem steep enough for being adequately explained by the adiabatic ascent of partially molten mantle plumes.

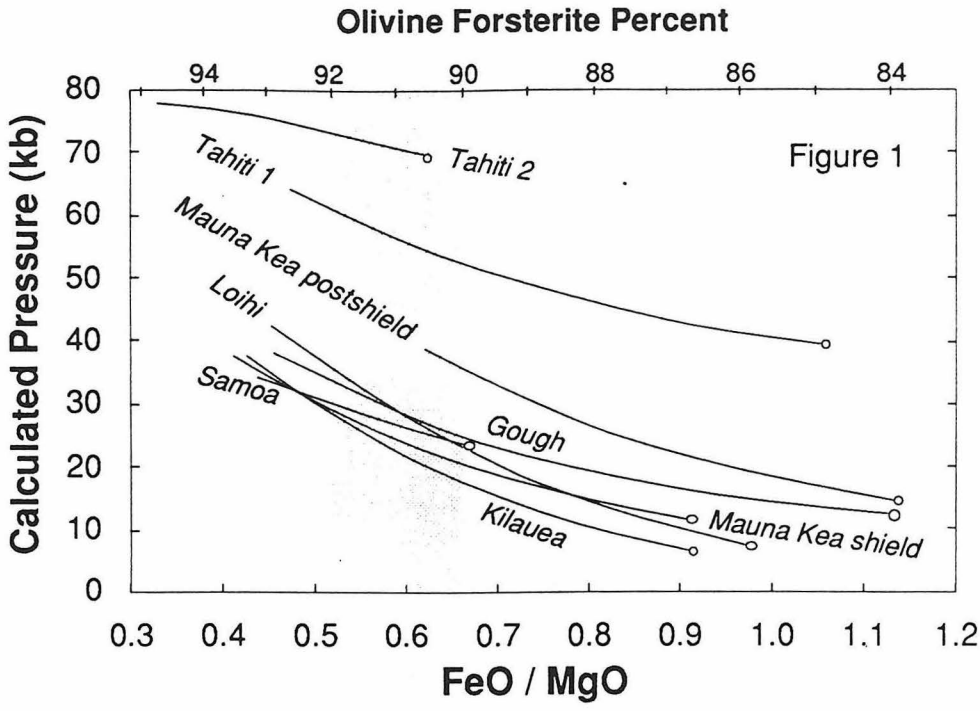
Olivine Forsterite Percent
94
92
90
88
86
84
Figure 1
Tahiti 1
Tahiti 2
Mauna Kea postshield
Loihi
Samoa
Gough
Kilauea
Mauna Kea shield
Calculated Pressure (kb)
80
70
60
50
40
30
20
10
0
0.3
0.4
0.5
0.6
0.7
0.8
0.9
1.0
1.1
1.2
FeO / MgO

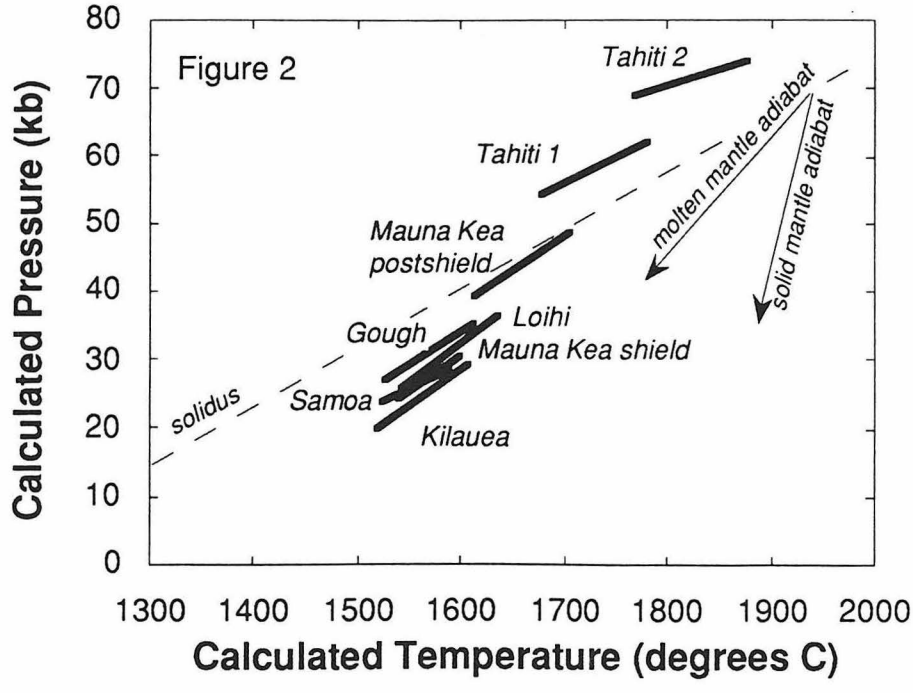
Figure 2
Tahiti 2
Tahiti 1
Mauna Kea postshield
Gough
Loihi
Mauna Kea shield
Samoa
Kilauea
solidus
molten mantle adiabat
solid mantle adiabat
Calculated Pressure (kb)
80
70
60
50
40
30
20
10
0
1300
1400
1500
1600
1700
1800
1900
2000
Calculated Temperature (degrees C)

PLUMES - The Standard Model

Don L. Anderson, Seismological Laboratory, California Institute of Technology, Pasadena, CA 91125, USA

1. The asthenosphere (=upper=convecting≡ depleted mantle≡ MORB source≡ DM ≡ primitive mantle - continental crust) represents the shallowest, sublithospheric mantle.
2. Enriched basalts must originate elsewhere.
3. The Continental Lithosphere (CL) is an ancient enriched reservoir where CFB originate or get contaminated by "plumes" coming from deeper. The CL is easily delaminated, replaced, displaced or depleted by plumes, extension or compression.
4. CL contaminates the So. Atlantic (Brazil) and Indian Oceans (India). Delaminated CL sits at the base of the upper mantle and provides OIB plumes.
5. The asthenosphere contains tongues, streaks, plums, schielen, flow channels, plume heads, CL etc. of enriched mantle (EM) at ridges, fracture zones, propagating rifts etc.
6. Recycled material is responsible for some plumes - this passes through DM without contaminating it, either on descent or ascent. DM is the shallowest mantle (except for plume heads, streaks, tongues, channels etc.)
7. Plumes originate in the lower mantle which is [primitive, enriched, recycled] material.
8. Plumes originate in the non-convecting mantle.
9. Plumes originate in D", a chemically distinct layer, but they are mainly thermal.
10. Plumes are fixed relative to one another.
11. The sources of heat, basalt and trace elements/isotopes are all the same. If the energy source is deep the isotopic signatures are deep (except for CL contamination).
12. Plumes are secondary instabilities, separate from the main flow.
13. Midocean ridges are passive upwellings, caused by plate separation.
14. Plate tectonics is driven by plumes.
15. Plumes represent about 10% of the global heat and mass flow.
16. Higher than atmospheric $^{3}He/^{4}He$ (except for MORB) implies primitive, promordial, unfractionated, undegassed mantle.

PLUMES - The Strawman

Don L. Anderson, Seismological Laboratory, California Institute of Technology, Pasadena, CA 91125, USA

1. In hotspots, as in Island Arcs, the source of basalt, the source of heat or energy, and the source of "contamination" (trace elements, isotopes) can all be different.
2. The source of basalt must be relatively deep (greater say, than 300-400 km) to satisfy tomography and provide the kind of stability that plumes seem to have. The heat source must be deeper since plumes are probably mainly heated from below. The "contamination" may be shallow. The direct evidence for plume depths (gravity, bathymetry, heat flow, tomography) can be satisfied in the upper 200 or 300 km of the mantle.
3. The lower mantle (LM) has higher viscosity than the shallow mantle and by thermal effects and boundary topography can provide a stable reference frame (hot upper mantle plumes over hot patches of LM). Subducted slabs are high viscosity and can also provide a reference system more stable than continents or ridges.
4. Sediments and altered oceanic crust are hard to recycle below 200-300 km because of dehydration of the slab and mechanical effects. The slab is de-metasomatized upon subduction, hydrating and enriching the shallow mantle (non-uniformly). This shallow recycled material from the slab eventually acts as an enriched (but not necessarily fertile) source for hotspots. The plume signature is acquired at shallow depths, even if the basalt and the heat are based much deeper. The hydrous mantle wedge flows readily but stays shallow.
5. Small melt fractions are also trapped in the shallow mantle (sub-crust, sub-lithosphere) by buoyancy, viscous, strength, permeability and thermal considerations. These contribute a distinctly different enriched component to be later tapped by plumes.
6. The shallowness of the various enriched components is attested to by the initial (enriched) products of rifting, ridge jumps, abandoned ridges (final products in this case), new hotspots, fracture zones, propagating rifts, uplifted peridotites (St. Peter-Paul, St. John) and the perceived need for a shallow EM in models that involve widespread asthenospheric contamination, an enriched CL, streaks, tongues, channels, plume heads in a "depleted asthenosphere". Plume heads alone eliminate the "depleted asthenosphere" every 10^9 years and fill up the shallow near-ridge mantle more often.
7. The depleted fertile (MORB) reservoir is below the EM (which may be enriched yet refractory) and is underlain by a non-uniform heat source (plume-like upwellings require strong bottom heating). The CMB is not a strongly bottom heated region unless the lower mantle is depleted in radioactivities.
8. The characteristics of IAB and BABB suggest a shallow origin for EM (OIB-like).
9. The lower mantle is refractory, depleted and infertile and intrinsically denser than the upper mantle (mainly because of CaO, Al_2O_3, Na_2O, SiO - contents). It contributes heat but not material to the upper mantle.
10. Plumes and ridges share the same basalt reservoir (the fertile mesosphere).
11. Depleted and enriched basalts differ because of their interaction with the shallow namtle and lithosphere.
12. The purest uncontaminated MORB is found at mature, rapidly spreading, slowly migrating ridges but all MORBs are mixtures.
13. Shallow contamination by EM is most pronounced for slowly spreading, rapidly migrating, new ridges.
14. For dying ridges or aborted rifts, the shallow EM (perisphere) can creep back in, laterally.

15. Rift and plume-like upwellings can be initiated by lithospheric effects as well as by hydrodynamic instabilities.
16. At depth all upwellings are depleted. Plumes may be the primary convective upwellings (which would give MORB-like products if the enriched shallow mantle were not present which it, by and large, isn't near mature ridges). Plumes can be MORB-like; upwellings at ridges can be enriched.

PRIMITIVE MANTLE PLUME ORIGIN FOR THE SIBERIAN FLOOD BASALTS AT THE PERMO-TRIASSIC BOUNDARY AND IMPLICATIONS FOR THE ORIGIN OF CONTINENTAL FLOOD BASALT PROVINCES

Asish R. Basu, Department of Geological Sciences, University of Rochester, Rochester, New York 14627

The well-known Dutch physicist, Onnes, once remarked "Door meten tot weten", which, literally translated, meant "Measure until understanding is achieved." In this brief report, I will review our recent measurements (1,2) of $^{40}Ar/^{39}Ar$ and Nd, Sr-isotopes along with the petrochemistry of the Siberian Flood Basalt Province (SFBP) to demonstrate that a comprehensive deep mantle plume origin for this flood basalt province can be established based on these measurements. Further, available geochemical data of the other younger than 250 Ma flood basalt provinces can also be understood in the light of our Siberian basalt data.

The SFBP constitutes one of the largest continental flood basalt (CFB) provinces in the world. Originally, covering an area of 1.5 $x10^6$ km^2 with an average thickness of 1 km, presently, it covers an area of 3.4 x $10^5 km^2$. These volcanic rocks are found principally in the great Tinguska basin, east of the Enisei River (Fig. 1), where they erupted through the Archean-Proterozoic Siberian Platform. Individua lava flows show variable thicknesses from a few meters to greater than 100 m, and they are interbedde with abundant pyroclastic deposits. Distinct suites of flows, laterally continuous over tens of kms, make up the lava stratigraphic column of the SFBP (Fig. 2). In the Noril'sk region (Fig. 1), 11 suites o petrologically distinct basalts have been recognized (Fig. 2), which can be correlated readily with lava elsewhere, such as in Putorana (Figs. 1, 2). An overwhelmingly greater part of the SFBP is in the Putorana region, which constitutes 90-95 percent of the bulk of the province. The total alkali versu silica diagram (Fig. 3) demonstrates that some of the Noril'sk group of rocks are more evolved than the Putorana samples, which plot mostly in the basalt field. It is important to note that the Putorana basalt erupted during the last two cycles of the five volcanic cycles believed to have formed the entire SFBP. It is also important that the Noril'sk eruptions are marked by central-type eruptions with short, irregular, cascade-like lava flows, implying relatively smaller magma chambers where assimilation-fractiona crystallization (AFC) processes could have been operational. In contrast, the Putorana basalts representing the same cycles as the Noril'sk, are the results of fissure-type eruptions with large lava volumes; fo example, a single flow of the Nadayanski flow of the Ayanski suite (Fig. 2) occupies an area of 270 km x 250 km with a maximum thickness of more than 100 m. Thus the Putorana eruptions were quick resulting in homogeneous basalt composition, inhibiting AFC processes to change magma compositions.

The rapid eruption of the SFBP can be documented with our preliminary measurements (1) of laser-heating $^{40}Ar/^{39}Ar$ data (Fig. 4), which indicate that the bulk of these basalts cover an extremely short time-interval (700,000±400,000 years) beginning at about 248 million years ago at mean eruption rates of greater than 1.6 km^3 yr^{-1}. This enormous eruption rate, over an area of ~ 1,500 km across compares favorably with eruption rates estimated for some of the other large CFB, including the Deccan Traps, the Karoo and the Columbia River Basalt (3), and implies a mantle plume origin for the bulk of the SFBP (4). Unlike the other CFB, the SFBP is not clearly related to any hotspot activity, although Morgan (5) suggests a possible relationship to the Jan Mayen hotspot. It is noteworthy that there is no major rifting associated with the SFBP, either prior or postdating the eruption. This observation clearly indicates that, at least for the SFBP, lithospheric extension was not a necessary precondition for the mantle plume initiation. Our $^{40}Ar/^{39}Ar$ data indicate also that the bulk of the SFBP magmatism coincided with the Earth's most profound faunal mass extinction (at the family level) event at the Permian-Triassic boundary - the boundary between the Paleozoic and Mesozoic Eras-estimated at 245-250 Ma (6).

The initial Sr and Nd-isotopic compositions of the Putorana and Noril'sk basalts of the SFBP (2 are shown in Fig. 5 and compared with the fields of Ocean Islands Basalts and MORB in this diagram The Siberian basalts define an array near the mantle correlation line and this array can be defined by a hyperbola. However, the majority of the Putorana basalts (70 percent) show a clustering of the data points near 0 to +2.5 and 0.7046 and 0.7052 for $\epsilon_{Nd}(t)$ and $(^{87}Sr/^{86}Sr)_I$, respectively. As the Putorana basalts comprise the bulk of the SFBP, these data, therefore, warrant a less depleted mantle component. which is near chondritic in Sm-Nd and Rb-Sr isotope characteristics, as the major source for the bulk of the SFB plume. It is also interesting to note the overlapping correspondence in Fig. 5 between the SFB and basalts of the ocean islands.

To quantitatively evaluate the role of assimilation fractional crystallization (AFC) processes in causing the chemical and isotopic variations of the SFB, it is possible to use the AFC equations (7) in conjunction with a plot of $(^{87}Sr/^{86}Sr)_I$ versus Sr-concentrations (Fig. 6). It is clear that most of the Putorana basalts cluster around initial $^{87}Sr/^{86}Sr$ ratios of 0.7045 and 0.7052 and Sr-concentrations of 150-220 ppm. The Noril'sk basalts define two arrays indicating that AFC processes were important in the evolution of these rocks. The Noril'sk curve calculated for $D_{Sr} = 0.01$ and $r = 0.05$, probably evolved by crystallizing olivine and pyroxene. The other AFC curve in Fig. 6, calculated for $D_{Sr} = 1$ and $r = 0.2$, evidently evolved by crystallizing plagioclase with subordinate amounts of olivine and pyroxenes. Two samples of picrobasalts in Fig. 6 (#19 and #42) do not follow the AFC curves and hence they are not genetically related to the other basalts falling on the AFC paths. In summarizing these observations, we can state that the volumetrically insignificant Noril'sk lavas of the SFBP show clear evidence of AFC; in contrast, the Putorana samples representing the bulk of the SFBP, do not show significant evidence of continental crustal contamination. Calculations of Ma/Mm^0, the ratio of mass assimilated to the initial mass of the magma, suggest that the Noril'sk basalts assimilated 3.6 and 12 percent crustal Sr, respectively, for the two AFC processes described above. Thus, we conclude that the initial isotopic ratios of Nd and Sr for the majority of the Putorana basalts are diagnostic of the mantle-source from which the bulk of the SFBP was derived.

Several recent studies on the CFB provinces have suggested the subcontinental lithospheres as a viable source for the basalts because they display a wide range of Nd, Sr-isotopic compositions. However, the available trace element and isotopic data also support an earlier suggestion (9) that the continental flood basalt volcanism is the result of plume activity derived from primitive mantle sources. The most important argument (10) in favor of this model is the fact that volume-weighted, major portions of several CFB, such as the Columbia River Basalts, cluster around $\epsilon_{Nd}(t) = 0$ and $(^{87}Sr/^{86}Sr)_I = 0.705$. Our new petrochemical and Sr, Nd-isotopic data (2) of the SFBP (Figs. 5, 6) also clearly demonstrate that the most voluminous portion of the SFBP in the Putorana section was derived from a mantle-source with near-chondritic Sr and Nd-isotopic signatures.

A plot of initial ϵ_{Sr} versus initial ϵ_{Nd} (Fig. 7) for all the major flood basalt provinces (8) younger than 250 Ma, including the SFBP (2), defines an array that runs parallel to the mantle correlation line between ϵ_{Nd} around 0 and +8. However, in the field of negative ϵ_{Nd} values, the data points fan out in hyperbolic fashion, paralleling between the contours of 1 and 2 Ga model crust formation ages and within the levels of a vertically layered crust with different Rb/Sr ratios. Thus, the overall Nd, Sr-isotopic patterns of the major flood basalt provinces can be modeled in terms of three end-members in the framework of an uprising primitive lower mantle plume that mixes by partial melting with the depleted mantle source of MORB (also present beneath the continental lithosphere) and finally incorporates some of the heterogeneous continental lithosphere component through AFC processes. In this model, the SFBP are sub-aerial analogue of ocean island basalts formed over a hotspot with an upwelling plume of primitive mantle composition. The striking negative linear relationship among the CFB data in Fig. 7 between $\epsilon_{Sr} = \epsilon_{Nd} = 0$ and the upper left hand corner (the MORB-field) of this diagram deserves scrutiny. This negative array is the so-called "mantle array" (11), initially defined from the Nd, Sr-isotopic data of oceanic basalts. However, this correlation is remarkably displayed also by the continental flood basalts and can be interpreted as a mixing relationship between a primitive mantle ($\epsilon_{Nd} = \epsilon_{Sr} = 0$) and MORB mantle source. From the consideration of a general mixing equation (12) applied to Nd and Sr-isotopes, such a linear mixing is possible only when the Sr/Nd ratios of the two reservoirs are equal. In this context, it is highly significant that the best estimates (13) of Sr and Nd concentrations in the primitive mantle (C1 chondrite, Sr = 19.5 ppm, Nd = 1.13 ppm, Sr/Nd = 17.3) and MORB (Sr = 128 ppm, Nd = 7.7 ppm, Sr/Nd = 16.6) support a very similar value for the Sr/Nd ratios in these two reservoirs. Therefore, the linear negative correlation observed for the CFB in Fig. 7 may represent the mixing process between a primitive deeper mantle plume and the upper mantle MORB-reservoir.

References

1. P.R. Renne and A.R. Basu, Science, submitted, 1991.
2. M. Sharma, A.R. Basu, and G.V. Nesterenko, Geochim. Cosmochim. Acta, in press, 1991.
3. M.A. Richards, R.A. Duncan, and V.E. Courtillot, Science, 246, 103-107, 1989.
4. I.H. Campbell and R.W. Griffiths, Earth Planet. Sci. Lett. 99, 79-93, 1990.
5. W.J. Morgan, in The Sea (ed. C. Emiliani), vol. 7, Chap. 13, 443-487, 1981, Wiley Intersciences.

6. G.S. Odin and W.J. Kennedy, C.r. Seances Acad. Sci. Paris 294, 453, 1982; A.R. Palmer, Geology 11, 503, 1983; G.S. Odin, in The Chronology of the Geological Record, N.J. Snelling, ed., (Blackwell, Palo Alto, 1985), 114-117.
7. D.J. DePaolo, Earth Planet. Sci. Lett. 53, 189-202, 1981.
8. S.R. Carter, N.M. Evensen, P.J. Hamilton and R.K. O'Nions, Nature, 281, 28-30, 1979; C.J. Allegre, B. Dupre, P. Richard, D. Rousseau, Earth Planet. Sci. Lett. 57, 25-34, 1982; R.W. Carlson, G.W. Lugmair and J.D. Macdougall, Geochim. Cosmochim. Acta 45, 2483-2500, 1981; R.W. Carlson, Geochim. Cosmochim. Acta, 48, 2357-2372, 1984; C.J. Hawkesworth, M.S.M. Mantovani, P.N. Taylor, and Z. Palacz, Nature, 322, 356-359, 1986; S.S. Hughes, R.A. Schmitt, Y.L. Wang, and G.J. Wasserburg, Geochem. J., 20, 173-189, 1986; J.J. Mahoney, in Continental Flood Basalts (ed. J.D. Macdougall), 151-194, Kluwer Academic Publish. 1988; R.V. Fodor, A.N. Sial, S.B. Mukasa and E.H. McKee, Earth Planet. Sci. Lett. 104, 555-567, 1990.
9. D.J. DePaolo and G.J. Wasserburg, Proc. Natl. Acad. Sci., USA, 76, 3594-3598, 1979.
10. D.J. DePaolo, Geochim. Cosmochim. Acta, 47, 841-844, 1983.
11. D.J. DePaolo, Neodymium Isotope Geochemistry: An Introduction, Springer Verlag, 187 p., 1988.
12. C.H. Langmuir, R.D. Vocke, G.N. Hanson and S.R. Hart, Earth Planet. Sci. Lett. 37, 380-392, 1978.
13. S.R. Hart and A. Zindler, in Mantle Convection, W.R. Peltier, ed., Gordon and Breach Science Publ. 261-387, New York, 1989.

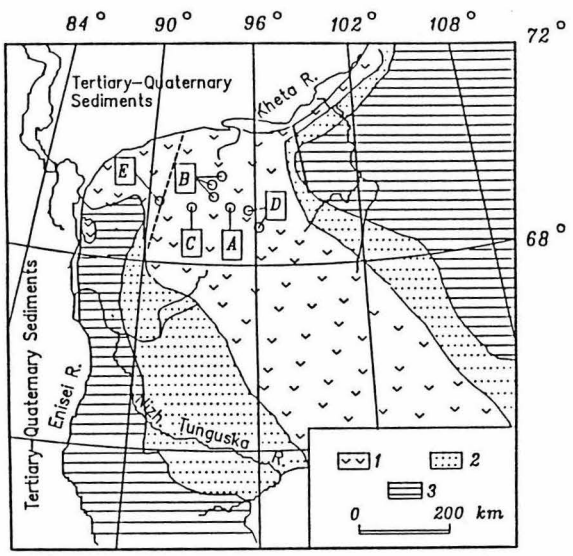

Figure 1. Schematic map of Permian-Triassic basaltic rocks from the Siberian Platform (modified from Zolotukhin and Al'mukhamedov, 1988) showing locations of the samples for this study. 1. Basaltic Trap, 2. Intrusive trap and tuffs, 3. Platform sedimentary sequence. Dashed line refers to the approximate boundary between the Norilsk and Putorana. Solid line refers to the boundary between the Putorana and Kotui to the northeast. Locations of samples analyzed in this study are indicated by A-D (refer to Fig. 2 for stratigraphic positions of samples): A. 1-8; B. 9-20; C. 21-27; D. 28-31; E. 32-47.

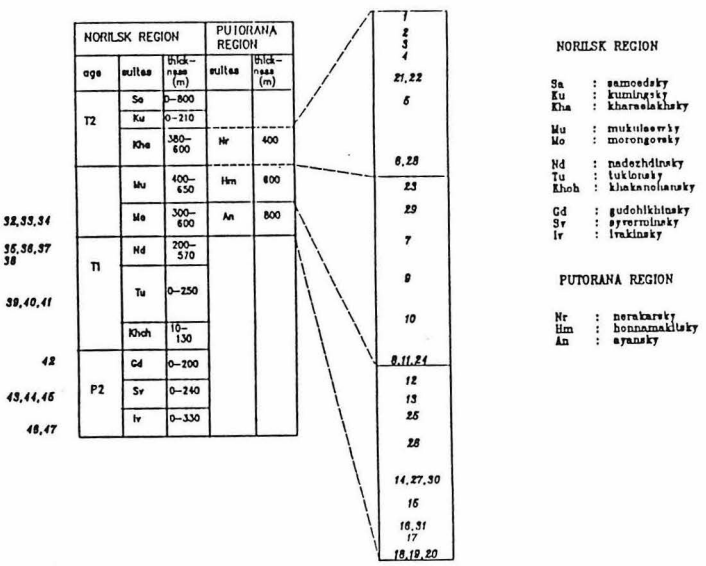

Figure 2. Composite volcano-stratigraphic cross-section of the Siberian basalts from Norilsk and Putorana regions showing approximate thickness of each suite in meters. Relative stratigraphic position of each of the samples studied are shown in italics. Stratigraphic boundaries between the suites are based on field and textural criteria and are considered to be tentative. The letters in the age column refer to P for Permian and T1 and T2 for Triassic, and are based on volcano-stratigraphic and geochronological correlations.

Fig.3

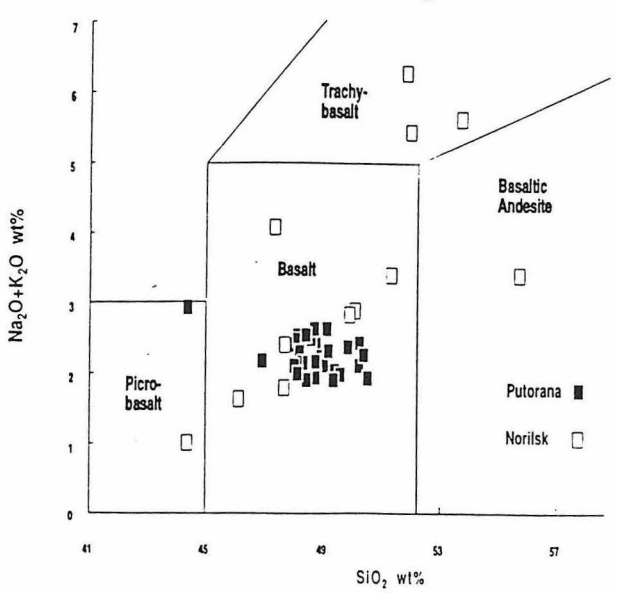

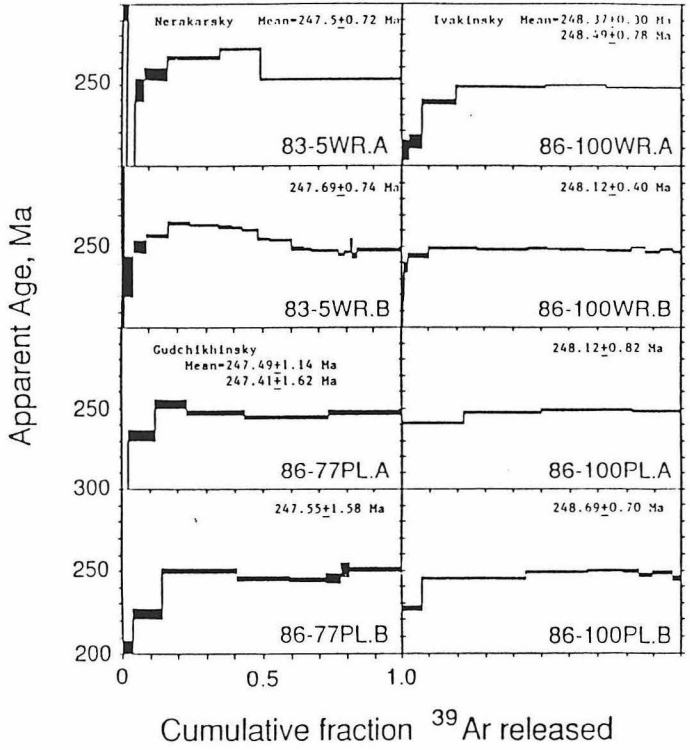
Nerakarsky Mean=247.5±0.72 Ma
Ivaktinsky Mean=248.37±0.30 Ma
248.49±0.78 Ma
83-5WR.A
86-100WR.A
247.69±0.74 Ma
248.12±0.40 Ma
83-5WR.B
86-100WR.B
Gudchikhinsky
Mean=247.49±1.14 Ma
247.41±1.62 Ma
248.12±0.82 Ma
86-77PL.A
86-100PL.A
247.55±1.58 Ma
248.69±0.70 Ma
86-77PL.B
86-100PL.B
Apparent Age, Ma
Cumulative fraction ^{39}Ar released

Fig. 6

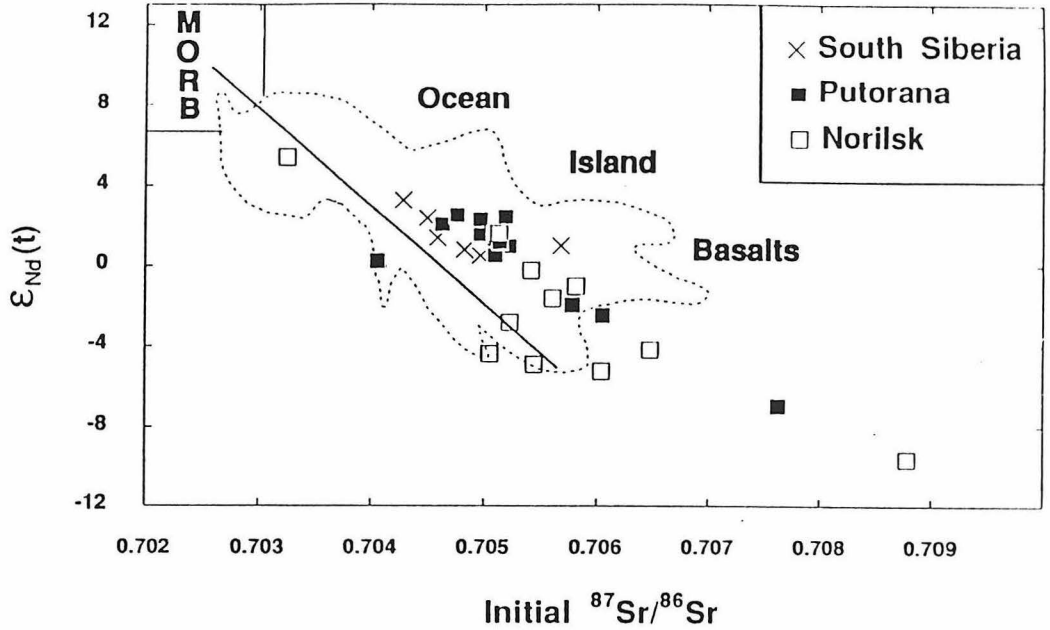
MORB
Ocean
Island
Basalts
South Siberia
Putorana
Norilsk
$\varepsilon_{Nd}(t)$
Initial $^{87}Sr/^{86}Sr$

Fig. 7

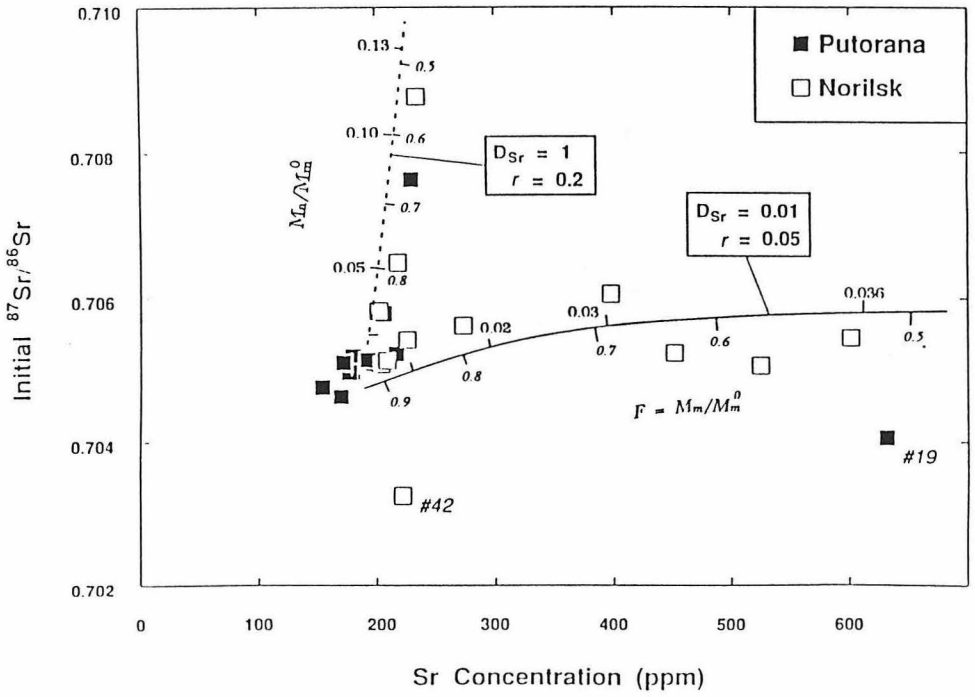
Putorana
Norilsk
D_{Sr} = 1
r = 0.2
D_{Sr} = 0.01
r = 0.05
M_m/M_m^0
$F = M_m/M_m^0$
#19
#42
Initial $^{87}Sr/^{86}Sr$
Sr Concentration (ppm)

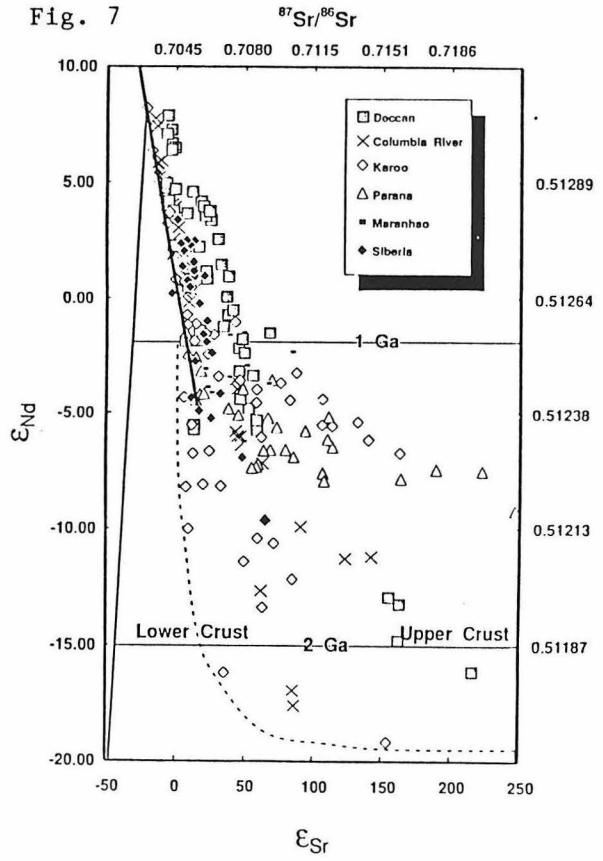
$^{87}Sr/^{86}Sr$
Deccan
Columbia River
Karoo
Parana
Maranhao
Siberia
1 Ga
2 Ga
Lower Crust
Upper Crust
ε_{Nd}
$^{143}Nd/^{144}Nd$
ε_{Sr}

Upper Mantle Temperature beneath the Mid Atlantic Ridge

by
Enrico Bonatti
Lamont-Doherty Geological Observatory
Columbia University, Palisades NY 10964

ABSTRACT

Information on the composition and thermal structure of the uppermost mantle underlying mid ocean ridges has been obtained from studies of peridotites recovered from the Mid Atlantic Ridge in lithosphere ranging in age from 0 to 30 m.y., from the Gibbs F.Z. at 52° N to the equator. The mineral chemistry of mantle-equilibrated phases olivine, orthopyroxene, clinopyroxene and spinel indicates broad regional heterogeneities in the composition of the uppermost mantle beneath the Mid Atlantic Ridge. The largest anomaly occurs between 34° N and 45° N, where the mantle-equilibrated phases are strongly depleted in incompatible elements, suggesting that the mantle has undergone a high degree of melting. This conclusion agrees with basalt data obtained by Schilling, Klein, Langmuir and coworkers. The strongly refractory upper mantle of the 34° N - 45° N region correlates with zero-age positive topographic and geoid anomalies, which are generally related to the influence of the Azores hot spot. A number of geothermometers were applied to the peridotite mineral chemistry data (including Wells and Lindsley 2-pyroxene geothermometers) in order to estimate variations in the temperatures of equilibration in the upper mantle in a profile along the Mid Atlantic Ridge. The estimated temperatures of equilibration are lower, or, at least, not higher in the 34° N - 45° N "hot spot" region than elsewhere along the the Mid Atlantic Ridge. These estimated temperatures probably reflect subsolidus closure temperatures and are probably related to cooling rates of the upwelling mantle. The lack of a mantle temperature anomaly in the "hot spot" region suggests the possibility that the Azores hot spot is a melting anomaly related to upper mantle composition rather than temperature.

A Non-Rayleigh-Taylor Instability in Upwelling Below Mid-Ocean Ridges

W. Roger Buck
Lamont-Doherty Geological Observatory of Columbia University
Palisades, New York 10964

Along sections of the axis of mid-ocean ridges topography and gravity are observed to vary with relatively uniform amplitude and wavelength. On slow spreading ridges (half spreading rates less that about 2 cm/yr) the amplitude of these variations is up to 500 m in topography and 20 mgals in gravity over wavelengths of 60 to 100 km. On fast spreading ridges amplitudes are lower by about an order of magnitude. The observations may be explained by either crustal thickness variations or density variations in the shallow mantle. The chemistry of rocks varies along ridge crests and in some areas the chemistry correlates with topographic variations. Both these observations have led to the suggestion that the delivery of melt to the crest of ridges is strongly variable along strike.

Several mechanisms to produce along axis variations in melt delivery have been proposed. An early suggestion was that melt pools in layers below the crust at ridges. This layer might periodically undergo a Rayleigh-Taylor instability, and the diapiric rise of the melt into the crust at a preferred wavelength, depending on the melt layer thickness, thus explaining crustal thickness variations. It is somewhat difficult to understand the physical conditions that would result in the pooling of melt in a thick layer given that the lithosphere at a ridge axis is in extensional failure and the melt might have readily available paths into the crust. Another way to produce along axis variations in melt delivery is for diapirs or plumes of melt and unmelted mantle to develop within the region of partial melting in the mantle. This can occur when melt segregates from the mantle residue via flow through a porous media. This mechanism is investigated in this paper.

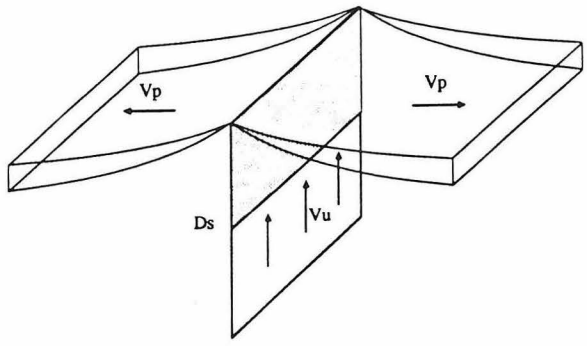

Figure 1. Geometry of an idealized ridge axis between two oceanic plates which are moving apart with velocities of magnitude Vp to the right and to the left. Under the ridge axis mantle upwells at a constant velocity Vu. At shallow depths under the ridge the upward velocity should decrease, but I ignore that complication. The shaded region is where pressure release melting is occuring and it extends down to depth Ds (the depth where the temperature of the upwelling mantle is first at the solidus temperature for that depth).

The way that lateral variations in the concentration of melt can lead to diapirism in the upwelling mantle can be explained simply. Figure 1 shows the geometry of the upwelling below a ridge. If a local area of mantle is upwelling at a slightly higher velocity than adjacent areas then the melt becomes more concentrated there. This occurs because the rate of melt production depends on the upwelling velocity. The melt percolates through the mantle at a rate velocity proportional to amount of melt is present. The only way for the melt percolation rate to equal the production rate is a faster region of upwelling is for the melt concentration to increase. Since the melt is less dense that the unmelted mantle, the region of faster upwelling is less dense than adjacent areas. The positive buoyancy can cause the region of slightly higher upwelling velocity to flow upward even faster. This instability can produce plume like upwellings within the melting region. Whether an instability develops depends on the viscosity of the mantle in the melting region and on how fast the melt percolates relative to the mantle (which depends on the melt porosity - permeability relation).

In this work the following variables, constants and relations are assumed. The density contrast $\Delta\rho$ between melt and mantle residue is 500 kg/m^3. The solid mantle viscosity is m. Vu is imposed upwelling velocity below the ridge and should be about equal to the plate spreading velocity. The melt velocity relative to the upwelling is ϕ Vr, where Vr is the reference velocity for melt flow. $Vr = kg\Delta\rho/\mu_{melt}$, where μ_{melt} is taken to be 10 Pa-s and k is the permeability for melt flow. $k= a^2\phi^2/b$ where a is the mineral grain size and b, which depends on the geometry of the pathways between mineral grains , and is taken to be 10^4. ϕ is the porosity, or the fraction of melt in a volume of mantle The density of the mantle residue changes linearly with the degree of melting with a reduction in density of 1 kg/m^3 for each percent of depletion. The melting begins at 90 km depth for the results illustrated here and the maximum degree of melting is taken to be 36%.

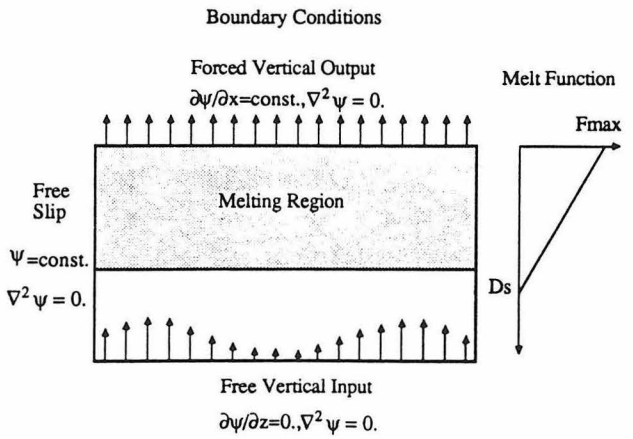

Figure 2. Set-up for 2-D calculations of flow through the melting region under a ridge axis. The flow boundary conditions are described in terms of the 2-D cartesian streamfunction. Within the melting region the rate of melting per unit decrease in pressure is assumed constant. The viscosity is kept constant throughout the numerical box.

Figure 2 shows the geometry and boundary conditions of the 2-D numerical calculations described here and Figure 3 illustrates some aspects of the results. The upwelling in Figure 3 has become diapirically unstable producing strong along axis variations in the rate of upwelling and in the concentration of melt in the asthenosphere. The pattern of streamlines is not steady in time because of the build up of depleted material pushed down by the flow in places. The low density depleted mantle can only be pushed so far before the flow adjusts. The spacing of the areas of melt concentration shows that the initially fastest growing wavelength of the instability is about twice the melt layer thickness. Figure 4 shows the results of a small number of such calculations for different parameters.

Also shown in Figure 4 are predictions from a crude linear stability analysis of this problem. To get an analytic estimate of these conditions requires that the wavelength of the instability be assumed. Taking this wavelength to be twice the thickness of the region where melting occurs yielded the predictions shown, which seem to match the numerical results. The analytic results let us estimate the stability conditions for parameter ranges that cannot be studied numerically.

The calculations indicate that an instability in the region of melting below a mid-ocean ridge can occur at both fast and slow upwelling rates (which scales with spreading rates) for plausible mantle viscosities (~10^{18} Pa-s). The mantle permeability cannot be too high or too low for this instability to develop, but for average grain sizes of 1 mm the instability is robust. The variations in the rate of delivery of melt to the ridge crest can explain the along axis variations in topography seen at slow spreading ridges.

It is worth noting that thermal instabilities, argumented by depletion related density changes is the other way that has been suggested to get along axis variations in melt production/delivery (Parmentier, E.M. et. al, EOS, v71, p627,1990). Preliminary numerical results using a temperature dependent rheology show that thermal instabilities develop only at lower than 10^{17} Pa mantle viscosity for even slow upwellings. So over about 6 orders of magnitude of assumed mantle permeability (or Vr) the melt buoyancy mechanism described here should be the dominant effect just under the ridge crest. More importantly the melt diapirism can happen at higher mantle viscosities which may be more realistic.

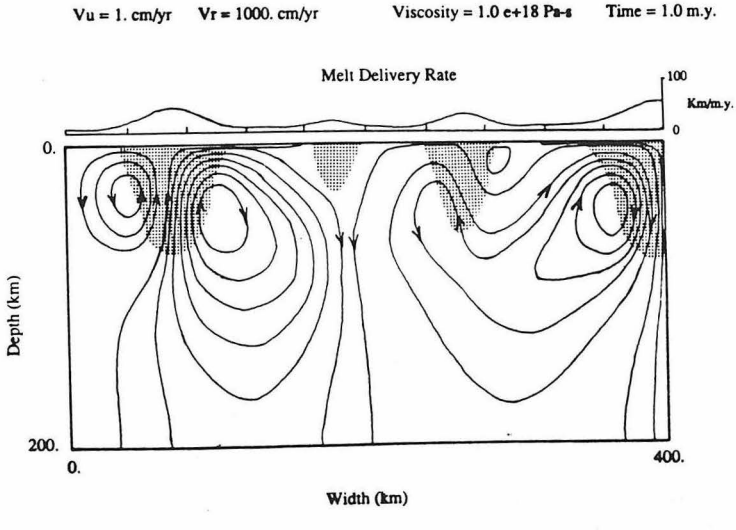

Figure 3. Illustration of one numerical calculation. Streamlines are shown as lines with arrows on them and the shaded areas have melt concentrations greater than 3% (i.e. $\phi > 0.03$). See text for details.

Since this instability is only weakly spreading rate dependent then why are large crustal thickness variations not seen at fast spreading ridges? Actually the reason can bee seen most clearly by looking at a very slow spreading ridge which has smooth topography - the Reykjanes ridge. There the spreading rate is lower than for any other part of the mid-Atlantic ridge but the crust is about twice as thick as is typical. It is thought that the lower part of the thick crust is hot enough to flow rapidly and so would obliterate any variations in crustal thickness that might be produced by mantle diapirs. For fast spreading ridges the crust is also thought to be hot (there is strong seismic evidence for this) so the crustal flow there could also mask the diapirs.

There may be evidence for the mantle diapirism even at fast spreading ridges. Away from the ridge where the upwelling is slower or does not occur the melt/mantle diapirs will die out. As they die out the old diapirs can leak melt into the lithosphere and crust. The off-axis effect of these diapirs should depend on the mantle permeability. In the numerical case illustrated in Figure3 there should still be significant 'leakage' of melt for 1-2 m.y. after the upwelling ceased. This small, spatially periodic melt flux might account for the observations of regularly spaced gravity undulations alligned in the absolute plate motion direction on parts of several fast spreading plates (Haxby, W.F. and J.K. Weissel, J. Geophys. Res., 91, 3507-3520, 1986.). The dribble of melt from the mantle away from the ridge would slightly thicken the crust above the formerly active diapirs. I call these DRIPUPS for Diapiric Ridge Instabilities Persisting Under PlateS. There effect is much like small hot spots and the aligned gravity variations may just be the tracks they leave. One important feature of these observations not previously explained is that the linear gravity anomalies are only seen on the side of a ridge crest trailing the absolute plate motion of the ridge. The DRIPUP model explains this asymmetry because only one plate overides the formerly sub ridge crest asthenosphere which has a small amount of extra melt left in it.

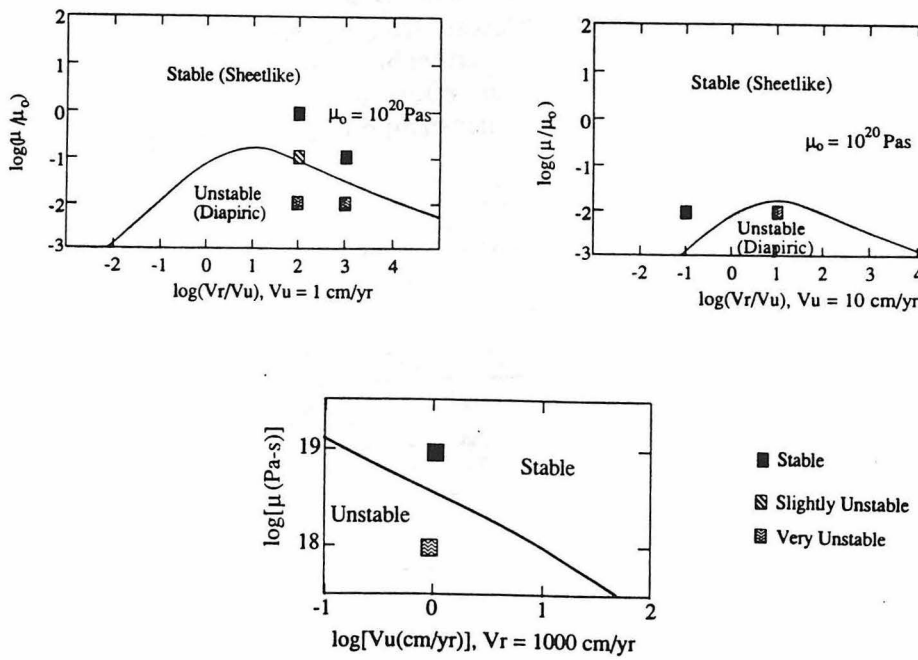

Figure 4. Results for a set of numerical calculations described in the text along with an analytic prediction of the conditions for the transition from stable upwelling (forming no diapirs of melt and mantle) to diapiric upwelling. The vertical axis always shows the log of the viscosity of the mantle and the horizontal axis shows the log of either the ratio of the reference Darcy velocity to the imposed upwelling velocity (Vr/Vu) for fixed values of the upwelling velocity or the upwelling velocity in cm/yr for a given value of Vr.

THE MANTLE ROLE IN MOUNTAIN-BUILDING: IMPLICATIONS FOR CRUST AND MANTLE EVOLUTION AS WELL AS HOT-SPOT DISTRIBUTION

Kevin Burke, University of Houston
(Currently at National Research Council)
2101 Constitution Avenue NW
Washington DC 20418

The huge extent of the world's two largest mountainous areas in western North America and Central Asia is suggestive of involvement of large volumes of flowing mantle because it is hard to see how continental crust and attached mantle lithosphere could be tectonized without involving the deeper mantle to build such large areas. The scale of mantle involvement at shallow depths is much less than in plate construction and consumption but it is possible that flow beneath these areas may trigger modifications in mantle circulation patterns. The two huge present day mountainous areas developed from smaller features close to plate boundaries and over a few tens of millions of years have extended about 1000km into the continents involved. The development of extensive mountainous areas is both sporadic and episodic in earth history (e.g. ref 1) so that perturbations of mantle circulation related to these phenomena are probably quite irregular.

Collisional extensive mountainous areas have been suggested to contribute to recycling of continental crust (1, 2, 3) by delamination, but this does not seem to be the case (except perhaps locally) in the type of mountainous area now represented in western North America. Places where lithosphere delamination has occurred (as in parts of Africa) may be marked by concentrations of hot-spot volcanism (Fig.2). In general hot-spot volcanism (defined as "non-plate-margin"volcanism) associated with the extensive mountainous areas in both Central Asia and western North America appears to be of shallow mantle origin with Yellowstone as a possible exception. Hot-spot volcanism in Arabia would also appear to be of shallow origin and linked to collision between Arabia and Asia because of time of initiation at about 13 ma and association with N-S trending rifts. Distinguishing hot-spots of profound origin from those of shallow origin is perhaps now becoming feasible.

REFERENCES

(1) L.D. Ashwal and Kevin Burke, African lithospheric structure, volcanism and topography Earth and Planet. Sci. Letters, 96 1989 8-14

(2) D.L. Turcotte, Geophysical processes influencing the lower continental crust IUGG symposium, Vancouver 1989 321-3329

(3) D. McKenzie and R.K. O'Nions, Mantle reservoirs and ocean island basalts, Nature 301 229-231, 1983

(4) Basaltic Volcanism on the Terrestrial Planets, LPI, Houston (1981)

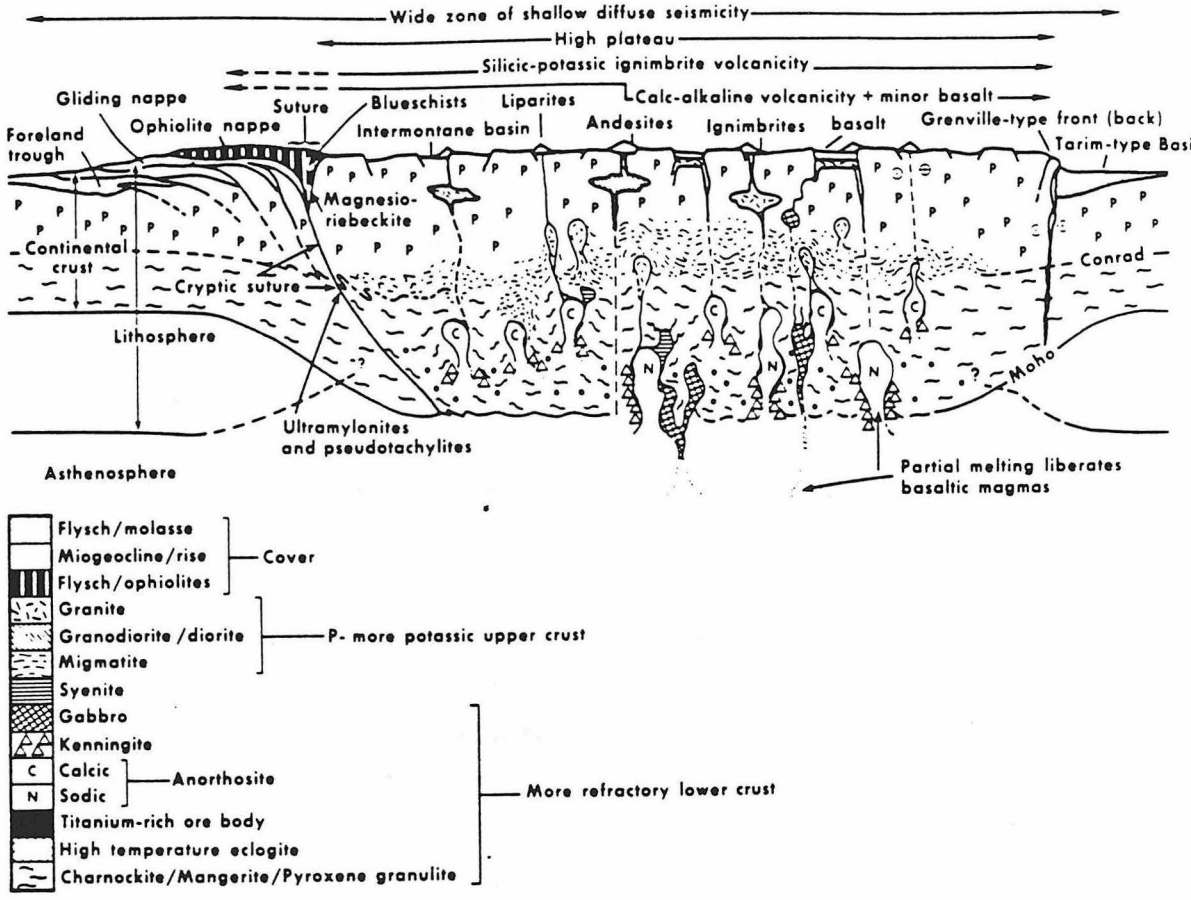

Fig.1 Continental thickening at collision: the continental crust below about the level labeled "Conrad" may be recycled into the mantle. Turcotte (ref.2) has suggested that a change in quartz rheology may control the level of delamination.

HOT SPOTS IN AFRICA PREDOMINANTLY IN REACTIVATED AREAS

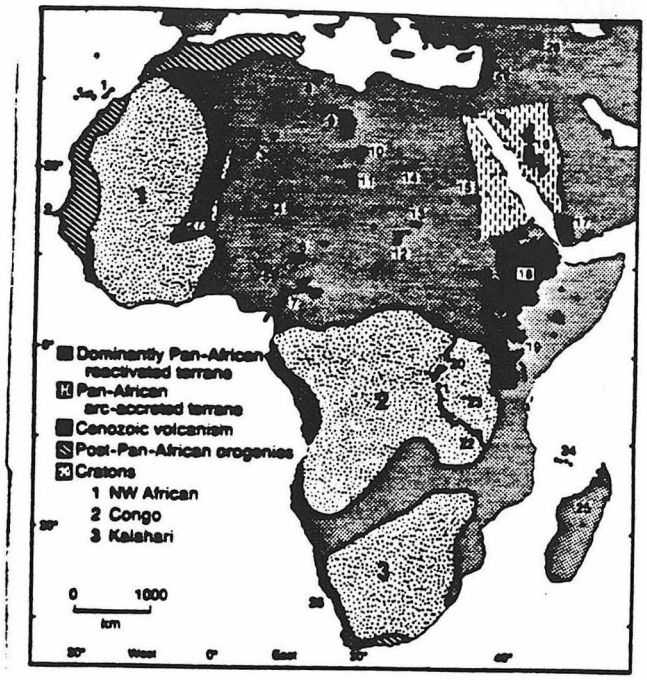

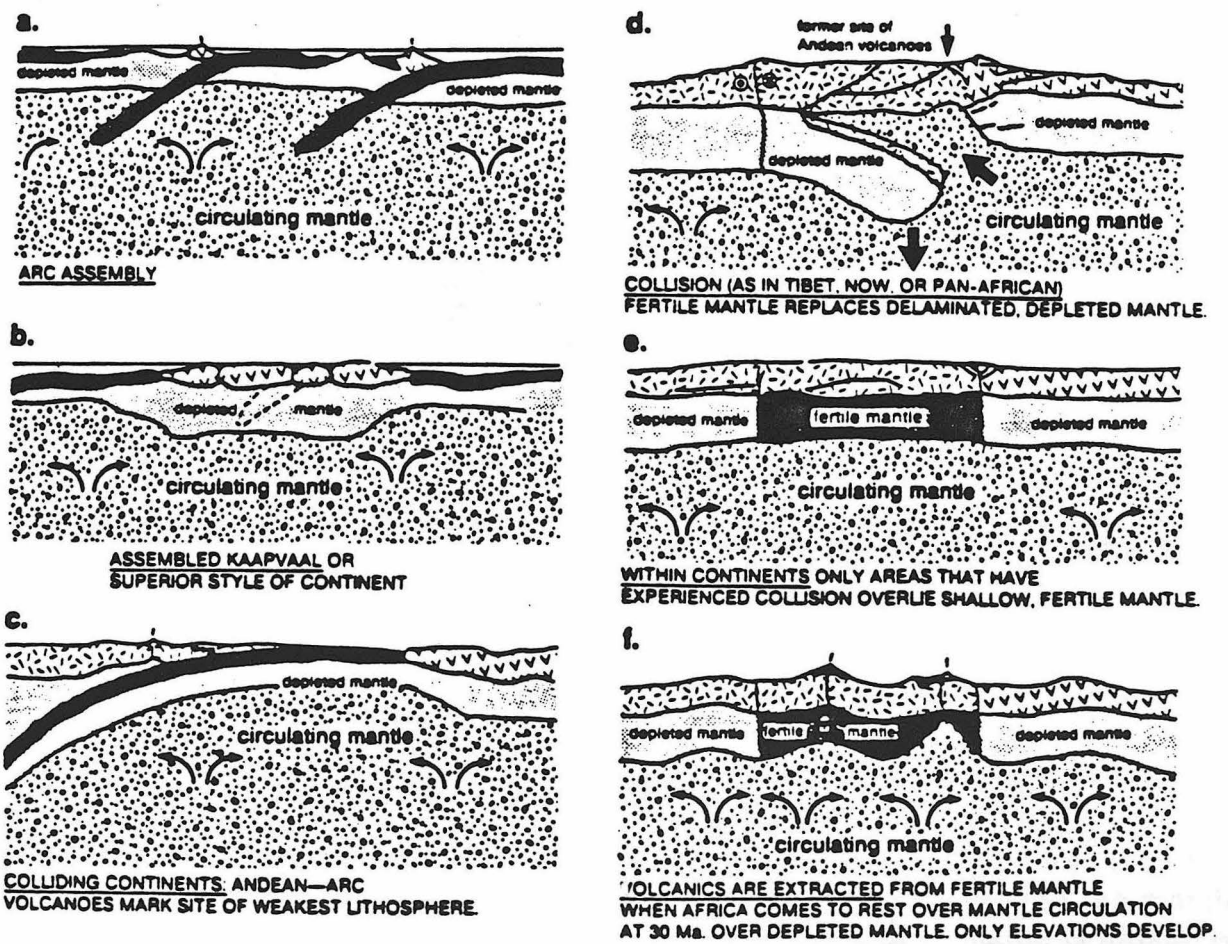

Fig. 2. Proposed sequence of events in the history of the African lithosphere. Generation of island arcs (a) and repeated collisions of such island arcs (b) result in assembled continent underlain by depleted mantle. Continued plate motions (c) result in Tibetan-style continental collision (d), during which depleted mantle is delaminated and replaced by "fertile" asthenospheric mantle. This results in laterally heterogeneous sub-continental lithosphere (e) in which only those parts of the crust having experienced Tibetan-style reactivation are underlain by fertile mantle. When Africa came to rest with respect to the mantle circulation pattern at about 30 Ma. heating from below produced volcanism only in reactivated areas underlain by fertile mantle lithosphere (f). Other areas responded to heating only by elevation increases.

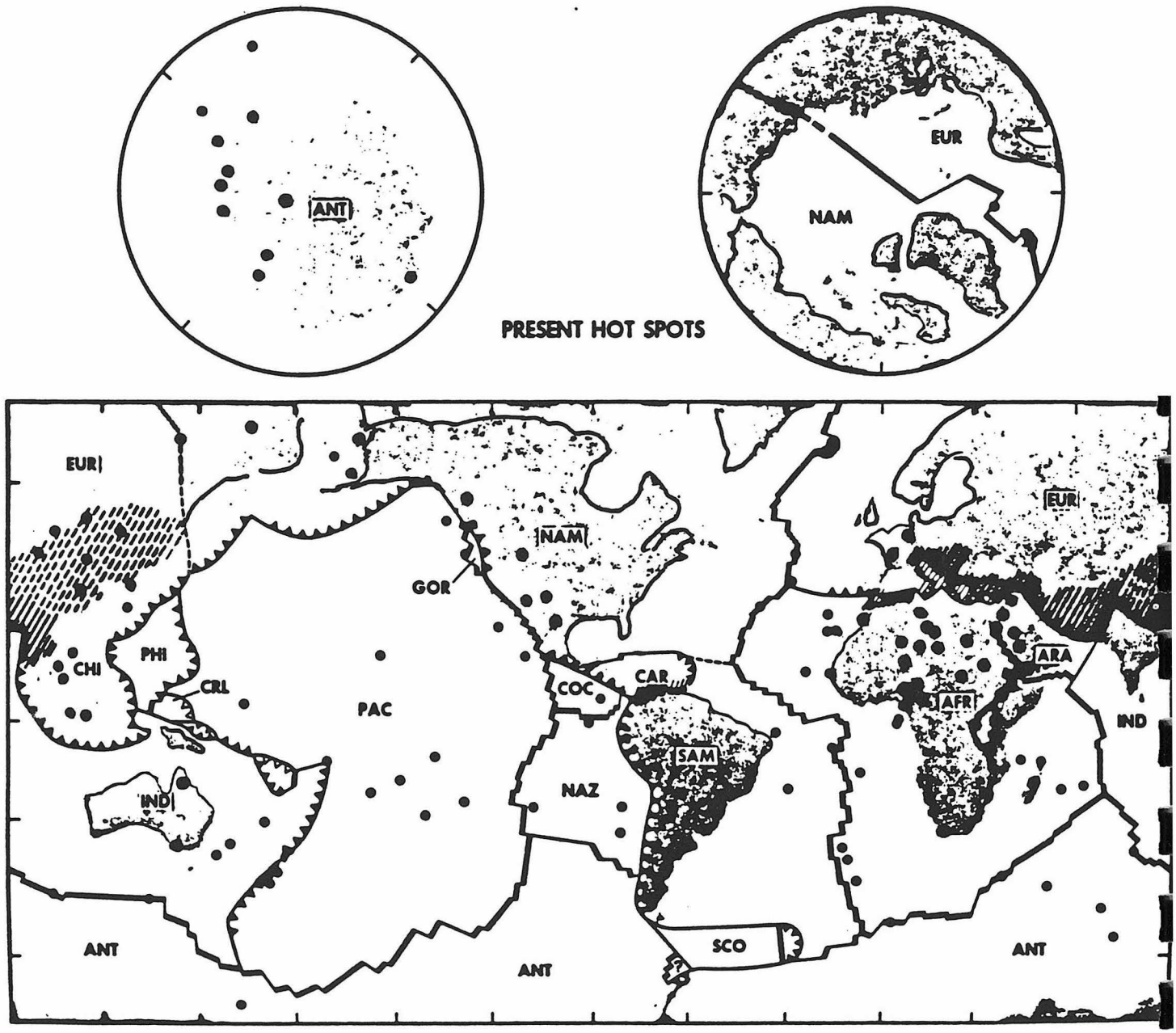

Fig.3 Hot spots (defined as non-plate-margin volcanism) are abundant but not uniformly distributed over the Earth. From Ref 4. It is becoming possible to be confident that some of these hot-spots are associated with "pressure release" (for example: some of those on the Arabian peninsula) while others may be associated with more profound mantle heterogeneities.

Stirring and Structure in Mantle Plumes

Ian Campbell and Ross Griffiths
Research School of Earth Sciences
The Australian National University

Continental flood basalts are the product of vast outpourings of basalt over a short period of time. A typical province covers an area 2000 x 2000 km and forms in 2 to 4 Ma. Morgan (1981) was the first to recognise that flood basalts formed over known hotspots and that they represent the first volcanic activity from that hotspot. These observations have lead to the suggestion that flood volcanism is produced by a new mantle plume.

Experimental studies in viscous liquids have shown that new, or "starting", plumes should consist of a large bulbous head followed by a narrow feeder conduit. Analysis of the plume flow by Griffiths and Campbell (1990) indicates that, if the plume ascent is driven by thermal buoyancy, the head will entrain the surrounding mantle as it rises. The head cools and enlarges, and develops a compositional zonation of source and entrained mantle (Figure 1). Uncontaminated, relatively hot material from the plume source continues to flow up the trailing conduit making the temperature of the plume axis greater than that of the remainder of the head.

The chronology, tectonics and geochemistry of flood basalts provinces fit well with the starting plume hypothesis. We attribute the sudden onset and short duration of continental flood volcanism, over an equant area 2000-2500 km across, to melting the plume head and its subsequent decline to a narrow chain of volcanic activity, ~200 km wide, to melting in the plume tail. A surface uplift of 500-1000 m is predicted but this gives way to subsidence due to lateral spreading of the plume head before the onset of the main period of volcanism. A period of enhanced subsidence is then predicted to occur as magma escapes from the mantle and loads the earth's surface, followed by slow subsidence over 10^9 years as the plume's thermal anomaly gradually decays. The predicted timing and duration of volcanism is strongly dependent on the assumed viscosity of the upper mantle. If the viscosity of the upper mantle is taken to be 3×10^{20} Pa s, the predicted time scale for the main period of volcanic activity is 4 Ma, in agreement with dating which indicates that the bulk of the magmas in each province were ejected within 2-3 Ma.

The model predicts that the high-temperature picritic melts associated with continental flood basalts are derived from hot, relatively uncontaminated plume-source mantle at the plume axis and that the more voluminous tholeiitic basalts are produced by melting of cooler hybrid mantle in the plume head. This explains for why the picrites of the Karoo and Deccan are strongly enriched in highly incompatible elements, consistent with melting of an enriched mantle source, whereas the associated basalts are weakly enriched in incompatible elements, consistent with derivation from a mixed enriched mantle–lower-mantle source (Figure 2).

Laboratory experiments have shown that plume conduits may also entrain as they rise if they become deflected from the vertical during their ascent through the mantle. The structure of a plume conduit that has entrained the overlying mantle is illustrated in Figure 3. An analysis of the entrainment shows that stirring of surrounding mantle

with plume source material can result in major modifications of the diameter, temperature and mass flux in plumes. This model is a departure from the axisymmetric vertical pipe models of plumes and predicts that the temperature in a defected plume will decrease with height, thus reducing the plume temperature in the upper mantle while allowing a sizeable temperature difference at the source.

The cooling of plume conduits, after they are deflected by plate motion, can lead to a lower maximum temperature and lower MgO contents of basalts along some linear hotspot tracks compared with picrites from their associated flood basalt provinces. The effects of entrainment depend primarily on the buoyancy (or heat) flux carried by the plume, with greater cooling for smaller fluxes. Strong continuing plumes such as Hawaii, Easter Island, Macdonald, Tahiti and Reunion are predicted to produce abundant picrites during the main period of volcanism. These will have MgO contents comparable to the picrites found in continental flood basalt provinces. Weak plumes such as Crozet, Bouvet and Juan de Fuca will give only cooler melts. Through entrainment long-lived plumes can sample the whole depth of the mantle from the source to the surface, and stirring within the plume leads to compositional zonation which may contribute to compositional heterogeneity in hotspot melts. We also predict that plumes originating at the core-mantle boundary and having buoyancy fluxes less than about $3 \times 10^3 N\ s^{-1}$ will not give surface hotspots, in good agreement with the lower limit of hotspot buoyancy fluxes inferred from seafloor topography.

Both starting plumes and continuing plumes represent an important mechanism for transporting material from the lower mantle to the upper mantle. When a starting plume reaches the top of its ascent it underplates the lithosphere forming a disk ~2000 km across and 200 km thick. The time scale for cooling of these disks is 1 Ga so that they remain buoyant and attached to the lithosphere. The situation with continuing plumes is similar. Plumes that underplate the oceanic lithosphere are carried away from spreading centres and will not normally take part in melting to produce MORB. They are returned to the lower mantle on a time scale of ~50 Ma when the plate to which they are attached is subducted back into the mantle. On the other hand plumes that ascend beneath continents will underplate the continental lithosphere. Some of this material may eventually find its way into the convecting upper mantle but most of it will be incorporated into the continental mantle lithosphere.

References

I.H. Campbell and R.W. Griffiths, 1990, Implications of mantle plume structure for the evolution of flood basalts, Earth Planet. Sci. Lett., 99, 79-93.

R.W. Griffiths and I.H. Campbell, 1991, On the dynamics of long-lived plume conduits in the convecting mantle, Earth Planet. Sci. Lett., 103, in press.

I.H. Campbell, R.W. Griffiths and R.I. Hill, 1989, Melting in an Archaean mantle plume: heads its basalts, tails its komatiites, Nature, 339, 697-699.

R.W. Griffiths and I.H. Campbell, 1990, Stirring and structure in mantle starting plumes, Earth Planet. Sci. Lett., 99, 66-78.

W.J. Morgan, Hotspot tracks and the opening of the Atlantic and Indian Oceans, in: The Sea, 7, The Oceanic Lithosphere, C. Emiliani, ed., pp. 443-487, Wiley, New York, N.Y., 1981.

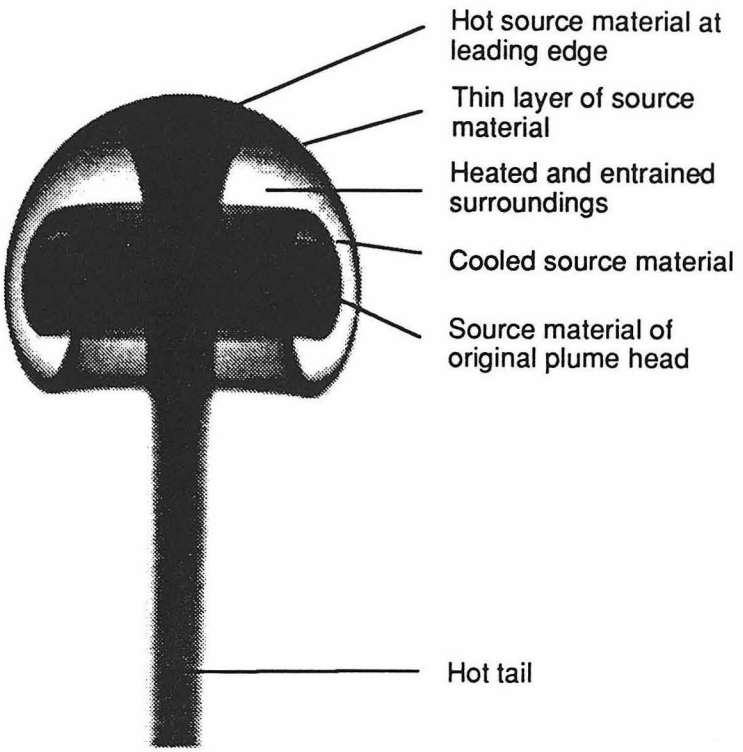

Fig.1. A photograph of a laboratory starting plume showing the structure caused by conduction of heat and consequent entrainment of surrounding fluid. Key features of the plume are labelled. Dark areas represent dyed material derived from the source, which becomes wrapped between layers of entrained mantle in a bulbous head. Hot source material is continuously supplied through the tail to the top of the plume head. The mean temperature in the head governs the dynamics of the plume ascent, and this temperature decreases as the volume of the head increases with time. The feeder conduit in these laboratory experiments is much broader, relative to the head, than is expected for mantle plumes because the viscosity of the hot conduit material in the experiments is only two orders of magnitude less than that of the surroundings, whereas the viscosity contrast in the mantle may be 10^{-2}-10^{-5}.

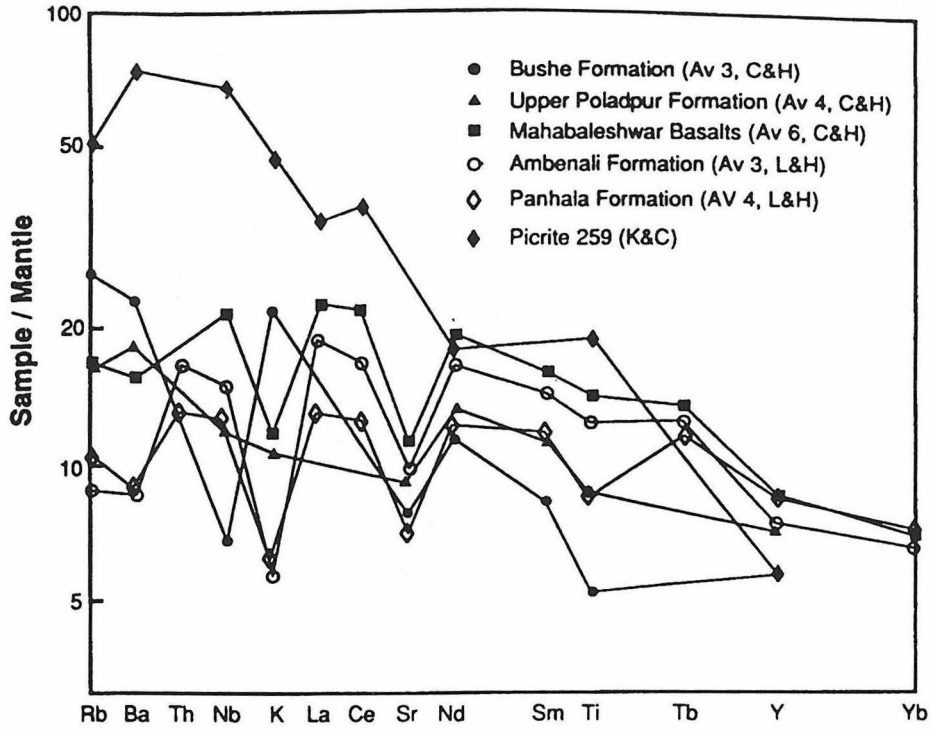

Fig.2. Mantle normalized trade element abundance patterns for the Bushe, Upper Poladpur, Mahabaleshwar, Ambenali and Panhala Formations and a picrite from the northern Deccan Traps.

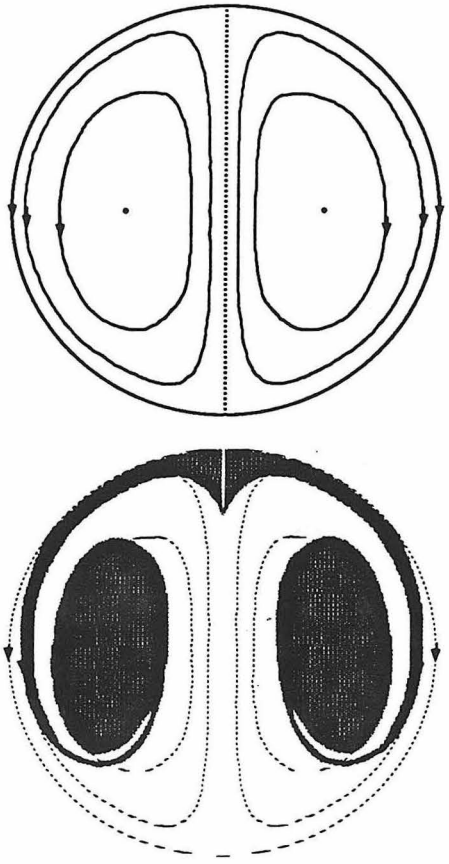

Fig.3. Diagrams showing (a) the form of non-axisymmetric recirculation (in a plane normal to the plume axis) resulting from horizontal deflection of plume conduits, and (b) the consequent distribution of source material in the conduit far above the source as determined from laboratory experiments.

An Estimate of Primary Magma Composition of Tholeiitic Basalt From Kilauea Volcano, Hawaii

David. A. Clague and William S. Weber
U. S. Geological Survey
Menlo Park, CA 94025

Estimates of the MgO content of primary Hawaiian tholeiitic magmas range from as low as 8 wt.% [1] to as high as 20-25 wt.% [2]. Most recent estimates fall in the range of 12-17 wt.% MgO [3-9]. These estimates are generally based on whole-rock compositions of lavas coupled with the compositions of the most forsteritic olivine phenocrysts observed. Volcanic glass provides the best estimate of magma compositions because it represents the melt composition at the time of quenching with only minimal changes that occur during the quenching process. Pillow-rim glasses from the submarine rift zone of Kilauea generally contain MgO<7 wt.% [10-12] whereas those of subaerially erupted tephras or of glass inclusions in olivine phenocrysts are as MgO-rich as about 10.0 wt.% MgO[13-14], although few are more MgO-rich than about 9 wt.%. The olivine phenocrysts contained by these lavas are generally restricted to compositions more fayalitic than $Fo_{88.6}$[13] for subaerially erupted lavas and more fayalitic than $Fo_{90.3}$[15] for submarine erupted pillow lavas. Glass sands from offshore Kilauea Volcano include glasses containing as much as 15.0 wt.% MgO that enclose olivine microphenocrysts as magnesian as $Fo_{90.7}$. These compositions are consistent with an average primary tholeiitic magma containing 17.1 wt.% MgO, but demonstrate that the primary magmas contain at least 15.0 wt.% MgO.

Tholeiitic basaltic glass was recovered in sandy turbidites in a box core collected near the base of the submarine East Rift Zone of Kilauea Volcano at 19°59.4'N, 154° 26.4'W and a depth of 5500 m during a U. S. Geological Survey cruise in 1988[16]. The layers contain a variety of unaltered submarine erupted (moderate to high S contents) glasses from Kilauea Volcano, as well as crystal fragments (mainly olivine), crystalline rock fragments, devitrified glass fragments, and rare radiolaria. Nearly all the glass sand grains lack any palagonite alteration rim, suggesting that the glasses are younger than a few thousand years. Microprobe analysis of more than 250 glass sand grains from this core demonstrate that nearly all the glasses from the surface sample, 9 cm, 15 cm, 21 cm, 26 cm, 29 cm, 31 cm, and 41 cm are within the range of compositions of the pillow lavas from the submarine East Rift Zone [10-12]. However, rare grains from the surface sample, 26 cm, 31 cm, and 41 cm, and common samples from the 55-58 cm layer have MgO>8 wt.%.

The unaltered glasses in the layer at 55-58 cm are dominated by a vesicular glass type containing 7.3-7.7 wt. % MgO, but having lower SiO_2 and higher TiO_2, K_2O, P_2O_5, and FeO than is present in most Kilauea glasses with similar MgO contents. This glass composition, although still tholeiitic, is trending towards alkalic basalt in its composition. Mixed in with this unusual basalt glass composition are a range of glass compositions ranging from an extreme differentiate containing about 1 wt.% MgO and 59 wt.% SiO_2 to tholeiitic glasses similar to those of pillow basalts dredged along the submarine rift [10] to the high-MgO glasses (Table 1). Glasses with MgO<7 wt.% define a multiphase fractionation trend characterized by decreasing CaO (Figure 1A) and Al_2O_3 with decreasing MgO produced by crystallization of olivine, clinopyroxene, and plagioclase in proportions of roughly 1:5:5[12]. Glasses with MgO>7 wt.% define olivine fractionation curves, which for FeO (Figure 1B) and SiO_2 are distinct from olivine-control lines. The glasses containing high S contents generally plot more-or-less along the olivine fractionation curves whereas the more degassed (lower S) glasses plot closer to olivine-control lines.

The high-MgO glasses constitute less than 1% of the glass sand grains in the 55-58 cm turbidite layer, but are important in that they contain up to 15.0 wt.% MgO (Table 1)

and enclose olivine microphenocrysts as magnesian as $Fo_{90.7}$ (Table 1). The microprobe analyses plotted in Figure 1 are not representative of the population of glass compositions in the turbidite layer, but instead overrepresent the high-MgO glasses which were preferentially selected for analysis using a ratemeter on the MgO scanner of the microprobe. These high-MgO glass compositions demonstrate that primary magmas at Kilauea are at least as MgO-rich as 15.0 wt.%. These glass compositions can be used to estimate eruption temperatures as high as 1316 °C based on the MgO contents of the glass and the experimental work of Helz and Thornber (17).

Table 1. Microprobe glass and olivine analyses, and an average calculated normalized composition for Kilauea primary tholeiitic magma

Sample	57-G7A Glass	57-35 Glass	57-15B Olivine	Primary Magma
SiO_2	48.4	49.0	40.7	48.3
Al_2O_3	10.6	11.9	-	10.3
Fe_2O_3	-	-	-	1.29
FeO	11.3	11.9	8.95	10.4
MnO	-	-	0.13	0.17
MgO	15.0	13.0	49.2	17.1
NiO	-	-	0.55	0.088
CaO	8.77	8.91	0.20	7.96
Na_2O	1.68	1.82	-	1.50
K_2O	0.31	0.28	-	0.26
P_2O_5	0.18	0.18	-	0.16
TiO_2	1.96	1.91	-	1.65
S	0.110	0.136	-	0.100
Cl	0.011	-	-	0.010
H_2O	-	-	-	0.50
Total	98.3	98.4	99.8	100.0
Fo	-	-	90.7	-

Figure 1. CaO (A), FeO* (B), and S (C) vs. MgO showing the high-MgO contents of many of the analyzed glasses. The glasses with MgO>7 wt.% plot along olivine fractionation lines on the CaO-MgO plot. The high-S glasses with MgO>7% also generally plot along olivine fractionation curves on the FeO-MgO plot, but the low-S glasses with MgO>7% have FeO higher than predicted by the olivine-fractionation curves. The glasses with MgO<7 wt.% plot along multiphase fractionation lines on both the CaO-MgO and the FeO-MgO plots. On the S-MgO plot, the pillow rim glasses (12) all contain less S than the model fractionation trends shown. The group of high-S glasses are relatively undegassed whereas the other glasses have undergone degassing of S and probably H_2O. Extrapolation of the trendline shown indicates that the S content of average primary Kilauea tholeiitic magma with 17.1 wt.% MgO is about 0.100 wt.% (1000 ppm).

Many of these glass sand grains contain small (≤30 μ) olivine microphenocrysts that are as magnesian as $Fo_{90.7}$. The compositions of the cores of the enclosed olivines are compared to the compositions of the host glasses in Figure 2 which shows that few of the olivine crystals

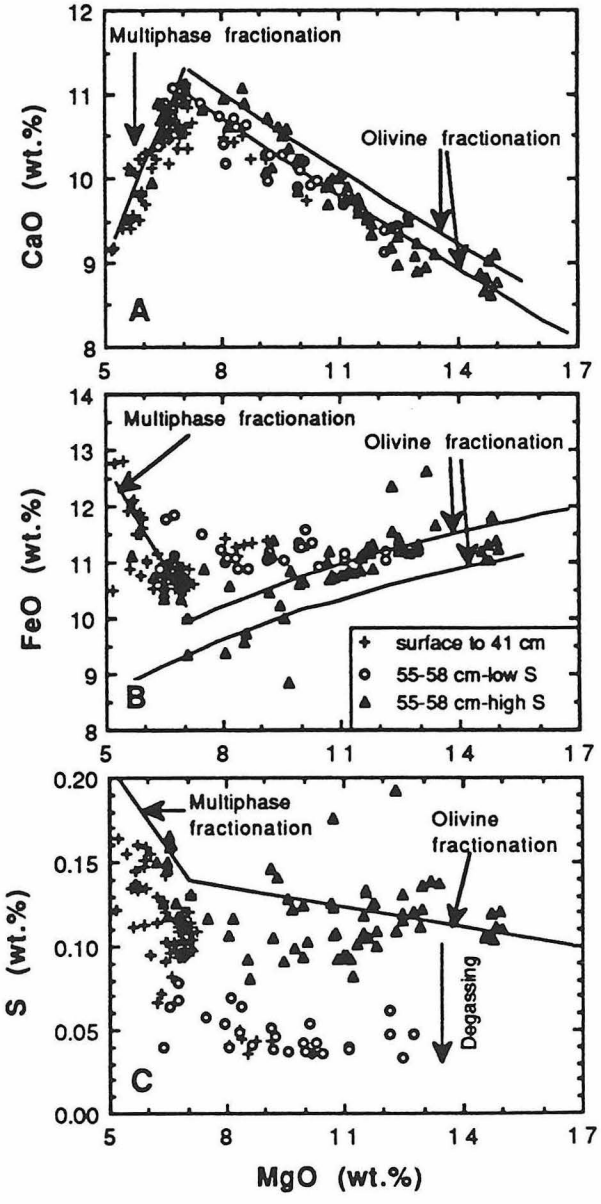

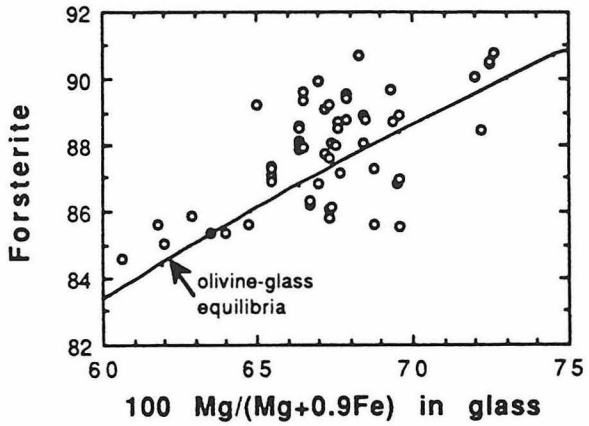

Figure 2.Forsterite content of the olivines plotted against 100Mg/(Mg+Fe2+) for the glasses showing that few of the olivine crystals are in equilibrium with the host glases.

are in equilibrium with the surrounding glass. Some of the olivine grains are more Fe-rich than the estimated equilibrium compositions; whereas the majority are more Mg-rich than expected for the melt composition. The Mg-rich olivines are probably acquired by the host melt from the base of the magma reservoir as the magmas move through the rift zone to the eruption site. The Fe-rich olivines may have settled into the higher MgO host melts from lower temperature parts of the magma reservoir overlying the zone where the high-MgO magmas reside. As these more Fe-rich olivine crystals sink through the increasingly hotter and denser magmas ponded at the base of the magma reservoir, the olivine is resorbed back into the melt and new, more Mg-rich, olivine is formed. Many of the glass compositions, particularly those with low S contents, have FeO contents that are higher than expected if the magma had simply crystallized olivine in equilibrium with the melt., possibly reflecting resorption of Fe-rich olivine by these glasses. Thornber and Huebner (18) have documented the reverse effect (a decrease in the FeO content of the glass) during quenching of glass containing olivine, because Fe-rich olivine is added to the rims of the olivine microphenocrysts as the compositions of the olivine and adjacent glass attempt to track the plummeting temperatures during quenching, thereby reducing the FeO content of the melt phase. Helz (19) has proposed that this effect is responsible for creating complex patterns of FeO concentrations in residual melts from Kilauea lava lakes. These two effects affect the compositions of these glasses but offset one another to some degree. We conclude that the high-MgO glasses do not precisely represent near-primary magma compositions.

The most forsteritic olivine composition can be combined with the glass compositions to estimate the composition of the magma with which the olivine would be in equilibrium. Several assumptions are required including the ratio of Fe^{2+}/Fe^{Total} in the melt, the distribution coefficient for Fe-Mg partitioning between olivine and melt, and that the olivine resorption and crystallization effects discussed above roughly balance each other. For illustration purposes we have used a ratio of $Fe^{2+}/Fe^{T}=0.9$, $K_D=0.3$, and the least squares fit through the dry normalized glass data (calculated with FeO and Fe_2O_3 calculated from $Fe^{2+}/Fe^{T}=0.9$) on an MgO-FeO diagram. The remainder of the estimated average primary magma composition is calculated from the least-square fits to the other oxides on MgO-variation diagrams and the estimated MgO content. The resultant normalized average primary magma composition for Kilauea Volcano contains 17.1 wt.% MgO and is given in Table 1.

The NiO content of the most fosteritic olivine microphenocrysts is significantly higher (0.55 wt.% vs. 0.38 wt.%) than that in olivine of comparable forsterite composition in lherzolite xenoliths, interpreted to be mantle residuum formed beneath ocean spreading centers. The high NiO contents of these olivines suggest that the source for Hawaiian tholeiitic basalt is enriched in NiO compared to the source beneath mid-ocean ridges. The primary magma is estimated to contain 690 ppm Ni (0.088 wt.% NiO) in order to be in equilibrium with the $Fo_{90.7}$ olivine. These NiO contents suggest that the mantle source (plume) for Hawaiian tholeiitic basalt has about 45% higher NiO than the source for MORB.

The S contents of many of the high-MgO glasses (avg. of 7 highest MgO glasses is 0.109 wt.% S) are higher than previous

estimates of the S content of primary Hawaiian tholeiitic basalt. The data presented here suggest that the pillow lavas[12] and at least one-third of the higher-MgO glasses have undergone some to substantial degassing of H_2O and S, and that only some of the highest-MgO glasses appear to be undegassed with respect to S, and presumably H_2O. The S content of the calculated primary magma composition is about 0.100 wt.%, or more than 20% higher than previously estimated from the submarine erupted pillow lavas [12].The H_2O content of the near-primary high-MgO lavas has not been directly measured, but is estimated from the S/H_2O ratio of the pillow lavas[12] and the S content of the high-MgO glasses to be about 0.5 wt.%.

The chemical characteristics of the near-primary high-MgO glasses indicate that the Hawaiian plume is hot in order to generate primary melts containing over 17 wt.% MgO (eruption temperatures estimated at 1358 °C), rich in NiO, and rich in volatiles.

References

1. Maaloe, S., *Lithos* **12**, 59-72 (1979).
2. Wright, T. L., *J. Geophys. Res.* **89**, 3233-3252 (1984).
3. Macdonald, G.A., & Katsura, T., *J. Petrol.* **5**, 82-113 (1964).
4. Irvine, T. N., *Yb. Carnegie Inst., Wash.* **76**, 454-461 (1977).
5. Basaltic Volcanism Study Project, Basaltic volcanism on the terrestrial planets. New York, Pergamon Press, 1286 p (1981).
6. Maaloe, S., & Hanson, B., *Cont. Mineral. Petrol.* **81**, 203-211 (1982).
7. Hofmann, A. W., Feigenson, M. D., & Raczek, I., *Contrib. Mineral. Petrol.* **88**, 24-35 (1984).
8. Wilkinson, J.F.G., & Hensel, H.D., *Contrib. Mineral. Petrol.* **98**, 326-345 (1988).
9. Nicholls, J., & Stout, M.Z., *J. Petrol.* **29**, 1031-1057 (1988).
10. Moore, J. G., *Am. J. Sci.* **263**, 40-52 (1965).
11. Garcia, M. O., Muenow, D., Aggrey, K., & O'Neil, J., *J. Geophys. Res.* **94**, 10525-10538 (1989).
12. Dixon, J.E., Clague, D.A., & Stolper, E.M.,*Jour. Geology* (in press).
13. Helz, R. T.,*In* Decker, R.W., Wright, T.L., and Stauffer, P.H., eds, Volcanism in Hawaii. *U.S. Geol. Surv. Prof. Paper* **1350**, 691-722 (1987).
14. Schwindinger, K. R., & Anderson, A. T. Jr, *Contrib. Mineral. Petrol.* **103**, 187-198 (1989).
15. Clague, D.A., Moore, J.G., Dixon, J.E., and Friesen, W.B., *J. Petrol.*(in press).
16. Clague, D. A., Holcomb, R. T., Torresan, M., & Ross, S., *U. S. Geol. Surv. Open-file Report* **89-109**, 33 p (1988).
17. Helz, R. T., & Thornber, C. R., *Bull. Volcanology* **49**, 651-668 (1987).
18. Thornber, C.R., and Huebner, J.S., *Am. Mineralogist*, 70, 934-945 (1985).
19. Helz, R. T., *In* Magmatic Processes: Physicochemical Principles, B. O. Mysen, ed., The Gechemical Society Special Publication No. 1, 241-258 (1987).

Caltech Mantle Plume Symposium, 2-4 May 1991

Crustal Structure and Emplacement Rates of the Kerguelen and Ontong Java Plateaus

Millard F. Coffin
Institute for Geophysics
University of Texas at Austin
8701 Mopac Blvd.
Austin, TX 78759-8345

The Kerguelen Plateau in the southern Indian Ocean and the Ontong Java Plateau in the western Pacific Ocean are the two giant, off-ridge, mafic igneous provinces on Earth, covering areas of ~1 x 10^6 and ~1.5 x 10^6 km^2, respectively. The total crustal thicknesses of both are not well known; limited refraction data suggests 15 to 23 km for Kerguelen (Recq & Charvis, 1986; Recq et al., 1990) and 39 km for Ontong Java (Furumoto et al., 1976). No deep seismic reflection data have been acquired over either feature. Igneous basement has been drilled at four sites on the Kerguelen Plateau; penetration was 54, 48, 38, and 34 m of primarily subaerial basalt flows (Schlich, Wise, et al., 1989). On the Ontong Java Plateau, basement penetration by drilling at three sites was 149, 26, and 9 m of predominantly submarine basalt flows (Kroenke, Berger, et al., in press). No deeper basement samples are available from either plateau. On the Kerguelen Plateau, dipping reflection sequences as thick as 7 km have been observed (E.C. Chudyk, pers. comm.), and have been interpreted to be primarily basalt flows. Refraction data from the Kerguelen Isles corroborate the thick upper igneous layer, and suggest that the overall crustal structure is similar to that of oceanic crust, with 8 to 9 km of 5.5 kms^{-1} layer 2, ~10 km of 6.6 to 6.8 kms^{-1} layer 3, overlying either 7.95 kms^{-1} mantle or a 7.2 to 7.5 kms^{-1} interpreted "underplated" or serpentinized peridotite layer (Recq & Charvis, 1986; Recq et al., 1990). Refraction data from the Ontong Java Plateau yield an average crustal structure of ~5 km of 5.5 kms^{-1} interpreted basalt flows, ~5 km of a 6.1 kms^{-1} layer, ~13 km of a 6.9 kms^{-1} layer, and ~13 km of a 7.6 kms^{-1} layer, all overlying 8.3 kms^{-1} mantle (Hussong et al., 1979).

The modern mid-ocean ridge system produces ~20 km^3 of new crust per year (RIDGE, 1988). Based on numerous radiometric and paleomagnetic analyses, crustal emplacement rates for the Deccan Traps in India have been estimated to have been ~1 km^3yr^{-1} (Richards et al., 1989). Based on two samples, one dated by K-Ar and the other by K-Ar, total fusion, and plateau ^{40}Ar-^{39}Ar, the Kerguelen Plateau is estimated to have been emplaced between ~114 (Leclaire et al., 1987) and ~110 Ma (Whitechurch et al., in press), yielding a crustal emplacement rate of 5 km^3yr^{-1}. Limited paleomagnetic and biostratigraphic evidence from ocean drilling samples suggests that the Ontong Java Plateau was emplaced over 3.5 my (Mahoney and Tarduno, 1990), yielding a crustal production rate of 11 km^3yr^{-1}. Initial radiometric dating of basalt samples suggests a similarly rapid emplacement of the Ontong-Java Plateau (Duncan, pers. comm.). If, however, the Kerguelen and Ontong-Java plateaus were emplaced in ~500,000 years, as has been proposed for the Deccan Traps (Courtillot, 1990), the crustal production rates would have been 40 and 78 km^3yr^{-1}, respectively, overwhelming the modern mid-ocean ridge production rate. The mantle "purging" which resulted in the rapid emplacement of the Kerguelen and Ontong Java plateaus appears unprecendented in what we know so far of the Earth's history, and has profound implications for mantle dynamics as well as potential global changes resulting from the massive heat, gas, and fluid fluxes accompanying the emplacements.

^{3}He IN MORB, BABB, AND OCEANIC AND CONTINENTAL HOTSPOTS: AN OVERVIEW AND THE CASE FOR PRIMITIVE MANTLE

H. Craig
Isotope Laboratory
Scripps Institution of Oceanography
University of California, San Diego
La Jolla, California 92093

It is now well-established that the ocean-wide MORB ^{3}He signature corresponds to $R/R_A = 8 \pm 1$ ($R_A = 1.4 \times 10^{-6}$ in air He) except in areas where the ^{3}He/^{4}He ratio is observed to be influenced by hotspots close to or on an oceanic spreading axis. The ratios in Back-Arc basalts and Arc volcanics are similar to those in MORB, except that the Arc volcanic lavas and gases are generally somewhat lower (R/R_A = 6 to 8 in most cases: Poreda & Craig, Nature, 1989) due to inclusion of some radiogenic or "crustal" He. In special areas such as the Banda Arc the ratios are very much lower (1 to 3 R_A; Hilton & Craig, Nature, 1989), due to a much larger proportion of crustal He, derived from subducting continental material. Indonesia is the classical (and so far only) case of a mid-arc transition from near-MORB to near-crustal ^{3}He/^{4}He ratios, corresponding to a transition from oceanic to continental crustal material in the single down-going slab below the archipelago.

The earliest investigations of helium in Ocean Island Basalts disclosed that some hotspots have ^{3}He/^{4}He ratios significantly greater than MORB (Craig & Lupton, EPSL 1976), while others have ratios lower than MORB values (Kurz et al., Nature 1982). We now have varying degrees of coverage (He in olivines or cpx phenocrysts, chilled glass from pillow margins, and/or volcanic gases or submarine hydrothermal vents) from a total of 40 hotspots (Data distribution: 35 SIO, 4 WHOI, 1 UCSB), as compared with less than half that number only eight years ago, so that it is possible to make some significant generalizations about the distribution of ^{3}He in hotspots from different regional and tectonic settings. In particular, we can distinguish "Low-^{3}He" from "High-^{3}He" hotspots (Craig & Rison, EOS 1982, 1983) based on MORB (R/R_A = 8) helium as the dividing line, if we include a significant number of hotspots that have MORB-type ^{3}He/^{4}He ratios in the "Low-^{3}He" division.

There are ~ 24 "Low-^{3}He" hotspots, with ratios ranging from 5.2 R_A (Tristan) to 8.5 R_A (Trindade), with a modal value = 8.0 × R_A. Most of these are oceanic islands in the Atlantic, on or near the Mid-Atlantic ridge; some are scattered around the borders of the Pacific (Norfolk, Guadelupe, "JDF", etc.). It is important to note that in a number of cases several islands in a hotspot

chain, or many flows in a single island, have been observed to have $^3He/^4He$ ratios less than or equal to MORB values, but eventually some flows on an island, or another island have been found to have "High-^{3}He" ratios. Thus it is possible that some hotspots currently appearing to be "Low-^{3}He" (e.g. the Marquesas and Gambiers in the south-central Pacific) **may** turn out to have some flows with "High-^{3}He" ratios, which would place them in that group according to my classification. However it is highly improbable that this will occur with the ~10 "Low-^{3}He" hotspots in the central Atlantic and in the Indian ocean, because so many of these islands have been analyzed and the pattern seems to be quite clearly established.

There are ~ 16 "High-^{3}He" hotspots known at present, with $^3He/^4He$ ratios ranging from 11.3 (SOC) to ~30 (HAW) × R_A. **No** hotspots are currently known (to me at least) with values in the "gap" from R/R_A = 8.5 to 11.3 × R_A that separates the two groups. There are data for five **Continental** hotspots: three (Yellowstone, Ethiopia, and Erebus, in the **High** ^{3}He group), and two ("Tariat" in Mongolia, and Rungwe in southern Tanzania at the intersection of the east and west branches of the East African Rift), in the **Low** ^{3}He group. In two of these continental hotspots, Yellowstone and Ethiopia, the current site of our volcanic gas measurements can be traced back along the hotspot track for some distance. In Yellowstone we (including W. Leeman and T. Cerling) have measured high ratios back along the Snake River Plain axis well into south-central Idaho (all in recent basalts) leaving no doubt that this is an actual hotspot track. In the same way, in Ethiopia we (including J. Lupton, and most recently P. Scarsi and A. Marinello from Palermo) have tracked the maximum ratios in the southern Ethiopian Rift back northward beyond Djibouti and well up into the Afar, with both volcanic gas measurements and basalt samples). However, in the McMurdo Region volcanoes of Antarctica, another High-He hotspot, the high ratios have so far been seen only at a single volcano out of six or seven sampled to date.

Although hotspots cluster near low-density residual geoid highs in the major ocean basins, they clearly show a bipolarity not seen in the simple geoid patterns. The "Low-^{3}He" oceanic hotspots form a cluster of at least 12 sites in the Atlantic and Indian oceans, over the region from Kerguelen and Heard Islands to the Azores, while the "High-^{3}He" hotspots form a cluster of 10 sites in the central Pacific, including and southward of the Hawaiian chain. These distributions clearly show a dominance of the most primitive undepleted mantle material in the central Pacific, as contrasted with sub-continental or slab material rich in radiogenic ^{4}He in most Atlantic and Indian Ocean hotspots.

It is now going on six years since White (Geology, 1985) defined a number of mantle "sources" for ocean basalts based on binary plots of the radiogenic isotope arrays of Sr, Nd, and Pb.

White showed that at least **four** components, defined by local extrema in the Sr -Nd - Pb isotopic arrays, are required as mixing endmembers for the observed OIB data. These components, originally defined by the island groups they most clearly represent, included in addition to depleted MORB, the St. Helena type, and two enriched-mantle types: the end-members of these "exterior" components are now often called (cf. Zindler and Hart in numerous thick papers) DM (they have an extra M), Hi-μ (or HM), and two kinds of EM (1 and 2) for the "enriched" components. By "exterior" components, I simply mean that these endmembers are defined by local **extrema** in the Sr - Nd - Pb isotopic arrays, and they are thus "real" components in the sense that they clearly correspond to actual lavas from actual hotspots.

White also defined another **possible** component of OIB's: a "primitive mantle" (PM) source, based on trends of data points for Hawaiian lavas that plot generally within the array interiors, and he posed a "crucial question": does "primitive mantle" actually exist as magma source, and is it actually sampled by oceanic volcanism? The possible PM source was defined by **interior** regions of the mantle arrays in all isotopic binary plots, and thus in contrast to the four "real" components described above, it is a **"virtual"** component in the sense that basalts of PM composition can be produced by simple mixing of the extremum sources.

Whether a PM reservoir is now present in the mantle is an open question: because it is an "interior" component of all Sr - Nd - Pb isotopic arrays, its existence cannot be established simply by use of these isotopes. In a very virtual sense, this is Gödel's Theorem (Monatshefte Math. Phys., 1931) for mantle geochemistry. Or, as Zindler and Hart point out (opera cit.) "we contend that no geochemical observation to date (1986 to 1989) demands this survival" (of "primordial" mantle material).

When He isotope ratios are added to the binary Sr -Nd - Pb array plots, a series of 3D plots is generated which can be conveniently centered in the horizontal plane (radiogenic arrays) on the MORB ratio of $8 \times R_A$. Then the data clearly show that the Hi-μ and EM1 exterior components lie **below** the MORB plane, with ratios as low as $5.2 \times R_A$ in the observed lavas (Cook Islands and St. Helena, and Tristan, Kerguelen, etc.). Hart and Zindler (opera cit.) consider that EM1 has "High-^{3}He" ratios, ~ $26 \times R_A$, perhaps representing ancient metasomatized mantle, but as noted above, the actual EM1-type OIB's (e.g. Tristan, Kerguelen) all have ratios much lower than MORB (~ $5 \times R_A$), and the EM1 source clearly plots **below** the MORB He plane in each 3-space. The same is true of Hi-μ data (e.g. Tubuai and Rurutu).

With respect to the "enriched" portions of the radiogenic isotopic arrays, in addition to the Yellowstone and Ethiopian data

(with high $^3He/^4He$ ratios but not very meaningful for comparison with OIB's), the only data until recently that plotted in the enriched Sr, "High-^3He" quadrants were the Samoan island data of Rison & Craig (EOS, 1982), plotted vs. Sr both by us and by Hart & Zindler and Zindler & Hart. These samples have a curious history: they are, for the most part, xenoliths from the **shield** lavas contained in **post-erosional** lava flows. The He measurements were made on the olivines and pyroxenes from the xenoliths, while the Sr isotope data (Wright and White, EPSL 1986) were measured on the enclosing basalts. Although He and Sr are generally "uncoupled" in basalts, Rison & Craig found a good linear correlation in their five samples, indicative of addition of a low 3/4 EM2 source to material with ratios (measured) up to at least 18 R_A. Strangely, however, the 87/86 ratios, ~ 0.7055 as a mean, are similar to the EM1 type lavas (e.g. Gough), so that these "hybrid" Samoan samples are not very significantly enriched vs. a PM or "bulk silicate earth" Sr composition. This led us, as well as Zindler & Hart, to propose that the high $^3He/^4He$ ratios were due to mantle metasomatism that had raised the ratios in an EM1 type material (e.g. Zindler & Hart, 1986, p. 534). If this seems confusing it is because it **is**: at that time it appeared that shield lavas of Samoa were **less** enriched than post-erosional lavas (Wright & White, op. cit.), but recent measurements by K. Farley at SIO have shown that this is not generally the case for the Tutuila lavas of Samoa. In fact, interpreted literally, the previous Samoan data are prima facie evidence for a "PM" component, but no "prima facie" interpreters were to be found because of the bastard nature of those particular samples of uncertain parentage.

Fortunately, better samples are now at hand (Farley, Natland, & Craig, in press) in which very highly enriched Sr ratios in Samoan lavas are coupled, and strongly and negatively correlated, with High ^3He ratios. These data leave little doubt that the observed He-Sr and Nd-Sr data measured by Farley et al. represent binary mixing arrays with a PM primitive mantle component that is alive and well and hiding in the lower mantle. That is to say, the "High-^3He" ratios that plot in the **enriched** Sr quadrant require a PM component **above** the MORB plane, unless the observed correlations are due to chance events.

That this is **not** the case is shown by the fact that we also have the **other** half of a symmetrical array (in Sr - He or Nd - He space). Poreda & Craig (in press) have studied samples from the north end of the Lau back-arc basin, across the Kermadec Trench from Samoa, that show a similar binary mixing array in the **High** ^3He, but **depleted** Sr, quadrant. The probability that these two arrays, representing two sets of lavas no more than 600 km apart and spanning a trench, **both** represent random patterns, is too low to be significant. We conclude that these are **both** mixing arrays, of the crucial PM component with EM2 and with DM.

If so, then spanning across the north end of the Kermadec trench, we have on the **one** side (NE) a binary PM - EM2 mixture of mantle sources, with the PM derived from a mantle plume, mixing with EM2 no doubt related to the downgoing subducted slab. And 600 km to the SW, on the **opposite** side of the Kermadec Trench, on the spreading axis (one of many in the Lau Back-arc Basin), we have a simple two-component mixture of PM with DM, the MORB source. The dynamics of this "plume splitting" at a convergent margin (for it is hard to believe in two independent plumes so close together, in these days of the 2000 km "warhead" plume vogue) are fascinating in the extreme. Perhaps the spreading on the Lau Basin axis is involved in pulling plume material toward the axial region where it mixes with the DM source of the BABB lavas, while most of a series of "plumelets" of PM intersect the slab on the other side and mix with the EM2 source. An important study now would thus be to see if it appears necessary to conclude that the PM component defined by the high $^{3}He/^{4}He$ ratios in each mixture, is indeed a single component mixing with different endmembers on either side of the trench.

Although the work by Farley et al. described here applies strictly only to the Samoan - Kermadec Trench region, it should be clear that once one admits a PM component in one region of the Pacific, one must expect it to rear its plumehead elsewhere in that ocean, and indeed in other oceans and in the continents. Continental hotspots (e.g. Yellowstone and Ethiopia) should therefore be fertile regions for further investigations of the use of He isotopes to escape the Gödelian Trap of the radiogenic mantle arrays. In the meantime let mantle geochemists rejoice that Samoa has at last "come of age" (Rison and Craig, EOS 1982) and has preserved such a rich heritage of mixtures with the Primitive Mantle source.

Supercontinental Fragmentation, Cambrian and Mesozoic - Plume Related?

I.W.D. Dalziel, Institute for Geophysics, University of Texas at Austin,
8701 Mopac Boulevard, Austin, Texas 78759-8345, USA.

The geometry and timing of supercontinental fragmentation in the Mesozoic is now well established. Magmatic provinces believed to be tectonically related to this event cover considerable areas of Laurasia and Gondwana. Some of them appear to be related to mantle plumes and have been suggested as the cause of break up. The geometry of the supercontinental fragmentation at the end of the Precambrian is far less certain, but manuscripts in press present evidence that western Laurentia rifted from East Antarctica-Australia (E. Moores, 1991, *Geology*; I. Dalziel, 1991, *Geology*), and that eastern Laurentia rifted from western South America during final amalgamation of the Gondwana supercontinent (I. Dalziel, 1991, *Geology*; P. Hoffman, 1991, *Science*). This provides a new framework within which to examine late Precambrian intracontinental magmatism that may have been related to supercontinental fragmentation. At first examination it appears to be much less extensive than its Mesozoic equivalent.

The contribution will examine hypotheses concerning the relationship between supercontinental fragmentation and magmatism. It will concentrate on the geologic evidence regarding break up, noting in particular the full extent of the magmatism in time and place, and the apparent control exerted by the prior history of the cratons.

Mantle Convection and the Role of Plumes

Geoffrey F. Davies
Research School of Earth Sciences, Australian National University
GPO Box 4, Canberra, ACT 2601 Australia

The inferred behavior of mantle plumes depends strongly on the context of mantle dynamics in which they are supposed to occur. Interpreting the physical and chemical observations of plumes thus requires that the general question of mantle dynamics be examined.

It is possible to infer the main characteristics of mantle convection using rather direct arguments from well-established observations. Plumes emerge from this approach as a clearly resolved but secondary convection mode transporting less than 10% of the earth's heat budget through the mantle. They most plausibly arise from a thermal boundary layer, and that boundary layer is most plausibly at the bottom of the mantle. They would thus control the heat loss from the core, and the observed poor correlation of plume location with plate configuration suggests that they do so, to first order, independently of the plate-scale flow. The relative importance of plumes through earth history will thus have been determined by their heat transport properties.

Two factors help to reconcile this picture of mantle plumes with observations of ancient chemical heterogeneities in the plume and MORB sources. One is the inferred increase in mantle viscosity with depth, and the other is that plumes would sample the lowermost mantle, which is lkely to be the most heterogeneous. While important aspects of this model remain to be quantified, alternative interpretations in terms of a layered mantle suffer important deficiencies and are poorly quantified.

An extended discussion is given by Davies and Richards [1].

Plate-scale Flow.

The defining property of plates, their strength, determines their role in the mantle convection system [2]. The plates organize the flow by trapping the driving negative buoyancy of the upper, cool thermal boundary layer, to be released into the mantle at subduction zones. Thus they determine where the main downwellings are and supress sub-plate-scale flow that might be driven by "dripping" off the boundary layer. The main flow associated with the plates is called here the "plate-scale flow".

The conductive cooling of the plates governs oceanic heat flow and topography, to first order. Oceanic heat flow accounts for about 85% of the heat loss from the mantle, so in terms of heat transport, the plate-scale flow is clearly the dominant convection mode. Correspondingly, the dominant "dynamic" topography of the earth - the mid-ocean ridge system - is also associated with the plates. It is remarkable that this topography is the result of a near-surface process (conductive cooling), and that the deeper mantle has only secondary effects on topography.

Plumes

Hotspot swells are a secondary but clearly defined form of dynamic topography. Their scale and association with isolated volcanic centers directly implies the existence of columnar, buoyant mantle plumes. The volume of hotspot swells also directly constrains the buoyancy flux and heat flux of plumes (with no assumptions about plume temperature). Collectively, plumes transport about 6% of the earth's heat budget to the base of the lithosphere (but only a fraction of this reaches the surface). They most plausibly arise from a hot, low-viscosity boundary layer at depth. Since core-cooling is estimated to release 5-10% of the heat budget, it is plausible that plumes come from the core-mantle boundary, as proposed by Morgan. On the other hand, they should be trasporting about 70% of the heat budget if they came from a thermal boundary layer at the 670 km transition zone (see below), and so an origin at this depth is implausible.

Thermal "Background" and Superswells

The depth of mid-ocean ridge crests (away from hotspots) varies by about a kilometer, most notably at the Australian-Antarctic discordance, south of Australia, where the crest is about 1 km too deep. Their large scale requires that these variations arise from the mantle, so they comprise a third form of dynamic topography. In any convecting fluid, small-amplitude, large-scale temperature variations always exist away from the thermal boundary layers, due to the incomplete homogenization of material from those boundary layers. Numerical models show that such variations can account for the scale and amplitude of the ridge-crest variations, especially if the deep mantle viscosity is higher (by a factor of around 100) than the shallow mantle.

Removal of the plate topography (square-root-of-age subsidence) from the sea floor reveals extensive broad undulations away from the ridge crests also. Most notable is a huge "superswell" extending for about 10,000 km through the central and western Pacific. It probably *is* Menard's Cretaceous Darwin Rise, still extant after 100 Myr.

The Role of the Transition Zone

The seismicity cutoff, stress orientations, contortions under Tonga and Marianas and the reflectivity of 670 km are not diagnostic, for or against mantle flow through the transition zone. Evidence for aseismic extensions of Wadati-Benioff zones is disputed. A chemical contrast remains disputed. Measured phase change buoyancies are too small to stop normal slabs. A neglected argument comes from the shapes of deep W-B zones: only two show significant deviation from smooth descent to 670 km.

The positive geoid over subduction zones is a more robust diagnostic [3]. In a fluid mantle, all mass anomalies are compensated by deflections of density interfaces. The observed geoid sign and amplitude requires that the deflections compensating slabs are *below* and *well-separated from* the slabs. A chemical interface at 670 km would be deflected and result in compensation

near to the slab, and so would yield too small a geoid signal. A viscosity increase at 670 km will transfer the compensating deflection to the core-mantle boundary, yielding the observed sign and amplitude.

The most direct and perhaps most robust constraint comes again from sea floor topography, or rather from the absence thereof. Heat would have to be conducted across a barrier at 670 km depth, giving rise to a hot thermal boundary layer at the base of the upper mantle. At least 70% of the earth's heat budget must flow through this level (there is not enough radioactivity or heat capacity in the upper mantle to supply the surface heat flow). Such a boundary layer would generate strong buoyant upwellings, with associated surface topography comparable to the mid-ocean ridges (generated by the negative buoyancy of the top thermal boundary layer). Numerical models have demonstrated this phenomenon, with results quite inconsistent with sea floor topography [4].

The plume flux is too small by an order of magnitude to account for the required flux. The broad, low-amplitude 'superswell' topography is of the wrong form to be due to other upper mantle modes: these should produce pervasive, 1-2 km amplitude, 1500-2000 km wavelength swells and troughs. Such features should be quite obvious, but none have been convincingly distinguished from hotspot swells and oceanic plateaus [5].

A hot thermal boundary layer is a basic feature of bottom-heated thermal convection, independent of material properties of the fluid. The resultant surface topography is attenuated at shorter wavelengths by a low-viscosity layer, but numerical modelling has shown that it is robust at plate scales even with a strongly developed low-viscosity layer [6].

Currently, the weight of quantified geophysical arguments is substantially against a barrier to mantle flow in the transition zone.

Chemical heterogeneity and plume sampling

Measurements of radiogenic isotopes in oceanic rocks has revealed heterogeneities in the mantle that require at least five source types and that have apparent ages averaging about 2 Gyr [7]. Plume-derived rocks (oceanic island basalts, OIBs) show more heterogeneity, with isotopic ratios spanning a range 2-3 times the range of mid-ocean ridge basalts (MORBs), although most of the trends in the former are also evident in the latter. Key trace element ratios (Nb/U) confirm this affinity betwen OIBs and MORBs [8].

How these observations can be reconciled with the mantle model deduced above has been discussed by Davies [9]. Several lines of evidence indicate that the deep mantle has a higher viscosity than the shallow mantle. This will slow the flow at depth, increase residence times and reduce stirring rates, thus enhancing the heterogeneity and age of the material, as demonstrated by quantitative models. Plumes from the core-mantle boundary will sample preferentially from the warmer, lower-viscosity boundary layer at the very bottom, where the greatest chemical heterogeneity is to be expected. Stirring in the vicinity of the boundary is less efficient than stirring in the body of the fluid. The Hawaiian plume flux could be sustained

for 100 Myr from a volume 700 km in diameter and only about 20 km thick. Some inefficient gravitational settling of the former oceanic crust component may occur on billion-year timescales. This may account for OIB trace element abundances, which are high relative to MORB, suggesting that their source may be enriched relative even to primitive concentrations.

MORBs, on the other hand, come from the uppermost mantle, which is expected to be the most homogenized and depleted, with the shortest residence times.

The occurrence of a primitive component of helium, in the form of higher $^3He/^4He$, in some OIBs is a puzzle for all models. It cannot be explained simply by appealing to a 'primitive' source, since the Nb/U ratios and lead isotopes of, for example, Hawaii, cannot be explained by a primitive component. The helium must be coming from somewhere else. In the present model, this could be a small amount of remaining relatively primitive mantle, or the core.

Neither can the occurrence of atmospheric noble gas isotopic compositions be interpreted in terms of a primitive mantle reservoir, as proposed by Allegre et al. [10]. There is a primitive neon component in the mantle that is not present in the atmosphere [11,12], so atmospheric composition cannot represent bulk earth or primitive composition. It has been suggested that atmospheric compositions in some OIBs are due to near-surface contamination [13].

References

[1] G. F. Davies and M. A. Richards, Mantle convection, submitted, 1991.
[2] G. F. Davies, J. Geophys. Res., 93, 10,451, 1988.
[3] M. A. Richards and B. H. Hager, J. Geophys. Res., 89, 5487, 1984; Hager, B. H., J. Geophys. Res., 89, 6003, 1984.
[4] G. F. Davies, J. Geophys. Res., 93, 10,467, 1988.
[5] G. F. Davies, J. Geophys. Res., 93, 10,481, 1988.
[6] G. F. Davies, Geophys. Res. Lett., 16, 625, 1989.
[7] W. M. White, Geology, 13, 115, 1985.
[8] A. W. Hofmann, K.P. Jochum, M. Seufert and W. White, EPSL, 79, 33, 1986.
[9] G. F. Davies, Earth Planet. Sci. Lett., 99, 94, 1990.
[10] C. J. Allegre, T. Staudacher and P. Sarda, EPSL, 81, 127, 1987.
[11] B. Marty, Earth Planet. Sci. Lett., 94, 45, 1989.
[12] M. Honda and I. McDougall, Nature, 1991.
[13] D. B. Patterson, M. Honda and I. McDougall, GRL, 17, 705, 1990.

A General Hot Spot Model Accounting for Known Lithospheric Structure

John R. Evans and H. M. Iyer

We propose a model of hot-spot dynamics and evolution in the lithosphere by combining teleseismic-tomography images with grain-scale upper-mantle melt geometries observed or inferred by other authors. We first describe the teleseismic results and our inferences from them, then proceed to a fairly detailed analysis of melt geometry and its affect on the movement of heat. Lastly, we describe our model and its implications.

Teleseismic tomography images of the Yellowstone-Snake River Plain (SRP) area reveal a deep-seated magmatic system. The upper mantle contains a persistent low-velocity anomaly extending from Yellowstone well into the eastern SRP, reaching a depth of 150 to 200 km throughout. The low is roughly 100-150 km wide along its whole length, and ends near the northeast edge of Yellowstone caldera. This low is offset consistently northwest from the axis of the hot-spot track; the anomaly beneath Yellowstone dips ~75° northwest from the caldera. We infer that this low-velocity body is an upper-mantle partial melt [*Iyer et al.*, 1981; *Evans*, 1982] of up to about 9% volume fraction of melt at Yellowstone. This estimate is based on the melt model of *Mavko* [1980], who computes the seismic effects of melt squirt within an interconnected network of melt tubes following grain edges. The observed anomaly weakens slowly to the southeast, implying a smaller melt fraction and lower heat content beneath older parts of the hot-spot track. The crust ages similarly, with that beneath Yellowstone highly anomalous [e.g., Benz and Smith, 1984] and that beneath the eastern SRP apparently healed [*Evans*, 1982; *Sparlin et al.*, 1982].

The Yellowstone upper-mantle anomaly is unlike any active non-hot-spot system known to us, but is similar to large anomalies observed beneath both Hawaii [*Ellsworth*, 1977] and Iceland [*Tryggvason et al.*, 1983]. We infer that hot spots are similar to one another but fundamentally different from other volcanoes. Because the upper-mantle anomaly is offset from the surface track at Yellowstone, we also infer that hot spots are controlled from the bottom up, with heat following a non-vertical path of least resistance to the surface. It is more difficult to explain such an offset if the hot-spot is controlled by shallower processes, such as rifting or crustal weakness. Hence we infer that the low-velocity anomalies observed are regions of percolating partial melt advecting heat rapidly from the asthenosphere to a shallower depth, from where other processes, dependent on the type of crust, move the heat to the surface.

We believe that the grain-scale geometry of partial melts and the effect of this geometry on the rate of heat movement are important to understanding hot spot behavior at lithospheric depths. *Waff* [1980] demonstrates that the millimeter-scale geometry of partial melts under upper-mantle conditions depends upon the pressure of the melt fraction relative to the pressure in the solid matrix. It is now widely accepted that basalt melt in unconfined equilibrium conditions forms a continuous network of channels along grain triple-junctions, leaving the grain faces dry. This is the melt geometry we believe exists beneath active hot spots. Waff points out that this connected-melt geometry requires that the melt pressure be below the solid-matrix pressure to compensate surface tension along the interface between solid and melt. The curvature of these solid-melt interfaces is convex-inward for dihedral angles less than 60°, as is the case in the upper mantle, so this surface tension pulls outward on the melt, lowering the melt pressure. If, in contrast, the melt pressure equals or exceeds the solid-matrix pressure, a contrary, outward-convex curvature must be introduced to the melt-solid interface. Creating net outward-convex curvature, while achieving the required dihedral angle at melt-solid-solid intersections, requires that the melt channels pinch out along the grain edges, forming disconnected blebs of melt along these edges (Figure 1). Though a great deal has been written about the connected-melt geometry, no subsequent work known to us or to H. Waff (personal communication, 1990) has addressed or contradicted Waff's model of disconnected, overpressured melt.

If a moving unperturbed lithospheric plate is heated from below, the heat conducts only a short distance into the base of the lithosphere before being swept away by plate motion. Conductive thermal models of this

sort yield regions of high temperatures only a few tens of kilometers thick at the base of the plate. Partial melting may occur in this heated basal region, but will not reach the surface as long as conduction dominates heat flow.

A region of small-fraction melting forming under these conditions cannot have lower pressure than the surrounding matrix. If an isolated bit of melt forms slowly under these conditions, it can form either a stable, isolated bleb of overpressured melt, with the pressure differential and the bleb geometry maintained by surface tension, or spread out along the grain edge, moving toward an interconnected melt geometry. In the latter case, the surface area, and therefore surface energy, increase. The stable, least-energy condition is the disconnected bleb, unless a large melt fraction is achieved, forcing the blebs to collide. (This forced interconnection happens somewhere between 5 and 22% volume fraction of melt [*Waff*, 1980].)

If low-pressure interconnected melt should form spontaneously, buoyancy will progressively reduce the pressure differential upward through the melt region. At some height of less than about 4 km above the base of the melt, the pressure difference drops to zero [*Waff*, 1980] and the melt must disconnect into isolated blebs. The ends of the connected channels at this depth are unstable, pinching off at one end (hence requiring high-pressure melt) but running on in the other (low-pressure melt). Since the disconnected geometry has lower surface energy and any negative pressure below the disconnection front can be eliminated rapidly by creep in the solid matrix, the disconnection front will propagate downward and eliminate the interconnected melt. The system remains disconnected and, therefore, thermally conductive. It remains in that state as long as the basal melt zone remains isolated (Figure 2*a*).

The situation changes radically if any melt pathway is established upward from the basal melt zone to a region where the melt pressure can remain stably below the solid-matrix pressure. The pressure differential between solid and melt increases downward because of buoyancy, permitting the melt to form an interconnected network. Negative feedback exists between this pressure differential and the melt-channel size—the channels constrict at greater depth, partially immobilizing the melt and reducing the differential-pressure gradient. This negative feedback creates a macroscopic equilibrium condition that maintains a column of interconnected melt of arbitrary height, the sort we infer exists beneath Yellowstone, Hawaii, and Iceland.

One place where a small negative melt pressure can exist indefinitely is the Earth's surface. A pathway between the surface and the basal melt zone can be provided by any pre-existing magmatic system with sufficiently deep roots. This triggering volcano might be carried over the basal melt zone by plate motion or might form in place, as in crustal rifting (Figure 2*b*). As soon as the pathway is established, a melt-interconnection front must propagate rapidly downward into the basal melt zone, expelling excess melt—a flood basalt—and establishing an equilibrium interconnected-melt zone (Figure 2*c*). With interconnection, the basal melt zone becomes an advective system moving heat rapidly by melt percolation—a large increase in the rate of heat movement. Now the heat source that created the basal melt effectively is applied to the top of the basal melt zone, melting the overlying lithosphere and expelling still more excess basalt as the melt zone builds upward (Figure 2*d*).

The mechanism of heat advection changes as the melt zone nears the surface. In oceanic environments, melt and heat are removed directly from the percolating zone through deep fractures, as inferred from Hawaiian microseismicity, for example. The response of continental crust is quite different. The large contrast in density and solidus temperature between basalt and silicic continental crust drive a heat-exchange process. At Yellowstone, silicic ash-flow tuffs are generated by fusion of lower-crustal rocks [*Doe et al.*, 1982]. Presumably, heat is exchanged between percolating basalt melt and crustal silicic melt at or near the Moho (Figure 2*e*). This silicic melt is buoyant and moves upward in the crust, perhaps as diapirs, forming upper-crustal magma chambers from which the ash-flow eruptions emanate (Figure 2*f*).

This lithospheric hot-spot model can be superposed on the adiabatic-upwelling model of *White and McKenzie* [1989]. Their model does not yet include the advective effects of percolating partial melt, while ours does so *via* our inferences from teleseismic observations. The adiabatic model qualitatively matches the observed anomalies at Yellowstone, Hawaii, and Iceland in that both imply upper-mantle partial melting. The adiabatic model differs in that the teleseismically observed feature has a narrower, more upright geometry and reaches shallower depths. (These differences cannot be attributed entirely to artifacts of the teleseismic technique.) There is no evidence of large "wings" of melt in a laterally spreading plume head, as predicted by adiabatic models, though a more compact form of that geometry cannot be ruled out. The teleseismic image is dominated by an upright low-velocity body. A near-vertical pipe of percolating partial melt reaching from the asthenosphere to a shallow depth would remove much of the heat responsible for the "wings".

A number of inferences can be drawn if our lithospheric model is correct; some of these are testable. Our model implies that most hot spots lie dormant for some period, conductively heating only the lower lithosphere. These "latent" hot spots first appear at the surface at some pre-existing magmatic or rift system. The depressurization and expulsion of excess melt at this place is marked by flood basalts. Hence, the common association between flood basalts, spreading centers or other magmatic systems, and hot spots is accommodated. The Yellowstone hot spot was released, for example, by a back-arc spreading center—the western SRP, Chief Joseph dike swarm, and northern Nevada Rift—and generated the Columbia River basalt and basalt deeply filling the western SRP. The association between mid-ocean ridges and hot spots is due simply to the fact that ridges are widespread magmatic systems that often serve to trigger hot spots—the hot spots need not induce the ridges.

REFERENCES

Benz, H. M., and R. B. Smith, Simultaneous inversion for lateral velocity variations and hypocenters in the Yellowstone region using earthquake and refraction data, *J. Geophys. Res.*, *89*, 1208–1220, 1984.

Doe, B. R., W. P. Leeman, R. L. Christiansen, and C. E. Hedge, Lead and strontium isotopes and related trace elements as genetic tracers in the upper Cenozoic rhyolite-basalt association of the Yellowstone Plateau volcanic field, *J. Geophys. Res.*, *87*, 4785–4806, 1982.

Ellsworth, W. L., Three-dimensional structure of the crust and mantle beneath the island of Hawaii, Ph.D. thesis, 237 pp., Mass. Inst. of Technol., Cambridge, 1977.

Evans, J. R., Compressional wave velocity structure of the upper 350 km under the eastern Snake River Plain near Rexburg, Idaho, *J. Geophys. Res.*, *87*, 2654–2670, 1982.

Iyer, H. M., J. R. Evans, G. Zandt, R. M. Stewart, J. M. Coakley, and J. N. Roloff, A deep low-velocity body under the Yellowstone caldera, Wyoming: delineation using teleseismic *P* wave residuals and tectonic interpretation, *Geol. Soc. Am. Bull., Part I*, *92*, 792–798, 1981.

Mavko, G. M., Velocity and attenuation in partially melted rocks, *J. Geophys. Res.*, *85*, 5173–5189, 1980.

Sparlin, M. A., L. W. Braile, and R. B. Smith, Crustal structure of the eastern Snake River Plain determined from ray trace modeling of seismic refraction data, *J. Geophys. Res.*, *87*, 2619–2633, 1982.

Tryggvason, K., E. S. Husebye, and R. Stefansson, Seismic image of the hypothesized Icelandic hot spot, *Tectonophysics*, *100*, 97–118, 1983.

Waff, H. S., Effects of the gravitational field on liquid distribution in partial melts within the upper mantle, *J. Geophys. Res.*, *85*, 1815–1825, 1980.

White, R., and D. McKenzie, Magmatism at rift zones: the generation of volcanic continental margins and flood basalts, *J. Geophys. Res.*, *94*, 7685–7729, 1989.

Figure 1 (*right*): Crystal-scale melt geometries for over-pressured and under-pressured melt (after *Waff, J. Geophys. Res.*, 1815–1825, 1980).

Figure 2*a-f* (*below*): General, partly schematic model of hot spots, illustrated for Yellowstone on a northeast-striking cross section along the hot-spot track.

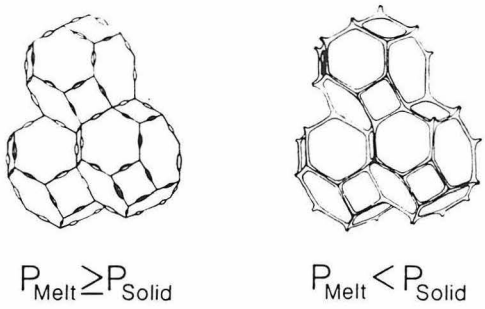

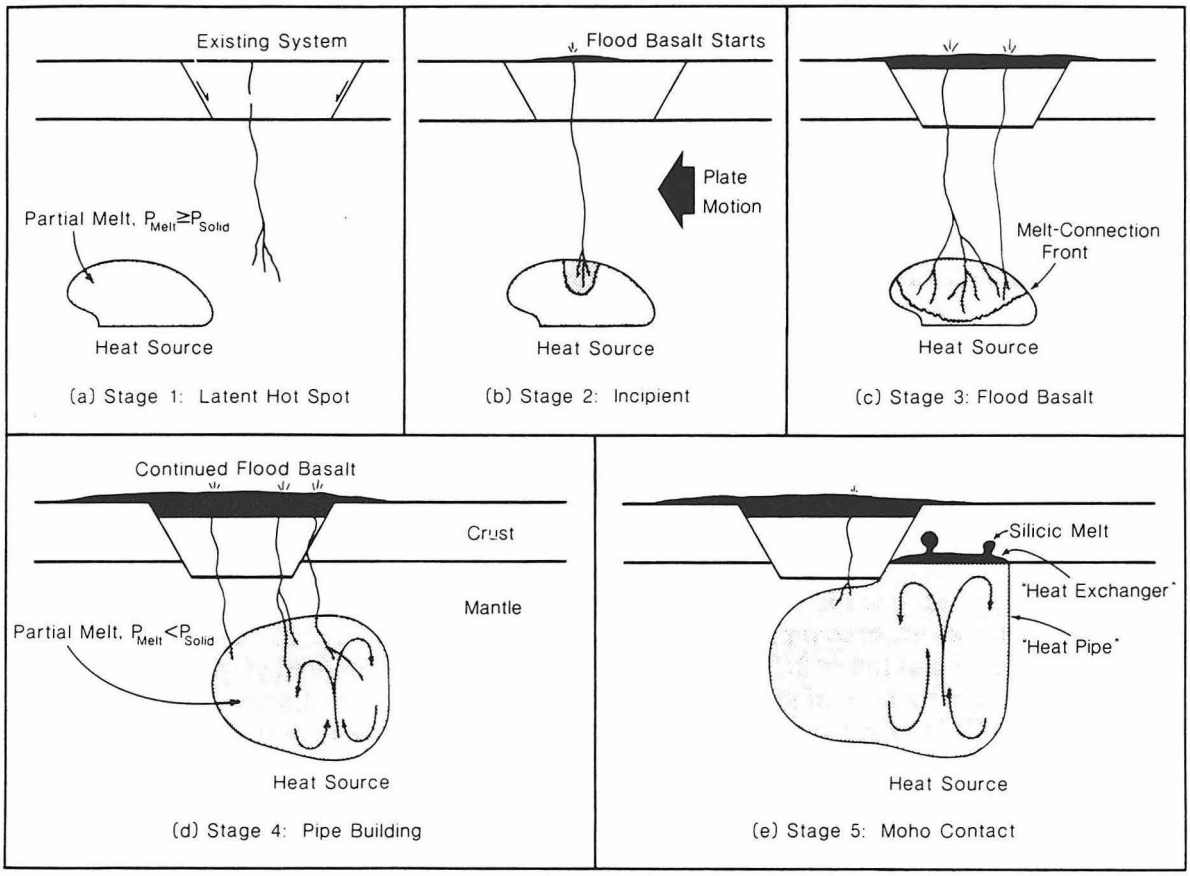

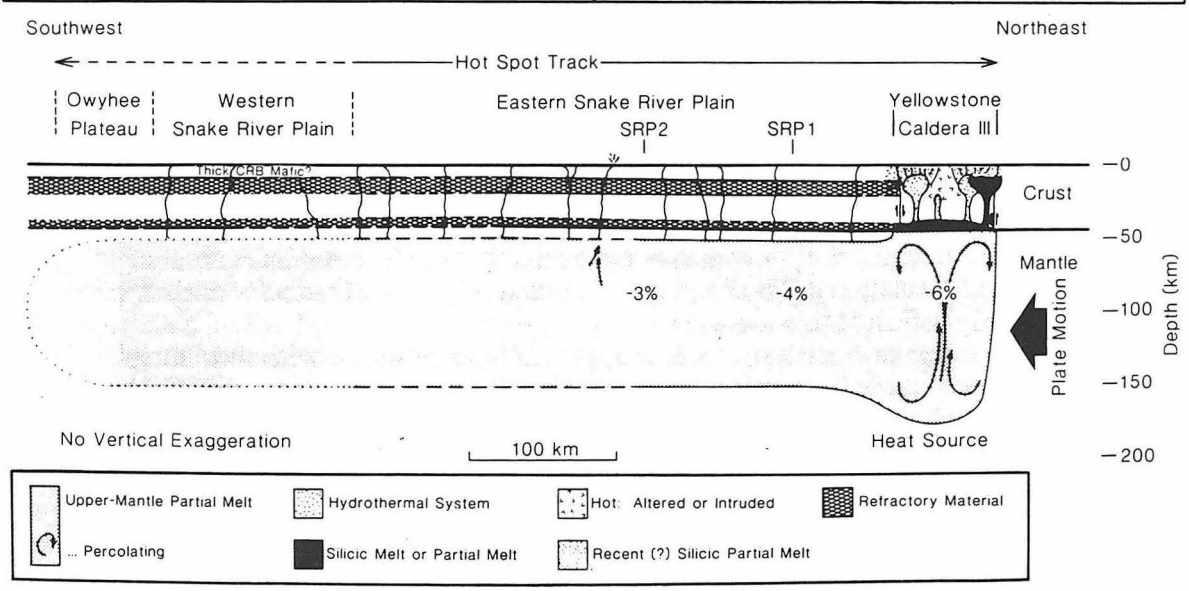

(f) Stage 6: Stable Continental Hot Spot

COMPOSITIONAL DIFFERENCES BETWEEN HAWAIIAN SHIELDS: SOURCE OR PROCESS RELATED?

Frey, F.A. (Mass. Inst. Tech.), Rhodes, J.M. (Univ. Mass.),
Garcia, M.O. (Univ. Hawaii), H.-J. Yang (Mass. Inst. Tech.)

The compositional characteristics of Hawaiian shield lavas can be used to understand physical and chemical processes associated with plumes. For example: (1) major element abundances can constrain the mean pressure and temperature of melt segregation from a diapir; (2) abundances of elements that are highly compatible in specific mantle minerals can constrain the residual mineralogy (e.g., Y and HREE reflect residual garnet); (3) abundances of incompatible elements are sensitive to the mean degree of melting; and (4) isotopic ratios of Sr, Nd and Pb and abundance ratios involving highly incompatible elements identify the presence of different source components.

The variable major element compositions of primitive MORB have been interpreted in terms of process (i.e. pressure, temperature and degree of melting) and source heterogeneties (e.g., Klein and Langmuir, 1987; Kinzler and Grove, 1991). MORB and Hawaiian shield lavas are tholeiitic basalt, but relative to MORB compositions Hawaiian shield lavas have lower Al_2O_3 and CaO contents, higher abundances of FeO^*, TiO_2 and incompatible elements, higher $^{87}Sr/^{86}Sr$ and lower $^{143}Nd/^{144}Nd$. Some of these differences, perhaps all, reflect differences in source composition. However, the lavas forming each Hawaiian shield also have distinctive compositions. Do these intershield differences reflect differences in plume composition, differences in proportions of source components such as plume and entrained asthenosphere, differences in melting process or the effects of shallow level contamination in the lithosphere?

Compositional differences between the adjacent and active Hawaiian volcanoes, Kilauea and Mauna Loa are well established. Relative to historic lavas from the Mauna Loa shield, the lavas forming the Kilauea shield have lower SiO_2 and higher CaO contents, higher abundances of incompatible elements such as TiO_2, K, Rb, Th, Nb and LREE, (Figures 1 and 2) and lower $^{87}Sr/^{86}Sr$ coupled with higher $^{143}Nd/^{144}Nd$ (Figure 3). During anhydrous melting of spinel and plagioclase peridotite with residual clinopyroxene, abundances of CaO increase and SiO_2 decrease with increasing extent of melting (e.g., Kinzler and Grove, 1991). Also, SiO_2 content decreases with increasing pressure of melting. Therefore the CaO and SiO_2 differences between Mauna Loa and Kilauea lavas could be interpreted as Kilauea lavas reflecting a higher mean degree of melting, possibly at a higher mean pressure; e.g., the plume source for Kilauea lavas may have a higher potential temperature leading to intersection with the solidus at a higher pressure and a larger mean degree of melting during ascent. In general, the mean pressure of melt segregation for Hawaiian lavas must be significantly greater than that inferred for MORB (e.g., <16 kbar, Klein and Langmuir, 1987, Grove and Kinzler, 1991) because the uniformity of Y and HREE abundances in primitive Hawaiian lavas is strong evidence for residual garnet (e.g., Hofmann et al., 1984). Therefore interpretation of the intershield differences in major element abundances requires experimental data for melts in equilibrium with garnet. Unfortunately, very few data are available but the low Al_2O_3 content of Hawaiian tholeiites relative to MORB and the similalr Al_2O_3-MgO trends for each shield (Figure 4) probably reflect residual garnet.

A higher degree of melting for Kilauea lavas is inconsistent with their relative enrichment in incompatible elements (e.g., Figure 1). Because the isotopic differences between historic Mauna Loa and Kilauea lavas require source differences, the abundances of incompatible elements may be source related. However, there is strong evidence that incompatible element abundances were affected by a recent mixing process. Specifically, relative to historic Mauna Loa lavas, historic Kilauea lavas have higher Rb/Sr (Figure 2), but lower $^{87}Sr/^{86}Sr$ (Figure 3). This paradox could be explained by mixing; e.g., Kilauea lavas may contain an incompatible element-rich component derived by incipient melting of

wallrock asthenosphere or lithosphere. This component could explain the relatively high Rb/Sr (Figure 2) and high incompatible element content of Kilauea lavas (e.g., Figure 1) accompanied by relatively low $^{87}Sr/^{86}Sr$ (Figure 3). In this scenario the larger volume Mauna Loa shield is more representative of the plume composition.

Important constraints on Hawaiian plumes and their interaction with wallrocks can also be provided by the longevity of the geochemical differences between Hawaiian shields. Many of the compositional characteristics of Kilauea and Mauna Loa lavas have persisted for 30 ka and perhaps 100 ka (e.g., Chen et al., 1991; Lipman et al., 1990); this requires long-lived uniformity in source compositions and processes and long-term independent magma ascent paths for the Kilauea and Mauna Loa magmatic systems. In apparent contrast, Kurz and Kammer (1991) have shown that Mauna Loa lavas older than 10 ka have lower $^{87}Sr/^{86}Sr$ than historic Mauna Loa lavas (~0.70360-0.70370 and approaching the ratios in Kilauea lavas). They suggest that the Mauna Loa plume has recently entrained asthenosphere with relatively high $^{87}Sr/^{86}Sr$; however, there is no apparent accompanying change in major or trace element abundances (Lipman et al., 1990; Rhodes, unpublished)..

Based on the Kilauea and Mauna Loa data sets, it is evident that: (1) historic lavas from each volcano contain different proportions of isotopically distinct components, and (2) abundances of incompatible elements were affected by a recent mixing process. However, it is not clear if the intershield differences in major element composition are process or source controlled. In order to more fully evaluate correlations between isotopic ratios and composition, we studied lavas from Koolau volcano, the Hawaiian shield that defines the high $^{87}Sr/^{86}Sr$, low $^{143}Nd/^{144}Nd$ end of the Hawaiian range (e.g., Figure 3 and Trull et al., 1990). In many respects Koolau tholeiites have compositional features like Mauna Loa lavas; specifically, Koolau tholeiites also have relatively high SiO_2, low CaO, and low abundances of TiO_2 and incompatible trace elements (Figure 4). They also have very high Al_2O_3/CaO (~1.5 compared to chondritic ~1.23, Figure 4), relatively high Na_2O and low FeO* contents (Frey et al., in preparation). These major oxide compositional features of Koolau lavas mimic the characteristics of melts segregated from a relatively cool diapir; i.e., segregation of melts formed by a low mean degree of melting at relatively low pressure (Klein and Langmuir, 1987).

CONCLUSIONS

1) The differences in radiogenic isotopes between Hawaiian shields requires isotopically distinct source components; perhaps different proportions of plume and entrained asthenosphere in each shield.

2) The compositional differences between Hawaiian shields persist for a large fraction of the volcano's shield stage.

3) Differences in major element composition are not correlated with differences in radiogenic isotopic ratios. Therefore, the intershield differences in SiO_2, CaO, TiO_2 and FeO* may be process related; i.e., they reflect derivation of each shield from separate plumes with different potential temperatures leading to melt segregation at different mean pressures and extents of melting.

4) Also abundances of incompatible elements are not correlated with isotopic differences. For example, Koolau lavas which define the high $^{87}Sr/^{86}Sr$, low $^{143}Nd/^{144}Nd$ end of the Hawaiian range are much more depleted in incompatible elements than Kilauea lavas. In particular, the inverse trend between Rb/Sr and $^{87}Sr/^{86}Sr$ defined by Kilauea and Mauna Loa lavas requires that the incompatible element abundances were affected by a recent mixing process, perhaps involving a high Rb/Sr melt formed by small degrees of melting.

5) In summary, plume models for Hawaiian Volcanoes must have the following characteristics: (a) an isotopically heterogeneous source, possibly reflecting variable mixing of plume and asthenosphere components; (b) a mechanism for creating variable abundance ratios of highly incompatible elements; (c) plumes that initiate melting at different depths and melt to varying extents; (d) very restricted lateral zones of magma generation; (e)

distinct and long-lived magma ascent paths. Several of these characteristics should be observable with detailed geophysical studies.

REFERENCES:

Basaltic Volcanism Study Project, Basaltic Volcanism on the Terrestrial Planets, Pergamon Press, New York, Chapter 1.2.6, 1981.

Chen, C.-Y., F.A. Frey, J.M. Rhodes and R.M. Easton, Long-term compositional variation of lavas from Kilauea Volcano, Hawaii: Evidence from the Hilina Basalt, EOS, Spring 1991 abstract.

Hofmann, A.W., M.D.Feigenson and I.Raczek, Petrogenesis of the Mauna Ulu eruption, Kilauea, 1969-1971, Contrib. Mineral. Petrol., 88, 24-35, 1984.

Kinzler, R.J. and T.L.Grove, Primary magmas of mid-ocean ridge basalts, Jour. Geophys. Res., in press.

Klein, E.M. and C.H. Langmuir, Global correlations of ocean ridge chemistry with axial depth and crustal thickness, Jour. Geophys. Res., 92, 8089-8115, 1987.

Kurz, M.D. and D.P. Kammer, Isotopic evolution of Mauna Loa volcano, Earth Planet. Sci. Letts., in press.

Lipman, P.W., J.M.Rhodes and G.B.Dalrymple, The Ninole Basalt - implications for the structural evolution of Mauna Loa volcano, Hawaii, Bull. Volcanol., 53, 1-19, 1990.

Trull, T., M. Roden, S.Hart, F. Frey, M. Garcia and M. Kurz, He-Sr-Nd-Pb isotopic compositions of Koolau basalts: more precise definition of the Hawaiian plume, EOS, 71, 657, 1990.

West, H.B., D.C. Gerlach, W.P. Leeman, and M.O. Garcia, Isotopic constraints on the origin of Hawaiian lavas from the Maui Volcanic Complex, Hawaii, Nature, 330, 216-220, 1987.

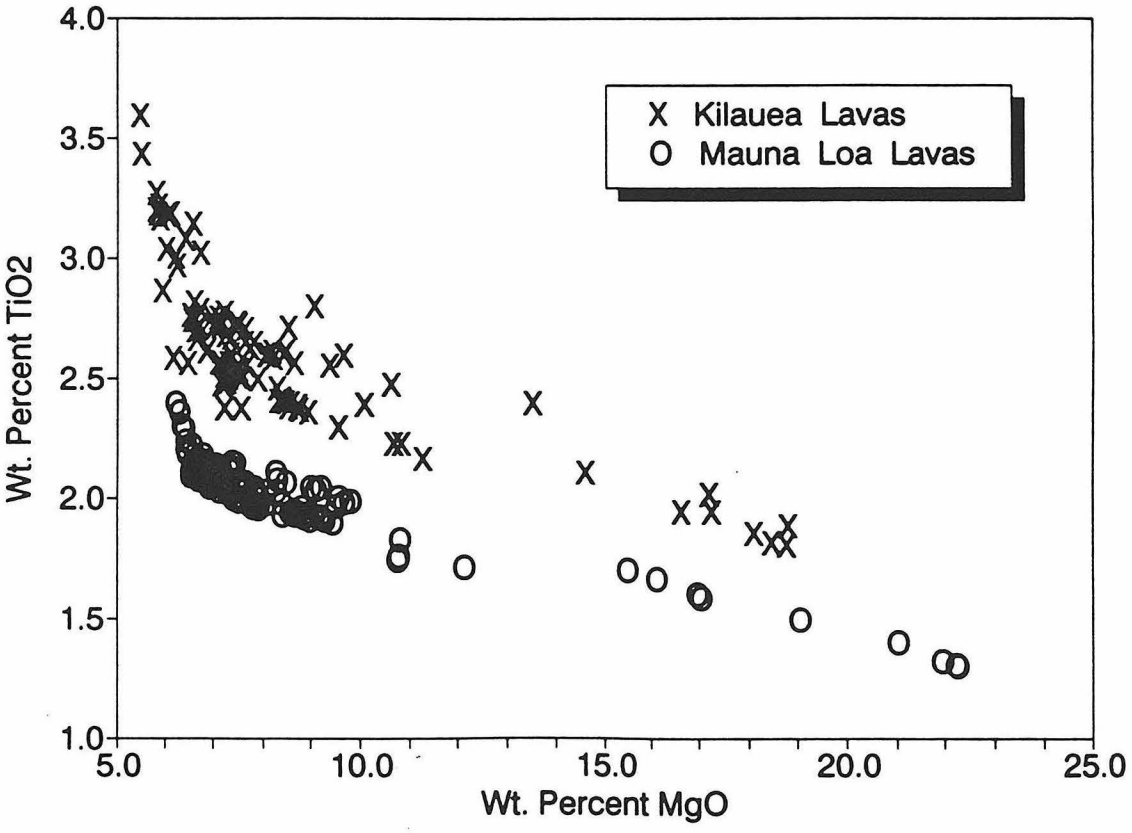

Figure 1. TiO_2 and MgO (wt.%) showing that Kilauea lavas are systematically enriched in TiO_2 relative to Mauna Loa lavas. Because this enrichment is independent of MgO

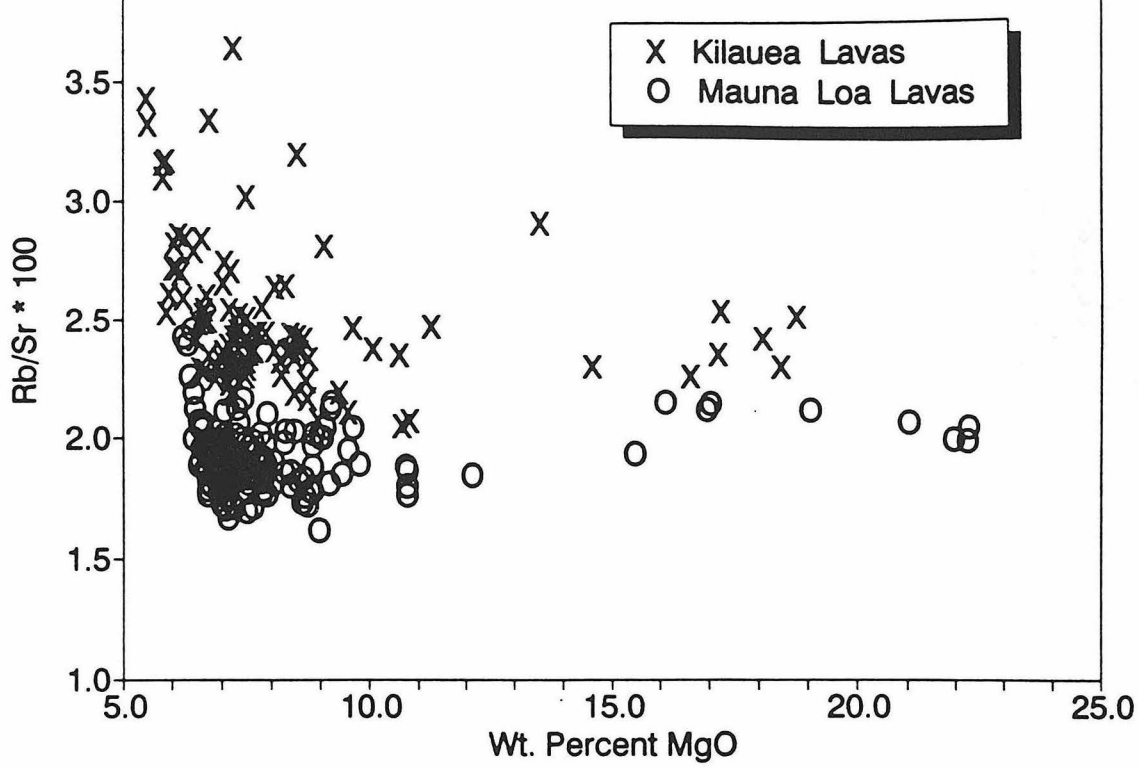

Figure 2. Rb/Sr versus MgO content (wt.%) showing that in general Kilauea lavas have higher Rb/Sr than Mauna Loa lavas although historic Kilauea lavas have lower $^{87}Sr/^{86}Sr$ than historic Mauna Loa lavas (see Figure 3).

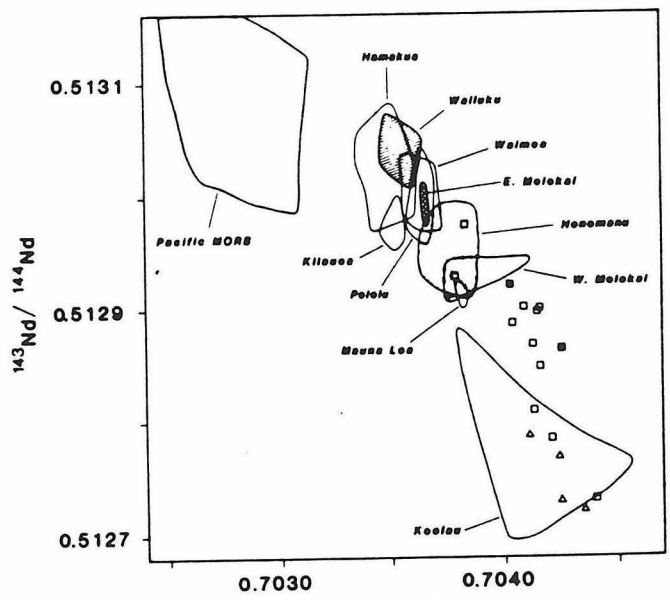

Figure 3. $^{143}Nd/^{144}Nd$ versus $^{87}Sr/^{86}Sr$ for Hawaiian tholeiites showing the distinct difference between the fields for historic Kilauea and Mauna Loa lavas, and the field for Koolau lavas which define the high $^{87}Sr/^{86}Sr$, low $^{143}Nd/^{144}Nd$ end of the Hawaiian field. Symbols show that lavas from two other volcanoes, Kahoolawe (squares) and Lanai (triangles) overlap with the Koolau field. Figure from West et al. (1987).

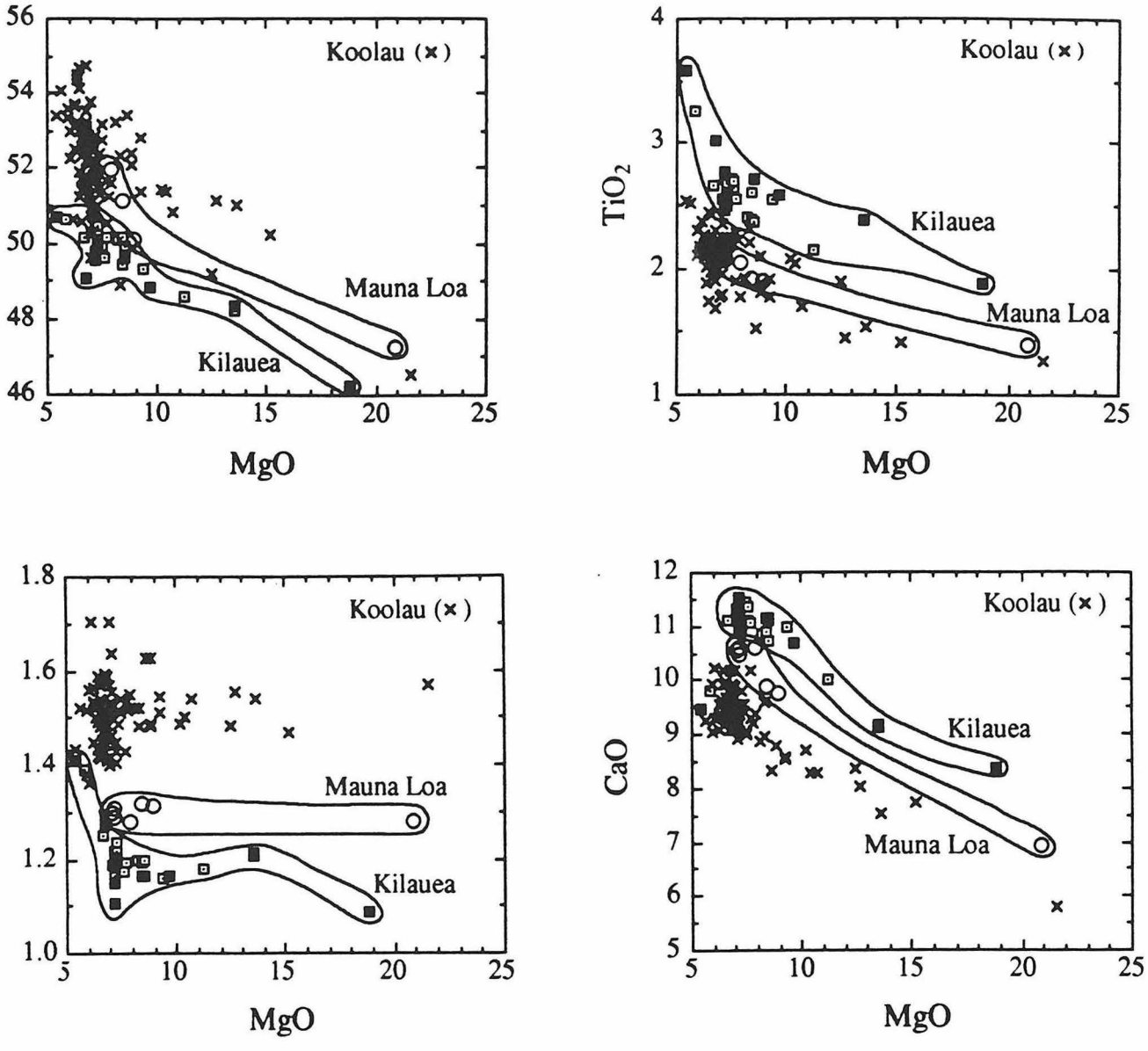

Figure 4. SiO_2, TiO_2, CaO and Al_2O_3/CaO versus MgO content showing that Koolau tholeiites have relatively high SiO_2 and low TiO_2 contents and overlap with Mauna Loa lavas. Although lavas from Kilauea, Mauna Loa and Koolau do not define different Al_2O_3-MgO trends (not shown), at a given MgO content Koolau lavas have lower CaO and higher Al_2O_3/CaO than other Hawaiian tholeiites. Koolau data from Frey et al. (in preparation). Mauna Loa and Kilauea data from (BVSP, 1981 and Rhodes, unpublished).

MANTLE PLUMES : WHAT SIZES, FROM WHAT DEPTHS ?
The constraints from seismic tomography, geoid and topography.

Claude FROIDEVAUX, Yanick RICARD, and Luce FLEITOUT
Ecole Normale Supérieure, Paris 75231, France

Two approaches based on dynamical modelling of the observed geoid have shed some light on the concept of mantle plumes. First, broad upwelling currents are predicted on the basis of the first seismic tomographic models of the upper and lower mantle. Second, the short wavelength geoid exhibits linear features sometimes interpreted as signatures of presently active convection rolls or, possibly, of past extensional tectonics. Here we shall argue that these geoid anomalies and their associated topographic expressions are best explained as tracks of small size hot spots.

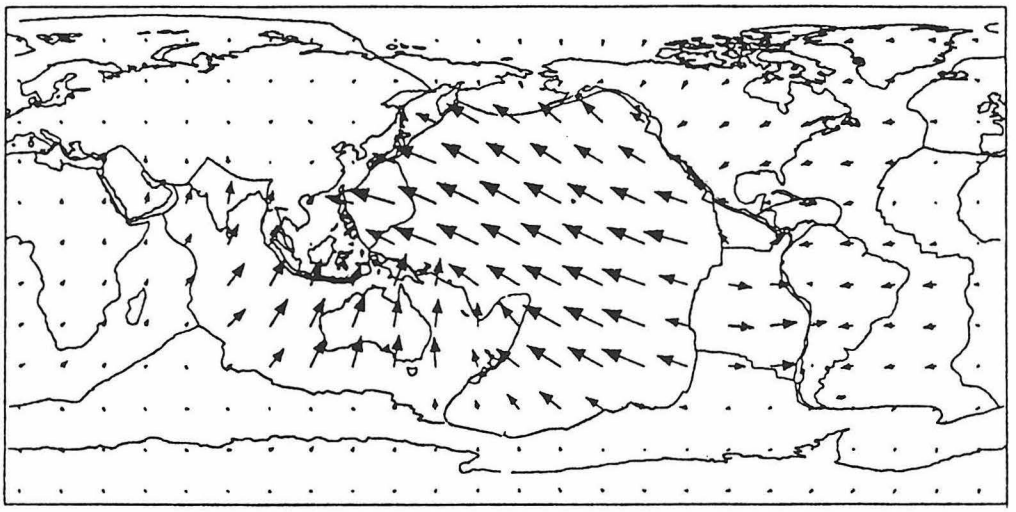

Fig. 1 Scale 10cm/yr →

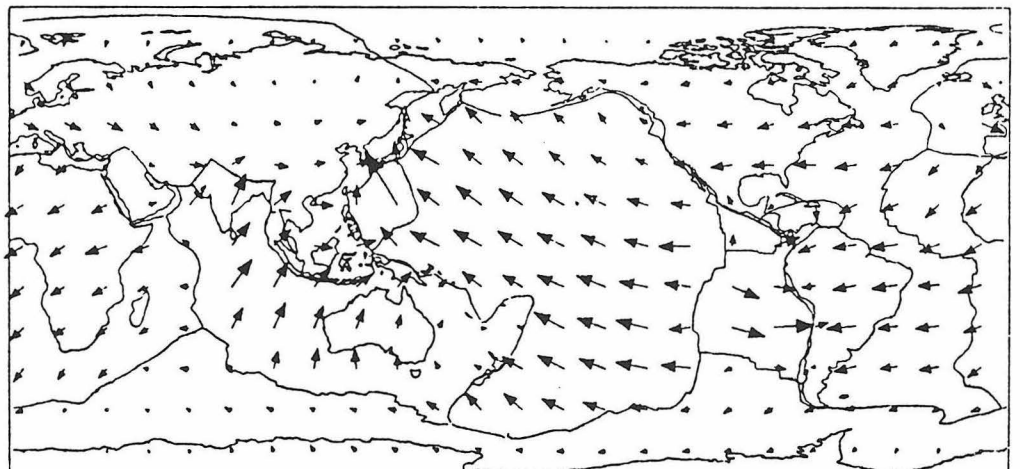

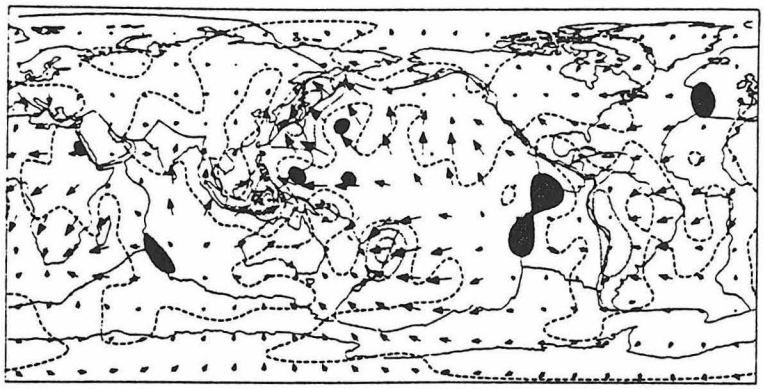

Depth 250km

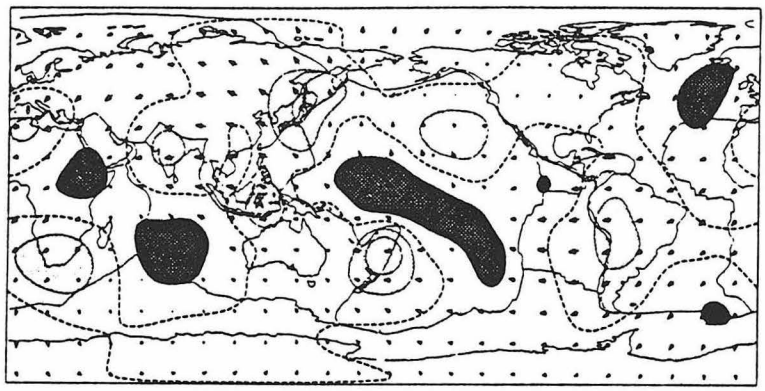

Depth 650km

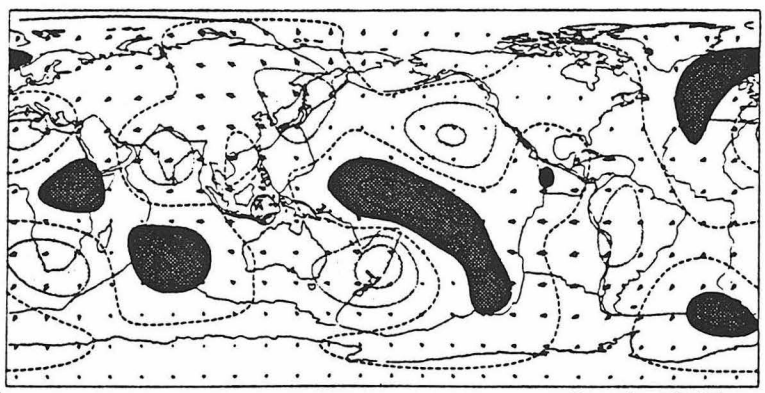

Depth 1250km

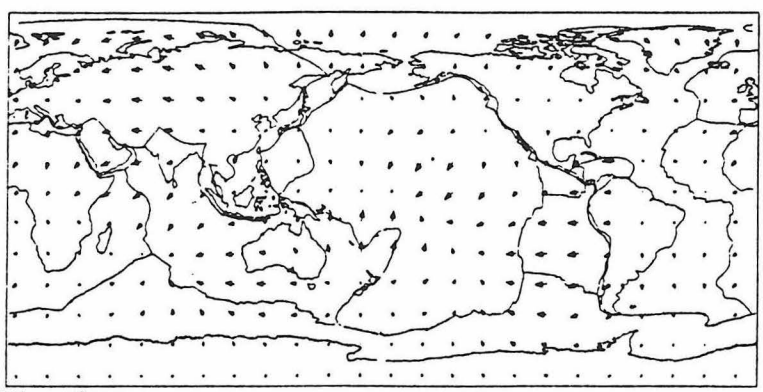

Depth 2900km

Fig. 2

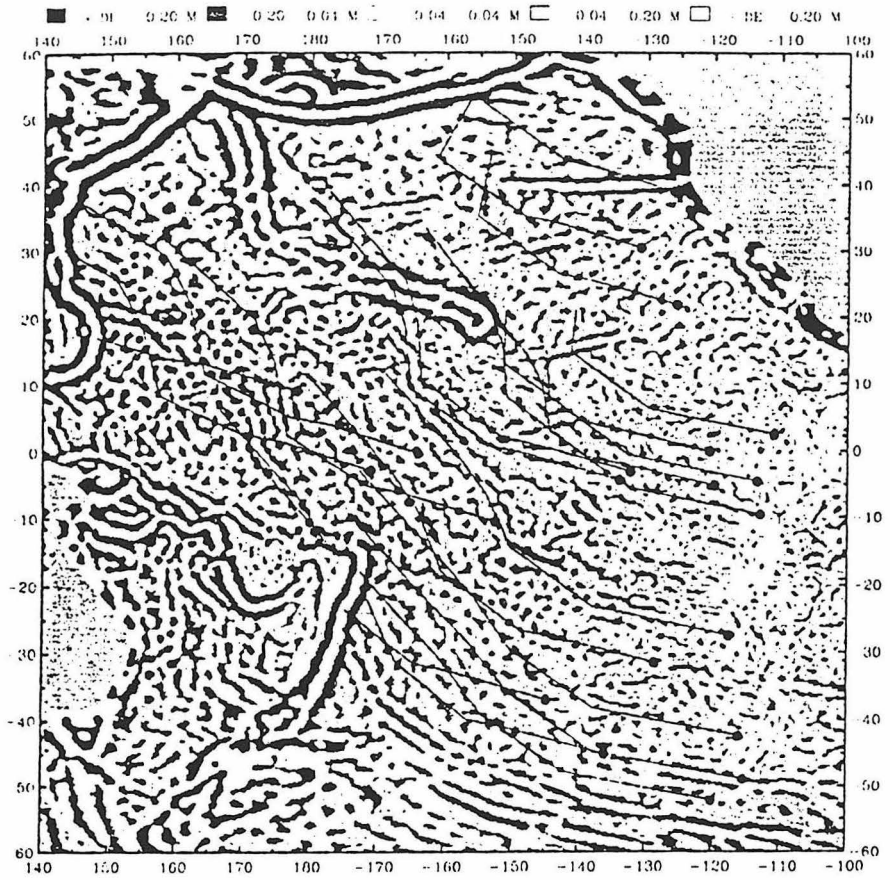

Fig. 3

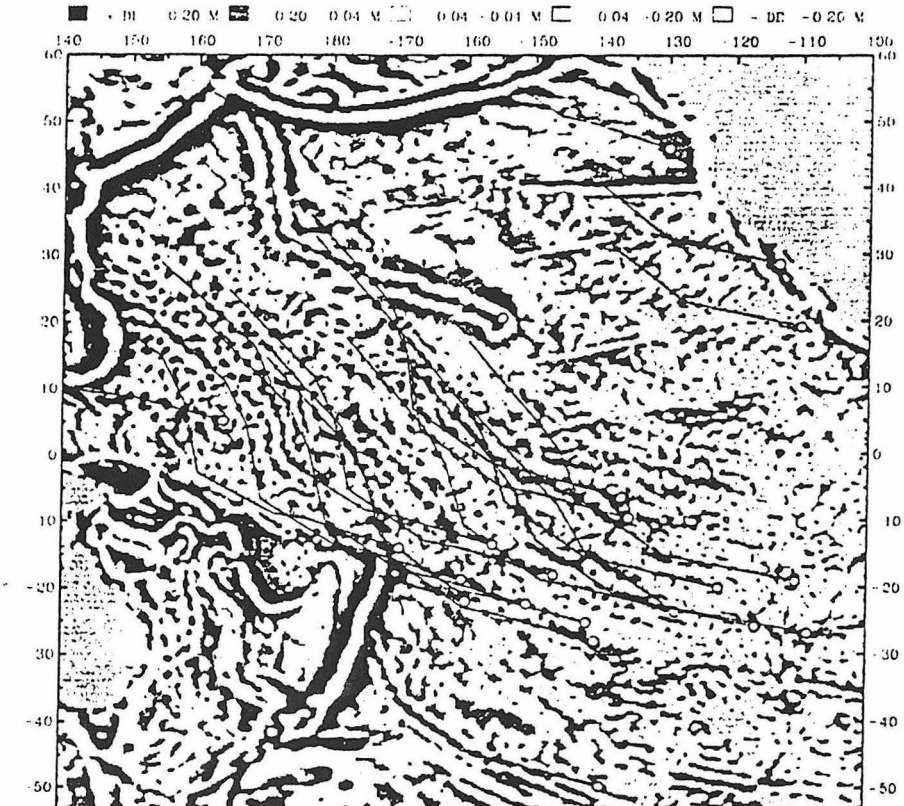

Let us start with the present tomography for the mantle (1) , which yields only the first 6 or 8 spherical harmonic degrees for the lateral variations of the seismic velocities. Assuming that these variations are mostly of thermal origine, one can derive a distribution of density variations, or internal loads for a viscous mantle, and compute the induced mantle circulation, and the predicted geoid (2). The latter compares well with the long wavelength measured geoid. What is the computed mantle circulation ?

Here are the results of a dynamic Earth model (3) characterized by a viscosity increase by a factor 50 between upper and lower mantle, and by the presence of rigid and freely moving surface plates. Figure 1 shows the plate tectonics velocities (top) and those predicted by the computation (bottom). For the fast moving plates the agreement is very satisfactory. The relevant point here is found in Figure 2, which depicts the computed 3D- circulation at various depths (4) (arrows give the horizontal velocity components ; dark, resp. lightly shaded areas, indicate the locations of vigorous up-or down-welling). The major upward flow beneath the central portion of the Pacific plate does not contribute much to plate motion, but deflects density interfaces near the Earth's surface or at depth which dominate the positive sign of the most prominent geoid maximum at this same location. Other upwellings between Iceland and the Indian Ocean are located closer to plate margins and contribute both to the other geoid high and to plate divergence. An interesting point is the geographical correlation between these broad size mantle plumes and the distribution of major hot spots, i.e. of mantle plumes of much smaller scales.

Let us now consider the short wavelength geoid (around 200 km). Figure 3 is a filtered geoid map over the Pacific (5). The tracks of 22 hot spots are drawn and correlate well with linear geoid highs. However, numerous similar lineations are present in this data. The arguments in favour of additional hot spot tracks, rather than presently active convection rolls are twofolds. First fossil plate velocities characterize many of these lineations. Second the associated topographic expressions, when they have been mapped, are more compatible with the existence of permanent dyke intrusions than with present thermal roll configurations. Figure 4 depicts some possible new hot spot tracks. The pattern emerging from this interpretation raises an interesting question regarding the small scale dynamical pattern of the upper mantle .

REFERENCES

1- WOODHOUSE, J.H., & A.M. DZIEWONSKI, Mapping the upper mantle : three-dimensional modeling of Earth structure by inversion of seismic waveforms, J. Geophys. Res., 89, 5953-5986, 1984.

NATAF, H-C., I. NAKANISHI & D.L. ANDERSON, Measurements of mantle wave velocities and inversion for lateral heterogeneities and anisotropy. 3 : Inversion, J.Geophys.Res., 91, 7261-7307, 1987.

2- RICARD, Y., L. FLEITOUT., & C. FROIDEVAUX., Geoid heights and lithospheric stresses for a dynamic Earth, Ann. Geophys., 2, 267-286, 1984.

RICHARDS, M.A., & B.H. HAGER, Geoid anomaly in a dynamic Earth, J. Geophys. Res., 89, 5987-6002, 1984.

FORTE, A.M., & W.R. PELTIER., Plate tectonic and aspherical Earth structure: The importance of poloidal-toroidal coupling, J. Geophys. Res., 92, 3645-3679, 1987.

RICARD Y., VIGNY C., & C. FROIDEVAUX : Mantle heterogeneities, Geoid and Plate Motion : A Monte-Carlo inversion., J. Geophys. Res., 94, 13,739-13,754, 1989.

3- RICARD,. Y., & C. VIGNY., Mantle dynamics with induced plate tectonics, J. Geophys. Res., 94, 17,543-17,559, 1989.

4- BAI WU MING, RICARD.Y., & C. FROIDEVAUX., On the origin of deviatoric stresses in the lithosphere, J. Geophys. Res., 199, in Press.

5- FLEITOUT. L., & C. MORICEAU., Short-wavelength geoid, bathymetry and the convective pattern beneath the Pacific Ocean, Geophys. J. Int., 1991, in Press.

FLEITOUT L., & C. MORICEAU., Topography and geoid anomalies due to density heterogeneities at the base of the thermal lithosphere. Application to oceanic swells and small wavelength geoid lineations, Geophys. J.Int., 1991, in Press.

Geochemical Evolution of a Plume Volcano: Lessons from Hawaii

Michael O. Garcia, Geology-Geophysics Department,
University of Hawaii, Honolulu, HI 96822

Introduction

A broad overview is presented here of the geochemical evolution of an idealized Hawaiian shield volcano. This approach is necessary because Hawaiian volcanoes grow so rapidly that they cover the lavas from earlier stages of development by 6-10 km of later lavas and this enormous pile sinks rapidly (2-3 mm/year; Moore and Campbell, 1987) below sea level. Thus, in the absence of a drill hole through an entire Hawaiian volcano, I have tried to find geochemical similarities between Hawaiian volcanoes that are in different states of development. The three active Hawaiian shield volcanoes, Loihi, Kilauea and Mauna Loa, have been used to make a composite Hawaiian volcano. Loihi is in the early stages of shield development (perhaps <100 Ka); Kilauea is in the main phase of development; Mauna Loa is in the waning stage of shield formation (Moore, 1990). The lavas recently produced by these volcanoes are chemically distinct but there are consistent geochemical trends in major and trace elements, and isotopes among the lavas from these volcanoes. The purpose of this contribution is to draw attention to this apparent geochemical evolution trend and to speculate on its implication for plume and melting processes.

Isotopes

The first issue we must address in constructing a composite Hawaiian shield volcano is: Are the lavas from the different volcanoes derived from a common source? Although various previous studies have emphasized the heterogeneities in the Hawaiian source (e.g., Staudigel et al., 1984), the isotopic ratio variations of shield lavas can be related to two principal components (West et al., 1987). The most primitive component (i.e. highest $^{3}He/^{4}He$ ratio) has the lowest $^{87}Sr/^{86}Sr$ ratio but highest $^{206}Pb/^{204}Pb$ ratio. This component may be from the plume. The other component may represent an impurity within the plume or may have been part of the lower mantle (i.e. beneath the MORB-source) that was entrained by the ascending thermally-drive plume (Griffiths and Campbell, 1990).

Whatever the source of the various components, for the active Hawaiian shield volcanoes there is an overall progressive increase in the $^{87}Sr/^{86}Sr$ and decrease in $^{143}Nd/^{144}Nd$ ratios from the youngest to oldest of the three active Hawaiian shield volcanoes (Fig. 1). The trend for $^{206}Pb/^{204}Pb$ ratios is different because Kilauea lavas have the highest ratios of any Hawaiian shield lavas, but both Loihi and Kilauea lavas have lower $^{206}Pb/^{204}Pb$ ratios than their much older sister, Mauna Loa (Fig. 1).

Major Elements

Now that we have shown that the source for Hawaiian shields seems to progressively evolve for at least some volcanoes (i.e. those currently active) the next question is what happens to their major and trace elements during the same period?

Garcia et al. (1989) demonstrated a systematic major element and volatile variation from Loihi through Kilauea to Mauna Loa using submarine glasses. Early stage lavas have higher CaO, FeO, TiO_2, Na_2O and K_2O and lower SiO_2 and Al_2O_3 contents at the same MgO then later stage lavas (Fig. 2), especially among lavas that

have olivine as their sole phenocrystic phase. This trend may be unrelated to changes in the proportions of the source components during the development of the volcanoes. Instead, it may be related to changes in both the percentage (increase) and depth (decrease) of the partial melting during the life of the volcano.

Two Elements

Ratios of trace elements are useful for fingerprinting distinct source components and in documenting the relative contribution of these components. Ratios of REEs in the lavas from the three active Hawaiian shield volcanoes define a linear variation that progressively varies from Loihi to Mauna Loa (Fig. 3). This variation could be due to a progressive increase in the degree of partial melting and/or differences in the composition of the two components that are mixed to form Hawaiian magmas. (A note of caution: not all trace element ratios show such a linear variation.)

Implications

The geochemical evolution of our composite Hawaiian shield volcano seems to involve the progressive variation of major and trace elements, and Pb, Sr and Nd isotope ratios. This variation could be related to the progressive increase in the amount of lower mantle that is entrained by the plume. However, the data are equally explained by a two-component plume with a progressive exchange in the proportions of the two components during the evolution of the plume. These simplistic models have a common theme. Each volcano is related to a separate "pulse" of the plume rather than all being derived from a heterogeneous plume. However as noted earlier, there are variations in Pb, Sr and Nd isotopic ratios in lavas from different Hawaiian volcanoes that require that the amount of the entrained lower mantle or of the two components in the plume must be variable with each plume pulse. The great variation is size of Hawaiian volcanoes [>42.5 x 10^3 km for Mauna Loa (Bargar and Jackson, 1974) to <10 km^3 for Mahukona Seamount] may be related to variations in volume of each discrete pulse of the Hawaiian plume. No other reasonable explanation has been made to explain the size variation of Hawaiian volcanoes. There is no relationship between the inferred extent of partial melting for the lavas from each volcano and their size (West et al., in review).

Concluding Remarks

Although there is the perception that the Hawaiian Islands are well studied and understood, this perception is only true relative to most other volcanic regions. We are beginning to recognize the important questions and better focus our studies to address them. However, the details of the processes that create these volcanoes are still poorly understood and we need the help of geophysical modelers (among others) to resolve these details.

References

Bargar K.E. and Jackson E.D., 1974, Calculated volumes of individual shield volcanoes along the Hawaiian-Emperor Chain. U.S. Geol. Surv. J. Res. 2, 545-550.

Garcia M.O., Muenow D.W., Aggrey K.W. and O'Neil J.R., 1989, Major element, volatile and stable isotope geochemistry of Hawaiian submarine tholeiitic glasses. J. Geophys. Res., 94, 10525-10538.

Griffith R.W. and Campbell I.H., 1990, Stirring and structure in mantle starting plumes. Earth Planet. Sci. Lett. 99, 66-78.

Kurz M.D. and Kammer D.P., 1991, Isotopic evolution of Mauna Loa Volcano. Earth Planet. Sci. Lett., in press.

Moore J.G. and Campbell J.F., 1987, Age of tilted reefs, Hawaii. J. Geophys. Res. 92, 2641-2646.

Moore J.G., Normark W.R. and Szabo B.J., 1990, Reef growth and volcanism on the submarine southwest rift zone of Mauna Loa, Hawaii. Bull. Volcanol. 52, 375-380.

Staudigel H.A., Zindler A., Hart S.R., Leslie T., Chen C.Y. and Clague D.A., 1984, The isotopic systematics of a juvenile intraplate volcano: Pb, Nd and Sr isotope ratios of basalts from Loihi seamount, Hawaii. Earth Planet. Sci. Lett. 69, 13-29.

West H.B., Garcia M.O., Gerlach D.C. and Romano J., in review, Origin of tholeiites from Lanai Volcano, Hawaii: Implications for geochemical heterogeneity in the source of Hawaiian lavas. Earth Planet. Sci. Lett.

West H.B., Gerlach D.C., Leeman W.P. and Garcia, M.O., 1987, Isotopic constraints on the origin of Hawaiian lavas from the Maui Volcanic Complex, Hawaii. Nature 330, 216-220.

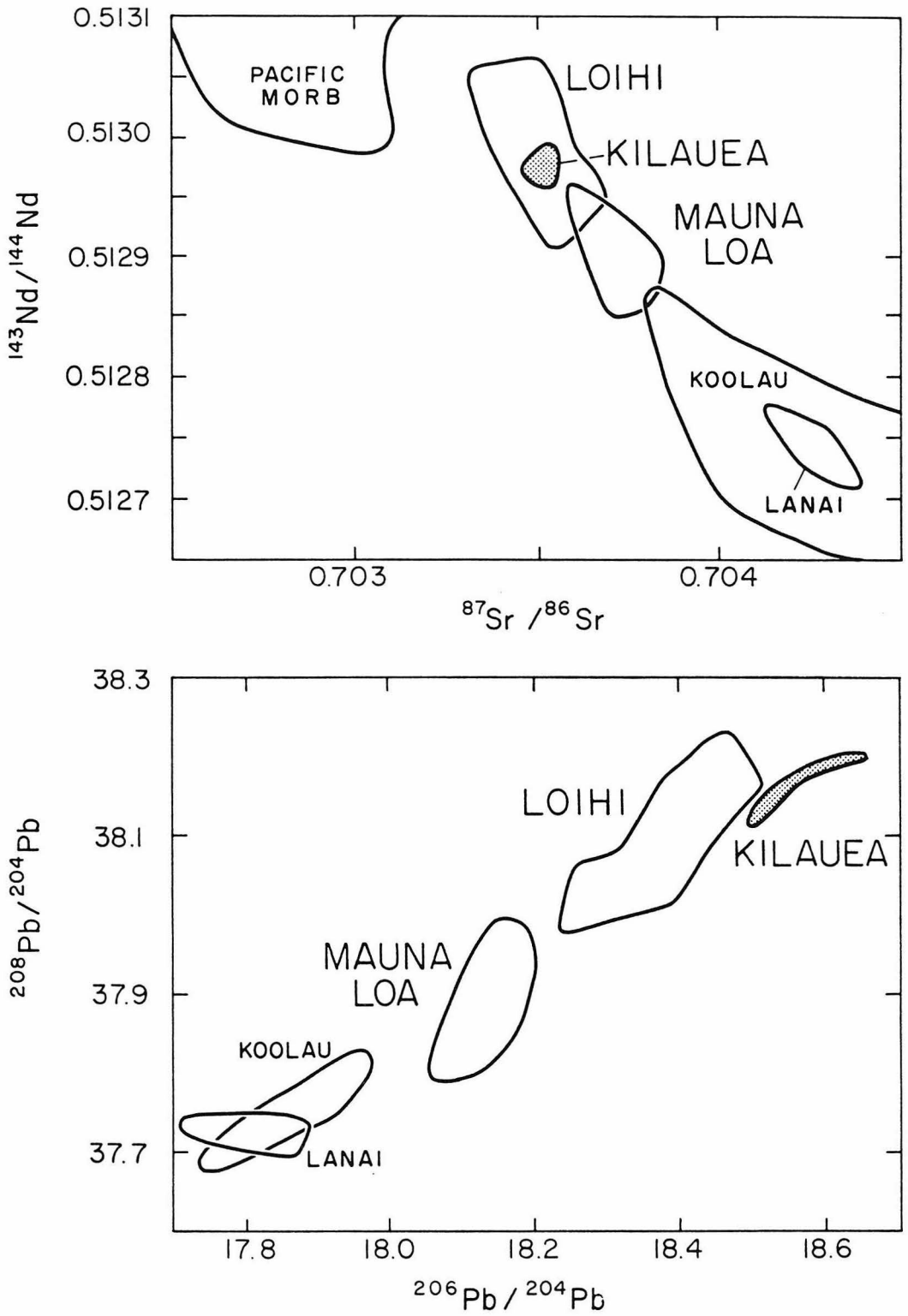

Figure 1. Sr, Nd and Pb isotope ratios for tholeiitic lavas from selected Hawaiian shield volcanoes. Data from West et al. (1987), Staudigel et al. (1984), Gurriet (1988), Kurz and Kammer (1991) and Garcia et al. (unpubl.).

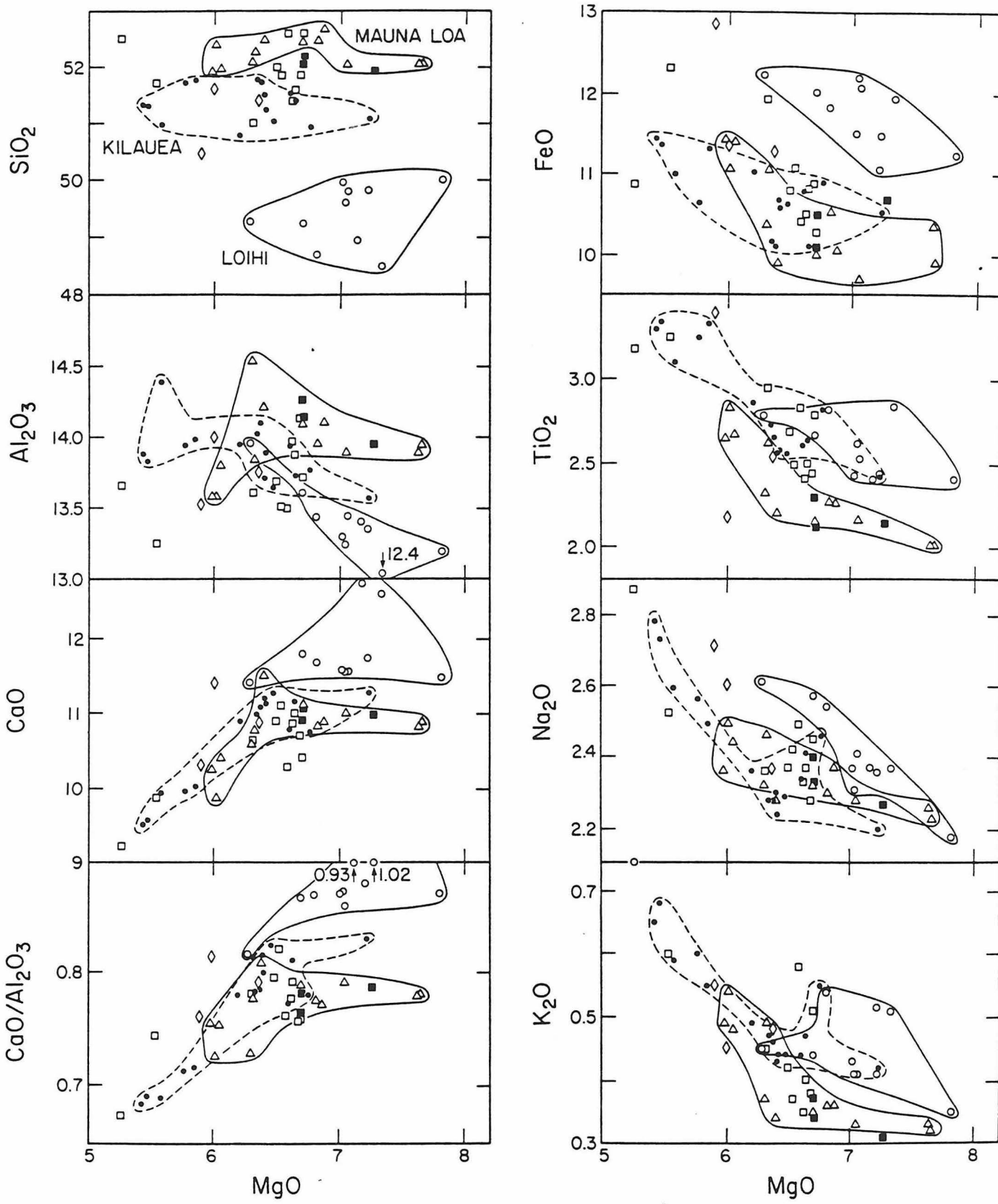

Figure 2. MgO variation diagram for submarine tholeiitic glasses from volcanoes from the island of Hawaii. Field for: Loihi (open circles); Kilauea (closed circles); and Mauna Loa (triangles). Data from Garcia et al. (1989).

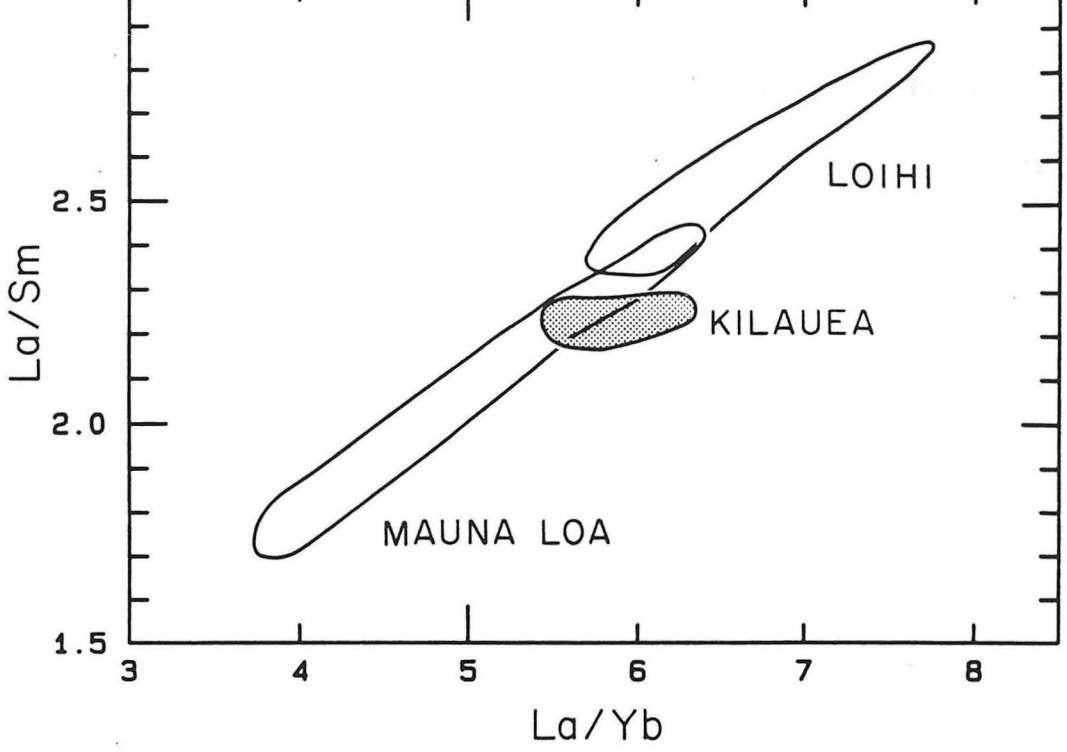

Figure 3. Ratio:ratio plot for REEs in tholeiites from Loihi, Kilauea and Mauna Loa (data from Gurriet, 1988).

An OIB-BABB-subcontinental lithosphere connection

James Gill, Fred Hochstaedter, Eduardo Malavassi, Qingquan Wang, Elisabeth Widom
Earth Sciences Board, UCSC, Santa Cruz CA 95064

Uppermost mantle becomes enriched relative to MORB beneath continents by subsolidus fluids and small melt fractions, as well as elsewhere in the mantle by sediment subduction or processes at the core-mantle boundary. We have studied northern hemisphere examples of basalts with EMI and EMII characteristics to evaluate this claim.

Lherzolite nodule-bearing Quaternary leucite basanites and lamproites from NE China have the isotopic characteristics of EMI (Wang and Gill, 1990). They are associated with early intra-continental rifting in a region of Paleozoic suturing between Archean shields. Their combination of high Mg# and high LILE concentrations indicates that their EMI isotopic characteristics are from the mantle. Their present-day and time-integrated Th/U (3.8-4.1) and Nb/Th ratios (10-12) are chondritic despite extreme enrichments in other incompatible elements, which precludes subduction-related processes. Positive correlation between $^{206}Pb/^{204}Pb$, U/Pb, and Nb/Zr ratios, for example, demonstrate that the EMI signature is most extreme in the lamproites and suggest that it is due to late Precambrian lithospheric metasomatism.

We studied the EMII component in alkali basalts of Sao Miguel, Azores, where the enriched component increases eastward towards Africa (Widom et al., 1990). Linear Sr-Nd-Th isotope mixing arrays but curved Sr-^{206}Pb arrays for these basalts indicate that the Azores EMII component is from subcontinental lithosphere rather than sediment. This constraint is possible because Th is the most incompatible isotopic tracer so that the potential variation in Sr/Th ratios between mantle and sediment is great. If the enrichment is young, it must have Sr/Th >200 which is inconsistent with bulk sediment. If the enrichment is Proterozoic or older, it must have $^{206}Pb/^{204}Pb$ >20 and the percent melting of the depleted mantle must exceed 5% during production of alkali basalt, neither of which is likely. Instead, the Azores EMII also seems to be from water-metasomatized subcontinental lithosphere.

Enriched mantle underlies island arcs and backarc basins despite the presence of subducting slabs which preclude plumes. Similarities in isotope and many incompatible trace element ratios between arc and ocean island magmas have long been cited as arguments for old enriched mantle above slabs (e.g., Gill, 1976, 1984; Stern and Ito, 1983; Morris and Hart, 1983). At issue are whether arcs and OIB reflect young versus old enrichments of similar kind, and whether most arcs involve *both*. At stake

is whether arcs prove that mantle enrichments are shallow and ubiquitous. Evidence for old enrichments in island arc magmas include Nd and Hf isotopic compositions more typical of OIB than MORB without consistent Pb and Be isotopic evidence of recent sediment involvement, and positive rather than negative correlations between Nd isotopes and elemental evidence of recent subduction-related metasomatism (e.g., Ba/La ratios).

Recently we documented a particularly clear example of old enrichment beneath Costa Rica (Malavassi and Gill, 1990). In the north, magmas are from depleted sources (high εNd) greatly affected by recent subduction (high $^{10}Be/^{9}Be$ and Ba/La), whereas the opposite characterizes the south. The transition occurs at the location of a change in the dip angle of the subducting Cocos plate which seems to coincide with the northern boundary of the Caribbean oceanic plateau. The shallow mantle beneath southern Costa Rica is characterized by old enriched mantle underlying that plateau, and by relatively little recently-subducted component.

This topic has remained contentious for two decades because of complexities attending subduction such as the following. *Some* recent enrichment is common in most arcs, especially at the volcanic front, for elements including Sr, U, and B. Old enrichments can be introduced by recent subduction; e.g., by subducting clastic sediments derived from OIB volcanoes. And for the same old enrichments to be present in both arc and OIB sources, refractory phases must preferentially retain HFSE during melting of enriched sources beneath arcs but not ocean islands. For recent suggestions by which to explain the tectonic dependence of refractory phases, see Reagan and Gill (1989) and Keleman et al. (1990). Nonetheless, enriched mantle arguably is present in representative noncontinental arc segments such as Fiji, the northern Marianas, and Costa Rica (Gill, 1984; Lin et al, 1990; Malavassi and Gill, 1990). If arcs look, sound, and fly likes ducks, they probably are ducks--stuffed with old mantle enrichments.

The occurrence of enriched mantle beneath backarc basins is even less expected and more striking. In the Lau, Mariana, Bonin, and Parece Vela basins, Pb has lower $^{206}Pb/^{204}Pb$ and/or higher $\Delta^{208}Pb/^{204}Pb$ ratios than in the adjacent arcs (e.g., Volpe et al.,1990; Loock et al., 1990; Hochsteadter et al., 1990; Hickey-Vargas, ms). That is, backarc magmas show more Pb isotopic evidence of apparent sediment involvement than do adjacent arc magmas. This is most extreme in the northern Lau Basin where the enriched component is most like EMII and underlies both the backarc and remnant arc (Volpe et al., 1988; Gill and Whelan, 1989; Loock et al., 1990). In the Philippine Sea plate examples, the most depleted N-type MORBs are the most like Indian Ocean MORB, including high $^{208}Pb/^{207}Pb$. Moreover, in this respect Philippine Sea BABB lie on a mixing

line between the arcs and the Chinese EMI component described at the outset.

Consequently, examples of northern hemisphere Dupal anomalies--in Philippine Sea BABB and Azores OIB--can be related to metasomatism of the lithosphere beneath adjacent continents. In general, the occurrence of old enriched mantle beneath arcs, and even more prominently in backarcs when arcs rift, indicates the ubiquity of enrichments in the shallow mantle. If incompatible element budgets even in tholeiites are dominated by small melt fractions and subsolidus fluids, as suggested by their large ^{226}Ra and ^{231}Pa excesses (Williams et al., 1991), then many sources of enrichment can create plume-like geochemical signatures, and cold fluids rather than hot advection may deliver the signatures to the melting sites.

References

Gill J. (1976) Evolution of the mantle: geochemical evidence from alkali basalt: comment. Geology 4: 625.

Gill J. (1984) Sr-Nd-Pb isotopic evidence that both MORB and OIB sources contribute to oceanic island arc magmas in Fiji. Earth Planet. Sci. Letters 68: 443.

Gill J. and Whelan P. (1989) Postsubduction ocean island alkali basalts in Fiji. J. Geophys. Res. 94: 4579.

Hickey-Vargas R. (ms) Isotopic characteristics of submarine lavas from the Philippine Sea: implications for the evolution of the Philippine tectonic plate and the genesis of arc and back-arc magmas.

Hochstaedter A.G., Gill J., and Morris J. (1990) Volcanism in the Sumisu Rift, II: subduction and non-subduction related components. Earth Planet. Sci. Letters 100: 195.

Keleman P.B., Johnson K.T.M., Kinzler R.J., and Irving A.J. (1990) High-field-strength element depletions in arc basalts due to mantle-magma interaction. Nature 345: 521.

Loock G., McDonough W.F., Goldstein S.L., and Hofmann A.W. (1990) Isotopic compositions of volcanic glasses from the Lau Basin. Marine Mining 9: 235.

Malavassi E. and Gill J. (1990) Along-strike magmatic variations at the southern terminus of the Central American volcanic arc. EOS 71: 1576.

Morris J. and Hart S. (1983) Isotopic and incompatible element constraints on the genesis of island arc volcanics from Cold Bay and Amak Island, Aleutians, and their implications for mantle structure. Geochim. Cosmochim. Acta 47: 2015.

Reagan M.K. and Gill J. (1989) Coexisting calcalkaline and high-Nb basalts from Turrialba volcano, Costa Rica: implications for residual titanates in arc magma sources. J. Geophys. Res. 94: 4619.

Stern R.J. and Ito E. (1983) Trace element and isotopic constraints on the source of magmas in the active Volcano and Mariana island arcs, western Pacific. J. Volcanol. Geothermal Res. 18: 461.

Volpe A.M., Macdougall J.D., and Hawkins J.W. (1988) Lau Basin basalts (LBB): trace element and Sr-Nd isotope evidence for heterogeneity in backarc basin mantle. Earth Planet. Sci. Letters 90: 174.

Volpe A.M., Macdougall J.D., Lugmair G.W., Hawkins J.W., and Lonsdale P. (1990) Fine-scale isotopic variation in Mariana Trough basalts: evidence for heterogeneity and a recycled component in backarc basin mantle. Earth Planet. Sci. Letters 100: 251.

Wang Q-Q. and Gill J. (1990) Geochemistry of K-rich mafic rocks in NE China. IAVCEI (Mainz) Abs.

Widom E., Gill J., Schmincke H-U., and Collerson K.D. (1990) Th-Sr isotopic correlations: Sao Miguel, Azores. IAVCEI (Mainz) Abs.

Willams R.W., Murrell M.T., and Goldstein S.J. (1991) Large ^{231}Pa enrichments in neovolcanic MORB measured by mass spectrometry. EOS 72.

Helium Isotope Variations Along Mid-Ocean Ridges: Implications for Mantle Heterogeneity

David Graham

Dept. of Geological Sciences, University of California,
Santa Barbara, CA 93106

Helium isotope studies have made fundamental contributions to the fields of mantle geochemistry and dynamics. Perhaps the single most important discovery is that some ocean island basalts (OIB) have high $^3He/^4He$ ratios compared to the source regions for mid-ocean ridge basalts (MORB). Rare gas geochemists usually refer to these OIB sources as "less degassed". Because ^4He is produced by the radioactive decay of ^{238}U, ^{235}U and ^{232}Th, mantle regions which are more extensively degassed have preferentially lost helium relative to heavier, non gaseous elements; they therefore have higher time-integrated $(U+Th)/^3He$ ratios and have evolved to lower $^3He/^4He$ ratios. Some geochemists disagree with this idea however, often suggesting that He is somehow "decoupled" from other, long-lived isotopic systems within the mantle, either by fluid-hosted metasomatism or because helium is a more *compatible* element than U and Th. If these arguments are correct, He will not be as reliable a tracer as Sr, Nd or Pb. Two lines of evidence from helium isotopes in MORB contradict the decoupled argument; 1) the presence of systematic relations between $^3He/^4He$ and $^{87}Sr/^{86}Sr$, and 2) an inverse correlation between local spreading rate and the variance of $^3He/^4He$ along mid-ocean ridge segments. These observations have implications for the origin and scale of heterogeneities in the upper mantle.

MORB are characterized by $^3He/^4He$ ratios between R/R_A = 6-9 (R_A = atmospheric ratio of $1.39x10^{-6}$). The fact that $^3He/^4He$ ratios are higher than the atmospheric ratio is unambiguous evidence that juvenile volatiles (i.e., volatiles which have never been at the Earth's surface) are still being released from the Earth's interior. Some hotspot volcanoes (such as those in the Hawaiian island chain, in Iceland and at Réunion Island) have $^3He/^4He$ ratios considerably higher than MORB values (R/R_A up to 32). Other hotspot volcanoes, such as those of Tristan da Cunha and Gough Island in the South Atlantic, have more radiogenic $^{87}Sr/^{86}Sr$ and $^3He/^4He$ than MORB.

Considering all MORB except those in the proximity of high $^3He/^4He$ hotspots (Iceland, Réunion and Bouvet), there is clearly a global, negative trend between $^3He/^4He$ and $^{87}Sr/^{86}Sr$ (Fig. 1). The He-Sr relation indicates that $^3He/^4He$ variations in the upper mantle are the result of ancient fractionation (> 1Ga) of $(U+Th)/^3He$. It also suggests the worldwide presence in the MORB source region (upper mantle) of chemical heterogeneities that are more radiogenic in both He and Sr. The global trend is reinforced by variations along individual ridge segments, such as within the Australian-Antarctic Discordance (Fig. 1). Furthermore, the coupled behavior of He and Sr isotopes suggests that in a time-integrated sense, He is more incompatible relative to U and Th, in a manner similar to the behavior of Rb relative to Sr.

There appears to be an increase in $^3He/^4He$ ratio with spreading rate, although a definable trend is at the limit of being statistically significant (Table 1; Fig. 2a). The spreading rate-weighted mean $^3He/^4He$ ratio is ~8.0 R_A. The variability in $^3He/^4He$ ratio (represented by the standard deviation of the population) along individual ridge segments increases with decreasing spreading rate (Fig. 2b). Similar observations have been made with respect to Sr isotopes [9-12]. Much of the change in variability occurs at slower spreading ridges, so that the observed trend is not formed simply by including samples from the fastest spreading ridges. There is no relationship between skewness (γ) and spreading rate (Table 1), and most of the populations are gaussian ($\gamma \equiv 0$). The data set used here only represents a first order, crude attempt to investigate possible trends; for example, the respective ridge segments have been treated equally despite different length scales. This means that with a more detailed analysis some groupings should be reduced even further; e.g., ridge segments opposite St. Helena and Tristan da Cunha in the South Atlantic show distinct isotope characteristics related to those off-axis hotspots [3].

It is noteworthy that small, near-axis seamounts from the East Pacific show a large diversity in isotopic compositions, including He [13], adjacent to ridges where the isotopic

variance is the least (Fig. 2). This supports the idea that some of the signal observed in helium isotopes along ridges is related to processes of melt generation and migration, as reflected by differences in spreading rate (or magma production rate). However, the observation that some ridge segments, in particular the AAD, do not follow the overall trend of average $^3He/^4He$ vs. spreading rate (Fig. 2a) displayed by most other segments is significant; it indicates that long-wavelength (>100 km) He isotope characteristics (e.g., the DUPAL anomaly) are largely produced by mantle source differences, and not by variability in melt generation processes acting upon a uniform distribution of upper mantle heterogeneities.

The above observations indicate that the upper mantle source of MORB is isotopically variable on a scale comparable to the scale of magma generation. These heterogeneities are globally dispersed and are usually more radiogenic in He and Sr. The heterogeneities may have their origin as reinjected crustal or lithospheric materials, which were isolated outside the upper mantle convective flow for long time periods (>1 Ga). The heterogeneities are more readily sampled by volcanism where magma production rates are low. This may result either because the processes of magma genesis (and/or mixing within magma chambers) are less efficient at averaging mantle compositions in those regions, or because lower spreading rates intrinsically reflect an increased abundance of small scale radiogenic "blobs" in the upper mantle, perhaps caused by more numerous plumes (or enriched OIB sources).

References

[1] Poreda, R., J.-G. Schilling and H. Craig (1986) Helium and hydrogen isotopes in ocean-ridge basalts north and south of Iceland. Earth Planet. Sci. Lett. 78, 1-17.

[2] Kurz, M. D., W. J. Jenkins, S. R. Hart and J.-G. Schilling (1982) Helium isotopic variations in the mantle beneath the central North Atlantic Ocean. Earth Planet. Sci. Lett. 58, 1-14.

[3] Graham, D. W., M. D. Kurz and W. J. Jenkins, J.-G. Schilling, G. Thompson and S. E. Humphris (1991) He isotope geochemistry of the South Atlantic. 2. MORB from 1°N-47°S. Earth Planet. Sci. Lett..

[4] Mahoney, J. J., J. H. Natland, W. M. White, R. Poreda, S. H. Bloomer, R. L. Fisher and A. N. Baxter, (1989) Isotopic and geochemical provinces of the western Indian Ocean spreading centers. J. Geophys. Res. 94, 4033-4052.

[5] Kurz, M.D., (1982) Helium isotope geochemistry of oceanic volcanic rocks: implications for mantle heterogeneity and degassing. PhD. Diss., MIT/WHOI.

[6] Graham, D. W., J. E. Lupton, E. M. Klein, D. Christie and D. Pyle (1990) Helium isotope geochemistry of the Australian-Antarctic Discordance. Geol. Soc. Australia 27, 41.

[7] Graham, D. W., R. Batiza and G. Thompson (1991) Helium isotope geochemistry of the Lamont Seamounts and the adjacent East Pacific Rise: implications for melt generation beneath mid-ocean ridges. in preparation.

[8] Lupton, J. E., Helium isotope variations in Juan de Fuca Ridge basalts. EOS 63, 1147, 1982.

[9] Cohen, R. S. and R. K. O'Nions (1982) The lead, strontium and neodymium isotopic structure of ocean ridge basalts. J. Petrol. 23, 253-279.

[10] Batiza, R. (1984) Inverse relationship between Sr isotope diversity and rate of oceanic volcanism has implications for mantle heterogeneity. Nature 309, 440-441.

[11] Allègre, C. J., B. Hamelin and B. Dupré (1984) Statistical analysis of isotopic ratios in MORB: the mantle blob cluster model and the convective regime of the mantle. Earth Planet. Sci. Lett. 71, 71-84.

[12] Holness, M. B. and F. M. Richter (1989) Possible effects of spreading rate on MORB isotopic and rare earth composition arising from melting of a heterogeneous source. J. Geol. 97, 247-260.

[13] Graham, D. W., A. Zindler, M. D. Kurz, W. J. Jenkins, R. Batiza and H. Staudigel (1988) He, Pb, Sr and Nd isotope constraints on magma genesis and mantle heterogeneity beneath young Pacific seamounts. Contrib. Mineral. Petrol. 99, 446-463.

Table 1

Mean, standard deviation and skewness for $^3He/^4He$ along mid-ocean ridges

Location	Spreading Rate (mm/y)	n	$^3He/^4He$ (R/R_A)	σ	γ	Data Sources
Kolbeinsey Ridge	18	5	11.04	0.67	0.22	1
Mohns Ridge	18	5	7.40	0.55	0.34	1
Reykjanes Ridge	19	17	13.90	1.71	-0.17	1
MAR 33-50°N	26	27	7.67	0.55	-0.16	2
MAR 2-47°S	38	46	7.88	0.54	-0.06	3
SW Indian Ridge	16	9	7.58	0.71	-0.48	4
Central Indian Ridge	50	10	8.28	0.54	-0.27	4,5
Carlsberg Ridge	58	5	8.44	0.26	-0.85	5
Austr-Ant Discordance	74	23	7.20	0.29	-1.16	6
Galapagos SC	64	5	7.93	0.52	-1.05	5
EPR 10-12°N	110	18	8.44	0.15	0.20	7
EPR 23°N	120	3	8.34	0.07	0.31	5
Juan de Fuca Ridge	60	18	8.21	0.35	0.07	8
Bouvet TJ	17	9	9.04	2.73	0.92	5

Uncertainties in spreading rate are typically ±10%.

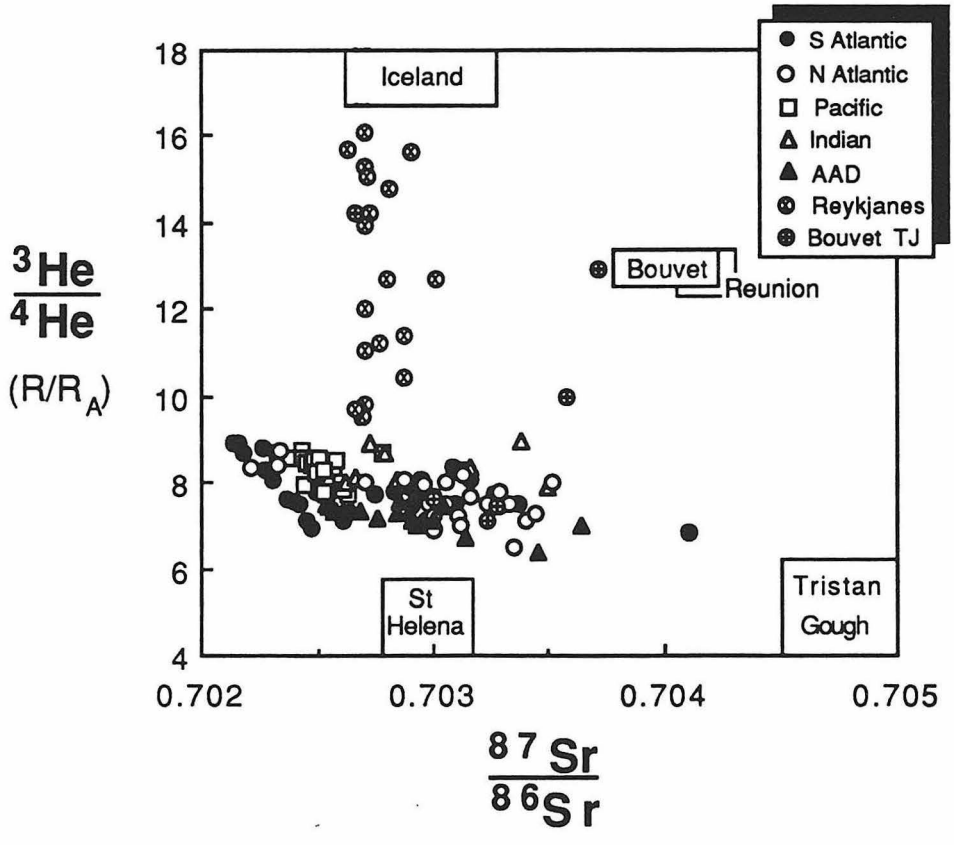

Figure 1. $^3He/^4He$ - $^{87}Sr/^{87}Sr$ diagram for mid-ocean ridge basalts and selected ocean islands. Data form an overall negative trend when ridge segments near the high $^3He/^4He$ hotspots of Iceland, Bouvet and Réunion are excluded.

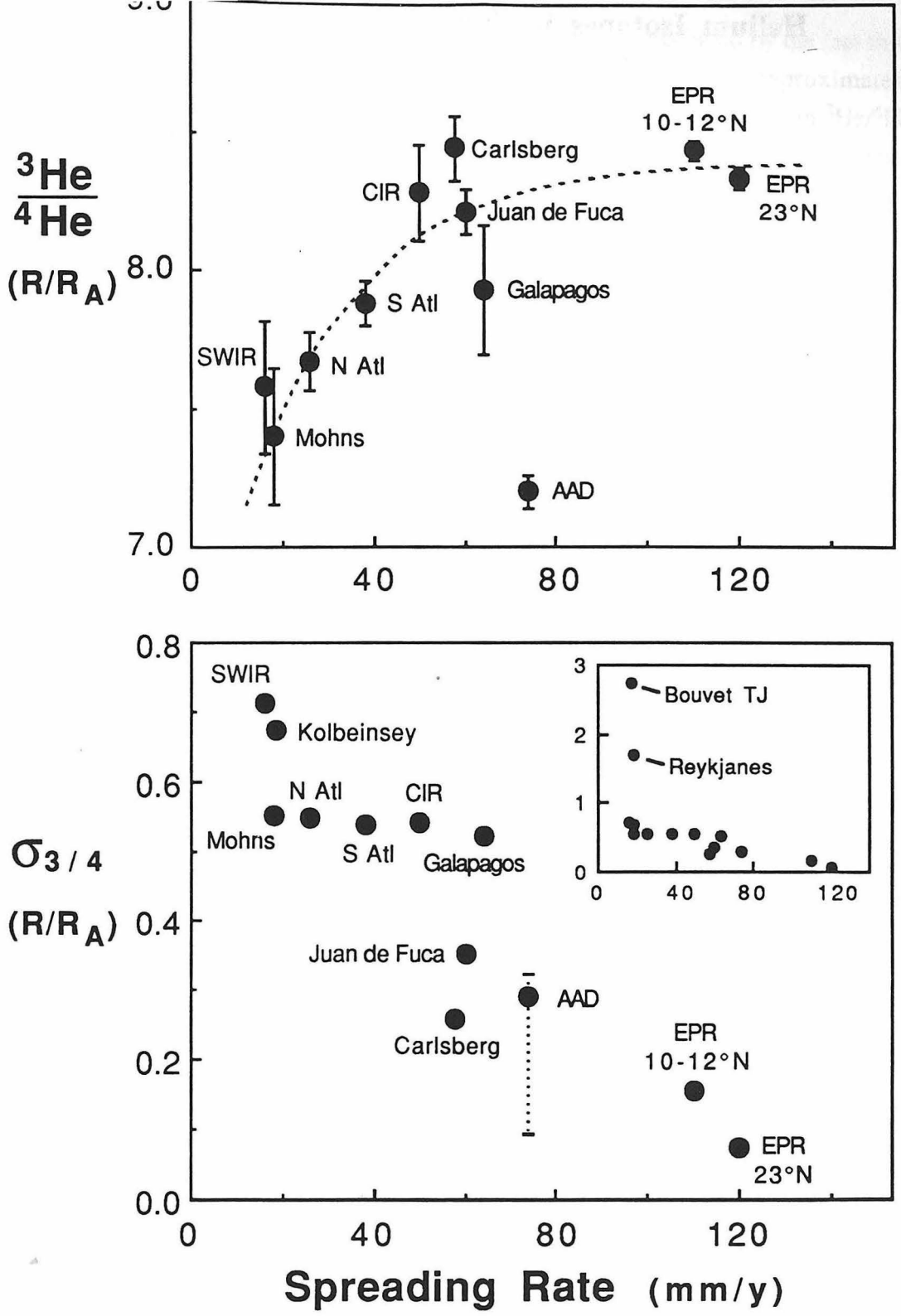

Figure 2. a. Mean $^3He/^4He$ vs. spreading rate for different ridge populations, excluding areas near high ^3He hotspots. Uncertainties are $\pm\sigma/\sqrt{n}$. b. Standard deviation of $^3He/^4He$ vs. spreading rate. Range shown for AAD depicts subgroups with "Pacific" and "Indian" characteristics.

Helium Isotopes in Submarine Tholeiitic Basalts from the Island of Hawaii

David Graham, John Lupton and Michael Garcia[1]

Dept. of Geological Sciences, University of California,
Santa Barbara, CA 93106

1. Hawaii Institute of Geophysics, University of Hawaii,
Honolulu, HI 96822

The variability of helium isotopes at ocean island volcanoes is of fundamental interest to volcanologists and geochemists. Because ^3He is one of the best tracers of primordial mantle material, variations in $^3He/^4He$ ratio are sensitive indicators of processes which accompany ocean island volcanism, such as mixing of magmas and/or source materials, assimilation and outgassing.

We have performed analyses of $^3He/^4He$, and He and Ne contents for a suite of tholeiitic basalts dredged from the submarine rift zones of Hawaii. Dredge locations are shown in Figure 1. Gases were released by melting basalt glass, or by *in vacuo* crushing of either glass or olivine phenocrysts separated by hand-picking under a microscope. These samples have been previously studied for major elements, volatile contents (water, chlorine and sulfur) and oxygen and hydrogen isotopes [Garcia et al., 1989], providing a good geochemical and petrologic framework within which to compare the helium results.

Elevated $^3He/^4He$ ratios of 10-28 R_A (R_A = atmospheric ratio of 1.39×10^{-6}) are observed in the studied samples, with the exception of one sample from Kohala which has a value of 7.9 R_A. The $^3He/^4He$ ratios reported here are in the range of previously reported values in the cases of Loihi Seamount, Kilauea and Mauna Loa, and are higher in the cases of Mauna Kea and Hualalai. Previous helium analyses of Kohala are unavailable.

Magmatic signatures are clearly present in all the samples analyzed, but not in all the phases. At Loihi, R/R_A ranges between 21.4-27.8 in three samples analyzed. At Kilauea and Mauna Loa, R/R_A ranges between 14.2-17.3 and 14.3-15.8, respectively, with typical glass He concentrations of $\sim 10^{-7}$ cc/g. One olivine-glass pair from Kilauea and three pairs from Mauna Loa display He isotopic equilibrium (Fig. 2). In contrast, glass samples from Mauna Kea, analyzed both by crushing and melting, have much lower $^3He/^4He$ ratios of 1.5-9.1 R_A and much lower He contents of $<5 \times 10^{-9}$ cc/g. However, helium released by crushing olivine phenocrysts from these same samples has R/R_A between 11.6-14.3 (Fig. 2), and the He contents are typically a factor of 4 to 5 higher than the He contents of the coexisting glasses. This indicates that while the Mauna Kea glasses have apparently been compromised for helium by outgassing, the magmatic signature has been preserved in the Mauna Kea olivines. Since the glasses have δD between -61 to -88 per mil (within the range of mantle values), assimilation of seawater-altered wallrock or post-eruptive alteration are unlikely to be responsible for the lower $^3He/^4He$ ratios. The timescale for radiogenic ingrowth to produce the glass-olivine disequilibrium is $\sim 10^4$-10^5 y. This timescale is too long to

be realistically associated with magma storage times, and is also precluded by the fact that mm-size olivines at magmatic temperatures reequilibrate with host melts on approximately decade timescales. Therefore, the most likely cause for the glass-olivine disequilbrium in $^3He/^4He$ appears to be efficient degassing of the magma upon eruption, followed by significant post-eruptive radiogenic ingrowth in the quenched glasses.

At Hualalai we have measured $^3He/^4He$ ratios between 19.6-19.9 R_A, and one olivine-glass pair shows He isotopic equilibrium (Fig. 2). No suitable glass was recovered from Kohala, but olivines from this volcano range between 7.9-13.2 R_A (Fig. 3). The single sample from Kohala with $^3He/^4He$ of 7.9 R_A is the only *tholeiite* from a Hawaiian volcano which has a $^3He/^4He$ ratio in the MORB range, other than lavas younger than 8,000 years from Mauna Loa [Kurz et al., 1987; 1990]. This finding is consistent with a temporal change toward MORB-like values (diagnostic of asthenospheric and/or lithospheric sources), for a very short time period, during the tholeiitic phase of Hawaiian volcanism [Kurz et al., 1987]. Our helium results also confirm the hypothesis that $^3He/^4He$ ratios higher than MORB values were present during the tholeiitic stage of development at all the volcanoes on the island of Hawaii.

Collectively, all the helium results to date for the subaerial Hawaiian volcanoes (Fig. 3) show minimal overlap (or none) with Loihi Seamount basalts (20-32 R_A). This emphasizes the importance of sampling the early submarine stages of island volcanism in order to obtain a representative and accurate picture of mantle plume characteristics.

References

Craig, H. and J. E. Lupton (1976) Primordial neon, helium and hydrogen in oceanic basalts. Earth Planet. Sci. Lett. 31, 369-385.

Garcia, M. O., D. W. Muenow, K. E. Aggrey and J. R. O'Neil (1989) Major element, volatile and stable isotope geochemistry of Hawaiian submarine tholeiitic glasses. J. Geophys. Res. 94, 10,525-10,538.

Kaneoka, I. and N. Takaoka (1978) Excess ^{129}Xe and high $^3He/^4He$ ratios in olivine phenocrysts of Kapuho lava and xenolithic dunites from Hawaii. Earth Planet. Sci. Lett. 39, 382-386.

Kaneoka, I., N. Takaoka and D. A. Clague (1983) Noble gas systematics for coexisting glass and olivine crystals in basalts and dunite xenoliths from Loihi Seamount. Earth Planet. Sci. Lett. 66, 427-437.

Kurz, M. D., W. J. Jenkins, S. R. Hart and D. Clague (1983) Helium isotopic variations in volcanic rocks from Loihi Seamount and the Island of Hawaii. Earth Planet. Sci. Lett. 66, 388-406.

Kurz, M. D., M. O. Garcia, F. A. Frey and P. A. O'Brien (1987) Temporal helium isotopic variations within Hawaiian volcanoes: basalts from Mauna Loa and Haleakala. Geochim. Cosmochim. Acta 51, 2905-2914.

Kurz, M. D., D. Colodner, T. W. Trull, R. B. Moore and K. O'Brien (1990) Cosmic ray exposure dating with in situ produced ^3He: results from young Hawaiian lava flows. Earth Planet. Sci. Lett. 97, 177-189.

Rison, W. and H. Craig (1983) Helium isotopes and mantle volatiles in Loihi Seamount and Hawaiian Island basalts and xenoliths. Earth Planet. Sci. Lett. 66, 407-426.

Torgersen, T. and W. J. Jenkins (1982) Helium isotopes in geothermal systems: Iceland, The Geysers, Raft River and Steamboat Springs. Geochim. Cosmochim. Acta 46, 739-748.

Vance, D., J. O. H. Stone and R. K. O'Nions (1989) He, Sr and Nd isotopes in xenoliths from Hawaii and other oceanic islands. Earth Planet. Sci. Lett. 96, 147-160.

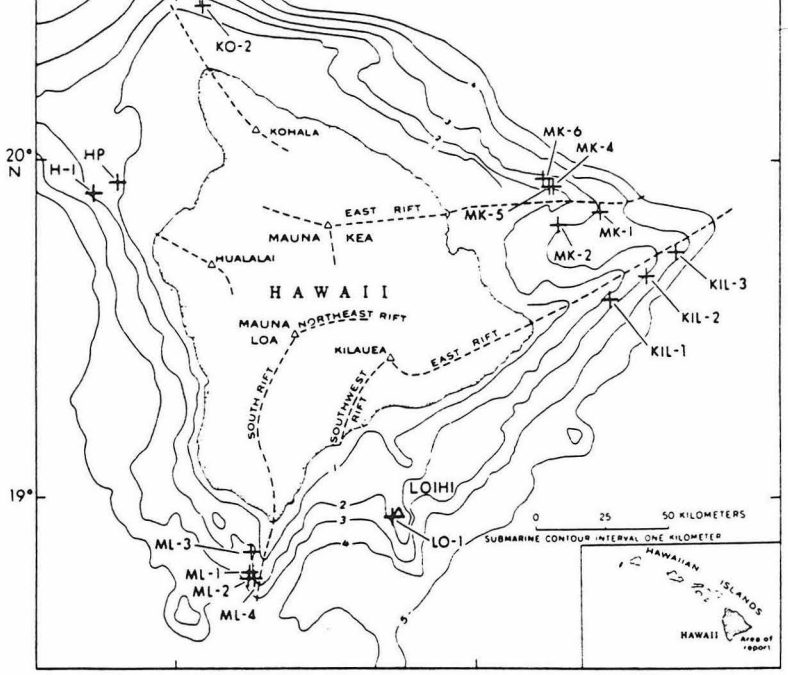

Figure 1. Map showing the five volcanoes that comprise the island of Hawaii, and Loihi Seamount. The summit of each volcano is marked by a triangle, and dredge haul locations are marked by crosses.

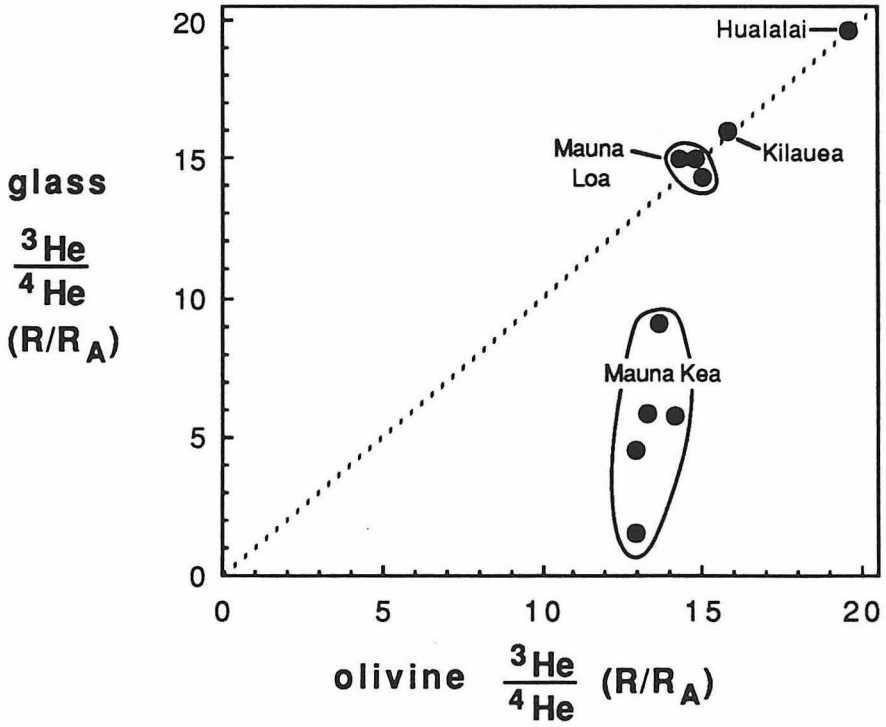

Figure 2. Comparison of helium isotope measurements in glasses and olivines from the same samples. Kilauea, Mauna Loa and Hualalai samples all display helium isotopic equilibrium between olivine and glass. However, 5 samples from Mauna Kea all show much lower $^3He/^4He$ in the glass compared to the olivines, suggesting that the magmatic signature in the Mauna Kea glasses has been compromised.

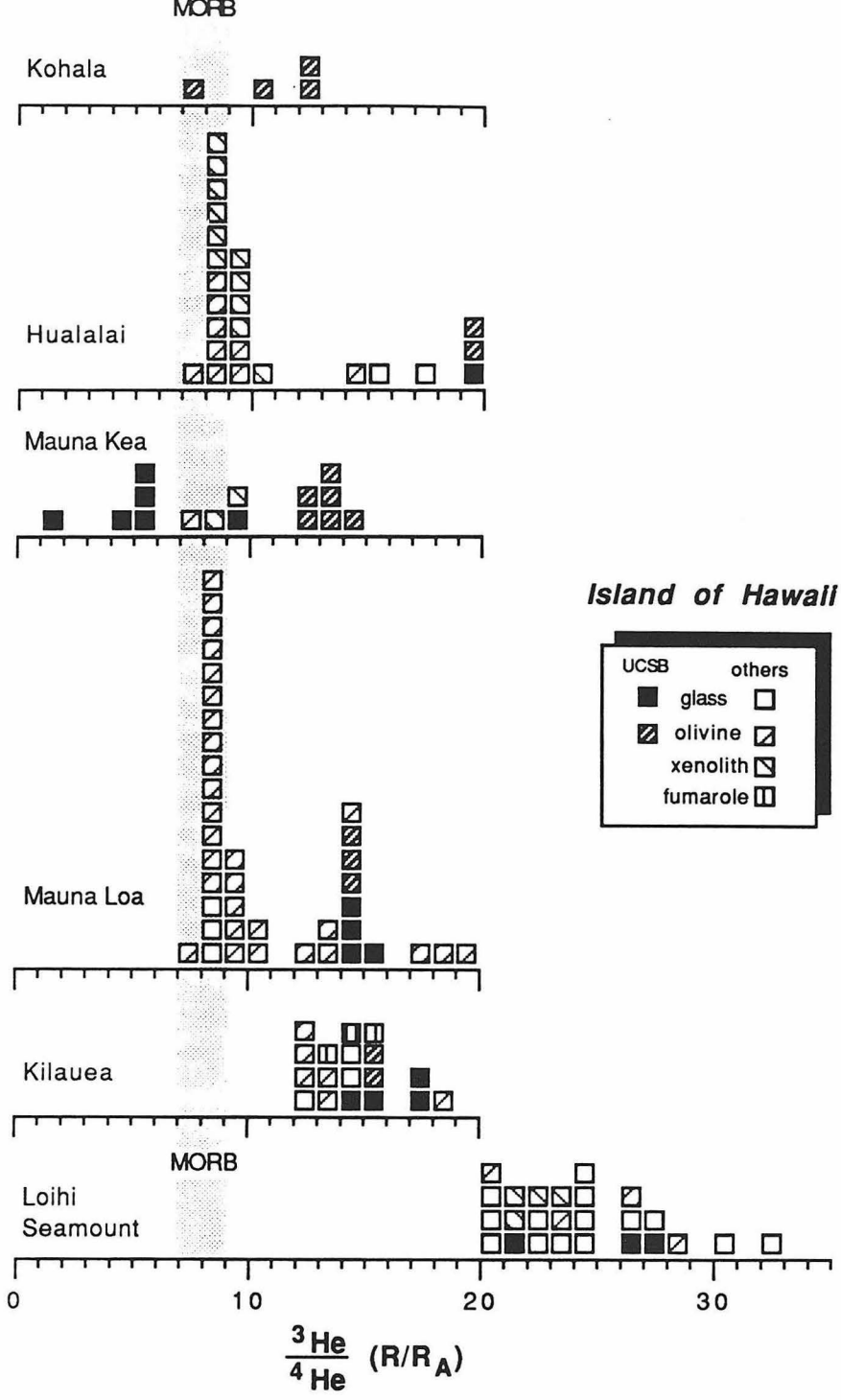

Figure 3. Histograms summarizing helium isotope measurements for Hawaiian volcanoes. Both tholeiitic and alkalic basalts are shown, along with data for xenoliths and for fumaroles. The only *tholeiites* with $^3He/^4He$ ratios in the MORB range are lavas from Mauna Loa that are younger than 30,000 years old, and a single sample from Kohala. Also, there appears to be no overlap of $^3He/^4He$ ratios for the 5 Hawaiian volcanoes with those for Loihi Seamount. Data are from the present study, and from Craig and Lupton (1976), Kaneoka and Takaoka (1978), Kaneoka et al. (1983), Kurz et al. (1983, 1987, 1990), Rison and Craig (1983), Torgersen and Jenkins (1982) and Vance et al. (1989).

Plumes, fossil plumes, pseudo-plumes and the Cameroon line.

Alex N. Halliday[1], J. Godfrey Fitton[2] and D.C. Lee[1]

[1]Department of Geological Sciences, University of Michigan, Ann Arbor, MI 48109-1063, U.S.A.

[2]Department of Geology and Geophysics, University of Edinburgh, Edinburgh, EH9 3JW, U.K.

The formation, separation and migration of small melt fractions and fluids in the mantle, by whatever mechanism, may generate geochemical features that resemble plumes in terms of trace element enrichments and isotopic anomalies. In many instances of intraplate magmatism the role of plumes is far from clear. However the tectonic and isotopic constraints on models for the origin of the Cameroon line, west Africa, are unusually strong, facilitating its use as a window through which to view mantle processes.

The Cameroon line is a 1600 km long chain of volcanoes and plutons extending from the continental interior of Africa to the Atlantic island of Pagalu (formerly Annobon). The line has been difficult to explain with conventional models of intraplate magmatism. The lack of any systematic migration in the focus of magmatism over the 65 Myr history of the Cameroon line is evidence against the direct involvement of a plume in the normal sense. Furthermore some small volcanic centers such as the island of Principe, have remained fixed sites of episodically-active volcanism for over 30 Myrs. Some authors have attempted to explain the Cameroon line in purely tectonic terms. However the Cameroon line is not associated with extension, and models that explain the feature in terms of lateral shear fail to account for mantle melting. The line has consistently maintained its geometry, without deflection across lithospheric features such as faults, and the continent/ocean boundary, for 65 Myrs.

The fact that Cameroon line magmatism has been so long-lived, and the episodic nature of volcanism on Principe in particular, provide evidence that there must exist some system of self-sustaining deep magma conduits that preferentially channel upper mantle melt flow. These reactivated conduits of preferential flow may be self-sustaining. Presumably the egress of magma through the mantle transfers heat such that subsequent batches of magma find the path of earlier melts the easiest to follow.

Clearly there has to be some process that is responsible for the initiation of this preferential flow path. One suggested mechanism is based on the similarity in size and shape between the Cameroon line and the neighboring Benue Trough (Fitton, 1980, Earth Plan. Sci. Lett. 51, 132-8). Fitton argued that the Cameroon line may represent the late magmatic expression of a thermal anomaly emplaced in the upper mantle in the Cretaceous and associated with the formation of the Benue Trough. In this model the Benue Trough represents a failed arm of a triple junction centered on the present day Niger Delta, which finally resulted in the separation of South America and Africa in this location at ca 125 Ma. Fitton suggested that the African plate was displaced away from the original asthenospheric upwelling associated with this triple junction, such that magmas rising from the asthenosphere erupted to one side of the Benue Trough, forming the Cameroon line. While such a link between the Benue Trough and Cameroon line is tenuous, it is interesting to note that the triple junction in the vicinity of the Gulf of Guinea coincides with the location of the St. Helena hotspot at 125 Ma. A rising plume from a mantle source similar to that responsible for magmatism on St. Helena, may therefore have triggered the formation of the Gulf of Guinea and conceivably the subsequent Cameroon line magmatism.

Isotopic and chemical data provide additional constraints on models for the Cameroon line, and the role that plumes may have played in modifying the mantle in this region. The Cameroon line magmas are clearly not derived from mantle lithosphere in the normal sense, since the basaltic lavas are broadly similar in oceanic and continental sectors (Fitton and Dunlop, 1985, Earth Plan. Sci. Lett., 72, 23-38). Furthermore new data from ultramafic xenoliths from the Cameroon line reveal that at least the uppermost lithospheric mantle is isotopically distinct from the lavas (Lee et al., 1991, Eos, in press). Isotopic data also reveal changes in the source of magma components with time in the Cameroon line. For example the volcanic rocks on Principe display an increase in $^{206}Pb/^{204}Pb$ and become progressively more nepheline normative. Such temporal variations in isotopic compositions have been explained (Halliday et al., 1988, J. Petrol. 29, 181-211) in terms of a rising hotzone or plume from a source similar to that of St. Helena magmas, that was incorporated into a downward propagating lithosphere. In the early stages of magmatism the hot plume-derived magmas resulted in melting and assimilation of lithosphere. As the lithosphere cooled further and the magma conduits became progressively lined with plume-derived components the "pure" HIMU plume component was tapped without contamination. Such a model presents the problem of reconciling a large (>1,200 km) plume head with persistent and episodic outpourings of relatively small volumes of magma. The thermal effects of large plumes in the upper mantle are commonly thought to be flood basalt provinces and triple junctions, rather than minor episodic eruptions of small degree partial melts. However, large volume melting of plumes may only be a feature of those that reach very shallow (<100 km, say) depths. Therefore the Cameroon line plume head, if it exists, is most likely relatively cool, has been rising slowly and is located at sufficient depth for only small degrees of partial melting. It must also be shallow enough to be tectonically coupled with the lithosphere, such that the magma conduits are not so distorted as to prevent their rejuvenation.

The recent (<10 Ma) Cameroon line basalts display an increase in $^{206}Pb/^{204}Pb$ and $^{208}Pb/^{204}Pb$ but not $^{207}Pb/^{204}Pb$, with proximity to the continent / ocean boundary (Halliday et al., 1990, Nature, 347, 523-8). This is readily explained in terms of geographical source variations in U/Pb and Th/Pb, provided the fractionation is relatively recent, ^{235}U having a much shorter half life than both ^{238}U and ^{232}Th. These data provide important supporting evidence for *young* (of the order of 10^8 years or less) trace element fractionation in the upper mantle associated with the continental margin. The magnitude of U/Pb and Th/Pb fractionation required to generate the change in $^{206}Pb/^{204}Pb$ and $^{208}Pb/^{204}Pb$ over 125 Ma, the time when the margin formed, is of the order of 5. Such a fractionation can easily be produced by small degrees (*ca* 1%) of fractional melting.

A reasonable model to explain these observations is that a plume head, emplaced at 125 Ma, and instrumental in the formation of the continent/ocean boundary, became zoned in U/Pb and Th/Pb ratio. A plausible explanation for this is mantle enrichment by upward melt percolation through the plume head itself as it compacted following emplacement. This would produce an upper zone of enriched material, the U/Pb ratio of which would decrease away from the center, as a function of the thickness of the plume head through which melt percolation occurred.

Pb Isotopic Constraints on Mantle Geodynamics: Observations from The Iceland Hotspot and Zero Age MORBs

Barry B. Hanan
Baylor Brooks Institute for Isotope Geology
San Diego State University
San Diego, CA 92182

Spatial variations in isotopic and incompatible element ratios in hotspot oceanic-island basalts (OIBs) and mid-ocean ridge basalts (MORBs) have revealed mantle source heterogeneities and provided constraints on present day mixing processes between the asthenosphere MORB source and hotspot-plume material (Schilling, 1973; Hart et al., 1973; White and Schilling, 1978; Dupré and Allègre, 1980, 1983; Allègre et al., 1984; Hamelin et al., 1984; Schilling et al., 1985; Hanan et al., 1986; Hanan and Schilling, 1989; Dosso et al., 1991). Iceland is the type locality for a ridge centered hotspot. Thermal plumes, produced by instabilities from hot boundary layers in the mantle, have long been proposed as the ultimate cause of hotspot volcanism. Morgan (1971) visualized the plumes as a continuous flow of material rising (2m/yr) from the deep mantle. The Greenland-Iceland-Faeroe plateau and ridge represents a good opportunity to study the evolution of a ridge-centered mantle plume in time and space and to further understand the relationship between hotspots, mantle heterogeneity and mantle dynamics. Temporal $^{87}Sr/^{86}Sr$ and REE pattern variations in Iceland basalts have been interpreted as episodes of binary mixing where a LILE and radiogenic isotope enriched mantle plume was progressively more diluted by the surrounding LILE-depleted asthenosphere MORB mantle source as it rises (Schilling, 1973; O'Nions and Pankhurst, 1976; Schilling et al., 1982). We have tested this model with Pb isotopes from Iceland Tertiary basalts (Hanan and Schilling, 1990). The Pb Isotope data for Iceland Tertiary basalts from two distinct paleo-rift zones spanning 14.1-2.2 Ma and from the Reykjanes Ridge and Neovolcanic zones of Iceland (0.7-0 Ma) require 3-component mantle source mixing (Fig.1).

The components are the ^{206}Pb-rich plume, the ^{207}Pb-rich asthenosphere, and ^{208}Pb-rich continental derived lithosphere material (Fig. 1). Fixed mass proportions between the ^{207}Pb and ^{208}Pb components are observed at 4 distinct periods of time (14.1-13.7 Ma, 13.7-7.5 Ma, 7.5-2.2 Ma and 0.7-0 Ma) resulting in 4 distinct, but converging, mixing arrays that help in constraining the Pb isotopic composition of the ^{206}Pb-rich plume component. Apparently the Iceland plume source has supplied material of relatively constant Pb isotopic composition throughout Iceland's 15 my history.

The Iceland ^{206}Pb-rich plume component shows maximum influence at 7.5 Ma, coincident with a maximum in volcanic production rate on Iceland and along the Reykjanes Ridge (Fig. 2). The ^{208}Pb-rich component is kindred to that of the Hebridean lithospheric keel (Menzies et al., 1987). The ^{208}Pb-rich component has a maximum influence at 13.7 Ma and decreases thereafter (Fig. 2). High $^{3}He/^{4}He$ recorded in modern Iceland basalts suggests a plume derivation from the lower mantle (Kurz, 1982, 1985; Poreda, 1986). The observed cyclic Pb isotope variations observed for the Tertiary Iceland basalts suggest a model where a chain of blobs rich in ^{206}Pb rise through and interact with a ^{207}Pb-rich asthenosphere which may have been contaminated by some delaminated continental lithosphere during the opening of the N-Atlantic. Alternatively, entrainment of the ^{208}Pb-rich component could have taken place during ascent of the plume through the 670-km discontinuity where recycled continental material may have accumulated.

The spatial Pb isotopic variations observed in MORBs from the Atlantic, Indian and Pacific oceans can be modeled by mixing of 3-components. Like the Iceland Tertiary basalts they consist of a ^{206}Pb-rich component, the ^{207}Pb-rich asthenosphere, and a ^{208}Pb-rich continental lithosphere component. In Figure 3, only MORBs with $(La/Sm)_N \leq 0.75$ are used to define the trends. These MORBs would normally be considered to be derived from the so-called LILE depleted asthenosphere. The three trends converge close to the ^{206}Pb-rich Iceland plume component (Fig. 3). The distinguishing characteristic for the three distinct trends is that fixed mass proportions are observed between the ^{207}Pb-rich and ^{208}Pb-rich components while the ^{206}Pb-rich component, common to all three trends, appears to be of relatively fixed composition. The Indian ocean has the highest proportion of the ^{208}Pb-rich component, the Pacific has least, and the Atlantic is intermediate. The Pacific trend can be modeled as a binary mix of the ^{206}Pb-rich and ^{207}Pb-rich components alone. These observations are consistent with the idea that the upper mantle itself consists of different provinces that are perhaps related to different convective flow patterns (Hamelin and Allègre, 1985; Hanan et al., 1986; Klein et al., 1988. The MORB Pb isotope data suggests a model where the asthenosphere underlying the Atlantic and Indian oceans has been variably contaminated by a ^{208}Pb-rich continental lithosphere derived component. The origin for this background contamination of the MORB asthenosphere is obscure and may be due to more than one mechanism. For example, broad radial dispersion of ^{208}Pb-rich and/or ^{206}Pb-rich plume material into the asthenosphere (Hanan et al., 1986), or delamination and entrainment of continental lithosphere material as the continents move over the asthenosphere during ocean basin development (Hanan and Schilling, 1990; Hawkesworth et al., 1986).

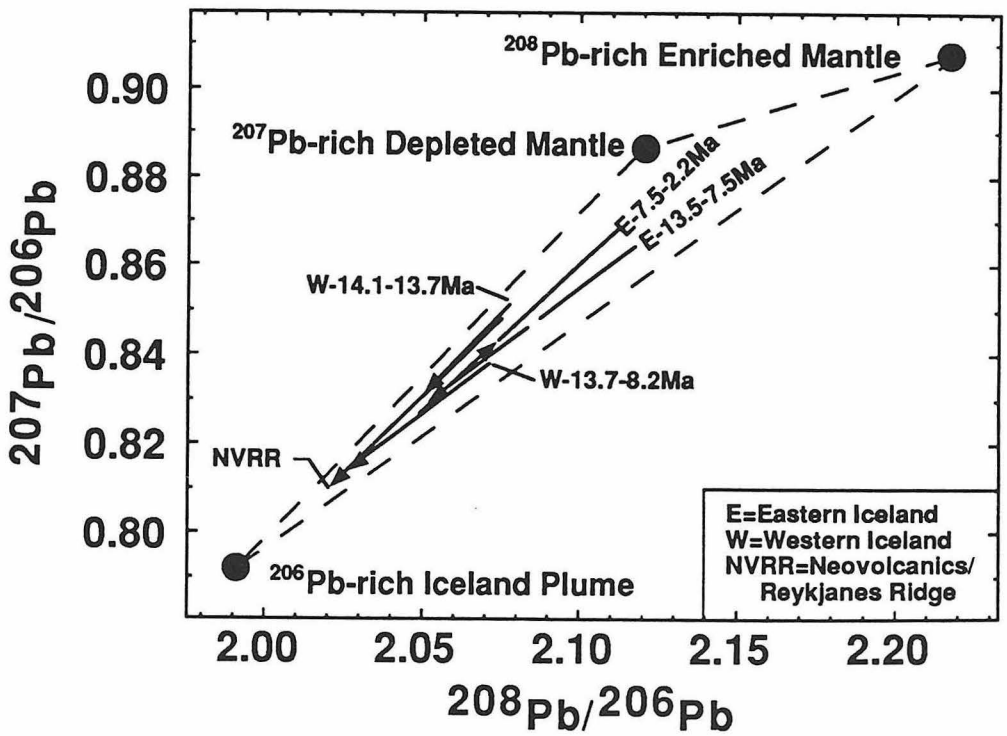

Figure 1. The three Pb isotope model endmembers were chosen so that they define a triangle that includes all of the Iceland Pb isotope data in Pb/Pb and relative ^{206}Pb-^{207}Pb-^{208}Pb isotopic space. The trends were determined by least squares linear regression of the Iceland Tertiary basalt data and the zero age data from the Reykjanes Ridge and Neovolcanic zones of Iceland (Sun et al., 1975; Sun and Jahn, 1975).

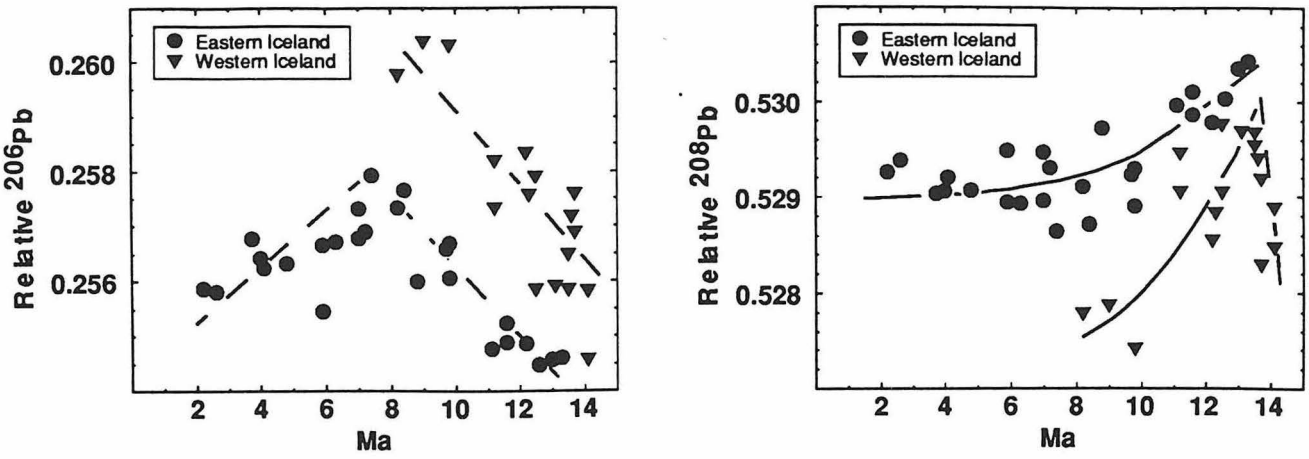

Figure 2 Relative Pb isotope temporal variation for the Iceland Tertiary basalts. The relative ^{208}Pb or $^{206}Pb = \{(^{208}Pb/^{204}Pb \text{ or } ^{206}Pb/^{204}Pb)\}/\{^{206}Pb/^{204}Pb + ^{207}Pb/^{204}Pb + ^{208}Pb/^{204}Pb\}$. The ^{206}Pb - rich Iceland plume component shows maximum influence at about 7.5 Ma. The ^{208}Pb-rich component has maximum influence at 13.7 Ma and decreases thereafter.

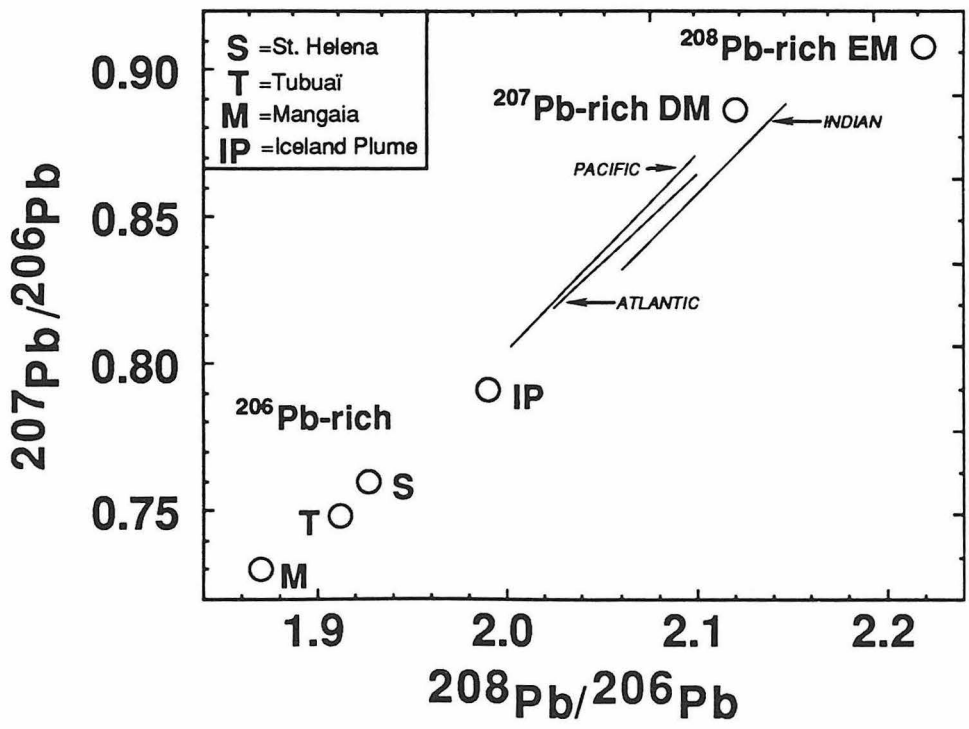

Figure 3. The trends were determined by least squares linear regression of data from Atlantic (Sun et al., 1975; Sun, 1980; Hanan et al., 1986; Dosso et al., 1991), Pacific (White et al., 1987; Hanan and Schilling, 1989), and Indian (Price et al., 1986; Michard et al., 1986; Ito et al., 1987; Dosso et al., 1987; Dupré et al., 1988) ocean MORB with $(La/Sm)_N \leq 0.75$. IP, EM, and DM are the same as shown in Fig.1. The averages for St. Helena, Tubuaï, and Mangaia are from Hart (1984).

REFERENCES CITED

Allègre, C.J. , Hamelin, B. and Dupré, B. (1984) Statistical analysis of isotopic ratios in MORB: the mantle blob cluster model and the convective regime of the mantle, Earth Planet. Sci. Lett. 71, 71-84.

Dosso, L., Hanan, B. B., Bougault,H. Schilling, J-G. and Joron, J-L. (1991) Sr-Nd-Pb Geochemical Morphology Between 10° and 17° North on the Mid-Atlantic Ridge: A New MORB Isotope Signature, submitted to EPSL.

Dupré, B. and Allègre, C.J. (1980) Pb-Sr-Nd isotope correlation and the chemistry of the N. Atlantic Mantle, Nature, 286, 17-22, 1980.

Dupré B. and C.J. Allègre(1983) Pb-Sr isotope variation in Indian Ocean basalts and mixing phenomena. Nature,303, 142-146.

Hamelin, B.H., B. Dupré and C.J. Allègre (1984) Pb-Sr isotopic variations along the EPR and MAR: A comparitave study, EPSL, 67, 340-350.

Hamelin, B. and C.J. Allègre (1985) Large scale regional units in the depleted upper mantle revealed by an isotope study of the South-West Indian Ridge, Nature, 315, 196-199.

Hanan, B. B. and Schilling, J-G. (1990) Dynamic Evolution of the Iceland Hot Mantle Plume: A Pb Isotope Perspective, Seventh International Conference on Geochronology, Cosmochronology and Isotope Geology, Canberra.

Hanan, B.B., Kingsley, R. H. and Schilling, J-G. (1986) Migrating ridge-hotspot interactions: Pb isotope evidence in the South Atlantic, Nature, 322, 137-144.

Hanan, B.B. and Schilling, J-G. (1989) Easter Microplate Evolution: Pb Isotope Evidence, J. Geophys. Res., 94, 7432-7448.

Hart, S.R., Schilling, J-G., and Powell, J.L. (1973) Basalts from Iceland and Along the Reykjanes Ridge:

Hart, S.R. (1984) A Large-Scale Isotope Anomaly in the Southern Hemisphere Mantle. Nature 309, 753-757.

Hawkesworth, C.J., Mantovani, M.S.M., Taylor, P.N. and Palacz, Z. (1986) Evidence from the Parana of south Brazil for a continental contribution to Dupal basalts. Nature 322, 356-359.

Klein, E. M., Langmuir, C. H., Zindler, A., Staudigel, H. and Hamelin, B. (1988) Isotope evidence of a mantle convection boundry at the Australian-Antarctic Discordance, Nature, 333, 623-629.

Kurz, M.D., Jenkins, W.J., Schilling, J-G., and Hart, S.R. (1982) Helium Isotopic Variations in the Mantle Beneath the Central North Atlantic Ocean. Earth Planet. Sci. Lett. 58, 1-14.

Kurz, M.D., Meyer, P.S., and Sigurdsson, H. (1985) Helium isotopic Systematics Within the Neovolcanic Zones of Iceland. Earth and Planet. Sci. Lett. 74, 291-305.

Menzies, M. A., Halliday, A. N., Palacz, Z., Hunter, R. H., Upton, B. G. J., Aspen, P. and Hawkesworth, C. J. (1987) Evidence from mantle xenoliths for an enriched lithospheric keel under the Outer Hebrides, Nature, 325, 44-47.

Morgan, W.J. (1971) Convection Plumes in the Lower Mantle. Nature 230, 42-43.

O'Nions, R.K. and Pankhurst, R.J. (1976) Petrogenic significance of isotope and trace element variations in volcanic rocks from the Mid-Atlantic, J. Petrology, 15, 603-634.

Poreda, R., Schilling, J-G., and Craig, H. (1986) Helium and Hydrogen Isotopes in Ocean-Ridge Basalts North and South of Iceland. Earth and Planet. Sci. Lett. 78, 1-17.

Schilling, J-G. (1973) Iceland Mantle Plume, Geochemical Evidence Along Reykjanes Ridge. Nature 242, 565-571.

Schilling, J-G., Meyer, P.S., and Kingsley, R.H. (1982) Evolution of the Iceland Hotspot. Nature 296, 313-320.

Schilling, J-G., G. Thompson, R. Kingsley and S. Humphris (1985) Hotspot - migrating ridge interaction in the South Atlantic. Nature 313, 187-191.

Sun, S-S. and Jahn, B. (1975) Lead and Strontium Isotopes in Post-Glacial Basalts from Iceland. Nature 255, 527-530.

Sun, S-S., Tatsumoto, M., and Schilling, J-G. (1975) Mantle Plume Mixing Along the Reykjanes Ridge Axis: Lead Isotopic Evidence. Science 190, 143-147.

Sun, S.S. (1980) Lead Isotopic Study of Young Volcanic Rocks from Mid-Ocean Ridges, Ocean Islands and Island Arcs. Phil. Trans. R. Soc. Lond. A297, 409-445.

White, W. M. and Schilling, J-G. (1978) The nature and origin of geochemical variation in Mid-Atlantic Ridge basalts from the Central North Atlantic, Geochim. et Cosmochim. Acta, 42, 1501-1516.

Plumes in Strongly Time-Dependent Convection: Effects from Depth-Dependent Properties and Thermal-Chemical Buoyancy

Ulrich Hansen, Institut fuer Geophysik Uni zu Koeln, D-5000 Koeln 41. F.R. Germany

David A. Yuen, Dept. of Geophysics and Geology and Minnesota Supercomputer Institute, University of Minnesota, Minneapolis, MN 55415

Conclusions and speculations about plumes which are presented in the following are mainly based on large-scale numerical computations:

Definition:

From a fluid dynamical point of view the expression "plumes" designate instabilities driven by density differences, emanating from boundary layers and having a "mushroom-" like appearance.

Origin:

Generally plumes can evolve in boundary layers of a system. Boundary layers are characterized by (almost) vanishing vertical velocities, i.e. by only diffusive transport of heat or concentration. No matter what the cause for the actual density difference of the plume is (thermal or compositional, phase boundary or combinations of there of), the presence of a boundary layer is required as a source region for a plume.

Evolution of plumes:

Under most simple circumstances, convection is driven by steady upwelling- and downwelling currents. Such currents display "plume characteristics" since they originate from boundary layer and they usually have a mushroom-like appearance. The vertical transport of heat and mass is governed mainly by such currents. From their size these currents are more comparable to ridges or subduction zones rather than to sharply localized features. We shall call this type of currents "master-plumes" indicating that they are driving a large scale circulation (L.S.C. in the following).

In the more realistic situation of strongly time dependent convection, instabilities of smaller scales evolve within the boundary layers of the flow. Their evolution is a result of a delicate balance between shear forces due to the L.S.C. and buoyancy forces with the boundary layer. Our calculations show that their fate is largely determined by the interaction of this smaller slave instabilities (SI's) with the L.S.C.(Hansen and Ebel, 1988; Hansen et al., 1990). The L.S.C. can bend the SI's or can even break them into several pieces, thus leading to a picture where a swarm of small patches can originate from one rising (or sinking) instability. Strongly time-dependent convection, typically characterized by the coexistence of "master plume" driving the L.S.C. and "slave-instabilities" driven by the L.S.C. can explain the broad variety in the characteristics of plumes by the immense richness of the dynamics of the flow. In this framework one need not to invoke a special source region or a special mechanism to explain the particular features of a plume. In other words: the difference between plumes may be only due to their different evolution histories and hence may not require any special type of reservoir.

The high Rayleigh number regime:

At Ra higher than about 5×10^7 plumes don't exist anymore for base-heated convection. Instead, disconnected droplet-like instabilities are observed (Hansen et

al.,1990). This change in the appearance of instabilities is connected with the transition to the regime of "hard turbulence." One definite conclusion is that mushroom-like plume structures, popularized today, did not exist at all in the early Earth.

Plumes in convection with depth-dependent properties:

Besides an increase of viscosity in the lower mantle, as has beeing expected for a long time, new laboratory results indicate a decrease of the coefficient of thermal expansivity α with depth and probably an increase in the thermal diffusivity χ. All those effects work in the same direction, i.e., they lower the thermal buoyancy or increase the dissipation, thus making convection more sluggish in the lower mantle. While, in constant property convection rising-depth-dependent properties are taken into account.

a) Decrease of the thermal expansivity (Anderson et al., 1990; Chopelas and Boehler, 1989). A decreasing α acts to concentrate the thermal buoyancy in the lower boundary layer within a few, strong upwellings. Conversely, the upper boundary layer still exhibits many instabilities which are drifting with the flow (Hansen, Yuen, Kroening, 1991). This leads to a configuration exhibiting almost stationary upwelling plumes in an otherwise strongly time dependent environment. While thermal anomalies of short wavelengths are present at the upper part, they disappeared from the lower mantle which is dominated by long wavelength anomalies.

Effects of depth-dependent viscosity:

An exponential increase of the viscosity with depth leads to almost the same "focussing" effect. Circulation patterns of larger aspects ratios, driven by strong upwellings are the result. A steplike increase of the viscosity, even three to four orders in magnitude, can not prevent instabilities from sinking into the lower or plumes form entering the upper mantle. Such effects are of purely transient character.

Plumes from a thermochemical boundary layer:

Thermochemical boundary-layers at the core-mantle boundary have been studied for a few years. Compositionally induced density differences can basically induce the following effects: a) they can enhance the thermally induced buoyancy or b) they can act in the opposite direction. Here, we discuss only the second case.

Plumes are able to escape from a thermochemical boundary layer if they can overcome the excess density which is due to the different composition. If plumes can escape they will deform the boundary layer (Hansen and Yuen, 1988; Hansen and Yuen, 1989a). They will also transport some of the chemically distinct material to the top. The ratio of themally induced driving- and compositionally induced restoring force is usually defined as (Rac: compositional rayleigh number) and is of paramount importance. In order to keep a dynamically supported topography on the CMB, R^{ρ} must neither be too low nor too high. In the case of the small R^{ρ}, the compositionally distinct layer would be immediately entrained by plumes in the lower boundary. If R^{ρ} is too high, plumes can not be formed. The dense layer would stay flat on the ground without being deformed (Hansen and Yuen, 1989a). We emphasize that there exists a narrow window for R^{ρ} within which plumes can be formed on the one hand, but do not entrain the dnese materials on the other. In order to derive an estimate, one must take into account every aspect which influences the buoyancy ratio R^{ρ} , namely the depth-variations of α and χ. Both factors lower the thermal buoyancy and do therefore shoft the optimal window for R^{ρ} towards lower values (Hansen and Yuen, 1989a). Besides the depth dependence of the material properties the mode of heating influences the window width for R^{ρ} . A substantial amount of internal heating leads to less

concentrated buoyancy in the lower boundary layer and therefore acts stabilizing on the dense layer. Like the depth dependent properties, it will lower the values for R^{ρ}

It has been shown that the type of boundary condition for the compostion at the bottom is extremely important (Hansen and Yuen, 1989b). Assuming that the dense layer is not recharged, either by subduction or by reaction between core and mantle, we obtain higher values of R^{ρ} required to prevent the layer from being immdeiately entrained. In this case values of R^{ρ} less than one may be sufficient to keep a chemically distinct layer, which is dynamically deformed at the bottom of the mantle.

Anderson, O.L., Chopelas A and R Boehler. Thermal expansivity versus pressure at constant temperature: a re-examination. Geophys. Res. Lett. 17,685-688, 1990.

Chopelas, A. and R. Boehler, Thermal expansion measurements at very high pressure, systematics and a case for a chemically homogeneous mantle. Geophys. Res. Lett., 16, 1347-1350, 1989

Hansen, U. and A. Ebel, Time dependent thermal convection-a possible explanation for a multiscale flow in the earth's mantle, Geophys. J., 94, 181-191, 1988.

Hansen, U. and D.A. Yuen, Numerical simulations of themal-chemical instabilities at the core-mantle boundary, Nature, 334, 237-240, 1988.

Hansen, U. and D.A. Yuen, Dynamical influences from thermal-chemcial instabilities at the core-mantle boundary, Geophys. Res. Lett. 16, 629-632, 1989a.

Hansen, U. and D.A. Yuen, Subcritical double diffusive convection at infinete Prandtl number, Geophys. Astrophys. Fluid Dynamics, 199-224, 1989b.

Hansen, U., Yuen, D.A. and S.E. Kroening, Transition to hard turbulence in thermal convection at infinite Prandtl number, Phys. Fluids A2 (12) 2157-2163, 1990.

Hansen, U., Yuen, D.A. and S.E. Kroening, Effects of depth dependent thermal expansivity on mantle circulation and lateral thermal anomalies, Geophys. Res. Lett., in press, 1991.

MANTLE PLUMES: INTERPRETING THE ISOTOPIC RECORD
(and other arcane pursuits)

Stan Hart
Woods Hole Oceanographic Institution
Woods Hole, MA 02543

The ZH isotopic taxonomy of oceanic basalts results in the identification of at least four mantle components (reservoirs), termed DMM, EM I, EM II and HIMU by Zindler and Hart (1986). These mantle components are mixed in various combinations to produce the observed isotopic variations in oceanic basalts. Fig. 1 shows the tetrahedron defined by these four end members in 3-D isotopic space, with the presently available Sr, Nd and Pb data set for 573 oceanic basalts plotted in the 87/86 Sr, 143/144 Nd and 206/204 Pb coordinate system. Inclusion of 207/204 Pb and 208/204 Pb would expand the dimensionality to five, or even 6 if 176/177 Hf is considered (for which only a limited data set exists, however). In n-dimensional space, the polygon containing the fewest vertices (n+1) is a simplex, and the oceanic data set would therefore require 6 or 7 end members to completely define it. Principal component (PC) analysis of this data set shows that the first three principal components account for 97% of the variance of the data set (Oschmann, 1991), a result in agreement with earlier work by Allegre *et al.* (1987) on a smaller data set. The clear implication is that the four end-members defined above are a sufficient description of the oceanic isotopic data set.

Fig. 1 shows progressive "viewpoints" of the data set, as the tetrahedron is rotated fore and aft. The view looking "edge on" into the DMM–EM I–HIMU base triangle shows that much of the data is clustered in, and just above, this plane (this plane is close in orientation to the "mantle plane" defined by Zindler *et al.*, 1982). This feature is borne out by the PC analysis, which shows that 94% of the variance is accounted for by just the first two eigenvectors. We will therefore use the view looking down onto the DMM–EM I–HIMU base triangle in our discussion of oceanic data arrays, mixing processes, etc. On a global scale, the DMM end-member is quite homogeneous (Ito *et al.*, 1987); for example, Atlantic and Pacific N-MORB have indistinguishable average values of Sr, Nd and 206/024 Pb (0.70260, 0.51316 and 18.40). Indian Ocean MORB are distinguishable from Atlantic and Pacific MORB, but still quite similar (0.70292, 0.51306 and 17.970). There appears to be little doubt that the DMM end-member is a reservoir, and that this reservoir is the upper-most mantle. In contrast to DMM, the other three end-members are strongly regionalized on a global scale, with the "purest" (most extreme) representatives of all three being confined to the DUPAL anomaly belt (approximately lying between the equator and

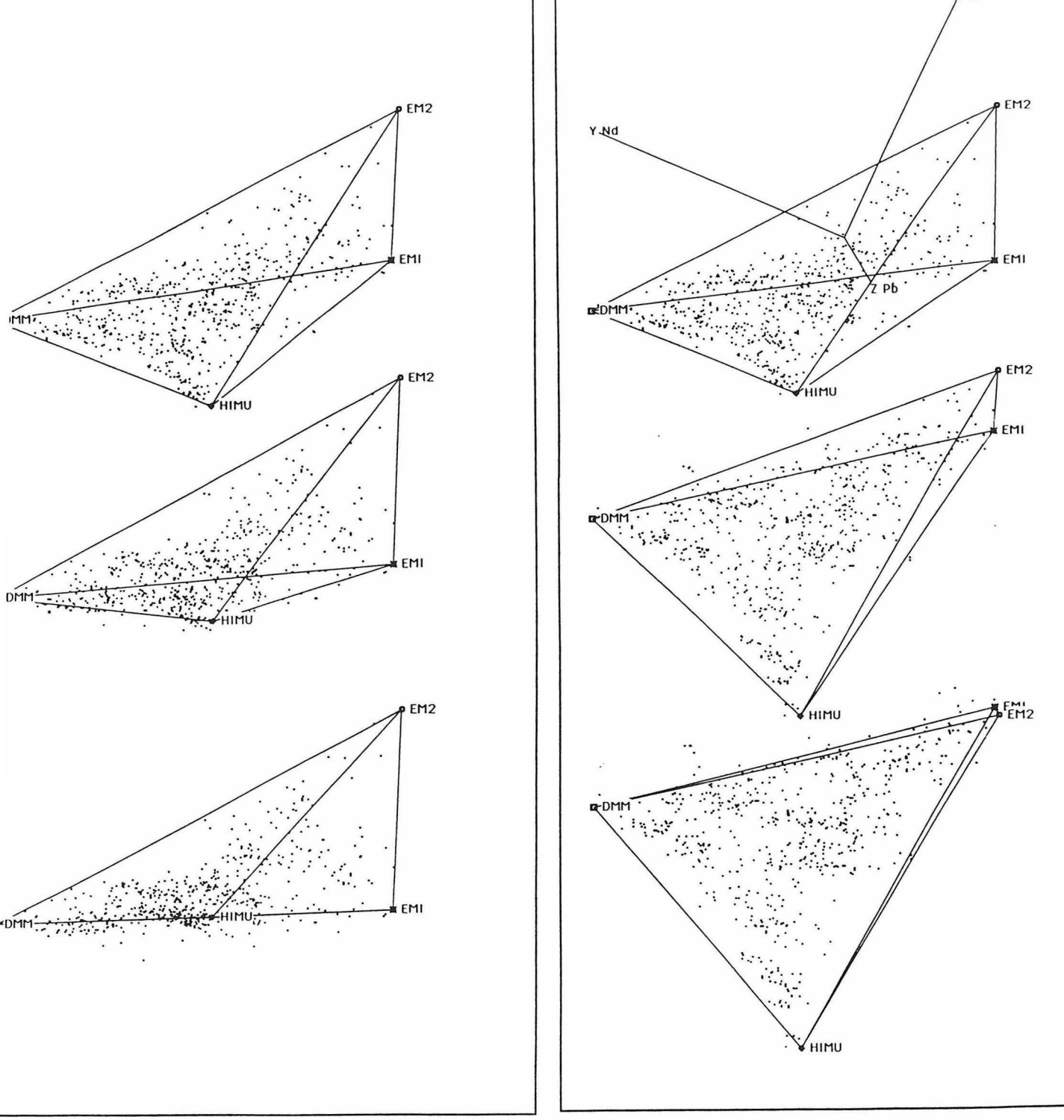

Fig. 1: Various "views" of the tetrahedron defined by the four mantle end members of Zindler and Hart (1986): DMM (depleted MORB mantle, HIMU (high U/Pb mantle), EMI (enriched mantle 1) and EM2 (enriched mantle 2). There are 477 OIB (oceanic island basalt) and 96 MORB (mid-ocean ridge basalt) plotted in terms of 87/86 Sr, 143/144 Nd and 206/204 Pb; these three coordinate axes are shown in the top "view." The left panel shows the tetrahedron as it is rotated back, demonstrating that a large fraction of the analyses plot near the base triangle (or

50°S). Polar regions appear to be free of significant EM I or EM II signatures; the south polar region is characterized by a significant HIMU signature.

As pointed out by Hart (1984, 1988) and Castillo (1988), the DUPAL anomaly belt shows a very convincing correlation (at low degree) with the geoid, the low velocity regions in the lower mantle, and the velocity anomalies in the core–mantle boundary layer (D"). I take this correlation as strong evidence for a lower mantle source/storage area for the DUPAL components, and thus as strong evidence that plumes originate from the core–mantle boundary (CMB) layer. Various considerations of the isotopic nature of the DMM, EM I and HIMU end members suggest that the relative concentrations of Sr, Nd, Pb and Hf in these mantle components are similar (30 to 50%), and that the relative abundances of Sm, U and Th in EM I and DMM are similar to the above as well, to within 10-20%. This agrees with the relative elemental abundances observed in basalts derived from these mantle reservoirs, and argues that these reservoirs cannot be radically different from each other in bulk (major element) composition (and therefore cannot be very different in intrinsic density). Plumes must therefore be driven by thermal, not compositional, buoyancy.

If thermal buoyancy drives plumes, their thermal entrainment of, and mixing with, the surrounding mantle may be important. Simple thermal modelling of plumes (for thermal contrasts of 300°K and viscosity contrasts of 10^2 - 10^3) suggests that plumes smaller than 100 km in diameter will entrain at least 20-40% host mantle during a one-shot transit from the CMB; long-lived conduits (such as Hawaii) should be highly diluted with host mantle, unless the conduit is very large (500 km?). Fig. 2 shows the isotope data for a number of oceanic hot spots, in an attempt to see if significant upper mantle (DMM) entrainment is present. Remarkably, all the hot spots which show elongated isotopic arrays are aligned in a "fan-pattern," with a focus near the DMM–HIMU join. There appears to be no evidence for mixing between the DUPAL components themselves, or if it exists it has been overwhelmed by the latest mixing toward the left side of the tetrahedron. However, the convergence point for these arrays is not DMM, nor "average" MORB mantle, as might be expected for entrainment of the upper MORB mantle.. Even Hawaii, which in Fig. 2 appears to head right into N-MORB, is rising off the plane, so that it projects above all but a few of the N-MORB shown. Thus, while there is ample evidence for mixing in many hot spots, as would be expected from thermal entrainment, and while these hot spots all appear to be mixing toward a common composition, this composition is not DMM or "average" N-MORB.

One conclusion might be that the upper mantle is not DMM (MORB-type). (Stop smiling, Don!) We prefer the idea that most of what is displayed in Fig. 2 is lower mantle entrainment (3/4 of the plume ascent is spent in the lower mantle, after all). If true, this is providing us with the first direct (?) indication of what the lower mantle is like geochemically: isotopically depleted, with Sr < 0.7030, Nd > 0.5129 and 206/204 Pb ~ 19.5 - 20.0. As a corollary, because few if any oceanic basalts actually plot in the "convergence" region of Fig. 2, we conclude that lower mantle is never sampled in "pure" form, suggesting the absence of significant whole mantle convection except that associated with the plume flux.

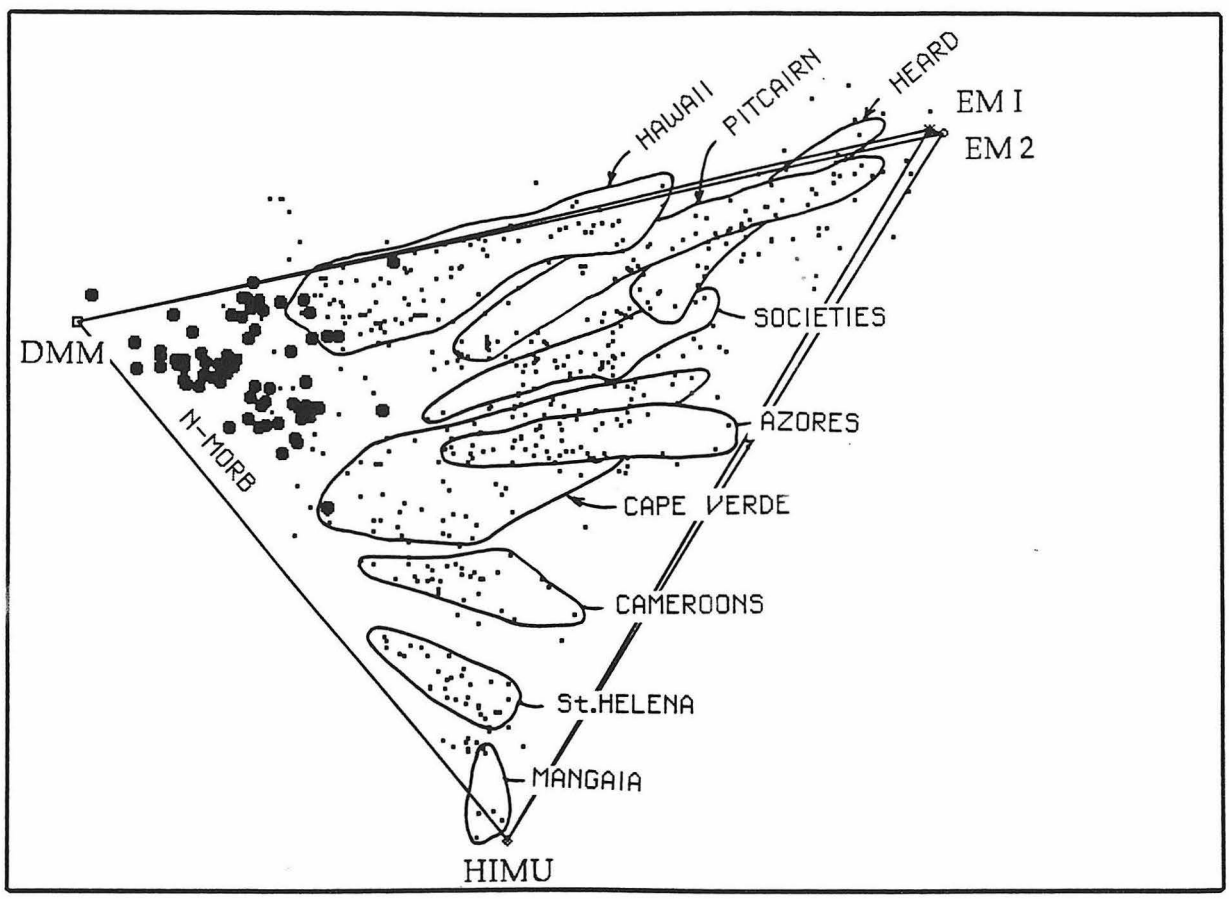

Fig. 2: View of the oceanic data set, looking down on the DMM–HIMU–EMI "mantle plane" (see Fig. 1 for orientation). Of the 96 MORB, 71 have 87/86 Sr < 0.7030, and are shown as large filled circles (N-MORB). Outline fields have been drawn around those islands which show the most elongated "cigar"-shaped data arrays (in 3-D). Fernando de Noronha and Walvis Ridge also show good arrays but were left off for clarity. Kerguelen, Marquesas and Samoa show fair arrays; all the other islands either show blobby distributions, or limited heterogeneity. Note that the field outlines enclose many points not necessarily belonging to that particular island (or island group). The tendency for the fields to converge or focus toward the left is apparent; DMM itself does not appear to be the prime focus however.

The origin of the species

A.W. Hofmann
Max-Planck-Institut für Chemie, Postfach 3060, 6500 Mainz, F.R. Germany

Mantle evolution is governed by two fundamentally different processes: (1) slow, mostly irreversible differentiation of the primitive mantle into two complementary reservoirs, continental crust and residual mantle; (2) rapid, reversible differentiation of the residual mantle into oceanic crust and lithosphere. The mean net rate of continental-crust production is only about 1.5 km^3/yr, and the present-day rate is lower than this and may be close to zero (Taylor and McLennan, 1985). The current mean rate of oceanic-crust production and destruction is 20 km^3/yr. Because of these gross differences in production rates and time scales of recycling, the overall differentiation can be approximated by simple, two-stage models.

The two differentiation processes are recorded by isotope and trace element abundances: most lithophile elements have similar bulk partition coefficients during both processes, and this creates simple and internally consistent abundance patterns of the main reservoirs, continental crust, residual mantle, and oceanic crust (Hofmann, 1988). However, a few elements discriminate strongly between continental and oceanic crust-forming processes, and they provide hard constraints on the origin of plumes. Nb and Ta are preferentially retained (probably via Ti-phases) in the residual mantle during continental crust formation, thus creating dramatically different concentration ratios of Nb/U = 10 and 47 in continental crust and residual mantle, respectively. Subsequent ocean crust and plume formation retains the high Nb/U = 47. Pb shows the opposite effect and is preferentially transferred to the continental crust, probably as a result of hydrothermal processes. This also creates dramatically different Ce/Pb ratios of Ce/Pb = 5 and 25 in continental crust and mantle residue, respectively. Again, subsequent ocean crust and plume formation retains the high Ce/Pb = 25 (Hofmann et al., 1986). These diagnostic element ratios thus require a common heritage for continental crust and island arcs on the one hand, and for oceanic crust and plume sources on the other. Their relative uniformity in the latter reservoirs shows that these reservoirs have been well homogenized since the formation of the first stage, the isolation of the most of the continental crust. This is a natural consequence of the high mean age of the continental crust and relatively short (1 Ga or less) convective mixing times in the residual mantle.

The common heritage of MORB and OIB suggests very strongly that they are all the result of the second differentiation process, namely the production and recycling of oceanic crust, where this recycled crust comprises not only the normal MORB-type but also "anomalous" elements such as oceanic plateaus and oceanic islands. The constraints provided by Nb, Ta, and Pb leave no room for present-day, primitive-mantle sources, and they permit only very small contributions of recycled continental material to plume sources. Isotope data, particularly those for He, Sr, and Nd, which are still frequently invoked in favor of primitive source reservoirs, are only permissive, not constraining, and thus do not require primitive source reservoirs. Several plumes contain negative ε(Nd) signatures, clearly revealing their non-primitive nature (cf Tristan with ε(Nd) = -3, Nb/U = 45, Ce/Pb = 30; Le Roex et al., 1990). All MORB contain substantial quantities of primordial ^3He, but no one would call the MORB sources primitive. The fact that many OIB contain higher $^3He/^4He$ ratios than MORB may mean that "new", primordial He has entered a degassed source, but it does not mean that source itself is primitive.

The contrasting time scales of the two processes are reflected by the isotopic ages of the reservoirs involved. Taylor and McLennan (1985) estimate that 2.5 Ga ago the continental crust had grown to within 70 to 90% of its present mass. The ages of mantle heterogeneities are less easily assessed. The oldest heterogeneities represented by "high-μ" basalts may be as old as 2 Ga, but most of the other plume sources are considerably younger (Goldstein and Chauvel, 1990).

The isotopic taxonomy for plume sources proposed by Zindler and Hart (1986) defines four species, HIMU, EM I, EM II, and PREMA, which are characterized by the most radiogenic Pb, the most unradiogenic Nd and Pb, the most radiogenic Sr, and the most common ("PRevalent MAntle") or average composition, respectively. The implication is that all oceanic basalts are derived from mixtures of these four species plus a fifth one, namely the DMM (depleted MORB mantle). Since then, much effort has gone into identifying the origin of the plume species. All sorts of source differentiation mechanisms have been suggested including various types of

recycling mechanisms involving fresh oceanic crust, altered oceanic crust, oceanic sediments, oceanic lithosphere, metasomatically altered lithosphere, continental lithosphere, internal igneous differentiation and so on. However, perhaps the first questions to be answered should be: Are these species real? Are they the only ones? Is there a unifying paradigm that ties all of them together? I start with the last question.

The continuous production of oceanic crust and lithosphere is by far the largest chemical differentiation mechanism currently occurring on Earth. This differentiated material reenters the mantle and introduces chemical heterogeneities that, given 10^8 to 10^9 years, will evolve into isotopic heterogeneities unless convective stirring is efficient enough to prevent this. The results of some model calculations notwithstanding, the evidence that isotopic heterogeneities do survive in the mantle is overwhelming. Indeed, suitable mixing times have been found in some calculations (Davies, 1990; Christensen, 1989). Moreover, while the extreme members of the HIMU species are clearly at least 1.5 Ga old, this need not be true for other plumes, most of which are probably significantly less than 1 Ga old (Goldstein and Chauvel, 1990). No matter, before introducing exotic mechanisms, any comprehensive theory for the origin of mantle heterogeneity and plumes should first account for the differentiated material *known* to enter the mantle by subduction.

Are the species real? Apparently they are, at least if we use Noah´s criterion that there ought to be at least two individuals of each species. We now have two essentially identical representatives of Z&H´s main three species, St. Helena (Atlantic) and the Australs (Pacific) for HIMU, Walvis Ridge (Atlantic) and Pitcairn (Pacific) for EM I, and Samoa (Pacific) and the Society Islands (Pacific) for EM II. Fig. 1 shows the isotopic evidence for this. Since there are several independent decay systems involved, a fortuitous coincidence of these pairs in all diagrams is rather unlikely. The similarities also extend to the chemical composition. Fig. 2 shows mantle-normalized chemical data for two typical HIMU basalts, one from Tubuai and the other from St. Helena. For 21 elements, the concentrations match within 20 % or better, 5 elements match within 30%, and only two elements, MgO and P_2O_5, show poor matches of 40 and 53%. Clearly, the difference in MgO is caused by different fractionation histories of the two melts and has little or no bearing on the source. The difference in P_2O_5 is not so easily explained, raising the suspicion of interlaboratory bias, a euphemism for systematic analytical error. Overall, the match is very close, considering the fact that incompatible trace elements can vary by a factor of ten or more in different OIB. Therefore, the sources of these two basalts have virtually identical chemical *and* isotopic composition, and the conclusion seems inescapable that they are indeed two specimens of the same species. The only alternative would be that the pairs were originally single individuals that were physically split, separated, and transported to take-off points beneath different oceans.

Are there other species? Barling and Goldstein (1990) have demonstrated that the Heard Island plume consists of closely constrained, binary mixtures between EM II and another species not previously identified. Similarly, LeRoex et al (1990) have shown that Tristan basalts, which come from the same plume as the EM I basalts of the Walvis Ridge but are isotopically distinct, form isotopic mixing trends which are parallel to but not connected with Walvis ridge compositions. Consequently, there are probably more species, or at least mutations, hidden in the interior of the scatter of the isotopic data.

What, then, is the origin of the species? The chemical and isotopic constraints are much better at eliminating bad hypotheses than in proving good ones. The eliminated hypotheses include any truly primitive mantle reservoir and any purely (continental) crustal reservoir. In addition, Hart and Staudigel (1989) have shown that strongly altered, recycled oceanic crust must also be eliminated. Why this should be so is not immediately obvious. Apparently, the subduction process and its concomitant volcanism is very effective in removing the altered parts of the oceanic crust from mantle circulation. The Be-B systematics of island arc volcanics recently investigated by Morris et al. (1990) confirm this inference.

The fact that most plumes contain hybrids of two or more mantle species strongly favors a single general mechanism for generating all of them. Therefore, if recycling of subducted material explains part of the origin of plumes, it may very well explain all of it. The quantitatively important volumes of subducted potential plume sources include (1) oceanic lithosphere, (2) normal oceanic crust, (3) enriched or fractionated oceanic crust, (4) oceanic basaltic plateaus, (5) oceanic islands, (6) pelagic and terrigenous sediments. If one of these can be recognized in

Fate of subducted reservoirs

(1) The **oceanic lithosphere** must ultimately serve as a future MORB source, with its uppermost, harzburgitic portion remaining refractory until it is sufficiently regenerated by blending with subducted oceanic crust and more fertile lherzolite.

(2) The so-called **"normal", depleted oceanic crust** is relatively thin and is easily stirred back into the depleted mantle. It is only rarely the main source component of plumes. However, the Iceland plume may be an example of this. Its Sr, Nd, and Pb isotopic compositions overlap the MORB field, and its source enrichment relative to present-day MORB is minimal.

(3) **Enriched oceanic** crust is a likely source of HIMU plumes. A magmatic differentiation during partial melting and subsequent fractionation which increases the Rb/Sr and U/Pb ratios by factors of two and the Sm/Nd ratio by about 30% will generate the isotopic composition of HIMU basalts from DMM in about 1.5 Ga. Alternatively, the high U/Pb and Th/Pb ratios required by this species may be generated by hydrothermal removal of lead from oceanic crust.

(4) **Oceanic plateaus** are probably created by plume heads first encountering the surface (Campbell and Griffiths, 1990). They owe their enormous volume to the entrainment of (non-plume) mantle into the ascending head. As a result, their chemistry is close to, but somewhat more enriched in incompatible elements than, normal MORB. Magmatic enrichment is enhanced by the presence of an oceanic lithosphere, which will keep melt segregation deeper and effective melt fractions smaller than at ocean ridges where there is no cold lid. Continental margins are not distinguished by large accretions of "scraped-off" plateau basalts, so these plateaus must normally be subducted and recycled into the mantle. When they are, they will be converted to voluminous packets of eclogite and higher-pressure equivalents. These may be the prime sources of the"garden variety," moderately enriched plumes such as Hawaii and other members of the PREMA species.

(5) **Oceanic islands** tend to be more severely differentiated primarily because of relatively low degrees of melting. OIB such as those from the Hawaiian chain possess the appropriate Rb/Sr, Sm/Nd, and (U,Th)/Pb ratios to create the main isotopic trends seen in OIB such as Tristan, if they are subducted and recycled. Such islands commonly have crustal thicknesses of 15 to 20 km, and I speculate that this enhances their chances of surviving the general stirring and becoming part of future plume sources.

(5) **Terrigenous sediments** have high $^{87}Sr/^{86}Sr$, $^{207}Pb/^{204}Pb$, low Nb/U and Ce/Pb ratios, and these features are found in EMII basalts. Mass balance calculations show that this sedimentary component contributes only a very small fraction of the source. Apparently most of the sediments are somehow lost during subduction, along with the altered parts of the igneous crust. Presumably these are incorporated into arc volcanics.

(6) **Pelagic clays** are distinguished by low U,Th/Pb and high Th/U ratios, and these might be incorporated in the sources of EM I basalts, which contain the least radiogenic Pb and the highest $^{208}Pb/^{206}Pb$ ratios of all oceanic basalts. However, present Nb/Th, Nb/U and Ce/Pb data are insufficient to confirm the presence of a sedimentary component in EM I.

The overall evolution of the mantle is recorded by the combined isotopic and chemical information. The distinct continental and oceanic arrays of Pb isotopes confirm the relative youth (< 2 Ga) of the mantle heterogeneities preserved in plumes. Recycling of continental material, irrespective of its importance during the early history of the earth, has been so small that the two isotopic arrays remain separate. The chemical tracers Nb/U and Ce/Pb distinguish even more sharply between continental and oceanic crust, and they constrain the nature of the enrichment processes as mainly "oceanic" (as originally proposed by Hofmann and White, 1980, 1982).

The relative uniformity of Nb/U in nearly all plumes and MORB provides an additional constraint: the residue of continent formation has had sufficient time to be homogenized by convection (since the instantaneous residue must be highly heterogeneous in Nb, U, and Nb/U). The more rapid oceanic differentiation process does not affect Nb/U and Ce/Pb, but it does fractionate the mother-daughter ratios of the long-lived decay systems. Therefore, the isotopic heterogeneities now sampled by plumes are mostly created by the "oceanic" process, and they are all comparatively young. An important corollary is that there is no detectable memory for any mantle layering created early in Earth history and preserved until today. If such layers exist, they are not sampled by any plumes! Even the most extreme isotopic and chemical heterogeneities carried by plumes are younger than this homogenization, and evidence for the course of the more ancient mantle history can only be found on the continents.

Barling, J. and Goldstein, S.L. (1990) Nature 348, 59-62.
Campbell, I.H. and Griffiths R.W. (1990) Earth Planet. Sci. Lett. 99, 79-93.
Chaffey, D.J. Cliff, R.A., and Wilson, B.M. (1989) in Saunders, A.D. and Norry, M.J.. (eds) Magmatism in the Ocean Basins. Geol. Soc. Lond. Spec Pub. 42.
Chauvel, C., Hofmann, A.W., and Vidal, P. (1991) ms. subm. to EPSL.
Christensen, U. (1989) Earth Planet. Sci. Lett. 95, 382-394.
Davies, G.F. (1990) Earth Planet Sci Lett. 99, 84-109.
Goldstein S.L. and Chauvel, C. (1990) ICOG VII Abstr. Geol. Soc. Australia Abstr. No. 27.
Hart, S.R. and Staudigel, H. (1989) Crust/Mantle Recycling at Convergence Zones. Kluwer.
Hofmann, A.W. (1988) Earth Planet. Sci. Lett. 90, 297-314.
Hofmann, A.W., Jochum, K.P., Seufert, M., and White, W.M. (1986) EPSL 79, 33-45.
Hofmann, A.W. and White, W.M. (1980) Canegie Inst. Wash. Yearb.79, 477-483.
Hofmann, A.W. and White, W.M. (1982) Earth Planet. Sci. Lett. 57, 421-436.
Le Roex, A.P., Cliff, R.A. and Adair, B.J. (1990) Jour. Petrol. 31, 779-812.
Morris, J.D., Leeman, W.P. and Tera, F. (1990) Nature
Taylor, S.R. and McLennan, S.M. (1985) The continental crust: its composition and evolution. Blackwell Scientific Publ. Oxford. 312 p.
Zindler, A. and Hart, S.R. (1986) Ann. Rev. Earth Planet. Sci. 14, 493-571.

Fig. 1. Comparison of 2 islands of each of the species HIMU, EM 1, and EM 2. Literature data.

Fig. 2. Comparison of trace element chemistry of basalts from Tubuai and St. Helena (HIMU). Data from Chaffey et al. (1989) and Chauvel et al. (1991).

Fig. 1

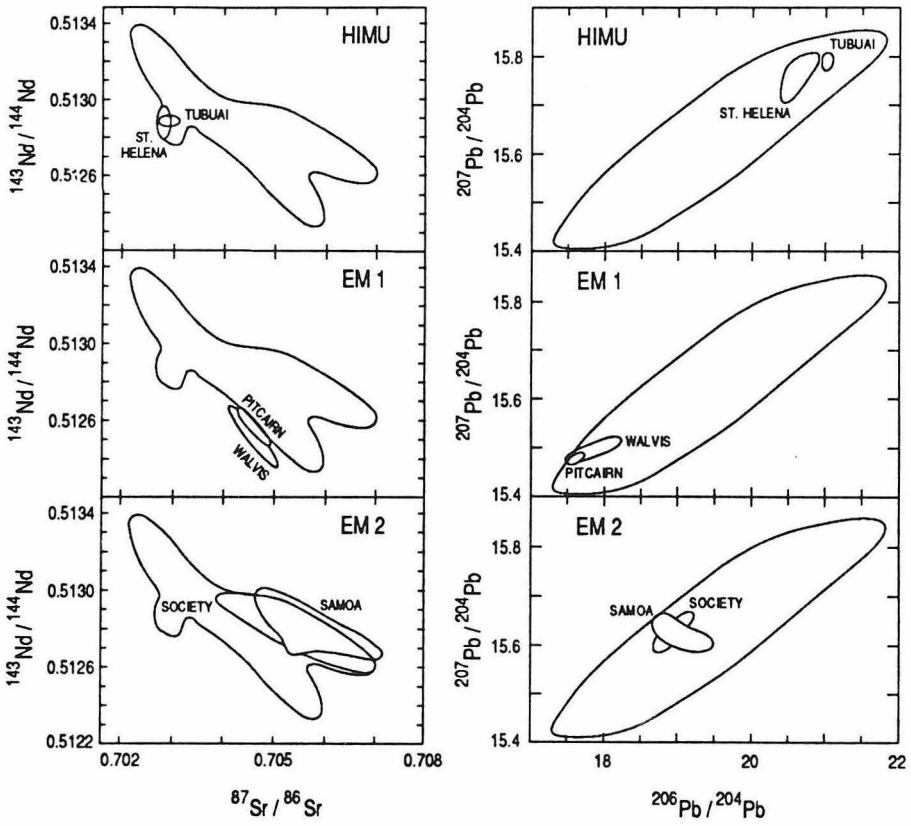

Fig. 2

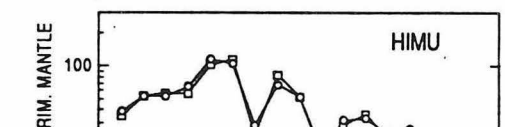

Plume tectonics

R.I. Hill, I.H. Campbell, G.F. Davies, and R.W. Griffiths
Research School of Earth Sciences, Australian National University,
PO Box 4, Canberra, ACT 2601, Australia

Introduction

Mantle plumes result in the emplacement of large volumes of hot material near the Earth's surface. Consequences can include the production of basaltic liquids [1,2], uplift of the superjacent surface [3,4], and large-scale anatexis of overlying continental crust [5]. A number of authors have documented a link between hotspots and continental break-up, leading to the suggestion that mantle plumes may play an important role in modulating the movements of the plates [6,7]. The purpose of this paper is to summarise evidence which may be used to assess the importance of mantle plumes in initiating thermal and tectonic reworking of the continents.

Dynamical framework

Fluid dynamics analog experiments [2-4] have shown that a new plume ascending through the mantle consists of a large spherical head trailed by a narrow pipe-like conduit (or "tail") that connects the top of the head to the source layer. Upon nearing the surface the head spreads to give a disc of hot material 1500-2500 km across and 100-200 km thick. Because of entrainment during ascent this disc consists of 20-40% source material and 80-60% entrained mantle. For the modern Earth, where the maximum temperature variation within basalt sources appears to be ~200°C {equivalent to a range in potential temperatures (T_P) of 1300-1500°C [8]}, average T_Ps within plume heads will be 1340-1380°C, while hot source material rising within the plume conduit can have T_P=1500°C. Positive buoyancy associated with emplacement of hot plume material can result in up to ~1000 metres of surface uplift [4], and uplift-induced horizontal deviatoric stresses may lead to extension of overlying crust [9].

The experiments allow the following inferences to be made about the scale and nature of plume-initiated continental reworking. 1) Two types of plume provinces should be recognisable, depending on whether the crust passes over a plume head or a plume tail. *Plume head provinces* are predicted to be equant and 1500-2500 km across, while *plume tail provinces* might be expected to have the bulk of volcanism and tectonism restricted to a narrow (<300 km wide) linear belt that is the surface projection of the underlying plume conduit (i.e., a hotspot track). 2) Both may contain basaltic magmatism. 3) Both are expected to be associated with extension. 4) Important uplift may predate both extension and initiation of basaltic magmatism. 5) Conductive heat transfer may play an important role in the development of both types of plume province because it may lead to weakening of the crust and uppermost mantle as well as to extensive crustal anatexis. We term the process of thermal and structural reworking above mantle plumes *plume tectonics*.

Plume head and plume tail provinces

Both types of plume province are recognisable in the geological record. Examples of plume heads include the Karoo, Deccan and North Atlantic Tertiary flood basalt provinces [1,10], and the Late Archaean granite-greenstone terrains of the Yilgarn Block of Western Australia [5]; plume tail provinces equate with the familiar hotspot tracks. Of the plume head examples, the Karoo and Yilgarn in particular have magmatic histories consistent with conductive heat transfer. A summary of the magmatic development is as follows. Partial melting within the rising plume head results in an early period of (often voluminous) basaltic volcanism [1,6,10]. Conduction of heat upwards away from the plume may result (after a time delay of 10-30 Ma) in the production of crustally-derived melts [5]. Such anatectic episodes may be voluminous but commonly are of short duration, ~5 Ma. Felsic magmatism may be followed by more mafic magmatism, and, after a further conductive time delay, by further episodes of lower-P or high-T crustal melting. Although the overall timescale for magmatism may be ~100 Ma, the bulk of magmatism is restricted to a few short periods of intense activity. The overall magmatic record of plume head provinces differs fundamentally from that of destructive margins (i.e., island and continental margin arcs), where melting results from injection of water into the mantle during prolonged subduction of hydrated oceanic crust [11] (Fig. 1).

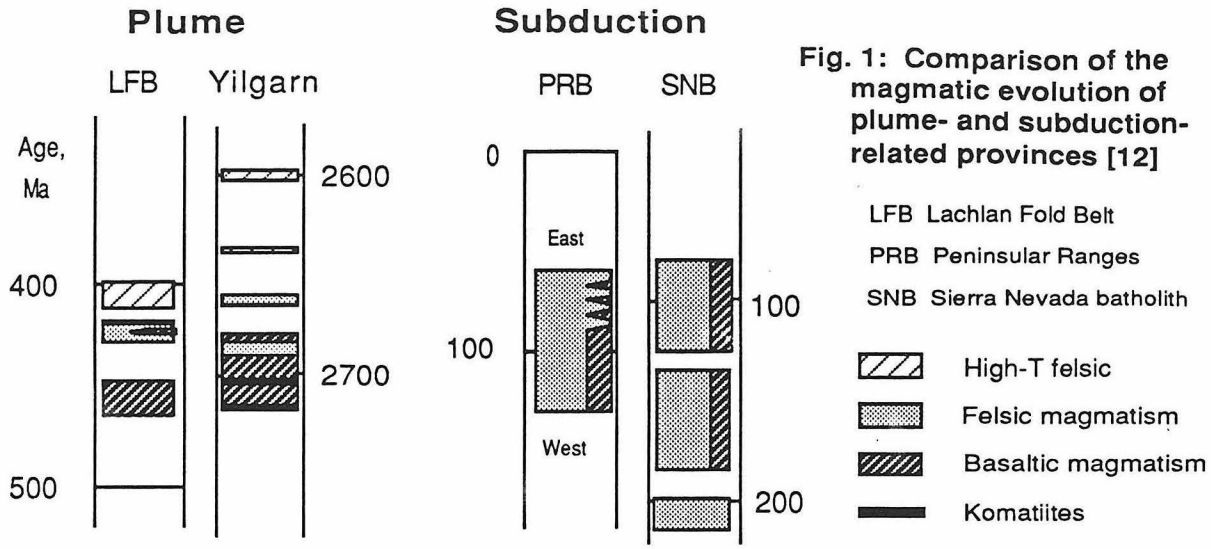

Fig. 1: Comparison of the magmatic evolution of plume- and subduction-related provinces [12]

Within hotspot tracks (plume tail provinces), the longevity of the main volcanic interval is related to the rate at which the overlying plate passes across the hotspot conduit. The province resulting from the Yellowstone plume (the Snake River Plain) provides an example. The Plain is a volcanic-filled graben atop a broad arch [13]. Early rhyolitic volcanism is superceded by basaltic volcanism, a main phase of felsic magmatism, and a final episode of plain-flooding basaltic volcanism. The entire volcanic history takes ~8 Ma at any one place [13], consistent with passage of North America at 25 km/Ma over a plume conduit 200 km across. Initiation of volcanism along the hotspot track is time-progressive, and although Yellowstone has only been active for 17.5 Ma, the geological evidence is that plume tails may persist for ~200 Ma [6]. Although lateral spreading of material from the top of the conduit may result in the production of a strip of hot plume material >1000 km wide [14], a striking characteristic of continental plume tail provinces is the restriction of evidence for major tectonic and magmatic reworking to a narrow (<200 km) volcanic- and sediment-filled trough atop a broad arch. Thermal subsidence of the arch may result in much more widespread later sedimentation. Formation of the graben has been suggested to result from removal of underlying crust through anatexis and eruptive dispersal [13]. The most obvious feature of plume tail provinces is the presence of a time-progressive chain of volcanic centres that may be many thousands of kilometres long. Although not always observed, the presence of high-T lavas such as picrites and komatiites derived through melting of hot material within the plume conduit is considered diagnostic of a hotspot track [15].

Plume tectonics and the development of stable continental crust

The observed internally differentiated crust of the Yilgarn craton of Western Australia has been argued to have formed by a two-stage process, with primitive continental crust of relatively mafic (basaltic andesite or andesite) composition undergoing plume-initiated reworking in Late Archean time to give a layered crust with an upper granitic layer overlying a more mafic residuum from partial melting [5,16]. The Yilgarn-derived model can be generalised, yielding the following conclusions. 1) Rapid production of internally differentiated crust over large areas, a characteristic feature of many continents, may result from thermal reworking above plume heads. 2) As the repeat time for passage of a particular piece of crust above a plume head is probably <1000 Ma, much of the episodicity in the geological and geochronological record of the continents may result from plume tectonic rather than plate tectonic processes.

Application to the late Cenozoic evolution of the Basin and Range province of the western U.S.

Late Cenozoic (post 30 Ma) extension and magmatism within the Basin and Range province has been suggested to have resulted from the presence of mantle plumes [13,17,18] We infer that much of the geological evolution of this region over the past 40 Ma results from the emplacement of first the Raton plume head ~28 Ma ago, followed by arrival of the Yellowstone plume at 17.5 Ma [19]. The

plume head model can satisfactorily account for initiation of uplift in the southern Rocky Mountains 36 Ma ago, the change from arc-type to bimodal volcanism that occurred in the southern Basin and Range 26-28 Ma ago, initiation of active extension in the southern Basin and Range 26-28 Ma ago and in the central and northern Great Basin ~17 Ma ago, the great increase in felsic volcanism 17-22 Ma ago, as well as many of the anomalous geophysical properties of this region.

Plume tectonics versus plate tectonics

Models of whole-mantle convection driven by the negative buoyancy of a cold, rigid surface boundary layer (the oceanic crust) are consistent with a wide variety of observations [20,21]. This plate-scale convective mode is responsible for most of the heat loss from the mantle, and >80% of the heat loss from the Earth [6]. Plumes are inferred to be derived from a thermal boundary layer resulting from heat loss from the core [1,6], and transport through the mantle 5-10% of the heat ultimately lost at the Earth's surface [14]. Because of their different origins, it is of interest to establish whether these two convective modes operate completely independently, or whether one can influence the other to any significant extent.

Geological observations which may be used to indicate the extent of the interaction between rising plume heads and overlying lithosphere, as well as between the two convective modes, have been summarised in [22]. These observations lead to a number of important conclusions. 1) Old lithosphere is resistant to displacement by rising plume heads. 2) Continental flood basalts are unlikely to have been derived through melting of old subcratonic lithosphere because it never gets hot enough. 3) Lateral temperature variations of up to 1000°C may be present in the uppermost mantle during a plume event. 4) Although arrival of a new plume may exert considerable influence on both the position and exact timing of break-up, rifting through to the formation of a new ocean basin occurs only if the plate-scale motions are already suitably arranged. An example of a plume which did not initiate continental break-up is that which yielded the flood basalts of the Siberian Traps. 5) Where a new plume "captures" an existing ridge, a new ridge is established near the centre of the plume within ~5 Ma. Because 5 Ma is insufficient to transfer enough heat to weaken the overlying mantle and crust, the dominant driving force for rifting must come from the plate-scale motions, but with a component coming also from the 500-1000 metres of uplift above the plume conduit. 6) Where rifting follows ascent of a plume into a slowly-extending region remote from pre-existing plate boundaries there is a delay of up to 40 Ma, presumably to allow sufficient heat to be conducted upwards to weaken the overlying mantle and crust. Examples include the opening of the central Atlantic ~25 Ma after arrival of the Fernando (Newark-Palisades) plume, and the rifting of Madacasgar away from southern Africa 40 Ma after arrival of the Crozet (Karoo) plume. 7) Rifts tend to be restricted to younger mobile belts unless rifting of an old craton is forced for geometric reasons; this is inferred to be the case because preferential emplacement of hot plume material beneath mobile belts results in greater uplift of the tectonically younger (and weaker) crust, and thus generation of greater horizontal deviatoric stresses.

Ridge jumping and ridge propagation contrast markedly with the formation of a completely new ridge, where the delay between plume arrival and break-up is 25-40 Ma. Although in both cases break-up only occurs when pre-existing plate motions are suitably arranged, the longer time scale observed for "true" break-up indicates that a second important role played by plume arrival may be to provide sufficient heat to change substantially the rheological properties of the uppermost mantle and crust, the strength of which has previously been preventing rapid extension [10].

Crustal production and crustal reworking

One of the most important products of the plate-scale motions (relatively low-density primitive continental crust) forms as a result of the injection of water into the hot mantle at subduction zones [11]. Without subduction of cold, dense, hydrated oceanic crust there would be no continental crust and no "granites" [23]. New continental crust, then, is a product of the plate-scale motions. The products of fluxed melting differ from those produced through decompression melting of near-anhydrous mantle: they are volatile, silica- and incompatible-element -rich, erupt at generally lower temperatures, and evolve through quite different mineral fractionation sequences compared to those of constructive margin or intra-plate basalts [12,24]. Magmatism associated with convergent margins is often characterised by the continued production of compositionally variable materials over time periods of many tens of Ma [25,26; Fig. 1], and although average compositions tend to be relatively mafic [27,28], they are more SiO_2-rich and thus less dense than basalt. Subsequent or later thermal and

tectonic reworking of this crust to produce the internally differentiated crust characteristic of stable continents results from both the plate-scale and plume processes. Because higher temperatures can be attained within crust overlying plumes, and because of the large areal extent of plume heads, it is possible that plumes play a more important role in the thermal reworking of continents than do plate tectonic processes.

Some geophysical implications

Because of the combination of thickness (100-200 km) and distance from the surface (>30 km) the thermal time constant of a plume head is large (200->500 Ma). Emplacement of a plume head can thus result in anomalously high surface heat flow for substantial time periods. Also, because the thermal time constant for a plume head is of comparable magnitude to the repeat time (~800 Ma), quasi-episodic emplacement of plume heads has the potential to play an important role in setting the temperature distribution within the uppermost mantle beneath the continents. This has broader scale geophysical implications; for example, the maximum possible sub-Moho temperature difference of 1000°C likely to result from plume emplacement can potentially lead to variations in uppermost mantle P_n velocities of 0.5 km/sec, and to correspondingly large variations in uppermost mantle viscosity.. As the bases of plume layers may occur at depths of 200-300 km, emplacement of plume heads may exert an important influence on the thermal structure and thus geophysical properties of much of the upper mantle. Ascent of plume heads may also play an important role in buffering the composition of the uppermost mantle [2].

References

[1] Campbell, I.H., and Griffiths, R.W., 1990, *Earth Planet. Sci. Lett.* **99**, 79-93. [2] Campbell, I.H., and Griffiths, R.W., this volume. [3] Griffiths, R.W., Gurnis, M., and Eitelberg, G, 1989, *Geophys. Jour.* 96, 477-495. [4] Griffiths, R.W., and Campbell, I.H., 1990, *Earth Planet. Sci. Lett.* **99**, 66-78. [5] Campbell, I.H., and Hill, R.I., 1988, *Earth Planet. Sci. Lett.* **90**, 11-25. [6] Morgan, W.J., 1981, *in* Emiliani, C., ed., The Sea, Volume 7: Wiley Interscience New York, 443-487. [7] White, R., and McKenzie, D., 1989, *Jour. Geophys. Res.* **94**, 7685-7729. [8] McKenzie, D., and Bickle, M.J., 1988, *Jour. Petrol.* **29**, 625-679. [9] Houseman, G., and England, P., 1986, *Jour. Geophys. Res.* **91**, 719-729. [10] Richards, M.A., Duncan, R.A., and Courtillot, V.E., 1989, *Science* **246**, 103-107. [11] Burnham, C.W., 1979, *in* Barnes, H.L., ed., Geochemistry of Hydrothermal Ore Deposits, John Wiley and Sons, New York, 71-136. [12] Stuart-Smith, P.G., Hill, R.I., Rickard, M.J., and Etheridge, M.A., Submitted to *Tectonophysics*. [13] Suppe, J., Powell, C., and Berry, R., 1975, *Am. Jour. Sci.* **275-A**, 1135-1147. [14] Davies, G.F., 1988, *Jour. Geophys. Res.* **93**, 10451-10466. [15] Campbell, I.H., Griffiths, R.W., and Hill, R.I., 1989, *Nature* **339**, 697-699. [16] Hill, R.I., Campbell, I.H., and Compston, W., 1989, *Geochim. Cosmochim. Acta* **53**, 1259-1275. [17] Morgan, W.J., 1971, *Nature* **230**, 42-43. [18] Wilson, J.T., 1990, *Jour. Geophys. Res.* **95**, 6611-6628. [19] Hill, R.I., Campbell, I.H., Davies, G.F., and Griffiths, R.W., To be submitted to *Geol. Soc. Amer. Bull.* [20] Davies, G.F., this volume. [21] Davies, G.F., and Richards, M.A., 1991, Submitted to *J. Geol.* [22] Hill, R.I., 1991, *Earth Planet. Sci. Lett.*, in press. [23] Campbell, I.H., and Taylor, S.R., 1983, *Geophys. Res. Lett.* **10**, 1061-1064. [24] Gill, J.B., 1981, Orogenic Andesites and Plate Tectonics: Springer-Verlag, New York. [25] Chen, J.H., and Moore. J.G., 1982, *Jour. Geophys. Res.* **87**, 4761-4784. [26] Silver, L.T., Taylor, H.P., Jr., and Chappell, B.W., 1979, *in* Abbott, P.L., and Todd, V.R., eds., Geol. Soc. Amer. 1979 Guidebook, 83-110. [27] McBirney, A.R., and White, C.M., 1982, *in* Thorpe, R.S., ed., Andesites: Orogenic Andesites and Related Rocks: John Wiley, New York, 115-135. [28] Silver, L.T., and Chappell, B.W., 1988, *Trans. Roy. Soc. Edinburgh: Earth Sci.* **79**, 105-121.

ENRICHED SHALLOW MANTLE BENEATH OCEAN BASINS - EVIDENCE FROM EVOLVED OCEAN ISLAND VOLCANICS

Kaj Hoernle; Department of Geology; University of California; Santa Barbara, CA 93106.

Compared to mid ocean ridge basalts (MORB), ocean island basalts (OIB) exhibit enriched characteristics, which has led to the concept of enriched mantle components (EM: very radiogenic Sr = EM2, and very unradiogenic Nd = EM1) and a high $^{238}U/^{204}Pb$ mantle component (very radiogenic Pb = HIMU) (cf. Zindler and Hart, 1986). The location of these mantle components is the subject of considerable controversy. Although usually excluded or ignored in studies of mantle geochemistry, evolved volcanics from ocean islands can potentially provide important information about the composition of the shallow mantle, if they have not been contaminated in the crust. We show that differences in isotopic composition between mafic and evolved volcanics from islands in the Atlantic, Pacific and Indian oceans cannot be explained by crustal contamination. Based on the observed isotopic differences, we propose that the evolved volcanics reflect contamination of melts from HIMU plumes by enriched material (EM) in the shallow mantle.

Based on their major element and to a large extent trace element compositions, more evolved ocean island volcanics (hawaiites-trachytes and tephrites-phonolites) can be derived from associated mafic compositions (alkali basalts, basanites and nephelinites) through fractional crystallization. On many ocean islands, the mafic and evolved volcanics have similar isotopic compositions, supporting a genetic relationship. On other ocean islands, however, temporally associated mafic and evolved volcanics have different isotopic compositions as illustrated in figures 1-3 (assuming of course that the available data from these islands is representative). Two possible explanations for these differences are (1) the mafic and evolved volcanics originate from isotopically distinct sources, or (2) the evolved volcanics have been contaminated during fractional crystallization (AFC). Several factors favor the second hypothesis. First, the mafic and evolved volcanics from several of the examples in figures 1-3 are from the same formation and are intercalated, suggesting a genetic relationship. Second, as is illustrated by the volcanics from Heard Island, Kerguelen Plateau and the Pliocene volcanics on Gran Canaria, Canary Islands, the range in isotopic composition of the evolved volcanics covers the range in the mafic volcanics and extends the field to more extreme (or enriched, for the examples given) compositions, consistent with at least some of the mafic and evolved volcanics being derived from the same source. Third, the evolved volcanics do not have compositions that could have been derived by direct melting of mantle peridotite. They also do not have isotopic compositions similar to crustal material, as shown below. For these reasons, we suggest that the differences in isotopic compositions of at least some of the examples in figures 1-3 reflect AFC.

An important question is where this assimilation occurred. Oceanic crust consists of three major components. The dominant component volumetrically is the igneous portion formed at the mid ocean ridge, which should have an isotopic composition similar to MORB. Seawater alteration can increase the $^{87}Sr/^{86}Sr$ ratio but will have little effect on the $^{143}Nd/^{144}Nd$ and $^{206}Pb/^{204}Pb$ ratios. As is evident from their high $^{143}Nd/^{144}Nd$ ratios, MORB and altered MORB do not have the appropriate composition to be the assimilant (figure 1). The second component is marine sediments. With the possible exception of Samoa, sediments also do not have the appropriate composition for the assimilant based on the trends formed on the $^{206}Pb/^{204}Pb$ versus $^{207}Pb/^{204}Pb$ isotope correlation diagram (figure 2). Intraplate submarine volcanics and intrusives, which are predominantly mafic based on samples recovered from dredges and xenoliths, represent the third component. In addition to thermal arguments against melting and assimilat-

ing significant amounts of mafic volcanics and intrusives, some of the evolved volcanics have the most extreme isotopic compositions yet found for an entire chain, for example Rarotonga (a phonolite has the least radiogenic Pb for the Cook-Austral chain) and Heard Island (a trachyte has the most radiogenic Sr and least radiogenic Pb on the Kerguelen Plateau). In addition to the crust not having an appropriate composition for the assimilant, evolved volcanics, even highly evolved phonolitic compositions, containing lherzolite xenoliths are common in continental settings, indicating that these magmas were derived from the mantle. These evolved volcanics can be derived from mafic volcanics through fractional crystallization at depths of 30-50 km (Irving and Price, 1981). Since the crust-mantle boundary (Moho) beneath most ocean islands is relatively shallow ($\leq$15 km), fractionation of ocean island magmas may be even more likely to occur in the mantle than fractionation of magmas erupted on continents.

If the evolved volcanics assimilated melts from mantle wall rocks, then the differences in isotopic composition between the mafic and evolved volcanics have important implications for the composition of the shallow mantle. With the exception of Principe (Cameroon Line) and possibly Mauna Kea (Hawaii), the evolved volcanics in figures 1-3 have more enriched (EM-like) compositions than the associated mafic volcanics, indicating the presence of enriched material in the shallow mantle beneath these islands. St. Paul's Rocks - an island near the mid Atlantic ridge composed primarily of spinel peridotite - and ultramafic xenoliths from ocean islands - such as Samoa (Cheng et al., 1988), Hawaii (Brouxel and Tatsumoto, 1988) and Kerguelen (Vance et al., 1989) - have isotopic compositions that are enriched relative to MORB, providing further evidence for enriched material in the shallow mantle beneath ocean basins.

On Principe, the more evolved volcanics have more radiogenic Pb and thus have more HIMU-like compositions. Interestingly, the continent-ocean boundary at the present site of the Cameroon Line probably passed over the St. Helena plume at 125 Ma. St. Helena, which has often been used as an example of the HIMU component, may have imparted it's signature on the lithosphere beneath the Cameroon Line (Halliday et al., 1988). Could passage of the lithosphere over earlier plumes, which may not always have left evidence of surface volcanism, or melts from the same plume, that formed older volcanoes in the chain, also have imparted the enriched (EM) signatures on the shallow mantle beneath the other ocean islands (Staudigel et al., 1991)? Clearly it is difficult to rule these possibilities out completely. Nonetheless, as pointed out above, some of the evolved volcanics have the most extreme isotopic compositions yet found for an entire chain, suggesting that at least in some places the enrichment may have been there previously. Furthermore, why are there not more examples of HIMU assimilation (assumming the data set in figures 1-3 is representative)?

With the exception of Principe and possibly Mauna Kea, the more mafic volcanics have more HIMU-like compositions and the evolved volcanics more EM-like compositions (figure 3). Based on this observation, we propose the following model. Enriched material is ubiquitous in the shallow mantle (Anderson, 1985), reflecting (1) remobilization of continental lithospheric mantle during rifting (Hawkesworth et al., 1986) and (2) dehydration and melting of sediments from the surface of subducting slabs. Melts from HIMU-like plumes, which originate from subducted crust at either the lower - upper mantle or the core - mantle boundary, fractionate within the shallow mantle and are, in some places, contaminated with enriched material.

FIGURES: Systematic differences are illustrated between the most mafic (solid symbols, shaded regions, and those regions designated with an M) and more evolved (open symbols and regions, and those regions designated with an E) volcanics from islands in the Atlantic, Pacific and Indian Oceans in isotope correlation diagrams: (1) $^{87}Sr/^{86}Sr$ versus $^{143}Nd/^{144}Nd$, (2) $^{206}Pb/^{204}Pb$ versus $^{207}Pb/^{204}Pb$, and (3) $^{206}Pb/^{204}Pb$ versus $^{87}Sr/^{86}Sr$. The data for ocean island volcanics, mantle endmembers (DM, HIMU, EM1 and EM2), Pacific and Atlantic mid ocean ridge basalt (MORB), and the marine sediment field are from the literature.

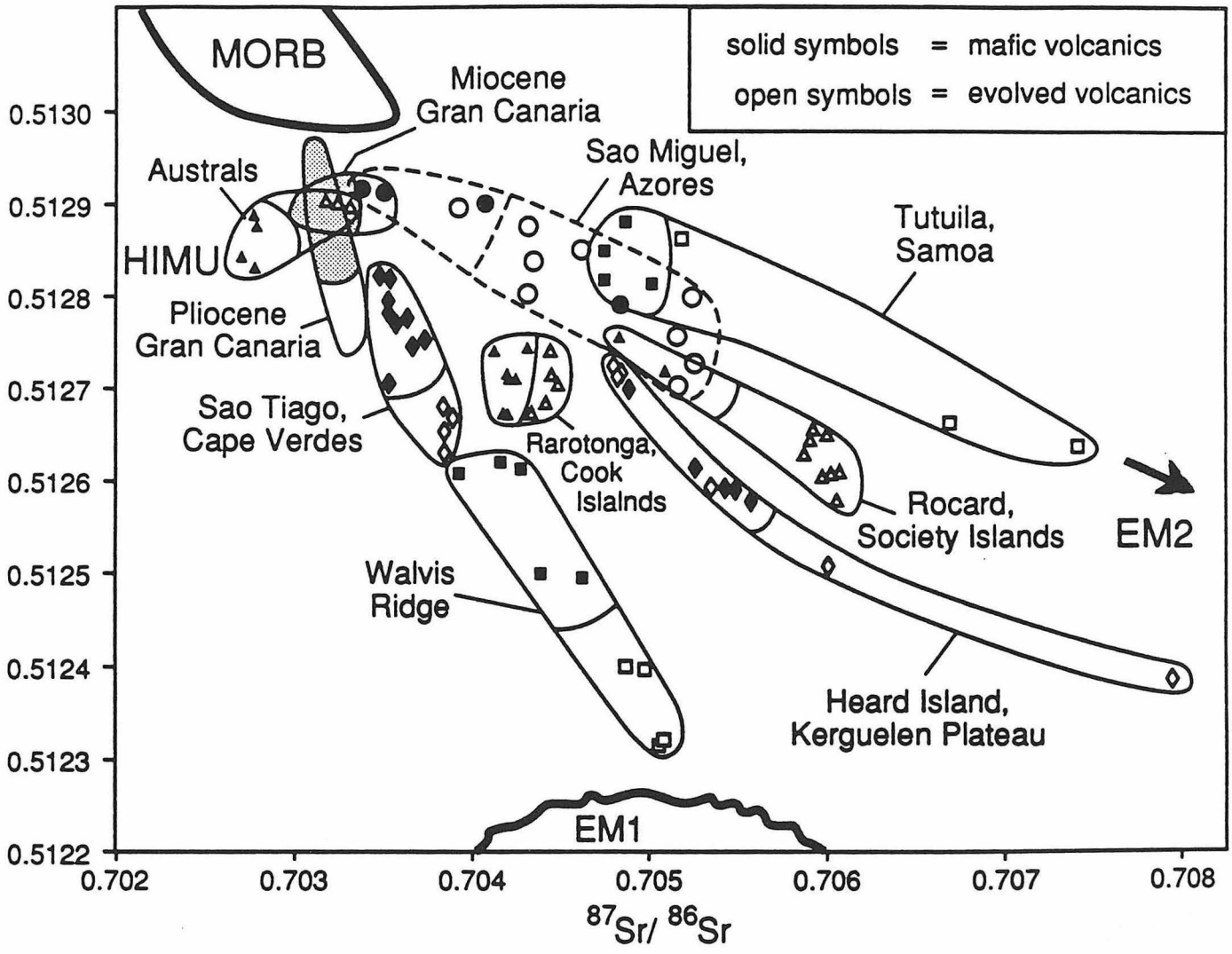

FIGURE1.

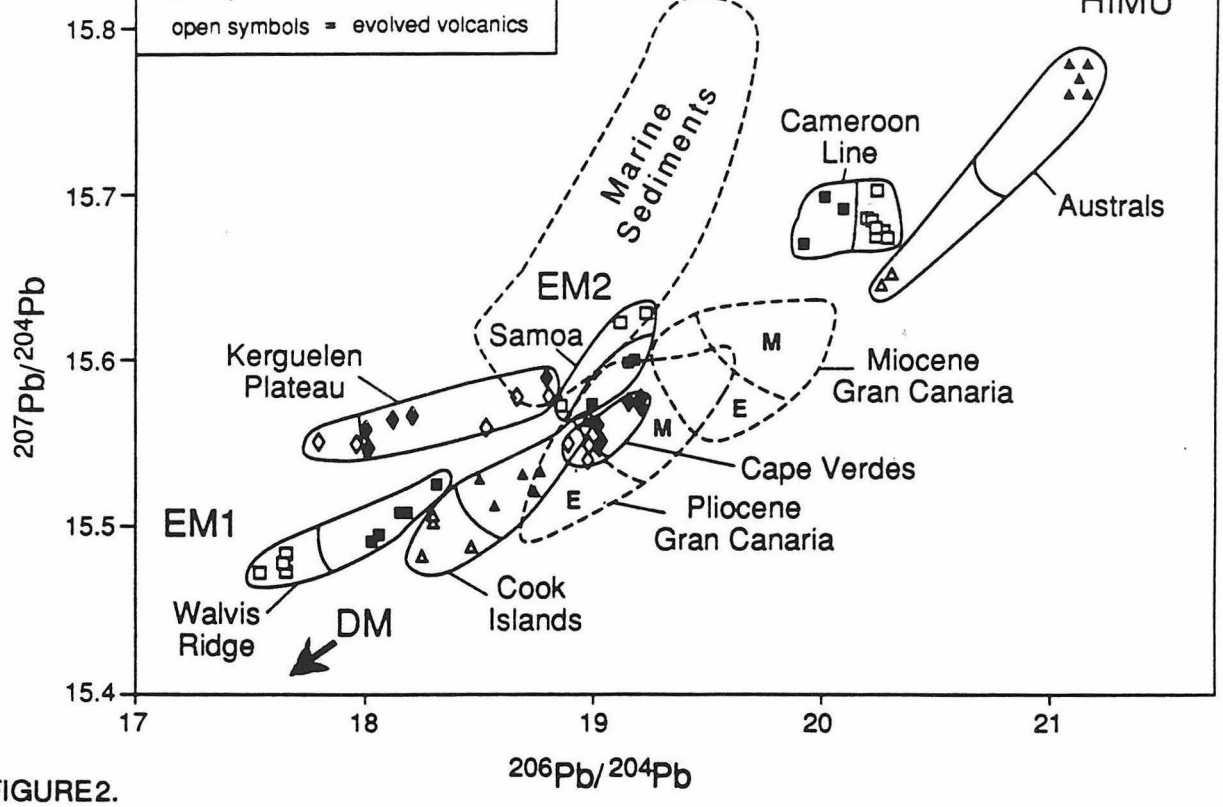

FIGURE2.

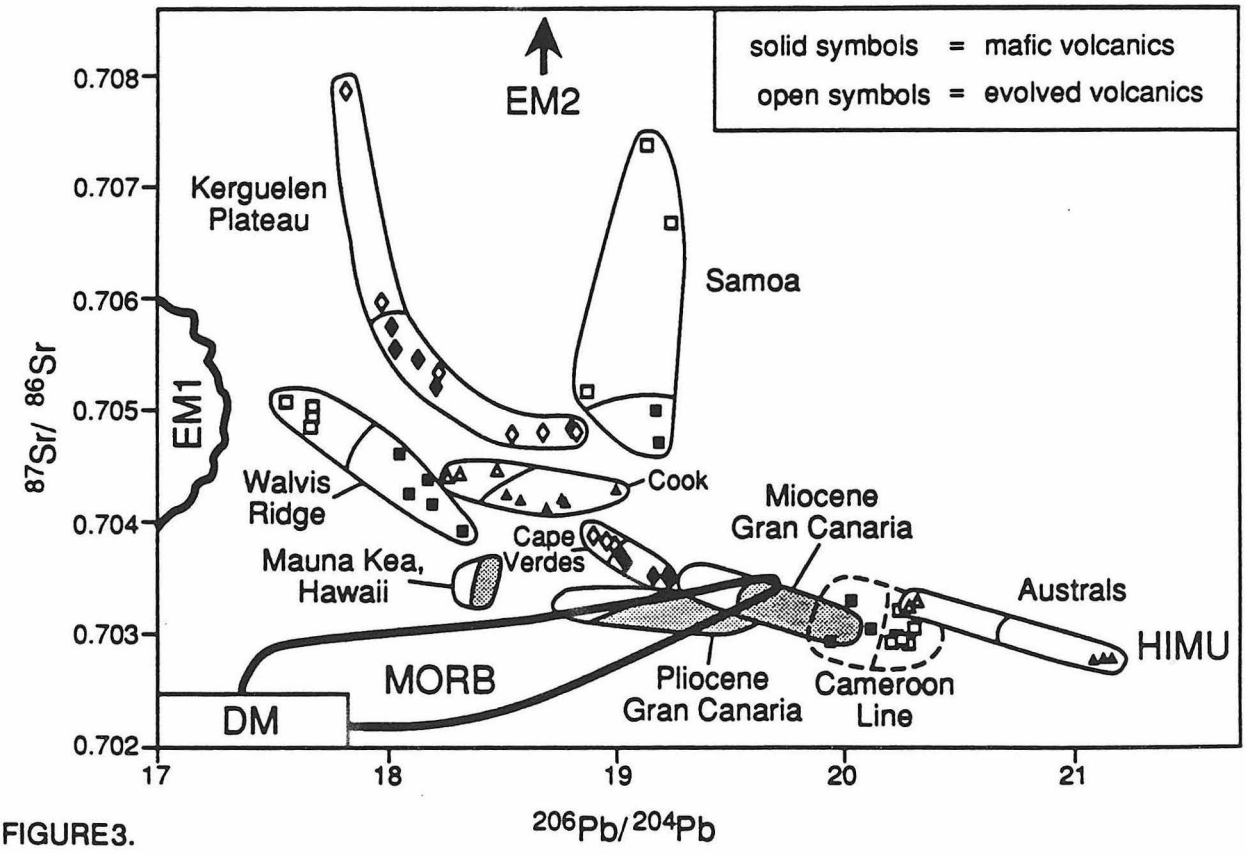

FIGURE3.

The Columbia River Basalt: A Mantle Plume or Back Arc Extension? Chemical, Isotopic and Tectonic Evidence.

P.R. Hooper[1] and C.J. Hawkesworth[2]

1) Department of Geology, Washington State University, Pullman, WA 99164
2) Department of Earth Sciences, Open University, Milton Keynes, MK7 6AA, U.K.

The Miocene continental flood basalts of the Columbia River Basalt Group (CRBG) form three subgroups, each derived from a different source: (1) The Main Series (~ 97% of the CRBG) include the sheet-flows of the Imnaha, Grande Ronde and Wanapum Basalts erupted rapidly in about 1.7 m.y.; (2) the Picture Gorge Basalts (PGB), which are contemporaneous with the Main Series, but geographically distinct, being erupted south of the Olympic Wallowa Lineament (OWL); and (3) The Saddle Mountains Basalt (SMB) which are smaller volume flows erupted later over a more protracted period (9 m.y.).

The PGB and other basalts erupted in NE Oregon south of the OWL in the last 20 m.y. are high-alumina olivine tholeiites (HAOTs) with a depleted MORB-like signature on which is superimposed an increased abundance of large ion lithophile (LIL) elements, including a notable Ba spike (Fig. B,C). This pattern is remarkably widespread throughout the Basin and Range extensional province and includes the most primitive basalts of the Cascades (Hart et al., 1984; Carlson and Hart, 1988; Fitton et al., 1988; Ormerod, 1988; Brandon, 1989; Donnelly-Nolan, in press). Many authors believe that this magma was derived from an enriched subcontinental lithospheric mantle (SCLM), probably the wedge of depleted mantle enriched in LIL elements by hydrous fluids generated by the dewatering of the underlying subducting slab. Fitton et al. (1988) and Ormerod (1988) interpret all the extension-related basaltic rocks of the Basin and Range province as mixtures of components derived from this SCLM and an asthenospheric mantle, as represented by the ne-normative small volume alkali basalts of the Geronimo or Lunar Craters volcanic fields in the center of the Basin and Range province (Figs. A and D).

Imnaha Basalt flows, the earliest eruptions of the CRBG, are relatively homogeneous isotopically and have a trace element profile distinct from HAOTs, but similar to OIBs Fig. A); that is, they carry the isotopic and chemical signature of a single asthenospheric source. Unlike the asthenosphere-derived central Basin and Range basalts, however, they are never ne-normative, are less enriched in incompatible elements (Fig. A) and have distinctive Nb/Zr and Nb/Ba ratios (Fig.D). This suggests higher temperatures and greater degrees of melting of the asthenosphere than required for the small Basin and Range flows. The Imnaha flows are isotopically and geochemically similar to Hawaii basalts with all those features expected of mantle plume eruptions. The voluminous Grande Ronde Basalt flows, which erupted immediately after the Imnaha, form linear isotopic and chemical arrays suggesting mixing of the Imnaha source component with a lithospheric (high SiO2, high K2O,?crustal) component.

The younger SMB flows, the third subgroup of the CRBG, have the distinctive isotopic signature of a source enriched some 2000 m.y or earlier, a source which can only be ascribed to the SCLM beneath the older cratonic crust of the Pre-accretionary North American Plate. In this they resemble the basalts of the Snake River Plain (Leeman, 1982; Carlson and Hart, 1988).

Whereas some have advocated a mantle plume origin for the CRBG (Duncan, 1982; Brandon and Goles,1988), others have preferred to equate the CRBG with volcanicity associated with the Basin and Range back-arc spreading (Carlson and Hart, 1988). **We conclude from the combined isotopic and chemical evidence now available, first, that it is possible to distinguish those volcanic rocks associated with Basin and Range lithospheric extension from the Main Series of the CRBG by their distinctive isotopic and chemical signatures. Second, that one of the primary mantle-derived components of the Main Series of the CRBG is similar to OIBs; a component derived from relatively large degrees of melting of the asthenosphere, and hence compatible with a mantle plume.** It also appears that the asthenosphere-derived magmas associated with the Basin and Range extension differ from those apparently associated with the plume only in parameters which are at least qualitatively explainable in terms of temperature and the degree of partial melting (total abundance of incompatible elements and such ratios as Nb/Zr and Zr/Y). Finally, it is apparent that if we accept a plume origin for the Main Series of the CRBG, the plume was able to mobilize and incorporate substantial proportions of a lithospheric component to form the large volumes of Grande Ronde Basalt.

If we accept a plume component in the initiation of the CRBG volcanism and assume that the plume involved is that now under Yellowstone, then we are left with some tectonic problems. Dominant among these are (a) the absence of an obvious hot spot track on either side of the center of the CRBG eruption (close to the triple state junction of Idaho, Oregon and Washington); (b) the apparent trace of the Yellowstone hotspot further south along the Snake River Plain; and (c) the accepted relative plate motions. Some of these problems have already been addressed by earlier advocates of a plume origin for the CRBG. Here we emphasize two arguments in support of the Yellowstone plume being responsible for the CRBG. First, that if the plume underlay the center of the CRBG eruption it would have been overridden in a short time by the massive continental block of the older North American plate which had only recently been thickened and welded by the intrusion of the Idaho batholith. This, we suggest, would have provided a formidable barrier to the direct penetration of the plume. The contrast between this and the thinner accreted crust through which the plume had earlier forced its way and also with the old tectonic boundary that now constitutes the Snake River Plain (Oregon-Nevada Lineament), is extreme and it seems not unreasonable that the plume would have been deflected to reach the surface by these two alternative paths rather than push straight through the massive batholith. In support of such a scenario is the dwindling rate of eruption of the CRBG after the huge eruptions of Grande Ronde Basalt with the increasing proportion of a lithospheric component throughout the

eruption of the Main Series and the increasing age of enrichment of that lithospheric component, all of which culminated in the eruption of the small flows of the Saddle Mountains and Snake River Basalts. These were entirely derived, apparently, from the ancient pre-accretionary lithosphere which surrounds, and presumably underlies, the Idaho batholith.

References:

Duncan, R.A.,1982, J. Geophys. Res., 87.

Brandon, A.D.,1989, J. Geophys. Res., 94.

Brandon, A.D. and Goles, G.G.,1988, Earth and Planet. Sci. Letts.,88.

Carlson, R.W. and Hart, W.K.,1988, In J.D. Macdougall (Ed.), *Continental Flood Basalts*, Kluwer Academic Publishers, Dordrecht.

Donnelly-Nolan, J.M., Champion, D.E., Grove, T.L., Baker, M.B., Taggart, J.E. and Bruggman, P.E., in press, J. Geophys. Res.

Fitton, J.G., James, D., Kempton, P.D., Ormerod, D.S., and Leeman, W.P,1988, J. Petrol., Sp. Vol.

Hart, W.K., Aronson, J.L., and Mertzman, S.A.,1984, Geol. Soc. Amer. Bull., 95.

Leeman, W.P.,1982, In Bonnischsen and Breckonridge (Eds.), *Cenozoic Geology of Idaho*, Idaho Bureau of Mines and Geology Bull., 26.

Ormerod, D.S., Ph.D. Thesis, Open University, U.K.,1988.

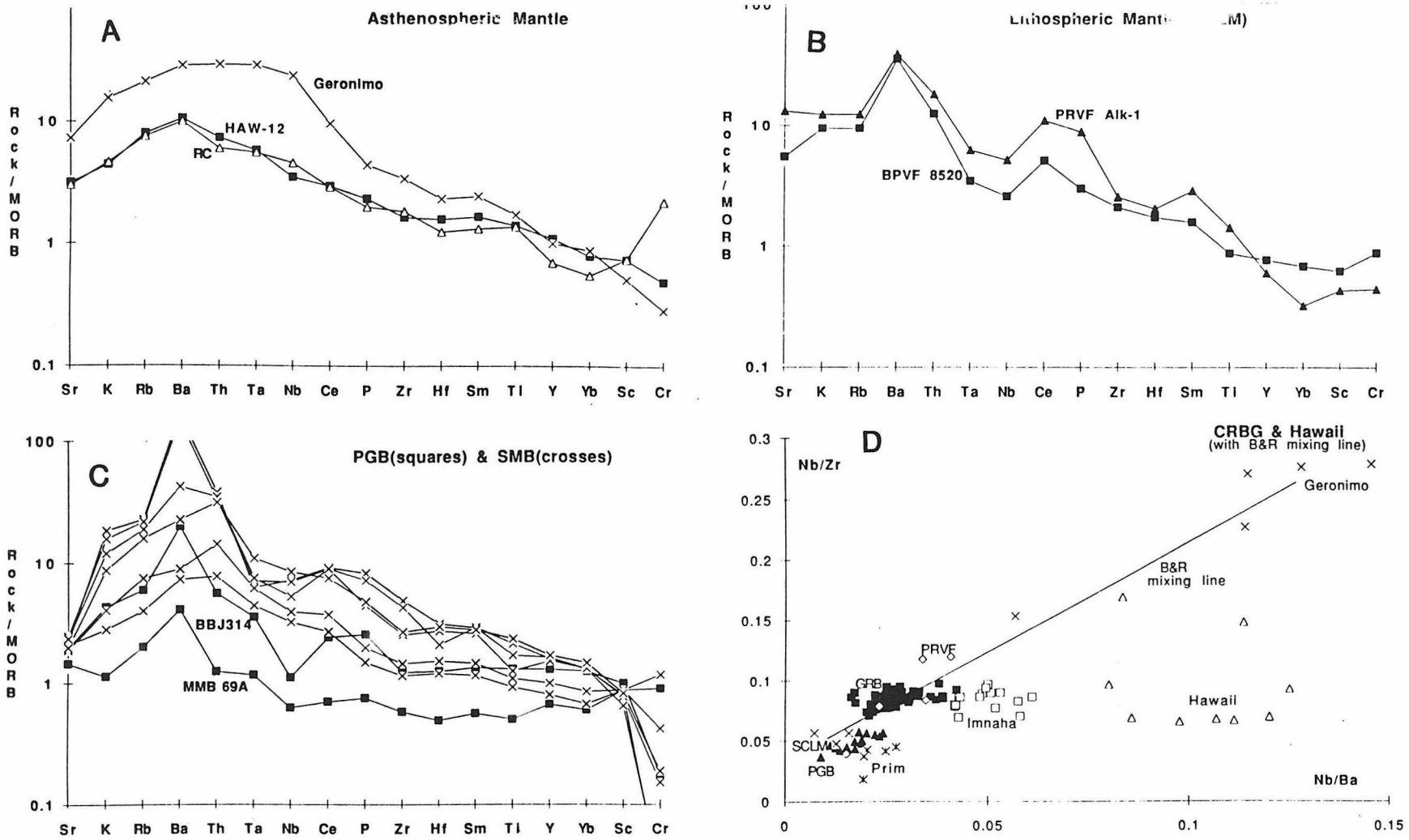

Fig. A. Spidergrams of alkali basalt from the central Basin and Range extensional province in Nevada (Geronimo Volcanics; Fitton et al., 1988), from Hawaii (BVSP, 1981) and an RC (Imnaha) flow from the Main Series of the CRBG. All three patterns are similar and typical of magmas derived from asthenospheric mantle. The flows from Hawaii and the Imnaha have much lower abundances than those of the small ne-normative flows of the Geronimo Volcanics, implying greater degrees of partial melting for the plume-related flows.

Fig. B. Typical spidergrams for olivine basalts from the margins of the Basin and Range extensional province. BPVF from the Big Pine volcanic field, Nevada (Ormerod, 1988) and PRVF from the Powder River volcanic field, south of OWL, NE Oregon (D.G. Bailey, 1990).

Fig. C. Spidergrams of Picture Gorge (PGB) and Saddle Mountains (SMB) Basalt flows of the CRBG. MMB 69A is a dike of primitive HAOT composition, BBJ 314 is a more typical flow of the Dayville Formation (M.M. Bailey, 1989).

Fig. D. Nb/Zr vs Nb/Ba plot of typical Basin and Range basaltic rocks (X) and the source mixing line that connects them (original data from Ormerod, 1988 and Fitton et al., 1988), with rocks of, or associated with, the CRBG. All flows of the PGB and the most primitive HAOTs (prim) of NE Oregon fall close to the SCLM endmember component of the B&R mixing line. Typical Powder River olivine basalts (PRVF) fall further up the mixing line close to Ormerods (1988) Big Pine volcanic field tholeiites. Basalts of the Main Series of the CRBG appear to lie on a trend with most of the Hawaii basalts (BVSP, 1981) which crosses the B&R mixing line. The PGB and Main Series subgroups of the CRBG have restricted and different Nb/Zr ratios

The Geometry of Thermal Mantle Plumes

Gregory A. Houseman

Department of Earth Sciences, Monash University, Clayton VIC 3168
(e-mail: greg@pegasus.earth.monash.edu.au)

The Earth's mantle convects. The lithospheric plates are an integral part and the most evident part of that convection system which includes the entire mantle. The convective flow is entirely driven by buoyancy forces, both negative buoyancy as found within the cold subducted slab, and positive buoyancy as found at mid-ocean ridges. Thermal buoyancy is distinguished from compositional buoyancy arising from systematic compositional variations. The buoyancy forces within the mantle are probably due mainly to lateral temperature differences and the interaction of the temperature field with the major phase transitions. Compositional buoyancy may play a major role in the convection system if it is responsible for a hypothesized separation of the convection system into two discrete layers with a boundary at about 700 km depth. Aside from this controversial hypothesis, which is the subject of conflicting geophysical and geochemical arguments, there is little evidence that compositional buoyancy plays any major role in the mantle convection system.

Mantle plumes are key elements of the plate tectonics theory, introduced to explain the linear seamount-island chains (hotspot trails) whose age increases linearly with distance from a presently active source characterised by elevated topography and heat flow, positive gravity and geoid anomalies, and volcanism. A mantle plume is a source of hot, perhaps partially molten, mantle material which presses upwards because of its excess buoyancy, heating and uplifting the overlying lithosphere by an elevation of order 1 km. Relative to the plates moving about the surface of the Earth, mantle plumes appear to form an almost fixed reference frame against which other plate motions may be measured. Plumes may be long lived (80 m.y. in the case of Hawaii) and they clearly mark sites of upwelling from deep within the mantle. An ocean ridge, on the other hand, does not in general remain located above a zone of hot deep upwelling within the mantle (1), although it may have originated in a continental rift located above a group of mantle plumes.

Experimental and numerical studies of convection in simple systems have clearly established the symmetry between hot and cold thermal structures in a layer heated from below. These studies have also shown that this symmetry is completely broken when the layer is heated internally; the flow is then characterised by concentrated downwelling structures embedded in a diffuse upward flow (2,3,4). Mantle plumes would necessarily owe their existence to compositional rather than thermal buoyancy if the mantle were entirely internally heated. Indeed, a very significant compositional buoyancy would be required for a plume to punch its way through an internally heated convecting layer without being dissipated by the thermally induced flow. It seems likely that mantle plumes are in fact of thermal origin and that their existence indicates a significant component of heat input to the base of the convecting layer. It is then a logical inference that mantle plumes together with subducted slabs are the principal hot and cold thermally buoyant structures within the convecting mantle. The concentration of mantle plumes in regions distant from subduction zones is one of the observations indicating the thermal origin of mantle plumes (5). Most of the other physical characteristics of mantle plumes are consistent with the inference that they owe their existence primarily to thermal rather than compositional buoyancy.

Linking thermal mantle plumes to basal heating immediately raises the question of which level we identify as the base of the layer and how much heat is input there. If the base of the layer is the core-mantle boundary (CMB) we have the difficulty of explaining why there is an unexpectedly large heat flow out of the core and why there is such a large number of relatively closely-spaced mantle plumes (6). Can all of the plumes be of thermal

origin in this case? The alternative hypothesis of a compositional boundary at 700 km and a 2-layered convection system avoids these problems, as the upper mantle layer would be predominantly heated from below and the plume spacing would be decreased by a factor of about 4 relative to the depth of the layer. With the layered hypothesis, upper and lower mantles convect separately, probably with some leakage. However, the layered mantle convection hypothesis runs into difficulties posed by the interpretation of seismic travel-time anomalies (7) and gravity anomalies (8). In my opinion this question of layered versus unlayered mantle convection is not yet satisfactorily resolved.

To investigate the geometry of the thermal structures that would be present in a 700 km thick mantle layer with a component of basal heating, I have carried out a set of numerical experiments using 3-D Cartesian geometry and assuming a constant viscosity fluid. These experiments illustrate time-dependent thermal convection where half of the total heat flow through the system is generated internally and the other half is input as a uniform heat flow through the base of the layer. The equations of incompressible flow are solved in a cell of dimensions ad x ad (horizontal) x d (vertical) where a is either 4 or 8, d is 700 km, and the solution is assumed to reflect in the side boundaries of the cell. The upper boundary is constant temperature, and both rigid and stress-free horizontal boundaries were considered. The Rayleigh number in these experiments is 587,000, about 1000 times the critical value for onset of convection, but significantly less than the values estimated for either upper mantle or whole mantle convection. The finite difference methods used to solve the three conservation equations that govern the behaviour of the above system in space and time (conservation of mass, momentum and energy) have been described previously (9).

Although these experiments are grossly over-simplified relative to the mantle, they permit some interesting observations about the geometry and time dependence of a class of hot thermal structures that are analogous to mantle plumes. Contrary to physical intuition or to the expectations generated by decades of 2-D numerical modelling, these thermal structures are neither axisymmetric nor sheet-like. The hot structures rise from the basal hot boundary layer as a network of connected vertical sheets (Figure 1a). But the most intense upwards flow occurs at the nodes where these sheets join together and, towards the top of the layer (Figure 1b), the dominant character of the upwelling is that of a connected group of hotspots, each with approximately cylindrical geometry. The cold sinking structures have more buoyancy than the hot rising ones because of the component of internal heating, but they have a complementary character which is sheet-like near the upper surface, evolving into cold spots near the base of the layer. The spontaneously arising experimental geometry of the near-surface thermal structures approximately reproduces the characteristic surface geometry of plate tectonics: linear or arcuate subduction zones separated by groups of hotspots.

These solutions have an interesting time-dependence characterised by the occurrence of boundary layer instabilities which typically form on the hot sheet structures and then get swept into the vertical flow associated with the thermal plumes. Analogous instabilities on the cold upper boundary layer also occur. The major thermal structures are relatively stable with respect to the small-scale thermal instabilities, so that a region of hot upwelling is likely to remain so for many overturn times. But these structures are continually modified by the effect of the boundary layer instabilities so that individual plumes are always competing for prominence and may flare up, fade away, or merge with other nearby plumes. The time dependence is best shown by animation, and a time-lapse video animation showing the time variation in a horizontal plane is available from the author. The a=8 solution shown here (Figure 1) may be compared with a previously published a=4 calculation (10). Although there is a tendency for hot or cold thermal structures to align themselves with the reflection boundaries at the sides of the cell, the structure within the interior of the 8x8x1 cell shows that these boundary artifacts do not seriously bias the thermal structures. Vertical velocity at depth 350 km is of order 1 cm/yr

in these calculations, and thus the time taken to traverse a 700 km thick layer is of order 70 m.y.

The impact of mantle plumes on the lithosphere may be highly variable. In the continental environment that impact may range from relatively minor uplift to extensive volcanism, continental rifting and the possible initiation of sea-floor spreading. The characteristic triple-junction signature of continental rifts (11) appears to be a consequence of the geometry of the uplift above thermal plumes. Although the uplift is approximately axisymmetric, the departures from axisymmetry reflect the geometry of the thermal sheets at the base of the layer and these sheets typically merge beneath the thermal plumes as 3 or 4 - armed triple-junctions. The highly non-linear rheology of the continental lithosphere ensures that the non-axisymmetric perturbation to the uplift function will be amplified, to concentrate the extensional deformation along radial arms oriented parallel to the hot sheets at the base of the layer, i.e. to form a characteristic triple-armed rift. Continental rifting is probably in many cases diagnostic of sub-lithospheric mantle plumes, and because the chronology of rifting can often be well constrained, there is some prospect of mapping the evolution over geological time of the thermal structures within the mantle by carefully mapping the evolution of the global distribution of rift structures. Although erosion and the general structural complexity of the continental crust may obscure much of the history of hot-spot activity, a failed continental rift may be a long-lived record of a mantle plume impinging on the base of the continental lithosphere.

In the oceanic environment large scale lithospheric deformation is unlikely and hotspot trails are the clearest indicators of thermal plume activity. Figure 3 shows some synthetic hotspot trails produced by moving an imaginary surface plate at a constant velocity above the time-dependent convection system (8x8x1) shown in Figure 1, and recording the locations of probable volcanic activity at any given time. Those locations are determined approximately by finding the locations of the local maxima of the temperature field in the horizontal plane, at depth z=d/4, and if the value of a local maximum is above a threshold value the location is plotted with a symbol representative of the time of activity. These synthetic hotspot trails are approximately linear and aligned with the plate movement vector, but the departures from linearity illustrate the consequences of the time dependent features of the convection circulation described above: adjacent trails merge and then split again into separate trails. Other hotspot trails are discontinuous, disappearing for some time and then reappearing.

In conclusion, these experiments illustrate a style of mantle convection with a component of heating from below, in which mantle plumes are a natural consequence of thermal buoyancy. Near the upper surface the plumes are approximately axisymmetric, but followed downwards the thermal structure evolves into a network of connected thermal sheets on the base of the layer. These thermal structures have a long term stability that is subject to continuing modification by small scale instabilities. The properties of these modelled plumes are consistent with the observed properties of mantle plumes even though the Rayleigh number used here is probably too small, and neither rigid plates nor variable viscosity have been included in the calculations. Supercomputer time for these calculations was provided by Leading Edge Inc. and the ANU.

(1) Houseman, G., *Earth Planet. Sci. Lett.*, **64**, 283-294, 1983.
(2) Carrigan, C.R., *Science*, **215**, 965-967, 1982.
(3) Houseman, G., *Nature*, **332**, 346-349, 1988.
(4) Bercovici, D., Schubert, G. & Glatzmaier, G., *Geophys. Res. Lett.*, **16**, 617-20,1989
(5) Weinstein S.A. and Olson, P.L., *Geophys. Res. Lett.*, **16**, 433-436, 1989.
(6) Vogt, P.R., *J. Geophys. Res.*, **86**, 950-960, 1981.
(7) Creager, K.C. and Jordan, T.H., *J. Geophys. Res*, **91**, 3573-3589, 1986.
(8) Richards, M.A. and Hager, B.H., *J. Geophys. Res.*, **89**, 5987-6002, 1984.
(9) Houseman, G.A., *Geophys. J. Int.*, **100**, 33-38, 1990.
(10) Houseman, G., *Geophys. J. Int.*, **102**, 15-24, 1990.
(11) Burke, K. and Dewey, J.F., *J. Geol.*, **81**, 406-433, 1973.

Fig 1a

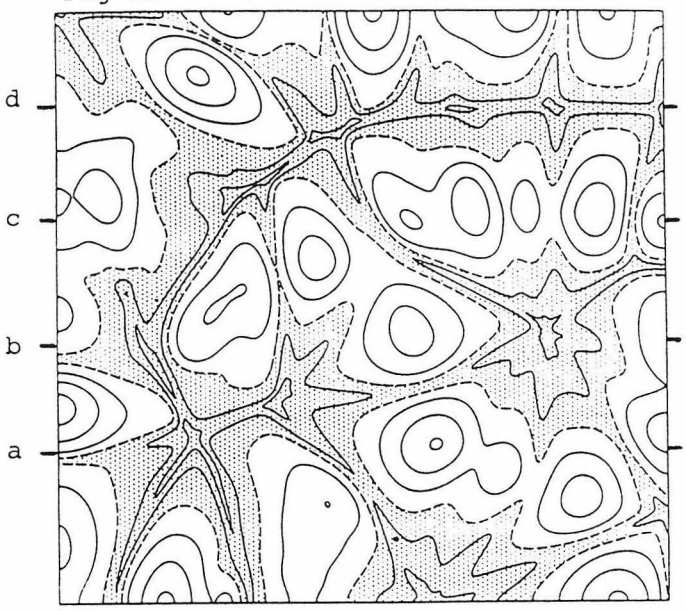

Fig 1b

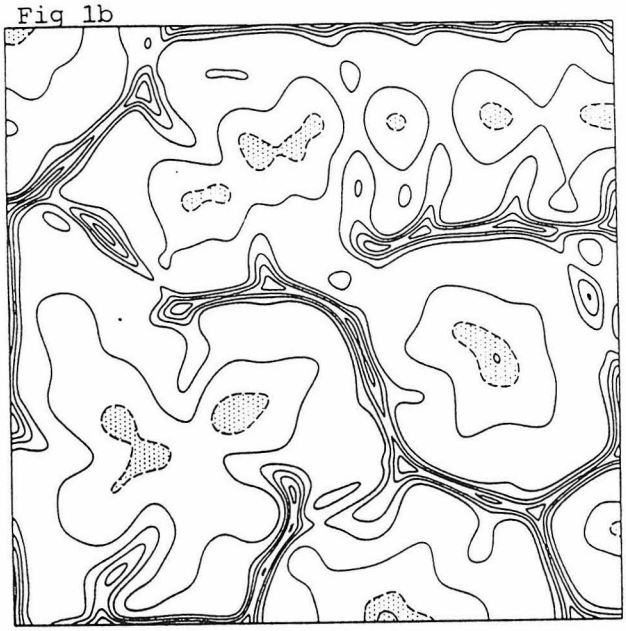

Fig 2

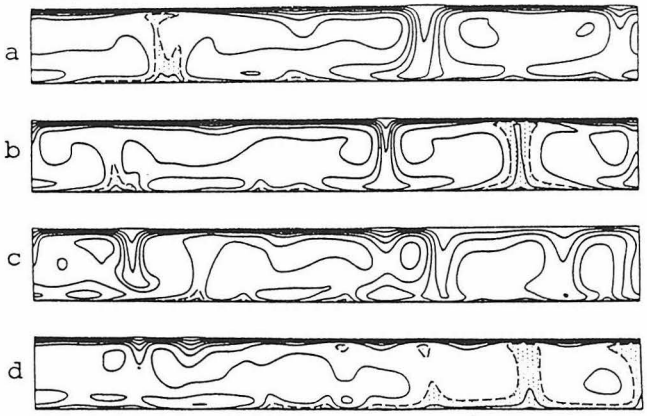

Fig 3

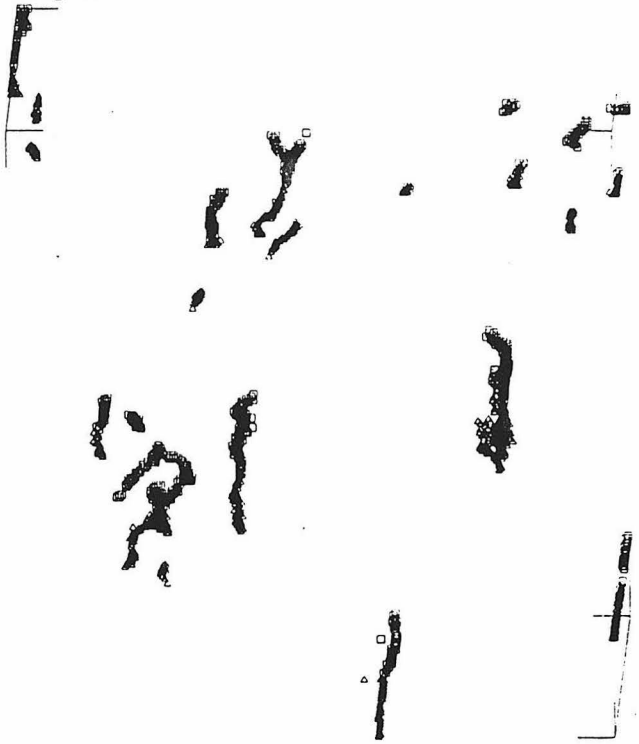

Figure 1. Contours of temperature in the horizontal planes (a) z = 0, the base of the layer, and (b) z = 28h, near the base of the upper thermal boundary layer (h = d/32). The arrows adjacent to (a) show the coordinates of the orthogonal sections in Figure 2. The contour interval is 300 degrees C, the T = 1800 degrees C contour is shown dashed, and temperatures hotter than 1800 degrees C occur in the stippled areas.

Figure 2. Contours of temperature in the vertical planes (a) y = 66h, (b) y = 112h, (c) y = 166h and (d) y = 216h (h = d/32). Other conventions are as in Figure 1.

Figure 3. Synthetic hotspot tracks generated by moving an imaginary plate over the convecting layer shown in Figure 1. The older part of each track is shown using a triangle and the younger half using a square symbol. Compare plume locations in Figure 1b with the upper end of the hotspot tracks. The plate velocity vector is shown as the line connecting the two right angles (down to the left). For this illustration, the square defined by the right angle brackets is 5,600 km across, the plate moves 1165 km, the elapsed time is 642 m.y. and average plate velocity is 1.8 mm/yr. A small plate velocity and large elapsed time are used here as the Rayleigh number of the convection is about 10 x lower than a realistic upper mantle estimate.

Young Western U.S.-Interior Tectonism and Volcanism: Hot or Wet?

Gene Humphreys, Ken Dueker and Francois Saucier

University of Oregon

Several aspects of western U.S. structure and activity that are peculiar and in need of explanation include:

-Most of the interior of the western U.S. has been elevated within the last 10-20 Ma, including:

Great Plains (stream incision, Trimble, 1980)
Rocky Mountains (deposition and drainage patterns, Dickenson et al., 1988)
Colorado Plateau (stream incision)
Great Basin (pollen-inferred climatic zonation, Axelrod, 1968)
Sierra Nevada (Disruption of topography, Christiansen, 1966)

Though the evidence from each region is not compelling, but in whole the evidence for young regional uplift is strong.

-Much of the volcanism during this time has been "active" (not attributable to extension), including:

Columbia River flood basalts (about 15 Ma).
Snake River Plain (since about 10 Ma).
St. George trend (young volcanism partially on the Colorado Plateau).
Jemez lineament (young volcanism trending obliquely across the Rio Grande Rift).

-Upper mantle structure (Figure 1 and 2) is very heterogeneous, and is:

discordant with recent tectonic activity, trending SW beneath the Great Basin
concordant with active volcanism, and co-incident with areas of high heat flow.

This structure is most reasonably interpreted as volumes of partially molten (low velocity) upper mantle juxtaposed against (high velocity) disrupted mantle lithosphere.

We present two general histories to account for these and other observations, which we term the hot and the wet hypotheses. Either one is plausible, as far as we know. These cast Yellowstone either as part of a greater "plume" event, or as a feature unrelated to plumes.

HOT

The recent uplift of western U.S. requires a massive influx of buoyancy. Western U.S. upper mantle is very slow and attenuating on average (Figure 3). These observations can be attributed to a regional inflation of unusually hot mantle. If so, because of the great area involved in this uplift and because the uplift pre-dates the Snake River Plain, St. George and Jemez volcanic trends, this unusually hot mantle required some time to ascend through the lithosphere and create the young active volcanism. We note that the low and high-velocity upper mantle structure defines a pattern of NE-SW oriented trends spaced a few hundred kilometers apart. Three possible processes to account for this include:

(1) The excessively hot mantle initiated convective destabilization of the lithosphere. If this were to occur, then the energetically favored flow pattern would be cylindrical rolls aligned with the upper mantle shear field (i.e., the absolute plate motion of the North American continent), causing NE-SW trending convective roll axes. These convective rolls would become disrupted near the western continental margin under the influence of the transform-induced flow field. Observations bear out this structure.

(2) The hot, buoyant mantle forcibly ascended in zones of inherited Precambrian weakness. In support, Precambrian structure appears to have the same trend (based on the orientation of geochemical patterns thought to sample upper mantle sources [DePaolo and co-workers] and on the location of a geophysically-inferred Precambrian crustal "flaw" associated with the Yellowstone trend [Eaton et al., 1975], and the western limit of the imaged upper mantle structure coincides well with the Sr-inferred western limit of Precambrian basement. A variation on this theme, supported by the same information, is that the entire upper few hundred kilometers of the mantle beneath the

uplifted region is relatively hot, and that (Precambrian) mantle compositional variations in solidus temperature (i.e., variations in "fertility") result in the imaged variations of inferred partial melt zones. (A problem with attributing Nevada upper mantle structure with Precambrian upper mantle structure is that the imaged upper mantle structure is about 200 km thick, whereas most of Nevada is, presumably, underlain by a Paleozoic thermal boundary layer that developed after this region was thermally disrupted in the late Precambrian.)

(3) The Yellowstone, St. George and Jemez trends are each the expressions of hot spots. Each volcanic trend would then represent individual members of a hot spot family; the causative plumes, in this case, would be bent over in the shear flow produced by the motion of North America over the more stable deep mantle, thus creating a set of parallel "tracks" that lack a well-defined time progression (this idea was supplied, though not necessarily endorsed, by Mark Richards).

WET

The region affected by young uplift, volcanism and tectonism is the same region that was affected by an unusual Laramide event about 75-50 Ma. During this event, arc magmaism was largely absent and whole-crust thrust faulting created mountains in the deep continental interior. We suggest (Figure 4), as have others, that the subducting slab during the Laramide was horizontal beneath western U.S., physically compressing the continental interior. Arc magmatism is commonly attributed to dehydration of the uppermost subducted slab within the asthenosphere at a depth of 100-125 km. Flat subduction, then, would prevent magmatism, and flat subduction for 25 million years would layer the bottom-side of western North America with large amounts of water-rich material. Uplift followed the Laramide by roughly 30 million years, such as may occur if the subducted slab was abandoned and thermally adjusted to its upper mantle setting. Uplift, under this wet hypothesis, requires either significant amounts of (1) hydration of uppermost mantle, or (2) water-induced partial melting and basaltic ascent and ponding at the base of the crust (i.e., underplating); because basalt is more buoyant than its parent, and because the rock depleted of basalt is also more buoyant (largely as a result of *Al* depletion [Jordan, 1975]), significant amounts of buoyancy can be created locally this way.

This mechanism does well in associating the co-incidence in the regions affected by the Laramide and recent uplift, and in providing a uniform mechanism for uplift from the Great Plains to the Sierra Nevada; not so apparent, however, is a means of creating the orientation and wavelength of the upper mantle structure and the volcanic trends (though perhaps compositional variations of Precambrian age influenced this in a manner similar to that suggested above).

Whatever the Yellowstone/Snake River Plain feature actually is, we do have a very well resolved image of the upper several hundred kilometers there (Figure 5). The low-velocity upper mantle beneath this volcanic province is steep-sided and extends to a depth of at least 200 km, but not significantly deeper than 250 km. Beneath the younger portions of this region the anomalous structure is stronger, narrower and appears to extend less deeply into the Earth.

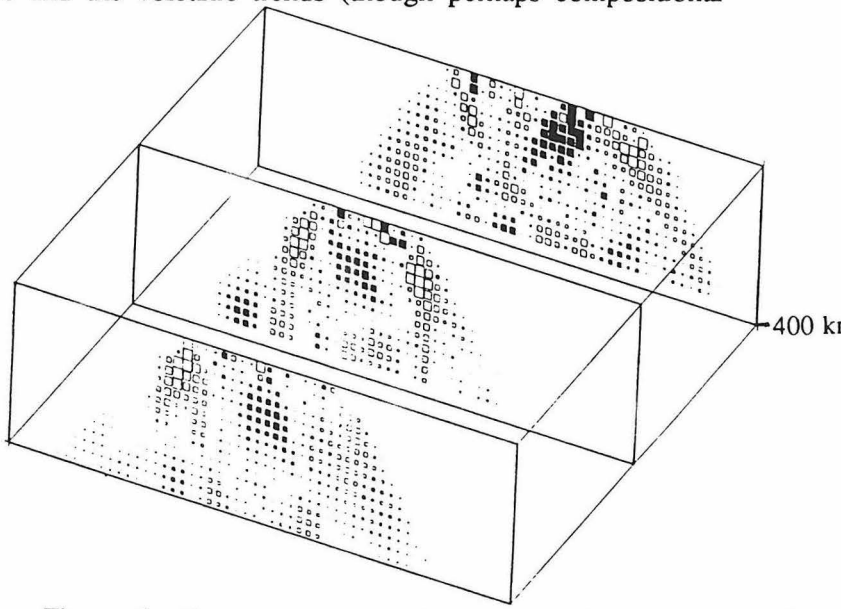

Figure 5. P-wave structure along the Yellowstone volcanic trend at the three cross sections indicated in Figure 3. Full symbol size indicates ±3% velocity variations. Note the confinement of the low velocities above 200 km

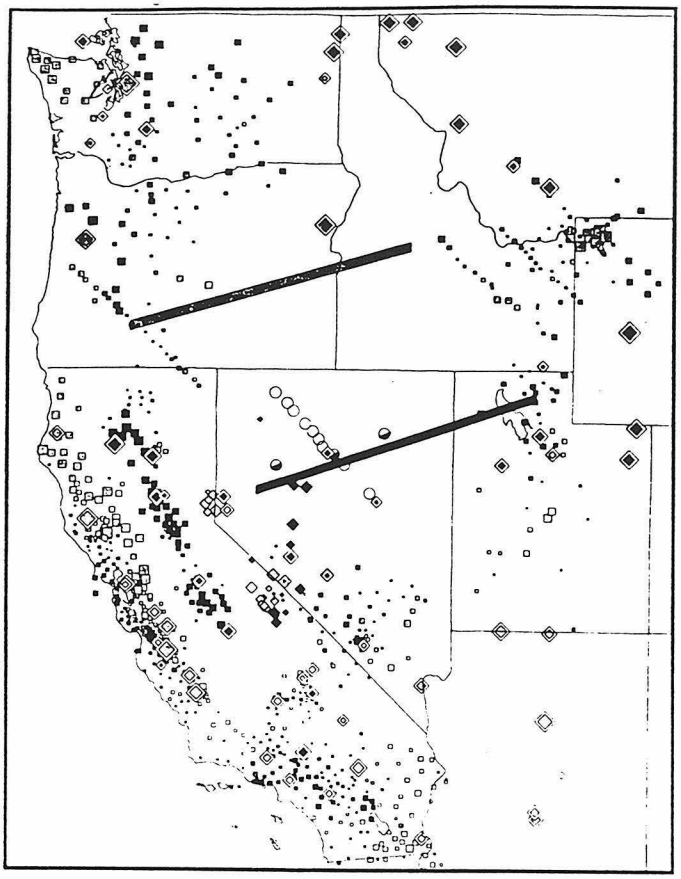

Figure 1. Average P-wave travel-time residuals from Humphreys and Dueker (in prep.). Largest symbol size indicated ± 0.6 s variations, with black and gray representing early and late arrivals, respectively. Such large residuals require large P-wave velocity variations in the upper mantle (e.g., ±3% P-wave variations in the 40-200 km depth range could produce these residuals). The outlined diamond symbols are ISC stations residuals from Dziewonski and Anderson (1983). The bold black and gray lines in the Great Basin represent fast and slow surface wave paths from Priestly and Brune (1982).

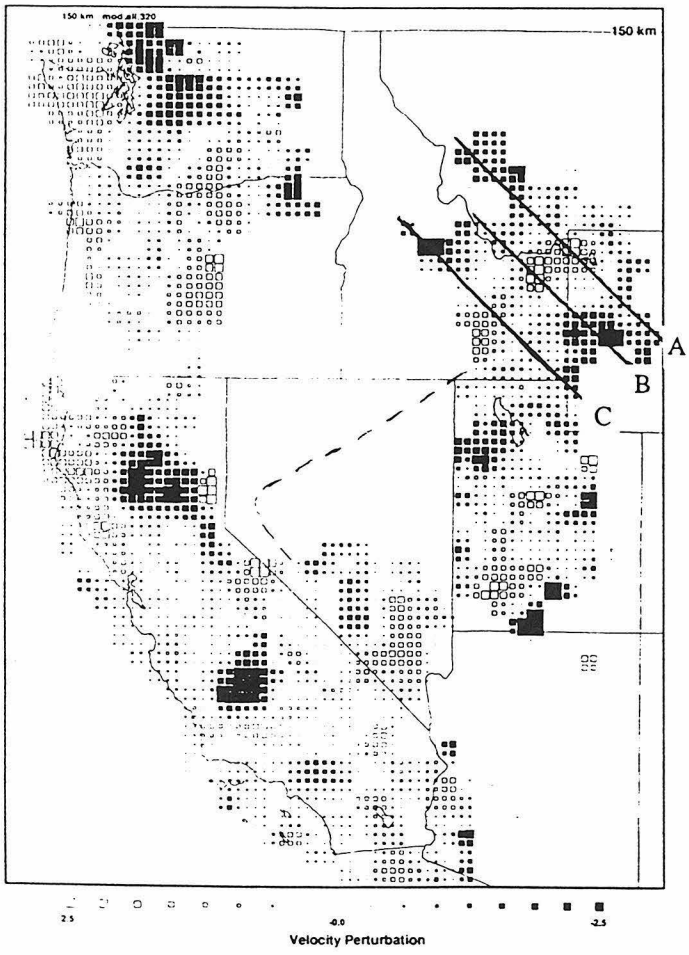

Figure 2. Upper mantle P-wave structure at 150 km depth (Humphreys and Dueker, in prep.) Filled and unfilled squares represent high and low velocities, respectively, with full symbol size indicating ±2.5% variations. The occurrence of such great P-wave variations necessitates great variations in the temperature and/or partial melt content.

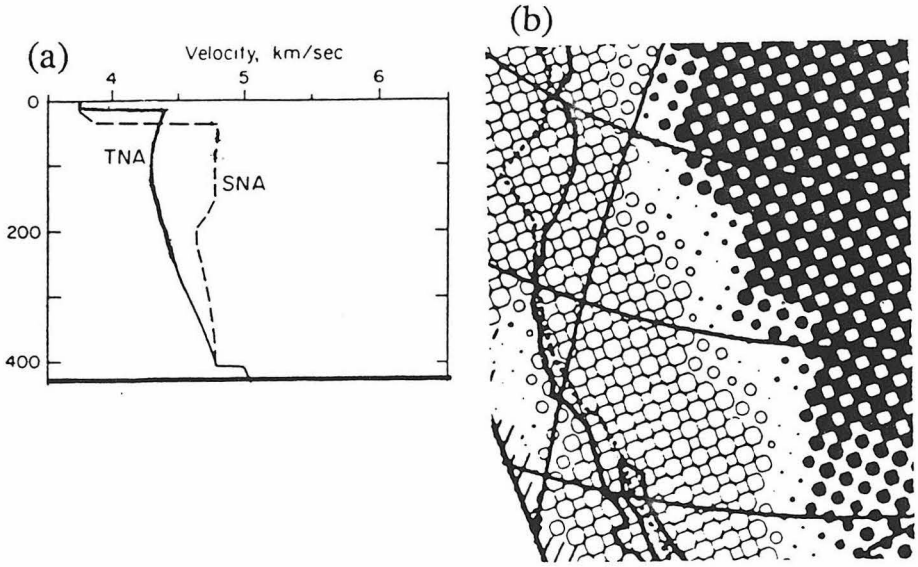

Figure 3. 1-D western United States upper mantle velocity structure. (a) 1-D S-wave velocity from Grand and Helmberger (1984). TNA, and SNA refer respectively to Tectonic North America (i.e, western U.S.) and Shield North America. The average velocity of 4.3 km/s for TNA in the 50-200 km depth range is considerably slower than worldwide average (e.g., PREM averages 4.46 km/s in this depth range). (b) Map view S-wave velocity structure in 0-160 km depth range (Grand, 1989). This image shows the boundary between TNA and SNA to lie approximately near the easternmost extent of Laramide deformation (i.e., the Rocky Mt. Front).

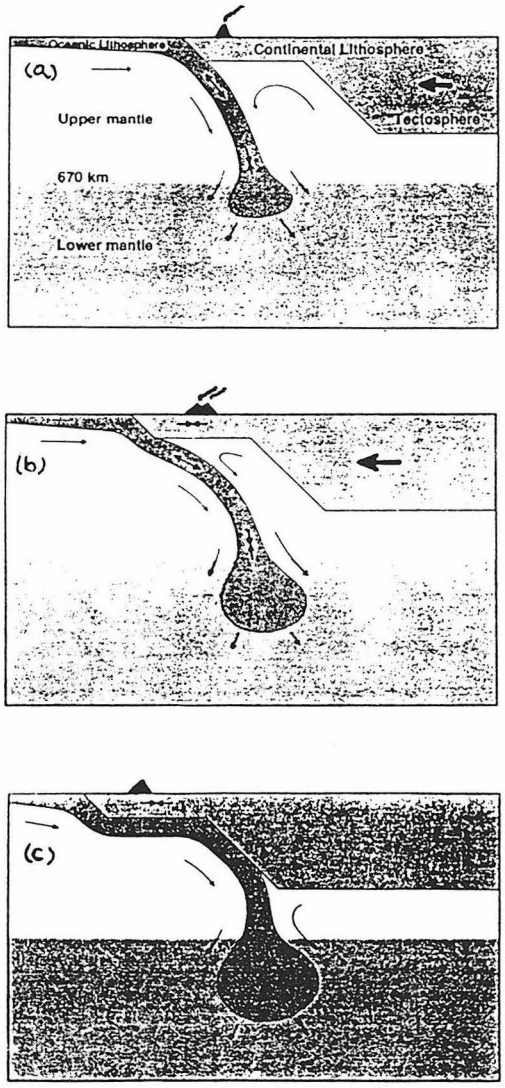

Figure 4. Schematic scenario of Laramide Orogeny from Saucier et al., (1988), based on results of numerical modeling.

(a) Pre-Laramide. Subduction occurring normally.
(b) Sevier (just prior to Laramide). The partial blockage of back-arc mantle re-supply caused by the non-convecting continental root magnifies back-arc suction and pulls up on the slab. This causes some eastward migration of the volcanic arc.
(c) Laramide. The slab has been pulled against the western North America lithosphere (and root), driving compression in the overlying lithosphere. Magmatic activity has been terminated, and the water associated with the slab may be deposited beneath the broad area affected by the Laramide.

IMAGING DEEP SEISMIC STRUCTURES BENEATH YELLOWSTONE, HAWAII AND ICELAND, PRESENT HOT SPOT LOCATIONS IN THREE GLOBAL TECTONIC ENVIRONMENTS

H. M. Iyer, J. R. Evans, G. R. Foulger[1], and B. R. Julian
U. S. Geological Survey, M.S. 977
345 Middlefield Road, Menlo Park, CA 94025

ABSTRACT

Seismic tomography is a powerful tool which is ideally suited to image hot spots and mantle plumes. To test existing theories of hot spots, specifically whether they are sustained by deep mantle plumes, we need to carry out tomographic experiments capable of delineating anomalous structures with horizontal dimensions of $100-200\ km$ extending to depths of at least the base of the upper mantle (ideally to the top of the core). We need a spatial resolution of the order of 20 km and velocity resolution of fraction of 1% in P and $1-2\%$ in S. With the current advances in instrumentation and analysis techniques it is realistic to visualize large-scale experiments to solve these fundamental problems. In particular, the enhanced instrumental and technical know-how and major collaborative efforts made possible by the advent of the IRIS/PASSCAL Consortium brings detailed multi-disciplinary seismological experiments of this scale feasible. In this poster, we propose experiments at three current hot spot locations: Hawaii, on an oceanic plate, Yellowstone, on a continental plate, and Iceland on a mid-oceanic ridge.

All three hot spots are currently volcanically active, accessible, and well studied. Extensive seismological studies of deep crustal structure using a variety of techniques have been carried out at each of them. However, exploration of the upper mantle has been rudimentary due to lack of adequate instrumentation. Our basic strategy is to operate dense arrays (with average spacing of approximately 20 km) of short-period seismographs interspersed with 3-component broad-band stations, to record P-waves, S-waves, and surface waves. To achieve this instrumentation density, several sequential deployments may be required. Analysis of the data can be expected to yield 3-dimensional images of

P- and S-velocity and P- and S-attenuation beneath the hot spots. Additional results include receiver functions and measures of anisotropy at the broad-band-station locations.

Since the island of Hawaii is only about 100 km in diameter, the proposed high spatial resolution can be achieved only to a depth of 150 km. However, by operating two rings of OBSs of 150 and 200 km diameter, the resolved depth can be increased to 300 km, albeit with lower resolution. Operating seismic stations on the other islands of the Hawaiian chain will enable reaching even greater depths and studying the aging process along the island chain. Since Iceland has an area of about 300 $km \times 400$ km it is feasible to probe deep into the upper mantle entirely with land stations. OBSs, if available can significantly increase this depth and/or extend observations along the ridge. At Yellowstone, on the other hand, the magnitude of the experiment is only limited by resources: instrumental, human, and financial. A practical experiment would be to operate several $600 - km$ long, northwest-striking profiles, eventually encompassing an area of 600 $km \times 600$ km centered on Yellowstone National Park.

The proposed experiments require major collaborative efforts between academia and U. S. Government organizations, and need international collaboration for the Icelandic experiment. The result of such an effort would be a superb data set. Analysis and interpretation of the data by various groups using a variety of powerful modeling and interpretive techniques will result in better understanding of the origin and evolution of mantle plumes and hot spots providing major constraints for geochemical and tectonic models.

[1]Department of Geological Sciences, University of Durham, England.

HOTSPOTS: INFERENCES FROM THEIR DISTRIBUTION, AND PLATE KINEMATICS

Donna M. Jurdy (Department of Geological Sciences, Northwestern University, Evanston, Illinois 60208-2150)

Michael Stefanick (Science Systems & Applications, Inc., Seabrook, Maryland 20706)

Hotspots show a very non-uniform distribution over the earth's surface that may be a clue to their origin. We have analyzed [*Jurdy and Stefanick,* 1990] 4 published hotspot catalogues of varying sizes (19-117) and compared these with synthetically generated random sets of corresponding sizes. Hotspot catalogues all show a hemispheric concentration. The cumulative distribution of each set about its center of mass shows a simple power law growth, with the number of hotspots growing approximately with the square root of area. This corresponds to a fractal dimension closer to 1 than 2 (Figure 1). All published sets show these characteristics to varying degrees. None of the randomly-generated sets of points have these characteristics. It is possible to define a simple shift of random sets that produces characteristics like the published catalogues; so, one possible explanation of the pattern is global counterflow balancing the surface motion toward the subduction zones. The possible relation of the hotspots to the locations of ridges and subduction zones is tested using large sets of randomly-generated points to estimate areas within given distances of the plate boundaries. The probability of finding the observed number of hotspots within 10° of the ridges is about what is expected.

For plate reconstructions a reference frame is needed to relate all the plates. We have tested [*Petronotis and Jurdy,* 1990] the fixity of the hotspot reference frame by reconstructing the Pacific plate relative to the African and Pacific hotspots using different approaches, and a combination of marine magnetic anomaly data and hotspot data, for 10, 15, 37, 48, and 61 Ma. Even when the uncertainties in the reconstructions are taken into account the results of the two approaches agree only for 10 Ma. Moreover, the match of the alternative reconstructions increasingly deteriorates with age. We have suggested as possible sources of error a) large uncertainties in the location of individual hotspots, b) increasing relative motion with age between coherent groups of Pacific and African hotspots, and c) a missing plate boundary in the relative plate motion circuit that ties the Pacific plate to other plates, possibly between East and West Antarctica. We conclude that the uncertainties in individual hotspot locations required especially for the older reconstructions are unreasonably large, but cannot distinguish between the remaining two explanations as to which may be the primary source of error affecting the reconstructions. If this discrepancy is due to shift of the Pacific hotspots relative to the African ones, then the calculated displacement is nearly anti-parallel to motion of the Pacific plate relative to its hotspots and in an amount of about

15-20% as much (Figure 2).

Paleomagnetic, hotspot, and mean-lithosphere frameworks are compared [*Jurdy*, 1990] for the Cenozoic Era. Errors in the relative motions of plate pairs accumulate to give uncertainties in reference frames. Uncertainties in the poles of the mean-lithosphere framework are estimated to be less than 1° and for the hotspot framework 1.1°, assuming a 50 km error in location of individual hotspots. The A_{95}'s for paleomagnetic data range from 1-5°. With these uncertainties the differences between the paleomagnetic and mean-lithosphere co-ordinate systems are not statistically significant, and the hotspot frame barely differs from the mean-lithosphere frame during the early Tertiary. On the other hand, the hotspot and paleomagnetic axes diverge in opposing directions in the mean-lithosphere framework, and can be distinguished. This difference can be attributed to the Pacific hotspots having more than 10° motion relative to the mean-lithosphere, whereas the African set does not statistically differ from the mean-lithosphere frame (Figure 3). A shift of the Pacific hotspots relative to those in the Atlantic would account for the differences in the reference frames.

Present-day hotspot locations may correlate with the positions of subduction zones 400-600 m.y. ago. To test the hypothesis of subduction origin, present hotspot densities are compared [*Jurdy and Wood*, 1989] with past subduction zones, using the Paleozoic reconstructions [*Scotese and McKerrow*, 1990] along with their assessments of the locations of subduction zones. This involves a considerable extrapolation back in time for the shift of the hotspots relative to Africa and the spin axis, but results in reconstructions having regions of maximum densities of present-day hotspots bounded by long-lived subduction zones, such as the Klamath arc and the Mongol-Kazakh trench (Figure 4). Thus, present-day hotspot distribution, plate kinematics, and paleomagnetic data are not inconsistent with the hypothesis of the subduction origin of hotspots.

Crough, S. T., and D. M. Jurdy, Subducted lithosphere, hotspots, and the geoid, *Earth Planet. Sci. Lett., 48*, 15–22, 1980.

Jurdy, D. M, Reference frames for plate tectonics and uncertainties, *Tectonophysics, 182*, 373–382, 1990.

Jurdy, D.M., and M. Stefanick, Models for the hotspot distribution, *Geophys. Res. Lett., 17*, 1965–1968, 1990.

Jurdy, D. M., and B. J. Wood, Are hotspots a Consequence of Ancient Subduction?, *Eos Trans. AGU, 70*, 1351, 1990.

Petronotis, K. E., and D. M. Jurdy, Pacific plate reconstructions and uncertainties, *Tectonophysics, 182*, 383–391, 1990.

Scotese, C. R., and W. S. McKerrow, *Paleozoic Biogeography and Paleogeography, Geol. Soc. Lond. Spec. Pub.*, Oxford Univ., London, 1990.

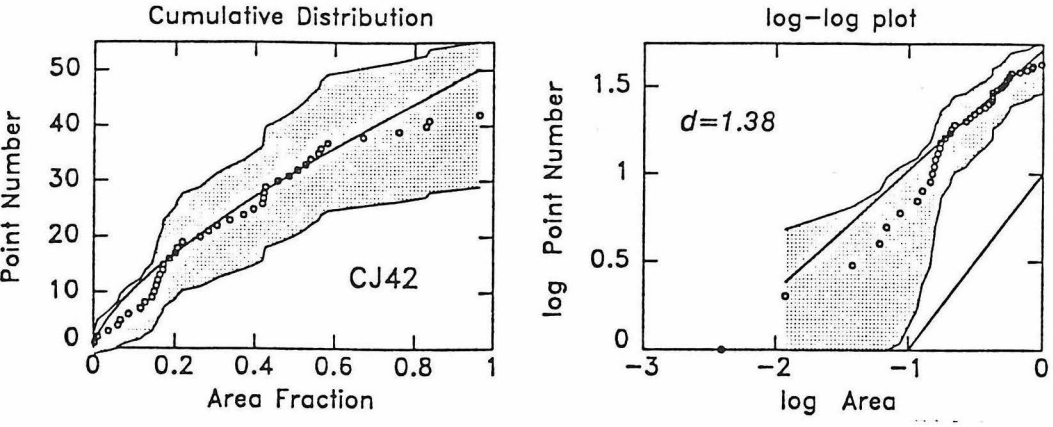

Fig. 1. Cumulative distributions of hotspots, ordinary (left) and logarithmic (right). A fitted power-law curve and its linear counterpart are shown together with a line of slope = 1. The shaded area is the uncertainty region, $\pm 2\sqrt{N}$ (two standard deviations). [from *Jurdy and Stefanick,* 1990] Crough and Jurdy [1980] set of 42 hotspots with center of mass at 9.2S, 36.6W.

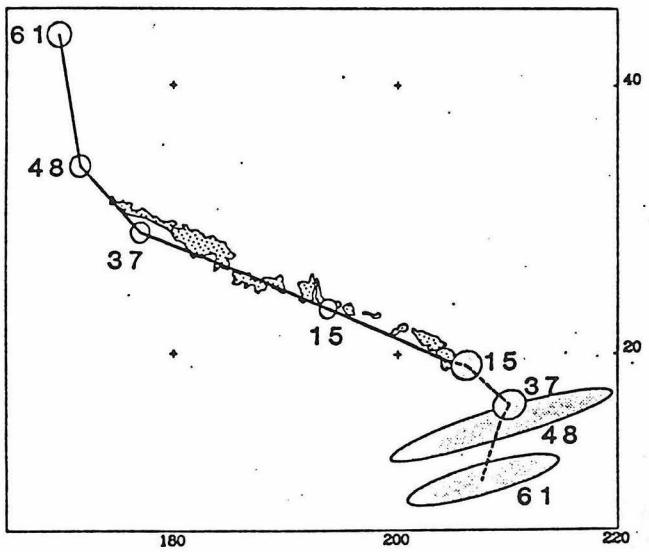

Fig. 2. Motion of the Hawaiian hotspot relative to fixed African hotspots (dashed line), assuming plate reconstruction parameters are known perfectly, is almost antiparallel to the motion of the Pacific plate relative to its hotspots (solid line) from 61 Ma to the present. This suggests mantle flow in response to plate motion may be affecting the fixity of hotspots. The outline of the Hawaiian chain corresponds to the 200 m bathymetric contour. [from *Petronotis and Jurdy*, 1990]

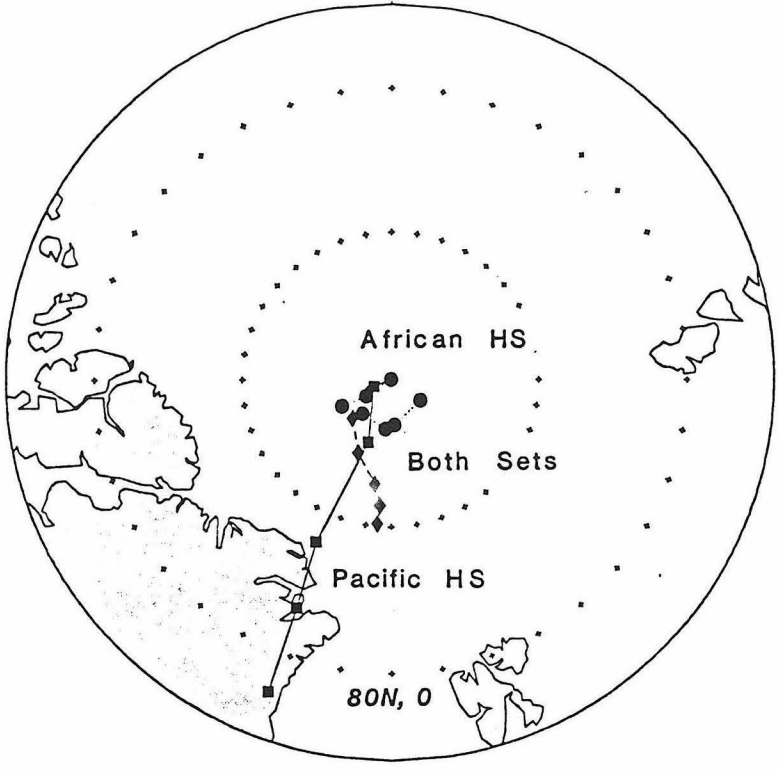

Fig. 3. Axes of hotspot frameworks shown in mean-lithosphere framework. The hotspot systems are shown as a single set (diamonds), the African set (circles) and the Pacific sets (squares), with the symbols shown every 10 m.y. The uncertainties associated with the axes are 0.4 ° for the mean-lithosphere and 1.1° for the hotspot frameworks. [from *Jurdy,* 1990]

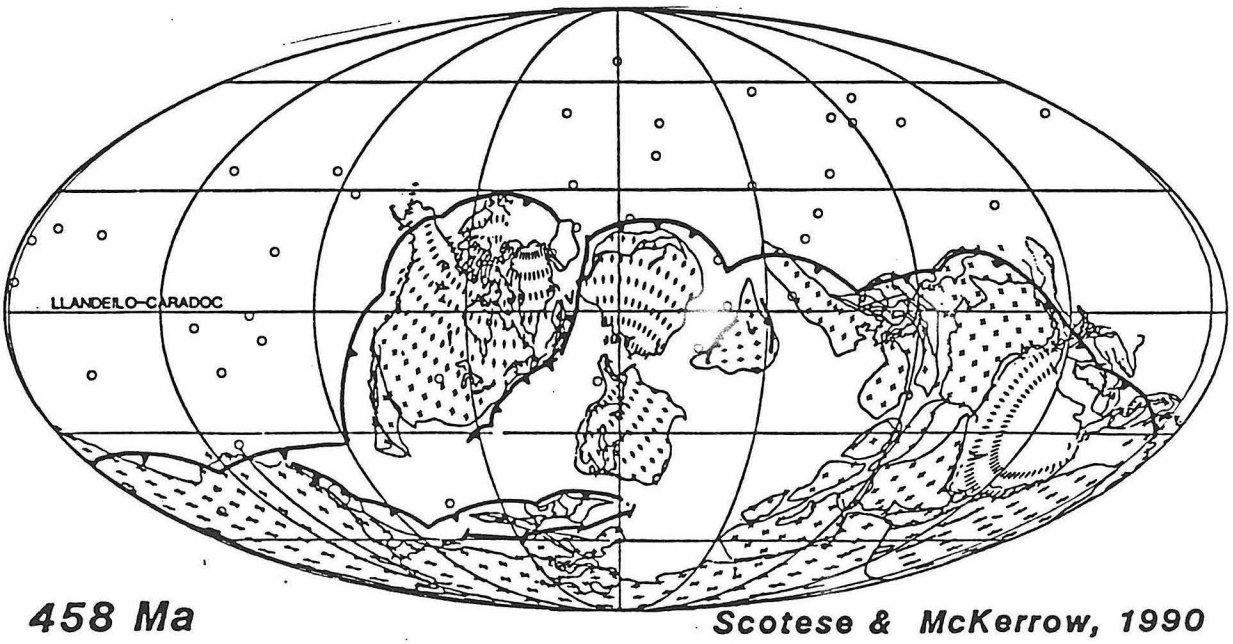

Fig. 4. Set of 42 hotspots positioned relative to paleogeography at 458Ma. Regions of

For: Caltech
Plumes Symposium
May 3, 1991

THE IMPLICATIONS OF VOLATILES AT DEPTH FOR PLUMES ON VENUS

W. M. Kaula
UCLA

The only good explanation for the extraordinarily greater retention of primordial inert gases by Venus, compared to Earth-- most notably, a factor of 80 in $^{36+38}$Ar-- is that the Earth suffered a much larger greatest impact (Cameron, 1983). Retention of so much argon implies retention of an even greater complement of water, because water is much more soluble in magmas than is argon (Zhang & Zindler, 1988). Most of this water must be at appreciable depth within Venus, because the high gravity: topography admittance ratios-- four times' the Earth's, on the average-- require an upper mantle stiff to a few hundred kilometers depth (Phillips, 1990).

A new indicator of high volatile retention in Venus is the abundance of sinuous flow features revealed by the Magellan imagery, which appear to require sulfur or carbonatite (Kargel et al, 1991).

The stiffness of Venus's upper mantle explains the absence of Earthlike plate tectonics (Kaula & Phillips, 1981). But Venus's mantle must be convecting-- otherwise, it could not sustain the prominences of Ishtar Terra, Aphrodite Terra, and Beta Regio. This convection is of sufficient vigor to deliver its heat close to the surface. However, the lack of plate-tectonic signature forbids this delivery being by sink-driven flows, like the Earth. The surface of Venus is thus shaped more by bulk properties of the mantle, and less by upper boundary-layer properties. A more regional character of mantle flow is an appealing explanation for lesser crustal formation on Venus, since magmatism is non-linearly proportionate to heat delivery.

It has been argued, however, that even if Venus's upper mantle is dry, to deliver its heat it would warm up enough to reduce the viscosity below that suggested by the high gravity: topography admittance ratio. Plumes are the evident mechanism to localize such warming, so that broad-scale stiffness is maintained-- but the popular candidate for the biggest plume, Beta Regio, has the greatest admittance ratio, equivalent to 400 km apparent depth of compensation.

The size and spacing of the major volcanic rises, such as Beta Regio and Eistla Regio, suggest sources that are more than 1000 km deep: perhaps near the core-mantle boundary.

The presence of appreciable volatiles would allow any instability to draw on a wide region, leading to a spacing of 1000's of kilometers (Sleep et al, 1988). Mild evidence of such fluidity deep in the Venus mantle is that the long wavelength part of the uncorrelated gravity field is appreciably less than predicted from Earth (Kaula, 1990). The problem is how a big upflow becomes stiff enough to sustain its large gravity signal; is it sweated-out by a "Stolper effect" (Stolper et al, 1981; Kaula, 1990)?

The abundant coronae suggest instabilities associated with shallower depths, perhaps the phase transition to perovskite, which would occur around 750 km deep in Venus. These also could be fostered by volatiles at depth. However, it is still to be sorted out how many of the coronae are recently active, because of the lack of degrading effects other than isostatic adjustment.

In any case, it is likely that plumes are a much more important heat delivery mechanism in Venus than in Earth, in part because of the absence of volatiles in the upper mantle, but also because of their presence in the lower mantle. The surface manifestation of contemporary plumes is most likely the large volcanic complexes: Asteria, Beta, Eistla, and Phoebe Regiones. How much of Aphrodite Terra, is a plume manifestation and how much convergent phenomema is yet to be settled; close examination of Ishtar Terra has revealed that characteristics of both can occur within an extent of less than 2000 km (Kaula et al, 1991). Venus could be like the Earth in that the highest topography is associated with downflows-- in part because of lower temperatures, and in part because of the influence of preexisting structures: "cratons".

Plumes undoubtedly deliver a greater proportion of heat to the surface in Venus than they do in the Earth; the question is how much relative to regional flows that exist because of the stiffness of the upper mantle.

REFERENCES

Cameron, A.G.W. 1983: *Icarus* **56**, 195.

Kargel, J.S., Komatsu, G., Baker, V.R., Lewis, J.S., Strom, R.G. 1991: *Lun.Pl.Sci.* **XXII**, 685.

Kaula, W.M. 1990: *Science* **247**, 1191.

Kaula, W.M., Bindschadler, D.L., Grimm, R.E., Smrekar, S.E., Roberts, K.M. 1991: *Lun.Pl.Sci.* **XXII**, 699.

Kaula, W.M., Phillips, R.J. 1981: *Geophys.Res.Let.* **8**, 1187.

Phillips, R.J. 1990: *J.Geophys.Res.* **95**, 1301.

Sleep, N.H., Richards, M.A., Hager, B.H. 1988: *J.Geophys.Res.* **93**, 7672.

Stolper, E.M., Walker, D., Hager, B.H., Hays, J.F. 1981: *J.Geophys.Res.* **86**, 6261.

Zhang, Y., Zindler, A. 1988: *EOS* **69**, 1294.

Relationship between Hotspots and Mantle Structure: Correlation with Whole Mantle Seismic Tomography

SHARON KEDAR, DON L. ANDERSON, DAVID J. STEVENSON (CALTECH)

We examine the relation between the locations of hotspots on the surface of the Earth and mantle structure as it appears from seismic tomography. In particular, we correlated the hotspots field with Tanimoto's 1989 shear wave velocity structure throughout the mantle, which is represented in spherical harmonics. A spherical harmonics representation of both fields enables us to perform a "degree by degree" correlation, and so to test the possible relations between features of the same scale in them. A statistical significance analysis is applied to these results. A similar analysis was performed by Richards, Hager and Sleep (1988) in studying the hotspots - geoid relations.

After correlating the hotspots with Tanimoto's model, two major phenomena were observed: 1. Very good correlation between the hotspots and slow (hot) regions in degree 2 in the bottom half of the lower mantle, which decays in the upper mantle (figure 1).

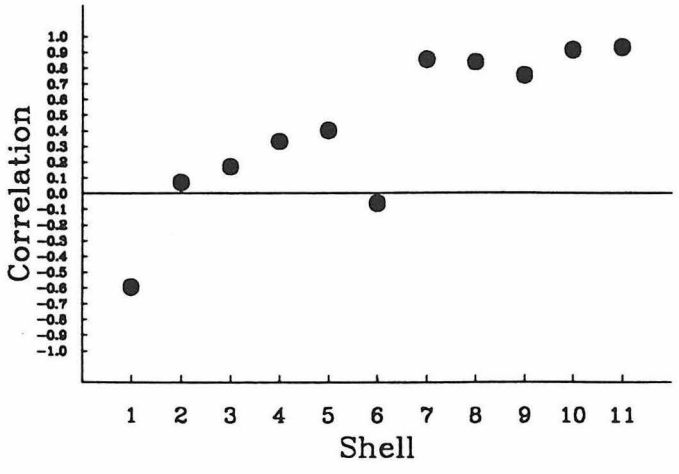

Figure 1: Variation of l=2 Correlation from the top of the mantle (shell 1) to the bottom (shell 11)

2. A good correlation in degree 6 in the deeper upper mantle (200-670 Km) and lack of such correlation below 670 Km (figure 2). These positive correlations are statistically significant (higher than 95% confidence level).

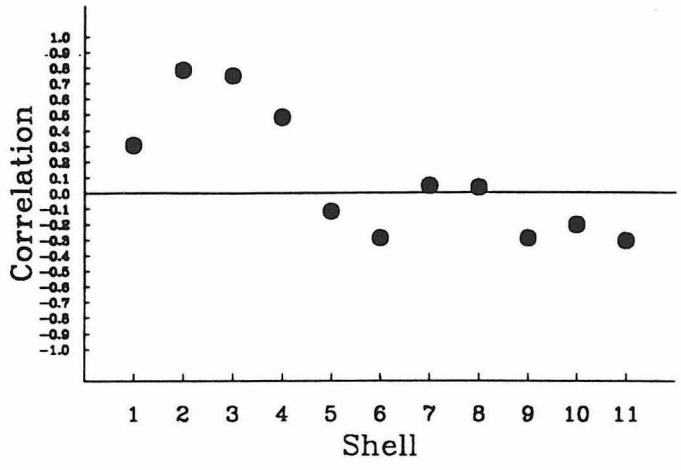

Figure 2: Variation of l=6 Correlation from the top of the mantle (shell 1) to the bottom (shell 11)

Moreover, they are also a peak in the amplitude spectrum. In other words, they describe a significant part of the hotspots field. The l=2 expansions of the lower mantle, and the l=6 expansion of the upper mantle are presented in figures 3 and 4 together with the corresponding expansions of the hotspots field.

The key to a better understanding of the resulting correlations lies not only in the good correlations but in the lack of them. The observations made here could suggest the possibility of two separate regions in the mantle which control different parts of the hotspots field. To check this possibility we excluded those hotspots which give a negative contribution to the $l = 6$ correlation in the upper mantle. The correlation of these excluded hotspots with the lower mantle gives a significant correlation for degree 2, which suggests we should look further in this direction.

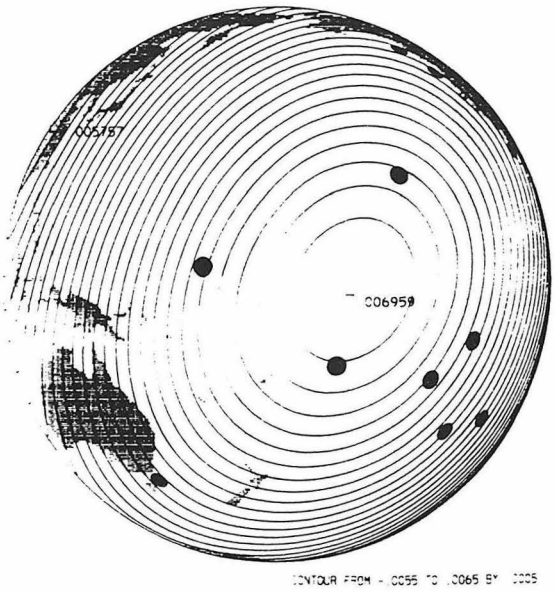

ower Mantle S-Velocity l=2

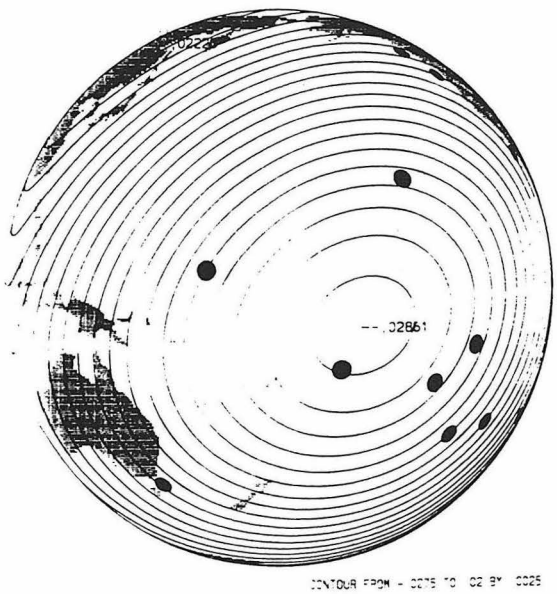

Lower Mantle S-Velocity l=2

figure 3

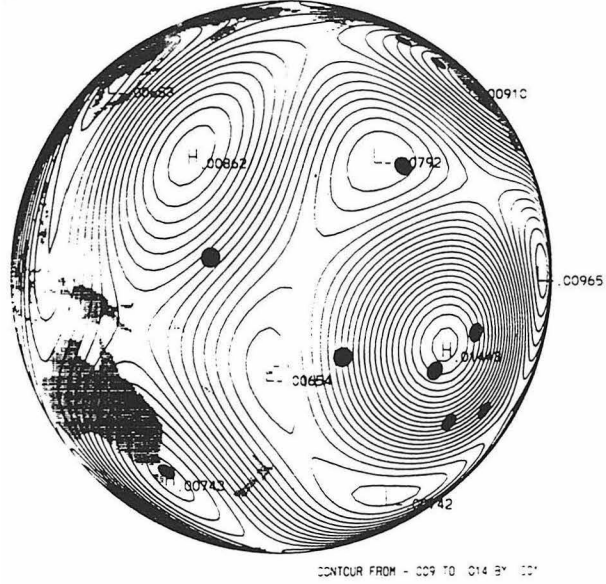

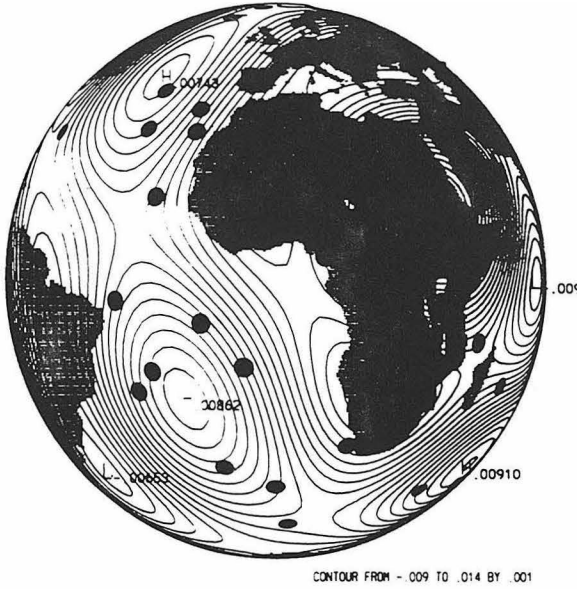

per Mantle S-Velocity l=6

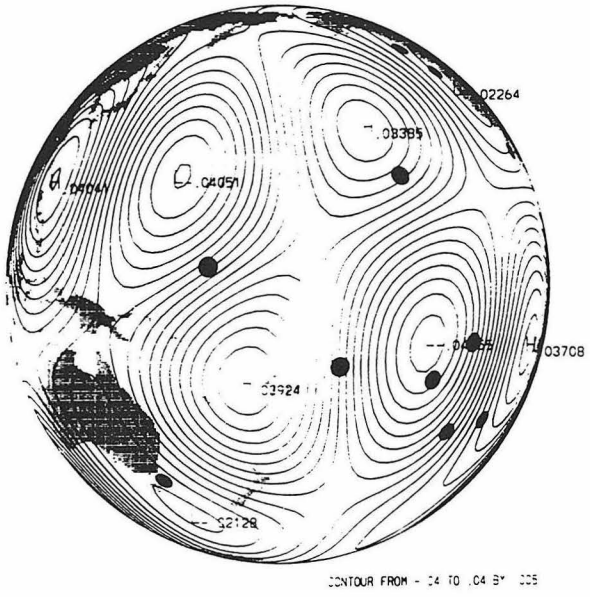

Upper Mantle S-Velocity l=6

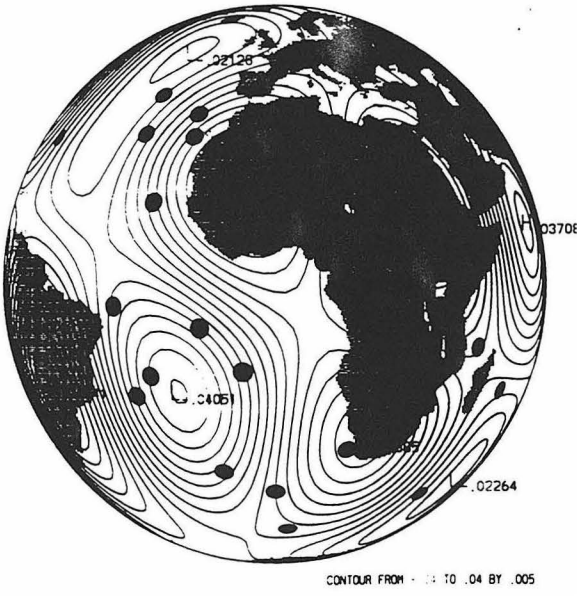

figure 4

Mantle Plumes and the 670 km Discontinuity

L. H. Kellogg
Department of Geology
University of California
Davis, CA 95616

Introduction

One outstanding question about the structure of the Earth's mantle is the nature of the seismic discontinuity observed at 670 km depth. From the viewpoint of dynamics, the relevant question is whether convection crosses this depth, or whether there is a barrier to convection at 670 km. From the viewpoint of chemistry, the question is whether the 670 km discontinuity corresponds to a phase change, a compositional change, or both. A phase change alone is consistent with either the existence or absence of a barrier to convection at 670 km depth, but a sharp variation in composition requires that the upper and lower mantle be convectively isolated to some degree. If the mantle is layered, "leaks" across the boundary would have significant geochemical consequences. Alternatively, the mantle may convect as a single layer in which heterogeneities collect at depth due to viscous stratification. A number of papers have recently suggested that the mantle is predominately layered with leaks in both directions.

Here I present the results of a finite-element model of plumes in a spherical, axisymmetric shell an internal compositional discontinuity at 670 km. When the density contrast between the materials is low, plumes originating in the lower mantle rise into the upper mantle. When the density contrast due to compositional variations equals the density contrast due to temperature variations, plumes do not cross into the upper mantle but there is some material transfer. The boundary between the two materials is deflected at upwellings and downwellings. Flow in the lower layer partly controls the geometry of the flow in the upper layer. Strong plumes in the lower layer induce downwellings where they impinge on the upper layer (shear-coupling), but as plumes mature and weaken, the flow in the upper layer reverts to thermal coupling, in which an upwelling overlies an upwelling. Increasing the density contrast between the two layers reduces the mixing and deflection of the boundary and causes shear-coupling rather than thermal-coupling.

Double-Diffusive Convection in an Axisymmetric Shell

To model the interaction of plumes from the core-mantle boundary with the 670 km discontinuity, I used a finite element model of double-diffusive convection in an axisymmetric, spherical shell. The material is incompressible and isoviscous, with variations in density due to thermal expansion and due to variations in composition.

The problem is governed by three dimensionless parameters. The Rayleigh number, $R_a = \alpha\rho\Delta T d^3/\mu\kappa$, measures the effect of thermal buoyancy, where α is the coefficient of thermal expansion, ρ is density, ΔT is the temperature drop across the shell, d is the thickness of the shell, μ is viscosity, and κ is the thermal diffusivity. The buoyancy number, $B = \Delta\rho_c/\rho\alpha\Delta T$, is the ratio of the density contrast due to compositional variations in the fluid, $\Delta\rho_c$, to the density contrast due to temperature variations, $\rho\alpha\Delta T$. The Lewis number, $L_e = \kappa/D$, is the ratio of the thermal to the chemical diffusivities. Time is scaled to the diffusional timescale d^2/κ. The governing equations were solved on a spherical axisymmetric shell using a Petrov-Galerkin finite-element method. The shell had an inner radius of 0.55 times the outer radius, and the solution was calculated on a hemisphere; that is, $0 \leq \theta \leq \pi/2$. There were 64 equal-sized elements in the radial direction and 129 in the azimuthal direction.

The dimensionless compositional field, C, indicates the presence of dense material; where $C = 1$ the material is most dense; where $C = 0$ it is least dense. Density is assumed to be linearly dependent on the temperature and the composition. The initial conditions for the composition were $C = 1$ for $r \leq 0.9$ and $C = 0$ for $r > 0.9$. The shell was heated from below and cooled from above with imposed temperatures at the inner and outer boundaries ($T = 1$ at $r = 0.55$ and $T = 0$ at $r = 1$). A perturbed conductive profile was used for the initial temperature. The Rayleigh number was $R_a = 10^6$, and the buoyancy ratios used were $B = 0.5$, $B = 1.0$, and $B = 2.0$. For all calculations $L_e = 100$. This value allows some diffusive mixing between the two materials and is low for the mantle; if chemical diffusion is controlled by the molecular diffusivity in the mantle, $L_e \gtrsim 10^{11}$. The model solutions are not applicable to the mantle for times approaching the diffusive timescale. The flow was time-dependent and the calculations were run for at least two full overturns.

Interaction of Plumes with a Compositional Boundary

When $B = 0.5$ (Figure 1a and b) plumes crossed easily into the upper mantle. Such a low buoyancy number was insufficient to maintain the lower mantle isolated from the upper mantle.

Increasing B reduced the mixing between the two materials (Figure 1c and d). When $B = 1.0$ the variations in density due to compositional gradients are about equal to the variations in density due to temperature gradients. There was some mixing, but in general the layers remained distinct. The plumes deflected the boundary up to a few hundred km (several elements.)

The time-dependent flow exhibited a combination of thermal and viscous coupling between the upper and lower layers. Plumes in the lower layer welled up and died back episodically. Over each strong upwelling in the lower mantle a downwelling developed in the upper mantle (Figure 1c). As the upwelling matured and weakened, a thermally induced plume developed in the upper layer (Figure 1d), entraining some lower mantle material with it. Upon later onset of a more rapid upwelling in the lower layer, the flow reverted to shear coupled convection.

Downwellings in the lower layer and upwellings in the upper layer entrained material from one layer to the other. Because the fluids were somewhat miscible ($L_e \neq \infty$) material of intermediate composition developed in these spots. In immiscible materials fine tendrils of the entrained material would be seen but in the present calculation these were smeared out by diffusion.

When the buoyancy number was increased still more ($B = 2.0$) there was even less interchange of material between the two layers (Figure 1 e and f). Flow in the upper layer was always shear-coupled to flow in the lower layer. The boundary between the two materials was deflected up to about 100 km by the upwelling plume. Although material of intermediate composition appeared at the boundary between the two fluids there was little entrainment and this material remained as a discreet layer between the upper and lower layers.

Discussion and Conclusions

The above calculations show that in order to maintain a distinctive composition in the lower mantle and prevent plumes in the lower mantle from rising into the upper mantle the buoyancy ratio must be at least 1, corresponding to a density change due to variations in composition of between 2% and 6%. Lower density contrasts allow massive exchange between the two layers. Even with a relatively large density contrast, however, plumes will deflect the boundary considerably. If the mantle is layered, some material may leak across the 670 km discontinuity. Some mixing occurs and material of intermediate composition develops at the boundary between the two regions. Plumes in the lower mantle will not penetrate into the upper mantle if $B \geq 1$. If the density contrast is just adequate to prevent plumes from rising into the upper layer ($B \approx 1$), the upper and lower mantle flows will be coupled in a complex time-dependent way, varying between shear and thermal coupling. If the density contrast is large ($B > 1$) plumes in the lower mantle will be shear-coupled to flow in the upper mantle and will induce local downwellings due to viscous drag.

Plumes in the upper mantle may be thermally coupled to plumes in the lower mantle in the manner seen in these calculations for $B = 1$. Thermal coupling would tend to stabilize the position of upper mantle plumes in a layered mantle relative to plates. Scaling the non-dimensional time of the calculations to the diffusional time d^2/κ, the upper mantle plume in Figure 1d had a lifespan of about 100 Myr.

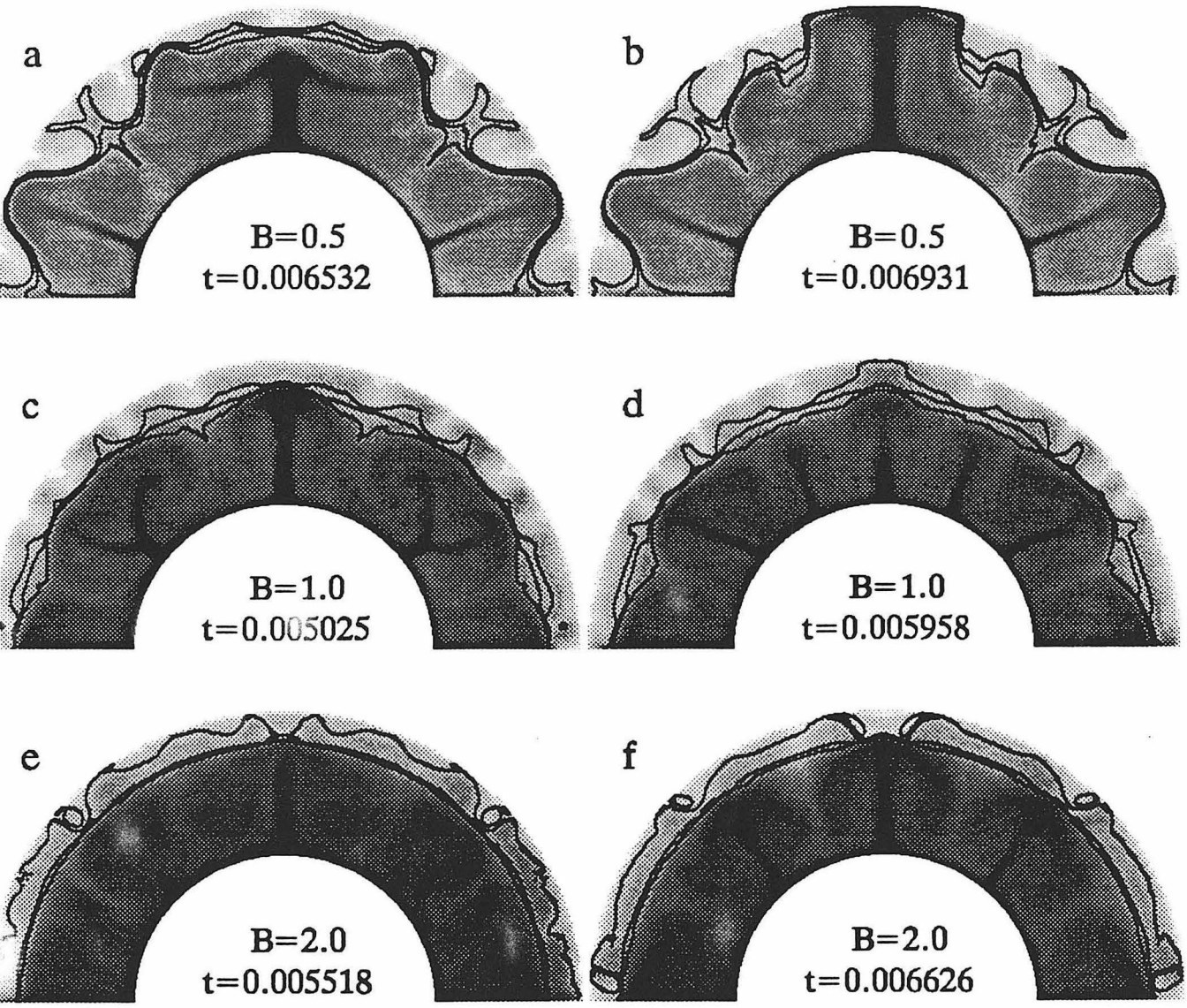

Figure 1. Convection in a spherical, axisymmetric shell. $R_a = 10^6$, and $L_e = 100$. The flow is axisymmetric about the central pole. Shades represent temperature ranging from $T = 0$ to $T = 1$ as shown. Lines are contours of C, the composition field, at intervals of 0.25. (a) $B = 0.5$, $t = 0.006532$ (b) $B = 0.5$, $t = 0.006931$ (c) $B = 1.0$, $t = 0.005025$ (d) $B = 1.0$, $t = 0.005958$ (e) $B = 2.0$, $t = 0.005518$ (f) $B = 2.0$, $t = 0.006626$

PLATE VELOCITY AND SUBDUCTION RATE: A KEY TO MANTLE DIFFERENTIATION?

SCOTT D. KING AND HUBERT STAUDIGEL

Scripps Institution of Oceanography, La Jolla, CA 92093

INTRODUCTION

Subduction of oceanic crust and possibly sediments and/or delaminated continental crust represents the largest known geochemical cycle in the solid earth. For this reason, it is not surprising that this process is called upon to explain at least some of the compositional diversity of Earth's mantle. Four mantle components are typically distinguished (following [*Zindler and Hart*, 1986]): the source regions of mid-ocean ridge basalts (MORB), the depleted MORB mantle ("DMM"), the enriched mantle components "EMI" and "EMII," and mantle material with unusually high 206Pb/204Pb ("HIMU"). "DMM" is generally accepted to be the result of continued extraction of mid-ocean ridge basalts. "EMI" and "EMII" are thought to be recycled continental lithosphere and recycled sediment respectively, and "HIMU" is often considered to be the direct result of recycling of oceanic crust. These end members may be found almost anywhere in the source regions of intraplate oceanic basalts, or they may be brought up as mantle xenoliths in many locations including oceanic and/or continental settings. However, extreme end members appear to be concentrated in the southern hemisphere, in the "globe-encircling" DUPAL anomaly [*Hart*, 1984], and in independent geochemical provinces in the south Atlantic, Indian Ocean or Pacific [*Staudigel et al.*, 1991].

The common coexistence of these end members suggests that they may have formed by a common geological process. Subduction is a very probable process capable of introducing enriched materials into the mantle, or at least providing the mantle with volatiles that may cause secondary mantle fractionation processes leading to some of these end members. The high abundance of end members in some regions of the earth suggests that these components are regionally concentrated, consistent with the current subduction zone distribution, leading us to speculate that subduction may be concentrated, both regionally and temporally, throughout geological time.

The distribution of recycled components in the mantle may be caused by two processes. Firstly, subduction zones appear to be relatively stationary over long periods of time [*Engebretson et al.*, 1990], concentrating recycled components in specific regions of the mantle. The second control relates to plate velocities in a subduction zone: the faster a plate is subducted the more delay in heating it experiences, and the longer its thermal equilibration time. Complete thermal equilibration will tend to remove alteration-related chemical additions to the oceanic crust (water, CO_2, alkalies), and large fractions of to-be-subducted sediment, making subduction a relatively inefficient recycling process. However, at very rapid subduction rates, it is conceivable that larger quantities of recycled elements are introduced into the mantle. Thus, orthogonal subduction at 10 cm/yr in the collision zone of the Australian and Eurasion plates, or even the higher plate velocities during the Cretacous, may provide the dominant fraction of the mantle heterogeneities. Even though we believe that geometric effects, as well as plate velocities, play a role in the effectiveness of the recycling process, in this paper we will provide some boundary constraints on how plate velocities affect the thermal structure of a subduction zone.

METHOD

We consider two simple analytic solutions for the heating of a subducted slab; pure conductive heating and uniform shear heating. While these models ignore potentially important processes, such as dehydration reactions, convective transport by fluid phases, and secondary convection in the mantle wedge, they illustrate the effect of plate velocities on the thermal structure of subducted oceanic crust. Pure conductive heating almost certainly underestimates the heating of the slab, because of the aforementioned processes increase the temperature within the slab. Shear heating, on the other hand, probably overestimates the heating of the slab (because of the large shear stress chosen). Therefore, these two models serve as end-members, with the Earth most likely somewhere in between.

For the conductive heating model, we use the error function plate cooling solution as our initial temperature distribution within the slab. We allow the top of the slab to be heated by warm mantle (1400 °C). The one-dimensional conduction equation is then solved using a harmonic expansion of the initial condition [*Carslaw and Jaeger*, 1959]. The geometry of the subduction zone is shown in Figure 1. The solution in the downdip slab direction, x, is given by $v_{\text{slab}} \times t$ where t is the time since that portion of the slab began subducting.

For the shear heating model, the temperature distribution in a descending slab with a uniform shear stress, ignoring convection in the mantle wedge, dehydration reactions, and multi-phase flow is given by *Turcotte and Schubert* [1973]

$$T = T_m \left(\frac{\pi x}{d_m} \sin\theta\right)^{1/2} \text{ierf}\, \frac{y}{2} \left(\frac{u}{\kappa x}\right)^{1/2} \qquad (1)$$

where T_m is the melting temperature, d_m is the depth at which melting occurs, x is the distance along the slab, y is the distance perpendicular to the slab, θ is the dip of the slab, u is the plate velocity, κ is the thermal diffusivity, and ierf is the first integral of the complementary error function. Once again, Figure 1 illustrates the geometry of the calculation.

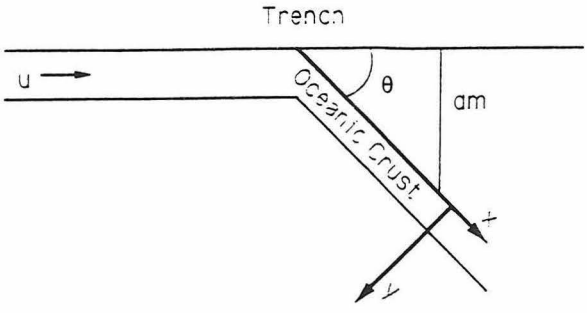

Fig. 1. Geometry of the subducting slab.

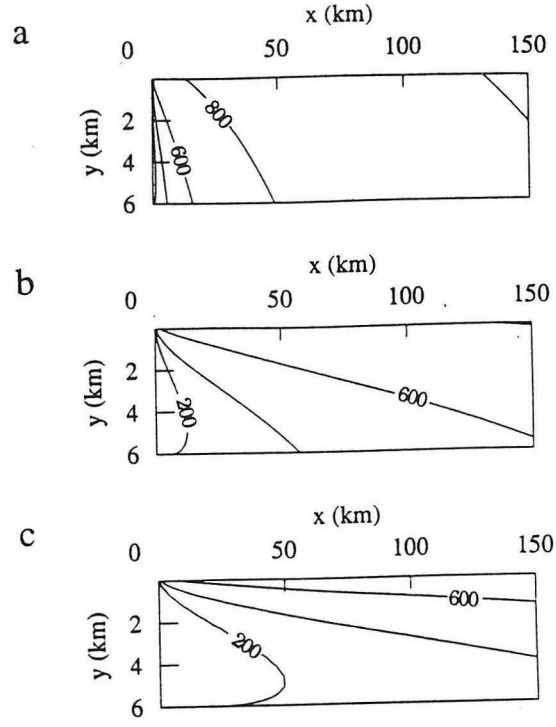

Fig. 2. Temperature distribution in the oceanic crust for the pure conductive heating model with plate velocities of a) 1 cm/yr, b) 10 cm/yr, c) 40 cm/yr. Temperatures are contoured every 200 °C. Refer to Figure 1 for the subduction zone geometry.

Discussion

The results of the conductive heating model are shown in Figure 2 for three different plate velocities representing slow (1 cm/yr), fast (10 cm/yr), and ultrafast (40 cm/yr) plate velocities. Figure 2 shows the variation of temperature along the slab mantle contact, x, and perpendicular to the slab mantle contact, y. The temperatures are contoured at 200 °C intervals. Assuming that there is little or no deformation of the slab, a horizontal line across one of these plots corresponds to a P-T path at a depth y from the top of the slab. We assume a diffusivity of 1 mm^2/sec, an interior mantle temperature of 1400 °C, and that the initial plate has cooled for 40 million years before subducting. Varying the initial plate cooling time, diffusivity, or mantle temperature has no effect on the qualitative behavior of the plots.

The effect of varying the plate velocity on the temperature profile of the slab is quite apparent, faster plate velocities result in colder slab temperatures at a given depth. This is clear from Figure 4, a plot of P-T paths followed by parcels 2 km below the slab surface plotted on top of a phase diagram for slab dehydration after *Drummond and Defant* [1990]. In all three models, the amount of heating within the slab decreases with time (depth) as evident by the increasing slope on the P-T diagram. This is because as the slab begins heating up, it cools the surrounding mantle, and thus the heat source for the slab is moving further away from the top of the slab with time (distance x). Because of this, the conductive heating model underestimates slab temperatures with depth. If convection in the mantle wedge were considered, then the mantle adjacent to the slab would become unstable, and the boundary layer which forms along the slab in the conductive case could not be maintained, more effectively heating the slab at depth.

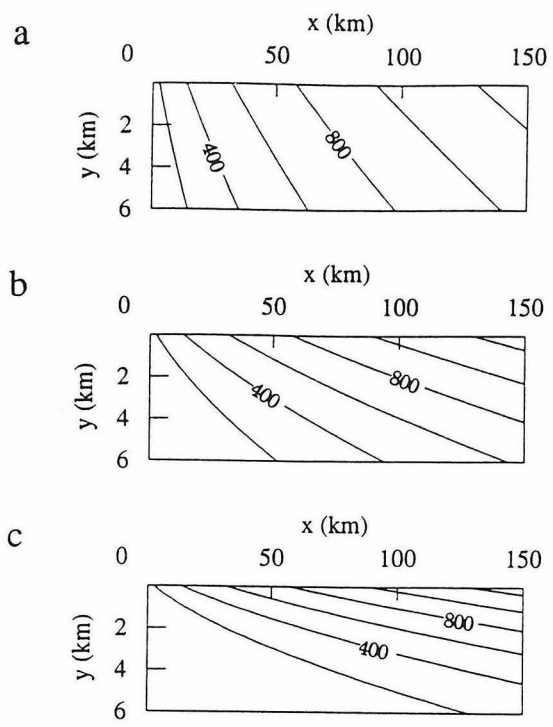

Fig. 3. Temperature distribution in the oceanic crust for the shear heating model with plate velocities of a) 1 cm/yr, b) 10 cm/yr, c) 40 cm/yr. Temperatures are contoured every 200 °C. Refer to Figure 1 for the subduction zone geometry.

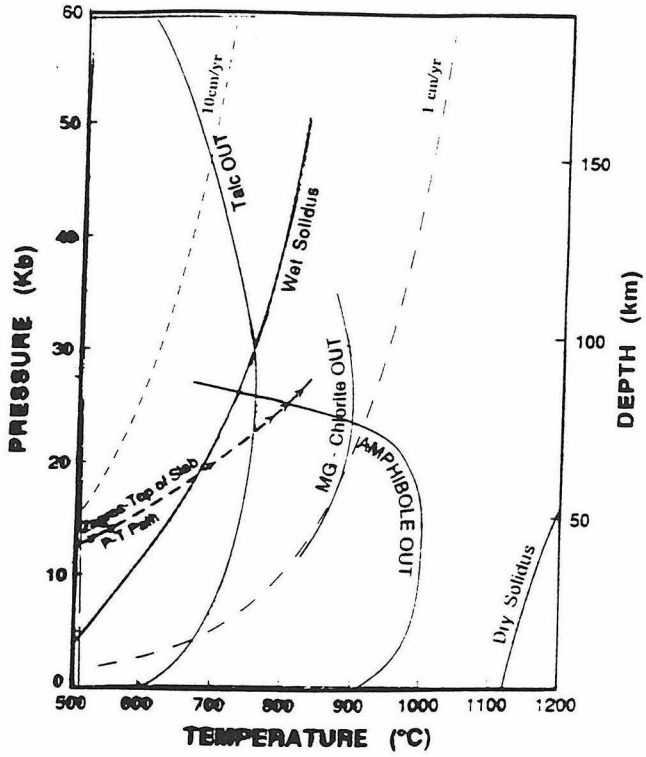

Fig. 4. P-T paths for the conductive heading models in Figure 2 at a depth of 2 km from the top of the slab plotted on a phase equilibria diagram after *Drummond and Defant* [1990]. The solid curve is for a plate velocity of 40 cm/yr, the short-dashed curve for 10 cm/yr, and the long-dashed curve is for 1 cm/yr.

The results of the uniform shear heating model are shown in Figure 3, again for the same three plate velocities as Figure 2. We assume T_m = 1400 °C, d_m = 150 km, θ = 45 °and κ = 1 mm^2/sec. While the shear stress required to produce the heating in this model is quite high (about 1.5 kbar), we point out that high shear stresses will heat the slab up faster, and thus these P-T paths may be unrealistically high. However, since convection in the mantle wedge is not considered in this model, the high shear stresses may mimic the effect of convection in the wedge. The difference between typical subduction rates (10 cm/yr) and a rate of 40 cm/yr (Figures 3b and 3c) is about 400 °C within the top 6 km of the slab. Even with this high rate of shear heating, it is possible that temperatures in the upper 6 km region of the slab will be low enough to inhibit slab dehydration until depths significantly below 150 km during periods of fast subduction velocities.

The P-T paths at a depth of 2 km for the shear heating model are shown in Figure 5. Notice that with the normal subduction velocity the P-T path follows the usual dehydration path, while a factor of four increase in subduction velocity decreases the heating and causes the slab to follow a steeper P-T path, possibly not dehydrating until depths greater than 150 km.

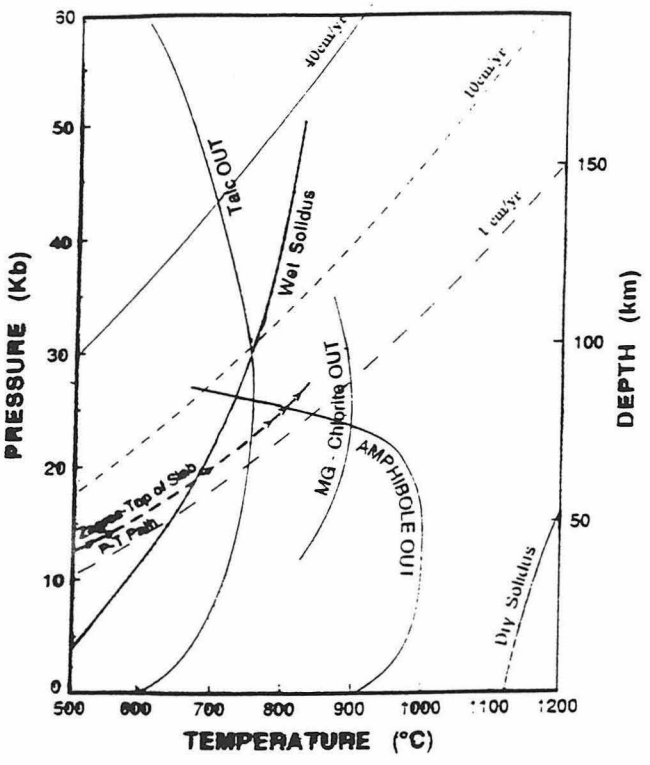

Fig. 5. P-T paths for the shear heating models in Figure 3 at a depth of 2 km from the top of the slab plotted on a phase equilibria diagram after *Drummond and Defant* [1990]. The curve for a plate velocity of 40 cm/yr is below the range of the plot, the short-dashed curve for 10 cm/yr, and the long-dashed curve is for 1 cm/yr.

Conclusions

These relatively simple calculations have shown that the P-T path of subducted materials significantly depends on plate velocities. For a given pressure the estimated temperature may vary by as much as 250 °C, between the plate velocities considered (40/10/1 cm/yr). Such differences drastically alter the phase equilibria of descending slab material, and therefore, its dehydration and partial melting characteristics. From these considerations, we conclude:

[1.] The amount and composition of metasomatic fluids and/or silicate melts extracted during subduction is critically dependent on slab descent velocities.

[2.] Some portions of the descending slab may not get an opportunity to outgas before it is transported beyond the volcanic front of a subduction zone.

[3.] The amount of recycled seawater or sediment components in subducted materials may, therefore depend on slab velocities.

[4.] Geoloogical periods with ultrafast plate velocities may preferentially contribute to mantle heterogeneities.

Finally, we believe we have shown convincingly that plate velocities influence the amount of material that can be extracted from subducted slabs. However, we emphasize that major controls of the thermal structure of descending slab materials, such as the relative proportion of frictional versus conductive heating and the thermal effects of slab dehydration and melting, are still not well understood.

References

Carslaw, H. S. and J. C. Jaeger, *Conduction of Heat in Solids*. 282 pp., Oxford University Press, London, 1959.

Drummond, M. S. and M. J. Defant, A Model for Trondhjemite-Tonalite-Dacite Genesis and Crustal Growth via Slab Melting: Archean to modern comparisons. *J. Geophys. Res.*, *95*, 21503–21521, 1990.

Hart, S. R., A Large Scale Isotope Anomaly in the Southern Hemisphere Mantle. *Nature*, *309*, 753–757, 1984.

Engebretson, D.C., K. P. Kelley, H. J. Cashman and M. A. Richards, Estimates for Subduction Parameters Since 180 Ma (abstract). *EOS Trans. AGU*, *71*, 1575, 1990.

Staudigel, H., K.-H. Park, M. Pringle, J. L. Rubenstone, W. H. F. Smith and A. Zindler, The Longevity of the South Pacific Isotope and Thermal Anomaly. *Earth Planet. Sci. Lett.*, *102*, 24–44, 1991.

Turcotte, D. L. and G. Schubert, Frictional Heating of the Descending Lithosphere. *J. Geophys. Res.*, *78*, 5876–5886, 1973.

Zindler, A. and S. R. Hart, Chemical Geodynamics. *Annu. Rev. Earth Platet. Sci.*, *14*, 493–571, 1986.

A Case for Catastrophic True Polar Wander in the Cambrian

Joseph L. Kirschvink[1] & Robert L. Ripperdan[2], [1]Caltech 170-25, Pasadena, CA 91125, USA; [2]Dept. of Env. Science, Weizmann Institute of Science, Rehovot, Israel.

Of all the periods in the Phanerozoic time scale, the Cambrian system is the most perplexing. Several lines of evidence which together suggest that the Cambrian Earth may have experienced a large, rapid episode of true polar wander (TPW) include: (1) The Cambrian is short. Once thought to have a duration approaching 100 Ma, stratigraphic Rb/Sr and U/Pb geochronometry now suggests a time span of about 20 Ma. (2) Lithostratigraphic analyses suggest that Northern Africa went from high to low and back to high latitudes within this time interval. North America at least moved into the carbonate belt during the early Cambrian. (3) Improvements in biostratigraphy, magnetostratigraphy, and carbon isotopic stratigraphy around the Precambrian-Cambrian boundary now allow precise correlations to be made between strata in Siberia, China, Morocco, Australia, and with somewhat less precision to North America. Isochronous poles from Australia and Africa demonstrate that they were moving separately in the late Precambrian. (4) Paleomagnetic poles, derived from biostratigraphically-dated units, suggest nearly 90° of APW for many, if not all, of these continents during Cambrian time. We interpret these effects as an episode of TPW resulting from the collision of East and West Gondwana during the early Cambrian. This suturing event would stop subduction of a large equatorial plate dipping under Africa (responsible at least in part for the Pan-African metamorphic events). Thermal warming of the orphaned slab then removes its mass anomaly, causing the magnitudes of the minimum and intermediate eigenvectors of the total earth moment of inertia tensor to switch, leading to a 90° TPW reorientation of the crust. The Cambrian sea-level transgression may then be the result of moving a large ocean basin from the polar region onto the equatorial buldge. Similarly, the enormously accelerated rates of organic evolution observed during Cambrian time may be the result of paleoenvironmental dislocation driven by TPW.

Helium isotopes in ocean island volcanoes: variability in time and space and some inferences about mantle plumes

Mark D. Kurz
Chemistry Department
Woods Hole Oceanographic Institution
Woods Hole, MA 02543

High $^3He/^4He$ ratios in oceanic basalts from some oceanic islands such as Hawaii and Iceland have been used to infer that the mantle sources have relatively high He/(Th+U), and are relatively undegassed. These high $^3He/^4He$ ratios, up to 32 times the atmospheric ratio (R_a) at Loihi seamount, are therefore consistent with the mantle plume model for Hawaii. The large range in $^3He/^4He$ ratios within and between Hawaiian volcanoes is now known to be related to temporal evolution, based on stratigraphic studies of Haleakala and Mauna Loa, and are also consistent with the plume model. However, the isotopic data from Mauna Loa shield building lavas shows a remarkable temporal evolution that requires three mantle sources within the last 15 kyr of volcanic eruptions. In the attached figure, the arrows indicate time evolution for Mauna Loa, as deduced from radiocarbon dating and stratigraphy. The earlier shield building lavas, which are presumed to be most representative of the mantle plume, have higher $^3He/^4He$ ratios. The younger samples define a trend toward lower $^3He/^4He$ and higher $^{87}Sr/^{86}Sr$ ratios, suggesting a lesser contribution from the mantle plume, and an end to shield building, at approximately 10 kyr before present. The isotopic composition of this material, having $^3He/^4He$ ratios similar to MORB (~8 R_a) with relatively high $^{87}Sr/^{86}Sr$ ratios (~.7040), is presumed to reflect variability within the plume itself, perhaps related to entrainment of the surrounding mantle. The historical Mauna Loa samples have similar $^3He/^4He$ ratios, but lower $^{87}Sr/^{86}Sr$ ratios, which is attributed to the Hawaiian lithosphere. These data demonstrate that the mantle sources of Hawaiian volcanoes vary on extremely short time scales, which probably relates to the axial geometry of the mantle plume.

The data from Haleakala are consistent with this model for isotopic evolution of Hawaiian volcanoes. As shown on the attached figure, the tholeiites have similar isotopic compositions to the earlier Mauna Loa tholeiites (i.e. plume related source) while the alkali basalts are similar to the historical Mauna Loa tholeiites in having $^3He/^4He$ ratios similar to MORB accompanied by lower $^{87}Sr/^{86}Sr$ ratios. The latter characteristics are assumed to be related to the lithosphere. However, the complex temporal evolution of Mauna Loa demonstrates that alkali basalts and tholeiites are not necessarily related by mixing processes.

Although there are very few data of this kind, other oceanic volcanoes do not necessarily display such temporal evolution. Helium data from Sao Miguel (Azores) have $^3He/^4He$ ratios that vary from MORB values to 3.5 R_a, which is the lowest value for an oceanic island. In this case, there is a strong relationship to tectonics, and no relationship to eruption age. As with the Hawaiian volcanoes, correlations between the isotopes of He, Sr, and Pb demonstrate that the low $^3He/^4He$ ratios are representative of the mantle source. The low $^3He/^4He$ ratios at Sao

Miguel are attributed to an ancient recycled sediment component in the mantle source. Helium isotopes are therefore useful tracers for recycled and undegassed sources in studies of mantle plumes, and show the importance of a chronological and tectonic framework for geochemical sampling.

Isotopic Evolution of Two Hawaiian Volcanoes

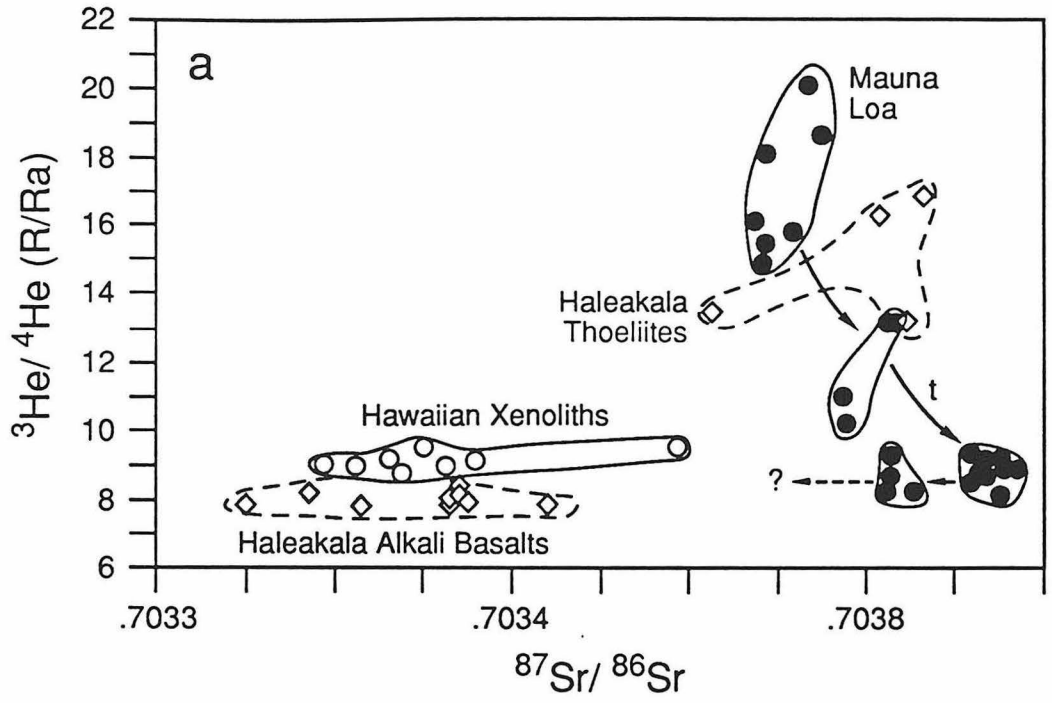

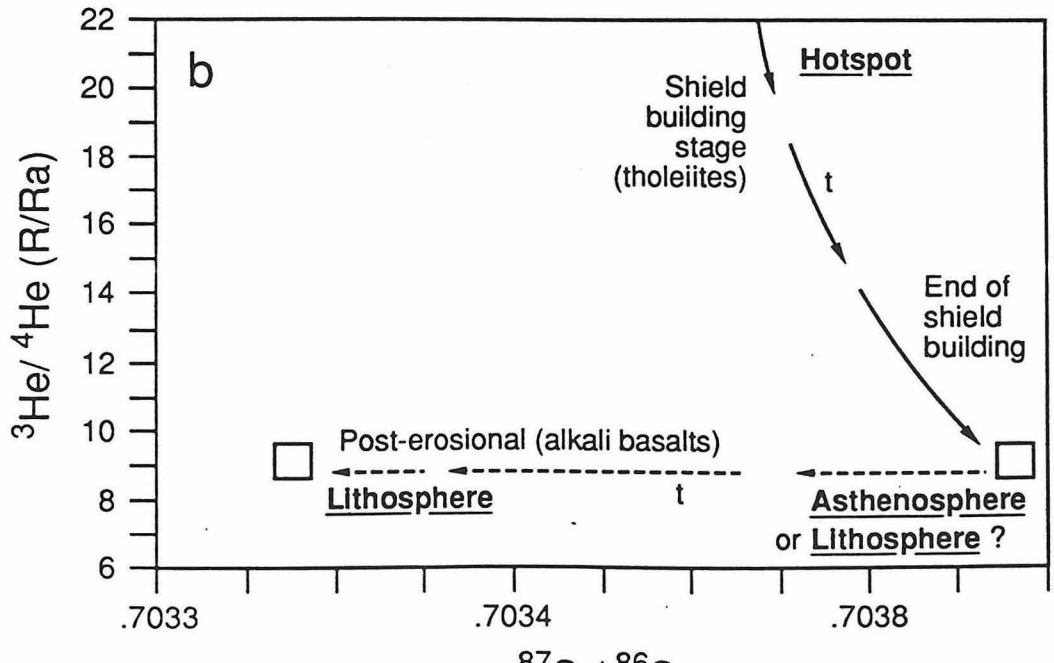

SUPER PLUMES STOP MAGNETIC FIELD REVERSALS

Roger L. Larson (Graduate School of Oceanography, University of Rhode Island, Narragansett, RI 02882; 401-792-6165; Telemail: R.LARSON)

Oceanic plateaus, seamount chains, and continental flood basalts are all proxies for deep mantle plume activity. A volume production history of these features for the past 150 Ma (Figure 1) shows a burst in volcanic activity coincident with the onset of the long Cretaceous normal magnetic polarity interval in the Early Cretaceous. I interpret this burst in volcanic activity as a rising super plume or plumes that initially erupted within the Pacific Basin, and then spread to other oceans. The initial burst in super plume activity decayed more or less continuously for the next 100 m.y. Plume activity reached a minimum level about 30 Ma that is approximately equivalent to activity prior to the initial burst. Thus, the "life cycle" of the super plume is 100 m.y.

Because the initial eruption of the super plume coincides with the onset of the long Cretaceous normal magnetic polarity interval, I conclude that the super plume episode stopped magnetic field reversals for about 40 m.y. in the following way. The super plume erupted from the super adiabatic layer at the base of the mantle called D" by seismologists. D" is currently about 100 km thick and has a vertical temperature gradient of about 10°K/km, probably a good approximation of its properties just prior to the Cretaceous super plume. Removal of high temperature material from D" to fuel the super plume thinned D" and raised its temperature gradient. This allowed heat to be transferred more rapidly by conduction across the core/mantle boundary. The outer core then convected more rapidly to restore this abnormal heat loss. The elevated convective activity of the outer core stopped magnetic field reversals by a process that is unclear, but probably related to the increased kinetic energy of the convection system. After the initial burst of activity the super plume decayed and temperature gradients began to restore to pre-super plume conditions. Sufficient restoration had occurred to allow magnetic reversals to begin again in the Late Cretaceous with a reduced frequency. Plume activity continued to decay and reversal frequency to increase until late Cenozoic time when present-day levels were approximately reached.

Figure 1 shows the history of magnetic field reversals plotted below the history of production of oceanic plateaus, seamount chains, and continental flood basalts for the past 150 Ma. The relative pattern of magnetic reversals for that period is well-known. The ocean plateau production history, which dominates the history of deep plume activity, is constructed using the assumption of Airy isostasy, so that their volumes can be calculated by knowing their topography and a "base level" from which that topography departs. They are dated mainly by scientific ocean drilling, or by direct sampling for the few that are exposed (e.g. Iceland). I assume in this study that the age of the oldest sediment recovered overlying basalt on top of a plateau represents the age of the plateau. This will yield minimum ages for these features, but the plateaus were probably built quickly by flood basalts fed from massive dike intrusions. The volumes of hot spot trails that formed islands and seamount chains were calculated in the same way as the plateaus and dated by a combination of dredging, drilling, and direct sampling. Continental flood basalts have been sampled directly for dating, and their volumes are estimated by geologic studies. It is likely that their volumes underestimate their plume sources relative to the oceanic features because only the extrusive sections are exposed for measurement, and significant plume material may have been "underplated" beneath the continental crust.

Except for some samples that are radiometrically dated, the deep plume production curve is correlated to the magnetic reversal time scale by biostratigraphic dates on both records. Production rates and reversal frequencies can be calculated by calibrating the biostratigraphic time scale to a radiometric time scale such as is shown in Figure 1. This radiometric calibration is well-known to a precision of about 2 m.y. back to the base of the Albian stage in mid-Cretaceous time. Calibration precision drops considerably prior to the Albian, an example being that the Aptian, which is the time of initial super plume eruption. This stage has a length varying from 6 to 12 m.y. on recently published time scales. As a conservative approach, the 12-m.y. Aptian is used in this study to minimize the initial peak in super plume activity. Any other recently published time scale calibration would result in a sharper, higher initial peak.

Subduction has destroyed much of the ocean crust in the Pacific Basin older than about 60 Ma that probably contained additional oceanic plateaus and seamount chains. It is especially likely that such material has been subducted at the western Pacific trenches, because mid-Cretaceous plateaus and seamounts are currently being subducted there. Also, structures interpreted as mid-Cretaceous plateaus from the Farallon plate have been obducted onto the western American coastline from northern California to Panama. To approximate the age and volume distribution of these plateaus, I have doubled the volumes of the existing plateaus older than 60 Ma in the western Pacific with the exceptions of the Line Islands and the Ontong-Java Plateau. The Line Islands are excluded because they approximate the age/volume of the Caribbean Basin, interpreted as a Farallon plate plateau that survived subduction. The Ontong-Java Plateau is excluded because its extremely large volume makes it unlikely that a plateau of that size could have been subducted.

The long Cretaceous normal magnetic polarity interval began in the early Aptian, with the youngest M-sequence magnetic anomaly, M0, dated paleontologically as earliest Aptian. The initial eruption of the super plume also occurred in the Aptian as evidenced by oldest paleontological dates on the Ontong-Java Plateau, Manihiki Plateau, Mid-Pacific Mountains (with one older Barremian date at DSDP 463), Hess Rise, Nauru Basin and East Mariana Basin, all currently located in the western Pacific. In addition the Parana Basalts of eastern South America, the world's most areally extensive continental flood basalts, are dated radiometrically at 120-125 Ma, and are clearly associated with the opening of the South Atlantic Ocean. Much of this plume activity continued for various lengths of time through the mid-Cretaceous when it became laterally more extensive with eruptions of Kerguelen Plateau, Broken Ridge, the Line Islands, Marshall Islands, Marcus-Wake Seamounts, and the Caribbean Basin. Although the total area affected by plume activity increased during this period, total volume output declined, probably both in response to the dissipating head of the super plume.

Inspection of a plot of the cumulative number of reversals versus geologic age (Figure 2) shows a pronounced flattening of that curve just prior to the long Cretaceous normal interval. This indicates a corresponding decrease in reversal frequency that started at M4 time (131 Ma). I interpret this decrease in reversal frequency as marking the initial "lift off" time of the super plume from D". The reversal frequency decrease should indicate super plume lift off quite precisely because outer core convection will respond quickly to a drastic change in the temperature structure just above the core/mantle boundary. The Ontong-Java Plateau is probably the surface expression of the rising head of the initial super plume because it is the largest of all oceanic plateaus and was constructed mainly in early Aptian time, 115-125 Ma. This gives a rise time for the initial super plumehead of about 10 m.y., and a rise velocity of 30 cm/yr. This is not

much faster than previous estimates and considerably slower than the rate ongoing plumes with existing "chimneys" can transport material (Loper and Stacey, 1983).

The manner in which the reversal process is controlled by convective flow in the outer core is poorly understood. Two models for alpha-squared dynamos have been proposed that predict magnetic reversal frequency would slow or stop if sufficient additional kinetic energy is imparted to the outer core. The first, called here the "helicity bias" model was proposed by Olson (1983) who supposed that field polarity is controlled by the dominant net helicity of the outer core convection system. Opposite-signed helicity is imparted to the system at its top and bottom, due to heat loss by conduction at the core/mantle boundary and heat gain by crystallization at the inner/outer core boundary. If heat loss by conduction were to increase, in this case due to super plume activity, then the system might be biased into that net helicity and the magnetic field locked into a long constant polarity interval. However, it is likely that the rapid turn over time of the outer core would allow inner core crystallization to compensate for this abnormal heat loss by increasing the rate of crystallization by the same amount. Thus, the helicity balance would be quickly restored and a long constant magnetic polarity interval would not result.

A second model for magnetic field stability resulting from increased dynamo activity characterizes the vigor of the convection system by its magnetic Reynolds number associated with its alpha effect (Olson and Hagee, 1989). Their examination of the long term behavior of azimuthally averaged core magnetic fields maintained by transversely isotropic induction as a function of Reynolds number showed that the duration of polarity epochs is extremely sensitive to the Reynolds number. Below some critical Reynolds number, essentially square wave reversals are produced. When the system velocity and its associated Reynolds number are raised above that critical value, the dipole field stabilizes and reversals no longer occur.

The inverse correlation of deep mantle plume activity with magnetic reversal frequency provides some guidance for future numerical modeling efforts of this type. It appears that increased dynamo activity associated with deep mantle plumes inhibits or actually stops the magnetic reversal process if sufficient additional energy is imparted to the convection system. Thus, future modeling studies that vary the level of convective activity in the system should search for solutions where increased convective activity reduces magnetic reversal frequency.

CONCLUSIONS:

1. **Super plumes stop the magnetic reversal process as follows:**
    a. **Super plumes rise from D" at the base of the mantle.**
    b. **This thins D" and raises its vertical temperature gradient.**
    c. **This increases heat conduction across the core/mantle boundary.**
    d. **This increases outer core convection to restore the abnormal heat loss.**
    e. **Increased convection stops the reversal process by a mechanism that is unclear, but probably related to the kinetic energy increase.**

QUESTIONS:

1. What is the mechanism by which increased outer core convective activity stops magnetic field reversals?

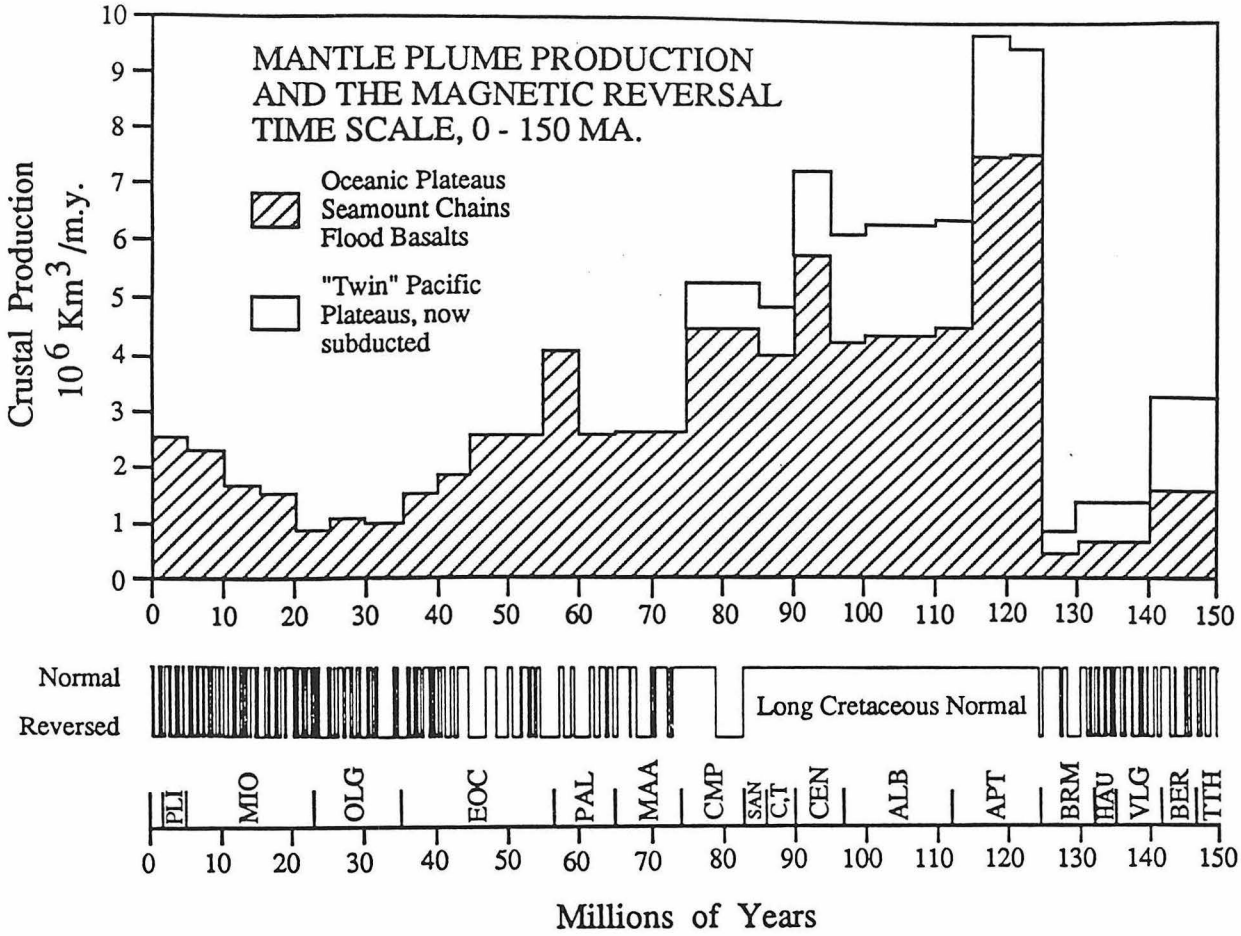

Figure 1. Oceanic plateaus, seamount chains and continental flood basalt production plotted with the magnetic reversal time scale as a function of geologic time according to Harland et al. (1990). "Twin" Pacific plateaus, now subducted, are equivalent to existing western Pacific plateaus older than 60 Ma except for Ontong-Java Plateau and the Line Islands.

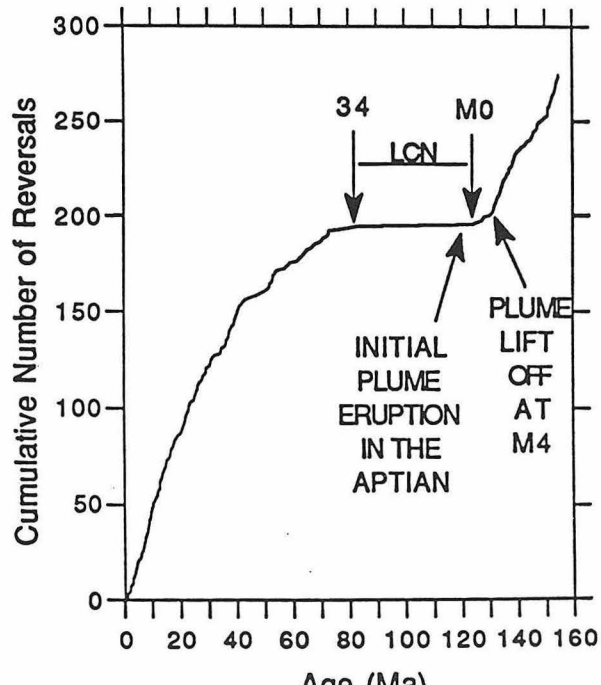

Figure 2. Cumulative number of magnetic reversals as a function of geologic time according to Harland et al. (1990). The slope of this curve is equivalent to magnetic reversal frequency. Magnetic reversals M0 and 34 bound the long Cretaceous normal (LCN) magnetic interval. The drop in reversal frequency at M4 time is interpreted as the time the initial super plume lifted off the core-mantle boundary.

THE SLAB PENETRATION CONTROVERSY

Thorne Lay, University of California, Santa Cruz

Determining the fate of subducted oceanic lithosphere is a fundamental problem in global geophysics, impacting the entire conceptual framework for deep earth dynamics. The most direct procedures available for addressing this issue are seismological, but important contributions also come from mineral physics, geodynamics, and geochemistry. This overview emphasizes seismological aspects of the ongoing controversy over whether subducting slabs penetrate into the lower mantle.

There are two basic attributes of subducting lithosphere that make it 'visible' to the seismologist. The first is that the relatively low temperatures of the slab allow abrupt elastic strain release in the form of earthquakes (caused by brittle slab deformation at shallow depths and mineral phase transformations at greater depths) to extend as deep as 700 km into the mantle. Earthquakes deeper than 700 km have not been observed, and the coincidence of the maximum depth of seismicity with the global 670 km velocity discontinuity has long been noted. The second aspect of the slab, also associated with its relatively low temperatures, is that elastic wave velocities in the colder slab material are expected to be faster than in the ambient mantle, producing a relatively high velocity tabular structure. Three-dimensional imaging of the velocity heterogeneity can thus potentially constrain the geometry of the subducted material even if seismicity does not illuminate it. This is the primary means by which to test whether slabs extend to greater depths than the 700 km seismicity cut-off.

The maximum depth of slab penetration into the mantle cannot be resolved by the intraplate seismicity alone, for it is well-established that thermal effects can suppress the mechanisms resulting in deep earthquakes. For example, slowly subducting lithosphere achieves higher slab temperatures at intermediate depths than rapidly subducting slabs, causing seismicity to terminate well-above the 670 km discontinuity, as is apparently the case for the Aleutian slab. Determining the leading edge of the slab then depends either on uncertain reconstructions of how much slab has been subducted or on seismic velocity imaging procedures. Even for slabs containing earthquakes to the maximum depth of 700 km, the likelihood that phase transformations associated with the 670 km discontinuity take place within the slab near this depth raises the possibility that the transformation process may eliminate the mechanisms for deeper events. What is fairly clear from the deep seismicity is that the slab does have some coherence as a strain-guide, with principle strain axes of deep events tending to align with the dip of the seismic distribution. The seismicity also reveals contortions of the slab environment, with evidence for both warping and imbrication of the slab (Tonga, Banda, Celebes) as well as several examples (Southern Kuriles, Peru, Izu, New Hebrides) of horizontal fingering of the slab. Recent attempts to infer the degree of strain deformation associated with the deepest slabs indicate that slab broadening takes place for at least some slabs, but the likelihood that deep seismicity accounts for only a small portion of overall slab deformation makes it difficult to account for the entire volume of slab material impinging on the 670 km discontinuity. As a result no consensus about the depth of penetration has emerged based solely on seismicity.

Imaging the velocity heterogeneity of subducting slabs and the surrounding mantle has played an increasing role in the effort to establish the fate of subducting material, but this approach has also led to inconsistent interpretations and controversy. Early seismological studies indicated that subducting slabs are faster than surrounding mantle at intermediate depths and provide a fairly continuous low attenuation conduit through which high frequency waves can traverse the upper mantle. Thermal models constructed for subducting slabs have shown that the thermal inertia of the slab is such that it is still several hundred degrees cooler than the surrounding mantle at great depths, which should be manifested in a fast seismic velocity, given the negative values of experimental

determinations of dVp/dT and dVs/dT. The fact that the slab has undergone chemical differentiation in its passage through the surface boundary layer complicates the prediction of slab velocity heterogeneity, as the differentiated slab may undergo a modified sequence of phase transformations relative to the surrounding mantle. This complexity is enhanced by the possibility of kinetically suppressed phase transformations, as has been observed experimentally for the olivine-β spinel transformation. Such kinetic suppression can lead to competition between thermal and chemical contributions to the slab anomaly, resulting in either decreased or enhanced total seismic velocity anomaly relative to the surrounding mantle. The complexity of the chemical processes, and the limitations of current experimental work on measuring velocity derivatives with pressure, temperature, and composition mandate that caution be used in 'predicting' the seismic velocity heterogeneity of the slab. As a result, there continues to be a strong dependence on empirical determinations of the slab heterogeneity, and variability in the physical interpretation of the seismic results.

Seismologists have developed several approaches to the problem of imaging velocity heterogeneity associated with deep subducting slabs. At first thought, it would seem to be a straightforward problem to reliably image slab velocity structure given that it is likely to be the strongest concentrated seismic velocity heterogeneity in the upper mantle; however, every seismic procedure has serious difficulties. One approach involves analysis of teleseismic residual spheres, or patterns of travel time anomalies for a particular event. The variation in path length within the subducting slab for different seismic raypaths can produce systematic slowly varying patterns of relatively early or late travel times. The main obstacle in this type of analysis is the fact that the source locations are not independently known, and much of the travel time pattern with respect to a tabular slab structure can mimic patterns due to errors in source location. As a result, even if the actual slab-induced anomalies are very large, the need to locate the event greatly suppresses the anomalies (Figure 1) and diminishes the intuitive relation between slab heterogeneity and travel time anomalies. In this approach it is necessary to process the synthetic calculations in the same

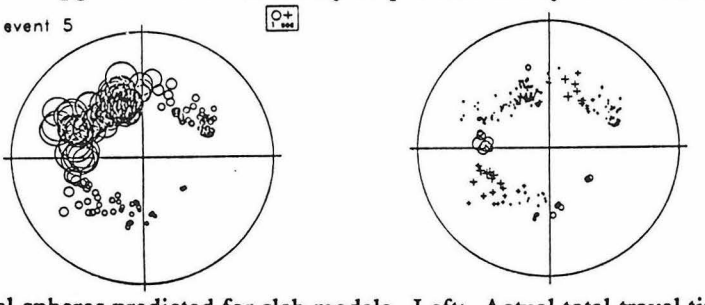

Figure 1. Residual spheres predicted for slab models. Left: Actual total travel time anomalies caused by the slab structure. Right: Observable anomalies after locating the event in a homogeneous earth model.

way as the data, essentially relocating the model predictions, before comparisons can be made. This reduces relative anomalies due to the slab structure to on the order of 1-2 sec for P waves and 4-6 sec for S waves. Reliable isolation of such small near-source contributions in the presence of larger anomalies caused by deep mantle and near-receiver aspherical structure poses great challenges.

Another seismic approach to the problem of imaging deep slab structure involves simultaneous determination of three dimensional velocity structure in the volume around deep seismicity, including relocation of the earthquakes. This application of seismic tomography has blossomed in the past decade, with both the accumulation of large travel time data sets and enhanced computer processing capabilities. The seismic data, often involving hundreds of thousands of travel time observations are inverted for relatively high resolution model parameterizations of heterogeneous structure around the slab (Figure 2).

Usually no a-priori geometry for the slab heterogeneity is imposed, so that any fast velocity image that emerges can be interpreted as the slab structure. The tomography for localized

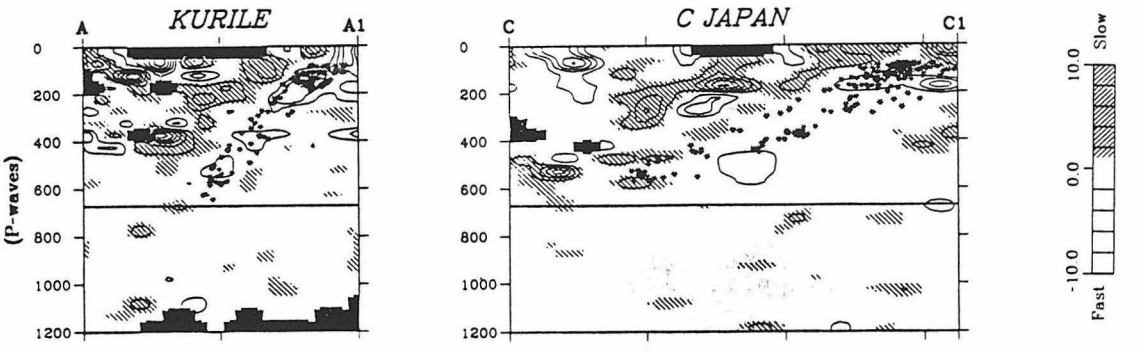

Figure 2. Velocity heterogeneity associated with subduction zones in the Kuriles (left) and Sea of Japan (right). Tomographic images from Hua-wei Zhou's thesis.

subduction zones may involve only data recorded by stations in the region above the slab (upgoing phases), or it may include or be limited to stations at large distances from the source (downgoing phases). Of the many difficulties with this approach, the primary one is the limitations of the data coverage, which seldom provides the crossing path coverage necessary to obtain high resolution of the seismic velocity structure. As a result, seismic images tend to streak out along the raypath directions. This is coupled with the strong trade-off with source location, which is poorly determined if only upgoing or downgoing phases are used. Any application using downgoing phases must eliminate the contributions from lower mantle and near-receiver heterogeneity as well. More subtle difficulties exist in the potential biases in the data sets due to measurement error associated with variable background noise properties, and effects of ray bending by the heterogeneous structure which leads to intrinsic non-linearity of the coupled source location/heterogeneity problem.

A third category of seismic investigations of deep slab structure involves utilization of complete waveform information rather than travel times alone. This includes analysis of amplitude focussing and defocussing or multipathing by lateral gradients in the slab velocity structure, and modeling of wave diffractions from the fast slab anti-waveguide structure. These approaches have gained attention as the limitations of travel time analysis have become clear, but suffer primarily from the complexity of modeling wave propagation in three-dimensional heterogeneous structures. The non-linear relation between velocity heterogeneity and secondary wavefield effects such as diffraction requires good initial starting models or simplified slab parameterizations. As with all of the other seismological procedures, isolation of the near-source effect requires that propagation effects distant from the source region be accounted for.

The depth of slab penetration has been addressed by each of these approaches, and in every case inconsistent interpretations have been advanced. Early residual sphere modeling showed that heavily filtered residual spheres corrected for distant propagation effects using low resolution aspherical models and averaged station residuals are consistent with predictions of a 5-7% fast velocity slab extending to depths of 1000 km or more in the Kurile, Japan, Marianas and Tonga subduction zones. Diminishing resolution of the structure due to ray bending effects precludes determining the maximum depth of penetration in residual sphere studies. More recent residual sphere analysis, which has both included greater coverage of the source focal sphere (to reduce the source location trade-off) and higher resolution aspherical models for distant travel time effects show far less regular slab anomaly patterns, with only intermittent evidence for high velocity anomalies below subducting slabs. Tomographic imaging has yielded comparable end-member interpretations, with some results favoring continuous high velocity structure extending to depths of at least 1000 km, while other results suggest horizontal flattening of

the slab, and even irregularity of the high velocity structure at intermediate depths. Waveform studies have demonstrated that some signals show strong distortions that are compatible with expected slab diffractions for deep mantle extensions of fast tabular structures, while it has proven very difficult to find the systematic patterns of amplitude variations expected for the simple slab models inferred from early residual sphere analyses.

Is it possible to reconcile the inconsistent seismic interpretations, and is progress being made toward such a resolution? The need for more reliable suppression of distant propagation effects for all of the seismic approaches has been clearly demonstrated, and recent work has focussed on developing empirical path calibrations for the seismic attribute being analyzed. Recent work has shown that much of the travel time variation that was modeled as a slab effect is caused by underprediction of distant effects (Figure 3). This is a manageable problem, with empirical calibrations or recent high resolution models improving the isolation of near-source effects. The general implication of work to date is that any deep slab extensions do not involve the strong velocity heterogeneity indicated by

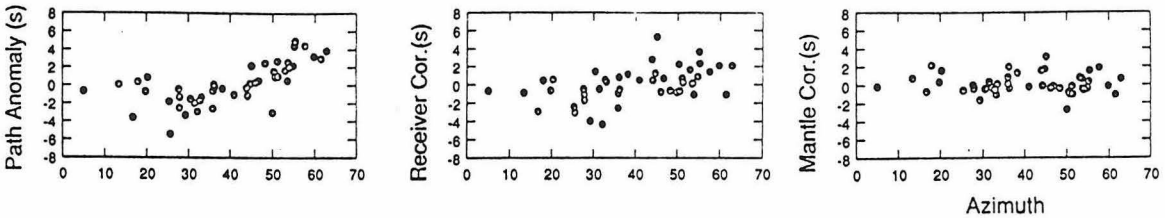

Figure 3. Example of observed S velocity anomalies from deep focus events. Left: Kurile data with no corrections. Middle: With standard station corrections. Right: With corrections from high resolution tomographic model.

early studies. Reduction of the slab heterogeneity can account for the absence of strong defocussing and diffraction effects, while still allowing waveform distortion for some geometries. But this also makes it all that much more difficult to resolve the question of whether slabs penetrate into the lower mantle at all. If the deep slab extension has indeed undergone the perovskite phase transformations near 670 km depth, it is only the thermal effect which will give a visible seismic velocity anomaly, and this may only be a few percent. If accompanied by strong slab distortion and broadening due to viscous resistance to penetration, the slab velocity gradients will be reduced, diminishing all seismic patterns for travel times, amplitudes, and waveform diffractions. Such a situation also increases the difficulty of discriminating between actual slab penetration and thermally coupled convection, which can produce continuous velocity anomalies. The question of what depth corresponds to the actual boundary between a chemically stratified upper and lower mantle must also be raised, since there is no compelling reason that it must coincide with the 670 km deep phase transitions. Thus, apparent penetration of the slab below 670 km may reflect either deflection of the boundary, penetration to a deeper chemical boundary, or actual whole mantle convection. Resolving this will not be trivial.

At present, it is reasonable to conclude that there is not yet a convincing demonstration of slab penetration into the lower mantle, nor is there a compelling refutation of this hypothesis. The combined seismological experience indicates that seismic velocity heterogeneity below the deepest earthquakes does exist, but is not as organized as indicated by early residual sphere analyses. Improved suppression of distant contributions to wavefield anomalies has tended to reduce near-source contributions, indicating that slabs are associated with less velocity heterogeneity and weaker velocity gradients. Only a few regions, such as the central Kuriles, appear to have high velocity extensions of the slab below 670 km, and this has not been unambiguously associated with the slab itself. More careful path calibration procedures are leading to improved resolution, but the reduction of deep slab anomalies may make the problem correspondingly more difficult.

The stabilization of hot plumes by variable mantle properties

A.M. Leitch, D.A. Yuen and C. Lausten

Dept of Geology and Geophysics and Minnesota Supercomputer Institute
University of Minnesota, Minneapolis MN 55415

In the world of two-dimensional convection simulations, a plume is a localized cylindrical *or* sheet-like upwelling or downwelling. As convective vigour increases, both hot plumes (upwellings) and cold plumes (downwellings) become time-dependent in their strength and position, leading to a convection pattern characterized by chaotically shifting convection cells.

We carried out numerical simulations in an axisymmetric spherical shell domain to investigate the influence of mantle properties which vary with pressure and temperature on this tendency towards chaotic behaviour. The simple boundary conditions we employed make these simulations particularly applicable to Venus, or the Earth prior to the formation of large continental plates.

We looked at the effect of a thermal expansivity α which decreased by a factor of 4.5 over the depth of the mantle, and a viscosity which increased with depth z and decreased with temperature T according to the simple formula:

$$\eta = \bar{\eta}\exp(-\ln 10(T-\bar{T}) + \ln 30(z - z_{mid})) \qquad (1)$$

This resulted into an overall increase in viscosity with depth of an order of magnitude, with high viscosity regions corresponding to the cold upper boundary layer and cold plumes, and low viscosity regions associated with the hot lower boundary layer and hot plumes. Our models also employed a thermal conductivity k which increased by a factor of 2.6 over the mantle.

A thermal expansivity α which decreased with depth by a factor of 3 was estimated from seismic measurements by Kaula [1]. Laboratory measurements by Chopelas and Boehler [2] predict a steeper change in the upper part of the mantle. The increase in k with depth is based on the lattice dynamics calculations of Anderson [3], and is supported by extrapolations of laboratory work [4] as set out in [1]. The viscosity structure of the Earth is much more uncertain [5] but an increase with depth of an order of magnitude or more is commonly proposed.

We used the finite-element code TWODEPEP [6] to solve the fully compressible anelastic liquid equations in an axisymmetric spherical shell geometry. The rheology was Newtonian and there was internal heating with a constant, chondritic concentration of heat-producing elements per unit mass. The boundary conditions at the surface and the core-mantle boundary (CMB) were free-slip and constant temperature. The equations and similar depth variations of α, k and ρ are set out in [7] for a cartesian geometry.

The vigour of convection is indicated by the Rayleigh number

$$Ra = \frac{\rho^2 c_p g \alpha \Delta T d^3}{\eta k} \qquad (2)$$

where the parameters are given in the table. The internal heating parameter $R = \rho H d^2 / k \Delta T$ used was 10.

We found that for $Ra = 3\times10^5$, which corresponds to a Newtonian viscosity of $10^{23}\ Pa\ s$, when α and η were constant the convection was already chaotic. On average there were about four cells, but their arrangement changed constantly.

When we introduced a depth-varying α, a two-cell convection pattern stabilized. There was a steady, vertical hot sheet plume at the equator and a time-dependent series of downwellings swept towards the poles. We note that the reverse flow situation, where there is cylindrical upflow at the poles and sheet downflow at the equator, is also stable, but the equatorial downflow is not steady.

The large aspect-ratio cells arise because low α at the CMB means a lower local Ra and so the boundary layer does not become unstable as readily. By the same token, the upper boundary layer becomes unstable more readily, but without the co-operation of the lower boundary layer in providing hot upflow, a convection cell cannot form. The hot plumes are steady and vertical because, due to variable α, they gain buoyancy as they rise. They tend to be "pulled up" from above and so rise straight. At the surface, they direct flow away from their weak roots. Conversely the cold plumes, vigourous at the surface, lose buoyancy and are easily swept sideways as they descend.

We increased the global Ra to 3×10^6 with variable α and found the pattern of convection became more disordered. For short periods, stable arrangements of 2, 3 and 4 cells were observed and hot plumes tended to be straighter and cold downwelling more numerous than for constant α. The higher Ra at the CMB allowed instabilities to develop in the lower boundary layer.

Next, we introduced the viscosity variation given in eqn (1) above. We recaptured the two-cell solution with equatorial upflow. The higher viscosity at depth stabilized the lower boundary layer, and the low viscosity channels cut by the hot plumes allowed them to rise straight, accelerating towards the surface. At this higher Ra the hot plume did exhibit an early instability: it weaved from side to side, directing the hot up-flow first to one hemisphere and then the next.

A global convection pattern arises due to the interaction of flow originating from the hot and cold boundary layers (surface and CMB). We have shown that depth-varying mantle properties, by changing the local properties of the boundary layers and the properties of the plumes as they move through the mantle, can have a significant effect on the aspect ratio of convection cells and the steadiness of plumes. In particular, variable α and η can lead to large cells and steady hot plumes.

Table 1. Mantle parameters used in simulations.

variable	name	value		
		average	TOP	CMB
c_p	specific heat	$1250\ J\ kg^{-1}$		
d	mantle depth	$2.8\times10^{6}\ m$		
g	acceleration of gravity	$9-10\ m\ s^{-2}$		
H	internal heat generation	$5\times10^{-12}\ W\ kg^{-1}$		
k	thermal conductivity	$6.6\ W\ m^{-1}\ K^{-1}$	4	10.5
α	thermal expansivity	$2\times10^{-5}\ K^{-1}$	3×10^{-5}	7×10^{-6}
η	viscosity ($Ra = 3\times10^{5}$)	$10^{23}\ Pa\ s$		
η	($Ra = 3\times10^{6}$)	$10^{22}\ Pa\ s$	3×10^{21}	3×10^{22}
ρ	density	$4500\ kg\ m^{3}$	3750	5200
ΔT	temperature difference	$2000-4000\ K$		

1. Kaula, W.M., "Material properties for mantle convection consistent with observed surface fields", *J. Geophys. Res., 85,* 7031-7044, 1980. 2. Chopelas, A. and Boehler, R., "Thermal expansion measurements at very high pressure, systematics and a case for a chemically homogeneous mantle", *Geophys. Res. Lett., 16,* 1347-1350, 1989. 3. Anderson, D.L., "A seismic equation of state II. Shear properties and thermodynamics of the lower mantle", *Phys. Earth Planet. Int., 45,* 307-323, 1987. 4. Schatz, J.F. and Simmons, G., "Thermal conductivity of earth materials at high temperatures", *J. Geophys. Res., 77,* 6966-6983, 1972. 5. Mulargia, F., Quareni, F. and Boschi, E., "Some rheological properties of the Earth's mantle", *Tectonophysics, 179,* 151-162, 1990. 6. Sewell, G. *Analysis of a finite-element method,* 154pp, Springer-Verlag, New York, 1985. 7. Leitch, A.M., Yuen, D.A. and Sewell, G., "Mantle convection with internal heating and pressure-dependent thermal expansivity", *Earth Planet. Sci. Lett., 102,* 213-232, 1991.

Possibilities for Mantle Plume Activity in Antarctica: Geochemical and Structural Characteristics of Cenozoic Volcanism

Wesley E. LeMasurier
Department of Geology
University of Colorado at Denver
Denver CO 80204

The Pacific sector of the Antarctic continent has been volcanically active for approximately the past 30 m.y. and continuing activity is known or suspected at roughly 14-19 volcanoes along this 5000 km segment of coast. The two largest volcanic provinces lie on opposite flanks of the West Antarctic rift system, on the coast of Marie Byrd Land (110°W-140°W) and along the west coast of the Ross Sea (~170°E, 71°-79°S). The largest volcanoes are 3000 m in relief and 1800 km^3 in volume, but large portions of some volcanoes are buried beneath the continental ice sheet. A seismic traverse across one of these indicates a 4500 m thickness of basalt buried beneath the ice, underlying 2000 m of exposed volcanic rock. All rocks in these two provinces are alkaline. Roughly 70%-90% are ne-normative basaltic rocks; the remainder are mainly trachytes, phonolites, comendites and pantellerites. Other alkaline volcanic centers occur discontinuously along the coast east of Marie Byrd Land (MBL), and northward along the Antarctic Peninsula. They are late Miocene to Holocene (7-0 Ma), widely scattered, and with two exceptions, small and entirely basaltic. A mantle plume source can be argued for the MBL province, and perhaps for the combined MBL and western Ross Sea (WRS) provinces, based on geochemical and structural characteristics described below.

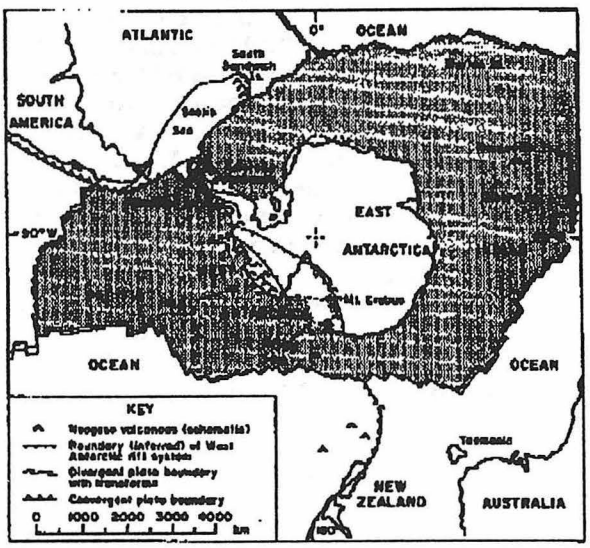

The Antarctic plate has been roughly stationary for the past 80 m.y. and is encircled by ridges and transform faults along 95% of its perimeter. The West Antarctic rift system is the major

currently active tectonic element within the plate. The axial part of the rift is a deep subglacial trough roughly 800 km wide that extends from the Ross Sea through the interior of West Antarctica to the base of the Antarctic Peninsula, a distance of 2500-3000 km (Fig. 1). Over large areas of this trough the rock-ice interface lies 1000 m below sea level, and maximum depths are -2500m. Seismic data and gravity modelling show that the crust is about 20 km thick beneath the trough, about 40 km thick beneath the Transantarctic Mountains on the south flank, and 32km beneath the MBL highlands on the north flank. It is not clear how much of the crustal attenuation beneath the trough has taken place during the present episode of rifting and how much during previous rift episodes in the late Cretaceous and possibly the Jurassic.

Geochemical characteristics of basaltic rocks have helped identify mantle plume candidates in West Antarctica (WA), by identifying those with sublithospheric source regions, but this approach is complicated by a surprising uniformity among basalt compositions. Basaltic rocks throughout WA occupy diverse tectonic environments and cover an area equivalent in size to the western cordillera from the Mexican border to southern Alaska. On the Antarctic Peninsula (AP), late Miocene-Pleistocene (7- <1 Ma) alkaline basaltic rocks were erupted <1 to 45 m.y. after the termination of subduction along the Pacific margin of the peninsula. In MBL, by contrast, alkaline basaltic volcanism has been semi-continuous from 25-30 Ma to the present, it occurs on the flank of a major rift system, and it began roughly 60 m.y. after subduction ended in this sector. Together, these Antarctic tectono-magmatic associations are analogous to the Basin and Range, Sierran, and Coast Range batholith provinces. Unlike the basalts of the western US, those in WA have consistent geochemical characteristics, with especially narrow ranges in $^{87}Sr/^{86}Sr$ (.7026-.7035), $^{143}Nd/^{144}Nd$ (.51286-.51299), and La/Nb (0.6-1.4) ratios, suggesting very limited input from "old" subcontinental lithosphere or crustal sources during magma genesis. However, there are significant differences in the relative and absolute abundances of the LILE and these divide WA into two discrete provinces. Basalts from the AP region have unusually high K/Ba and K/Rb ratios (50-140 and 500-1500 respectively) and marked Ba depletion (Ba/Nb 2.5-8.0; Ba ppm 66-320) relative to MBL basalts, which have LILE distributions within the range for OIB (K/Ba <40, Ba/Nb 5-20). This geochemical contrast is accompanied by a roughly three-fold increase in the age range of volcanic activity and an estimated three orders of magnitude increase in the volume of eruptive products, upon entering MBL.

The spatially constrained differences in geochemistry, and in the volume and duration of volcanic activity, are best explained by a plume-related origin for MBL basalts, whereas alkaline magmatism in the AP is in some way causally related to the cessation of subduction. Plume activity has already been proposed to explain tectonic doming and associated spatial patterns of volcanism in MBL. Most MBL geochemical characteristics are shared by the volcanoes of the WRS,

suggesting the possibility that a large plume head, consistent with the scale of the White and McKenzie model, underlies the West Antarctic rift system and is responsible for the tectonic and volcanic activity of the entire rift system. The uniformity of basalt compositions throughout WA may be related to uniformly slow rates of extension, by analogy with the Basin and Range province, where basalts most like those in WA are associated with the slowest extension rates in the region.

Although geochemical characteristics of Antarctic basalts are compatible with a very large plume head, the associated structural characteristics and thermal implications are more complicated. The best stratigraphic datum available for measuring plume related uplift is the West Antarctic erosion surface (WAES), a very low relief surface exposed throughout most of coastal West Antarctica but not found in the western Ross Sea. In MBL, the WAES cuts rocks as young as 80 Ma and is overlain by 25 Ma volcanics. Its age and origin are better constrained by the characteristics of a closely related erosion surface in New Zealand and the Campbell Plateau (NZ/CP), which were part of MBL before 85 Ma. Evidence from both surfaces indicates that erosional levelling was caused by fluvial erosion followed by subsidence and marine planation, during a 10-15 m.y. interval that followed the 85 Ma breakup of the MBL-NZ/CP block. The estimated magnitude of the subsidence conforms closely to the White and McKenzie model for non-volcanic rifting, and is compatible with the lack of volcanic activity in Antarctica accompanying breakup. Thus, if Cenozoic volcanism associated with the West Antarctic rift system is plume related, the plume is new, and was probably initiated in early Oligocene time.

The magnitude of plume related uplift in Antarctica is most easily measured in MBL, where the WAES has been block faulted and domed in the late Cenozoic, and where two spatial and chronologic patterns of volcanism are closely related to doming. The patterns include (1) a centrifugal migration of felsic activity away from the center of the dome, along rectilinear volcanic ranges, over the past 18 m.y., and (2) a pattern in which the ages of basal volcanic rocks resting on the WAES become older with increasing elevation of erosion surface remnants. The oldest of the basal volcanics is about 25 Ma, and rests on the WAES at an elevation of 2700 m, at the crest of the dome. Both patterns indicate that block faulting and uplift were related to volcanism. Assuming that the WAES formed at sea level, and that uplift began with the inception of volcanism, the magnitude of plume related uplift is apparently 2700 m, minus any isostatic response to erosional denudation and deglaciation. Beyond 150 km from the dome crest, block faulted remnants of the WAES are exposed at 400-1000 m elevations throughout WA. In the WRS region, Jurassic and older basement rocks stand at maximum elevations just over 4000 m in the Transantarctic Mountains (TAM). Fission track studies suggest that the TAM have risen at about 100 m/m.y., averaged over the last 60 m.y. Volcanism began here about 25-35 Ma. In the absence of a reliable stratigraphic horizon it has not been possible to estimate whether uplift was episodic, or in any way related to

volcanism, but the relief from the floor of the trough to crest of the TAM is impressive enough to suggest that a large, if unquantifiable, amount of uplift accompanied volcanism here.

Comparison of the uplift in MBL with the White and McKenzie model for volcanic-related rifting shows that 2700 m of uplift is roughly twice that expected for their maximum cases of plume related heating of the asthenosphere and lithospheric thinning. The magnitude of isostatic uplift in response to erosion seems minimal in this region. The WAES is remarkable for its lack of erosional dissection over large areas, and extremely slow rates of erosion are indicated by the rectilinear (fault bounded) outlines of many nunataks and the common occurrence of 5-10 m.y. old volcanic cones with perfectly preserved constructional form. There is evidence in the ages and distribution of hydrovolcanic deposits that the ice sheet stood 300-400 m higher than todays level between 30-70 Ka, and a possibility that ice level was 1000m higher than today about 5-8 Ma. Neither event seems capable of accounting for much of the uplift in MBL. Thus, it appears that uplift in MBL exceeds that predicted for mantle plume associated volcanism and rifting, even assuming conditions that, in the White and McKenzie model, would be associated with high rates of extension and flood basalt volcanism. No Cenozoic flood basalts have been found in the rift system, although the aeromagnetic work of Behrendt suggests that large volumes of basalt may lie beneath the ice in the axial part of the rift.

The characteristics of the rift trough offer an interesting contrast to those of the flanks. The great depth of the trough and its geometry, combined with seismic evidence that the crust is continental, and surface evidence that the ice sheet is an ineffectual agent of erosion, all suggest that the ice is graben fill. If this is true, then a substantial proportion of graben collapse has taken place within the past 30 m.y. (the approximate age of the ice sheet), contemporaneous with volcanism on the rift flanks. For comparative purposes it is helpful to crudely estimate what the rift axis might look like in a temperate region, with sedimentary graben fill. If one doubles the density of the present ice fill and halves its thickness, valley floors would lie roughly at sea level. A comparable situation in the western U.S. would leave the Sierra Nevada at its present elevation but reduce valley floors in the Basin and Range province to sea level. This seems difficult to reconcile with a very large, newly initiated plume head.

In conclusion, basalt geochemistry throughout the West Antarctic rift system, and the spatial patterns of volcanism and uplift in Marie Byrd Land, all suggest a relationship to mantle plume activity, and the characteristics of the West Antarctic erosion surface suggest a newly initiated plume. However, the rift flanks seem anomalously high and the trough anomalously low for a single large new plume, and the flood basalt fields that might validate the expected thermal regime of such a plume are well concealed, if they exist at all.

Abstract of a presentation at the Mantle Plume Symposium at Cal Tech, May 2-4, 1991

Models of mantle plumes

David E. Loper
Geophysical Fluid Dynamics Institute
Florida State University
Tallahassee. Florida

The paradigm of mantle plumes has become increasingly popular in the past five years as more evidence has accumulated concerning their internal structure and their expected imprint on the surface. The prototypical model of a plume is a persistent vertical conduit of hot, low-viscosity material extending from the base of the mantle to the base of the lithosphere, up which hot buoyant material rises. In the following, I will investigate the theoretical existence of such model plumes, the possibility and plausibility of their occurrence in the mantle, the way they get started and alternative explanations for the geophysical evidence in favor of such plumes.

The existence of plumes, as structures which might occur in variable-viscosity flow, has been investigated by the complementary approaches of mathematical analysis and experimentation. Loper and Stacey (1983) showed that a cylindrical plume exists as a self-consistent structure in variable-viscosity flow provided: (1) temperature or compositional variations occur such that the viscosity of the fluid medium varies by several orders of magnitude, (2) there is a (roughly constant) supply of low-viscosity material at depth, sufficient to maintain a flow of material up the plume. The existence of plumes was first demonstrated experimentally in 1975 by Whitehead and Luther, and since then by a number of others.

Plumes in the mantle are possible if the two conditions listed in the previous paragraph are satisfied. It is known that the viscosity of mantle material varies strongly with both temperature and with composition (particularly fluxing agents such as H_2O and CO_2). Most studies of plumes assume them to be due to the action of temperature, but metasomatic (i.e., compositional) plumes are also possible. Temperature differences of at least several hundred degrees are needed to obtain significant ($\sim 10^2$) viscosity variations. Such differences are known to occur within the mantle; the temperature difference across the lithosphere is about 1000 K. It is less obvious that there is a possible supply of hot material at depth, but if the Earth is cooling as thermal-history calculations predict, heat escaping from the core would likely produce a hot thermal boundary layer at the base of the mantle that could supply the necessary hot material for plumes. The temperature jump across this layer is very uncertain; 800K is a favorite number, but this may be in error by a factor of two or more. In spite of this uncertainty, it must be concluded that a supply of low-viscosity material for plumes is likely to exist at the base of the mantle.

It was shown by the theoretical analysis of Yuen and Peltier in 1980 that a diffusively thickening buoyant, low-viscosity bottom boundary layer (such as that believed to exist at the base of the mantle) becomes progressively more dynamically unstable with time, and they argued that the bottom boundary layer in the mantle is likely to be unstable to the formation of plumes. Furthermore, Loper, McCartney and Buzyna (1988) have demonstrated experimentally that discrete narrow plumes of buoyant low-viscosity material (such as water) can emanate from a broad source region lying below a more dense, more viscous fluid (such as syrup). Thus plumes are a plausible structures in such situations.

The plausibility of plumes in the mantle is a somewhat more subjective matter, depending on one's opinion (prejudice) concerning the structure of the mantle and on the plausibility of alternative explanations for the data which seems to support the occurrence of plumes in the mantle. There is sufficient data in accordance with both requirements, described above, and the salient predictions of the mantle plume model, described below, to support the contention that mantle plumes plausibly occur within the mantle.

A plume is initiated as a spherical cap of low-viscosity, buoyant material rises through the surrounding medium, trailing a conduit up which additional buoyant material flows; this is characterized by the balloon-on-a-string model. This model predicts that as the new plume rises to the surface and encounters a moving lithospheric plate, the signature will consist of a large volcanic outpouring (a flood basalt) followed by a chain of progressively younger volcanoes extending from the flood basalt to the site of a presently active hotspot volcano. If the plume is 'stationary', the orientation of the volcanoes will be dictated by the motion of the plate. The Hawaiian plume has two of these three features (the chain of volcanoes and the currently active volcano), but location of the flood basalt marking the origination of the plume is obscured by the Aleutian and Kuril-Kamchatka trenches. It may not be coincidental that the Emperor seamount chain intersects these two trenches at a cusp; the cusp might be the topological remnant of the intersection of the flood basalt with the (initially uncusped) trench.

Perhaps a better example of the geological remnant of the rise of a new plume is seen in India and the Indian Ocean. The Deccan traps were extruded rather quickly some 66 Myr ago. Trailing south from this flood basalt, in accordance with the northward motion of the Indian plate, is found a sequence of progressively younger volcanic islands: the Laccadives, the Maldives and the Mascarenes. At the termination of these features lies Reunion Island, with Piton de la Fournaise, a currently active hotspot volcano. There are a number of other such coupled features found on the surface of the earth, including the Columbia River basalts, the volcanic features along the Snake River plain and Yellowstone.

The concordance of theoretical, experimental and observational evidence of plumes provides a strong argument for their existence within the mantle. Alternative explanations for the observed volcanic features are less convincing. The suggestion that the chain of volcanic islands is the result of a propagating rift in the ocean floor which allows upper-mantle material to well up to the surface fails to explain why the volcanic edifices rise much higher than the midocean ridges, and why the geochemical signature of these volcanoes is distinct from MORBs. Similarly, any other shallow mechanism cannot explain the distinctive elevation and geochemistry of hotspot volcanics.

It has been suggested recently (Alt, et al, 1988; Rampino and Stothers, 1988) that flood basalts and their associated hot-spot volcanism can be initiated by the impact of a comet or meteor at the surface of the Earth. This hypothesis appears to require that the disturbance at the surface initiates the development of a plume from depth, since there is no plausible way that the distinctive geochemistry of hot-spot volcanics can be produced by a source restricted to the upper mantle. But if our ideas of the thermal and dynamical structure of the mantle are correct, there is apparently no way for plumes to be initiated by any surface disturbance (Loper and McCartney, 1991). This argument also rules out plume initiation due to plate reorganization, lithospheric thinning, plate fractures, etc.

The remaining question is the depth of the source of mantle plumes. The fact that the source region must be able to supply material with a viscosity several orders of magnitude less than the surrounding mantle rules out the formation of plumes from a general upwelling within the mantle. The 650 km discontinuity has been suggested as a possible source of plume material, but there is no seismic evidence of a low viscosity region at that

depth. A stronger argument (Davies, 1988) against an origin at 650 km depth is that the heat flux, geoid and bathymetry signatures of plumes are inconsistent with an origin at that level. For example, if convection in the mantle is layered, then plumes from 650 km depth would carry virtually all of the heat from the core and lower mantle to the surface. But the heat flux up plumes is estimated (Sleep, 1990) to be about 2.5×10^{12} W, less than 10% of the mantle heat flux, and far less than needed to cool the lower mantle. However, this observationally based value of plume heat flux is remarkably close to independent estimates of the present rate of cooling of the core of 3×10^{12} W (Loper, 1991).

Furthermore, the observed fixity of hotspots is difficult to explain if they arise from a mobile boundary layer at 650 km depth and rise through a vigorously convecting upper mantle. On the other hand, hotspot fixity is a natural consequence of plumes rising from the base of the mantle. The base of the mantle is in contact with a virtually inviscid core, and hence is not subject to any basal shear stress. This means that there is little vertical shear of horizontal flow in the lower mantle. Also, if the heat from the core is conveyed to the surface by plumes, the bulk of the lower mantle is unaffected by this bottom heating. That is, the lower mantle convects principally in response to the descent of cold material from above. Loper (1985) calculated that penetration of cold slab material into the lower mantle causes a relative drift between hotspots of about 5 mm/yr, which is in accord with observed drifts.

If plumes penetrate the mantle from base to lithosphere, then they are perforce a form of convection through the 650 km discontinuity, and the concept of the mantle convecting in two distinct layers is severely weakened, if not invalidated. Moreover, the fixity of hotspots tells us much about the structure of mantle convection. In particular the sharp bend in the Hawaiian-Emperor chain is geometrically possible only if the region of shear between the Pacific Plate and the underlying mantle is 200 km thick at most (Griffiths & Richards, 1989), and the portion of the upper mantle lying below this shear zone is virtually stationary. This is in direct conflict with models of layered mantle convection in which the upper mantle is in a state of vigorous convection, and provides strong evidence in favor of whole-mantle convection.

References

Alt, D., Sears, J. M., and Hyndman, D. W. (1988) Terrestrial maria: The origins of large basalt plateaus, hotspot tracks and spreading ridges. *J. Geology*, **96**, 647-662.

Davies, G. F. (1988) Ocean bathymetry and mantle convection 1. Large-scale flow and hotspots. *J. Geophys. Res.*, **93**: 10467-10480.

Griffiths, R. A. and Richards, M. A. (1989) The adjustment of mantle plumes to changes in plate motion. *Geophys. Res. Lett.*, **16**: 437-440.

Loper, D. E. (1985) A simple model of whole-mantle convection. *J. Geophys. Res.*, **90**: 1809-1836.

Loper, D. E. (1991) The nature and consequences of thermal interactions twixt core and mantle. *J. Geomag. Geoelectr.*, to appear.

D. E. Loper and K. McCartney (1991) Impacts as a cause of geomagnetic field reversals or flood basalts, to appear in GSA Special Paper 247 - *Global catastrophes in earth history: An interdisciplinary conference on impacts, volcanism, and mass mortality*, V. L. Sharpeton and P. D. Ward, Eds.

Loper, D. E., McCartney, K. and Buzyna, G. (1988) A model of correlated episodicity in magnetic-field reversals, climate, and mass extinctions. *J. Geol.*, **96**: 1-15.

D. E. Loper and F. D. Stacey (1983) The dynamical and thermal structure of deep mantle plumes. *Phys. Earth Planet. Inter.*, **33**, 304-317.

Olson, P., and Nam, I. S. (1986) formation of seafloor swells by mantle plumes. *J. Geophys. Res.*, **91**: 7181-7191.

Rampino, M. R., and Stothers, R. B. (1988) Flood basalt volcanism during the past 250 million years. *Science*, **241**, 663-668.

Sleep, N. H. (1990) Hotspots and mantle plumes - some phenomenology. *J. Geophys. Res.*, **95**, 6715-6736.

White, R. S., and McKenzie, D. P. (1989) Magmatism at rift zones: the generation of volcanic continental margins and flood basalts. *J. Geophys. Res.*, **94**: 7685-7730.

Whitehead, J. A., and Luther, D. S. (1975) Dynamics of laboratory diapir and plume models. *J. Geophys. Res.*, **80**: 705-717.

Yuen, D. A., and Peltier, W. R. (1980) Mantle plumes and the thermal stability of the D" layer. *Geophys, Res. Lett.*, **7**: 625-628.

Plume Observations: How Much are They Contaminated by Lithospheric Effects?

MARCIA McNUTT
Department of Earth, Atmospheric, and Planetary Sciences
Massachusetts Institute of Technology, Cambridge, MA 02139

Conventional plume wisdom (CPW) dictates that
(1) the orientation of volcanic chain traces the absolute motion of the lithospheric plate with respect to the hot spot;
(2) the intermittent nature of most hot spot traces marks the waxing and waning of plumes;
(3) variations in isotope geochemistry of hot spot lavas reflects heterogeneity at the plume source.

More detailed observations suggest that the lithosphere may be more instrumental in controlling the orientation, intensity, and chemistry of hot spot volcanism than what is implied by CPW. However, based on observations of plume-type volcanism on oceanic lithosphere, the filtering effect of the lithosphere cannot easily be interpreted in terms of a lithospheric vulnerability factor.

Orientation of Hot Spot Traces

In violation of CPW, some hot spot chains, notably the Marquesas, depart by as much as 30° from the azimuths of other coeval Pacific traces (Figure 1). The Pitcairn and Louisville chains are both suspected to be reoriented from the CPW direction towards that of nearby fracture zones. There is good evidence in the Hawaiian, Musician, and Marquesas chains for the production of hot spot ridges where the hot spot crosses a fracture zone (Figure 1). In the Marquesas, we suspect that the non-CPW orientation is caused by channeling of magma along the direction of an older lineation coeval with the Line Islands. In these cases, there appears to be a limit of a few hundred kilometers to the distance over which the plume magmas can be deviated that may be related to the dimensions of the plume source. Thus preexisting lithospheric structure is unlikely to cause major departures from CPW orientation over a long distance, but it does limit our ability to detect subtle changes in plate motion direction and rate.

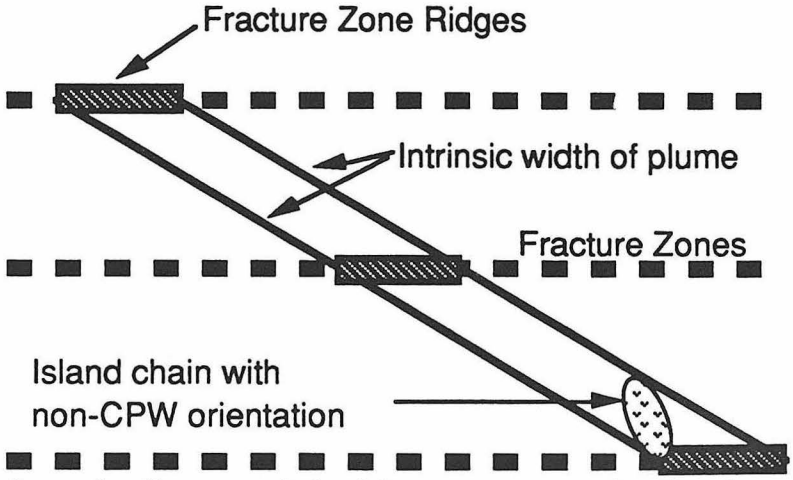

Figure 1. Schematic diagram of the Marquesas area, showing how the non-CPW orientation of the island chain and the location of fracture zones ridges relate to the theoretical path of the hot spot according to CPW.

Episodicity of Plumes

The examples of deviation of plumes along fracture zones noted above are frequently associated with an increased volume of volcanism. The extreme case is the Marquesas hot spot for which the fracture zone ridges represent the only surface expression of volcanism along its early Tertiary path (Figure 1). Similar phenonena occur when hot spots cross older traces of plume activity. Therefore, plate structure does modulate plume output.

A very important, but not yet entirely understood, example of plume modulation by the lithosphere is the segmentation of off-rige volcanism across fracture zones. Statistics of seamount abundances show that distributions change across fracture zones, and some hot spots appear to even turn on or turn off as they cross fracture zones. Some of these observations must be interpreted with care, particularly for older volcanic chains for which the disappearance of the hot spot trace might simply be explained as the result of a near-ridge hot spot crossing onto the opposing plate and thus leaving its trail somewhere else (Figure 2). A possible explanation for the segmentation of hot spots by fracture zones is that plumes might produce more or less volcanism when they cross a fracture zone to lie beneath younger or older lithosphere, respectively. The observations do not always support this theory, but one must again be cautious in the case of near-ridge hot spots (Figure 2).

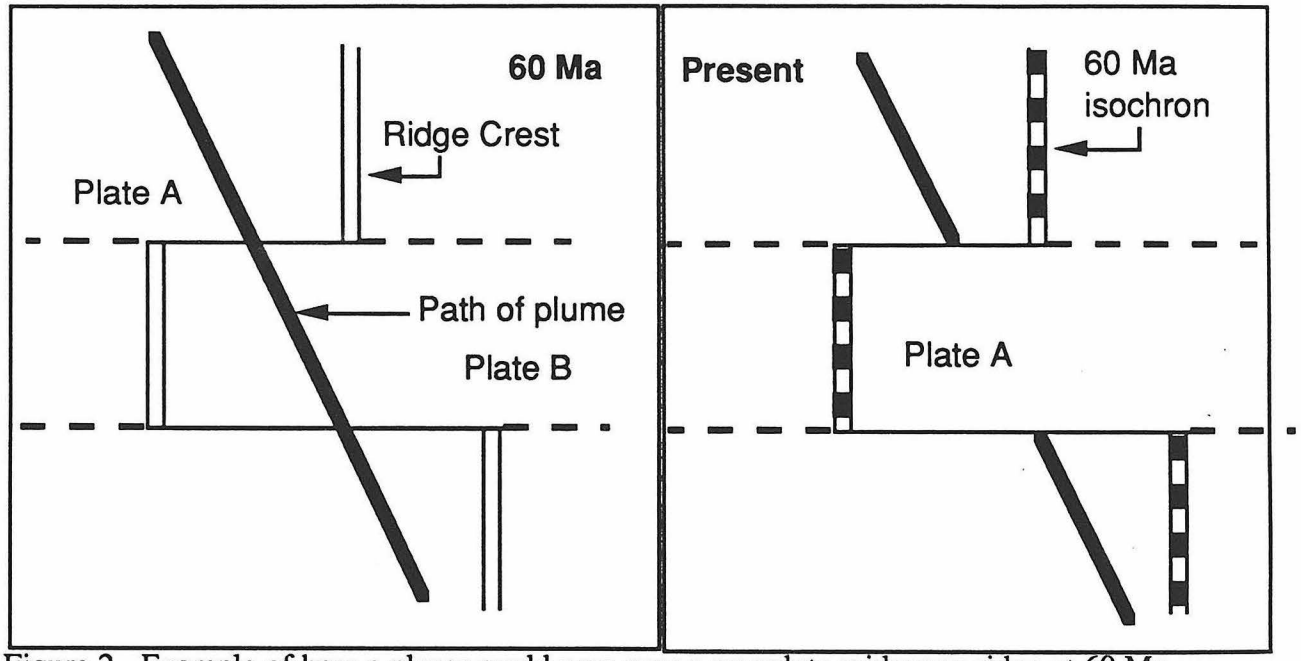

Figure 2. Example of how a plume could pass near a crenulate midocean ridge at 60 Ma, and thus appear at the present to turn on and turn off because part of the hot spot trace is left on Plate B. The sense of offset on the northern fracture zone is such that the apparent turning off of volcanism occurs beneath the younger plate. Without knowledge of how the age of the hot spot compares to that of the underlying plate, these observations could be interpreted as younger lithosphere being less vulnerable to hot spot volcanism.

Geochemistry of Plume Magmas

Others at this symposium are certainly more competent that I am to comment on the subject of geochemistry of plumes. Individual hot spots do tend to have characteristic geochemical fingerprints, often expressed in terms of mixing of isolated end-member components. If these distinctive components all reside in the convecting mantle, as dictated by CPW, their persistence has strong implications for mantle mixing times and scales. If the plume melts interact with the lithosphere, however, the possibility exists that one or

more of the components resides within the plate, and therefore does not mix with the mantle on account of its higher viscosity. Some of the short-term (few million years) temporal variation of the geochemistry of individual hot spots (e.g., Samoa main shield versus post-erosional stages) may be explained by the contamination of plume material with remelted rocks from a geochemically layered lithosphere.

Vulnerability of the Lithosphere

The question remains as to whether the lithosphere exerts first-order control on the global distribution of hot spots, and therefore their pattern cannot be used to infer the fundamental structure of upwelling in the mantle. Based solely on the distribution of hot spots, it is difficult to choose between the mantle- and lithospheric-control hypotheses, because there are exceptions to the predictions of both models. However, using Sleep's [*JGR*, 1990] recent quantification of hot spot flux, it is possible to assess whether the exceptions to each rule are significant in terms of the mass and heat carried by hot spots.

Figure 3 shows histograms of hot spot flux as a function of various parameters likely to represent the lithosphere's ability to act as a barrier to hot spot penetration. Because Sleep's hot spot compilation omits some examples on continental lithosphere (on account of the difficulty in defining a reference level for elevation, geoid, and heat flow from which excess plume flux can be estimated), I have concentrated on the flux from just the oceanic hot spots and normalized the flux to the area of oceanic lithosphere represented in each histogram category. The flux from plumes is discharged without regard to the age of the overlying plate (Figure 3a), except for the two youngest age bins which display an excess of flux near ridge (<5 Ma) and a compensating deficit on young lithosphere at 5 to 23 Ma. I interpret this as either capture of a nearby ridge by a plume or entrainment of the flux from a nearby plume to the flux at the ridge.

The flux liberated as a function of velocity of the plate also shows no tendency for rapid plate motion to inhibit the flux from hot spots (Figure 3b). Plotting the flux as a function of the "lithospheric vulnerability parameter" which increases linearly with plate thickness and as the square root of plate velocity, again shows that most of the hot spot flux penetrates lithosphere that is predicted to have low vulnerability for volcanism (Figure 3c). The one parameter that does appear to be sensitive to plate vulnerability is the average flux of the hot spots (Figure 3d). Feeble hot spots simply do not occur on lithosphere with low vulnerability (large thickness and/or rapid drift velocity).

In fact, the impression from Figure 3c is that lithosphere of low-vulnerability, by virtue of its rapid motion (Figure 3b) rather than old age (Figure 3a), is, ironically, the site for most of the global flux of hot-spot volcanism. This conclusion is entirely dictated by the large flux from Hawaii and the Superswell hot spots of French Polynesia, which together account for 45% of the global flux. This correspondence between rapid plate motion and large plume flux may also hold for a prior period of rapid plate motion at 70-100 Ma when volcanism from Superswell hot spots produced the "Darwin Rise" seamount chains in the northwest Pacific. If indeed mantle circulation (as indicated by the global geoid pattern) controls the distribution of plume flux, then the large discharge of plume flux through rapidly drifting plates with low vulnerability may imply that upwelling drives rapid plate motion.

This link between hot spots and plate speed is quite distinct from earlier suggestions that plumes must be part of a broad mantle flow driven by plate motions because they cluster near midocean ridges and avoid subduction zones. I now question the evidence used to support this latter theory. The present analysis demonstrates that the ridge-related entrainment of flux is only a local phenomena (Figure 3a; 23 Ma in time≈1000 km in distance), and plumes near subduction zones might easily be mistaken for island-arc type volcanism. Indeed, some arc systems show isotopic and trace element signatures derived from a plume source.

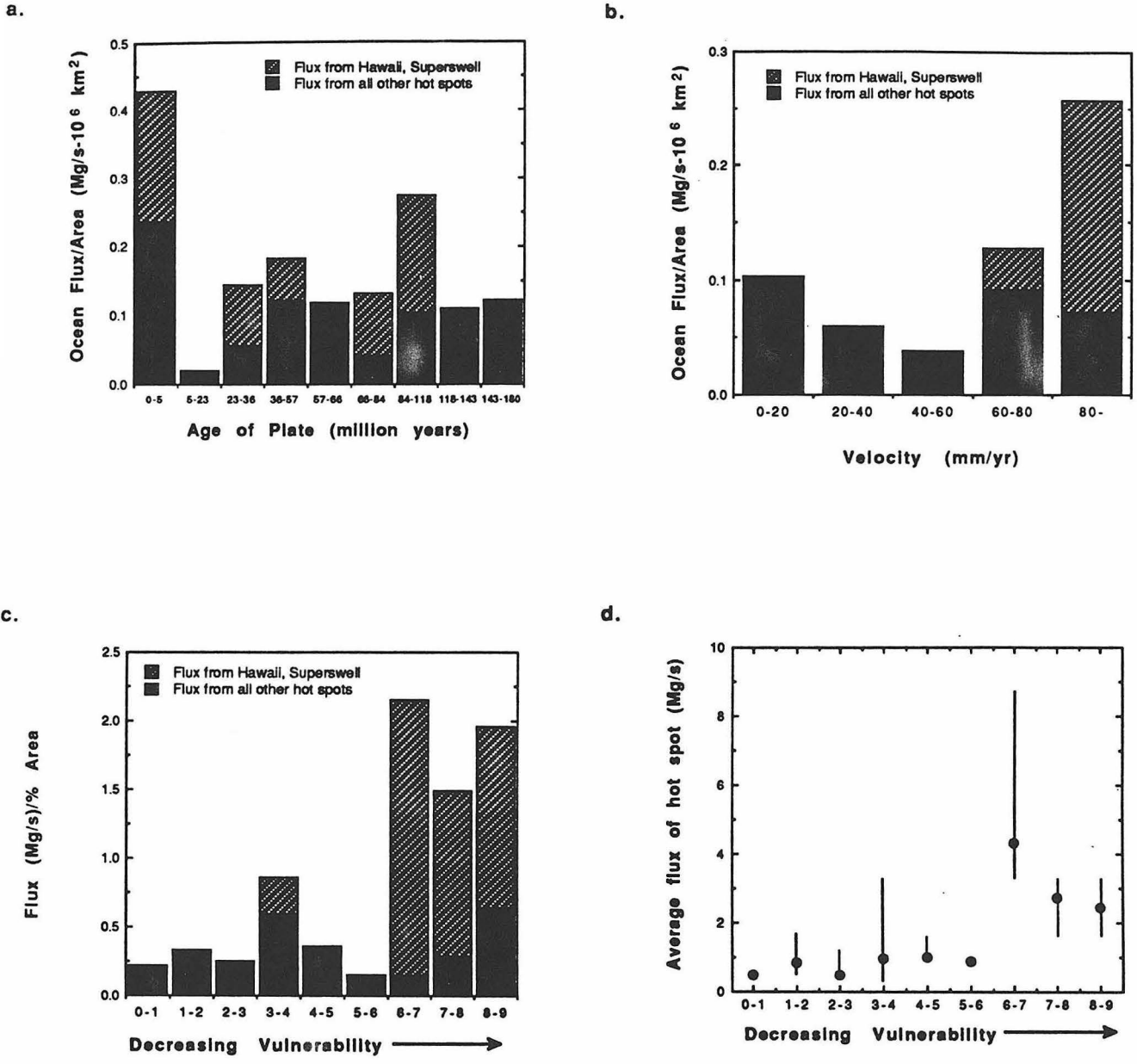

Figure 3. (a) Distribution of the flux from oceanic hot spots as a function of age of the overlying plate. Flux is normalized by the total area of oceanic lithosphere in each bin. (b) Same as (a), except that flux is plotted as a function of absolute velocity of the overlying plate with respect to the hot spot frame of reference. (c) Same as (a), except that flux is plotted as a function of the dimensionless vulnerability of the lithosphere, defined as $(\pi u/kd)^{1/2}l$, in which u is plate velocity, k is the thermal diffusivity of the lithosphere, d is the characteristic spacing of thermal perturbations (assumed constant), and l is the thickness of the lithosphere. (d) Average flux of oceanic hot spots as a function of the vulnerability of the lithosphere. Vertical bars show the total range of values in each vulnerability category.

CONTINENTAL LOWER LITHOSPHERE - AN INSIGNIFICANT RESERVOIR FOR FLOOD VOLCANISM.

Martin A. Menzies,
Department of Geology, Royal Holloway and Bedford New College, University of London, Egham, Surrey TW20 OEX, England

Several features inherent to the post-Archaean lithospheric mantle need to be considered if one invokes paticipation of this reservoir in the genesis of continental flood basalts. These include :

(1) Chemically enriched lithospheric mantle exists beneath Archaean crust but there is no conclusive evidence for laterally and vertically continuous enriched reservoirs beneath post-Archaean terrains. Moreover it appears that even beneath Archaean crust enriched mantle is restricted to the vicinity of magmatic conduits and is not widespread. Compilation of xenolith data indicates that en route to the surface flood basalts will encounter a broadly "oceanic" reservoir in the post-Archaean lithospheric mantle.

(2) Asthenospheric melts (MORB and OIB) have frequently crystallised within the lithospheric mantle as a fossilised hydrofracture system. The melt conduits are armoured against contamination from the surrounding lithospheric mantle by reaction zones (metasomatic and enrichment fronts). If such conduits can be thought of as an analogue for the plumbing system of cfb provinces it is apparent that such chemical buffers are complex hybrids that protect the melt from inheriting the isotopic characteristics of the surrounding lithospheric mantle.

(3) Studies of Pyreneean orogenic massifs indicate that continental tholeiites ($^{87}Sr/^{86}Sr > 0.705$) were themselves the source of metasomatism and modification of the Phanerozoic mantle lithosphere. Consequently their derivation from the lithospheric mantle is highly unlikely.

(4) In the garnet stability field migration of very small volume melts (plume or asthenosphere) is evident as metasomes in garnet peridotites and micro-inclusions in diamonds. Studies of these metasomes (e.g. MARID) again indicate transformation of all aspects the lithospheric mantle (i.e. petrology, chemistry and redox state) by the melt and not contamination of the asthenospheric melt by the lithosphere.

(5) The "aged" isotopes required to contaminate deep mantle melts in the production of flood basalts are resident within the mechanical boundary layer (MBL) separated from the asthenosphere by the thermal boundary layer (TBL) which has an isotopic composition similar to the asthenosphere. Therefore the presence of the TBL greatly reduces the volume of the "aged isotope reservoir" in the MBL beneath post-Archaean crust (<< 100 km.).

(6) Recent considerations by geophysicists argue for very small contributions (< 1%) from the lithospheric mantle. Several authors have regarded < 1% contamination of cfbs by the crust as insignificant from a petrogenetic standpoint. Similarly one could argue that contamination of an asthenosphere-derived melt (MORB or OIB) by < 1% of the lithospheric mantle is insignificant.

One can conclude fom these observations that the lithospheric mantle was not involved in the genesis of continental flood basalts to any great extent but may act as a source for small volume alkaline magmas with unusual isotopic chemistry (e.g. lamproites, kimberlites etc.). Therefore the chemically enriched characteristics of flood basalts must be sub-lithospheric in origin if it can be shown that they are not imposed on the chemistry of a mantle-derived melt during high level contamination with crust.

Large-Scale Mantle Heterogeneity Revealed by H_2O and Trace Elements in MORB

Peter Michael, Department of Geosciences, The University of Tulsa, Tulsa OK 74104

INTRODUCTION

Ratios of elements that have different bulk solid/liquid partition coefficients but similar chemical properties (e.g., La/Sm, Nb/Zr) are often used to determine the extent to which a MORB or OIB source is enriched or depleted. Ratios of two incompatible elements that have similar bulk solid/liquid partition coefficients but different chemical properties can reveal new information about mantle heterogeneity and mantle differentiation (Hofmann et al., 1986). Bougault et al. (1990) recently showed that the ratio of a high field strength element (Nb) and large ion lithophile element (K) was constant for depleted to enriched MORB within a given region, but that the ratio varied significantly between regions. Regardless of the depleted or enriched nature of the source, the K/Nb ratio is characteristic for MORB from a region. K/Nb ratios of MORB from the Explorer Ridge, N.E. Pacific (Michael et al., 1989) are slightly different than ratios in MORB from the East Pacific Rise at 28°-34°S (Michael, 1988; and unpublished), supporting Bougault et al.s' observations and indicating further regional diversity of basalt sources (Figure 1).

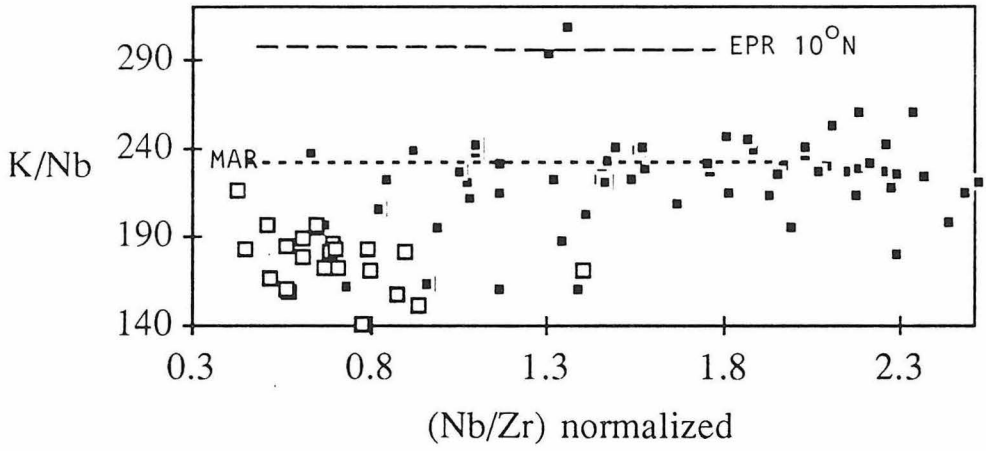

FIGURE 1: K/Nb versus Nb/Zr (normalized using values from Sun, 1980). Open squares are MORB from the EPR, 28°-34°S (Michael, 1988 and unpublished). Filled squares are MORB from the Explorer Ridge, N.E. Pacific (Michael et al., 1989). Uncertainties are small for most points but are significant for samples with low concentrations of Nb: especially open squares at the left of the diagram. Dashed lines at K/Nb = 325 and K/Nb = 235 correspond to averages of MORB from the EPR 10-13°N and from the MAR 10-17°N, respectively (Bougault et al, 1990).

H_2O and REE

In a similar way, the ratio of H_2O, (a volatile species) and a rare earth element can be calculated (Figure 2). (It is necessary to consider only those basalts that have erupted at sufficient water depth not to have exsolved a hydrous vapor phase, and basalts that have not been contaminated significantly by assimilation of altered oceanic crust). The H_2O/Ce ratio decreases slightly, and the H_2O/Nd ratio increases slightly with increasing Nb/Zr or La/Sm. The H_2O/La ratio decreases significantly with increasing La/Sm. Despite its slight dependence on enrichment, the H_2O/Ce ratio is used below instead of the H_2O/(Ce+Nd) ratio Michael, (1988) because it is easier to calculate and more data are available. The ratio

H_2O/Ce is roughly constant for depleted through enriched MORB from the northeast Pacific at 175±60 (Figure 2). Basalts from Hawaii (Loihi) and from seamounts near the EPR, and MORB from the Galapagos Spreading Center, the southern EPR, the southern MAR, the SW Indian Ridge and the America-Antarctic Ridge also fall mostly within this range (Michael, 1988). Notably, both enriched and depleted MORB from the MAR north of the Oceanographer Fracture Zone (MAR-nOc) have *significantly higher H_2O/Ce ratios* : 290±50. Within any region, there is moderate variation in this ratio, partly due to analytical uncertainty. However, the H_2O/Ce shows only a gentle dependence on the degree of mantle enrichment as expressed by ratios such as Nb/Zr or La/Sm. On the other hand, the ratio H_2O/K_2O is steeply and negatively correlated and the ratios H_2O/Zr and H_2O/Sm are steeply and positively correlated with Nb/Zr or La/Sm (Michael, 1988). The H_2O/Ce ratio is thus similar in nature to the K/Nb ratio (Bougault et al. 1990) and the Nb/U ratio (Hofmann et al, 1986).

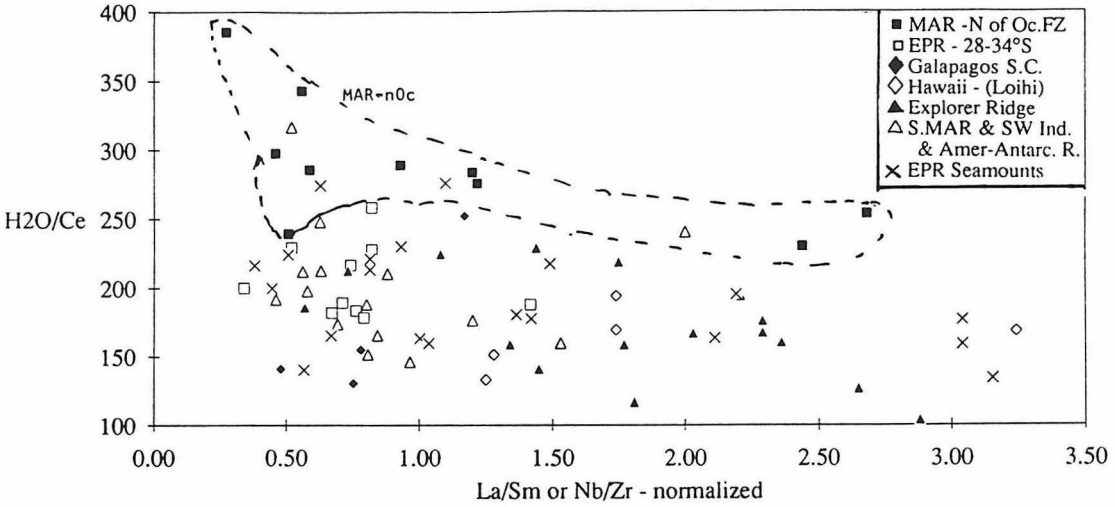

Figure 2: H_2O/Ce versus chondrite normalized La/Sm or Nb/Zr. Data sources are: Galapagos Spreading Center: Byers et al., (1983 & 1984); Schilling et al., (1983a); Clague et al., (1981). Perfit et al., (1983). EPR 28-34°S: Michael, (1988), Michael and Schilling, unpublished. Explorer Ridge: Michael, (1988); Cousens et al., (1984). MAR north of Oceanographer FZ: Poreda et al., (1986); Schilling et al., (1983b); Michael, (unpublished). MAR south, America-Antarctic Ridge and SW Indian Ridge: LeRoex et al., (1983; 1985); Humphris et al., (1985). Michael, (1988). Loihi: Byers et al., (1985); Frey and Clague, (1983). Near-EPR Seamounts: Aggrey et al., (1988); Allan et al., (1988); Batiza and Vanko (1984). The H_2O/Ce ratio decreases slightly with increasing La/Sm or Nb/Zr for most groups, indicating that Ce behaves slightly less compatibly than H_2O.

DISCUSSION

Considering the variety of plume sources that may contaminate the MORB source (as revealed by radiogenic isotope ratios), it is surprising that there is such homogeneity of the H_2O/Ce ratio for enriched MORB (and OIB) from several regions. One would expect a range of high and low H_2O/Ce ratios for enriched MORB, corresponding to relatively "wet" or "dry" enriched (plume) components: that the diagram would show linear arrays fanning outward from relatively uniform values for depleted MORB. Instead, depleted and enriched MORB from many areas share similar ratios and there is at least one region with a significantly different ratio. One possible exception to this is the Galapagos S.C. where a single enriched MORB has higher H_2O/Ce than depleted MORB from that region.

The intriguing difference between MAR north of Oceanographer FZ and all other ridges cannot be related to spreading rate, since basalts from the slow-spreading southern MAR, SWIR and AAR fall within the range of Pacific MORB. For the MAR-nOc mantle, H_2O behaves like Ce or Nd during mantle enrichment/depletion (as it does in the Pacific) because the ratio H_2O/Ce is constant. But the value of the constant is *different* for MORB from the MAR-nOc. The rare earth element analyses in the compilation have been published mostly by Schilling and co-workers, so it is unlikely that interlaboratory analytical bias accounts for the distinctive ratios of the MAR-nOc MORB.

Assuming that there are no analytical biases, there are at least two possible explanations for the constancy of H_2O/Ce between enriched and depleted MORB and for the differences between MORB from the MAR-nOc and the rest of the global spreading system. The valid model may also be useful in explaining the regional variations in K/Nb noted above and by Bougault et al. (1990).

Model 1. Enrichment (i.e., formation of the plume component) is an autometasomatic (i.e., silicate melt enrichment) process of depleted mantle, and there is a fundamental difference between the composition of the mantle beneath the MAR-nOc and most of the rest of the global spreading system. This difference would be older and larger in scale than the formation of the plume component in the suboceanic mantle, since it is a characteristic shared by enriched and depleted MORB from the MAR-nOc. This would imply that plumes are locations where extra heat has led to convective upwelling, small extents of melting, and redistribution of elements to form enriched zones within a depleted matrix. The enriched zones themselves are derived merely by autoenrichment within the mantle, with no introduction of new or exotic material. The autometasomatism must be a long-term process in order to account for the isotopic characteristics of depleted through enriched basalts. The model also implies that the H_2O content of MAR-nOc mantle was higher overall, before the formation of the Iceland or Jan Mayen plumes. Thus, both enriched and depleted MORB share the higher H_2O contents. Curiously, there appears to be little difference in other trace element and isotopic systematics between the MAR-nOc and other plume-MORB regions.

If autometasomatism is responsible for producing the enriched or plume component, then the most likely distribution of basalt sources in the mantle would be a depleted zone beneath an enriched upper mantle, contrary to the most popular conceptions of mantle plumes and mantle stratification. A corollary of this model is that there should be more highly depleted as well as enriched basalts associated with mantle plumes. High ^3He plumes might be locations where both heat and He were contributed to the mantle, but not necessarily anything else.

Model 2: Depleted MORB are derived from mantle sources which are mixtures of depleted and enriched components: mid-ocean ridges never sample a "pure" depleted mantle. This model requires that pure depleted mantle has very low abundances of incompatible elements, and that the source of even the most depleted MORB contains a small amount of an enriched component. The sparse enriched component however imparts its trace element signature on the depleted source. Different incompatible element ratios between plumes would then be responsible for the regional differences of H_2O/Ce (or K/Nb) in both

enriched and depleted MORB. This model requires that enriched components are very well dispersed throughout the entire MORB-producing mantle and suggests that they are more concentrated near plumes. Unlike Model 1, Model 2 allows the enriched component to be an "exotic" component such as subducted slabs, lower mantle, continental lithosphere, etc.

Preliminary numerical modelling suggests that it may be difficult for an enriched component to impart its characteristic H_2O/Ce ratio on highly depleted mantle without causing the source to appear distinctly enriched. The same is not true for the K/Nb ratio.

COMPARISON OF K/Nb, H_2O/Ce AND ISOTOPIC RATIOS

Comparisons of MORB from different regions is very preliminary because there are very few samples for which trace element and isotopic data of the required accuracy exist. MORB from the Explorer Ridge and EPR 28-34°S have overlapping H_2O/Ce ratios (Figure 2) and slightly different K/Nb ratios (Figure 1). There is not enough difference to see a relationship. Many of the MORB from the southern MAR, SW Indian Ridge and American-Antarctic Ridge have high K/Nb ratios (leRoex et al., 1983, 1985). Yet their H_2O/Ce ratios are similar to MORB from Explorer Ridge and EPR 28-34°S. H_2O/Ce ratios do not seem to be related in an obvious way to K/Nb. The northern MAR and Explorer Ridge both lack a DUPAL isotopic signature (Hart, 1984) yet they have distinctly different H_2O/Ce ratios. Meanwhile, the southern MAR, SW Indian Ridge and AAR contain a DUPAL signature but have similar H_2O/Ce ratios as the Explorer Ridge MORB. The only hint of a correlation is between K/Nb and DUPAL isotopic signature. A larger body of very precise trace element data for MORB world wide will help establish whether there are any correlations of the trace element and isotopic ratios. The correlations will yield important information about the origin of enriched components in the mantle.

Aggrey, K.E., Muenow, D.W. and Batiza, R., (1988), *Geochim. Cosmochim. Acta* **52,** 2115-2119.

Allan, J.F., Batiza, R. and Lonsdale, P. (1988) in *Seamounts, Atolls* 255-282. Amer. Geophys Union Monograph

Batiza, R. and Vanko, D. (1984) *J. Geophys. Res.* **89**, 11,235-11,260.

Bougault, H., Joron, J.L., Dosso, L. and Romeur, M. (1990) Trans. Amer. Geophys. Union **71**, 1702-3.

Byers C.D., Muenow D.W. and Garcia M.O. (1983) *Geochim. Cosmochim. Acta* **47,** 1551-1558.

Byers C.D., Christie D.M., Muenow D.W. and Sinton J.M. (1984) *Geochim. Cosmochim. Acta* **48,** 2239-2245.

Byers C.D., Garcia M.O. and Muenow D.W. (1985) *Geochim. Cosmochim. Acta* **49,** 1887-1896.

Clague D.A., Frey F.A., Thompson G. and Rindge S. (1981) *J. Geophys. Res.* **86,** 9469-9482.

Frey, F.A. and Clague, D.A. (1983) *Earth Planet. Sci. Lett.* **66**, 337-355.

Hart, S.R. (1984) *Nature* **309,** 753-757.

Hofmann, A.W., Jochum, K.P., Seufert, M. and White, W.M. (1986) *Earth Planet. Sci. Lett.* **79,** 33-45.

Humphris, S.E., Thompson, G., Schilling, J-G. and Kingsley, R.H. (1985) *Geochim. Cosmochim. Acta* **49**, 1445-1464.

le Roex A. P., Dick H. J. B., Erlank A. J., Reid A. M., Frey F. A. and Hart S. R. (1983) *J. Petrol.* **24,** 267-318.

le Roex A. P., Dick H. J. B., Reid A. M., Frey F. A., Erlank A. J. and Hart S. R. (1985) *Contrib. Mineral. Petrol.* **90**, 367-380.

Michael P. J. (1988) *Geochim. Cosmochim. Acta* **52**, 555-566.

Michael, P.J., Chase, R.L. and Allan J.F. (1989), *J. Geophys. Res.* **94,** 13895 - 13918.

Perfit M.R., Fornari D.J., Malahoff A. and Embley R.W. (1983) *J. Geophys. Res.* **88,** 10551-10572.

Poreda R., Schilling J.-G. and Craig H. (1986) *Earth Planet. Sci. Lett.* **78,** 1-17.

Schilling, J.-G., Kingsley, R.H. and Devine, J.D. (1983) *J. Geophys. Res.* **87,** 5593-5610.

Schilling J.-G., Zajac M., Evans R., Johnston T., White W., Devine J.D. and Kingsley R. (1983b) *Amer. J. Sci.* **283,** 510-586.

Sun, S.-S. (1980), Phil. Trans. Roy. Soc. Lond. **A297**, 409-445.

The Coupling Between Mantle Plume Activity and Geomagnetic Reversal Frequency

Peter Olson
Department of Earth & Planetary Sciences
The Johns Hopkins University
Baltimore, MD 21218

March 29, 1991

Long term variations in the frequency of geomagnetic polarity reversals correlate with long term variations in hotspot activity over the last 150 Ma. Initiation of a small number of thermal plumes in the D" layer at the base of the mantle during Cretaceous times has been proposed as the mechanism for coupling these seemingly unrelated phenomena. Here I present calculations showing how the core might respond to a *cooling pulse* brought about by plume initiation just above the core-mantle boundary. These calculations predict that geomagnetic polarity reversal frequency is *inversely* related to the rate of core cooling, and that increases in cooling rate due to plume formation can produce geomagnetic polarity superchrons. The calculations suggest several independent tests of this model.

In this symposium, Larson [1991] presents evidence that the rate of intraplate volcanism, as indicated by the volumes of crust added at oceanic plateaus and in continental flood basalt provinces, was about a factor three higher during the Cretaceous geomagnetic polarity superchron, compared with rates immediately before and after. The Cretaceous superchron commenced about 130 Ma. It was followed by a large spike in the rate of intraplate volcanism near 120 Ma, mostly due to formation of the Ontong-Java plateau on the Pacific plate. Intraplate volcanism remained anomalously active for about 60 Myr, the duration of the polarity superchron. Since that time, both the reversal frequency and intraplate volcanic activity have returned to pre-Cretaceous levels.

It is not intuitively obvious why geomagnetic polarity epochs should be altered by changes in intraplate volcanism. One way the two phenomena might be linked is through mantle plume activity. Results of numerical calculations of thermal plume formation to show that plume initiation in the D" layer at the base of the mantle results in a 60 Myr pulse of increased heat transfer from the core to the mantle. In addition, calculations of self-reversing spherical dynamos, in which the effects of convection in the outer core are represented parametrically by an anisotropic α-effect, demonstrate that *increasing* the vigor of core convection can actually *decrease* the frequency of geomagnetic reversals, by stabilizing the dipole field in one polarity state. These results indicate that the Cretaceous superchron could have been caused by initiation of a small number of thermal plumes at the core-mantle boundary (CMB), producing a pulse of increased core heat loss and vigorous core convection. After the plumes rise through the mantle, partial melting of the plume heads results in a period of increased hotspot activity. The final state consists of stationary plume conduits, reduced core-mantle heat flow, lower rates of hotspot volcanism, and more frequent polarity reversals.

Figure 1 shows results from a numerical calculation by Olson, Schubert, and Anderson [1991] of axisymmetric thermal plume formation in a strongly temperature-dependent viscous fluid, heated from below. Parameters values used in the calculation are given in the figure caption, and were chosen to model the thermal conditions in the lower mantle. In this calculation, a circular portion the lower boundary is heated, producing a plume with a steady-state heat transport of 400 GW, approximately the present-day strength of the Hawaiian hotspot.

The most significant result of the calculation is the evolution of the plume structure with time. The plume separates from the thermal boundary layer as a large, nearly spherical diapir, with a narrow conduit of heated fluid

at its center. The conduit remains intact after separation, providing a low resistance path for the heated fluid to travel rapidly from the boundary layer to the diapir. The final steady-state structure is a narrow conduit fed by converging flow in the thin basal thermal boundary layer.

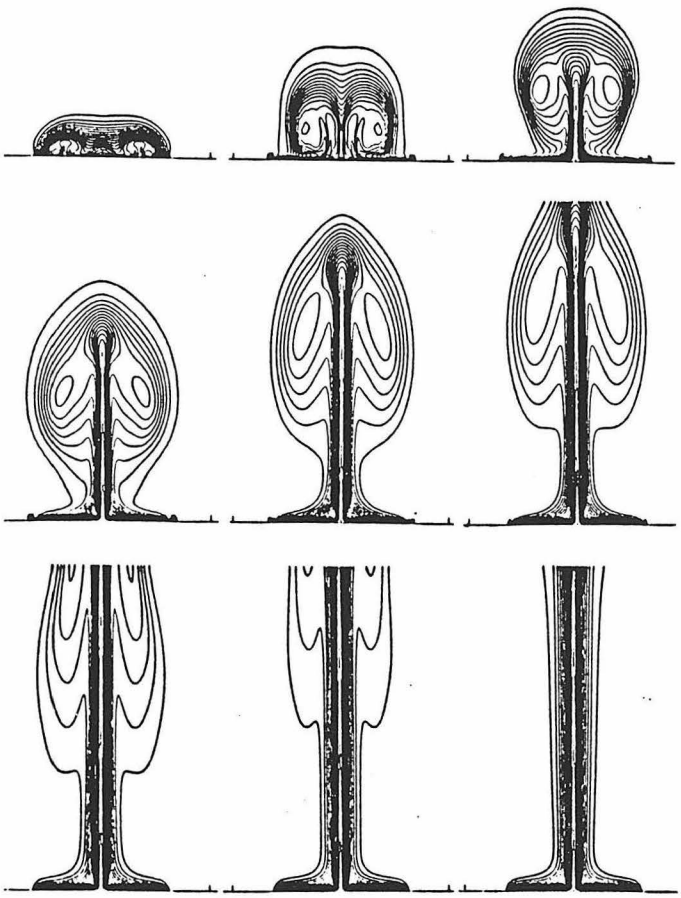

Figure 1: Initiation of an axisymmetric plume in a temperature-dependent viscous fluid. The initial fluid temperature and viscosity are 3000 K and 10^{22} Pa s, and 3800 K and 10^{22} Pa s at the base. The heated region is 600 km in radius and the Rayleigh number based on this radius is 5228. Snapshots of the temperature field contoured in 50 K intervals are at times t=1.6, 2.2, 2.5, 2.9 , 3.3, 4.1, 5.0, and 10.0 $\times 10^{15}$ s.

Figure 2a is a time series of the average heat flow over the heated portion of the lower boundary, and figure 2b shows time series of vertical velocity at two heights above the lower boundary. A 60 Myr pulse in basal heat flow occurs during plume initiation. The peak heat flow is approximately twice the final steady-state value. Comparing the time of peak heat flow in figure 2a with the diapir arrival times in figure 2b indicates a 40-50 Myr lag time between the basal heat pulse and the arrival of the diapir at the surface. Assuming the core responds quickly to the heat flow pulse, and assuming volcanic activity commences when the leading diapir reaches the lithosphere, this calculation indicates a delay of 40 Myr or more between onset of the superchron and the increased hotspot activity.

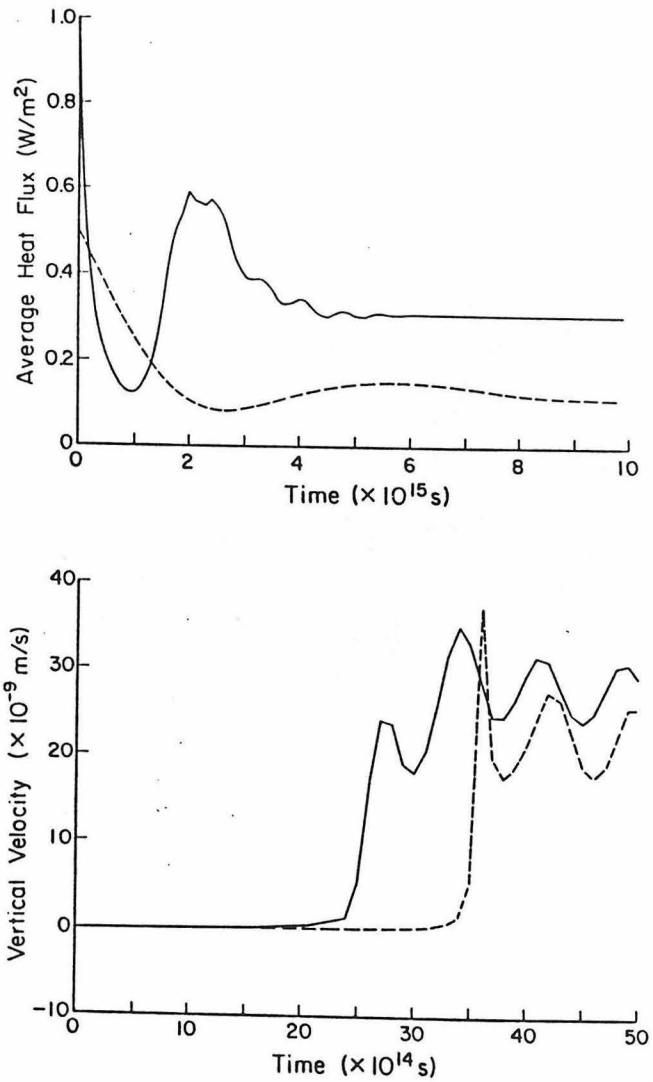

Figure 2: (a): Average heat flow on the heated basal region versus time for the plume shown in figure 1 (solid curve). (b) Vertical velocity versus time at 600 km (solid curve) and 2200 km (dashed curve) above the heated base for the plume shown in figure 1.

Observed rates of geomagnetic secular variation indi-

cate outer core fluid velocities are orders of magnitude larger than mantle convection velocities, so the core adjusts rapidly to changes in CMB heat flow, compared to the mantle. It is likely the core responds to CMB heat flow variations by adjustments in the *amplitude* of convection, rather than by changes in the *pattern* of convection. This is particularly true if the dominant energy source for core motions is freezing and chemical differentiation at the inner core boundary (ICB). Inner core freezing depends on the *total* CMB heat loss rate; the spatial distribution of mantle plumes responsible for the heat loss is probably irrelevant. Core convection is affected by several forces, but its overall structure is dominated by the Coriolis acceleration. Both experimental and numerical simulations of rotating spherical convection demonstrate that nearly two-dimensional, geostrophic flow is strongly favored in the outer core, with the motion constrained to planes parallel to the equator, as shown in figure 3. Because the flow is essentially two-dimensional, its magnetic induction is strongly anisotropic.

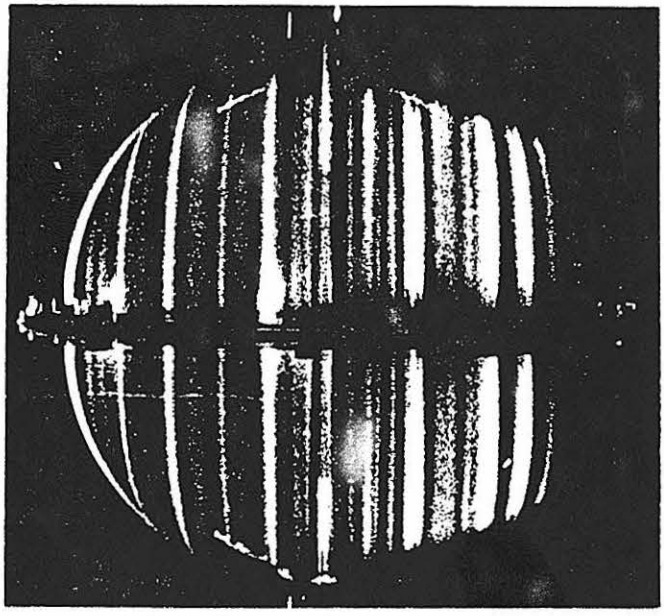

Figure 3: Experimental simulation of thermal convection in a rapidly rotating spherical shell, with inner and outer radii in proportion to the inner and outer core radii, at Rayleigh number 10^9 and Taylor number 10^{12}. The columnar structure of the flow is illuminated by a plane of parallel light reflected off neutrally buoyant flakes in the fluid. Rotation is left to right and the illuminated plane is just foreword of the inner core.

Busse [1975] demonstrated the magnetic induction by this style of convection is *transversely isotropic*, with a principle symmetry axis parallel to the spin axis. Dynamos generated by anisotropic induction tend to be largely dipolar, symmetric about the spin axis, and self-reversing. The period between reversals is extremely sensitive to the amplitude of convection (Olson and Hagee, 1990).

Figures 4 and 5 show the reversal behavior of a zonal-averaged, nonlinear mean-field dynamo model with anisotropic induction, calculated for the style of convection shown in figure 3.

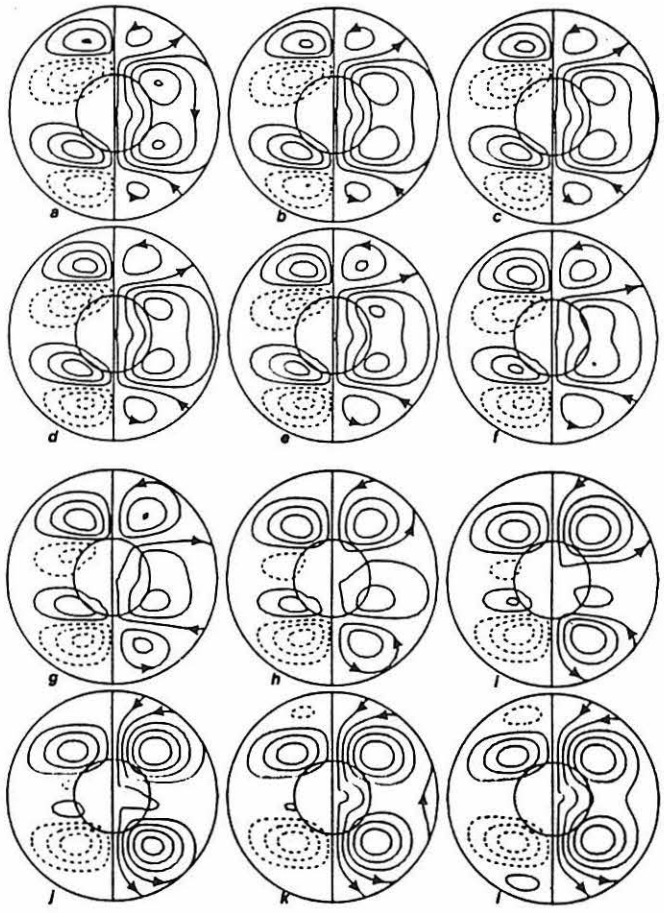

Figure 4: Axisymmetric field structure within a spherical mean-field dynamo with transversely isotropic α^2-induction, during a polarity reversal, at magnetic Reynolds number $Rm_\alpha = 60$. Outer circle represents CMB, inner circle the ICB. Left half of each frame shows contours of the toroidal field amplitude; right half shows lines of force of the poloidal field. Time step is approximately 1400 yr.

Reversals occur periodically if the magnetic Reynolds number Rm_α has a fixed value. The frequency of rever-

sals in this dynamo model varies inversely with magnetic Reynolds number, from 4 Myr^{-1} at $Rm_\alpha = 40$ to about 0.1 Myr^{-1} at $Rm_\alpha = 75$. For $Rm_\alpha > 80$, the dynamo does not reverse at all. The field amplitude between reversals increases slightly with R_α as well.

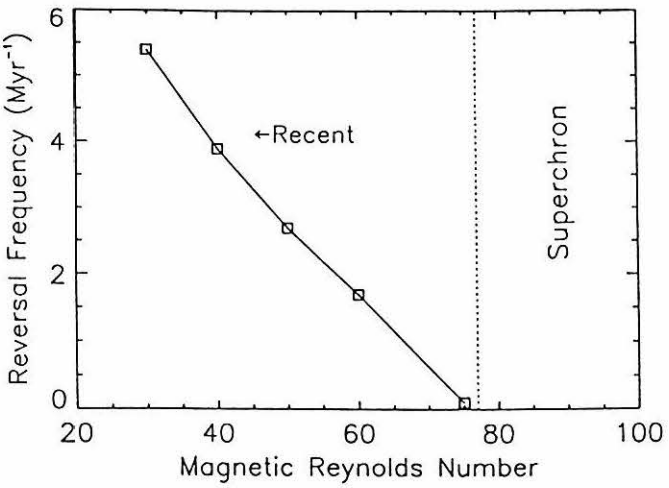

Figure 5: Reversal frequency versus magnetic Reynolds number for the dynamo model shown in figure 4.

Since Rm_α is proportional to the product of fluid velocity and vorticity, it is essentially a parameterization of the amplitude of core convection. When core convection is vigorous, as expected during plume initiation in the D" layer, polarity reversal frequency is relatively low (or even zero). When CMB heat loss is small and core convection is weak, polarity reversal frequency is relatively high, as it has been in the last few Ma. During times high reversal frequency, small, incidental fluctuations in CMB heat loss can probably account for the observed irregularity in polarity epoch duration.

The connection between long term geomagnetic field behavior and hotspot activity, through the mechanics of deep mantle plumes, can be tested further in a number of different ways:

1. Plumes starting in D" require several tens of Myr to rise through the whole mantle. The phase lag between superchron onset and increased hotspot activity gives the plume travel time.

2. Superchrons have higher than average magnetic field intensity, according to my calculations of self-reversing dynamos.

3. The model predicts the Devonian superchron was also a period of anomalous hotspot activity. Direct evidence might be found in flood volcanism at old continental margins. Indirect evidence might be found in the sea level record.

4. *Speculation*: Plate boundary reorganization and continental breakup are related to these events. Perhaps changes in the pattern of lower mantle convection is ultimately responsible for all of the long term variability in the Earth.

References

Busse, F.H., Geophys. J. Roy. Astron. Soc., 42, 437, (1975).

Larson, R.L., this Volume (1991).

Olson, P. and V.L. Hagee, J. Geophys. Res., 95, 4609, (1990).

Olson, P., G. Schubert, and C. Anderson, J. Geophys. Res., in press, (1991).

Helium, Plumes, and Mantle Reservoirs

E.R.Oxburgh
Department of Earth Sciences
Downing Street
Cambridge, UK

Helium is an extremely useful tracer for a variety of geological processes: its naturally occuring isotopic ratios vary over about four orders of magnitude in terrestrial materials (Table); it is inert and does not participate in chemical reactions; it is not retained by the atmosphere, and the atmospheric inventory of 5ppm is largely the result of contemporary terrestrial degassing.

Typical 3He/4He compositions

Terrestrial radiogenic He	1 E-8
Terrestrial atmosphere	1.4 E-6
MORB glasses, phenocrysts	1.2 E-5
Hot spot extrusives and xenoliths	0.8 to 4.4 E-5
Gas-rich chondritic meteorites	1 to 2 E-4
Solar helium	4 E-4

Of the two isotopes of helium ^{4}He is the more abundant in all natural situations and is generated by the decay of unstable isotopes of U & Th, the elements that are responsible for around 80% of the Earth's radiogenic heat production. The rare isotope ^{3}He was for the most part incorporated in the Earth at the time of its formation although a small amount is generated by the ^{6}Li(n,α) reaction.

Helium escapes from the Earth's mantle at mid-ocean ridges, continental rifts, major faults, and all sites of active igneous activity. Although its distinctive composition makes the presence of mantle-derived He easy to identify, its flux from the solid Earth is hard to measure and in the oceans has been done only for the ocean ridges.

Helium is present in the upper mantle at very low concentrations (eg. << 1E-6 cm^3 STP gm^{-1}) but it is stripped and concentrated by processes of magma generation. At ocean ridges about 2.5 E+21 atoms He are released per m^3 of basalt erupted.

Although the ridge He flux cannot represent the total oceanic flux (He is lost at hot spots and in island arc volcanism) it probably accounts for around 80% and, given that both ^{4}He and heat are generated by U,Th decay, it may be compared with the oceanic heat flux - the observed oceanic value is about 4E+10 ats ^{4}He W^{-1}, significantly less than the production ratio of about 8E+11 atoms ^{4}He W^{-1}. This implies either that a substantial component of the heat flux is not radiogenic or, more likely, that radiogenic ^{4}He is being retained within the Earth while the associated heat is being released. This is consistent with the geochemical observation that the upper mantle (the source of Mid-ocean ridge basalt) is too depleted in heat producing elements (U *ca.*5 ppb) to account for more than a small fraction of oceanic heat flow. It therefore appears that heat is convected through the upper mantle while helium is not.

Although there is relatively little He in the upper mantle that which is sampled at mid-ocean ridges appears to be rather uniform and contrasts markedly with that at hot spots which is more variable in isotopic composition and often richer in 3He. Hot spot ^{3}He/^{4}He values as high as 4.4 E-5 are close to values expected for He incorporated in the primordial Earth when allowance is made for shift of the ratio by the addition of radiogenic ^{4}He during the history of the Earth.

It is therefore useful to consider the possibility of a lower mantle that is both the source of ^{3}He-rich He for hot spot volcanism and the repository of radiogenic ^{4}He that has accumulated during the history of the Earth. This can be addressed by considering various primordial U,Th / ^{3}He ratios for the lower mantle and the isotopic evolution of lower mantle helium over time. It is evident that a ratio of around 2000 allows ^{3}He / ^{4}He to evolve from *ca.* 2 E-4 to 4 E-5 over 4.5ga. This conclusion is not much affected if a solar starting ratio of ca. 4 E-4, rather than a planetary value is chosen. Choice of a suitable U,Th content allows derivation of an initial total He content that may be compared with that of other materials. Taking a U content of 20 ppb (and Th / U *ca.*3) gives an initial He content of 2.9 E-06 cm^3 STP gm^{-1}. This is much less than the He contents of gas-rich chondrites (1E+02 to 1E+04 cm^3 STP gm^{-1}) and strongly suggests that the lower mantle was substantially degassed early in the history of the Earth.

It is therefore plausible that hotspot helium is derived from a relatively undepleted lower mantle and that it may be delivered to the surface by some process involving plume flows through the upper mantle. It is also necessary to find a process that is capable of maintaing the ^{3}He / ^{4}He of the upper mantle at its uniform value of

1.2E-5. Magma generation at ridges effectively strips He from that part of the upper mantle that is processed, and subsequent *in situ* He growth from residual U & Th will have a composition ca. 1E-08. Maintainance of the upper mantle value of 1.2E-05 therefore requires the continuous addition of a small amount of He rich in ^{3}He presumably from the lower mantle. This could happen by some diffuse entrainment process at the interface between upper and lower mantle wherever this may be, or by incorporation of material invoved in major plume flows. An important characteristic of this process is that it appears not to permit regular or systematic relationships to be established between He composition and other patterns of chemical or isotopic variation.

In conclusion, the evidence from He isotope studies requires that hotspot He be derived from a source other than the upper mantle and arguably one that has remained relatively undisturbed since the formation of the Earth; it could plausibly be derived from an lower mantle of undifferentiated material that contains most of mantle heat production and is accumulating radiogenic He. A quantitative study of a families of internally consistent models including some with assumptions and conclusions similar to those above has recently been published by Kellogg & Wasserberg.

VENUSIAN HOT SPOTS AND PLUMES

R.J. Phillips and R.E. Grimm, Dept. Geol. Sci., SMU, Dallas, TX 75275

Introduction. One of the principal hypotheses on the nature of venusian tectonics is that it is dominated by the effects of convective plumes rising in the mantle, impinging on the lithosphere, and producing hot spots — areas of volcanism and uplift created by the magmatic, thermal and dynamic effects of the plumes (*1, 2, 3*). Two major elements of this model are: (i) that large-scale horizontal motion of the lithosphere does not take place or is, at most, a minor process (*3*), and (ii) that Venus loses most of its heat through lithospheric conduction, which is enhanced at the thin lithosphere associated with hot spots (*4, 5*).

The hot-spot/plume hypothesis was first suggested from several lines of evidence drawn from both morphological and geophysical observations from the Pioneer Venus mission. Many of the large topographically elevated areas in the tropical and subtropical latitudes of Venus are quasi-circular and isolated and have large apparent depths of isostatic compensation (> 100 km). If the heat source concentration in Venus is like that in the Earth (*1*), these levels of apparent compensation are deeper than can reasonably be expected for passive support; they must be supported, at least in part, dynamically, that is, by convective upwellings in the mantle.

Any model attempting to describe the global tectonics of Venus must explain the following major observations:

(1) Elevations on Venus belong to a unimodal population with most of the surface lying within a kilometer of the level of the vast venusian plains (*6*). High-standing areas occupy a small fraction of the surface area (*7*) and are for the most part associated with the Equatorial Highlands (Atla, Beta, Eistla, Phoebe, Asteria Regiones, and Aphrodite Terra) (*2*). Here the regional morphology is best described as broadly aligned topographic rises. Beta and Eistla Regiones display large-scale rifting and shield volcanism (*8, 9*). Ovda Regio in western Aphrodite Terra has plateau-like topography and Magellan images reveal evidence of compressional tectonism (*10*). The other major region of elevated topography is Ishtar Terra, centered about the prime meridian at high northern latitudes. The western portion of this region, Lakshmi Planum, is surrounded by linear mountain belts. There are also a number of basins lying about a kilometer beneath the mean planetary elevation. Some (e.g., Sedna and Guinevere Planitae) are elongate, extending for thousands of kilometers along strike.

(2) Long-wavelength free-air gravity anomalies are highly correlated with large-scale topographic features, indicating large depths of apparent isostatic compensation (*11*). However, the compensation depths are quite variable (*12*), indicating that more than one mechanism may be involved or that a single mechanism has a complex behavior.

(3) Images acquired by the Soviet Venera missions, by the Arecibo Observatory, and most recently by the Magellan mission, reveal a variety of tectonic features (*13, 14, 15, 16*). Widespread faulting, ridge belts, the intricate structure of mountain ranges on Ishtar Terra, major elevated regions of intense crosscutting faults (tessera), and enigmatic circular structures up to 1000 km in diameter (coronae) are observed. These same data sets show that volcanism operates on different scales and styles and pervasively modifies the surface of Venus (*17*).

The inventory of impact craters mapped also holds implications for the resurfacing history of the planet (*18*).

Below we review briefly the hot-spot/plume concept and raise major questions regarding its shortcomings. A longer discussion is found in (*19*).

Significance of Plumes. We suggest that plumes on Venus come in two varieties: (type 1) those arising from the core-mantle boundary and (type 2) those arising from within the mantle, either from instabilities associated with internal convection (include chemical plumes associated with partial melting) or from internal phase or compositional boundaries.

As the significance of type 1 plumes depends on the amount of heat removed from the core, we consider the nature of the venusian magnetic field to obtain a crude assessment of this quantity. The magnetic dipole moment of Venus is less than 1/25000th of the terrestrial moment (*20*); Venus does not possess a geodynamo-generated magnetic field. The magnetic moment scales linearly with planetary rotation rate (*21*), so that the 243–day rotational period of Venus does not appear to account for its lack of a dipole field. In order to generate a geodynamo, the liquid portion of a planetary core must have sufficient energy sources to be convecting. Heating by exothermic freezing of the liquid core combined with the secular cooling is the most likely source of energy enabling core convection and driving the Earth's present-day geodynamo (*22*). The absence of a magnetic field suggests that Venus does not have a freezing inner core, as plausible parameterized convection solutions demonstrate (*22*). The implication is that the heat flux from the venusian core is less than that for the Earth. In turn, we would expect that the thickness of the core/mantle thermal boundary is greater and the effective Rayleigh number of the mantle is lower for Venus. In comparison to the Earth, venusian plumes may have larger horizontal dimensions because the effective mantle viscosity may be higher, plumes may be rarer, and their transient phase may be more long-lived. The horizontal dimension of a plume head scales linearly with the diameter of the induced topographic swell (*23*). If the Hawaiian swell is representative of terrestrial hot-spot features, then major plumes on Venus (e.g., those associated with Beta, Eistla, and Thetis Regiones) are about three times the radius of their terrestrial counterparts. We suggest that the majority of heat escaping Venus may be internally generated in the mantle and be delivered in spatially and temporally variable zones of weak mantle upwelling (including type 2 plumes), which is manifested at the surface by broadly distributed volcanism in the rolling plains, as fields of small domes (*24*), and as coronae (*25*). In the absence of seafloor spreading and subduction, the effects of type 1 plumes should dominate the surface tectonics and large-scale topography of the planet, however, because of their large and concentrated buoyancy flux and because their effects are not muted by a low viscosity zone.

Plume Evolution. Originally, all of the Equatorial Highlands were interpreted to result from plumes, although possibly in different stages of evolution. More recently, (*26*) it was suggested that various features represented a specific evolutionary sequence in the interaction of a plume with the lithosphere, the development path being exhibited by differences observed from Beta Regio (youngest) to Thetis Regio to Ovda Regio to the Artemis Chasma region to the semicircular region west of Ovda Regio (including Hestia Rupes). In this sequence, the topography and style of volcanism and magmatism is a function of the depth of the ascending plume head, which can be traced through the apparent depth of isostatic compensation (ADC). Early in the sequence

(Beta Regio), the ADC is large, the lithosphere is rifted and otherwise deformed in response to the normal and shear stresses associated with uplift (*27*), and volcanism is limited because the plume head is subject to high lithostatic pressures. As the plume head ascends (Thetis Regio, then Ovda Regio), the ADC decreases, and the decrease in pressure leads to large volumes of partial melt, substantial addition of crust, and flood-basalt volcanism (*26*). For example, if the plume head temperature is elevated an additional 200° C above the ambient mantle temperature, then about 20 km of new crust could be generated if the plume head ascends to within about 60 km of the surface. Consistent with these concepts, comparisons of western to central Eistla Regio for age, as inferred from Magellan crater counts, and ADC values show that the younger region, central Eistla, also has the shallower ADC (*9*).

As the plume head penetrates the base of the lithosphere, magmatic activity will eventually decrease as the equilibrium fraction of partial melt is attained. Flattening of the plume head will lead to a decrease in buoyancy pressure, diminishing dynamic support and leading to partial collapse of topography. Additional topography will be supported by isostatically thickened crust and thermally thinned lithosphere (*5*). Thus topography will evolve from a broad swell supported dynamically by the plume to the development of a crustal plateau compensated by lithospheric mechanisms and associated with an abating component of dynamic uplift . Ultimately, the former site of mantle upwelling will be marked by a plateau alone. Such plateaus will have a finite lifetime, as continued slow creep will eventually diminish the plateau topography to the point where the former plateau is indistinguishable from surrounding rolling plains, and deformational units are broken up and buried by plains volcanism (*28*). Simple viscous relaxation calculations indicate that crustal plateau lifetimes are of order 0.5 - 1.0 billion years. Thus a plume or hot-spot cycle will include (i) creation of dynamic topography and accompanying deformation associated with uplift, (ii) generation of a crustal plateau, (iii) collapse of dynamic support, and (iv) slow creep relaxation of the plateau.

The ADC values for highland features appear to be resolved into two broad groups associated with different phases of the hot-spot cycle (*12*): (i) highland features (Nokomis Montes, Gula Mons, Atla, Asteria, Bell, Beta, and Sappho Regiones) that have large ADC values, implying a large component of dynamic compensation and only a modest crustal component, and (ii) highland features (Ovda, Phoebe, Tellus, Thetis, and Ulfrun Regiones) that have only a moderate ADC, implying significant support in the lithosphere by crustal and thermal compensation mechanisms. Four of the seven features in the first group can be described morphologically as broad domes capped with steeper peaks or small plateaus; four of the five features in the second group plus Asteria Regio in the first group can be described as plateaus.

Issues. The apparent lack of a low viscosity zone beneath the venusian lithosphere (*27*) implies that plumes can more directly interact with the lithosphere, making Venus an excellent laboratory to study plume dynamics. However, there are major questions raised by this model for Venus that must be addressed before Venus is wrapped up in a tidy plume package.

1. Topographically low areas on Venus also have large apparent depths of isostatic compensation, suggesting that with the same set of assumptions applied to highland features, lowlands must be dynamically supported. The equivalent understanding in terms of evolution and tectonic consequences is not well understood.

2. It has been suggested (*29*) that high regions on Venus may mark the sights of mantle *downwellings*, resulting from inward flow and thickening of crust.
3. Highland features such as Lakshmi Planum and Ovda Regio contain compressional terrain, including orogenic belts, which must be accounted for in any plume evolution model (*30, 31*).
4. Preliminary indications from Magellan are that the transient phase of plume activity would have to last several hundred million years. This may be consistent with a high viscosity mantle (relative to Earth), which could also lead to the large lateral dimensions of plumes as inferred from the size of topographic swells.
5. The plume model rests on the tenet that Venus contains heat sources similar to the Earth and that we can apply the results of laboratory rheological measurements to real planets.

References. 1. R. J. Phillips and M.C. Malin, *Annu. Rev. Earth Planet. Sci.* **12**, 411 (1984); 2. R. J. Phillips, W. M. Kaula, G. E. McGill, M. C. Malin, *Science* **212**, 879 (1981); 3. R. J. Phillips and M. C. Malin, in *Venus*, D. M. Hunten, L. Colin, T. M. Donahue, V. I. Moroz, Eds. (Univ. of Arizona Press, Tucson, 1983), pp. 159-214; 4. R. E. Grimm and S. C. Solomon, *Geophys. Res. Lett.* **14**, 538 (1987); 5. P. Morgan and R. J. Phillips, *J. Geophys. Res.* **88**, 8305 (1983); 6. G. H. Pettengill *et al.*, *J. Geophys. Res.* **85**, 8261 (1980); 7. H. Masursky *et al.*, *J. Geophys. Res.* **85**, 8232 (1980); 8. G. E. McGill, S. J. Steenstrup, C. Barton, P. G. Ford, *Geophys. Res. Lett.* **8**, 737 (1981); 9. R. E. Grimm and R. J. Phillips, *Lunar and Planet. Sci. XXII*, 497 (1991); 10. R. S. Saunders *et al.*, *Lunar and Planet. Sci. XXII*, 1169 (1991); 11. W. L. Sjogren *et al.*, *J. Geophys. Res.* **88**, 1119 (1983); 12. S. E. Smrekar and R. J. Phillips, *Earth Planet. Sci. Lett.*, in press (1991); 13. V. L. Barsukov *et al.*, *J. Geophys. Res.* **91** D378 (1986); 14. A. T. Basilevsky *et al.*, *J. Geophys. Res.* **91**, D399, (1986); 15. D. B. Campbell *et al.*, *Science* **246**, 373 (1989); 16. S. C. Solomon *et al.*, *Science*, in press (1991); 17. J. W. Head *et al.*, *Science*, in press (1991); 18. R. J. Phillips *et al.*, *Science*, in press (1991); 19. R. J. Phillips, R. E. Grimm, M. C. Malin, *Science*, in press (1991); 20. C. T. Russell and O. Vaisberg, in *Venus*, D. M. Hunten, L. Colin, T. M. Donahue, V. I. Moroz, Eds. (Univ. of Arizona Press, Tucson, 1983), pp. 873-940; 21. F. H. Busse, *Phys. Earth Planet. Inter.* **12**, 350 (1976); 22. D. J. Stevenson, T. Spohn, G. Schubert, *Icarus* **54**, 466 (1983); 23. P. Olson and I. S. Nam, *J. Geophys. Res.* **91**, 7181 (1986); 24. J. C. Aubele and E. N. Slyuta, *Earth Moon Planets* **50/51**, 493 (1990); 25. E. R. Stofan and J. W. Head, *Icarus* **83**, 216 (1989); 26. R. R. Herrick and R. J. Phillips, *Geophys. Res. Lett.* **17**, 2129 (1990); 27. R. J. Phillips, *J. Geophys. Res.* **95**, 1301 (1990); 28. A. Nikishin, *Earth Moon Planets* **50/51**, 101 (1990); 29. D. L. Bindschadler and E. M. Parmentier, *J. Geophys. Res.* **95**, 21,329 (1990); 30. R. E. Grimm and R. J. Phillips, *Geophys. Res. Lett.* **17**, 1349 (1990); 31. R. E. Grimm and R. J. Phillips, *J. Geophys. Res.*, in press (1991).

Hot Spots, Hot Lines, and Magmatism from Plume-modified Lithosphere

Stephen Paul Phipps, Geology Department, 251 Hayden Hall, University of Pennsylvania, Philadelphia, PA, 19104-6316

Some alignments or belts of mantle-derived magmatism are well explained by the mantle plume or hot-spot hypothesis (for example, the Hawaii-Emperor chain). These belts are characterized by regular progression and cessation of magmatism at a velocity compatible with the motion of the plate bearing the magmatic centers (Wilson, 1963; Morgan, 1971, 1983).

Other belts of mantle-derived magmatism, especially on continents, do not show such regularity. They exhibit some combination of: (1) great longevity of magmatism in one location; (2) simultaneity of magmatism over much of the belt; (3) belt geometries inconsistent with plate motion over mantle-fixed hot spots; and (4) indicated plate motions inconsistent with those reliably deduced from other data (Okal and Batiza, 1987; Phipps, 1988). These belts of mantle-derived magmatism are better termed "hot lines" than "hot spots" (Bonatti and Harrison, 1976).

Some continental hot lines--for instance, those in southeastern North America--can be explained by the emplacement by plumes of enriched (and probably melt-fertile) material in the thick continental lithosphere during rifting (Phipps, 1988) (Fig. 1).

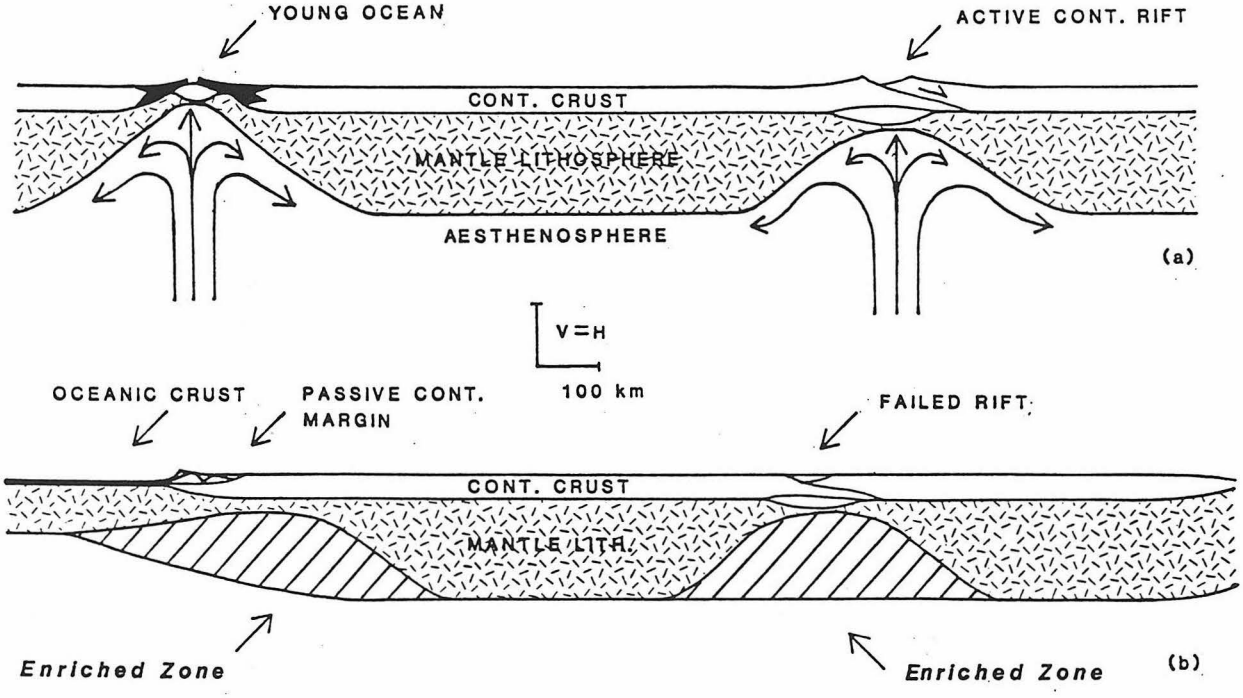

Figure 1. Plumes emplacing enriched mantle material in the continental lithosphere during rifting.

This material translates with the plate; magmatism can be triggered by later thermal or tectonic disturbances in the lithosphere, including increased convective activity (such as in the U.S. Gulf Coast ??) and continental collisions (such as in the U.S. 38th-parallel belt ??) (Phipps, 1988 and in preparation).

The hot-line phenomenon is not restricted to the continental lithosphere, however. Some hot lines--the Cameroon Line, for instance--cross continent-ocean boundaries (Fitton and Dunlop, 1985; Halliday and others, 1988), and some lie entirely within oceans, such as the Cook-Austral island chain (Okal and Batiza, 1987, p. 7). In some cases, the onset of magmatism in these belts shows an approximately linear progression, but magmatism persists rather than subsiding as the onset locus moves laterally. In other cases, magmatism is associated with rifting. These phenomena suggest that mantle plumes may emplace melt-generating material in oceanic as well as continental lithosphere. If the plate is moving, emplacement may occur directly above the plume--along its track. If it is relatively stationary, enriched mantle material may be emplaced in the lithosphere after flowing laterally down pipes beneath rift arms radiating from the crustal swell above the plume (Fig. 2) (Phipps, in preparation).

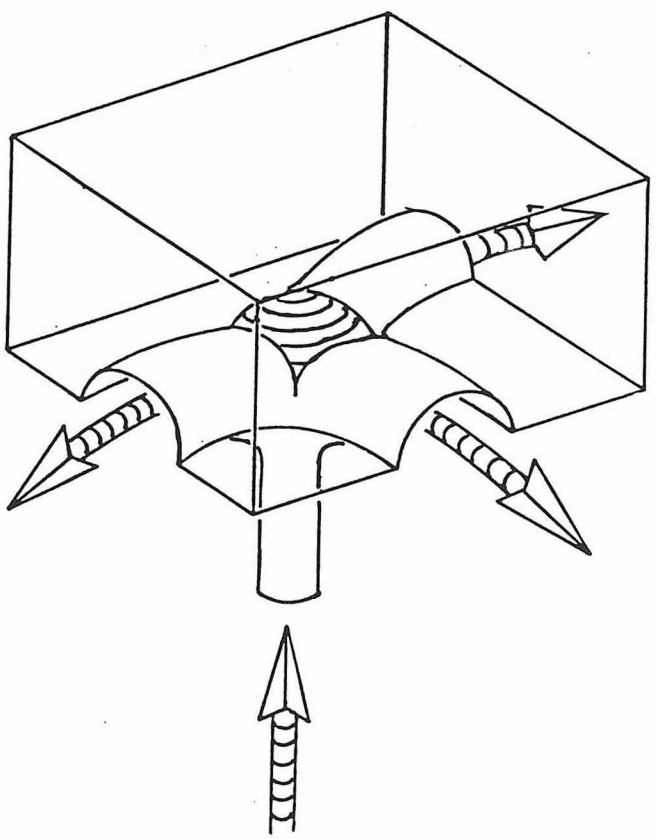

Figure 2. Plume emplacing enriched material in mantle lithosphere by piping beneath three-armed rift.

Moreover, even such well defined hot-spot traces as the Hawaii-Emperor chain show some hot-line characters, for instance, persistent magmatism as witnessed by the relatively young volcanism at Haleakala on Maui, on Hawaii, and on Loihi (Jackson, 1976; Okal and Batiza, 1987). To some extent, this may be explained by long emptying and cooling times for deep and/or large melt-gathering systems and magma chambers. However, especially in the case of persistent eruption of little-differentiated magmas, it may be a result of magma generation from within the altered lithosphere. The small volume and largely MORB-type source for some of these magmas suggest that in these cases the alteration may be thermal rather than chemical (Chen and Frey, 1983).

Thus, there may be an entire range of phenomena from hot spots to hot lines of varying persistence, which may all be related to mantle plumes through lithospheric alteration by plume-track formation or by rifting. Hot-line phenomena may tend to be more conspicuous in thicker continental lithosphere, and/or for less voluminous plumes, which may be less thoroughly depleted in magmas during their initial rise, and which therefore have a long-lasting chemical effect on the lithosphere above them. More voluminous plumes, or those rising beneath relatively thin oceanic lithosphere, may undergo more efficient melt extraction, and their effects on the lithosphere after their passing may be principally thermal and of shorter duration.

Models that explain hot-line magmatism by the motion of lithosphere-scale fractures over melt-productive zones in the aesthenosphere (Bailey, 1980, 1983) are unlikely because (1) annealing is likely to heal the deep regions of such fractures in geologically short times, and (2) even if fractures could be maintained, they are unlikely to be of much benefit to rising magmas at these depths (Phipps, in prep.). This is so because, for the rapid ascent velocities of such mantle-derived melts as alkali olivine basalts, lamproites, and kimberlites, even quite deep regions of the lithosphere will behave as brittle solids. At lithospheric depths, most of the strength of such materials--in this case, their resistance to hydrofracturing--depends on confining pressure, not on cohesion, which is the only aspect of the strength affected by the hypothesized pre-existing fractures. Strength variations because of grain-size differences between annealed ductile shear zones and adjoining, less-sheared country rock offer the most likely mechanism by which the deep zones of old fractures might localize

mantle-derived magmatism. Even this mechanism seems likely to affect the locus of hot-line magmatism only secondarily; the primary control probably comes from chemical modification of the mantle lithosphere.

References Cited

Bailey, D.K., 1980, Volcanism, Earth degassing, and replenished lithosphere mantle: Philosophical Transactions of the Royal Society of London, Series A, v. 297, p. 309-322.

Bailey, D.K., 1983, The chemical and thermal evolution of rifts: Tectonophysics, v. 94, p. 585-597.

Bonatti, E., and C.G.A. Harrison, 1976, Hot lines in the Earth's mantle: Nature, v. 263, p. 402-404.

Chen, C.-Y., and F.A. Frey, 1983, Origin of Hawaiian tholeiite and alkalic basalt: Nature, v. 302, p. 785-789.

Fitton, J.G., and H.M. Dunlop, 1985, The Cameroon line, West Africa, and its bearing on the origin of oceanic and continental alkali basalt: Earth and Planetary Science Letters, v. 72, p. 23-38.

Halliday, A.N., A.P. Dickin, A.E. Fallick, and J.G. Fitton, 1988, Mantle dynamics: A Nd, Sr, Pb, and O isotopic study of the Cameroon line volcanic chain: Journal of Petrology, v. 29, Part I, p. 181-211.

Jackson, E.D., 1976, Linear volcanic chains on the Pacific plate: in Sutton, G.H., M.H. Manghnani, and R. Moberly, eds., The Geophysics of the Pacific Basin and its margins, American Geophysical Union Geophysical Monograph 19, p. 315-335.

Morgan, W.J., 1971, Convection plumes in the lower mantle: Nature, v. 230, p. 42-43.

Morgan, W.J., 1983, Hotspot tracks and the early opening of the Atlantic: Tectonophysics: v. 94, p. 123-139.

Okal, Emile A., and Rodey Batiza, 1987, Hotspots: The first 25 years: in Keating, B.H., P. Fryer, R. Batiza, and G.W. Boehlert, eds., Seamounts, Islands, and Atolls: American Geophysical Union Geophysical Monograph 43, p. 1-11.

Phipps, S.P., 1988, Deep rifts as sources for alkaline intraplate magmatism in eastern North America: Nature, v. 334, p. 27-31.

Phipps, S.P., in preparation, Mantle plumes and deep rifts: Sources of lithosphere-fixed mid-plate volcanism [working title]: to be submitted to Earth and Planetary Science Letters (??), 31 pp. and 4 figs. in ms.

Wilson, J.T., 1963, Evidence from islands on the spreading of the ocean floors: Nature: v. 197, p. 536-538.

Early Cretaceous plateau basalts, EM1 from the lower mantle, and the origin of the Dupal anomaly

Malcolm S. Pringle

U.S. Geological Survey, Menlo Park, CA 94025.

Abstract. Four large flood basalts of the southern hemisphere were a focus of excess volcanism in the Early Cretaceous. Geodynamic constraints require a lowermost mantle source for these basalts; since all four plateaus have an EM1 (Enriched Mantle 1 of Zindler and Hart) isotopic signature, EM1 must be a significant component of the lowermost mantle. The DUPAL isotopic anomaly may be best described as a geographic superposition of at least three separate anomalies, which places much less severe contraints on mantle convection than Hart's original globe-encircling model. Only two of the four Early Cretaceous plateaus represent the initiation of hot spot tracks which are still active today.

The Early Cretaceous volcanic event recognized by anomalous basaltic volcanism in the world's oceans represents a first order modification of plate tectonics as a global geodynamic process. Using the Pacific plate as the most complete record of this event (Figure 1), Early Cretaceous basaltic volcanism reflects almost a threefold increase in the amount of heat released by mid-ocean ridges and hot spots. Mid-ocean ridge ocean crust production was about twice what it is today. Most significantly, hot spot or intraplate volcanism made up about 50% of the total ocean crust production compared to the Cenozoic average of 10%.

Four large plateau or flood basalts in the southern hemisphere represent a significant fraction of this Early Cretaceous volcanism (Figure 2). The Parana and Etendecka flood basalts of Brazil and Namibia erupted in what is today the south Atlantic Ocean. Manihiki and Ontong Java plateaus formed in the south Pacific Ocean. The Kerguelan Plateau grew in what is today the south Indian Ocean. The volume of volcanism represented by these plateaus is enormous: Ontong Java plateau alone is 50 million km^3, about 50 times the volume of the Deccan Trap flood basalts, while all four plateaus total approximately 90 million km^3. The Early Cretaceous event may be more analogous to the large volcanic provinces observed on Mars and Venus rather than recent volcanism observed on Earth.

Age control is still incomplete for each of these flood basalt provinces but suggests progressive volcanism from east to west around the globe: 135-130 Ma for Parana-Etendecka, 125-115 Ma for Manihiki and Ontong Java, and c. 115 Ma for Kerguelen. While it is beyond scope of this paper to speculate on the ultimate cause of the unique mantle event which formed these plateaus, we can say that the its surfacial expression began c. 135 Ma, peaked c. 125 Ma, and finished c. 115 Ma.

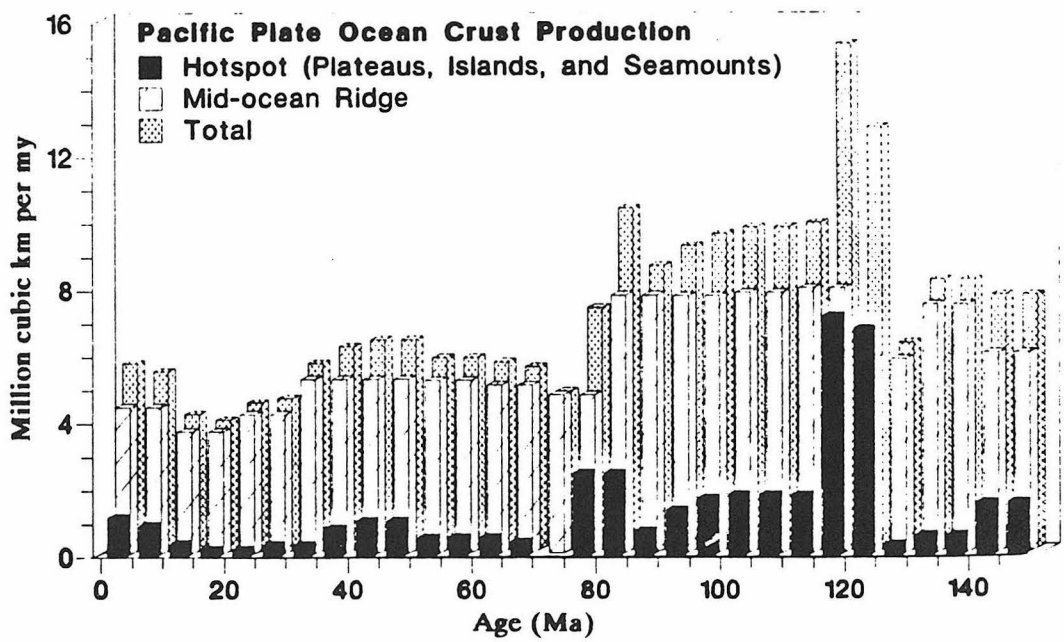

Figure 1. Basalt production as a function of time for the Pacific plate. Note the increased volcanism throughout the Cretaceous, and especially the maximum between 115-125 Ma.

Isotope Geochemistry. Most of the variation in the isotopic composition of the mantle can be described by combinations of four end member compostions: ***d***epleted ***M***ORB ***m***antle (DMM), ***e***nriched ***m***antle ***1*** (EM1), ***e***nriched ***m***antle ***2*** (EM2), and ***hi***gh μ (HIMU) using the terminology of Zindler and Hart (shown in $^{87}Sr/^{86}Sr$ vs $^{206}Pb/^{204}Pb$ space in Figure 3). The actual location in the mantlte of these four components is a subject of intense debate, and the isotopic composition of EM1 and EM2 is similar to the isotopic compostition of lower and upper continental crust, respectively.

Figure 3 also shows the isotopic compostion of the Early Cretaceous plateau basalts and of the recent through Cretaceous basalts from the South Pacific Isotpic and Thermal Anomaly (SOPITA) of Staudigel et al. EM1 is the principal isotopic component of each of the four Early Cretaceous plateaus basalts. Because Ontong Java and Manihiki plateaus were erupted in an oceanic environment, the EM1 component there cannot represent contamination from continental crust or sub-continental upper mantle. The Parana-Etendecka and Kerguelen provinces were involved in the breakup of continental masses and it may be difficult to distinguish continental contamination from mantle source components for these basalts. However, since the modern equivalents of these hot spots are located far from the continents and are still erupting EM1 (Tristan da Cuna and Heard/Kerguelen, respectively), I conclude that the EM1 found in those basalts is also representative of a mantle source region not affected by continental influence.

The original location of the EM1 plateaus of the Pacific, Ontong Java and Manihiki, is significantly south of both the DUPAL anomaly maximum of Hart and the South Pacific Isotopic and Thermal Anomaly (SOPITA) of Staudigel et al. (Figure 2). Therefore, the mantle source of these EM1 plateaus and the isotopically anomalous regions of the present day Pacific must also be distinct. Only two islands of the SOPITA today have lavas with some component of an EM1 signature: Pitcairn and Raratonga. Little is known about the evolution of the Pitcairn hot spot, i.e. how long EM1 basalts have been erupted. However, the 100 Ma equivalent of Raratonga, Hemler Seamount in the Magellan Seamounts, has an EM2 rather than an EM1 mantle source signature. I suggest that the mantle source of these isolated islands of the SOPITA is distinct from the EM1 source of the Early Cretaceous flood basalts.

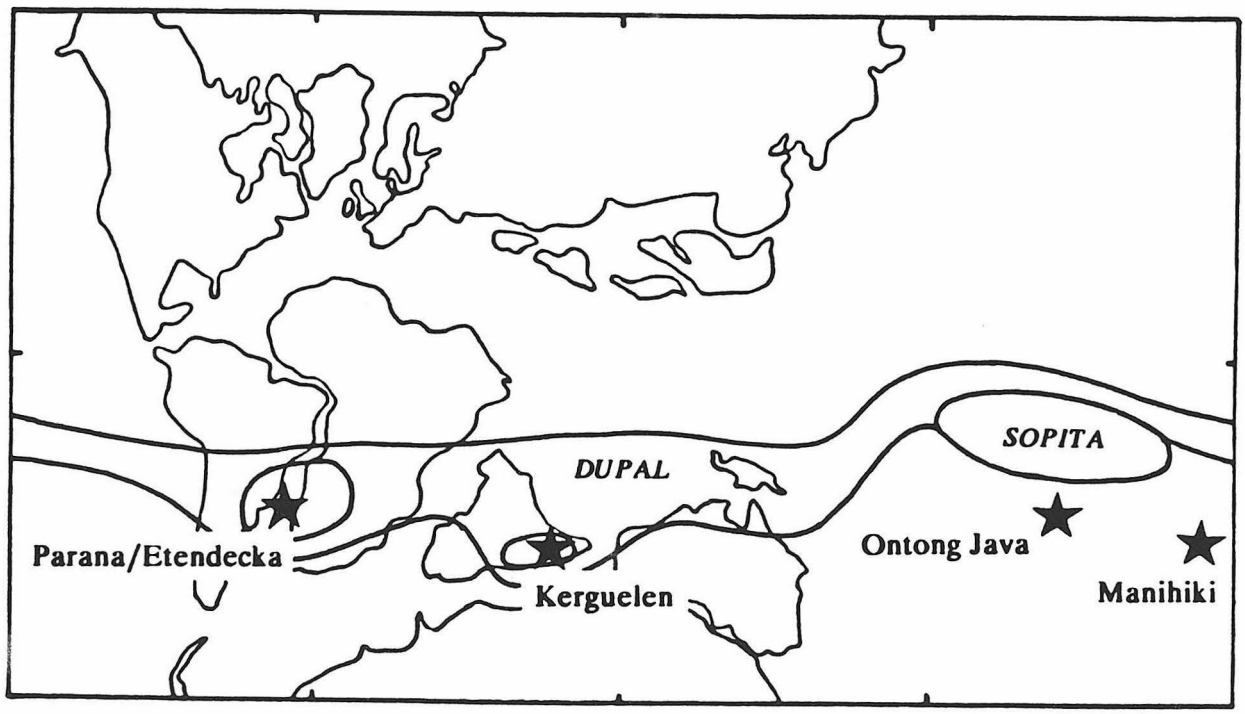

Figure 2. Reconstructed plate and Early Cretaceous plateau positions at M0 time (about 120 Ma), with the present day location of the DUPAL and SOPITA isotopic anomalies. Note that Ontong-Java and Manihiki plateaus were erupted in an oceanic environment, far from any source of continental contamination. The Kerguelan and Tristan da Cuna hot spots, however, were associated with the initial breakup of South America-Africa and India-Antartica(Australia), respectively. The Cretaceous SOPITA, as recorded by the volcanism of the Darwin Rise, is north of and distinct from the Ontong Java and Manihiki hot spots.

Of the principle mantle isotopic components (Figure 3), EM1 is the closest in composition to hypothetical primordial mantle, requiring an ancient (> ~2 Ga) enrichment of only 5-15% from primitive mantle compositions. Also, other than a few isolated islands in the south Pacific, EM1 is found only in the long-lived and stable hot spot environments: the four plateau basalt provinces discussed here, and the Hawaii and Reunion/Deccan hot spots.

Geodynamics. Morgan, Richards et al., and others have suggested that flood basalts originate from large diapirs or plume "heads" representing the initiation of mantle plume activity, while hot spot tracks represent magmatism from the subsequent plume conduit or "tail". Plumes must originate from a thermal and/or compositional boundary layer; for mantle plumes, the only plasible sources are the transition zone discontinuities at 400 and 650 Km and the core/mantle boundary (CMB) region. Assuming a spherical source and 20% partial melting, one can make and estimate of the size of the diapir which formed each of the Early Cretaceous flood basalts.

The 50 million km^3 Ontong Java Plateau would require 250 million km^3 of mantle material, forming a diapir 780 km in diameter which simply cannot fit in the upper mantle and must orginate in the CMB region. Similarly, Kerguelen, Manihiki, and Parana/Etendecka would require mantle diapirs 620, 400, and 240 km in diameter. While it is possible to fit the smaller of these diapirs entirely within the upper mantle, one would have to call upon 20% melting of almost the entire upper mantle in that portion of the globe, which I find very unlikely. Therefore, I conclude that all four Early Cretaceous flood basalts originated as mantle diapirs near the CMB.

The lowermost 200-300 km of the mantle, layer D", has reduced seimsic velocity gradients, is laterally heterogeneous, may contain one or more discontinuities, and has the highest thermal gradient of any terrestrial boundary layer. D" may also represent a chemically distinct layer, and I suggest that it is the reservoir from which the EM1 component of the Early Cretaceous flood basalts is sampled. The diapirs or plume heads which formed the smaller of these flood basalts could originate entirely from within this region, especially if D" has a higher basaltic component than typical mantle (D" has been proposed to include ancient subducted lithosphere). However, the largest of the flood basalts must have originated from mantle diapirs which also sampled lower mantle material above D", even before any thermal entrainment of overlying mantle during ascent. One would then expect basalts from the largest plateaus to have isotopic compostions diluted away from the purest EM1 end member basalts, precisely what is observed for Ontong Java.

All lavas with an EM1 isotopic component do not necessarily have a lower mantle source. Anderson has argued that hot spot basalts have enriched sources in the *upper* mantle, with the lower mantle providing thermal energy but no mass transfer. It is likely that EM1 represents a shallower mantle source in some lavas, such as the sub-continental mantle in South Africa or the EM1 South Pacific islands discussed above. I do conclude, however, that the source of the large Early Cretaceous flood basalts, as well as the four long-lived stable hot spots which have recently erupted EM1 (Heard/Kerguelan, Tristan da Cuna, Reunion, Hawaii), is in the lowermost mantle.

Hot Spot Tracks. Only two of four the Early Cretaceous flood basalts-- Parana/Etendecka and Kerguelen -- mark the inception of hot spot tracks which are still active today. The melting anomalies which formed the two Early Cretaceous Pacific plateaus -- Ontong Java and Manihiki -- are no longer active. No hot spot track can be traced to Manihiki Plateau. The Louisville Ridge in the south Pacific has been proposed as a hot spot trail originating at the Ontong Java hot spot, but its trace seems to disappear about 20 Ma. Therefore, not all plateau building/flood basalt events establish a stable plume source which feeds a long-lived hot spot chain.

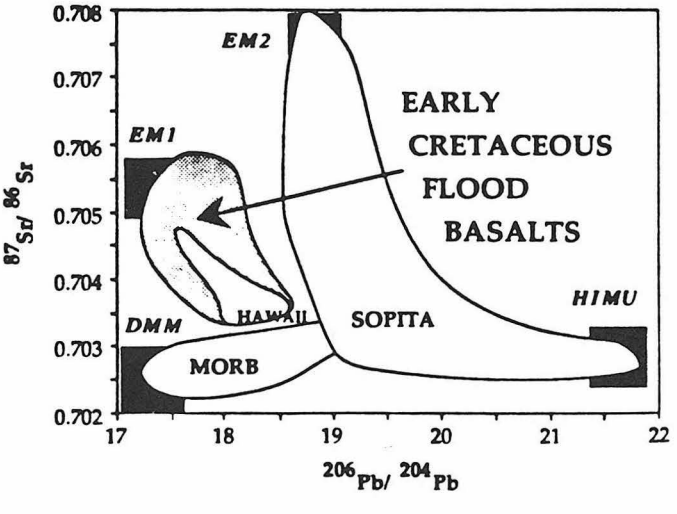

Figure 3. Sr vs Pb isotopes, including the field for the four Early Creatceous plateau or flood basalts, the four main mantle components of Zinder and Hart, and the SOPITA field of Staudigel et al. (excluding the mixing toward EM1 at Pitcairn and Raratonga).

Seamount lavas along the Louisville Ridge do not have an EM1 isotopic signature. While seamounts older than about 70 Ma have been subducted, younger seamount lavas exhibit more typical plume compositions. I would propose that EM1 lavas are not found along the Louisville ridge because the Ontong Java plume head (1) was a detached diapir instead of a plume "tail" initiation event and/or (2) had tapped all the EM1 available in the lower mantle source region. The Louisville ridge could have been formed by a melting anomaly created in the mantle wake of the Ontong-Java plume head, and the more typical plume source materials would be from mantle located above the source of the EM1 material. Also, the volume of volcanims would decrease as the amplitude of the wake diminished with time, precisely what is seen for the Louisville Ridge.

Southern Hemisphere Isotopic Anomalies. The DUPAL isotopic anomaly was defined by Hart as a globe-encircling band centered around 30°S (Figure 2), combining the earlier observations of Dupre and Allegre in the south Indian and Atlantic Oceans and of Hedge in the south Pacific Ocean. Castillo observed that this DUPAL anomaly may not be globe-encircling and that the DUPAL anomaly maxima appear to be located above two large scale, lower mantle, low seismic velocity regions (LVR). Located beneath the south Atlantic/south-west Indian Ocean and the south Pacific Ocean, these two LVR's (presumably hotter) are separated by high seismic velocity regions (presumably colder) in the lower mantle beneath Australia and South America. Castillo concluded that the source of DUPAL signature lavas may be hotter, upwelling regions of the lower mantle described by the LVR's, or at least that the LVR's provide the thermal anomaly necessary for the production of DUPAL signature lava from the upper mantle sources.

However, as defined, the DUPAL anomaly combines two of the principal mantle ocean island basalt (OIB) isotopic components -- EM1 and EM2 -- and does not include the third -- HIMU (Figure 3). The Atlantic/Indian ocean DUPAL maxima is principally an EM1 anomaly, with HIMU basalts also present in the Atlantic. The the Pacific DUPAL maxima is principally an EM2/HIMU anomaly (more completely described by Staudigel et al.'s SOPITA) and does not include the original location of Ontong Java and Manihiki plateaus (Figure 2). In detail, then, the DUPAL anomaly of the southern hemisphere is really the combination of several distinct isotopic anomalies, associated geographically perhaps only by chance: (1) an EM1 source from the lower mantle initially brought up by (and focussed in the area of) the four Early Cretaceous flood basalt provinces, (2) an EM2 component associated with continental breakup in the south Atlantic and Indian Oceans, also associated with Early Cretaceous events, and (3) a mixed source from relatively shallow anomalous mantle in the south Pacific, i.e. Staudigel et al.'s SOPITA, which includes all three OIB components and is probably the result of focused subduction over time into that region of the upper mantle. The global distribution of HIMU basalts has yet to be investigated in a systematic manner.

Viewing the isotopicaly anomalous Southern Hemisphere mantle as a combination of distinct sources places less severe constraints on mantle convection than Hart's original globe-encircling DUPAL model. A lower mantle source is not required for many hot spot basalts. However, EM1 is an important component of the lower mantle, perhaps the main component of D" at the base of the lower mantle. The Early Cretaceous plateaus represent a significant mass transfer from the lower mantle which is still occurring beneath the south Atlantic and Indian oceans today. The model for the south Pacific mantle is not as clear -- the upwelling regions of the south Pacific LVR may provide only the heat necessary for SOPITA basalts without requiring any new input of lower mantle material. A more complete model of mantle convection awaits (1) a careful delineation of the southern hemisphere isotopic anomaly for *each* of the OIB components, and (2) the development of a geochemical test to distinguish lower and upper mantle source material.

Questions:

- Do at least some plumes transfer mass between the upper and lower mantle?
- Does the south Pacific correlation of the present day SOPITA with the LVR of the lower mantle represent mass and/or thermal transfer between the upper and lower mantle?
- Is EM1 a significant component of the lower mantle? Does the concentration of distinct isotopic anomalies in the southern hemisphere (1) reflect a regional geochemical heterogeneity in lower mantle composition or (2) is it simply the result of an Early Cretaceous event in the southern hemisphere which sampled part of a more homogeneous mantle?
- Why do some flood basalt / oceanic plateau building events mark the initiation of long-lived, stable hot spot tracks while others do not?
- What did happen in the Early Cretaceous mantle?

Correlation of Hotspot Isotopic Data with Mantle Tomography

Terrill W. Ray and Don L. Anderson

Isotopic data have been gathered from igneous rocks at areas believed to be hotspots. These data include ratios of $^{208}Pb/^{204}Pb$, $^{206}Pb/^{204}Pb$, $^{207}Pb/^{204}Pb$, $^{87}Sr/^{86}Sr$, and $^{143}Nd/^{144}Nd$. The lead ratios are typically expressed as deviations from the reference lines given by:

$$(^{207}Pb/^{204}Pb)_{NHRL} = 0.1084(^{206}Pb/^{204}Pb)+13.491$$

$$(^{208}Pb/^{204}Pb)_{NHRL} = 1.209(^{206}Pb/^{204}Pb)+15.627$$

The expressions for these deviations are given by:

$$\Delta 7/4 = [(^{207}Pb/^{204}Pb)-(^{207}Pb/^{204}Pb)_{NHRL}]x100$$

$$\Delta 8/4 = [(^{208}Pb/^{204}Pb)-(^{208}Pb/^{204}Pb)_{NHRL}]x100$$

For the strontium and neodymium ratios, the following expressions are used:

$$\Delta Sr = \{[(^{87}Sr/^{86}Sr)-0.7]-[(^{87}Sr/^{86}Sr)_{REF}-0.7]\}x10^4$$

$$\Delta Nd = \{[(^{143}Nd/^{144}Nd)-0.51]-[(^{143}Nd/^{144}Nd)_{REF}-0.51]\}x10^4$$

$$(^{87}Sr/^{86}Sr)REF = .70368$$

$$(^{143}Nd/^{144}Nd)REF = .512907$$

This is the same system for lead used by Hart (1984). The baseline strontium and neodymium ratios, used above, are the median values of the strontium and neodymium isotopic ratios used in this study. The "standard" for strontium is from the Comores hotspot, and the neodymium "standard" is from St. Helena.

All of these isotopes and their parent elements are incompatible, entering melts preferentially, but the important aspects of these elements are their relative incompatibilities. It is expected that melts extracted from primitive mantle material would have higher U/Pb, Th/Pb and Rb/Sr ratios than primitive mantle owing to the greater incompatibility of the parent elements as compared to the daughter elements. Conversely, the higher incompatibility of neodymium as compared to its parent, samarium, would result in a lower Sm/Nd ratio in the melt.

Castillo (1988) claimed that the Dupal anomaly correlated well with low velocity regions in the lower mantle. In addition, all degree except 2 and 3 in the tomography were discarded. This study examines the quantitative significance of this correlation with the lower mantle, and, since the correlation is to be done depth by depth, it should be possible to determine the depths at which these correlations occur. Additionally, correlations in the upper mantle and at other degrees will be found and evaluated.

Procedure: Hart (1981) gives a list of 43 hotspots with all three of the lead ratios listed above and a subset of 37 of these with the strontium ratios. Zindler et al (1982) gives a list of 12 hotspots with the neodymium isotopic data, Gill (1984), Vidal et al (1984), Roden et al (1982) and Richardson et al (1982), bringing the total number of hotspot neodymium data points to 18. The data was then expanded into spherical harmonics to degree 18 using a code developed by Robert Clayton. The data exhibit a spectrally flat signature with only a small possible peak in degree 10 for the lead data. A plot of the 18 degree expansion showed that the expansion becomes invalid prior to degree 18. The Tanimoto (1990) tomography expansion is only available to degree 6, so the higher degrees in the isotopic data are thrown out, resulting in

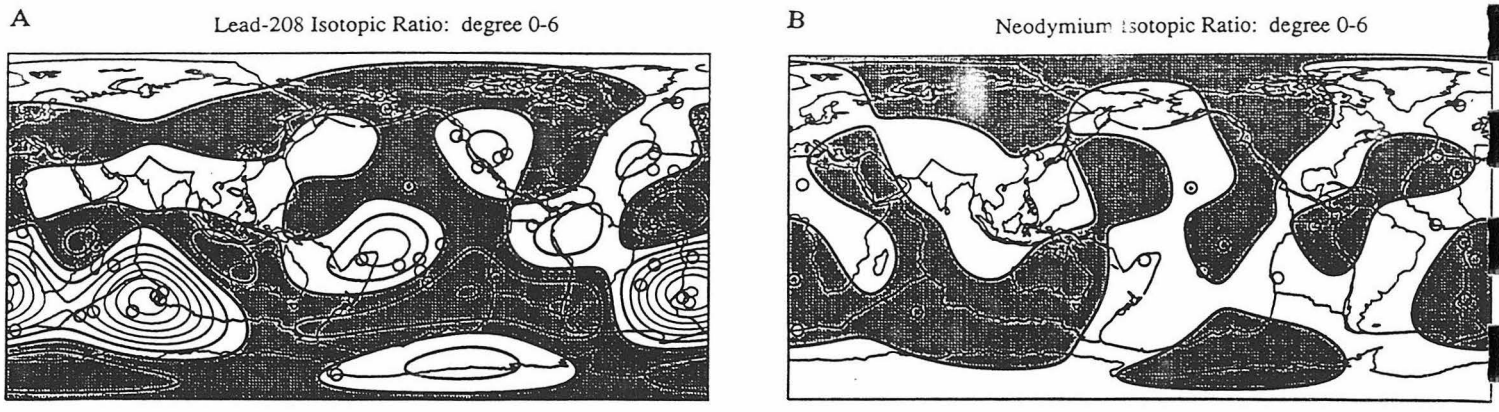

Figure 1: Degree 0 through 6 spherical harmonic expansions of A) Δ8/4 and B) ΔNd. Shaded areas are regions of negative values. Circles show the locations of data points.

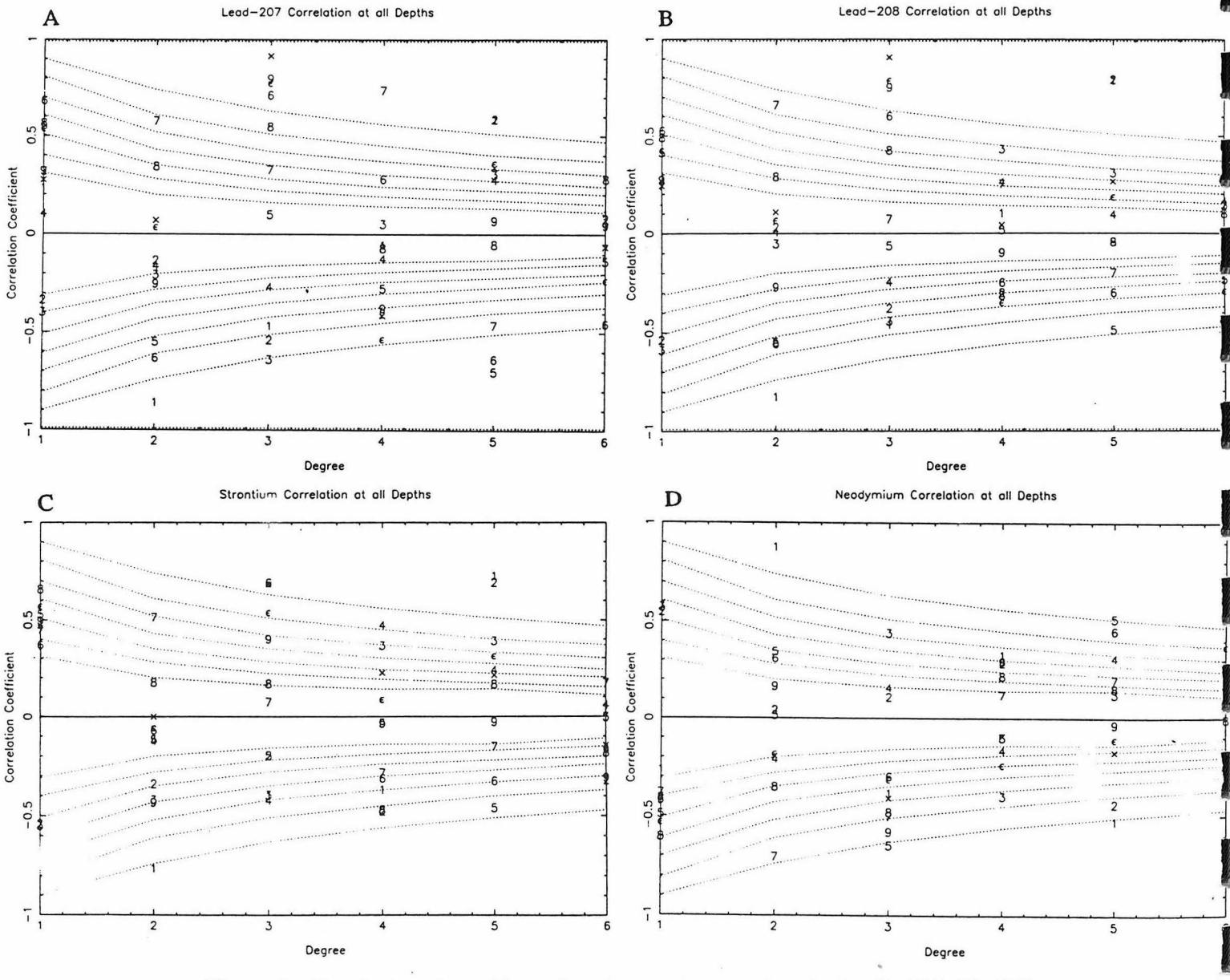

Figure 2: Correlation plots of isotopic values against mantle velocity A) Δ7/4, B) Δ8/4, C) ΔSr, D) ΔNd. Positive correlations represent high isotopic values correlating with slow regions or low values correlating with fast regions. Dotted lines are confidence levels in increments of 10% from 90% to 30%. The numbers indicate the layer of the Tanimoto (1990) tomography at which the correlation is calculated with x representing layer 10 and ε denoting layer 11.

potentially substantial power loss because of the flatness of the power spectra. Figure 1 shows plots of the Δ8/4 and ΔNd expansions through degree 6.

Cross-correlation between the isotopes indicates that the lead isotopes correlate very strongly with each other, and that neodymium and strontium have fairly good anticorrelation. Gerlach (1990) has noted strontium - neodymium anticorrelation and used it to argue for upper mantle heterogeneities. The lead - strontium cross-correlation shows relatively little correlation between the isotopes except for a strong negative correlation in degree 2. Neodymium, on the other hand, has a strong positive correlation with the lead in degree 2 with little correlation elsewhere.

The Tanimoto (1990) tomography model is a model of mantle velocities based on long-wavelength S-waves. There are eleven layers to this model. For convenience, I refer to layers 1 through 3 (0 - 670 km) as the upper mantle, layers 4 through 8 (670 - 2088 km) as the middle mantle, and layers 9 through 11 (2088 - 2891 km) as the lower mantle.

Results: Figure 2 shows plots of the correlation coefficients for each of the four isotopic ratios. First, we see that there are strong correlations between isotopic maps and the lowest part of the mantle (2088 - 2891 km). This is a large scale (degree 3) correlation, and is very strong in the lead isotopes and somewhat weaker in the strontium and neodymium isotopes. This suggests that some large scale deep mantle structure may control the geochemical composition of magmas erupted at the surface. However, there is a paucity of correlations at any other degree in this region of the mantle.

The near-surface degree 5 isotopic signature seems to correlate quite well with the slow areas in the shallow mantle, consistent with these being reservoirs for erupted magma. The larger-scale correlations in degree 2 in the upper mantle are less easily understood. Further complicating matters in degree 2 is the fact that lead and strontium both correlate positively with upper mantle tomography but anticorrelate with each other. The same problem arises with the negative degree 2 neodymium correlation with the tomography and the positive cross-correlation with lead in that same degree. The relationship of these degree 5 and degree 2 structures in the upper mantle to the degree 3 structure in the lowest part of the mantle is unclear.

The middle portion of the mantle exhibits several scales of structure relating to the isotopic maps. Structures from degree 2 to degree 6 are apparent, which could suggest a bridge from the degree 3 lower mantle structure to the degrees 2 and 5 upper mantle structures. The fact that the degree 2 and degree 5 correlations in the middle mantle are opposite sense of the correlations in the upper mantle gives this idea some difficulty. A strong degree 3 correlation occurs with the lead and strontium isotopes in layer 6 of the tomography (1284 - 1555 km). This correlation is of the same sense as the deep mantle correlation, and may therefore be a shallower expression of the structure in the lowest mantle which correlates with the isotopes. However, with regard to the lead isotopes, the layer 6 correlation is weaker than the lowest mantle correlations, and, except for very weak correlations in layer 8, there are no other degree 3 correlations evident.

Further work in this area needs to be done. There are MORB isotopic data which can be correlated in the same manner both as a separate data set and as part of a combined MORB - hotspot data set. A correlation of these isotopic maps with the geoid could also provide some relations to mantle dynamics and structure. There are also higher resolution tomography maps of the shallow mantle available, and the flat power distribution of the isotopic data suggest that important things may occur at higher degree harmonics.

References

Allegre, C. J., B. Dupre, B. Lambret, and P. Richard (1981) "The subcontinental versus suboceanic debate, I. Lead-Neodymium-Strontium isotopes in primary alkali basalts from a shield area: the Ahagger volcanic suite." *Earth and Planetary Science Letters* 52:85-92.

Anderson, D. L. (1989) *Theory of the Earth* 366 pg. Blackwell.

Castillo, P. (1988) "The Dupal anomaly as a trace of the upwelling lower mantle." *Nature* 336:667-670.

Gerlach, D. C. (1990) "Eruption rates and isotopic systematics of ocean islands: further evidence for small-scale heterogeneity in the upper mantle." *Tectonophysics* 172:273-289.

Gill, J. B. (1984) "Sr-Pb-Nd isotopic evidence that both MORB and OIB sources contribute to oceanic island arc magmas in Fiji." *Earth and Planetary Science Letters* 68:443-458.

Hart, S. R. (1984) "A large-scale isotope anomaly in the Southern Hemisphere mantle." *Nature* 309:753-757.

Richardson, S. H., A. J. Erlank, A. R. Duncan, and D. L. Reid (1982) "Correlated Nd, Sr, and Pb isotope variation in Walvis Ridge basalts and implications for the evolution of the mantle source." *Earth and Planetary Science Letters* 59:327-342.

Roden, M. K., S. R. Hart, F. A. Frey, and W. G. Melson (1984) "Sr, Nd and Pb isotopic and REE geochemistry of St. Paul's Rock: the metamorphic and metasomatic development of an alkali basalt mantle source." *Contributions to Mineralogy and Petrology* 85:376-390.

Tanimoto, T. (1990) "Long-wavelength S-wave velocity structure throughout the mantle" *Geophysical Journal International* 100:327-336.

Vidal, P., C. Chauvel, and R. Brousse (1984) "Large mantle heterogeneity beneath French Polynesia." *Nature* 307:536-538.

Zindler, A., E. Jagoutz, and S. Goldstein (1982) "Nd, Sr, and Pb isotopic systematics in a three-component mantle: a new perspective." *Nature*. 298:519-523.

A Mantle Plume Initiation Model for the Formation of Wrangellia and Other Oceanic Flood Basalt Plateaus

Mark A. Richards[1], *David L. Jones*[1], *Robert A. Duncan*[2], *and Donald J. DePaolo*[1]

[1]Dept. of Geology and Geophysics, Univ. of California, Berkeley, CA 94720
[2]College of Oceanography, Oregon State University, Corvallis, OR 97331

The origin of large oceanic basalt plateaus, such as Ontong-Java or Kerguelen, has not been successfully explained by plate tectonic processes or by normal hotspot activity. We suggest that these provinces form during the initial activity of mantle plumes; the huge volumes of basalt are generated by partial melting of a large plume head rising beneath the oceanic lithosphere. Hence, submarine basalt plateaus are the oceanic equivalents of continental flood basalt provinces.

The stratigraphy and structure of *in situ* oceanic plateaus is still poorly known, so we must rely on an uplifted and exposed plateau for geological, petrological, and geochemical evidence in support of the model. We argue that the Wrangellia terrane, which was accreted onto the continenal margin of North America during the mid-Cretaceous and is an uplifted oceanic basaltic plateau, has the requisite features. This terrane contains a 3000-6000 meter thick section of greenstone (originally tholeiitic basalt), exposed over a vast area of at least several hundred thousand square kilometers, bounded above and below by Triassic marine sediments. These formations rest upon a Paleozoic island arc complex which had matured and subsided well before eruption of the Triassic basalts. The particular features of this terrane that suggest a plume head origin are the conspicuous lack of evidence for extension in the underlying strata, extremely rapid eruption of the basalts over a period of only a few million years, rapid uplift preceeding eruption, and slow subsidence back to submarine conditions after the cessation of volcanism.

Radiometric and fossil dates on samples obtained from deep-ocean drilling and dredging on the Kerguelen and Ontong-Java plateaus are also consistent with the hypothesis that these plateaus represent the initial plume head activity of the Kerguelen and Louisville Ridge hotspots, respectively. The Kerguelen plateau formed at about 115 Ma adjacent to and contemporaneous with the Rajmajal traps of eastern India. Preliminary results also indicate that most of the Ontong-Java plateau was formed at about 120 Ma at the approximate reconstructed position of the Louisville Ridge hotspot. We suggest a similar relationship between the active Galapagos hotspot and the late-Cretaceous (80-90 Ma) basalts and greenstones of the eastern and circum-Caribbean basin.

A plume-head origin of at least some large oceanic plateaus would confirm an important prediction of the plume initiation model for flood basalt provinces, i.e., that they should occur in the oceanic basins. The Wrangellia example suggests that these igneous outbursts form buoyant (unsubductable) blocks or microplates which are an important component of crustal addition along continental margins. More detailed studies of oceanic plateau structure, exposed spectacularly in cross-section in the Wrangellia terrane, should yield insight into the nature of mantle plume and flood basalt activity, both oceanic and continental.

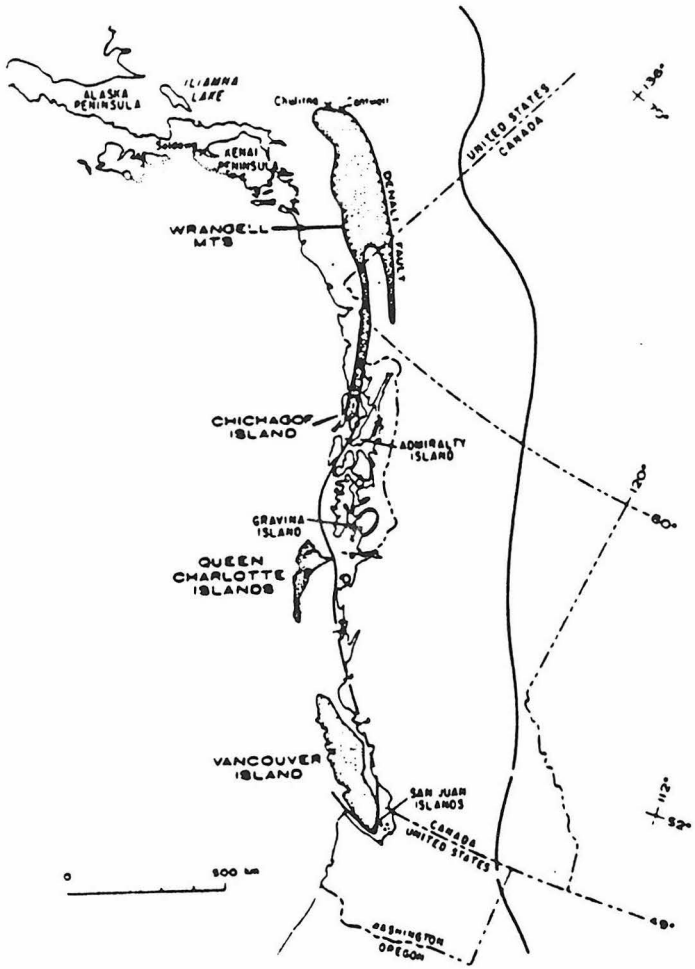

Figure 1: Location map of Wrangellia. The stippled areas have been proposed as pieces of Wrangellia. The heavy line shows the western limit of Triassic rocks related to the North American craton. (Adapted from Jones et al., 1977.)

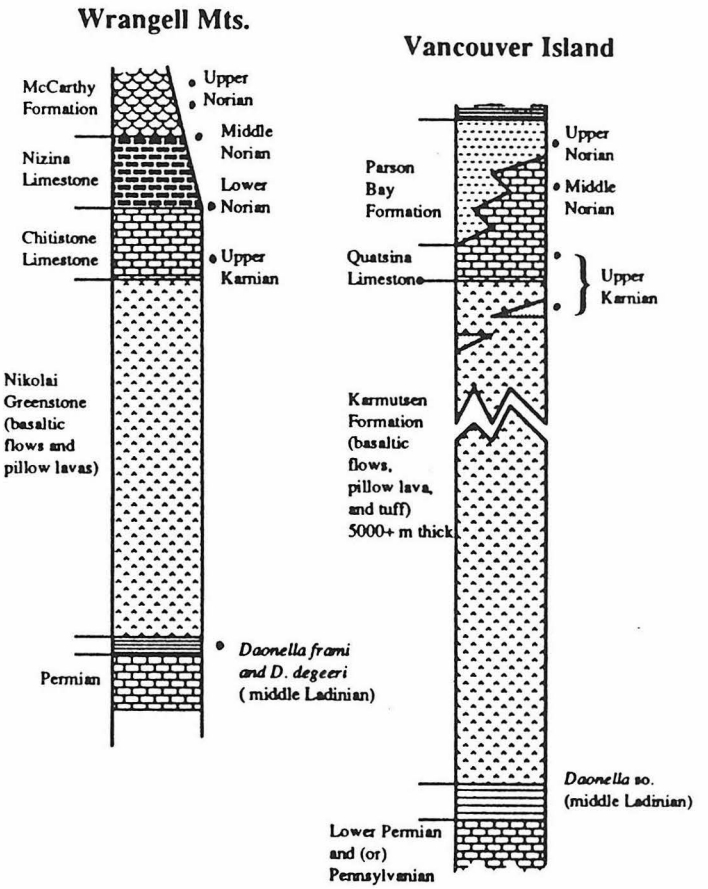

Figure 2: Diagrammatic stratigraphic columns showing the Triassic rocks of Wrangellia exposed in the Wrangell Mountains and on Vancouver Island. Occurrence of age-diagnostic fossils indicated by black dots.

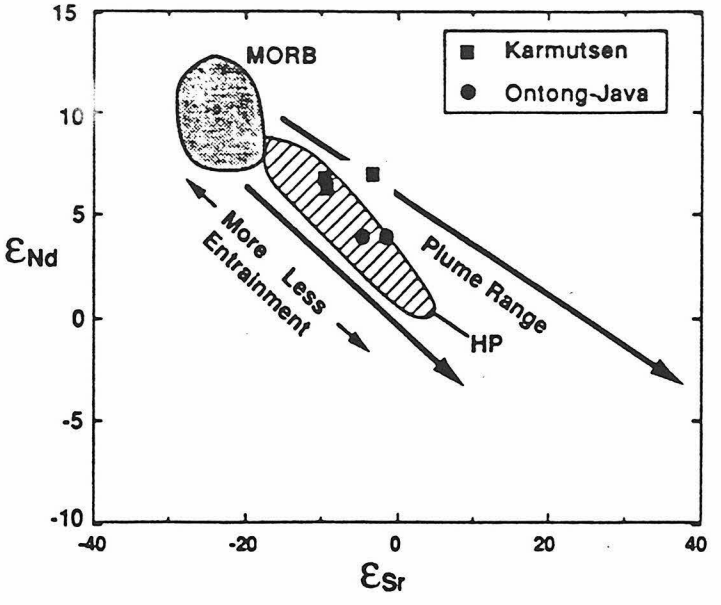

Figure 3: Nd and Sr isotopic compositions of basalts from the Karmutsen Formation, Vancouver Island (Samson et al., 1990) and from the Ontong-Java plateau (Spencer and Mahoney, 1991). Fields of MORB and Hawaiian lavas (HP) shown for comparison. Large arrows envelope the compositions of most plume-derived basalts, and small arrows show the effect of entrainment of upper mantle material. Hawaiian data show that any or all of three factors -- entrainment efficiency, lithospheric melting, and plume composition -- can vary with time, so it may be difficult to fingerprint plumes geochemically. The few Karmutsen and Ontong-Java basalts measured have compostions compatible with a plume origin.

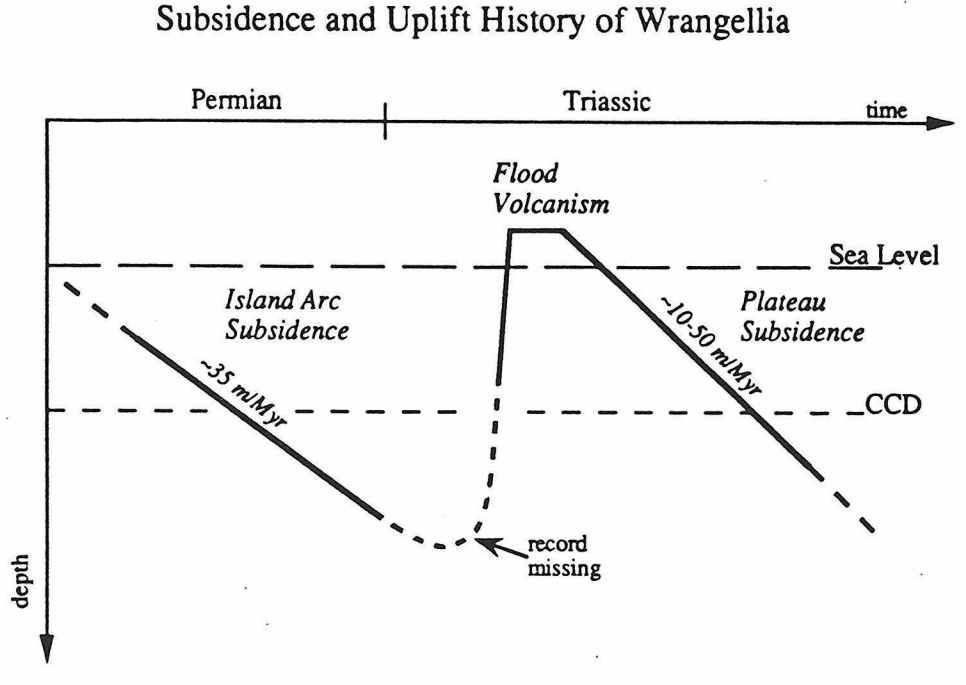

Figure 4: Schematic subsidence and uplift history of Wrangellia as deduced from analysis of the strata (fossil ages) underlying and overlying the Nikolai and Karmutsen greenstones.

GEOLOGIC CONSTRAINTS ON VENUS HIGHLAND STRUCTURE AND EVOLUTION, R.S. Saunders[1], J.W. Head III[2], R.J. Phillips[3], S.C. Solomon[4], R. Herrick[3], R. Grimm[3], E.R. Stofan and D.L. Bindschadler[5]
[1] Jet Propulsion Laboratory, Calif. Institute of Technology, Pasadena, CA 91109; [2]Department of Geological Sciences, Brown University, Providence, RI 02912; [3]Southern Methodist University, Dallas, TX 75275; [4]Massachusetts Institute of Technology, Cambridge, MA, 02139; [5]Dept. of Earth and Space Sciences, UCLA

Venus has many highland regions suggested to have formed by mantle plumes, although alternative hypotheses (e.g., downwelling, crustal spreading) have been proposed. The morphology of highland regions on Venus varies from a high plateau surrounded by mountain belts in Ishtar Terra [1,2], highly deformed tessera or complex, ridged terrain in Tellus and Alpha Regiones [3, 4] to volcanism and rifting in Beta Regio [5-7]. Magellan systematic radar mapping of Venus is revealing distinct tectonic patterns in highland regions. Western Ishtar Terra exhibits an overall morphology that may be generally characteristic of major highland areas elsewhere. The basic pattern is a marginal tectofacies comprising linear mountains and an interior tectofacies that is more chaotically deformed and flooded by plains forming volcanism. The westernmost part of Aphrodite Terra exhibits roughly similar arrangements of tectonic elements. Two western lobes of the equatorial highlands have been examined and a preliminary map of tectofacies compiled. This area includes Hestia Rupes, an interior region and the southern ridge which is similar to Hestia Rupes in overall topography and the western part of Ovda Regio. The region lies along the equator between approximately 55 and 100 degrees east longitude. Aphrodite Terra, previously imaged only by low resolution Pioneer Venus radar, has been the subject of much analysis based on low resolution Pioneer Venus Orbiter radar mapping, and is expected to reveal important information on the formation and evolution of highland terrains on Venus.

Pioneer Venus topography indicates that Ovda is a 2000 x 3500 km highland region rising over 4 km above the surrounding plains. Its interior is relatively plateau-like, with steep outer margins. Pioneer Venus roughness and reflectivity data indicated that the surface may be composed of tessera-like terrain [8], while PVO gravity data gave a relatively shallow depth of compensation at Ovda [9]. Several theories have been proposed for Ovda Regio based on Pioneer Venus data. Aphrodite was initially interpreted to be composed of ancient crustal material, representing a continent-like region [10]. This hypothesis would suggest that Aphrodite should be rather uniformly cratered and ancient. We note that this ancient crust idea begs the question of how the crustal material of the highlands formed. Head and Crumpler [11] proposed that Ovda was the site of new crust formation and spreading analogous to a terrestrial spreading center, identifying a central trough and

cross-strike discontinuities interpreted as transform faults. This theory implies that the age of the surface should increase away from the E-W axis of spreading. However, none of the features such as medial rift, fracture zones, etc. that characterize Earth's mid ocean ridges are present. Given the Magellan images, we do not identify features characteristic of terrestrial spreading centers, and would not propose Ovda as an analogue of those features.

A number of workers [12-14] have proposed that Aphrodite formed by hotspots, with individual regions within Aphrodite representing hotspots of varying ages. Depending on the model for hot spot evolution, and how the variations in apparent depth of compensation are interpreted, one model would predict that Ovda has the oldest surface in Aphrodite [12] and the age of the highlands increases from west to east while another interpretation would have the youngest surfaces in Ovda [13] These hypotheses are testable with Magellan data.

In fact the latter hotspot or mantle plume model, called "blob tectonics" appears to fit some of the new observations of Ovda in the Magellan images. Based on the modest free-air gravity signal and the plateau-like nature of the topography, the blob tectonics model (1) predicts that Ovda Regio is undergoing or has recently undergone massive resurfacing, creating a several kilometer thick crustal cap. Possible sources of tectonic deformation at this stage in the model are 1) those associated with emplacement of massive amounts of lava, such as slumping or ductile detachment and thermoelastic effects, 2) thrust faulting in the interior of the underlying dynamic support has begun to subside (membrane stress effect), and 3) isostatic spreading of the crustal block. These deformational mechanisms are, of course, overprinted on any preexisting tectonic structures. Overall, the blob tectonics model predicts that Ovda should be geologically young, implying a low crater density.

Compression and crustal thickening might also result from downwelling of cold mantle [15,16]. This mechanism may provide the compression and crustal thickening at the margins of the highlands and produce the uplift. At present, the detailed tectonic analysis that would distinguish between mantle upwelling and mantle downwelling has not been performed for any of the highland areas.

Preliminary Magellan data reveal that Ovda Regio is characterized by highly deformed terrain. Linear ridges spaced approximately 10-20 km apart characterize the interior of Ovda. The interior is characterized by very high reflectivity. Some of the ridges are cut by troughs. Some of the ridges resemble terrestrial fold belts, and are interpreted to be compressional in origin. The outer slopes of Ovda are characterized by blocks of tessera-like complexly deformed regions surrounded by smooth deposits interpreted to be volcanic in origin. The region includes extensive lava plains that embay the deformed uplands.

The latest stage of volcanism, also extensive, appears to have formed on rather steep regional slopes and flowed down off the flanks of the present highlands. Finally, Ovda appears to have a low density of impact craters.

The preliminary tectofacies of Ovda are defined as follows:

C	CRATER MATERIAL	Includes all sub units of craters, ejecta, wall, floor, peaks.
P	PLAINS, UNDIVIDED	Smooth, radar dark planar surface. Interpreted to be basalt.
R	LINEAR RIDGE TECTOFACIES	Linear, rounded ridges cross-cut perpendicularly by narrow troughs, probably graben. Generally fold-like appearance. Ridges typically 8-15 km wide and 30-60 km long. Marginal unit in Western Ovda Regio, in contact with plains.
Ri	IRREGULAR RIDGE	Similar to R but having irregular curving ridges and few cross fractures.
T	LINEAR TROUGH TECTOFACIES	Generally appears cross-fractured, with at least one well-developed system of straight, parallel troughs, 10 to hundreds of km long and a few hundred meters to a few km wide, interpreted to be graben.
B	BLOCK FRACTURED TECTOFACIES	Irregular raised blocks, more or less equidimensional, 15-75 km, separated by curvilinear troughs. Blocks are highly fractured by graben but regionally there are few long fractures.

References [1] L. Crumpler et al., Geology, 14, 1301, 1986; [2] V.L. Barsukov et al. J. Geophys Res., 91, 378, 1986; [3] D.L. Bindschadler and J.W. Head, J. Geophys. Res., 95, 21329, 1990; [4] D.B. Campbell et al., in press, Science, 1990; [5] G.E. McGill et al., Geophys Res. Lett.,8, 737, 1981; [6] D.B. Campbell et al., Science, 226, 167, 1984; [7] E.R. Stofan et al., GSA Bull.,101, 143, 1989; [8] D.L.Bindschadler et al., Geophys. Res. Lett., 17, 171 1989; [9] W. Sjogren et al., J. Geophys. Res., 85, 8295, 1980; [10] H. Masursky et al., J. Geophys. Res., 85, 8232, 1980; [11] J.W. Head and L. Crumpler, Science, 238, 1380, 1987; [12] R.S. Saunders et al., Eos, Trans. AGU, 69, 1295, 1988; [13] R. Herrick and R.J. Phillips, Geophys. Res. Lett., 17, 2129,

1990; [14] E.R. Stofan and R.S. Saunders, Geophys. Res. Lett., 17, 1377, 1990 [15] D.L. Bindschadler et al., Geophys Res. Lett., 17, 1345, 1990 [16] D.L. Bindschadler and E.M. Parmentier, JGR, in press.

Notes from RSS:

Images and maps illustrating this abstract will be shown as a poster at the conference.

I have used an old term, tectofacies, to describe the map units that have been delineated. I am extremely reluctant to introduce any more jargon to add to the confusion of things like tessera and coronae, not to mention rupes and mons, planitia and regios. However, there is no present basis for determining lithology and stratigraphy in the Magellan radar images except in some limited cases. All we can see is the tectonic imprint on surface rocks that may be pretty much all the same stuff for all we know. The term tectofacies was first used by Sloss et al. (1949, Integrated Facies Analysis, GSA Memoir 39, p. 91-123) for "a group of strata of different tectonic aspect from laterally equivalent strata." This term may be of little use on Earth where we can make detailed geologic maps. I think the term and the concept may be useful for Venus.

The list of authors represents those Magellan scientists who have contributed to the ideas expressed. I will deny vigorously that we have reached any general consensus about how to approach the task of understanding Venusian highlands, nor do I mean to represent that we have any notions that we understand what is going on.

Acknowledgements: This work was performed, in part, at the Jet Propulsion Laboratory, California Institute of Technology, under contract with NASA.

Mantle Plume - Migrating Ridge Dynamics

J-G Schilling (Graduate School of Oceanography, University of Rhode Island, Kingston, RI 02881)

We report on the interaction and dispersion of mantle plumes in the upper mantle, using the spatial distribution of isotope ratios in basalts from mid-ocean ridges and ocean islands as tracers of mantle dynamics - much like dyes are used to follow flow patterns and mixing conditions in laboratory fluid-dynamic experiments. This is possible since mantle plumes are isotopically distinct from the asthenosphere which normally feeds the mid-ocean ridges.

Several plume dispersion models are currently being debated, for instance:

1. The blob cluster model which suggests that the breakup and dispersion of mantle plumes is directly proportional to the convective rate of the upper mantle, as measured by the spreading rate of mid-ocean ridges (Allègre et al. 1984). It implies a direct link between mantle convection and relative plate motions and an inverse relationship between spreading rate and Nd-Sr-Pb isotopic variance in MORBs.

2. Sleep's 1990 model considers intraplate plumes (e.g. Hawaii) injected into the low-viscosity zone (LVZ) underlying the rigid lithosphere. The dispersion of the plume is not entirely radial but influenced by the plate drag.

3. We have pursued the "*mantle plume source - migrating ridge sink model*" (MPS-MRS), which suggests that the migrating ridge is fed and dynamically affected by a preferential plume flow along a thermally induced channel at the base of the lithosphere caused by the hot plume from the time it was ridge-centered. When ridge-centered, the preferential flow takes place along the ridge axis, symmetrically about the plume (Vogt 1971, Schilling 1973 & 1985, Morgan 1978). Mixing of the plume with the asthenosphere takes place by entrainment and in the melting zone.

4. Plumes tilted significantly in the upper-mantle by plate drag or by deeper return flows may enhance entrainment of the surrounding mantle and detachments of blobs once a critical tilt angle is reached (Skilbeck and Whitehead 1978, Whitehead 1982, Olsen and Singer 1985, Geist et al. 1988, Richards and Griffiths 1988 and 1989). We have investigated this model as a possible alternative to the MPS-MRS model.

Whatever dispersion mechanism is considered, it is now well documented that mid-ocean ridges migrating away from hot mantle plumes are geochemically and dynamically affected by plumes discharging over long periods of time (t) and ridge migration distances (x). A flow connection between plumes and migrating ridges has been established from the following surface observables: (i) tracks of constructional volcanism (Morgan 1978), (ii) along-ridge geochemical anomaly width (W) and associated excess ridge elevation (ΔE) (Schilling 1985), (iii) the tagging of plumes from mixing vectors in multi Nd-Sr-Pb-He isotope space representation of basalt compositions (Hanan et al.1986). The empirical relationships $W=1010\text{-}24.5\ x^{1/2}$ and $\Delta E=2.42 \cdot 10^{-3} W$ (with W and ΔE in km), established from 7 hotspots in the North and South Atlantic, the Galapagos and the Sala y Gomez plumes beneath the Nazca plate and the Afar plume (Schilling 1985), suggest that these plumes would become purely intraplate when the migrating ridge distance is of the order of 1700 ± 250 km.

Plume fluxes: With the use of the above tracer information and the concept of buoyancy flux developed for intraplate plumes by Richards et al. 1988, Davies 1988, and Sleep 1990, we have developed two independent methods for constraining plume fluxes (or discharge rates into migrating ridges). *Method I*, which makes use only of the geochemical anomaly width (W), the associated full spreading rate (S) and lithosphere thickness (H), is given by: $Q_p = k_1 HSW/2$ (I)
where k_1 is a coefficient which takes into account the fraction of the plume which does not enter the accretion process and is dispersed into the LVZ.
Method II, which makes use of the ridge elevation anomaly maximum ($\Delta E(o)$) and the buoyancy flux, is given by: $Q_p=[k_2\ \Delta E(o)\ S\ W(\rho_m-\rho_w)]/[2\rho_m \alpha \Delta T]$ (II)

where ΔT is the mean excess temperature of the plume relative to the asthenosphere, α the thermal expansion coefficient (3×10^{-5} K^{-1}), ρ_m and ρ_w the density of the asthenosphere (3300 kg/m^3) and water (1000 kg/m^3). The coefficient k_2 corrects for the contribution of thicker crust to the elevation anomaly using the Airy compensation model. The volumetric flux of the 13 plumes investigated by this method are compared with those of Sleep (1990) in Table 1, using first $k_1=k_2=1$, H=100 km and ΔT=225°C. The estimated fluxes by our two methods and Sleep's method based on intraplate uplifts correlate well for plumes located at a distance (x) more than 200 km from these migrating ridges. Accordingly, we interpret that in this case $k_1=k_2=1$ and the plume discharge rates measured at these migrating ridges represent essentially the entire plume flux discharged into the LVZ. However, in the case of the ridge-centered plumes (and when $x < 200$ km), simple kinematic models, taking into account plate drags and isotopic gradients resulting from mixing, suggest that $k_1 \leq 1.5$, and for compensating for thicker crust $k_2 \approx 0.5$. Our listed "*best estimate*" are based on a simple average of our two methods with $k_1=k_2=1$ for distant plumes with $x > 200$ km, and a weighted average using $k_1=1.5$ and $k_2=0.5$ for ridge-centered plumes (and when $x < 200$ km). The volumetric flux of the 13 plumes investigated range from 0.4 km^3/yr for the Great Meteor and 3 km^3/yr for Kerguelen. For comparison, Hawaii, the largest currently active plume flux monitored, is 9-12 km^3/yr (Sleep 1990).

Excess temperature of plumes: By equating the plume flux method I and II given above, we have solved for the mean excess temperature of plumes, which is given by: $\Delta T = [k_2 (\rho_m - \rho_w) \Delta E(o)] / [k_1 H \rho_m \alpha] = 232 (k_2/k_1) \Delta E(o)$
with ΔT in [°C] and $\Delta E(o)$ in [km]. The excess temperature of the 13 plumes range from 140°C for the Azores and 300°C for the Galapagos, with the ridge-centered Iceland and Afar plume equal to 263°C and 224°C, respectively (Table 1). Again we used $k_1=k_2=1$ for plumes with $x > 200$ km, and $k_1=1.5$ and $k_2=0.5$ for plumes with $x < 200$ km. The range compares well with estimates made by independent published methods. These vary from 100°C for Iceland (Schilling 1973), to a maximum of 300°C for Hawaii (Wyllie 1988), and mostly 200-250°C (McKenzie 1984, Davies 1988, Klein and Langmuir 1987 and Sleep 1990). The ΔT at the center of plumes may be 1.25 to 1.6 times higher than the means previously quoted (Sleep 1990).

There is no relation between the excess temperature of these 13 plumes and their distance from the migrating ridges where these ΔT's were investigated. This suggests the rapid establishment of a quasi-steady thermal-state condition at shallow depth between the plume, the LVZ and the growing and aging lithosphere.

The lowest ΔT found for the Azores, corresponds to a low $^3He/^4He$ "*wet*" plume highly enriched in volatiles (Schilling et al 1980), which Bonatti (1990) has qualified as "*not so hot*" on the basis of geothermobarometry of peridotites from the region. Otherwise, there are no relationships between the ΔT of these plumes and their geochemical and isotopic nature, such as DUPAL, non-DUPAL, HIMU and high or low $^3He/^4He$ characters.

Had some of these plumes derived from the core/mantle boundary, others possibly from the 670-km discontinuity, and some from shallower depth by some kind of metasomatism, one would have expected larger variations, since the ΔT of thermal plumes are likely to be proportional to their depth of origin (e.g. Griffiths and Campbell 1990). Within the uncertainties in ΔT's involved, it would seem that a common depth of origin and source of heat for these 13 plumes is likely, namely the core/mantle boundary. Perhaps, the geochemical and isotopic diversity of plumes, and their temporal variation so far noted may then reflect (i) the layered nature and timing of the recycled lithosphere material accumulating and forming the D" layer, (ii) the mode of subsequent plume detachments, and (iii) the complexities of the entrainment process, particularly across the 670-km discontinuity where some recycled material may also accumulate.

Plume tilting versus MPS-MRS models: The geochemical anomaly width (W) facing the Reunion, Crozet, Kerguelen plumes range between 750-900 km. According to the empirical relationships previously established, one would expect near ridge-centered plume configurations, when in fact the three observed hotspot-ridge distances (x) are in the range of 1100 to 1800 km! However, if the distance (x) is measured with respect to the near-ridge satellite islands consistently associated with these plume - migrating ridge systems, namely Rodrigues, Marion/Prince Edward and St. Paul/Amsterdam, the range becomes 85 - 275 km, and the W vs $x^{1/2}$ correlation is not violated within the uncertainties involved.

Could it be that the migrating ridge, the satellite island and the off-ridge hotspot reflect detachments of blobs from a single tilted plume conduit?

This possibility was investigated using both the 2-layer shear flow and the return flow models and the theory described by Richards and Griffiths (1988), combined with (i) the flux constraints previously discussed, (ii) the required deflection distances between the migrating ridge, the satellite island and/or the off-ridge hotspot. The *radius* of the plume was left as a free parameter for determination. The plume radius constrained by this approach range 200-16400 km for the two-layer shear flow model assuming a viscosity contrast η_1/η_2 of 50 for the underlying mantle relative to the LVZ assumed to be 100 km thick. A thicker LVZ decreases somewhat the radii required, but generally not to reasonable values. For the return flow model, the radius required would range from 200 to 1575 km. These radii are clearly excessive and reflect the very large surface deflections needed in the first place. For comparison, the radius of the plume conduit for Hawaii is estimated at 75-80 km on the basis of the curvature of the Hawaiian-Emperor seamount chain (Duncan and Richards 1991). The two tilting models are rejected on this basis as well as on the lack of consistency in the direction of the tilts required by plate kinematics. For example, in the case of the shear flow model, plumes underlying the same African plate in the South Atlantic and the Indian Ocean should all be tilted in the direction of the absolute African plate motion. This is not the case. The geochemical anomalies on the MAR are all located West of the Circe, St Helena and Tristan off-ridge plumes, whereas the anomalous Mid-Indian Ocean Ridge segment is located east of the Reunion plume. Similar inconsistencies can be found with plumes underlying the Nazca and the Antarctic plates.

However, in all the cases studied, the geochemical anomalies are always located on the ridges that are migrating away from these plumes, which strongly suggests that migrating ridges, which act as sinks, have the power of capturing plumes towards them. In our view, this argument strongly supports the MPS-MRS model and the development of a thermally-induced channel at the base of the lithosphere (groove- and parabolic-like) along which the plume is preferentially dispersing from the time these migrating ridges were ridge-centered. Using Turcotte and Oxburgh's (1967) thermal boundary layer model and a mean ΔT of the plume of 200°C, we estimate this thermal-groove to be about 30 km deep for a fully developed lithosphere 100 km thick, and only 3 km deep near the migrating ridge axis where the lithosphere is only 10 km thick. The pressure gradient required to maintain this lateral flow is provided by the dynamic pressure of the plume. Assuming a Poiseuille type of conduit plume flow, 100 km in diameter, 1000 km long, with a 3 km^3/yr flux and a viscosity of $3x10^{18}$ Pa s, the mean pressure drop required would be 116 Pa/m, corresponding to a hydraulic head of 3.5 km. This is not impossible, since an inviscid plume from the core/mantle boundary with a density contrast of 33 kg/m^3 would have an hydraulic head of 29 km (Sleep et al. 1988).

There is ample evidence that plumes feeding migrating ridges can have other important dynamic and tectonic effects, besides uplift. They can generate propagations of rifts, the development of transient microplates, and induce rift jumps backs towards the plume, and as a result, large transform fault offsets. Spatial isotopic tracer variations across these transform fault discontinuities testify that

conduit plumes do not disperse radially into the LVZ, but are preferentially channeled as the MPS-MRS model predicts (Schilling et al. 1982). The only time plumes may disperse radially into the upper mantle may be when an initial plume head reaches and flattens against a rather stationary plate such as beneath a subcontinental lithosphere. Evidence for a vestige of the dispersal of St. Helena and Tristan plume heads under the Gondwana continental lithosphere has been detected along the MAR between 20°S - 40°S (Hanan et al. 1986). Also, Nd-Sr-Pb isotope tracer variations along the Gulf of Aden and Red Sea suggest that the head-part of the Afar plume may have recently been flattened and radially dispersed (Schilling et al. 1991).

Plume	Ridge Anomaly	W (km)	ΔE(o)† (km)	S (cm/yr)	Qp (Sleep) (km^3/yr)	Qp (I)	Qp (II)	$\bar{Q}p$*	ΔT (°C)
North Atlantic									
Jan Mayen (JM)	71°-73°N	668	2.2	1.66	-	0.55	1.26	0.73	170
Iceland (I)	60°-66°N	923	3.4	1.9	1.98	0.88	3.08	1.43	263
Azores (Az)	33°-40°N	1094	1.8	2.46	1.56	1.35	2.50	1.63	139
Great Meteor (GM)	34°-36°N	323	1.1	2.38	0.71	0.38	0.44	0.41	255
South Atlantic									
Circe (C)	7°-11°S	393	1.2	3.87	-	0.76	0.94	0.85	278
St. Helena (SH)	15°-16°S	208	0.9	3.93	0.71	0.41	0.38	0.40	209
Tristan (T)	35°-40°S	565	0.7	3.85	2.4	1.09	0.79	0.94	162
Red Sea/Gulf of Aden									
Afar (Af)	42°-51°E	1000	2.9	1.91	1.7	0.96	2.86	1.43	224
Pacific Ocean									
Galapagos (G)	95°-87°W	880	1.3	6.02	1.4	2.65	3.56	3.10	302
Sala Y Gomez (SG)	25°-28°S	350	0.85	8.0	4.67	1.40	1.23	1.31	197
Indian Ocean									
Crozet (Cr)	43°-46°S	788	2.38	1.62	0.71	0.64	1.57	1.10	552
Kerguelen (K)	33°-40°S	862	1.0	6.72	0.71	2.90	2.99	2.94	232
Reunion (Re)	12°-22°S	892	0.75	4.63	2.69	2.06	1.60	1.83	174

* $\bar{Q}p = [Q_p(I)+Q_p(II)]/2$ with $k_1=k_2=1$ for x>200km and $k_1=1.5$ and $k_2=0.5$ for x<200km.

† ΔE = Maximum excess elevation relative to 2.9 km normal mean depth (Vogt 1976).

References

Allègre, C.J., et al., *Earth Planet. Sci. Lett.* **71**, 71, (1984).

Bonatti, E., *Science*, **250**, 107, (1990).

Davies, G.F., *J. Geophys. Res.*, **93**, 10,467, (1988).

Duncan, R.A. and M.A. Richards, *Rev. Geophys.*, **29**, 31, (1991).

Geist, D.J., et al., *Nature*, **333**, 657, (1988).

Griffiths, R.W. and I. H. Campbell, *Earth Planet. Sci. Lett.*, **99**, 66, (1990).

Hanan, B.B., et al., *Nature*, **322**, 137, (1986).

Klein, E.M. and C.H. Langmuir, *J. Geophys. Res.*, **92**, 8089, (1987).

McKenzie, D., *J. Petrol.*, **25**, 713, (1984).

Morgan, W.J., *J. Geophys. Res.*, **83**, 5355, (1978).

Olson, P. and H. Singer, *J. Fluid. Mech.*, **158**, 511, (1985).

Richards, M.A. and R.W. Griffiths, *Nature*, **342**, 900, (1989).

Richards, M.A. and R.W. Griffiths, *Geophys. J.*, **94**, 367, (1988).

Richards, M.A., et al., *J. Geophys. Res.*, **93**, 7690, (1988).

Schilling, J.G., *Nature*, **314**, 62, (1985).

Schilling, J-G., *Nature*, **242**, 565, (1973).

Schilling, J-G., et al., *J. Geophys. Res.*, submitted, (1991).

Schilling, J-G., et al., *Phil. Trans. R. Soc. Lond. A*, **297**, 147, (1980).

Schilling, J.G., et al., *J. Geophys. Res.*, **87**, 5593, (1982).

Sleep, N.H., et al., *J. Geophys. Res.*, **93**, 7672, (1988).

Sleep, N.H., *J. Geophys. Res.*, **95**, 6715, (1990).

Turcotte, D.L. and E.R. Oxburgh, *J. Fluid Mech.*, **28**, 29, (1967).

Vogt, P.R., *Earth Planet. Sci. Lett.*, **29**, 309, (1976).

Vogt, P.R., *Earth Planet. Sci. Lett.*, **13**, 153, (1971).

Whitehead, J.A. Jr., *Geophys. J. R. astr. Soc.*, **70**, 415, (1982).

Wyllie, P.J., *J. Geophys. Res.*, **93**, 4171, (1988).

Three-Dimensional Models of Venusian Interior Dynamics

Gerald Schubert
Department of Earth and Space Science
University of California
Los Angeles, CA 90024

Recent numerical models of three-dimensional thermal convection (e.g., Schubert et al., 1990; Glatzmaier et al., 1990; Travis et al., 1990) suggest that the primary convective structures in the Venusian mantle should be hot upwelling cylindrical plumes and cold downwelling sheets and cylinders. This theoretical prediction is supported by the detailed view of the surface of Venus provided by Magellan (e.g., Head et al., 1991; Solomon et al., 1991) that reveals prominent geological features plausibly interpreted as surface expressions of mantle upflow plumes and downflow sheets and cylinders. Possible surface expressions of mantle plumes are Beta Regio (Kiefer and Hager, 1991) and the numerous coronae (Schubert et al., 1990; Stofan et al., 1991) widely distributed over the surface of Venus. Possible surface expressions of cylindrical mantle downflows are western Ishtar Terra and the low-elevation plains regions of Atalanta and Lavinia Planitia (Bindschadler et al., 1990), while Aphrodite Terra and Sedna and Guinevere Planitia may be the surface manifestations of sheetlike mantle downflows. Beta Regio and the coronae are plausibly related to mantle plumes because of their circularity and hotspot-like characteristics such as elevated topography and volcanism. The compressional mountain belts around Lakshmi Planum in western Ishtar Terra and along the northern margin of Aphrodite Terra are the primary features suggesting association with mantle downwelling.

Notably absent from the surface of Venus is a linear network of rises similar to the system of midocean ridges on Earth. This is in agreement with numerical models of convection that are devoid of sheetlike upwellings (e.g., Bercovici et al., 1989) and consistent with the inference that the midocean ridges on Earth are secondary passive features associated with the rigidity of tectonic plates (Schubert, 1991). The lithosphere of Venus is apparently not as thick or rigid as that of the Earth. Accordingly, primary mantle convective features are more readily expressible in the surface geology of Venus than they are on Earth, and Venus' lithosphere does not impose any secondary mode of deformation on its mantle. The Earth's tectonic plates impose a mode of sheetlike upwelling on the mantle under the midocean ridges that is incompatible with the primary mode of plumelike upwelling. The Earth's plates also suppress any surface expression of cylindrical mantle downwelling as may be occurring beneath western Ishtar Terra on Venus. Mantle convection on Earth and Venus contrast interestingly in that one shows the influence of multi-rheological behavior (nonviscous plates above a viscous interior), while the other shows the consequences of a predominantly simple viscous rheology.

References

Bercovici, D., Schubert, G., Glatzmaier, G.A. 1989. Three-dimensional, spherical models of convection in the Earth's mantle. *Science* 244: 950-955.

Bindschadler, D., Schubert, G., Kaula, W.M. 1990. Mantle flow tectonics and the origin of Ishtar Terra, Venus. *Geophys. Res. Lett.* **17**: 1345-1348.

Glatzmaier, G.A., Schubert, G., Bercovici, D. 1990. Chaotic, subduction-like downflows in a spherical model of convection in the Earth's mantle. *Nature* **347**: 274-277.

Head, J.W. et al. 1991. Venus volcanism: Initial analysis from Magellan data. *Science,* in press.

Kiefer, W.S., Hager, B.H. 1991. A mantle plume model for the equatorial highlands of Venus. *J. Geophys. Res.* submitted.

Schubert, G. 1991. Numerical models of mantle convection. *Ann. Rev. Fluid Mech.* in press.

Schubert, G., Bercovici, D., Glatzmaier, G.A. 1990. Mantle dynamics in Mars and Venus: Influence of an immobile lithosphere on three-dimensional mantle convection. *J. Geophys. Res.* **95**: 14,105-14,129.

Solomon, S.C., et al. 1991. Venus tectonics: Initial analysis from Magellan. *Science,* in press.

Stofan, E.R., Bindschadler, D.L., Head, J.W., Parmentier, E.M. 1991. Corona structures on Venus: Models of origin. *J. Geophys. Res.* submitted.

Travis, B., Weinstein, S., Olson, P. 1990. Three-dimensional convection planforms with internal heat generation. *Geophys. Res. Lett.* **17**: 243-246.

Spherical Harmonic Correlation of Pangea and Subducted Slab with Global Seismic Tomography

Craig W. Scrivner and Don L. Anderson (Division of Geological and Planetary Sciences, California Institute of Technology, Pasadena, CA 91125)

A map of continental Pangea, circa 180 Ma, was digitized and expanded numerically in spherical harmonics to degree $l = 8$ (Figure 1). Also, an estimate of the distribution of lithospheric slab subducted since 180 Ma was obtained from plate reconstruction maps, and this area of distribution was digitized and expanded in spherical harmonics to $l = 8$ (Figure 2). The distribution of subducted slab was determined by overlaying successive map reconstructions of the subduction zones from 180 Ma to the present and digitizing the area which fell between the extreme positions of the trenches over that time. Subduction zones appeared to shift direction, backtracking over themselves instead of moving in a constant direction away from their 180 Ma positions. This indicates changes in relative plate motions that were not clearly indicated on the maps used. The areas of Pangea and the subducted slab were digitized to 5° by 5° resolution. The power spectrum of the spherical harmonic expansion for Pangea indicates the dominance of the degree 1 component (Figure 3). The power in degree 3 is most likely the result of the Tethys Sea which cuts into the eastern margin of Pangea. The power spectrum for the expansion of the subducted slab peaks for degrees 2 and 3 (Figure 6). Both of these expansions were correlated with the 11 depth layers (Table 1) of Tanimoto's (1990) global seismic S-wave and Love wave tomography for degrees $l = 1$ to 6. For his tomography, the degree $l = 2$ has the largest power in all layers except shell 5, where $l = 3$ is strongest. Tanimoto is concerned that aliasing may occur for the layers 4 to 6. The correlation between the expansion of Pangea and Tanimoto's tomography is strongest for degree 1 at the bottom of the upper mantle with a correlation coefficient of $r = -0.90$ (Figure 4, see note concerning the sign of correlations). Degree 3 shows a high correlation at the top of the lower mantle with $r = 0.82$ for shell 5 (Figure 5). The high power coefficient at degree 3 for shell 5 in Tanimoto's tomography lends added weight to this correlation. The reversal of sign in the correlation for degree 3 relative to degree 1 is interesting. The correlation between the expansion of the subducted slab and Tanimoto's tomography are strongest for degrees 2 and 3. Degree 2 shows its strongest correlation, $r = -0.79$ at the bottom of the lower mantle; there is a somewhat weaker correlation at the bottom of the lower mantle (Figure 7). Degree 3 has a strong correlation of $r = -0.70$ at the top of the lower mantle (Figure 8). Overall, the correlations of these two degrees indicate a strong tomographic signal from cold, fast material around the 670 km discontinuity.

Previous researchers have reached conflicting conclusions about the path of subducting slab. The primary argument concerns whether the slab cross the 670 km discontinuity. This is a significant point because the answer is strongly dependent on the nature of the boundary, and so would clarify many issues if it were known. Attempts to use seismic ray travel-time anomalies of deep earthquakes to image the dip of the slab further down have not all reached the same results. Fischer et al. (1988) find a near-vertical dip, Zhou et al. (1989) find a sub-horizontal dip at the depth of the 670 discontinuity. Recent discussions of mantle chemistry (Anderson 1989, and Ringwood and Irifune 1988) seem to favor the slab dipping to horizontal, though some slabs might punch through steeply and reach the bottom of the mantle. The problem has also been modeled experimentally in the lab by Kincaid and Olson (1987), and, depending on the density variation across the discontinuity, different regimes of subduction were found – from near vertical dip for no density variation, to horizontal dip for a large density variation. This experimental work generates other useful questions as well, about the significance of dip angle and trench migration. Richards and Engebretson (Fall 1990 AGU Abstract) correlate seismic tomography to sinking slabs, but only for the lower mantle body wave tomographies of Dziewonski (1984) and Hager and Clayton (1988). Their correlation for degree 3 with these tomographies is about the same as the correlations presented here for degree 3. However, their correlations for degrees 1 and 2 are higher. For these degrees, the correlations presented here are highest in the upper mantle and suggest that a significant fraction of the subducted slab is going no deeper than the 670 discontinuity.

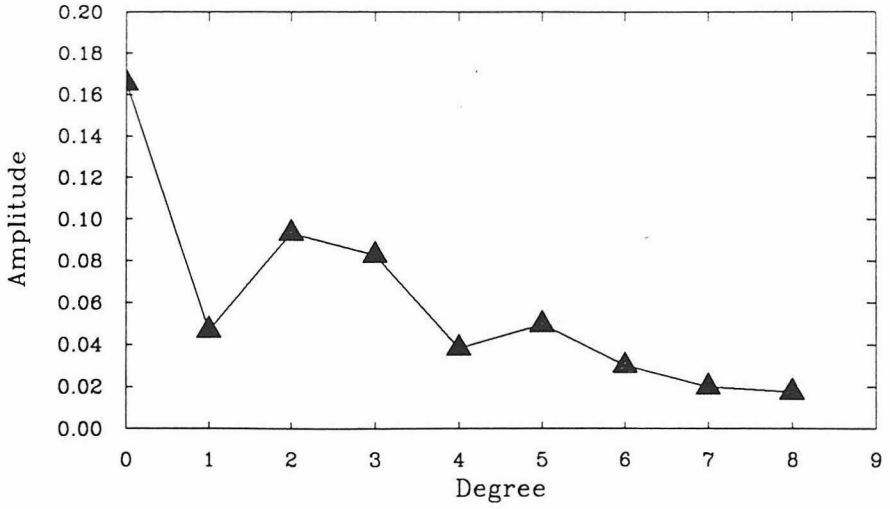

Figure 6: Amplitude spectrum of subducted slab expanded in spherical harmonics to degree $l = 8$. The circum-Pacific slab produces the power at degree $l = 2$, and the Tethyan subduction trench (now the Alpine/Himalayan collision zone) is the source of the power in $l = 3$.

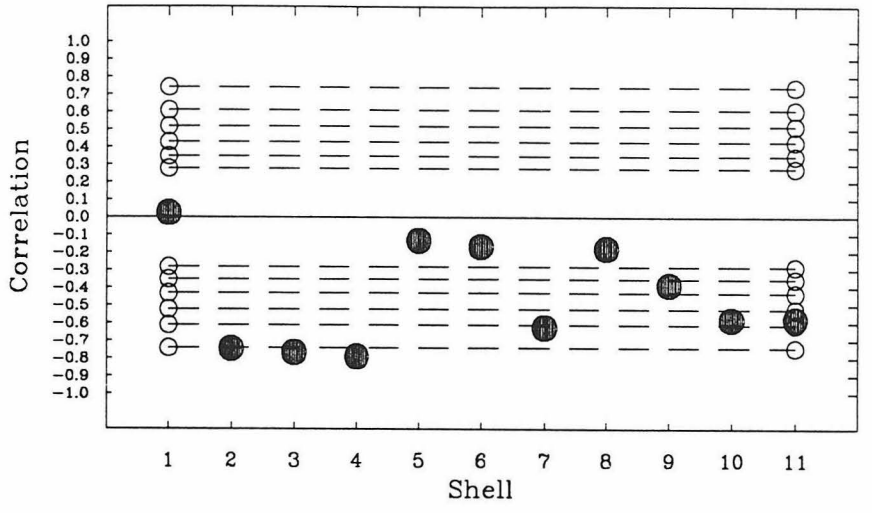

Figure 7: Degree 2 correlation of tomography with subducted slab for shells 1 to 11

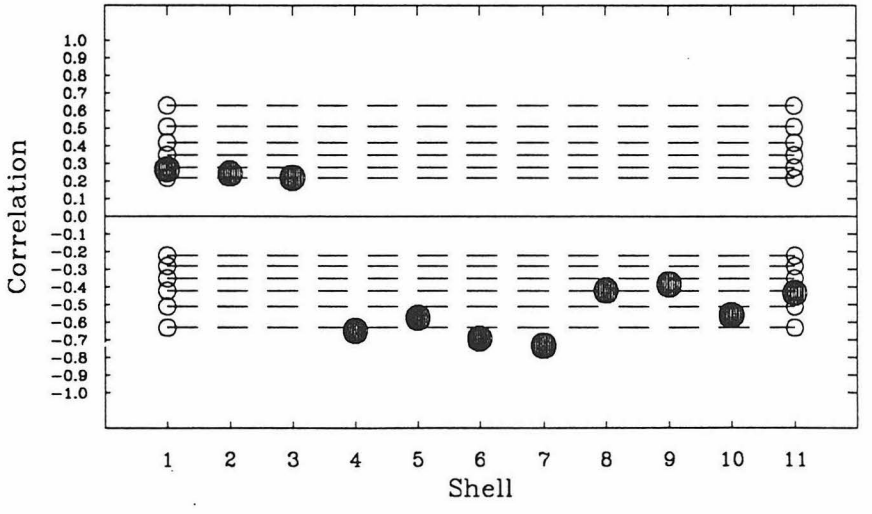

Figure 8: Degree 3 correlation of tomography with subducted slab for shells 1 to 11

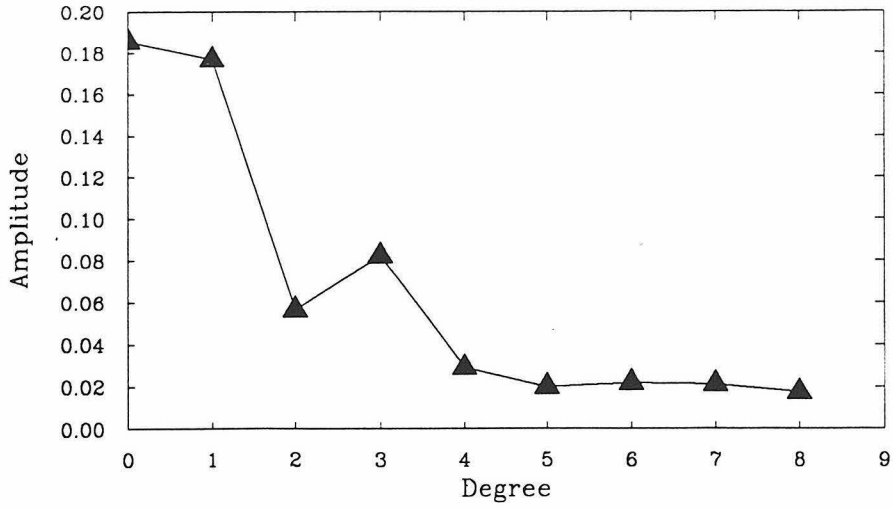

Figure 3: Amplitude spectrum of Pangea expanded in spherical harmonics to degree $l = 8$. The Tethys seaway is responsible for power in $l = 3$

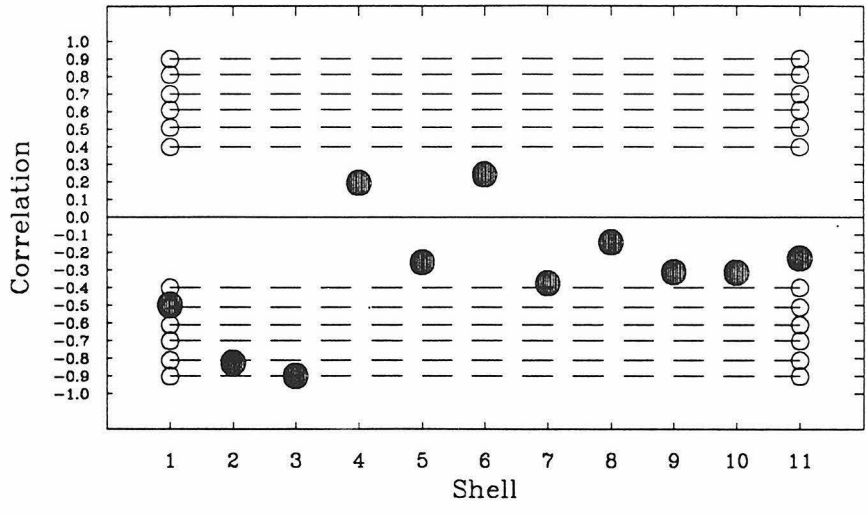

Figure 4: Degree 1 correlation of tomography with Pangea for shells 1 to 11 **Note**: For All Plots, negative correlation values indicate cold, seismically fast mantle material. Dashed lines indicate correlation confidence levels, varying from 50% to 95%

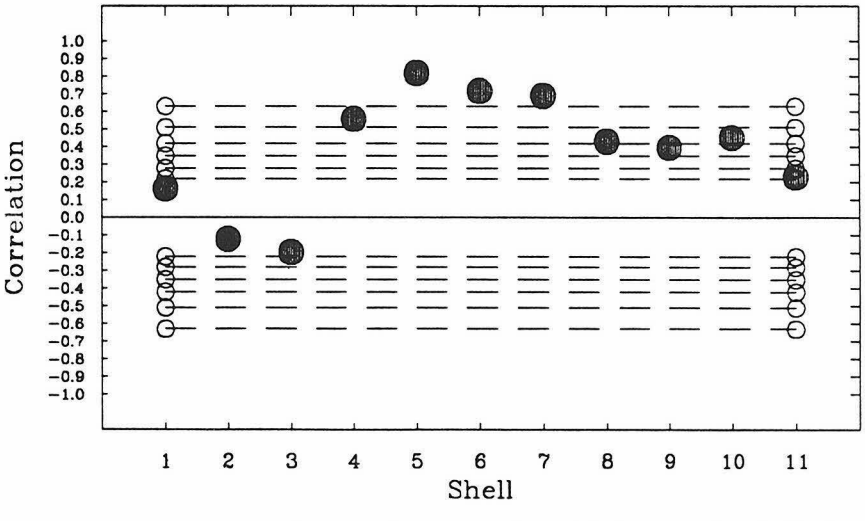

Figure 5: Degree 3 correlation of tomography with Pangea for shells 1 to 11

Shell #	Top	Bottom	Depth
1	6371	6151	220
2	6151	5971	400
3	5971	5701	670
4	5701	5349	1022
5	5349	5087	1284
6	5087	4816	1555
7	4816	4555	1816
8	4555	4283	2088
9	4283	4012	2359
10	4012	3741	2630
11	3741	3480	2891

Table 1: Shells in Tanimoto's Mantle Tomography (in km)

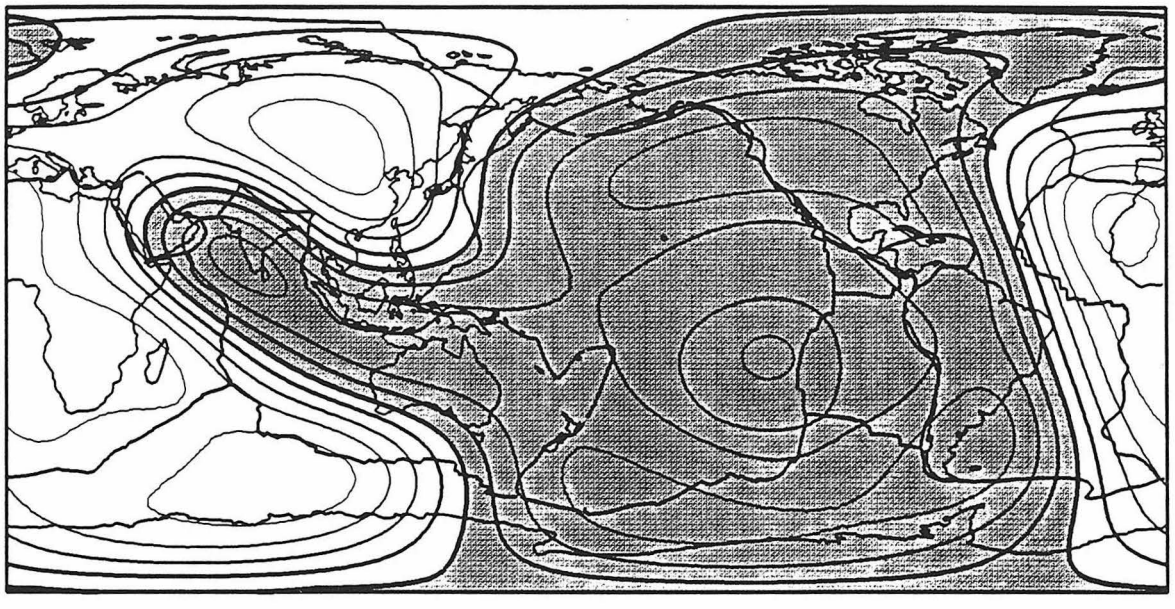

Figure 1: Spherical harmonic expansion of Pangea for degrees $l = 1$ to 8. White areas are positive contours (continental mass of Pangea)

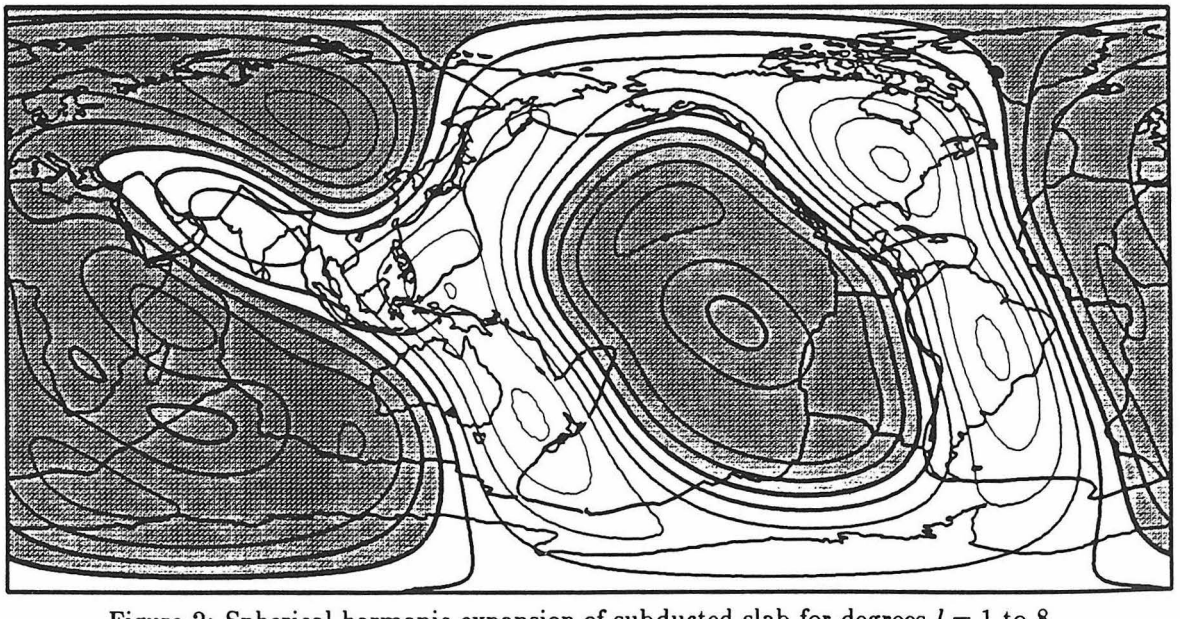

Figure 2: Spherical harmonic expansion of subducted slab for degrees $l = 1$ to 8.

Time dependence of mantle plumes

by

Norman H. Sleep
Department of Geophysics
Stanford University
Stanford CA 94305

Several hotspot tracks have persisted on the order of 10^8 years which is long enough for changes in the flux of the underlying plumes to become observable. The flux of off-ridge marine hotspots can be determined directly from the relief of the hotspot swell. The flux is then conveniently expressed as buoyancy flux $B \equiv \overline{WE}\,\rho_m - \rho_w V_P$ where $\overline{WE}$ is the cross sectional area of the swell, ρ_m is mantle density, ρ_w is water density, and V_P is track velocity. This flux is directly proportional to the excess heat flux from the plume. The buoyancy flux of older swells is obtained by determining the original cross sectional area by correcting for thermal subsidence. The volume flux of on-ridge hotspots is obtained for the volume of material supplied by the plume to the length of ridge axis which is strongly affected.

Hotspots which cross ridge axes constitute a special problem which gives some information about the dynamics of ridge-plume interaction. When a hotspot approaches sufficiently near a ridge axis, plume material is entrained into the axis. Entrainment is fairly efficient even when the expected track position is still away from the axis because the addition of plume material to the ridge axis suppresses the passive upwelling which would normally occur beneath the ridge. Kinematically the track appears to jump to the ridge axis creating a gap in the track. Such a gap is best demonstrated by the jump of the New England seamount track to the on ridge Corner seamounts. The Tristan track has recently jumped off axis. For the purposes of determining the flux, such entrainment has the positive effect that the ridge axis efficiently gathers plume material so that the submarine plateau created at the ridge axis records plume flux. Conversely, the gap in the track might be misinterpreted as a weakening of flux. For example, the flux I have given (JGR, 95, 6715-6736, 1990) for Tristan is too low by a factor of two because the effects of the jump were not recognized. The preferred flux 3.4 $\mathrm{Mg\,s^{-1}}$ makes this plume the strongest one outside of the Pacific basin.

The flux history of isolated plumes is easiest to determine. Iceland has stayed the same since soon after the initial plume head arrived at the surface. The Galapagos hotspot has also not changed for the part of the track recorded in the Pacific basin. Hawaii, the strongest plume, has grown stronger. Louisville has weakened drastically. Réunion and Tristan have weakened somewhat.

Flow associated with with plate tectonics is important in controlling the evolution of the basal boundary layer and hence the flux history of plumes. Plumes by themselves tap the basal boundary and locally deplete it. However, flow associated with the density contrast from relief on the top of the basal boundary layer as well as flow associated with plate tectonics can locally thicken the layer and allow a strong plume to strengthen with time. These inferences were confirmed by analytical finite-element calculations in cylindrical geometry.

VENUS: GLOBAL AND REGIONAL TECTONICS. Sean C. Solomon, Dept. of Earth, Atmospheric, and Planetary Sciences, M.I.T., Cambridge, MA 02139; James W. Head, Dept. of Geological Sciences, Brown University, Providence, RI 02912; William M. Kaula, Dept. of Earth and Space Sciences, U.C.L.A., Los Angeles, CA 90024; Dan McKenzie, Bullard Laboratories, Cambridge University, Cambridge CB3 OEZ, England; Barry Parsons, Dept. of Earth Sciences, Oxford University, Oxford OX1 3PR, England; Roger J. Phillips, Dept. of Geological Sciences, Southern Methodist University, Dallas, TX 75275; R. Stephen Saunders, Jet Propulsion Laboratory, Pasadena, CA 91109; Gerald Schubert, Dept. of Earth and Space Sciences, U.C.L.A., Los Angeles, CA 90024; Steven W. Squyres, Center for Radiophysics and Space Research, Cornell University, Ithaca, NY 14853; and Manik Talwani, Houston Area Research Center, The Woodlands, TX 77381.

Introduction. Radar imaging and altimetry data from the Magellan mission have revealed a diversity of deformational features at a variety of spatial scales on the Venus surface [1]. The radar images from Magellan constitute an improvement in resolution by at least an order of magnitude over the best images previously available [e.g., 2,3]. In this paper we discuss what those images, and their interpretations, are revealing about the styles of lithospheric deformation on Venus, the inferred mechanical properties of the lithosphere, and their implications for the tectonic history of the planet. We first give an overview of patterns of tectonic deformation of Venus, and we then focus on the question of identifying potential sites of present and past mantle upwelling.

Tectonic Features. The *plains* of Venus record a superposition of different episodes of deformation and volcanism. This deformation is manifested in areally distributed strain of modest magnitude and in zones of concentrated lithospheric extension and shortening. In areas of distributed deformation, the characteristic spacing between tectonic features (graben, small ridges, or narrow lineations) ranges from 1 km or less to tens of kilometers. The strain patterns are commonly coherent over hundreds of kilometers, implying that even many local features reflect a long-wavelength processes.

Much of the strain in lowlands regions is concentrated into *deformation belts*, intensely deformed linear to curvilinear regions 50-100 km wide and hundreds of kilometers long separated by radar-dark and less deformed regions of plains a few hundred kilometers across. The deformation belts stand hundreds of meters higher than the surrounding plains, indicating that they are products of lithospheric shortening and crustal thickening. There is also an approximate correlation between radar brightness, indicative of intensity of deformation, and total relief, presumably a measure of crustal shortening. A number of older linear features show offsets and changes in trend where they cross deformation belts, indicating that some horizontal shear has accompanied shortening.

Mountain belts, observed to date only in Ishtar Terra, represent still greater degrees of lithospheric shortening and crustal thickening. Modest horizontal shear has accompanied compression in several mountain belt regions. Magellan images have for the first time revealed widespread evidence for lateral extension and gravitational collapse of mountainous terrain. Relationships between compressive and extensional structures indicate that lateral spreading has occurred both during and following active crustal convergence. Magmatic and volcanic activity has accompanied the lateral extension in several mountainous terrains and adjacent regions.

Venus displays two principal geometrical variations on large-scale lithospheric extension: the quasi-circular *coronae* and *broad rises* with linear rift zones. Coronae are circular to oval structures 200-1000 km in diameter having a generally elevated interior and a narrow deformed annulus of concentric ridges [2,4]. Broad rises are typically 1000-3000 km in diameter and quasi-circular in planform; where rift zones are present such features are 50 to several hundred kilometers wide, up to thousands of kilometers in length and up to 5 km in relief. Both coronae and rifted rises are sites of significant volcanic flux, and both have been attributed to convective upwelling in the

underlying mantle [e.g., 4,5].

Some of the most complexly deformed terrain are the *tesserae*: broad, elevated, radar-bright regions characterized by two or more sets of intersecting linear features [2]. Magellan images of tesserae to date reveal pervasive deformation at a variety of scales, ranging from tens of kilometers down to the limit of radar resolution. Tesserae display significant (5 km or more) local relief as well as limited volcanism confined to the outer margins and isolated interior pockets of smooth and therefore comparatively undeformed plains.

Overview of Observations. A number of generalizations may be made about tectonic styles on Venus on the basis of Magellan data analyzed to date. Examples of both horizontal shortening and horizontal extension are abundant on the Venus surface at scales ranging from the 1-km scale that characterizes the spacing between tectonic features in a number of regions to the 1000-km scale that governs the large scale physiography of major structures and the spatial coherence of many smaller scale patterns of strain. Horizontal shear has evidently occurred in the lowland deformation belts and in the mountain belts, but such shearing tends to be broadly distributed and to accompany horizontal stretching or shortening. No clear examples have yet been documented of long, large-offset strike-slip faults such as those typical of oceanic and some continental areas on Earth.

The various scales of deformation arise from the complicated mechanical and dynamical structure of the Venus interior. The 10-30 km scale is plausibly attributed to the response of a strong upper crustal layer, while the deformation of a strong upper mantle layer can account for tectonic features with characteristic scales of a few hundred kilometers [6]. The scale of a few hundred to a few thousand kilometers, particularly if evident in the long-wavelength gravity as well as the topography, is likely dominated by mantle convection and its associated dynamic stresses and heat transport. The scale of a few kilometers and less involves either internal deformation of the upper crust or tectonic disruption of a thin surficial layer decoupled thermally or mechanically from the remainder of the otherwise strong upper crust.

In general, compressive features are more evident than extensional features in the areas viewed to date by Magellan. To some extent this is coincidental, in that there are many large highland regions thought to be sites of lithospheric extension that have yet to be imaged. The prevalence of compressive structures, however, may be in part because compression is accompanied by crustal thickening and uplift, and the elevated terrain is less susceptible to resurfacing by volcanic burial. Extensional fault systems, in contrast, and large rift systems in particular, may show a tendency for self-erasure, in that significant lithospheric stretching should lead to pressure release melting in the mantle [7] and volcanism that will act to bury the tectonic evidence for extension. In the absence of significant weathering and erosion, the lifetime of high topography is limited by ductile flow in the thickened lower crust that must at least partly support the topographic relief once active compression ceases. The widespread evidence for lateral extension in the mountains of Ishtar Terra documents the tendency for such ductile flow to occur. The very steep regional slopes (20-30°) marking some of the edges of Lakshmi Planum and the front ranges of the mountain belts provide evidence that dynamical processes have been recently operative.

We have seen no evidence to date for tectonic behavior similar to terrestrial oceanic regions, i.e., nearly rigid lithospheric plates with horizontal dimensions of 10^3-10^4 km and active deformation confined to plate boundary zones a few kilometers to tens of kilometers across. Nor have we seen analogues to oceanic fracture zones or to deep sea trenches. Rather much of the tectonic behavior on Venus appears to be reminiscent of actively deforming continental regions on Earth, with deformation distributed across broad zones one to a few hundred kilometers wide separated by comparatively stronger and less deformed blocks having dimensions of hundreds of kilometers. On Earth, the continental lithosphere in tectonically active areas is weaker than typical

oceanic lithosphere because of the greater thickness of more easily deformable crust. Because of the much greater surface temperature on Venus, the lithosphere on Venus should behave in a weak manner for crustal thicknesses less than are typical of continental regions on Earth.

In general, the intensity of deformation and state of preservation of tectonic features on Venus are strong functions of local topographic relief. Elevated regions tend to be areas of thicker crust and therefore a thicker layer of weak lower crust susceptible to ductile flow. Such regions thereby serve as concentrators of regional lithospheric strain, such as the lowland deformation belts and the mountainous terrain. Elevated regions, particularly areas uplifted by compression and crustal shortening, are also less susceptible to volcanic resurfacing and thus are more likely to preserve records of deformation spanning one or more episodes of significant strain. We suggest that much of the surface of Venus may have only two possible fates: volcanic burial and comparatively long-term preservation as relatively elevated and intensely deformed terrain. The first fate is represented by the abundant volcanic plains. The second fate may be primarily represented by tessera terrain.

Plumes on Venus? A major challenge in unravelling the evolution of Venus is to understand the interaction between mantle convection and the lithosphere. The strong correlation between long-wavelength gravity and topography and the large (100-400 km) apparent depths of compensation of relief for many upland regions [8] suggests that these long-wavelength variations are signatures of mantle dynamics [9,10]. Furthermore, the large apparent depths of compensation and considerations of probable lithosphere thickness on Venus point to the absence of a low-viscosity zone beneath the lithosphere [11,12], in contrast to the viscosity structure in oceanic regions on Earth [13]. The lack of a low-viscosity zone, possibly a result of the dehydration of the upper mantle of Venus [14], allows mantle dynamic stresses to couple strongly to the overlying lithosphere and can thus contribute significantly to surface topography and tectonic deformation [12,15].

These considerations raise the question as to whether the geometry of upper mantle convection on Venus may be discerned directly from measurements of topography and gravity and observations of lithospheric deformation and igneous activity. In numerical models of three-dimensional convection in constant-viscosity spherical shells with Rayleigh numbers at about 100 times the critical value, convective upwelling occurs dominantly in the form of cylindrical plumes, with the number and characteristic spacing of plumes a function of the relative fraction of basal and internal heating [16]. With parameters appropriate to the Venus mantle and with 20% of the heating supplied from below, a figure consistent with the heat flux from the core given by parameterized convection models of Venus thermal evolution [17], such calculations indicate that about 20 plumes are active at any one time [18], although this result is likely to be quite sensitive to such model assumptions as choice of Rayleigh number and viscosity structure.

Localized centers of mantle upwelling are likely to be characterized by broad topographic rises and geoid highs [19], by uplift and extension of the lithosphere, and by consequent pressure-release melting and surface volcanism [7,20]. Plumes arising from instability of the bottom boundary layer to upper mantle convection are likely to be transient features on geological time scales [7,21], so that a sequence of events associated with an individual plume on Venus can be anticipated, including initial uplift, voluminous igneous activity, and collapse and relaxation during the waning of plume-delivered heat and magma [5,22]. Because of the probable strong coupling of mantle convective stresses to the lithosphere, mantle flow patterns should have predictable associated patterns of surface deformation [12,15]. Such diagnostic patterns may be difficult to discern, however, because thin-skinned deformation enabled by a ductile lower crust may in some situations dominate the observable tectonic features [23].

Long-wavelength topography and geoid anomalies on Venus are characterized by a number of broad highs such as might be produced by 10-20 distinct centers of approximately cylindrical

upwelling [10,11], although specification of the geoid is presently limited by the uneven resolution of gravity information with latitude and the necessary truncation of harmonic representations. A number of these highs correspond to the broad rises, 1000-3000 km across, identified from radar imaging as centers of volcanism and tectonic activity [1,3,24], also consistent with sites of active mantle upwelling. Many of the details required to associate particular regions on Venus with mantle flow patterns, however, remain to be worked out. For instance, there is not presently an agreement as to whether the volcanic plateau Lakshmi Planum in Ishtar Terra is located over a region of mantle downwelling, as might be suggested by the large-scale convergence implied by the formation of the bounding mountain belts [25,26], or over a region of mantle upwelling, as might be suggested by the pervasive volcanism [27,28] and aspects of the long-wavelength gravity anomaly [29]. As noted above, coronae have also been suggested as sites of mantle upwelling [4], although coronae have lesser characteristic dimensions (200-1000 km) and are greater in number than the broad highland rises, and coronae do not have a discernible gravity anomaly at present resolution. The relative ages of different coronae and the distribution of those coronae recently or even presently active have not been determined. If both broad rises and coronae are products of mantle upwelling, then multiple scales of mantle convection are indicated and the two forms of upwelling must presumably have different controlling geometries and buoyancy fluxes. A physical explanation for the different morphologies of the two classes of features has yet to be elucidated.

A complementary question is the location of sites of mantle downwelling. Theoretical models of mantle convection suggest that downwelling should occur in sheets or cylinders [16, 18], and it has been suggested that much of the downwelling is localized beneath the lowland planitiae [5,30]. The lowlands are also sites of pervasive plains volcanism [31], however, which would not be expected over regions of convective downwelling and lower than average upper mantle temperatures. Clearly, further measurements by Magellan of global topography and gravity and delineation of large-scale patterns of volcanism and tectonics and their temporal relationships will provide important new constraints on these issues. It is likely that new models linking magmatism and surface deformation to patterns of interior flow will also be needed.

References: [1] S.C. Solomon et al., *Science, 252*, in press, 1991; [2] V.L. Barsukov et al., *PLPSC 16th*, D378, 1986; [3] D.B. Campbell et al., *Science, 246*, 373, 1989; [4] A.A. Pronin and E.R. Stofan, *Icarus, 87*, 452, 1990; [5] R.J. Phillips et al., *Science*, in press, 1991; [6] M.T. Zuber, *PLPSC 17th*, E541, 1987; [7] R. White and D. McKenzie, *JGR, 94*, 7685, 1989; [8] S.E. Smrekar and R.J. Phillips, *EPSL*, in press, 1991; [9] R.J. Phillips et al., *Science, 212*, 879, 1981; [10] B.G. Bills et al., *JGR, 92*, 10335, 1987; [11] W.S. Kiefer et al., *GRL, 13*, 14, 1986; [12] R.J. Phillips, *JGR, 95*, 1301, 1990; [13] E.M. Robinson et al., *EPSL, 82*, 335, 1987; [14] W.M. Kaula, *Science, 247*, 1191, 1990; [15] R.J. Phillips, *GRL, 13*, 1141, 1986;[16] D. Bercovici et al., *Science, 244*, 950, 1989; [17] D.J. Stevenson et al., *Icarus, 54*, 466, 1983; [18] G. Schubert et al., *JGR, 95*, 14105, 1990; [19] B. Parsons and S. Daly, *JGR, 88*, 1129, 1983;[20] D. McKenzie and M.J. Bickle, *J. Petrol., 29*, 625, 1988; [21] M.A. Richards et al., *Science, 246*, 103, 1989; [22] R.R. Herrick and R.J. Phillips, *GRL, 17*, 2129, 1990; [23] S.E. Smrekar and R.J. Phillips, *GRL, 15*, 693, 1988; [24] G.E. McGill et al., *GRL, 8*,737, 1981; [25] W.S. Kiefer and B.H. Hager, *LPS, 20*, 520, 1989; [26] D.L. Bindschadler et al., *GRL, 17*, 1345, 1990; [27] A.A. Pronin, *Geotectonics, 20*, 271, 1986; [28] A.T. Basilevsky, *Geotectonics, 20*, 282, 1986; [29] R.E. Grimm and R.J. Phillips, *GRL, 17*, 1349, 1990; [30] M.T. Zuber, *GRL, 17*, 1369, 1990; [31] A.L. Sukhanov et al., *Map I-2059*, USGS, 1989.

Where is the OIB source? Further constraints from arcs

Robert J. Stern, Center for Lithospheric Studies, U. Texas at Dallas
Sherman H. Bloomer, Dept. of Geology, Boston University
Julie Morris, Department of Terrestrial Magnetism, Carnegie Institution of Washington

There are few good constraints on how deep in the mantle the sources of ocean island basalt (OIB) lie. The fact that OIB are erupted at hotspots - the surficial expression of plumes - coupled with the inference that these hotspots remain fixed over 10^7 - 10^8 years, has led to the consensus that OIB sources lie deeper than the depth of mantle convection. This is widely interpreted to be the deep mantle (<670 km). However the growing recognition that the lithospheric plates are driven by body forces ('slab pull' and 'ridge push') and not by basal shear from convecting upper mantle opens the possibility that non-convecting mantle extends to very shallow depths. There is thus presently no basis to preclude the possibility that OIB mantle - and the roots of hotspots - lie as shallow as the upper asthenosphere.

Convergent margins present us with some of the few constraints on the depth of OIB mantle. Because the subducting lithosphere acts as a physical and thermal barrier to the ascent of mantle directly beneath it, the mantle components in arc magmas sample the top 100 - 150 km of the mantle. Once components added from 1) the subducted slab and 2) the sub-arc crust are removed, the composition of arc basalts can be used to constrain the composition of the upper 100-150 km of the mantle. The second effect can be greatly minimized by concentrating on arcs built on oceanic crust (intra-oceanic arcs). Removing the first effect - the subduction component - is much more difficult because the multiple sources and processes possible in subduction zones makes forward modelling dangerously dependant on the initial assumptions. In most instances, unique solutions are not feasible and this is reflected in the literature on arc magmagenesis. We discuss two perspectives based on isotopic studies of arc samples to obtain new insights into the question of whether the mantle beneath arcs is like OIB or MORB.

The first perspective comes from studies of boninites. A consensus exists that boninites manifest melting due to hydration - by the fluid that carries the subduction component - of otherwise dry and ultradepleted harzburgite. The corollary is that the LIL and LREE abundances and Sr, Nd, and Pb isotopic compositions of boninites are determined by the elemental inventory of this fluid. Our studies of the trace element and isotopic composition of Eocene boninites from the Mariana arc lead us to conclude that the subduction component in this case carried Sr, Nd, and Pb stripped out of typical N. Pacific OIB-type mantle (Fig. 1,2), with perhaps only water and the alkali metals having originated in the slab itself. It appears that the hydrous fluid released by dehydration of the slab, re-equilibrated with OIB-type mantle beneath the Eocene Mariana arc.

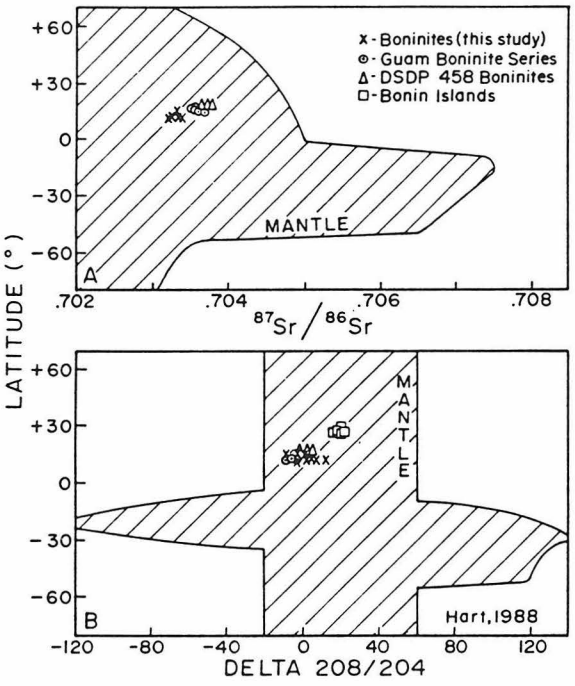

Fig. 1: The isotopic composition of Mariana and Bonin boninites vs. the sources of OIB as a function of latitude (after Hart, 1988).
(a) $^{87}Sr/^{86}Sr$ vs. latitude;
(b) Δ8/4 vs. latitude.

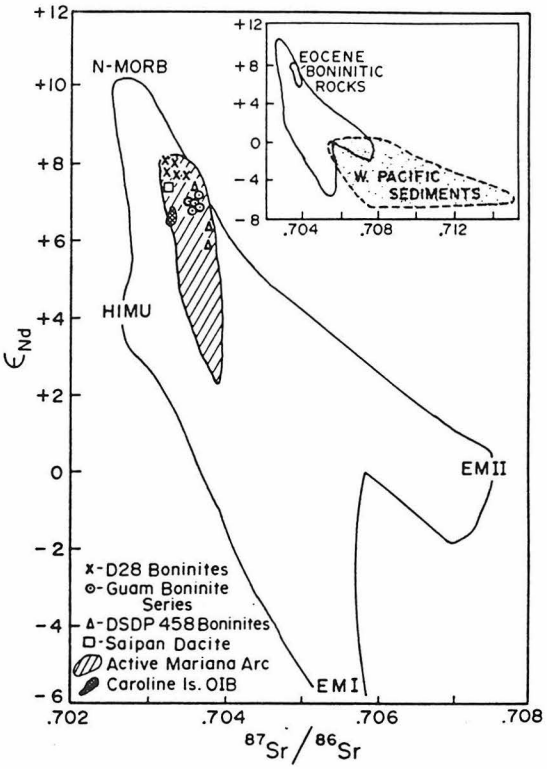

Fig. 2: Sr- and Nd- isotopic composition of Mariana forearc boninites and related rocks. Insert field shows the isotopic composition of Western Pacific pelagic sediments, the oceanic mantle, and the boninite field.

Another perspective comes from comparing the isotopic composition of modern intra-oceanic arc/back-arc basin systems with that of the local OIB-type mantle. This is especially appropriate because the most important heterogeneities in the Pacific trend E-W while the

arcs trend N-S, so that OIB characteristics can be grossly predicted. We focus on the Mariana system, where any OIB component should be similar to that of the northern Pacific (or perhaps the Indian) Ocean, and the Tonga-Kermadec-Lau system, where any OIB-component should have DUPAL-type signatures, at least in the north. Recent Mariana arc and back-arc basin lavas have Sr- and Nd- isotopic compositions that are indistinguishable from those of Hawaiian and Caroline Island OIB, extending towards EM I (Fig. 3). Mariana Sr- and Nd- isotopic compositions are distinct from W. Pacific pelagic sediments and from many of the Cretaceous seamounts (which formed to the south and have strong DUPAL signatures). Certainly the data from the Mariana system is most compatible with a model whereby the source of these melts has a mantle OIB component.

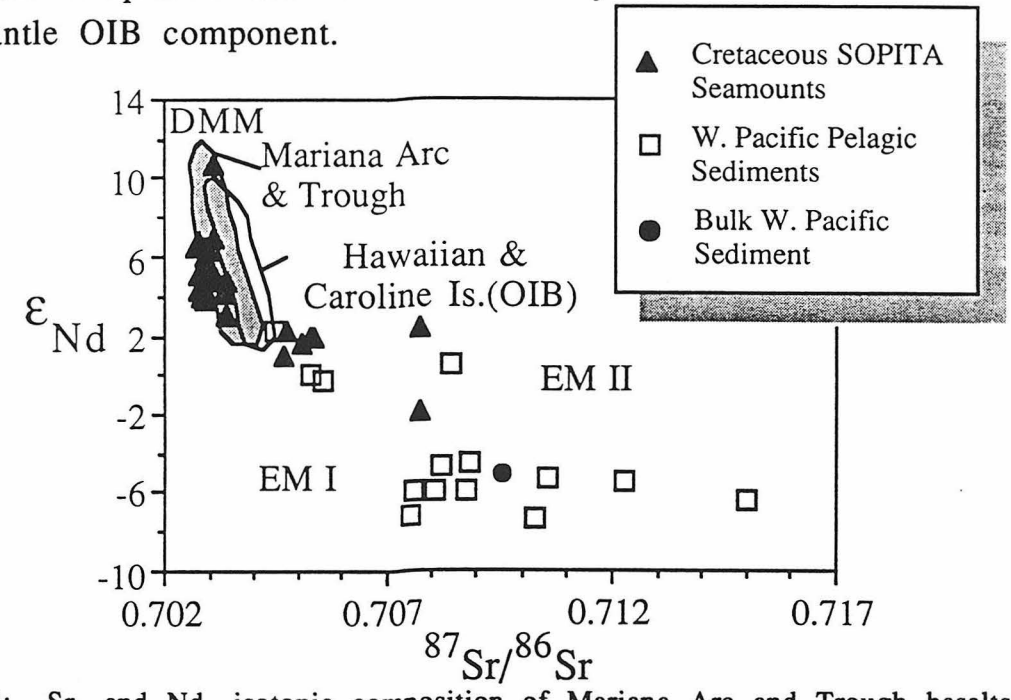

Fig. 3: Sr- and Nd- isotopic composition of Mariana Arc and Trough basalts, compared with N. Pacific OIB sources (Hawaiian and Caroline Islands) and sources on the subducted slab (W. Pacific pelagic sediments (Lin and Stern, in revision) and Cretaceous SOPITA seamounts (Staudigel et al., 1991).

Finally, we examine the Lau-Tonga-Kermadec system in the S. Pacific. Sr- and Nd- isotopic data for this system extend towards Samoan OIB (Fig. 4). Samoan OIB extends towards EM II as do the arc and back-arc data, in contrast to the pattern for the Marianas. Samples from the arc and back-arc closest to Samoa have the strongest isotopic similarities to Samoan OIB. In order to explain unusual basalts on Fiji, Gill and Whelan (1989) proposed that DUPAL-type mantle has been drawn into the northern part of the Lau-Tonga-Kermadec system;

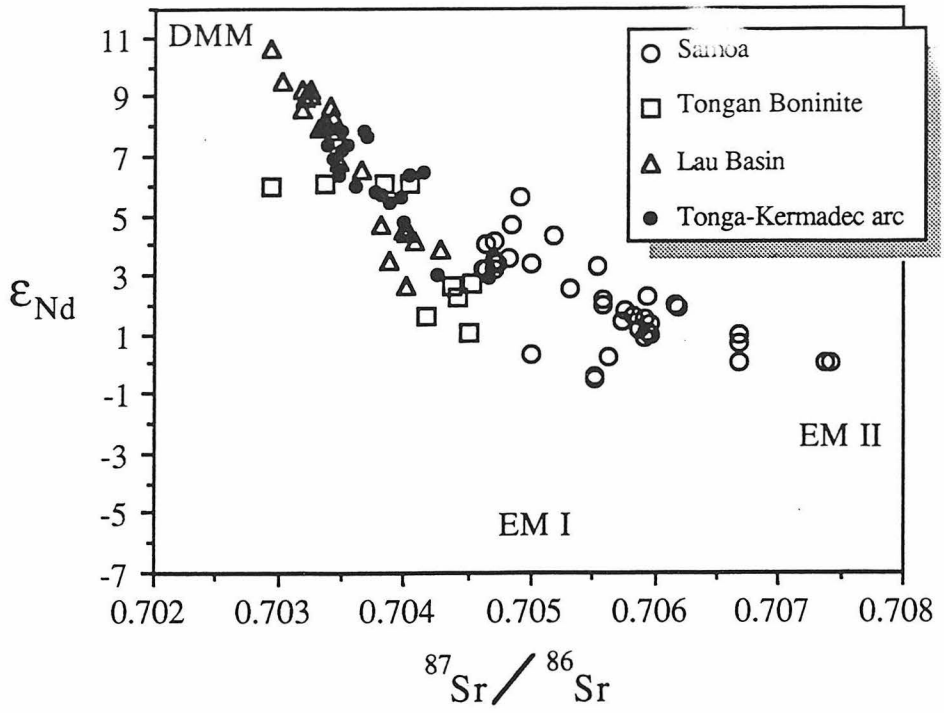

Fig. 4: Sr- and Nd-isotopic composition of Recent lavas of Samoan OIB (Wright and White, 1987), Tongan boninite (Falloon et al., 1989), Lau Basin basalt (Volpe et al., 1988), and the Tonga-Kermadec arc (Ewart and Hawkesworth, 1987).

similar mantle seems to underly much of the northern part of the Lau-Tonga-Kermadec system.

These perspectives are consistent with the interpretation that an OIB-type mantle is present beneath arc systems of the Western Pacific. We recognize that combinations of subducted sediments, fresh and altered oceanic crust and OIB-seamounts could also yield these signatures, but if subduction were responsible for the enriched characteristics, such signatures should be stronger in the arc and would not lead to the isotopic homogeneity observed in intra-oceanic arc/back-arc systems. Application of Occam's Razor and the Principle of Least Astonishment leads us to favor the idea that the dominant control on the isotopic composition of these systems is contributions from large OIB reservoirs that must extend to the top of the asthenosphere beneath arcs.

Ewart, A.E., and Hawkesworth, C.J., 1987. J. Petrol. 28, 495-530.
Falloon, T.J., Green, D.H., and McCulloch, M.T., 1989. in Crawford, A.J. (ed.) Boninites Unwin Hyman, 357-395.
Gill, J., and Whelan, P., 1989. JGR 94, 4579-4588.
Hart, S.R., 1988. EPSL 90, 273-296.
Staudigel, H., Park, K.-H., Pringle, M., Rubenstone, J.L., Smith, W.H.F., and Zindler, A., 1991. EPSL 102, 24-44.
Volpe, A.M., Macdougall, J., and Hawkins, J.W., 1988. EPSL 90, 174- 186.
Wright, E., and White, W.M., 1987. EPSL 81, 151-162.

CORONAE: PLUMES ON VENUS

E.R. Stofan
California Institute of Technology, Jet Propulsion Laboratory, Pasadena, CA.

D.L. Bindschadler and G. Schubert
University of California, Los Angeles, CA.

Mantle plumes have been suggested to be significant to lithospheric heat transfer on Venus. Coronae, first identified in Venera 15/16 data of Venus (1-3), are thought to be one surface manifestation of mantle plumes or hotspots (4). Magellan data have revealed a large number of new coronae in previously unmapped regions of Venus, and the higher resolution of the Magellan data has revealed significant new information on the detailed morphology of these features (5).

Coronae are circular to elongate features with maximum widths of 160-1060 km, characterized by an annulus of concentric compressional and/or extensional features. Ridges and troughs in the annulus vary in length and tend to be spaced 5-15 km apart. Corona annulae vary in width from about 30 - 90 km. The interiors of coronae are geologically complex, and vary a great deal from corona to corona. Many coronae are characterized by interior radial graben, while others are dominated by volcanic flows and edifices. Most coronae are 0.5-2.0 km higher than the surrounding region and are surrounded by an annular moat. Coronae topographic profiles are that of domes, plateaus or plateaus with central topographic lows. A few coronae have virtually no topographic signature.

An evolutionary sequence for coronae was determined by detailed studies of the features in Venera 15/16 data (2, 3). Initially, coronae are characterized by uplift and radial fracturing. This is followed by volcanism, annulus and trough formation. In the latest stages of formation, topographic degradation and continued volcanism occur. This sequence and the basic morphologic and topographic characteristics of coronae are most consistent with formation by mantle plumes followed by gravitational relaxation.

The distribution of coronae and their relationship to other features that may be related to mantle plumes, such as highland regions, are currently being analyzed in the Magellan data. Coronae tend to form dominantly in clusters in lowland plains regions. They also tend to form near large volcanic shields and in regions associated with extensional deformation that are interpreted to form by mantle plumes. Coronae may represent transitional features between large-scale volcanic constructs/calderae and major highlands forming over upwellings.

Significant questions regarding the origin of coronae remain. These include the detailed nature of upwellings related to corona formation. What is the size of and the density (or temperature) anomaly associated with the "plume head" or rising diapir that causes the initial uplift? Do coronae often "self destruct" by volcanic flooding caused by pressure release melting of the rising diapir? Do the geological and morphological characteristics of coronae offer constraints on the source region for plumes on Venus?

References

1) V.L. Barsukov et al., JGR, 1986. 2) E.R. Stofan and J.W. Head, Icarus, 1989. 3) A. Pronin and E.R. Stofan, Icarus, 1990. 4) E.R. Stofan et al., JGR, in review, 1991. 5) S.C. Solomon et al., Science, 1991.

* Contributions to the work described here were made by the other members of the Magellan Corona Science Analysis Team: D.L. Janes, V.L. Sharpton, and S.W. Squyres.

Correlation between plate motion and tomography

Toshiko Takata and Don L. Anderson (Caltech, Pasadena, CA 91125)

The driving force of plate motions is considered to have a correlation with the upper mantle, but the correlation with the lower mantle is not clear. There might be a heat source in the lower mantle or on the top of the outer core, in addition to ridge spreading, or slab pull force that may originate in the upper mantle.

In this paper, seismic tomography at all depths, which represents the mantle heterogeneity and structure, and the plate velocities, crustal age and boundary spreading and convergence rate, which represent the plate motion, crustal thickness, and boundary position, respectively, are correlated in order to investigate the mechanism of the driving force of plate tectonics with respect to the mantle structure.

We used the method of Richards and Hager(1988) to obtain the correlations between two functions expanded with spherical harmonics.

Tanimoto(1990) model was used for the seismic tomography of the entire mantle. These data were expanded in terms of the spherical harmonics up to l=m=6 mode for 11 layers of the mantle.

For the correlation of plate velocity with tomography, we used the data of plate velocity of HS2-NUVEL1(Gripp and Gordon,1990). Vector direction of these data is ignored and this function is expanded up to l=m=6 with spherical harmonics(figure 1).

A high negative correlation in the lower mantle, a high negative correlation above 670km discontinuity and positive(above layer 5)-negative(layer 6,7)-positive(layer 10,11) correlation pattern in the lower mantle in l=4 are observed(figure 2). These results indicate that the lower mantle structure has also a correlation with plate motions, that 670km transitional boundary can be seen clearly in this correlation, and that there might be a three layers structure in the lower mantle in mode l=4.

For the correlation of crustal age with tomography, the crustal age of the oceans and the continents by Sclater et al.(1981) are used. Data points of crustal age are expanded with the same method as the case of the plate velocity(figure 3).

There is a high positive correlation in the upper mantle above the 670km discontinuity(figure 4). It might be related to the difference of mineralogy of continental and oceanic crust. The pattern of the positive correlation in l=3 and negative correlation in the higher modes in the lower mantle is somewhat opposite to the pattern in the upper mantle. This result might indicate the different pattern of the distribution of the horizontal anomaly of the compositional materials in the upper mantle from that in the lower mantle.

For the correlation of boundary rate with tomography, the spreading and convergence rate of NUVEL1 (DeMets et al. 1990) are used. The velocity is equal to zero at the non-boundary place, positive on the ridge, and negative on the trench, and absolute velocity is used to weight the boundary rate(figure 5).

A strong negative correlations in layer 4 which is the top of the lower mantle is observed(figure 6). There is also negative-positive-negative correlation in the lower mantle which can be seen in the case of the plate velocity in l=4. This might be related to the mantle convection structure as stated in the case of plate velocity.

From these analyses, three main results can be noted. One is a clear evidence of 670km discontinuity. The good correlation of the old crust and high seismic velocity in the upper mantle, the good correlation of slow plate velocity and high seismic velocity at the bottom of the upper mantle, and the high correlation of the boundary rate and tomography under the discontinuity support the existence of the 670km boundary of compositional material.

Secondary, the good correlation between the high seismic velocity and low plate velocity in the lower mantle suggests the existence of the correlation of the lower mantle to the plate motion.

Finally, in the lower mantle, three layers structure of the material anomaly can be seen with respect to the correlation of the plate velocity and the boundary rate with the tomography in $l = 4$. This indicates that the mantle convection might have three layers in the lower mantle with $l = 4$ mode.

References

DeMets et al.(1990) GJI, 101,425-478. Gripp and Gordon(1990) GRL, 17, 8, 1109-1112. Richards and Hager(1988) JGR, 93,7690-7708. Sclater et al.(1981) JGR, 86, 11535-11552. Tanimoto(1990) GJI, 100,327-326.

Figure Captions

Figure.1:Map of the plate velocity reconstructed from the coefficients of spherical harmonics up to $l = 6$.

Figure.2:The correlation between the plate velocity and the tomography. Horizontal axis is l mode and Vertical axis is the depth layer of the mantle(from 1:surface to 11:CMB). High positive correlations(high plate velocity and high seismic velocity, and vice versa) are expressed with the dotted area and negative correlations(high plate velocity and low seismic velocity, and vice versa) are expressed with the shaded area.

Figure.3:Map of the crustal age reconstructed from the coefficients of spherical harmonics up to $l = 6$.

Figure.4:The correlation between the crustal age and the tomography. High positive correlations(old crust and high seismic velocity, and vice versa) are expressed with the shaded area, and negative correlation (new crust and low seismic velocity, and vice versa) are expressed with the dotted area.

Figure.5:Map of the boundary velocity reconstructed from the coefficients of spherical harmonics up to $l = 6$.

Figure.6:The correlation between the boundary velocity and the tomography. The representations are the same as figure 5.

Figure.1

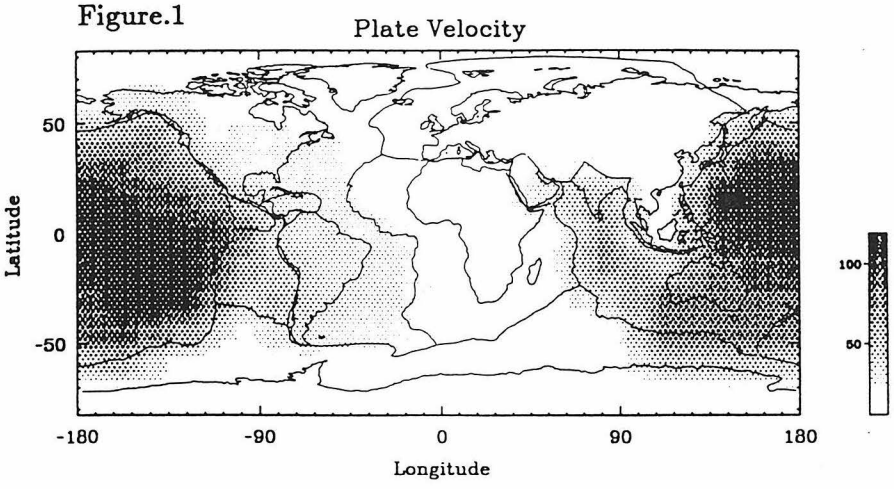

Figure.2

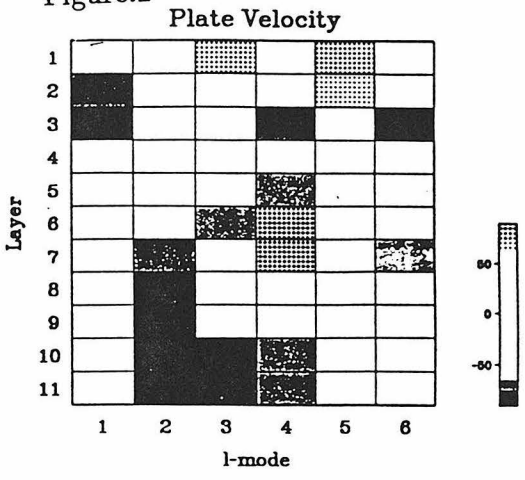

Figure.3

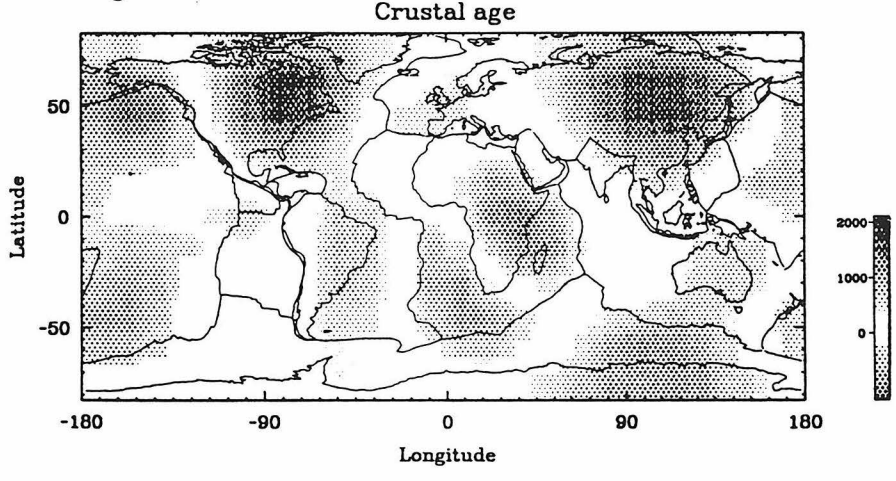

Figure.4

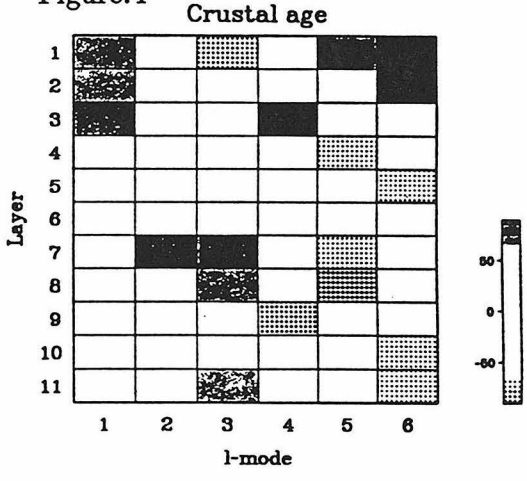

Figure.5

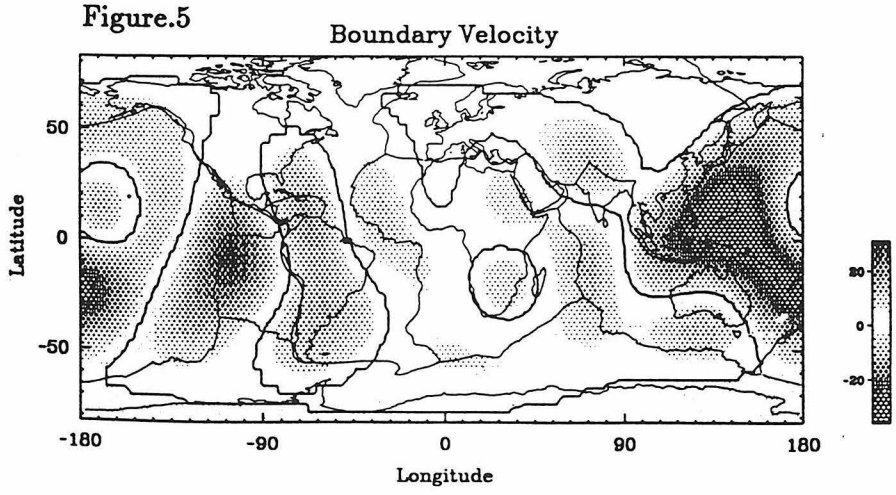

Figure.6

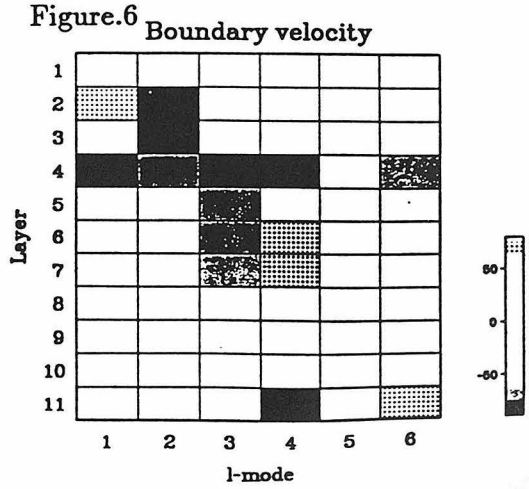

Long wavelength characteristics of Earth structure

Toshiro Tanimoto and Hiroshi Inoue

Seismological Laboratory 252-21
California Institute of Technology

Considerable efforts have been paid to analyse digital seismic network data and ISC (International Seismological Center) data during the last decade. Although there are still uncertainties in seismic maps, some consistent results for long wavelength characteristics of Earth's heterogeneity have emerged. We briefly summarize those features in this paper.

Figure 1 shows spectral amplitudes of mantle P-wave heterogeneity as a function of harmonic degree (horizontal wavenumber). The results are from Inoue et al. (1990) based upon ISC data and each line corresponds to a particular depth. As a reference, a line for l^{-1} is given by dash line. Geoid is shown by a chain line. The figure demonstrates that seismic heterogeneity spectra (amplitude) varies as l^{-1}, while geoid varies as l^{-2} (Kaula's rule). The geoid data, however, may not be relevant to deep structure at least for higher l (>10). This is because variation of topography can explain this feature. Topography produces a surface density anomaly of ρh, where ρ and h are density and topography. The geoid can then be written $N=(4\pi Ga)/g(2l+1)*\rho h$ and since topography h varies as l^{-1}, l^{-2} dependence is expected for N. Furthermore, geoid and topography have fairly good correlation as shown in Figure 2 (from l=2 to 36), which supports the surface origin of geoid signal for higher l. Note that SEASAT maps generally support this. The l^{-1} dependence seems to be an important feature of mantle heterogeneity that must be explained by any modeling efforts.

Figures 3a and 3b shows the variation of total heterogeneity amplitudes as a funciton of depth. Variations from five studies are shown, all of which show peaks at top, decrease with depth and a secondary peak at the bottom. Most of lower mantle shows relatively small heterogeneity. There are a factor of few differences among various studies but overall trend seems consistent. Locations of boundary layers are indicated at top and bottom of the mantle in these figures, and the figure also indicates that average level of heterogeneity is about twice as much higher in the upper mantle than in the lower mantle. These results must be further confirmed with more recent results, but place an important constraint on the differences between upper and lower mantle.

Since overall spectra of heterogeneity follow l^{-1}, lower harmonic components are of considerable importance. We have noted that $l=2$ components are generally the largest throughout the mantle; but the pattern of anomaly produced by $l=2$ components are quite different between upper and lower mantle. Correlation among 11 layers in the mantle, for which 1 is the shallowest and 11 is the bottom layer (D"), are given in Figure 4. The results from two models, MDLSH in Tanimoto (1990) and M84A (Woodhouse'and Dziewonski, 1984) plus L02.56 (Dziewonski, 1984) are shown here. White circles denote positive correlation and black negative correlation. Circles along the diagonal components are 1. Note the lack of correlation or negative correlation between layers 1-4 and 5-11. It is important to note that the largest component of the model ($l=2$) does not show correlations.

Depth slices at the equatorial plane are shown in Figures 5a and 5b. Figure 5a contains components $l=1$ to 3, while Figure 5b contains $l=1$ to 6. Dark areas are fast velocity and white areas are slow. The figures basically support that locations of fast velocity anomlies in upper and lower mantle are shifted with respect to each other. It seems to suggest that there are important qualitative differences between upper and lower mantle.

Figure 1: Spectral amplitudes of heterogeneity are plotted as a function of harmonic degree (l). As a reference, the diagonal dash line for l^{-1} is shown. Geoid follows l^{-2} trend, the well-known Kaula's rule. Higher harmonic parts ($l>10$) can be explained simply by topography. Note the good correlation of geoid and topography in Figure 2.

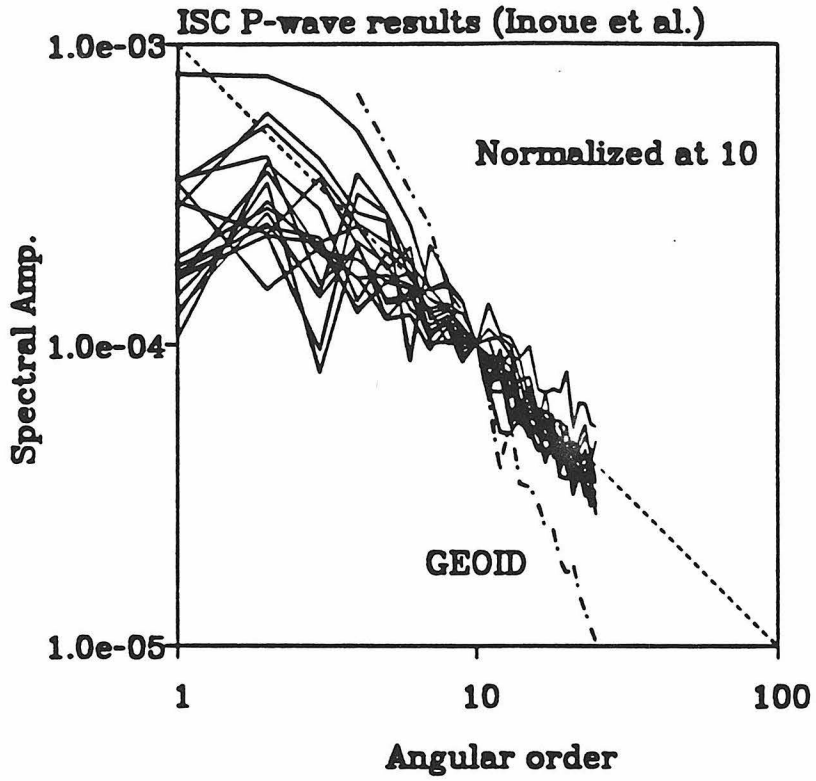

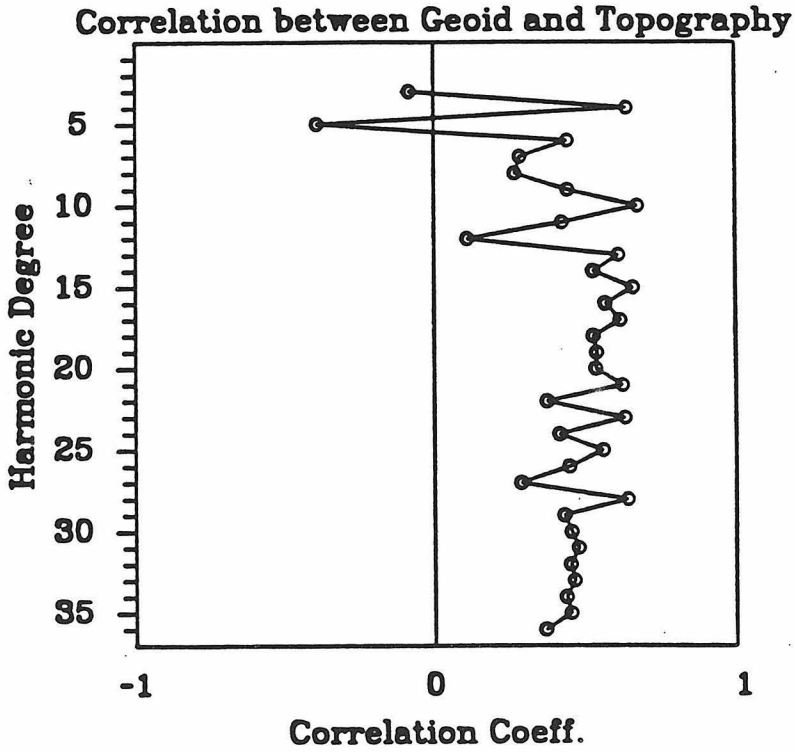

Figure 2: Correlation coefficients as a funciton of l between geoid and topography.

Figure 3a: RMS variation (total heteorgeneity) as a function of depth. Two models are from Tanimoto(1990,MDLSH) and Inoue et al.(1990). Note the peaks both at the top and the bottom of the mantle, which suggests the locations of boundary layers there.

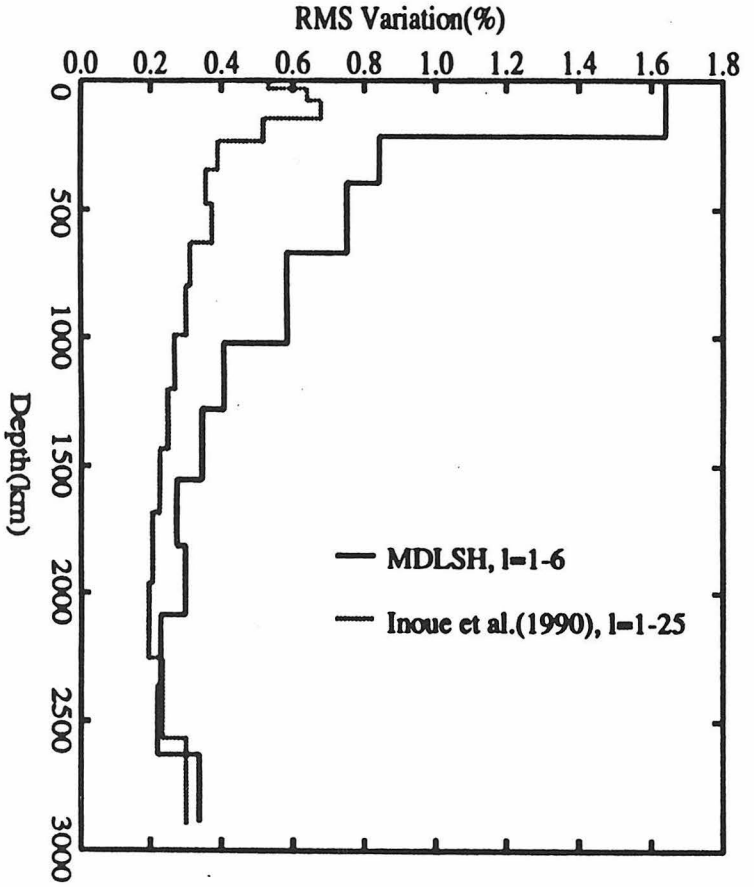

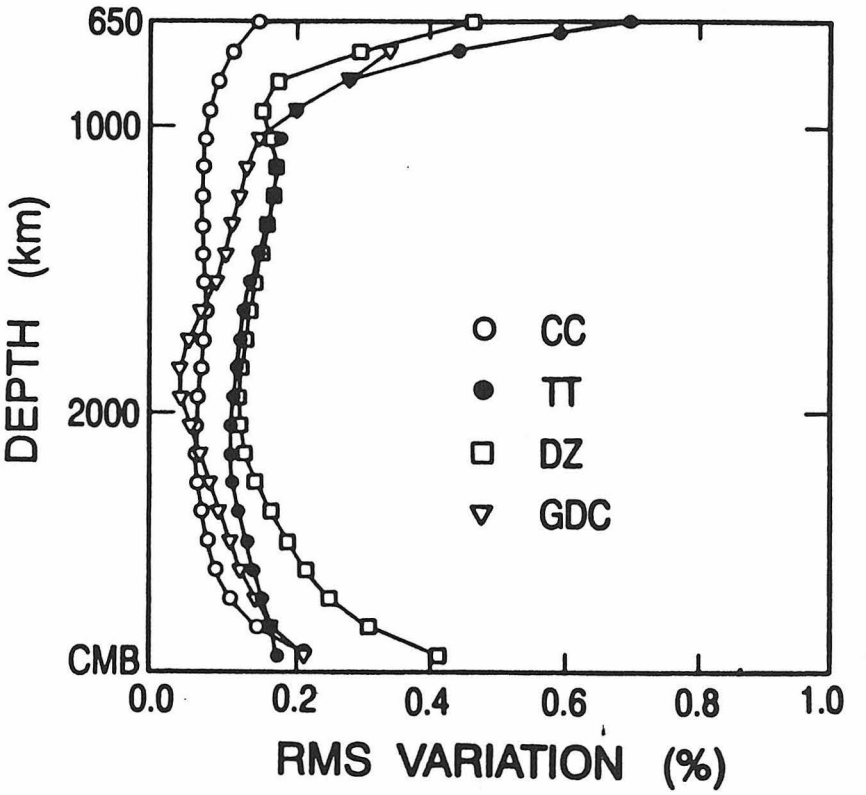

Figure 3b: RMS variation of four models in the lower mantle. CC is Clayton and Comer (1983), TT is the same with MDLSH, DZ is L02.56 (Dziewonski, 1984) and GDC is by Gudmundsson et al.(1990). Note that all models show small heterogeneity in the mid- lower mantle.

Figure 4: Cross correlations of l=2 component among 11 layers in the mantle. The eleven layers are from the top (1) to the bottom (11) of the mantle and have thicknesses of about 250-300 km. Both MDLSH and composite M84A plus L02.56 model demonstrate the *lack* of correlation between upper and lower mantle.

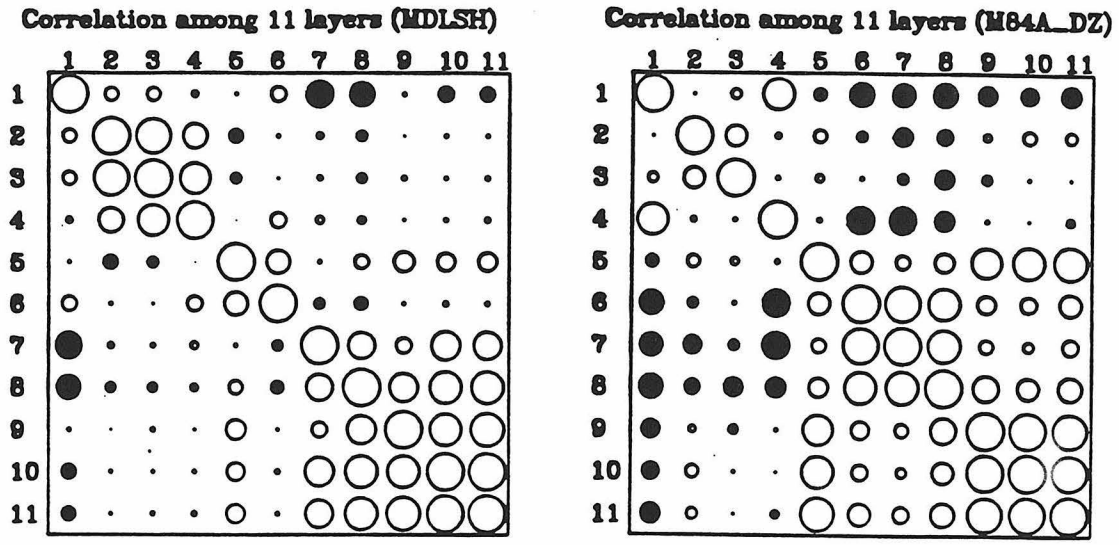

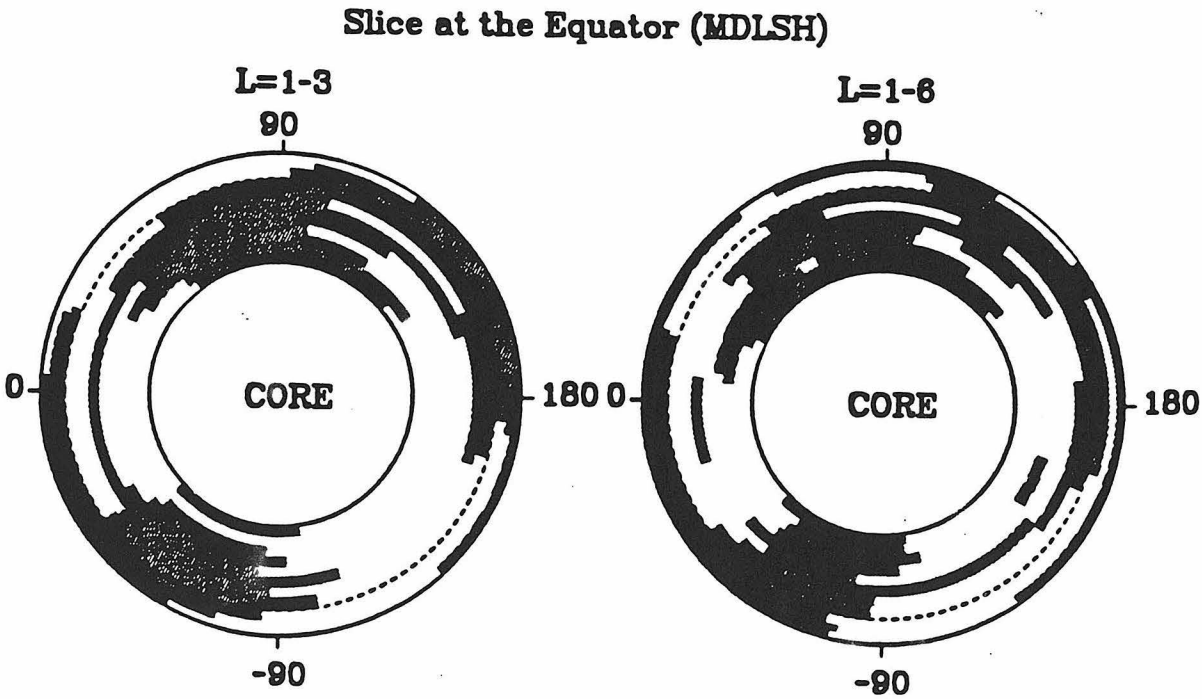

Figure 5a and 5b: Depth cross sections of MDLSH at the equator. The left figure contains spherical harmonic components from l=1 to 3, while the right figure contains from l=1 to 6. Because of the l^{-1} dependence of spectra, those low harmonic components are dominant. Dark areas are fast velocity and white areas are slow. It is clear that fast velocity anomalies in the lower mantle are shifted with respect to those in the upper mantle.

MANTLE PLUME VOLCANISM AND THE FORMATION OF ONTONG JAVA PLATEAU

John A. Tarduno
Scripps Institution of Oceanography, La Jolla, California 92093-0215
William V. Sliter
U.S. Geological Survey, Menlo Park, California 94025
Helmut Mayer
Scripps Institution of Oceanography, La Jolla, California 92093-0220
Ocean Drilling Program Leg 130 Shipboard Scientific Party

Abstract. Data from Leg 130 of the Ocean Drilling Program suggest that much of Ontong Java Plateau formed in a brief (< 3 m.y.) portion of the Early Aptian (~121-124 Ma). Eruption rates as much as one order of magnitude greater than those of continental flood basalt provinces are implied. The data are compatible with a mantle plume origin, possibly forming in response to thermal characteristics of the lower mantle recorded by long-term (100 m.y.) variations in geomagnetic reversal frequency. The high rate and massive volume of volcanism may have driven oceanic anoxia and contributed to CO_2 buildup, the latter creating the Cretaceous greenhouse climate.

1. Introduction

Recent studies of continental flood basalts have isolated two aspects important in understanding their potential relationship to mantle processes. Continental flood basalts appear to record the oldest volcanism on tracks of hotspots, suggested to have sources fixed in the mantle, and the duration of volcanism requires eruption rates much greater than any contemporary volcanic process (*1*). To explain these observations, a model has been proposed by several authors suggesting that continental flood basalts form when the "head" of a deep mantle plume initially penetrates the lithosphere. A critical test of this model requires detailed information from the ocean basins since the initiation of hotspots by mantle plumes in the past should have also left a profound mark on the oceanic lithosphere. The obvious candidates for records of oceanic hotspot initiation are Cretaceous oceanic plateaus of the Pacific basin, some of which backtrack to active hotspots. Previous deep sea drilling of these plateaus, however, has failed to penetrate deeply enough to evaluate adequately the nature of basaltic basement. For example, thick flows that characterize rapid eruptions had never been recovered. Data constraining the duration of volcanism independent of the mantle plume model were unavailable. Leg 130 of the Ocean Drilling Program recently drilled two basement sites (Sites 803 and 807) on the largest of the oceanic plateaus, Ontong Java, to address some of these questions. For the first time a thick (28 m) flow was recovered yielding physical evidence for flood basalt volcanism comparable to that of the major continental flood basalt provinces. In addition, new paleomagnetic and paleontologic data can be used to date the initiation and duration of volcanism.

2. Initiation and Duration of Volcanism

Drilled in a small basement graben that likely sheltered the site from early erosion, Site 807 provides the best paleontological (minimum) basement age derived from overlying sediments. Limestone directly overlying basalt yield foraminifera of the *Globigerinelloides blowi* Zone indicating an Early Aptian age. This age is similar to the ages of sediments overlying basement at DSDP Sites 289 and Sites 288 on the plateau. Paleomagnetic analyses of basalts recovered at Sites 807 indicate constant normal polarity consistent with magnetization during the Cretaceous Normal Polarity Superchron. Excluding the possibility of the removal of reversed polarity chron M0, a possibility minimized by the basement structure at Site 807, these new data suggest that much of the Ontong Java Plateau (OJP) formed in a brief period (< 3 m.y.) of the Early Aptian. The volume of the Ontong Java Plateau has been calculated as exceeding 50 x 10^6 km^3(*2*). Combined with our estimates of OJP volcanism, this suggests an eruption rate of some 17 km^3/yr, more than one order of magnitude greater than eruption rates calculated for continental flood basalt provinces such as the Deccan Traps. If correct, the rapid and massive eruption of OJP should be recorded at sites close to the plateau as intrusives and extrusives. Drilling of Jurassic oceanic crust surrounding Ontong Java Plateau in the Nauru Basin has provided evidence of such activity, which has been dated as occurring during Early Aptian times (*3*). Importantly, the volcanism younger than basement appears limited to the Early Aptian providing addition support for the cataclysmic formation of the Ontong Java Plateau.

3. Geomagnetic Reversal Frequency and Plume Volcanism

Geomagnetic reversal frequency can act as a proxy measure of lower mantle conditions since mantle cooling controls the thermal characteristics of the core where the geodynamo is maintained. If mantle plumes are generated in the lowermost mantle, it may be useful to examine this proxy measure to understand the generation of a mantle plume possibly responsible for the Ontong Java Plateau. Reversal frequency defines a long term (100 m.y.) variation which may reflect long-term mantle convection (*4*). This variation is largely unaffected by recent changes in geomagnetic time scales (Fig. 1). When the timing of Ontong Java volcanism is compared with reversal frequency, it is seen to fall precisely at the beginning of the Cretaceous Normal Polarity Superchron. Unlike models which seek to relate plume volcanism to times of increasing reversal frequency or as the causal factor in stopping reversals during the Cretaceous Normal Polarity Superchron, it is proposed that OJP volcanism may reflect a long term variation in mantle convection which enters a mode where plume generation is encouraged. In fact at least two other potential plume events (Manihiki Plateau, Rajmahal Traps-Kerguelen Plateau) also occur during the Early Aptian.

4. Ontong Java Eruption and Cretaceous Global Change

Many authors have noted the occurrence of a broad period of increased volcanism during the Cretaceous Normal Polarity Superchron. The new data from ODP Leg 130 suggest much of this volcanism is related directly to the eruption of the Ontong Java Plateau during a brief portion of the Early Aptian. It is likely that this rapid and massive volcanism influenced Cretaceous global climate. We briefly list some poten-

tial consequences: 1. OJP volcanism corresponds precisely with anoxic facies in the Tethys (Selli horizon) that have been shown to be global by paleomagnetic (*5*) and paleontological correlations (*6*). When mantle plumes penetrate oceanic lithosphere they may drive oceanic anoxia through either rapid sea level change or ocean chemistry change. 2. The rapidity of volcanism and release of volatiles may have contributing to Cretaceous greenhouse conditions. 3. Although larger than the Deccan Traps, a major extinction event does not fall within the duration of OJP volcanism. Mass extinction events may need an addition external driving force and/or the damage to the biosphere is limited when mantle plumes first erupt in the oceans.

5. Conclusions and Speculation

1. Much of Ontong Java Plateau formed in less than 3 m.y. representing the majority of previously postulated Pacific mid-Cretaceous volcanism.
2. Eruption rates were several times to an order of magnitude larger than continental flood basalt provinces.
3. Long term (100 my.) cycles of mantle convection appear to control long-term variations in reversal frequency and possibly the sporadic occurrence of plume volcanism.
4. The rate of OJP volcanism contributed to oceanic anoxia and CO_2 buildup, the latter resulting in the Cretaceous greenhouse climate.

6. References

1. M.A. Richards, R.A. Duncan and V.E. Courtillot, *Science* **246**, 103 (1989).

2. G. Schubert and D. Sandwell, *Earth and Planet. Sci. Lett.* **92**, 234 (1989).

3. R. Moberly *et al.*, *Init. Rep. Deep Sea Drilling Proj.* **89**, 167 (1986) .

4. R.T. Merrill and P.L. McFadden, *Science* **248**, 345 (1990).

5. J.A. Tarduno, W.V. Sliter, T.J. Bralower, M. McWilliams, I. Premoli Silva, J. Ogg, *Geol. Soc. Am. Bull.* **101**, 1306 (1989).

6. W.V. Sliter, *Geology* **17**, 909 (1989).

7. P.L. McFadden and R.T. Merrill, *J. Geophys. Res.* **89**, 3354 (1984).

8. W.B. Harland, W.B., A.V. Cox, P.G. Llewellyn, C.A.G. Pickton, A.G. Smith and R. Walters, 131 pp., *A Geologic Time Scale*, (Cambridge Univ. Press, New York, 1982).

9. W.B. Harland, R.L. Armstrong, A.V. Cox, L.E. Craig, A.G. Smith and D.G. Smith, *A Geologic Time Scale 1989*, 263 pp., (Cambridge Univ. Press, New York, 1990).

10. J.A. Tarduno, J.A., *Geology* **18**, 683 (1990).

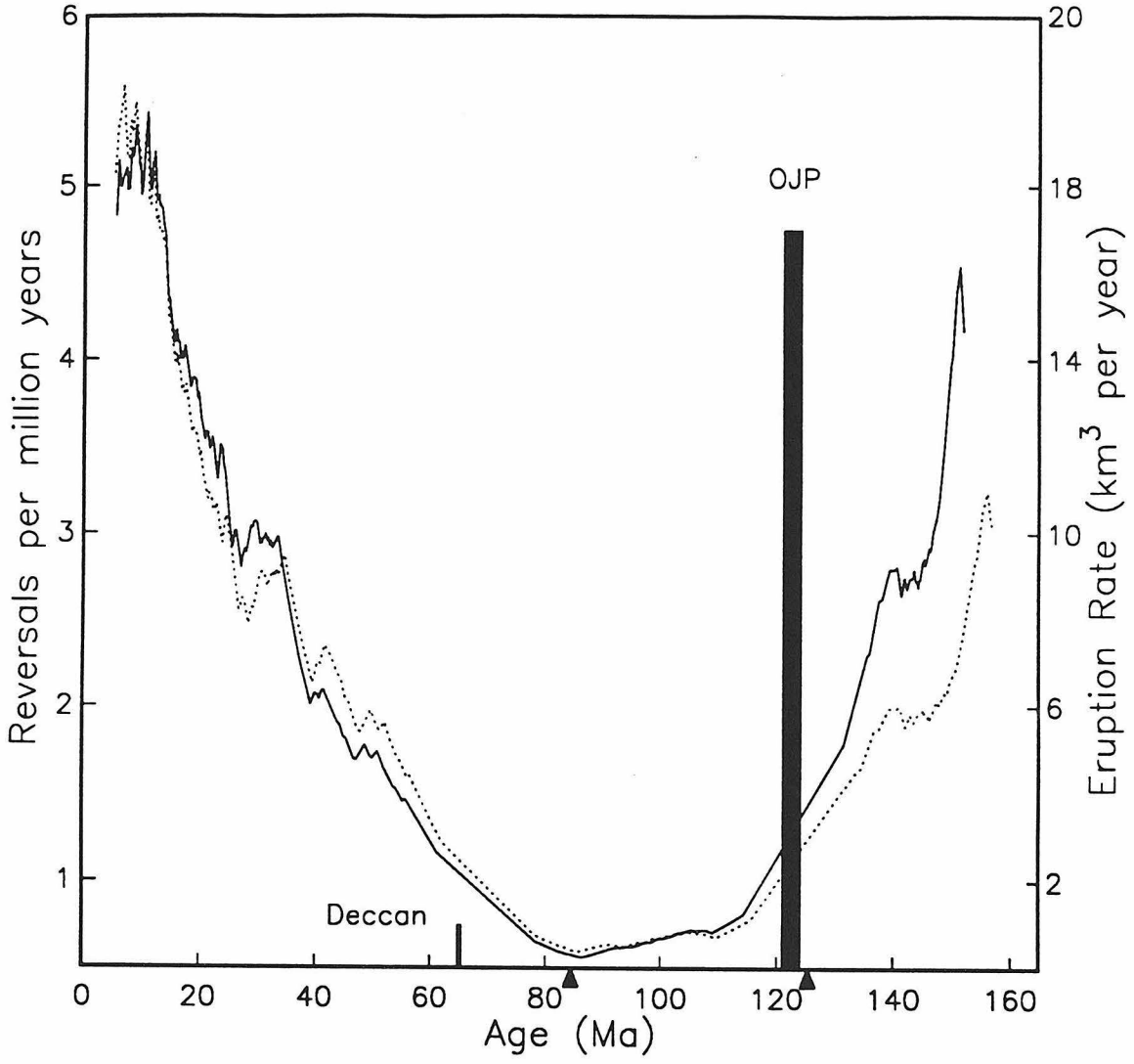

Fig. 1. Geomagnetic reversal rate per million years versus age for two recent time scales with the addition of a short polarity event in the Late Aptian (*10*). Frequency calculated by a sliding window of 25 polarity intervals shifted by one reversal for each estimate modified from (*7*). Solid line, Harland *et al.*, 1989 (*9*); dotted line, Harland *et al.*, 1982 (*8*). Solid triangles mark location of the Cretaceous Normal Polarity Superchron using the Harland *et al.*, 1989 time scale. Also shown versus the Harland *et al.*, 1989 time scale is eruption rate for the Deccan Traps (*1*) and Ontong Java Plateau.

DUPAL anomaly in the Sea of Japan: A plate recycling model for OIB sources

Mitsunobu Tatsumoto, US Geological Survey, MS 963, Box 25046, Denver, CO 80225, U.S.A.

Abstract: Volcanic rocks from the eastern Eurasian plate margin have enriched isotopic signatures. Ulreung and Dog, two islands in the sea of Japan, show typical DUPAL characteristics with extremely high Δ 208/204 Pb (up to 160) and enriched Nd and Sr isotopic compositions (ε_{Nd} = -3 to -5, $^{87}Sr/^{86}Sr$ = ~0.705). This is the first discovery of a typical DUPAL signature in the northern hemisphere. The Δ 208/204 Pb values are higher than those associated with the DUPAL anomaly in the southern hemisphere (up to 140). These findings support the idea that EMI originates from the subcontinental mantle lithosphere. We suggest a model which employs shallow plate-recycling as asource of oceanic basalts.

In an attempt to account for our Sr-Nd-Pb isotopic data, we will use Hart's nomenclature [1] as a frame of reference in the subsequent discussion: depleted mid-oceanic rodge basalts (MORB) mantle (DMM), enriched mantle (EMI & EMII), and high 238U/204Pb (HIMU). DUPAL is the enriched component (EMI) with low $^{206}Pb/^{204}Pb$, $^{87}Sr/^{86}Sr$ >0.705 and Δ 208/204 Pb >+60. The origin of the DUPAL isotopic anomaly found in basalts from the Indian Ocean [2] is still in dispute. The major interpretations have emphasized local mantle enrichment, delaminated subcontinental lithosphere, and (more or less) pristine deep mantle. McKenzie and O'Nions [3] speculated that the EMI component may have originated from the mantle portion of the lithosphere that was delaminated from the thickened continental lithosphere and incorporated into the convective flow. On the other hand, because continental mantle xenoliths do not show high $^{208}Pb/^{204}Pb$ values with corresponding less radiogenic $^{206}Pb/^{204}Pb$, Hart [1] rejected their mantle lithosphere hypothesis and placed the source of EMI at the core/mantle boundary.

Two oceanic plates are being subducted under the Japanese arc: the Pacific plate beneath NE Japan, and the Philippine Sea plate beneath SW Japan. Development of a deep seismic zone is clearly observable for the Pacific plate, but it is not clear for the Philippine Sea plate. The crustal thickness increases from NE to SW. The Sea of Japan is considered to be a typical back-arc basin. A continental plateau extends eastward from the middle portion of the Korean Peninsula toward the Yamato Bank. We have studied Sr, Nd, and Pb isotopes in volcanic rocks from Ulreung and Dog islands on the flank of the plateau, and dredged samples from a buried ridge (Yamato Basin Ridge; YBR) in the sea of Japan [4]. The results are compared with those from Japan and northeastern China.

The Nd and Sr relations and Pb isotopic compositions from this area are compared in figures 1and 2. The data from the Japanese volcanic rocks are clearly separated into two compositional groups: a depleted composition from NE Japan and an enriched composition from SW Japan. The Nd-Sr data from NE China do not plot in the enriched field as an extension of the data from Japanese rocks as $^{206}Pb/^{204}Pb$ decreases from NE Japan to inland China, but instead they show a large variation along the mantle array from MORB-like to near bulk-earth compositions. The Ulreung and the Dog rocks (Ul-Dog) plot close to the SW Japanese data. The ε_{Sr} values of the Ul-Dog rocks are all positive (except one sample) and all ε_{Nd} values are negative. Dredged YBR samples show depleted characteristics (plotting close to Hawaiian basalts and Mariana back-arc basalts) and the ε_{Nd} and ε_{Sr} are positive and negative, respectively. It is clear that all the $^{208}Pb/^{204}Pb$ values from the eastern Eurasian continental margin are distinctly higher than the data trend of oceanic basalts from the northern hemisphere, NHRL [5]; among them, Ul-Dog rocks are extremely high in $^{208}Pb/^{204}Pb$ values.

The Δ 208/204 Pb versus $^{87}Sr/^{86}Sr$ and ε_{Nd} are plotted in Figure 3. It is distinctive that Δ 208/204 Pb values of Ul-Dog basalts are extremely high (120 to 150) compared to SW Japan (40 to 130) and Chinese rocks (50 to 100). The Δ 208/204 Pb values of the Ul-Dog samples are larger than in those of DUPAL rocks from the southern hemisphere (60 to 140). On the other hand, Δ 208/204 Pb of Wudalianchi leucite basalts, located far to the west of the Tan-Lu fault in northeastern China, are only 70 to 80 [6], indicating that the DUPAL anomaly is most pronounced at the Eurasian continental margin. High $^{208}Pb/^{204}Pb$ values are also found from high P-TiO_2 basalts of the Parana flood basalt of Brazil. We interpret the high $^{208}Pb/^{204}Pb$ values to be a continental signature, resulting from time-integrated high Th/U ratios in the source in contrast to MORB source with low Th/U ratios over a comparable timespan.

We may assume that oceanic and continental asthenospheres are similarly depleted and that their isotopic signatures are not grossly different (although they both are isotopically heterogeneous). They may be similar to PREMA (prevalent mantle) with an average of $^{206}Pb/^{204}Pb \approx 18.2$-$18.4$ [8]. We may further assume that $^{206}Pb/^{204}Pb$ values can be used as an index that reflects the contribution of (old) sub-continental mantle lithosphere to asthenospheric magmas, and that the contributions increase from the Pacific front toward inland China. Then, it can be said that the $^{206}Pb/^{204}Pb$ value of 18.0 for the dredged YBR basalts reflects the sub-continental asthenosphere with little contamination from sub-continental mantle lithosphere at the spreading ridge in the Sea of Japan. On the other hand, the $^{206}Pb/^{204}Pb$ value of 17.0 for Wudalianchi (China [6]) may indicate a larger contribution from an old lithospheric mantle to the basalts. Because the $^{87}Sr/^{86}Sr$ values of Ul-Dog samples are not as high as Samoa and Society island rocks [9], and the $^{206}Pb/^{204}Pb$ values are lower and $^{208}Pb/^{204}Pb$ values are very high, it would be logical to suspect the involvement of an early (>1 b.y.) differentiated, enriched part of the lithosphere. However, Hart [1] rejected this idea, because xenoliths in continental basalts do not show high $^{208}Pb/^{204}Pb$ characteristics.

Results of our Chinese xenolith study [10] are indeed consistent with Hart's contention . Xenoliths and megacrysts (spinel peridotites) from Kuandian, Hanluoba, and Minxi in eastern China show lower $\Delta^{208/204}$ Pb values than the host basalts. Because these xenoliths are estimated to originate from about 100 km depth, these results indicate that upper parts (100-150 km) of the sub-continental lithospheric mantle or keel of the continental crust have a less distinct EMI signature. Thus, we conclude that lower portions of the mantle lithosphere have had high Th/U ratios for a long time (>1 Ga) and, consequently, high $^{208}Pb/^{204}Pb$ values have been acquired.

The stabilization of the crust at the Sino-Korean paraplatform occurred in Archean time (~2.7 Ga), and the sub-continental lithosphere has grown since then. A simple two stage calculation indicates that if a source with $^{238}U/^{204}Pb$ (μ) = 8.1 and $^{232}Th/^{238}U$ (κ) = 3.8 differentiated at 1.0 Ga, then μ = 9.3 and κ = 6 are required for the second stage in order to reach the observed Pb isotopic composition. If the differentiation was at 2.7 Ga from a μ=8, and κ=3.8 source, then μ=8.8 and κ=4.6 are required. In any case, these calculations indicate prolonged high κ values to account for the observed high $^{208}Pb/^{204}Pb$ values.

It is not certain how the EMI component was created near the subduction system, whether the cause was invasion of subducted material, magmatism, or metasomatism. Oceanic sediments near the trench have low U/Pb and high Th/U ratios compared to ordinary crustal values. It may be possible that continental lithosphere was metasomatized with slab-derived fluids or subduction-related processes that caused Th enrichment in the lower portion of mantle lithosphere. However, it must be granted that metasomatism had occurred at an earlier time (>1 Ga), probably during continental accretion and not during the present subduction process. We prefer the explanation that mantle differentiation may have caused heterogeneous local enrichment of Th (~20%) relative to U in the lower portion (~200 - 250 km) of the mantle lithosphere, such as by underplating of eclogite layers that represent trapped basaltic magma.

Plate recycling model : The lithosphere is a relatively cool layer attached to the crust and overlying the convective asthenospheric mantle. From the isotopic similarity of oceanic and continental basalts, it is commonly thought that there is small chemical difference between continental and oceanic asthenosphere and that the lithosphere slides upon the asthenosphere (continental drift). The thickness of the lithosphere is ~100 km for oceanic regions and up to 200-250 km for stable continents. It is commonly accepted that the EMII component is continental crustal material, recycled via oceanic sediments [11]. Above, we found that EMI exists at a lower portion of the sub-continental lithosphere at the eastern Eurasian continental margin. We believe this lower portion is the source for the EMI component. Our proposal is similar to that of McKenzie and O'Nions [3]; the source of EMI is a deep sub-continental mantle lithosphere that is thickened by plate collision. However, the mantle lithosphere at a continental margin must be different, instead of thickened middle continental deep mantle lithosphere. Also, we believe that an important feature of our proposal is that the lithosphere at the continental margin may have a better chance to be incorporated into the convective mantle system. It is interesting that the EMI signature has been reported (at least in $\Delta^{208/204}$ Pb values) for basalts from Parana [7] and Deccan [12] as well as in the Columbia basalts [13], all of which erupted at or near continental margins. This observation strongly supports our contention that EMI is stored in the sub-continental mantle near continental margins and is not from a slightly modified primitive bulk-earth component stored for a long time without recycling in a core/mantle boundary layer.

As a consequence, we propose that the sources for the three components required to account for the isotopic characteristics of oceanic basalts are recycled components: continental crustal materials for EMII, perhaps via oceanic sediments; a lower sub-continental mantle lithosphere for EMI; and a high U/Pb oceanic crust for HIMU. The oceanic lithosphere with the other two components (EMI & II) has been subducted into the mantle over geologic time and has formed a layer such as the mesosphere boundary layer [14] or a megalith

[15]. We envision a mantle model similar to that proposed by Allegrè and Turcotte [14], except that a delaminated mid-continental mantle lithosphere is the source for EMI (Fig. 4). We maintain our previously proposed whole Earth differentiation model [16, 17] and that the lower portion of the mantle is more depleted. Ocean island basalts (OIB) originate through mixing of diapirs from the mesosphere boundary layer with depleted upper mantle material. The 1.8 Ga Pb isotope trend observed for MORB [16] may be caused by mixing DMM with melt from recycled lithospheric components.

REFERENCES:

[1] Hart, S. R. (1988) Earth Planet. Sci. Lett. 90, 273-296. [2] Dupré, B. and Allegrè C. J. (1983) Nature 303, 142-146. [3] McKenzie, D. and O'Nions, R. K. (1983) Nature 301, 229-231. [4] Nakamura Y. and Tatsumoto M. (1991) Geochim. Cosmochim. Acta (submitted). [5] Hart, S.R. (1984) Nature 309, 753-757. [6] Basu, A. R., Wang J.-W. Huang W. K., Xie G.-H., Tatsumoto, M. (1991) Earth Planet Sci. Lett. (in press). [7] Hawkesworth, C. J., Mantovani M. S. M., Taylor P. N., and Palacz Z. (1986) Nature, 322, 356-359. [8] Zindler, A. and Hart, S. (1986) Annu. Rev. Earth Planet Sci. 14, 493-571. [9] White W. M. and Hofmann A. W. (1982) Nature 296, 821-825. [10] Tatsumoto M., Basu, A. R., Wang J.-W. Huang W. K., Xie G.-H. (1991) in prep. [11] Hofmann A. W. and White W. M. (1982) 57, 421-436. [12] Allegre C. J., Dupre B., RichardP.,rousseau D., and Brooks C. (1982) Earth Planet. Sci. Lett. 57,85-92. [13] Church S. G. (1985) Bull. Geol. Soc. Am. 96, 676-690. [14] Allegrè C. J. and Turcotte, D. L. (1985) Geophys. Res. Lett. 12, 207-210. [15] Ringwood A. E. (1982) J. Geol. 90, 611-643. [16] Tatsumoto, M. (1978) Earth and Planet. Sci. Lett. 38, 63-87. [17] Anderson D. L. (1983) J. Geophys. Res. 88, B41-B52.

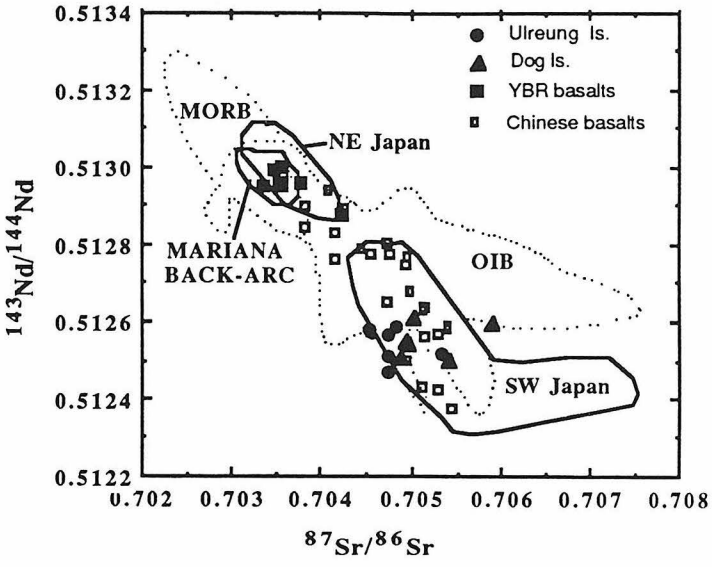

Figure 1. Nd versus Sr diagram for rocks from the eastern Eurasian plate margin.

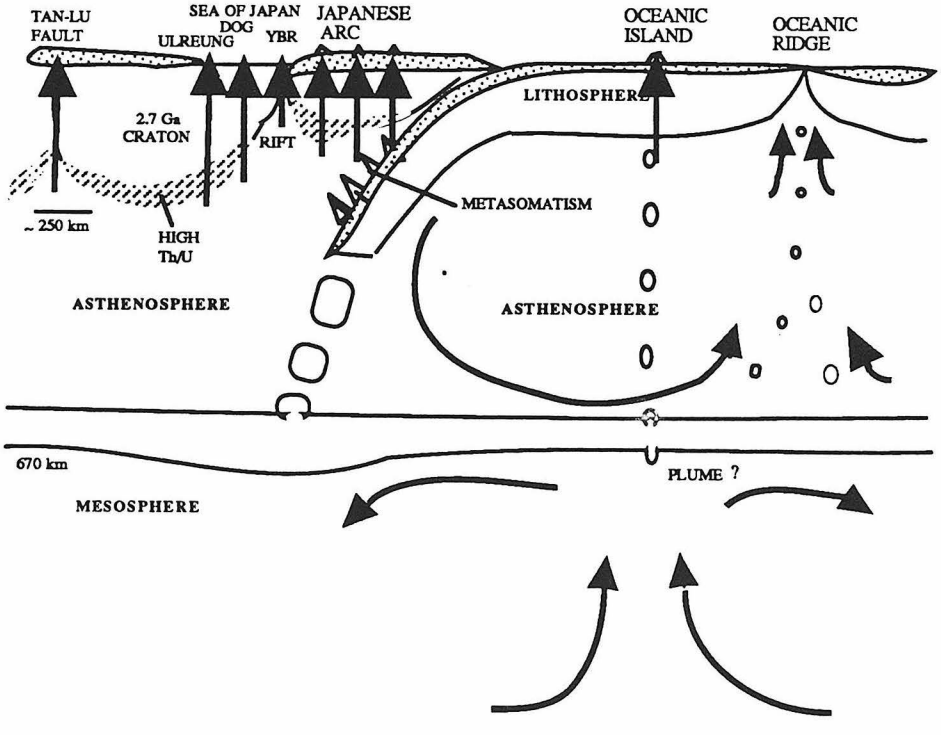

Figure. 4. Sschematic diagram illustrating plate recycling.

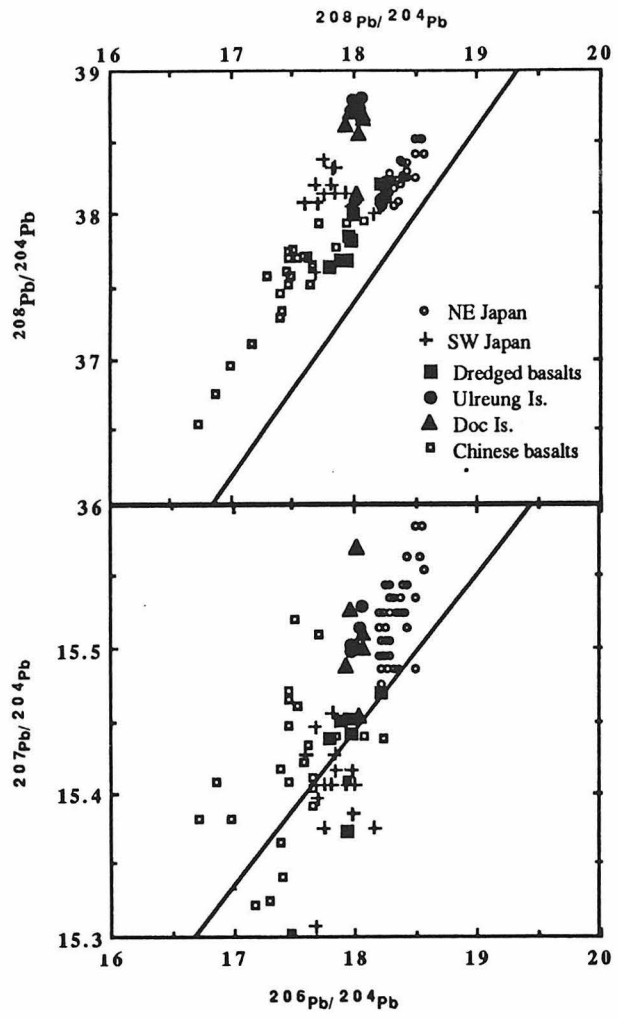

Figure 2. Combined diagram of $^{207}Pb/^{204}Pb$ and $^{208}Pb/^{204}Pb$ versus $^{206}Pb/^{204}Pb$.

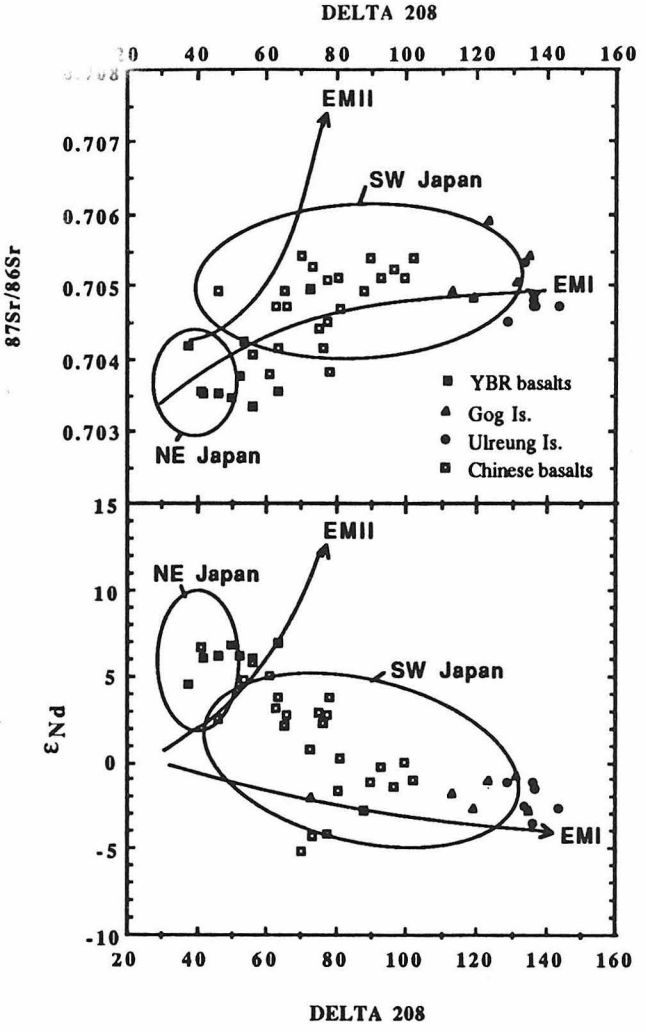

Figure 3. $^{87}Sr/^{86}Sr$ and ε_{Nd} versus $\Delta^{208}Pb/^{204}$ Pb plot for volcanic rocks from the eastern Eurasian plate margin.

Convective Evolution of a Chemically-Stratified Fluid Heat from Below: Application to Mixing Within the Upper Mantle

Micol Todesco
Frank J. Spera

Department of Geological Sciences and Institute for Crustal Studies, University of California, Santa Barbara, CA 93106

The possibility that the upper mantle at depths less than 670 km is chemically as well as mineralogically layered has been repeatedly and extensively discussed in the past 20 years. One idea is that sublithospheric upper mantle above 400 km is dominantly harzburgitic and of relatively low density compared to majoritic and clinopyroxene-rich piclogite which occupies the transition region from 400 to 670 km depth. We have studied the gravitational stability of the "harzburgite over piclogite" arrangement (light above heavy) in order to better understand the convective mixing dynamics of a two-layer upper mantle when heated from below. The calculations are simplified by ignoring the effects of compressibility, viscous dissipation, phase change and three-dimensional effects. The aspect ratio of the domain is 3:1 and boundary conditions have been chosen to approximate conditions in the sublithospheric mantle at depths between 100 and 670 km. The dimensionless parameters of this problem include the thermal Rayleigh number based on the heat flux into the piclogitic layer ($Rq = \alpha g q d^4 / \kappa k \nu$) , the ratio of the chemical to thermal buoyancy ($R\rho = (\Delta\rho/\rho_0)k/\alpha q d$) and the temperature and composition-dependence of the viscosity of the fluid assumed to be Newtonian. Here α, g, d, κ, k, ν, $\Delta\rho$, ρ_0 represent the expansitivity, gravity, total depth, thermal diffusivity, thermal conductivity, kinematic viscosity, isothermal difference in density between the two layers and density of the piclogitic layer, respectively. The upper boundary of the computational domain (the asthenosphere-lithosphere contact) is considered rigid whereas the bottom boundary is slippery; all boundaries are impermeable with respect to heavy component. Three measures of the extent and thoroughness of mixing are used to quantify mixing; these include the variance of the C field, a simple two-point spatial correlation function for composition and the average composition within each layer. The spatial correlation method enables one to assign a length scale associated with chemical heterogeneity (L*). The adimensional variance, sometimes called the intensity, may be used to define a mixing time. Simulation at fixed Rq but with $\Delta\rho/\rho_0$ = 0,2,4,8% have been carried out for periods of time equivalent to the age of the Earth. Some results are summarized in the figures below which are relevant to the isoviscous case. Inclusion of T and C-dependent viscosity breaks symmetry and produces finer-scale mixing features. However, the critical $\Delta\rho/\rho_0$ which separates mixed states from poorly mixed ones remains at ≈4%.

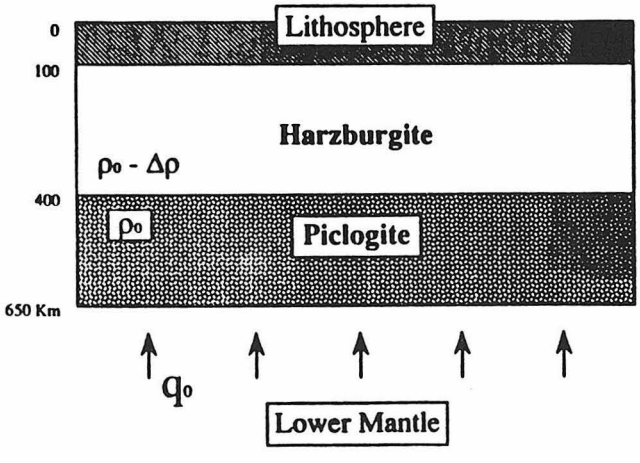

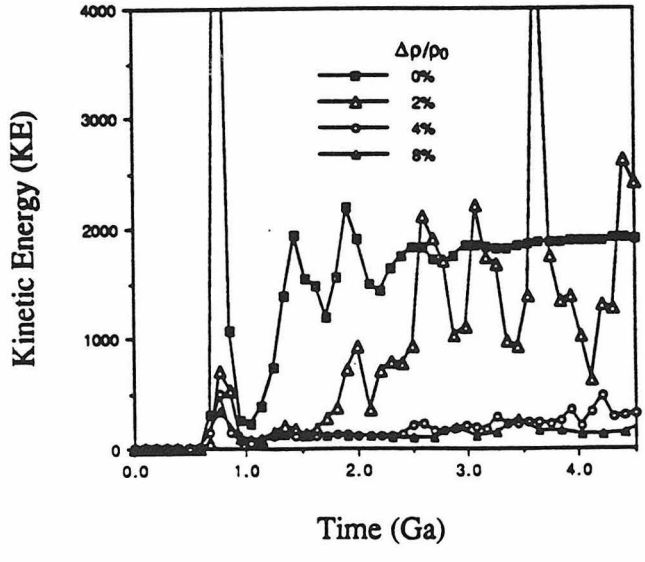

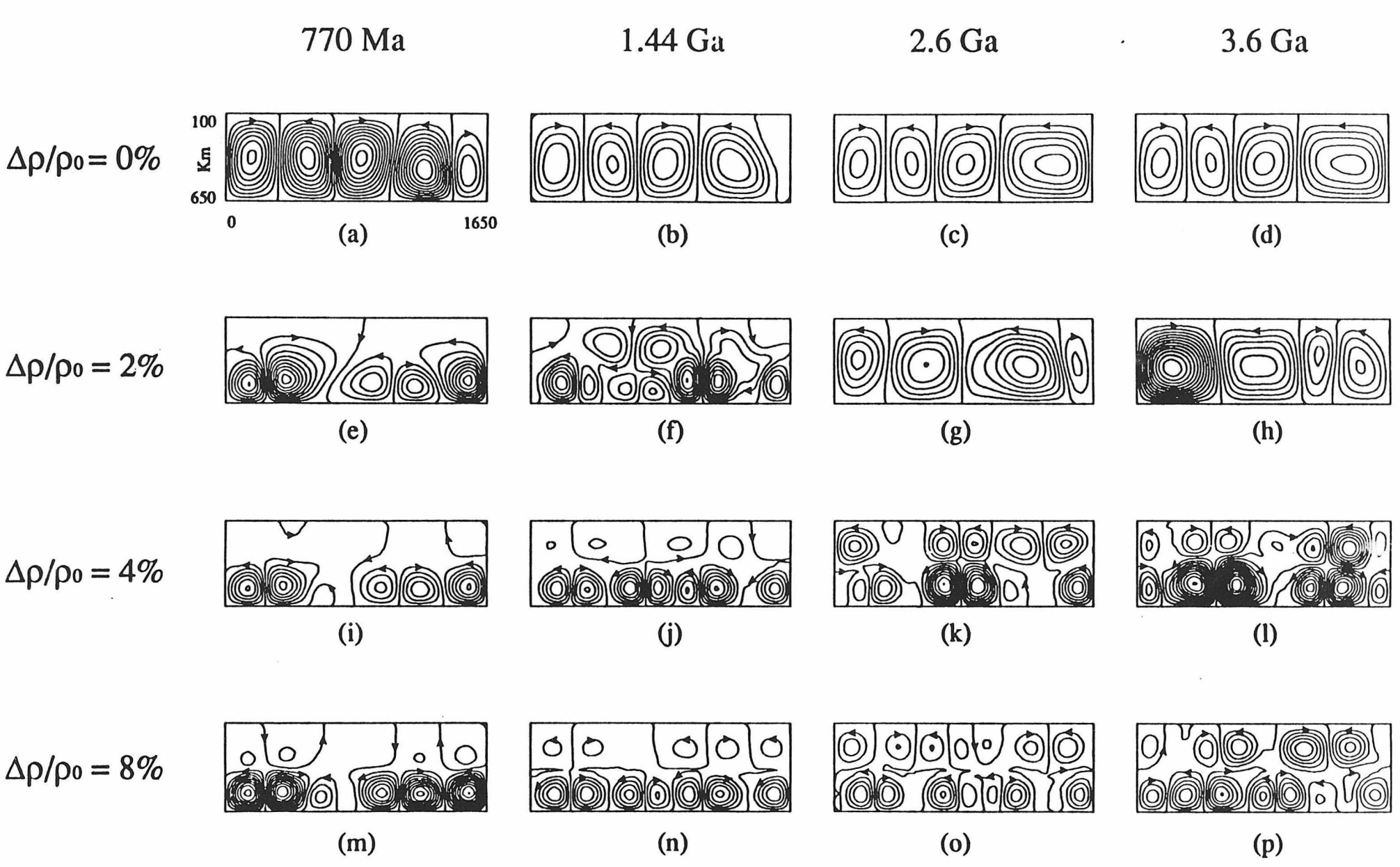

Stream Function

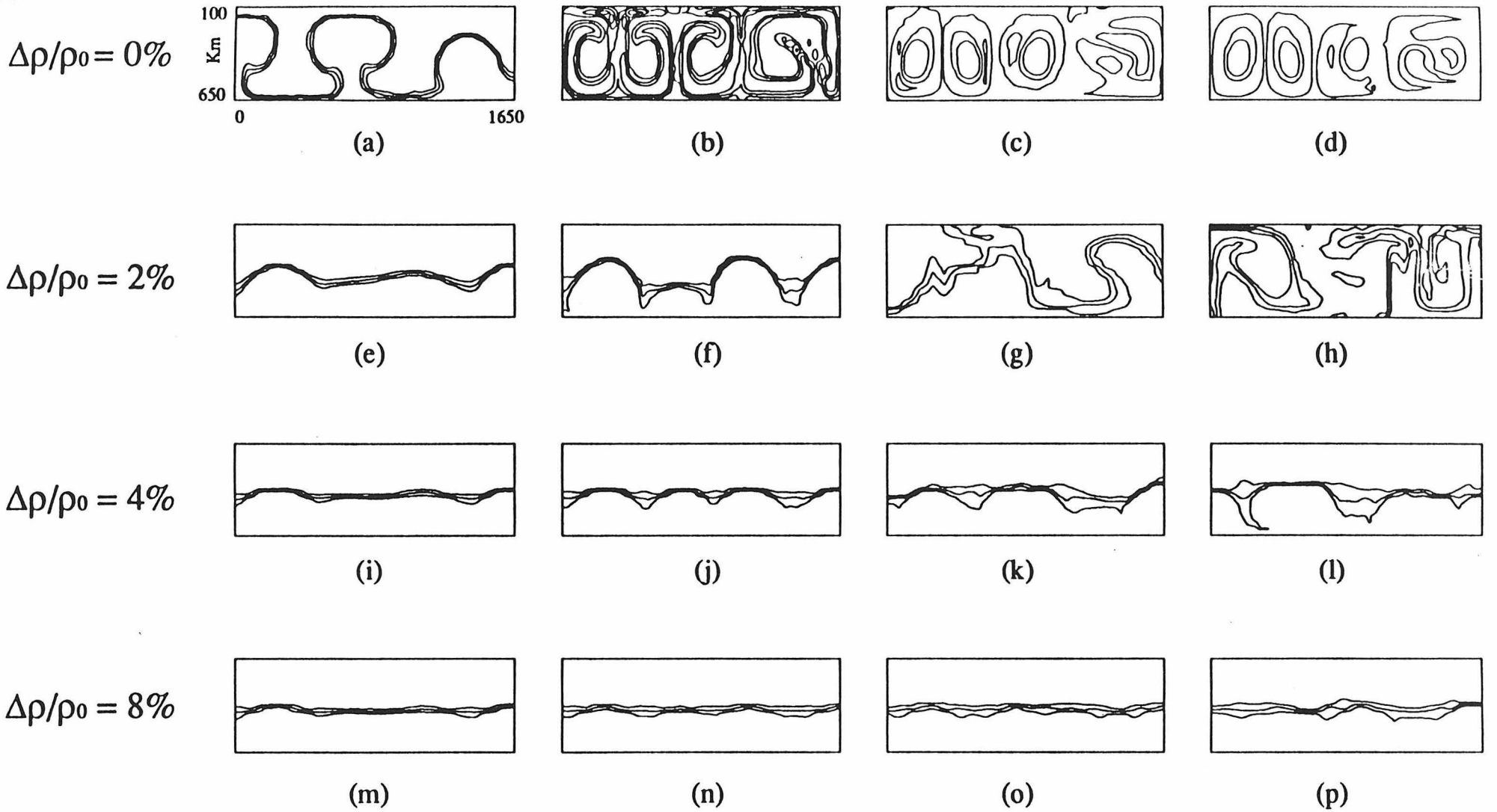

Compositional Field

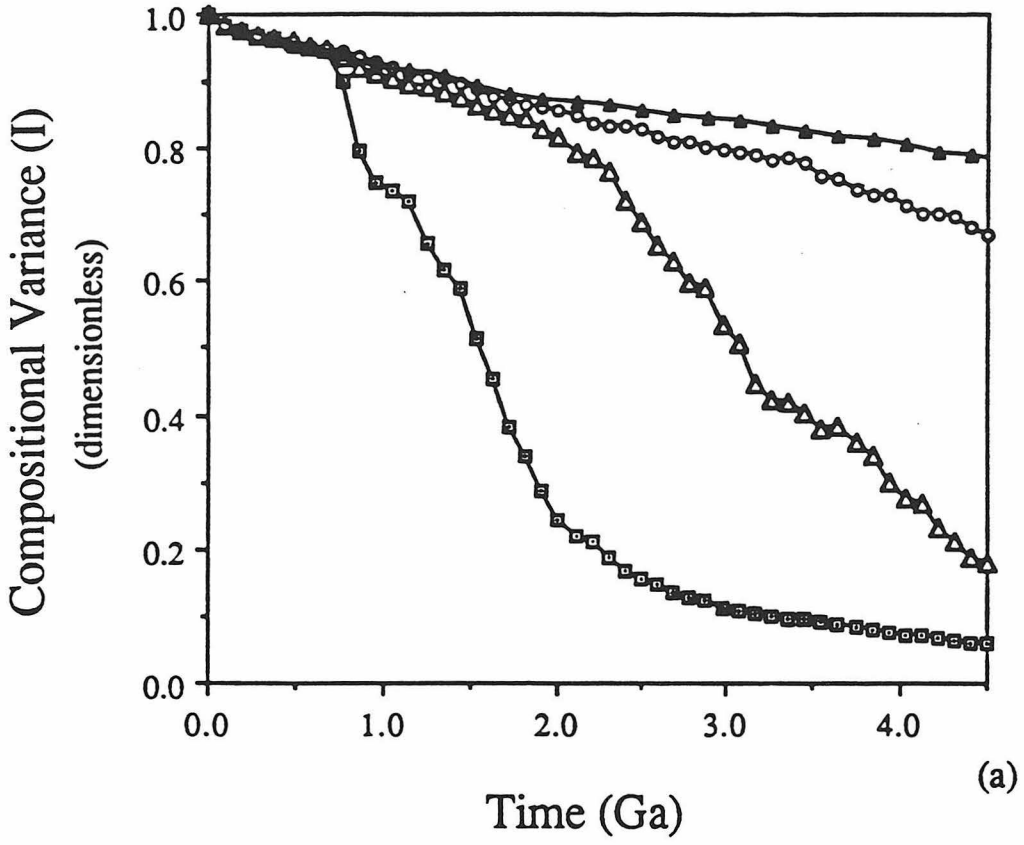
Compositional Variance (I)
(dimensionless)
1.0
0.8
0.6
0.4
0.2
0.0
0.0
1.0
2.0
3.0
4.0
Time (Ga)
(a)

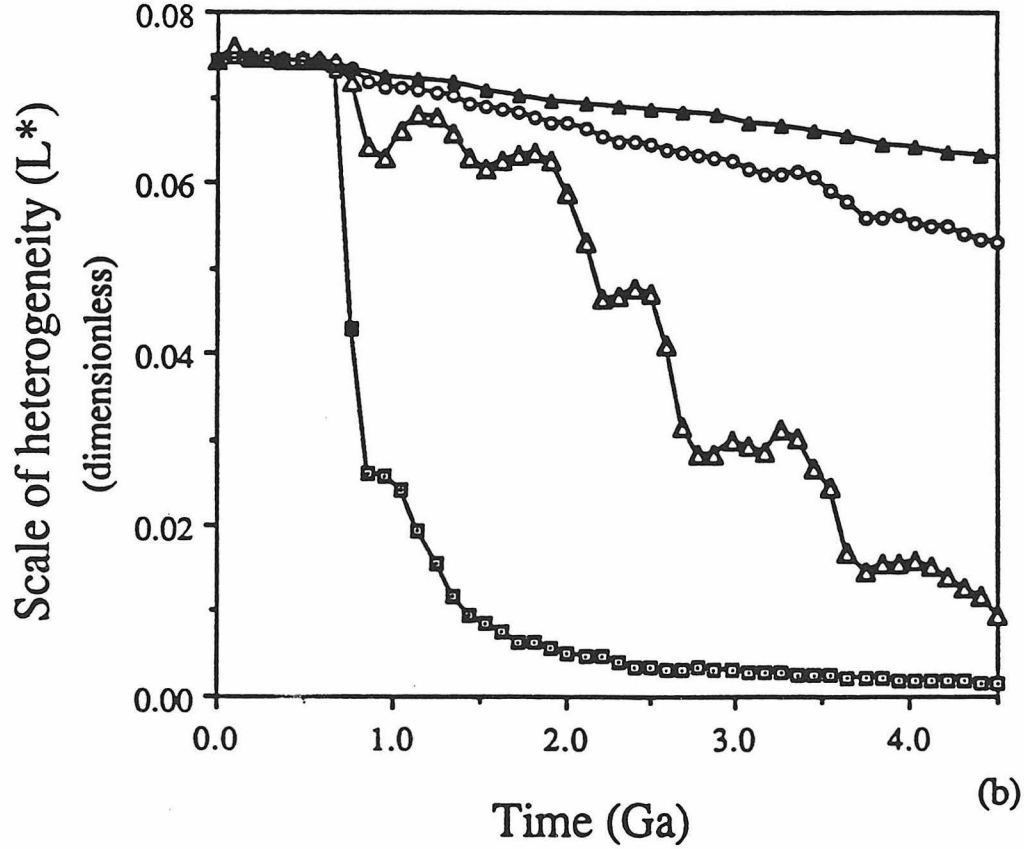
Scale of heterogeneity (L*)
(dimensionless)
0.08
0.06
0.04
0.02
0.00
0.0
1.0
2.0
3.0
4.0
Time (Ga)
(b)
Δρ/ρ0
0%
2%
4%
8%

Intraplate volcanism: Associations with plumes and other sources.
D. L. Turcotte, Department of Geological Sciences, Cornell University, Ithaca, NY 14853

The essential feature that interests us is intraplate volcanism or "hotspots" because intraplate volcanism does not fit into the plate tectonic hypothesis. The association of intraplate volcanism with plumes is attractive for a number of reasons. The linear progression of the Hawaiian-Emperor island-seamount chain is impressive and can be explained by a (nearly) fixed mantle plume with the Pacific plate riding over it. Other plume tracks are in accord with the plume hypothesis to a greater or lesser extent. The plume hypothesis is also consistent with our understanding of thermal convection. When a hot thermal boundary layer thickens it becomes unstable and forms an ascending plume.

While it appears appropriate to associates a substantial fraction of the intraplate volcanism with mantle plumes it is doubtful that it is the only cause. Volcanism is pervasive in the western United States. The Snake River-Yosemite system may be attributable to a plume, but the remainder probably can be attributed to the delamination of the lithosphere. Passive rifting and/or delamination may be a substantial source of intraplate volcanism. It is highly unlikely that mechanical failures of the lithosphere that result in continental rifts are always associated with plumes anymore than the passive spreading associated with normal mid-ocean ridges is associated with plumes.

I would like to proposal a working hypothesis for most (but not all) intraplate volcanism. It involves a number of postulates, some of which are more controversial than others.

i) Mantle convection is layered at the 650 km seismic discontinuity. The upper mantle is a partially mixed, depleted mantle reservoir. Plumes are generated by the instability of the hot thermal boundary layer at the base of the upper mantle. The Rayleigh number of the convecting mantle is sufficiently high that thermal convection in it is turbulent. This leads to a fractal distribution of plume or blob seizes. The Hawaiian plume represents one of the largest in the statistical distribution. The most numerous plumes are small bobs, many of these do not complete the ascent through the upper mantle and others underplate rather than penetrate the lithosphere. The largest plumes can entrain some lower mantle material. The strongest argument for layered mantle convection is the low thorium-uranium ratio associated with MORB. Such a low ratio could not be associated

with a near uniform, whole mantle reservoir. There are other observations supporting layered mantle convection, but convincing arguments can also be made in support of whole mantle convection.

ii) Chemical heterogeneities associated with intraplate volcanism come primarily from two sources, subducted material and crustal contamination. MORB is generally quite uniform and is consistent with a reasonably well mixed, depleted reservoir. Ocean island basalts (OIB) and anomalous MORB (i.e. Iceland, Azores, etc.) generally have enriched signatures that several authors attribute to three sources associated with subducted and delaminated material that has not been significant mixed. The anomalous isotopic signatures require 1.5 - 2.5 Gyr to develop and it is very unlikely that any segment of the mantle can be isolated for these lengths of time. The anomalous isotope signatures can be associated with subducted upper and lower crust and continental lithosphere where the anomalies developed. It has long been recognized that continental volcanics suffer considerable contamination from the crustal rocks which they pass. I suggest that the anamolous signatures of continental floods basalts and other continent volcanics can be attributed to this contamination rather than mantle metasomatism or other mantle reservoirs.

Abstract of a presentation at the Mantle Plume Symposium at Caltech, May 2-4, 1991

On Moving Mountains

by J. Tuzo Wilson
Department of Physics
University of Toronto
Toronto M5S 1A7, Canada

The land surface has provided an excellent time scale and economic benefits, but knowledge of the Earth's internal behavior has been to explain tectonics. New information from ocean floors and the interior show that fluid flow in the mantle breaks the thin and brittle lithosphere into plates by three classes of faults defined by laws of physics. Plate motions produce three corresponding types of mountains. Collisions between plates of different compositions (i.e. seafloor, continents, etc.) at different angles of incidence and by different modes of subduction produce many sub-classes. The second major type forms along coastal transform faults. Mantle plumes uplift the third type and anchor them relative to the mantle so that they migrate across plates and leave tracks. Over two dozen are active in oceans and a dozen of which the tracks are obscure on six continents and New Zealand. Neglected methods help to identify tracks. Plumes also feed and lubricate ranges, like the Wasatch Uplift, which migrate. Coordination of data from land, oceans and the interior enables physics to be applied to revise tectonics. That provides an astonishingly different view of Earth's behavior which is of far more value in solving problems.

A SURFACE-WAVE TEST OF THE LITHOSPHERE REHEATING MODEL FOR HOTSPOT SWELL FORMATION

Mark T. Woods and Emile A. Okal

Dept. of Geol. Sciences, Northwestern Univ., Evanston IL, USA;

> · · · If the lithosphere is thin beneath the Hawaiian chain, then the surface wave velocities along the chain should be unusually low. If, on the other hand, the lithosphere has normal thickness · · · then the velocities will be normal.
>
> *Detrick and Crough* [1978]

The Problem: What causes the uplifted swell surrounding active, oceanic hotspots?

- Examples: Azores, Réunion, Tahiti, Hawai'i. We shall concentrate on the type-example of such a feature, the Hawaiian Swell.

Previously Available Observational Constraints:

- Shape and Depth Anomaly. The relatively narrow aspect of the swell (600 km), elongated downstream from the active volcanism on Hawai'i, and in the direction of Pacific plate motion, suggests formation by hotspot processes. The maximum height above the "unperturbed" oceanic floor is the same as for normal, 25 m.y. old oceanic lithosphere, which yields a "depth anomaly" of about 1 km.

- Subsidence Rates. The measured rates of subsidence along the Hawaiian Swell appear to fit a square-root of age function, where the lithosphere age is 25 m.y. This well documented feature [*Detrick and Crough*, 1978] yields a subsidence rate that is about three times faster than predicted by the standard cooling model for 100 m.y. old oceanic lithosphere.

- Gravity and Geoid Signatures. Inversion of potential field data over the swell yield apparent depths of compensation that lie between 40-60 km deep. This depth suggests that the lithosphere is thinner than would be expected given the 100 m.y. crustal age.

- Heat Flow Characteristics. Older surveys of heat flow along the swell [*Von Herzen et al.*, 1982] indicated a possible elevation of 12 $mW\,m^{-2}$ above background values between Hawai'i and Midway Atoll. Recent surveys, however, fail to show a clear anomaly over either the Hawaiian Swell [*Von Herzen et al.*, 1989], or the postulated South Pacific Superswell [*Stein and Abbott*, 1990]

The Model: The above constraints are commonly used to support a model for swell formation in which the Pacific plate is reheated during its passage over the Hawaiian hotspot (*see Fig. 1*). Details differ among various incarnations of this model [*e.g. Von Herzen, et al.*, 1982; *Crough*, 1983] but they generally hold that the lower lithosphere is heated to asthenospheric temperatures so that the total lithosphere is thinned to about 50 km. As conduction is too slow

a process to thin the lithosphere in less than 100 m.y., some convective "erosion" must be invoked. The increased density contrast between the perturbed and unperturbed plate then leads to uplift of the recognizable swell, and as the plate continues past the upwelling plume, it cools conductively and again subsides with the usual square-root of age relationship.

The Test: As suggested by *Detrick and Crough* [1978], the dispersion of seismic surface waves offers a good test of the lithosphere reheating model. If the lithosphere has indeed been thinned during its passage over the Hawaiian hotspot, then Rayleigh wave group and phase velocities should be relatively slower along the swell than generally accepted for 100 m.y. old lithosphere [e.g. *Mitchell and Yu*, 1980; *Nishimura and Forsyth*, 1989]. The difficulty with this test was that seismic stations have existed only on Hawai'i, preventing two station measurements along the swell. Therefore in December of 1988 we installed a three-component station on Midway (MWY). The station has response characteristics similar to those of GEOSCOPE stations operating in the classical BRB mode [*Romanowicz et al.*, 1991], and has provided data suitable for dispersion analysis (*see Fig. 2*), and a variety of other investigations.

The Results: Two-station analyses of four Rayleigh waveforms recorded by MWY and KIP on Oahu for interstation group velocity yields maximum values $U_{max} \sim 4.09 \pm 0.01$ kms^{-1} at $T \sim 44$ s along the swell. If we compare the observed dispersion curves with age-dependent regionalized dispersion curves (*see Fig. 3*), we find that they are consistent with values for oceanic lithosphere having ages $50 \leq t \leq 110$ Ma (consistent with the crustal age t_c inferred from magnetic lineations between Hawai'i and Midway). The reheating model predicts, however, that they should match the regionalized curves for lithosphere with ages $20 \leq t \leq 50$ Ma (equivalent to the range of the lithosphere's reset thermal age t_{th} from Oahu to Midway), because the lithosphere is presumed to be thinner. The simplest interpretation of these comparisons is that the lithosphere has not been appreciably thinned by the hotspot.

This conclusion appears to be supported by a shear velocity model of the swell, obtained by inverting the group velocities (*see Fig. 4*) with a starting model consisting of an ocean, a single crustal layer, a high-velocity upper mantle lid, and a three-layer low-velocity zone (LVZ) overlying a halfspace. We assumed that all layers were flat, with constant, isotropic velocities. Fitting the observed dispersion curve using this parameterization, required that the shear velocity in the uppermost layer of the LVZ increase from 4.20 km s^{-1} to 4.49 ± 0.02 km s^{-1}, which is consistent with values found in the lid. The shear velocities in the two deeper layers of the LVZ remained, however, within one σ of their starting value.

The resolving kernels demonstrate that the data's bandwidth was sufficient to resolve the velocity structure down to ~ 100 km. The lid and the uppermost layer of the LVZ (layers 3 and 4), having large, compact kernels, were clearly resolved, but the deeper layers, having smaller, broader kernels, were not.

Where Do We Go From Here? Although these simple experiments offer strong constraints on the thickness of the lithosphere along the Hawaiian swell, and appear to contradict the simple reheating model, it cannot yet be discarded.

- First, more waveforms, especially from larger earthquakes, need to be examined to verify our results. The restrictive geometry of the experiment limits, however, the usefulness of many large events occurring around the Pacific rim. Investigation of Love waves from suitable earthquakes would also add important information.

- Second, the analysis of phase velocities would introduce additional, albeit dependent, constraints for reliable inverse models.

- Third, the question of anisotropy needs to be examined. It is clear that isotropic shear velocities cannot account for the observations; nevertheless it is possible that the anisotropic structure of the oceanic lithosphere may be able to explain why the observed group velocities are higher than those predicted by the reheating model. Particularly interesting are the depth extent of the anisotropic layers, and how effectively the relict fast NE-SW directions may have been reset to the current NW motion of the Pacific plate.

- Fourth, continued theoretical work is required to refine, as far as is warranted by observation, the reheating model. In particular, two related questions should be addressed: 1) Is convective erosion of the lithosphere necessary to explain the rapid uplift of the swell and the isostatic compensation depths? 2) If erosion is necessary, is there a plausible temperature buffering mechanism that could explain the apparent lack of heat flow anomaly over the swell?

References

Crough, S. T., Hotspot swells, *Ann. Rev. Earth Planet. Sci., 11,* 165–193, 1983.

Detrick, R. S., and S. T. Crough, Island subsidence, hot spots, and lithospheric thinning, *J. Geophys. Res., 83,* 1236–1244, 1978.

Mitchell, B. J., and G. K. Yu, Surface wave dispersion, regionalized velocity models, and anisotropy of the Pacific crust and upper mantle, *Geophys. J. R. astron. Soc., 63,* 497–514, 1980.

Nishimura, C., and D. Forsyth, The anisotropic structure of the upper mantle in the Pacific, *Geophys Jour, 96,* 203–226, 1989.

Romanowicz, B., J.F. Karczewski, M. Cara, P. Bernard, J. Borsenberger, J.M. Cantin, B. Dole, D. Fouassier, J.C. Koenig, M. Morand, R. Pillet, A. Pyrolley, and D. Rouland, The GEOSCOPE Program: Present Status and Perspectives, *Bull. Seismol. Soc. Am., 81,* 243–264, 1991.

Stein, C., and D. Abbott, Heat flow constraints on the South Pacific Superswell, *J. Geophys. Res.,* in press, 1990.

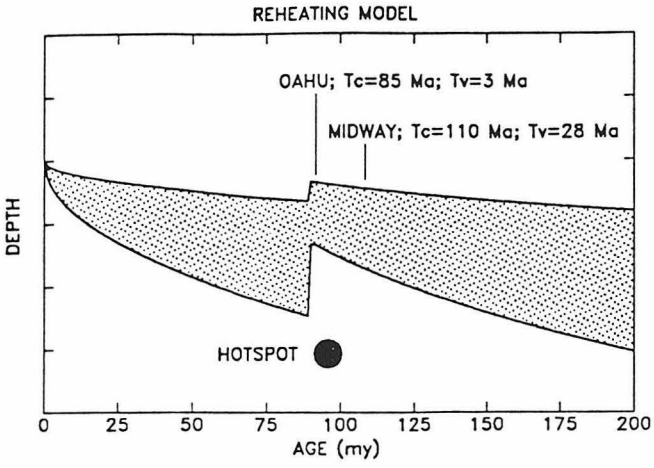

Fig. 1. Cartoon of lithosphere reheating model. Lithosphere thickens with age until it passes over hotspot, where it is thinned and rises isostatically, forming swell. Thereafter, lithosphere cools and again thickens; swell subsides. Positions of O'ahu and Midway are indicated, showing values of crustal age t_c, established from seafloor magnetic lineations, and age of volcanic edifices t_v, established radiometrically [after *Detrick and Crough*, 1978].

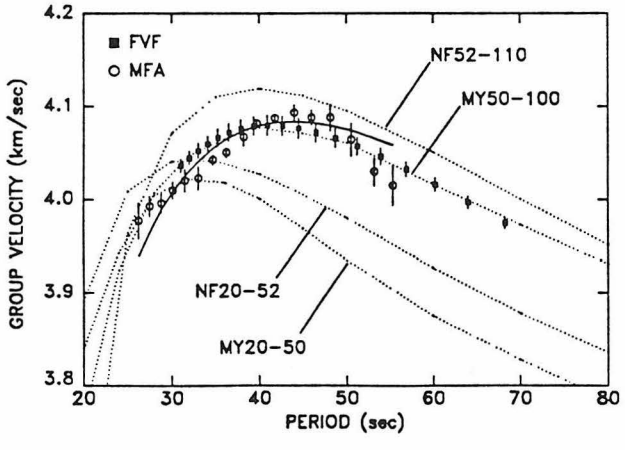

Fig. 3. Summary of Rayleigh wave group velocities observed along Hawai'ian Swell. Symbols: average values (± 1 standard error) of individual curves from four earthquakes, constructed using MFA or FVF techniques. Dashed lines: pure-path dispersion curves for age provinces in the Pacific Ocean Basin. Curves with MY prefix from *Mitchell and Yu*, [1980]; curves with NF prefix from *Nishimura and Forsyth*, [1989]; numbers following prefix correspond to ages spanned by curve. Solid line: fit to observations from inverse model (Table 3, Figure 4).

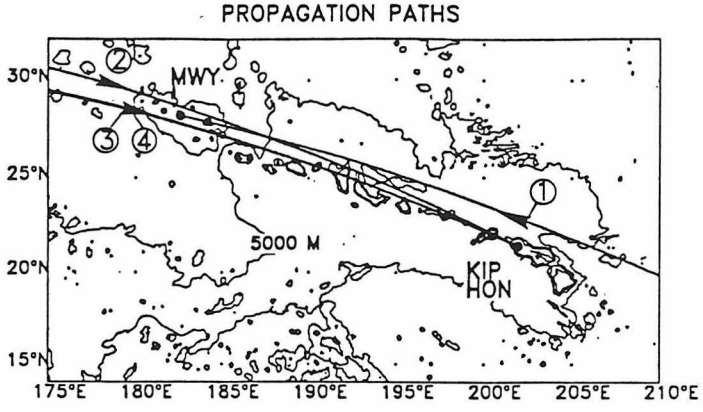

Fig. 2. Geometry of experiment showing Hawai'ian Swell, seismic stations, and propagation paths. Swell delineated by 5000 m contour of SYNBAPS bathymetric values. For clarity, propagation paths terminate at second station along great circle; arrows show propagation direction. Path numbers correspond to event numbers in Table 1.

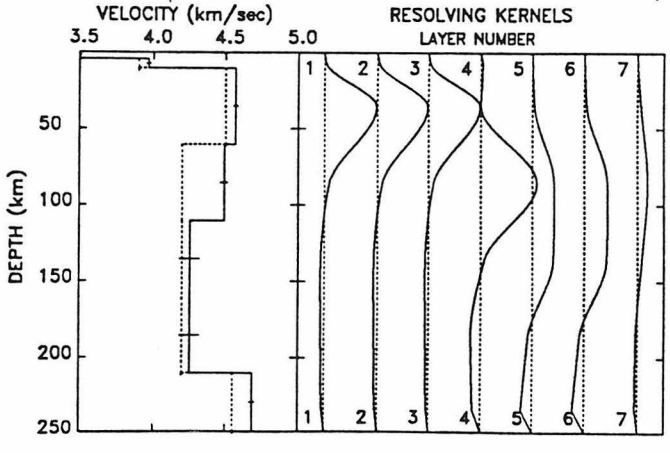

Fig. 4. Shear velocity model for Hawai'ian Swell, obtained by inverting group velocities. Dashed line is 7-layer starting model; solid line is final result (Table 3). Resolving kernels demonstrate that only the lithosphere (layers 3 & 4) is well resolved. The solution is particularly insensitive to the ocean and crust (layers 1 & 2). The large change between the starting and final velocities for layer 4 suggests thick lithosphere between Midway and O'ahu.

DOES OCEAN WATER REACH MANTLE PLUME SOURCES? IF SO WHAT ARE THE CONSEQUENCES?

Peter J. Wyllie
Division of Geological and Planetary Sciences, California Institute of Technology, Pasadena, CA 91125, USA.

Plume basalts contain H2O and CO2, with possible sources: (1) the primordial Earth, (2) subducted lithosphere in deep mantle storage, or (3) the lithosphere. The depth at which volatile components dissolve in melt in a rising plume has consequences for trace element distributions.

The subduction of volatile components from the hydrosphere is a distinctive feature of convergent plate boundaries. These components are contained in the sediments and altered basalt and gabbro and serpentinites of the oceanic crust, and in hydrated peridotite of the subducted lithosphere or overlying mantle wedge. Large volumes of volatile components are removed by underplating of sediments at the accretionary prism, and by diagenetic and low grade metamorphic reactions. Rocks of blueschist or greenschist facies are carried deeper, and they experience a series of progressive metamorphic reactions, with facies inverted because of the thermal structure.

The broad picture was clear in the early 1970s: most of the H_2O stored in minerals of subducted oceanic lithosphere is lost through dehydration or melting reactions by a depth of about 100 km, or 150 km in favorable circumstances. What is known can be illustrated with old figures (Wyllie, 1973, 1979, 1984) and reference to recent treatments (e.g. Kesson and Ringwood, 1989; Peacock, 1990; Davies and Stevenson, 1990). **THE CRITICAL QUESTION IS WHETHER ANY HYDROUS MINERALS SURVIVE IN THE SUBDUCTED LITHOSPHERE DOWN TO DEPTHS WHERE DENSE, HIGH-PRESSURE HYDROUS MINERALS BECOME STABLE.**

The depths to which hydrous minerals can be carried is a function of their phase relationships (within their host rocks, not as isolated minerals), and the temperature variation as a function of depth and time within the subduction zone. Phase boundaries for the common hydrous minerals of the host rocks have been measured, and those for other candidates proposed as water carriers if not determined can be calculated. The thermal structure varies as a function of slab geometry, and time, with significant differences between a young subducted slab, and more mature slabs, and for a slab of young, warm lithosphere close to a ridge when subduction occurs. Temperature variations are represented in two ways: (1) The thermal structure at any time can be depicted by a set of isotherms, and variations with time are shown by a series of such diagrams. (2) Individual depth-temperature trajectories can be computed for specific parts of a subducting slab, and time variations can be shown by different trajectories, similar to the curves in Figs. 1 and 3. The positions of dehydration reactions are correspondingly illustrated by: (1) The dehydration fronts in mantle cross-sections, obtained by plotting the positions of dehydration reactions on the thermal structure maps as in figs. 2 and 4, and (2) The depths of dehydration of minerals located in particular parts of subducted lithosphere, given by the intersections of depth-temperature trajectories with dehydration boundaries, as in Figs. 1 and 3.

Many thermal structures have been calculated for subduction zones. Two early versions covering a wide range of possible conditions provide the dehydration fronts shown in Fig. 2. Fig. 3 shows three bands for the temperature variation within a 5 km-thick ocean crust, OT and TMJ, corresponding to curves in Fig. 1, and the third band, ADS, corresponding to a calculation in which the crust is strongly cooled by endothermic dehydration reactions, even cooler than Peacock's (1990) coolest trajectory for 200 my old lithosphere, which is near values of Davies and Stevenson (1990). Very high thermal gradients exist in the subducted oceanic crust, with cooler rock situated below warmer rock.

Figures 2 and 4 show the positions of dehydration fronts where H_2O is released from the most common hydrous minerals expected in the three subducted materials. Fig. 2 shows the maximum depths to which the hydrous minerals could be carried if H_2O was available, and Fig. 4 shows the orientation of the dehydration fronts in the subducted crust. The positions of the reaction boundaries vary as the thermal structure changes, and the serpentinite reaction (DG) (approximately equivalent to extrapolation of the greenschist facies boundary) may be stretched out through a considerable depth interval, or compressed into a much shorter interval (Wyllie, 1979, 1984). Amphibolite breakdown, on the other hand, is a pressure-sensitive reaction under these conditions (Figs. 1 and 3), and its position within the oceanic crust can change

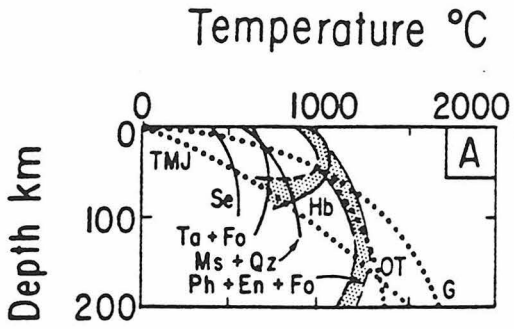

FIG. 1. Dehydration reactions, and estimated depth-temperature trajectories (TMJ, OT, G) along upper boundary of subducted lithosphere slab. Compare with Fig. 3. Se = serpentine, Ta = talc, Fo = forsterite, Ms = muscovite, Qz = quartz, Ph = phlogopite, En = enstatite, Hb = amphibole (Wyllie, 1973, Fig. 3A).

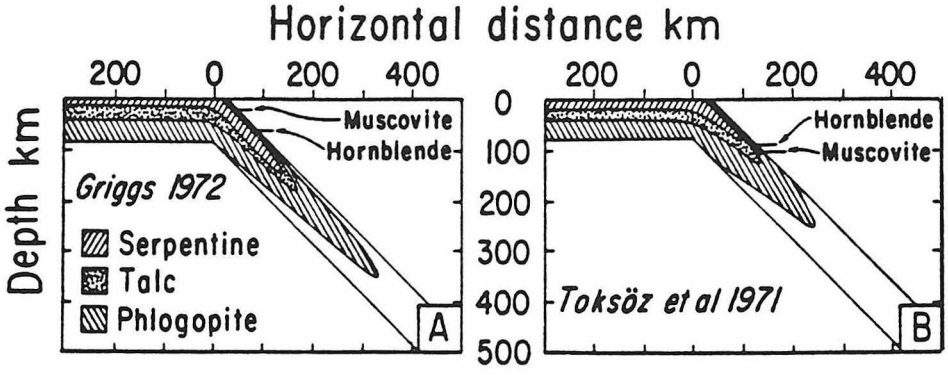

FIG. 2. Schematic cross-sections through subducted slab, showing maximum depths to which hydrous minerals can be carried, if the host-rock composition is appropriate (with H_2O), according to two thermal structures (see G and TMJ in Fig. 1 for slab-surface trajectories). For a view of the dehydration fronts (metamorphic facies boundaries) within the oceanic crust, see Fig. 4. (Wyllie, 1973 Fig. 7).

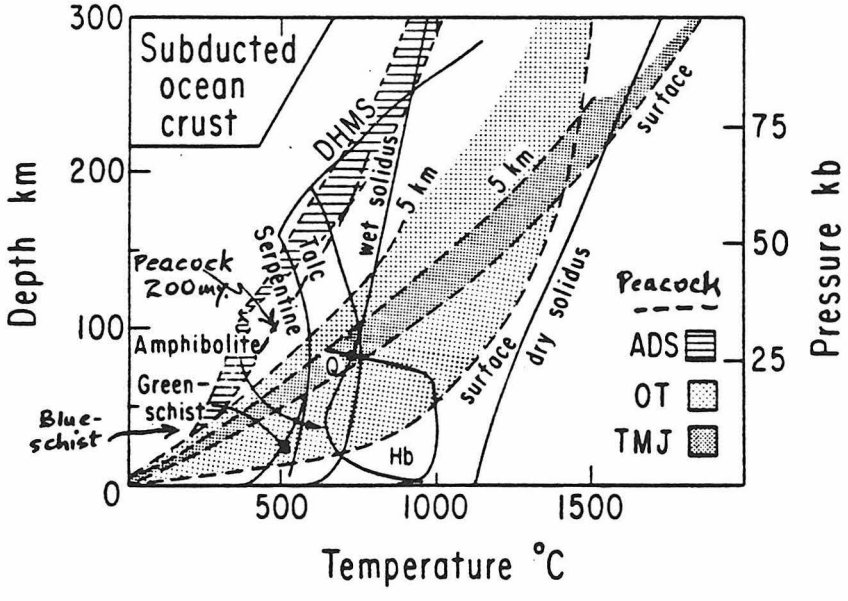

FIG. 3. Phase boundaries for subducted oceanic crust of gabbro, enclosing bodies of serpentinite. The shaded bands give temperature distribution across a 5-km thick subducted crust according to three investigations. Compare OT and TMJ with Figs. 1 and 2. ADS trajectories are even cooler than the coolest calculated by Peacock (1990). Selected dehydration reactions as in Fig. 1, plus dense hydrous magnesian silicates (DHMS), compared with solidus curves dry and wet. Note the blueschist, greenschist, and amphibolite facies. Compare dehydration fronts and facies in Fig. 4 (Wyllie, 1979, Fig. 15).

through only a limited range.

Pelagic clays yield micas when metamorphosed, and breakdown or melting of muscovite + quartz may represent the conditions for almost complete dehydration of pelagic sediments, at depth less than 100 km (Fig. 2). For the coolest slabs (Peacock, and ADS in Fig. 3), mica could survive to somewhat greater depths.

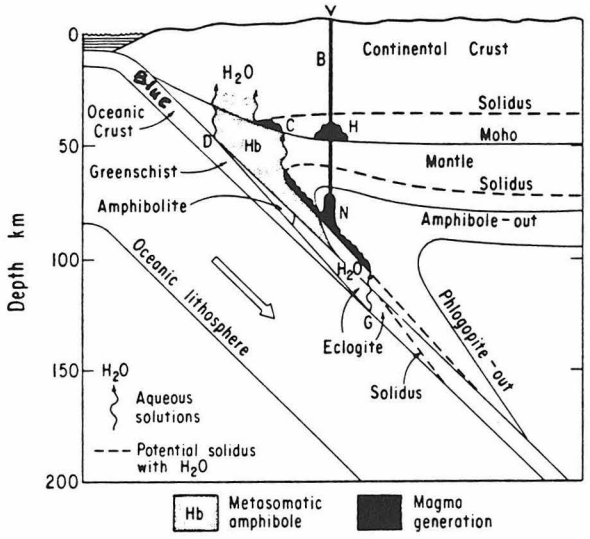

FIG. 4. Selected reaction boundaries plotted on subduction zone thermal structure, for cool subducted crust and warm mantle wedge, based on dehydration reactions in Figs. 1 and 3. Compare Fig. 2. Note the greenschist dehydration front, DG, corresponding also to serpentine dehydration. The amphibolite dehydration front is the short line between amphibolite and eclogite facies. Melting begins if H_2O migrates across the dashed solidus curves. Reaction positions change with thermal structure (Wyllie, 1984, Fig. 5).

Amphibolite dehydration or partial melting at depth near 80 km yields anhydrous eclogite. Serpentinite bodies in the bottom of the oceanic crust may carry water to depth G in Fig. 4. The geometry of the serpentinite boundary, DG (Fig. 4), is sensitive to the thermal structure, but it appears to be difficult to force the position of point G any deeper than 180 km (see the coolest trajectory, ADS, in Fig. 3). If the subcrustal oceanic lithosphere does become hydrated by deep penetration of ocean near the ridges or trenches, serpentine and talc appear to be limited to shallower than 180 km even in the centers of the coolest lithosphere slabs (Fig. 2A). Phlogopite is the only common hydrous mineral with a greater depth range. As shown in Figs. 1 and 4, phlogopite in oceanic crust or overlying mantle (formed possibly by reaction with solutions or melts from the subducted slab; Wyllie, 1984, Fig. 6) could reach a maximum depth of about 180 km, where it would dehydrate or melt. The deeper field for potential phlogopite within the center of the subducted slab is unlikely to be realized in depleted, low-K harzburgite.

THERE HAS BEEN SPECULATION THAT OTHER HYDROUS MINERALS FORMED AT LOW TEMPERATURES MIGHT SURVIVE TO GREATER DEPTHS IN: (1) BLUESCHIST FACIES PELAGIC CLAYS, AND (2) BLUESCHIST FACIES GABBROIC CRUST (PEACOCK, 1990), AND (3) SUBCRUSTAL SERPENTINIZED HARZBURGITE (KESSON AND RINGWOOD, 1989). THERE IS A REAL PROSPECT THAT CARBONATE MAY ESCAPE DISSOCIATION OR MELTING FOR LONG-TERM RESIDENCE IN THE MANTLE (HUANG ET AL., 1980).

Peacock (1990) listed the following candidates for pelagic clays and gabbros: phengite, glaucophane, chlorite, lawsonite, stilnomelane, clinozoisite, epidote, laumontite, lawsonite, margarite, prehnite, waikarite, and zoisite. Stern and Wyllie (1973) studied a pelagic red clay at 30 kbar and found only one subsolidus hydrous mineral at 675°C, a phengitic mica. However, the occurrence of other blueschist minerals at lower temperatures along the trajectories ADS and Peacock (Fig. 3) remains a possibility. Schreyer et al. (1991) considered newly sythesized high pressure hydrous minerals such as MgMgAl-pumpellyite. Candidate minerals proposed have not yet been demonstrated to be stable in suitable bulk compositions to appropriate pressures and temperatures, but the prospect exists.

There is a family of dense hydrous magnesian silicates stable only at high pressures (DHMS in Fig. 3), which include: Phase A, a 10 angstrom phyllosilicate, and clinohumite. If hydrous minerals being subducted survive until they enter this region then, when they dehydrate, some water can be recaptured in DHMS for transportation to greater depths. Kesson and Ringwood (1989) appealed to dehydration of serpentinite through the depth interval of 150-300 km, proposing that subcrustal serpentinite is carried deep enough to enter the DHMS field, with more dehydration occurring to 400 km. Fig. 4 shows that even with the coolest oceanic crust (ADS), serpentine and talc are completely dehydrated between about 160 km (top) and 180 km (bottom) before the dense hydrous magnesian silicates (DHMS) become stable. However, the P-T trajectory for the deepest crust is very close to reaching the DHMS field as dehydration is

completed, and if serpentine is present within lithosphere beneath the oceanic crust, this cooler lithosphere could follow a trajectory passing directly from serpentinite into the stability field for DHMS, where dehydration of the serpentinite and talc would leave some bound water in DHMS.

THE EVIDENCE SUPPORTS A CONCLUSION THAT NORMALLY THE SUBDUCTED OCEANIC LITHOSPHERE IS COMPLETELY DEHYDRATED BY A DEPTH OF 150 KM. THE ONLY PROSPECTS FOR DEEPER SUBDUCTION OF SMALL QUANTITIES OF OCEAN WATER APPEAR TO BE IN THE OLDEST, COOLEST LITHOSPHERE, IF: (1) SOME HYDROUS MINERALS FROM THE BLUESCHIST FACIES ESCAPE DEHYDRATION OR MELTING, OR (2) EXCEPTIONALLY DEEP HYDROTHERMAL ALTERATION OF SUBOCEANIC MANTLE CARRIES H_2O THROUGH SERPENTINE AND TALC FIELDS TO ONE OF THE DHMS MINERALS.

The mantle wedge is a site where the lithosphere is thoroughly impregnated by solutions and, under some conditions, by hydrous siliceous melts (Fig. 4).

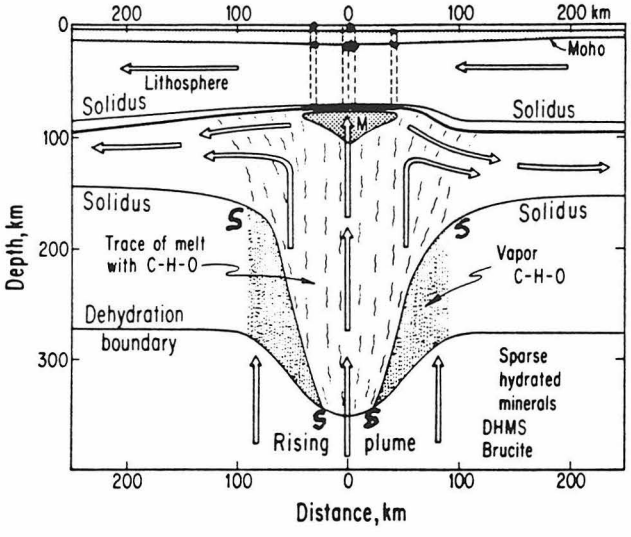

FIG. 5. Distribution of vapors and melts in mantle plume obtained by superimposing extrapolated phase boundaries for peridotite-H_2O-CO_2 on isotherms in plume thermal structure. The locations of phase boundaries vary with temperature and oxygen fugacity, but the general structure persists. In a rising plume, volatile components are released from solids at depths below about 300 km. The cylindrical plume contains a core with a trace of interstitial volatile-rich melt, and a sheath of vapor. There is a small kernel at the top of the plume, M, where significant melting occurs, forming picrite. See Wyllie (1988) for assumptions and construction.

Consider now the reversal of subduction, with a mantle plume carrying volatile components from the interior toward the surface. The DHMS boundary in Fig. 3 confirms that water if present deeper than 300 km would be stored in minerals, as indicated in Fig. 5 (if oxygen fugacity is low enough, a vapor with CH_4 or even H_2 may be present). Volatile components are released as the plume crosses the DHMS boundary (follow P-T trajectories from high to low pressure in fig. 4), and the vapor rises with the plume until it crosses the solidus, where it becomes dissolved in a trace of melt. The melt is rich in volatile components and incompatible elements. The line around the shaded area M corresponds to the solidus for dry peridotite, and significant melting with generation of picritic melt occurs only in this limited volume. The distribution of trace elements and isotopes within and above the plume are influenced by the different partition coefficients between minerals and (a) vapor, (b) volatile-rich melt, and (c) picrite. Trace element concentrations in volatile-rich melt are set at different pressures as a function of the slope of the solidus boundary (S-S), i.e. as a function of distance from the center of the plume. These differences would persist in the melt reaching the lithosphere at different distances from the plume center.

REFERENCES. Davies & Stevenson,1990,Preprint. Huang et al.1980.Am.Min.65,285. Kesson & Ringwood,1989.Chem.Geol. 78,83. Peacock,1990.Science,248,329. Schreyer et al.1991.47-64 in "Progress in Metamorphic & Magmatic Petrology". Stern & Wyllie,1973.Contr.Min.Pet.42,313. Wyllie,1973.Tecton.17,189. Wyllie,1979.Am.Min.64,469. Wyllie,1984.PEPI,35,12. Wyllie,1988.J.G.R.93,4171.

VARIOUS MECHANISMS FOR GENERATING DIAPIRIC STRUCTURES IN THE MANTLE

David A. Yuen, Wuling Zhao, and Andrej V. Malevsky

Department of Geology and Geophysics and Minnesota Supercomputer Institute, University of Minnesota, Minneapolis, MN 55415

Mantle plumes are commonly thought of as being continuous tall cylindrical structures with a mushroom cap at the top. These ideas are drawn from steady-state numerical and laboratory experiments conducted under moderate Rayleigh number conditions. There are, in fact, no firm seismological evidences supporting the existence of narrow continuous plumes in the mantle. It has been known for a long time that thermals or diapirs, which represent detached boundary layer instabilities, can be generated in heated plate experiments. In the last couple of years a great deal of fundamental understanding on the role played by diapiric structures in convection has come from work done in the physics community (Sano, Wu, Libchaber, 1989; Castaing et al., 1989) on the transition to hard turbulence in thermal convection. This transition first studied for low Prandtl number fluids has been demonstrated to occur for infinite Prandtl number medium by the two-dimensional numerical simulations of Hansen, Yuen and Kroening (1990). For stress-free boundary conditions and basal-heated Newtonian convection this transition occurs between Ra of 10^7 and 10^8. At these high Rayleigh numbers the heat-transfer mechanism changes from one characterized by mushroom-like plumes to one consisting of disconnected ascending instabilities. Plume-plume collisions in high Ra convection also serve to amplify the vigor of diapiric instabilities at high Ra. This type of diapiric instability is a distinct mode of heat transfer which is characteristic of the hard turbulent regime.

These basic fluid dynamical results can help us to understand the nature of plume dynamics in strongly time-dependent situations in the mantle. They show that when a certain Rayleigh number is exceeded, diapiric structures would prevail. Effects of internal-heating, compressibility, variable viscosity and depth-dependent thermodynamic properties would merely shift the threshold value for the surface heat flow above which diapiric structures would

develop. For base-heated Newtonian convection this occurs at Nusselt number of around 40.

Diapiric instabilities can develop spontaneously when there is a sudden increase in the effective local Rayleigh number by means of (1.) a dramatic increase in α via a phase-transition (2.) local reduction in viscosity in a stress-dependent viscosity. We have studied these two possibilities by numerical modelling. The problem of phase-transition in mantle convection has traditionally been studied with a single phase-change at 670 km depth (e.g. Christensen and Yuen, 1985; Machetel and Weber, 1991). However, there are other phase boundaries in the upper mantle which must be considered because of the interactions between them. Recent theoretical (Fei, Saxena and Navrotsky, 1990) and experimental (Boehler and Chopelas, 1991) data have shown the existence of a triple point in the phase-diagrams for both the Mg_2SiO_4 and $MgSiO_3$ systems near the 670 km discontinuity. Such a triple point, C in Fig. 1, would have dramatic effects on plume dynamics, as very hot plumes can go through the zero Clapeyron slope path (line 4 in Fig.1) virtually unscathed and further boosted by the large increase in α from density decrease. We have developed a formalism for treating multiple phase-transitions in thermal convection, which include the effects of density changes in the momentum equation and latent heat release in the energy equation. The boundary conditions at the top and bottom are fixed temperature and stree-free. Periodic boundary conditions are employed along the vertical edges of an aspect-ratio three box. We have studied both single and multiple phase-transitons. Our results indicate the importance of considering both depth-dependence of thermal expansivity and multiple phase-transitions with triple point in phase-transitions problems in mantle convection. Both $\alpha(z)$, depth-dependent expansivity, and triple point in the phase-diagram (see Fig. 1) would encourage diapiric instabilities and allow much more mass flux across the 670 km discontinuity than models with constant α and only one negative Clapeyron slope (e.g. Christensen and Yuen, 1985; Machetel and Weber, 1991).

Studies of time-dependent convection with non-Newtonian rheology (strain-rate proportional to some power of the deviatoric stress) are extremely difficult because of the demanding numerical accuracy and long computational time involved. We have studied this problem by using a method based on characterictics-based technique with Lagrangian formulation of the substantive derivative for the temperature. Bi-cubic splines are used for spatial discretization. The transition to the disconnected plume regime (see Fig. 3) occurs

much lower Nu, between 20 and 25, than for Newtonian rheology. Non-Newtonian hot plumes exhibit much greater curvature in their upward trajectory and are strongly attracted by the descending flows at the top. Their tendency towards diapiric formation is greater than for Newtonian rheology. Viscosity fields in the turbulent regime become strongly mixed and assumes a granular character.

References:

Boehler R. and A. Chopelas, Geophys. Res. Lett. in press, 1991.

Castaing, B. et al., J. Fluid Mech., 204, 1-30, 1989.

Christensen, W.R. and D.A. Yuen, J. Geophys. Res., 90, 10291-10300, 1985.

Fei, Y., Saxena, S.K. and A. Navrotsky, J. Geophys. Res., 95, 69515-6928, 1990.

Hansen, U., Yuen, D.A. and S.E. Kroening, Phys. Fluids, A2 (12), 2157-2163, 1990.

Machetel, P. and P. Weber, Nature, 350, 55-57, 1991.

Sano, M., Wu, X.Z. and A. Libchaber, Phys. Rev. A, 40, 6421-6432, 1989.

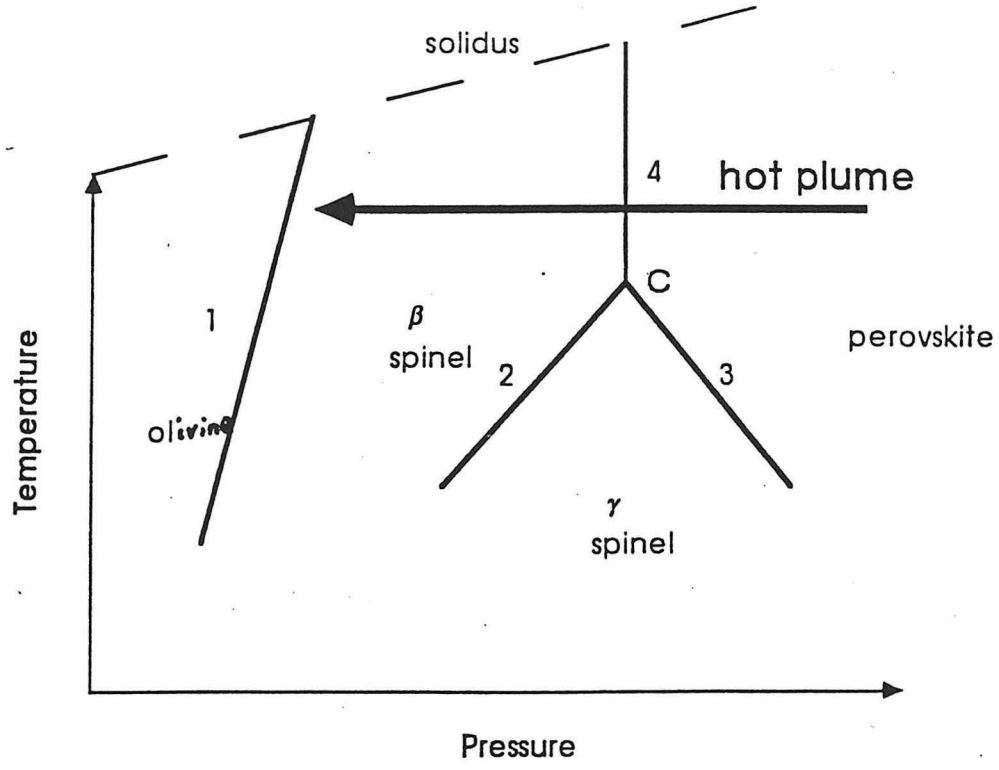

ig.1 Schematic diagram of multiple phase transitions with inverted Y triple point. Triple point C is located near the 670 km discontinuity and at temperatures between 2000 and 2400 K (Fei, Saxena, Navrotsky, 1990; Boehler and Chopelas, 1991). 3 is the proverbial negative Clapeyron slope used for the 670 km discontinuity. Note trajectory of hot plume may miss the negative Clapeyron slope.

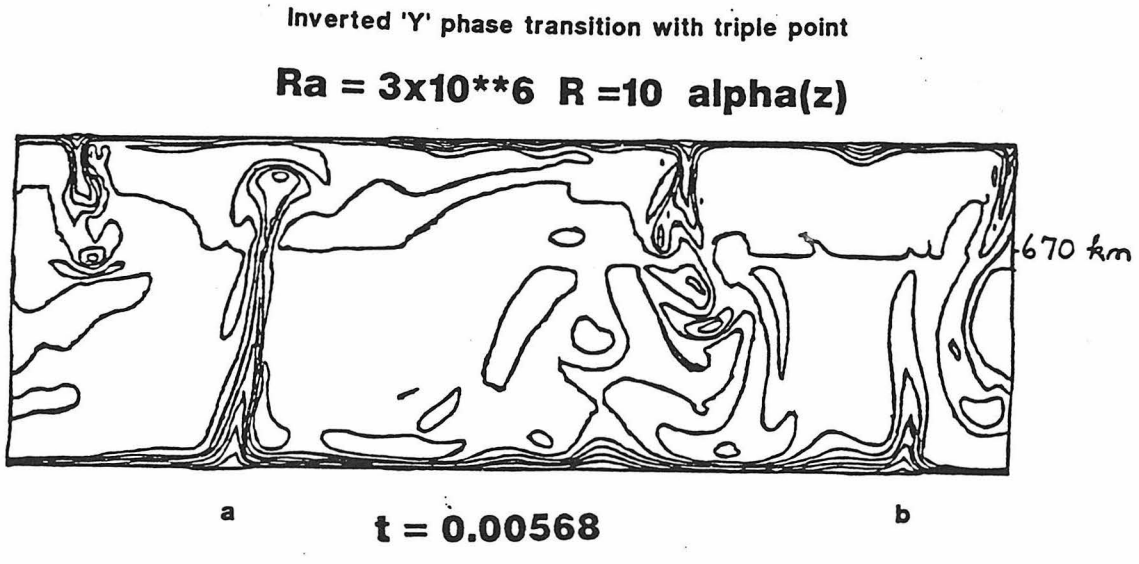

Fig.2 Temperature fields of convection with multiple phase-transitions with the inverted 'Y' triple point present. Instant is after five overturns. Note plume "a", being hotter can penetrate by passing through line 4 in Fig.1, while the colder plume "b" is stopped by the negative Clapeyron slope, line 3 in Fig.1.

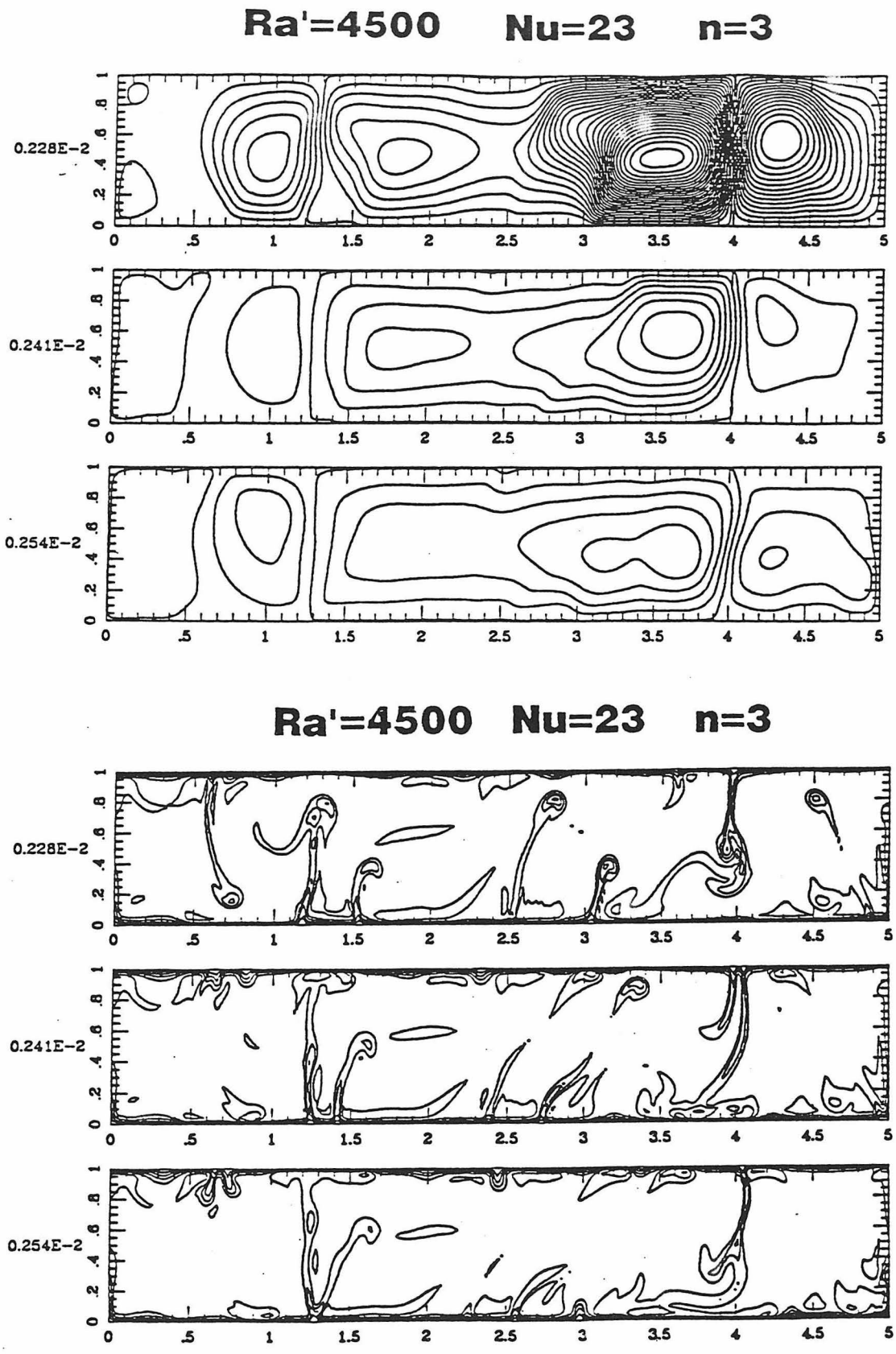

Fig.3 Streamlines and temperature fields in strongly time-dependent non-Newtonian convection in the disconnected-plume (turbulent) regime. Note the stark contrast in spatial heterogeneities of the streamlines from the first instant to the second one. Diapiric instabilities are bent by the large-scale flow.

Ridges and hotspots: perspectives from global tomography

Yu-Shen Zhang and Toshiro Tanimoto

Seismological Laboratory 252-21
California Institute of Technology

Resolution in global tomography has improved to a level of about 1000 km due to a rapid increase of digital data during the last decade. We have started to see various important tectonic features in some detail. We will attempt to summarize our current observations for ridges and hotspots.

Depth cross-sections of our recent S-wave velocity results, perpendicular to three ridges, are shown in Figures 1. These are stacked sections over 30 degrees along the ridge axis and the axis is aligned at the center of the figures, denoted by arrows. The velocity scale (in percent) is given on the bottom of figures. Contours are at every 0.5 percent and patterns change every percent. The most notable feature in these figures is the concentration of very low velocity anomalies (less than -1 percent) in the top 100 km. The minimum velocity is shallower than 50 km. Ridges are located above slow velocity regions, but in general we cannot see any features which suggest active upwelling. The fastest spreading East Pacific Ridge does have a 0.5 percent contour which extends to about 200 km in depth, but this could be interpreted as induced upwelling due to very fast spreading.

S-wave velocity at four depths under the ridge axes as a function of spreading rate are shown in Figure 2. Depths vary from 36 to 100 km and the possible contaminations from hotspots and triple junctions are avoided. It is clear that the shallow results (36 and 60 km) strongly correlate with spreading rate, but correlations decrease for deeper results and vanish at 100 km. Melt fraction due to decompression melting should increase with spreading rate, thus this trend can be understood as simple decompression effects. Both Figures 1 and 2 suggest that ridges are mainly passive features, and faster spreading ridges tend to induce deeper upwelling currents.

On the other hand, low velocity anomalies associated with hotspots are relatively deep. Figure 3 shows our S-wave velocity at two major hotspots. We will show more results in the conference. They all show low velocity anomalies, but the minimum velocity is located typically between 100 and 200 km depths. Differences in depth from low velocity anomalies at ridges are clear. They suggest that plume heads are creating low velocity anomalies below the lithosphere. Stems of plumes are presumably narrower than our resolution (1000 km), thus making them impossible to detect in these plots.

From these observations, we make the following conjecture: the depth of the low velocity anomaly can serve as a criterion to distinguish the nature (passive or active) of upwelling. If it is shallow, a passive mechanism is suggested, while deep anomalies suggest active mechanisms. With this in mind, we created two cross-sections in North-East Africa (Fig. 4). One is along the Red Sea and the other is perpendicular to it and crosses the East African Rift. Note that the north and south ends are denoted in the figure, as well as the locations of the Red Sea. The Red Sea is associated with a low velocity anomaly as expected, but the anomaly is clearly deeper than those for ridges. Active upwelling is clearly indicated and furthermore, the shape of the low velocity anomaly suggests that materials may be fed by hotspots at the southern end (Afar). The cross-section for the East African Rift also suggests an active origin, fed by a deeper low velocity anomaly from the South-West (under Africa). These results may be a useful tool to identify origins of other continental rifts.

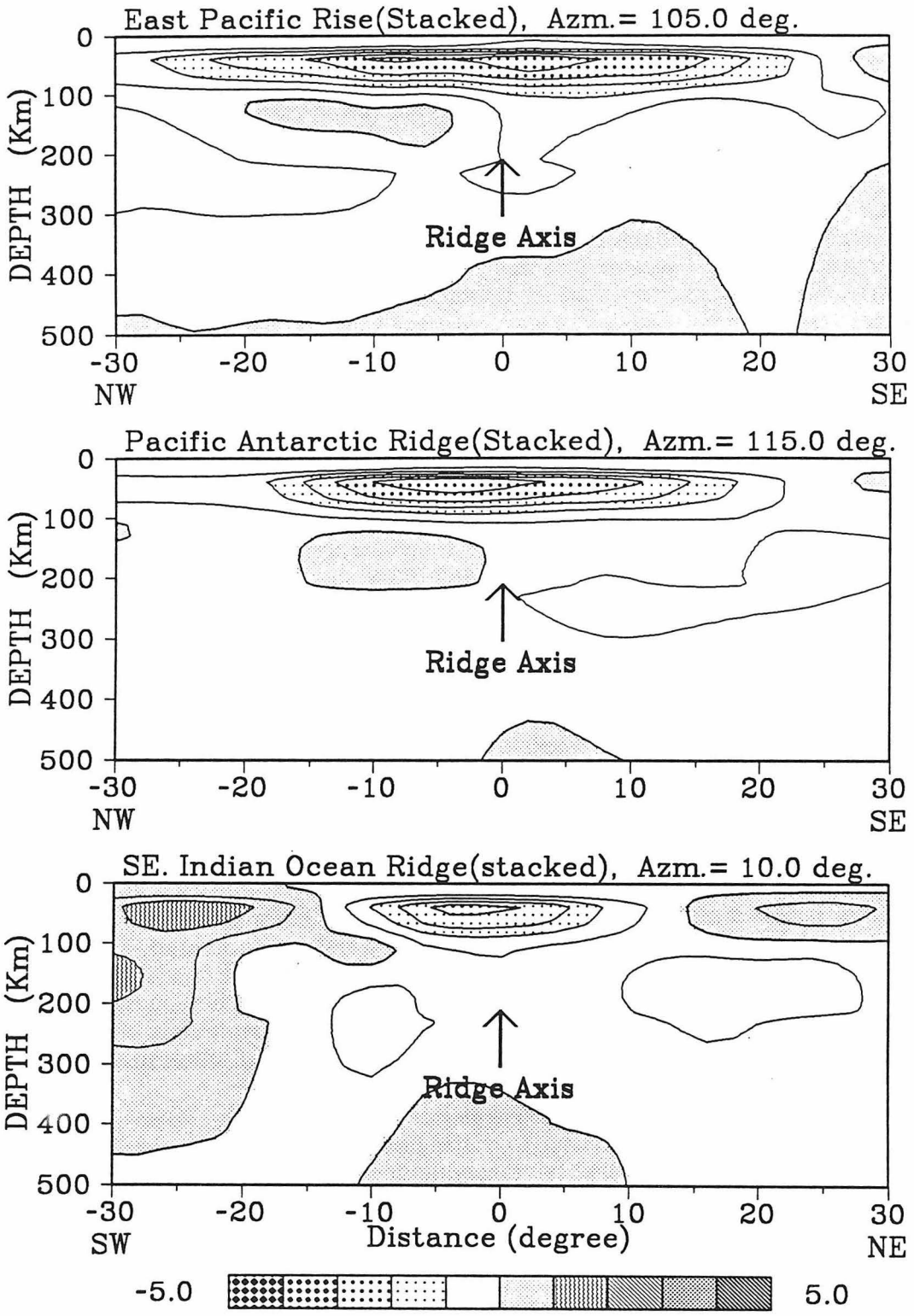

Fig. 1. Cross-sections of S-wave velocity results for East Pacific Rise, Pacific Antarctic Ridge and South-East Indian Ocean Ridge, respectively. These are stacked sections over 30 degrees along the ridge axis. The ridge axis is aligned at the center of the figure, denoted by arrow. The azimuth (clockwise from north) of each section is shown on top. The velocity contours are at 0.5 percent and patterns change every percent.

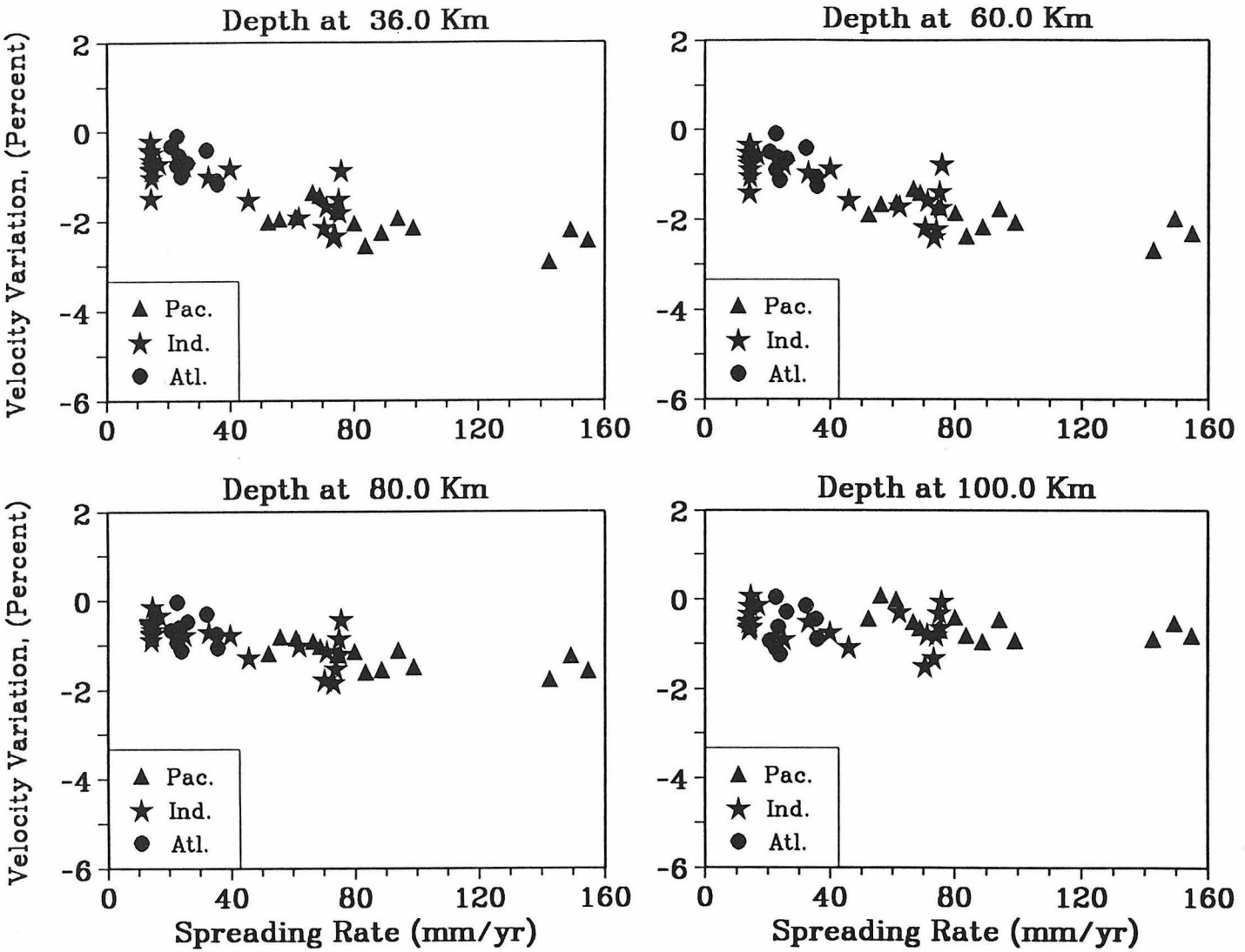

Fig. 2. S-wave velocity at four depths under the ridge axes as a function of spreading rate. Each point means an average velocity stacked over 8 degrees along the ridge axis. Different symbols are used to distinguish ridge in different oceans.

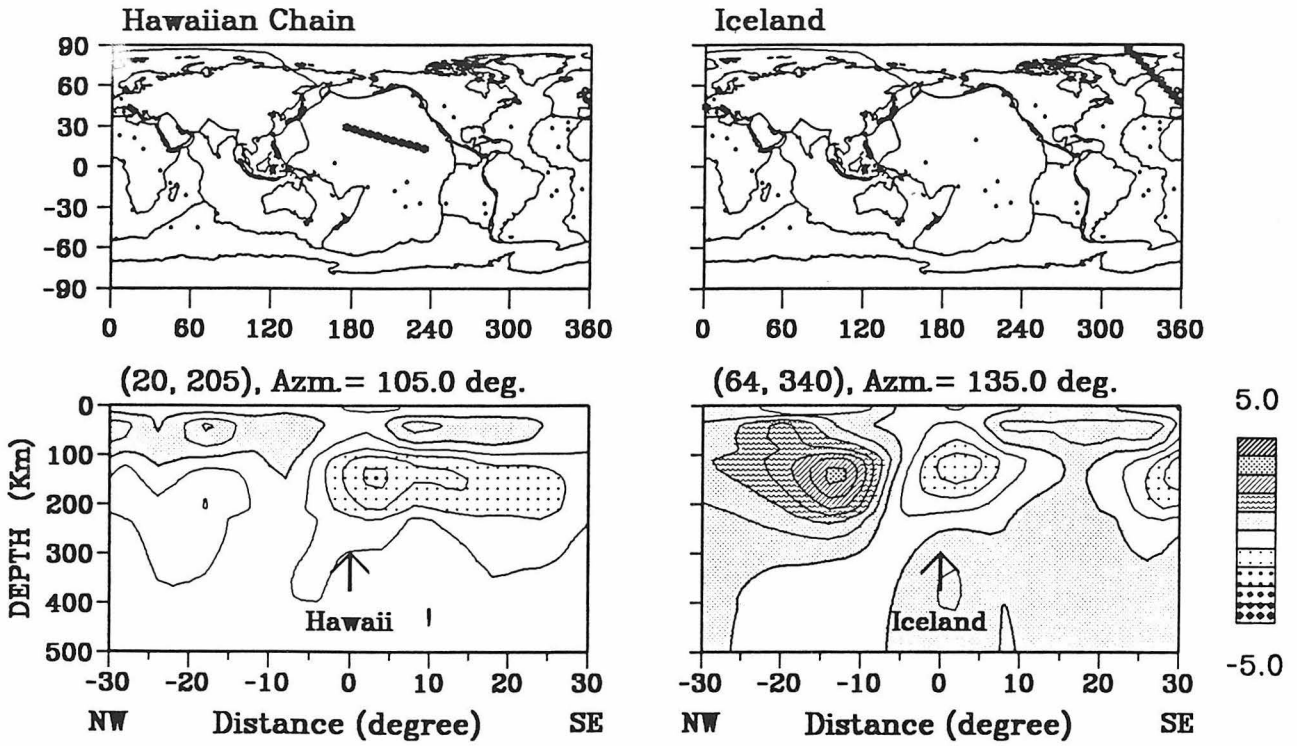

Fig. 3. Lower parts are two vertical cross-sections of S-wave velocity results at Hawaii and Iceland hotspots. The latitude, longitude of the center point, and the azimuth of the cross line are given in the figures. The directions of the line are also shown at bottom. Top parts give locations of the cross lines (star line). The velocity scale is same as in Figure 1.

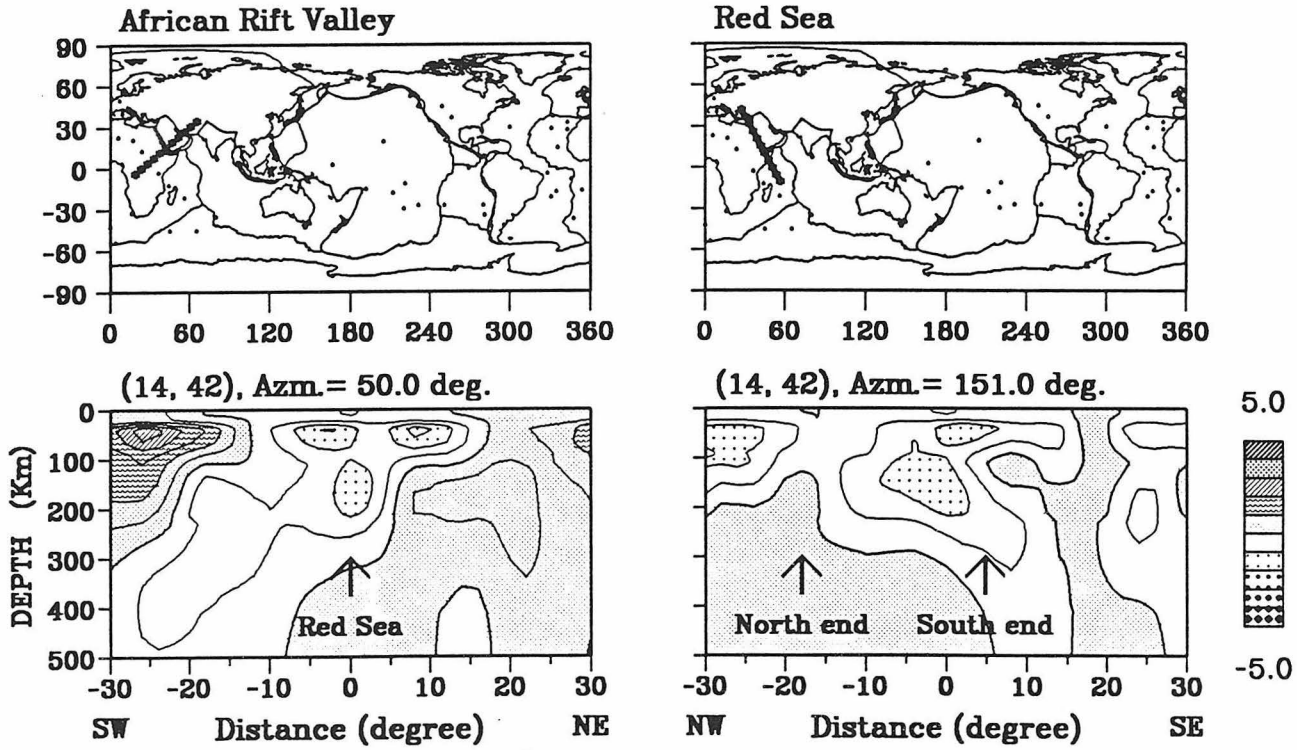

Fig. 4. The same as Figure 3 but for African Rift Valley and Red Sea cross-sections. These two cross-sections are almost perpendicular.

Oceanic Lithosphere: perspectives from Love wave phase velocity

Yu-Shen Zhang and Toshiro Tanimoto

Seismological Laboratory 252-21
California Institute of Technology

Global Love wave phase velocity variations are constructed for periods between 80 and 200 seconds by using approximately 9,000 paths from 971 events (with $M \geq 5.5$). The block parameterization approach ($5^o \times 5^o$ near equator) is used in this study. With improved resolution of about 1000 km, we attempt to study the oceanic lithosphere structure by using these results, because they are very sensitive to structure variation in the upper 200 km near the surface.

Using Sclater et al.'s oceanic age map (1981), we assigned an age to each 5 degrees by 5 degrees block in the Pacific, Atlantic and Indian oceans. We also corrected the age map based upon the resolution kernel at each block. Figure 1 shows the age versus Love wave phase velocity distribution for the Pacific Ocean at different periods. There is some scatter in the data, but the increase of phase velocity with age is apparent. There are similar features for the Indian and Atlantic oceans. The average phase velocities at ten million year intervals were calculated and plotted in Figure 2. One standard deviation is also shown in the figure. The number in parenthesis at the bottom is the number of blocks for a given age interval. In the conventional model, plates are believed to cool, subside and thicken during the first 60-80 Ma, but the development of secondary small scale convection or viscous shear stress heating below the lithosphere causes plate thickness to remain constant. On the contrary, our results indicate an increase in phase velocity for all oceans from the ridge to areas older than 100 Ma.

Using PREM as a starting model, we calculated theoretical phase velocity dispersion curves, and attempted to fit the observation by varying the thickness of the lithosphere and S-wave velocity of different layers. The final model for the Pacific Ocean is shown in Figure 3. Topography and crustal corrections are included in the analysis. Theoretical phase velocity variation curves are plotted with solid lines in Figure 2. They suggest that the lithosphere continuously thickens with age up to about 150 Ma, and does not stop thickening after 60-80 Ma.

Figure 4 is the age-phase velocity curves for the Pacific, Atlantic and Indian Oceans at period 100 s. There are two distinct features in these curves: (1) convergence of phase velocities for plate older than 100 Ma, and (2) systematic differences in plates of younger ages. The convergence of phase velocities beyond 100 Ma probably means that the lithospheric thicknesses are approximately the same for all oceans for old ages. The differences at younger ages implies a failure of scaling derived from a simple thermal boundary layer model for oceanic plates. Average heat flow data in young oceans decrease from the Pacific Ocean to the Indian Ocean, and then the Atlantic Ocean. They have been mainly explained by hydrothermal circulations. But our surface wave results indicate that the thermal differences in the mantle are required.

In order to understand the evolutions of lithosphere on different side of ridges, we examined the phase velocity variations. Figure 5 shows age-phase velocity curves on different sides of the Mid-Atlantic Ridge. We have added data from all areas of the Atlantic ocean. The phase velocity gradients are different for each side. Similar features occurred in other oceans, but the Atlantic Ocean shows this feature more clearly. Different hotspot concentrations is one possible explanation for the asymmetry. There are different thermal states on different sides of ridges, resulting perhaps in different lithospheric thickening rates.

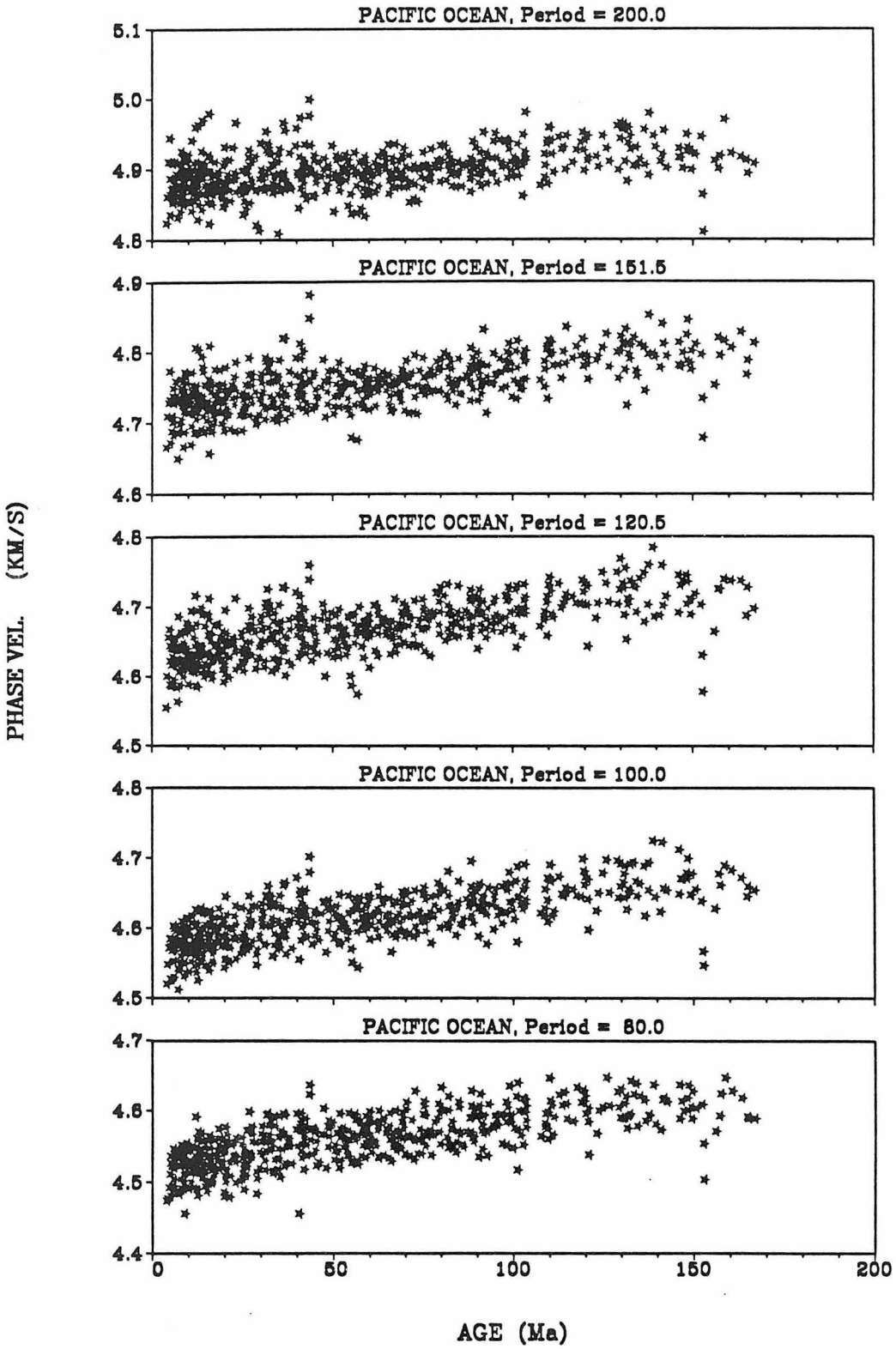

Fig. 1. Velocity distributions in the Pacific Ocean for periods from 80 to 200 s.

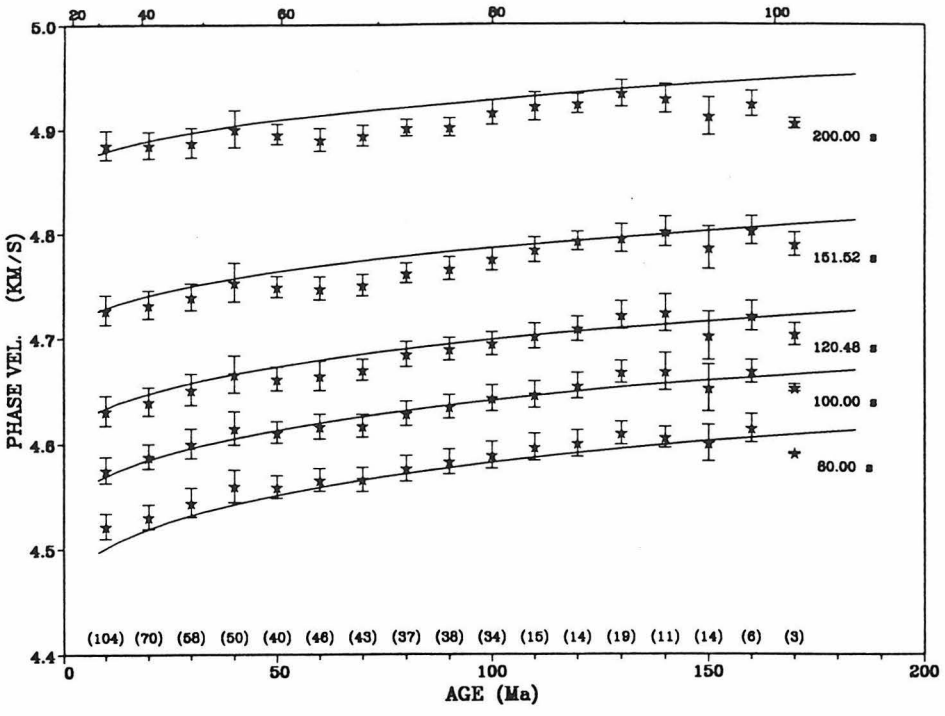

Fig. 2. Average phase velocity at ten million year intervals with one standard deviation for the Pacific Ocean. Solid lines are theoretical phase velocity curves for model in Figure 3.

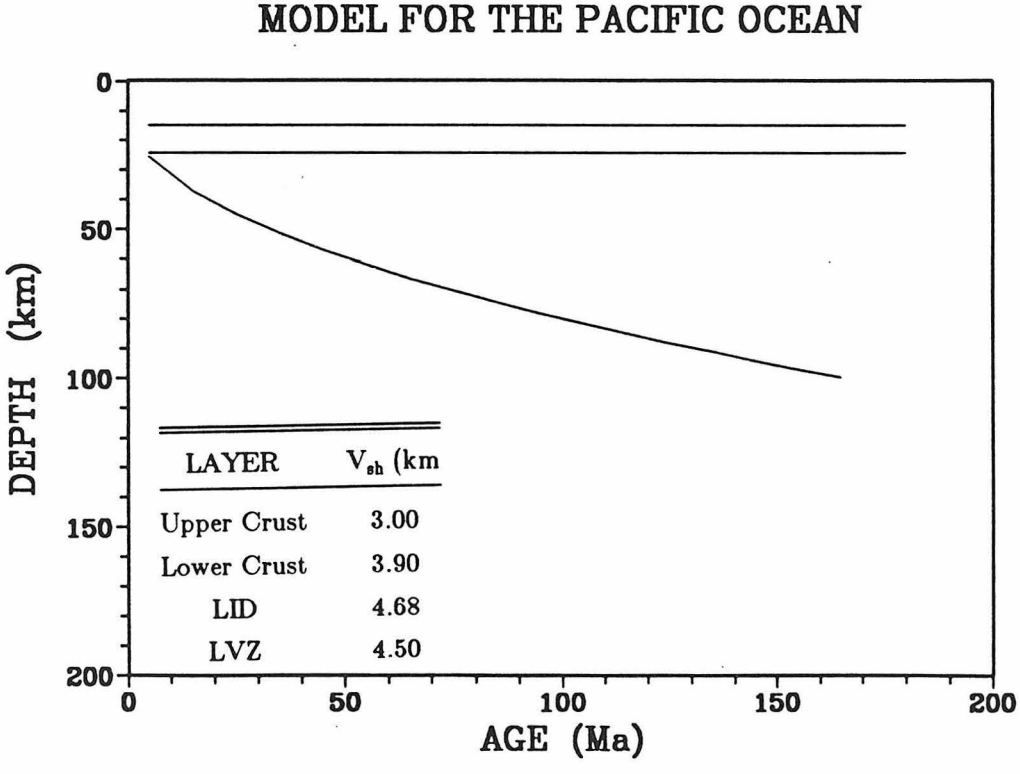

Fig. 3. Model for the Pacific plate. The thickness of the lithosphere is proportional to the square root of the age. The corresponding velocities for each layer are also given in the figure.

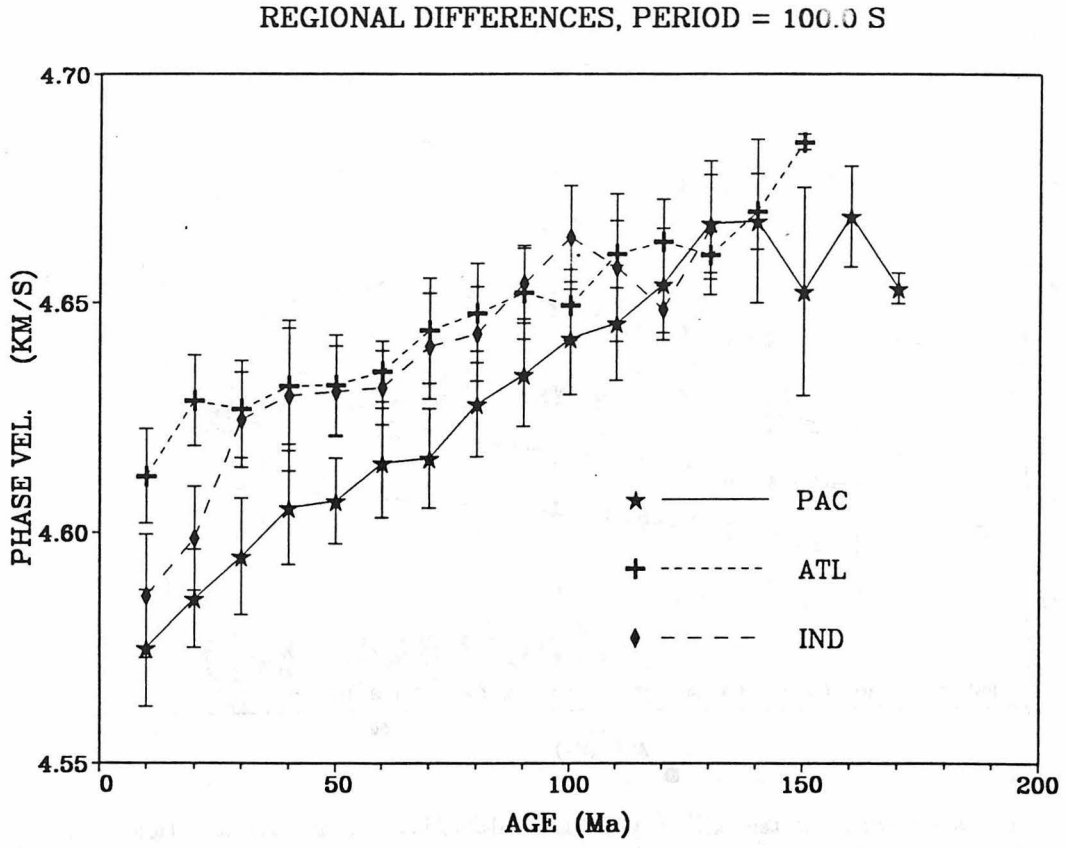

Fig. 4. Average phase velocity and one standard deviation in every ten million years for three oceans at period 100 s.

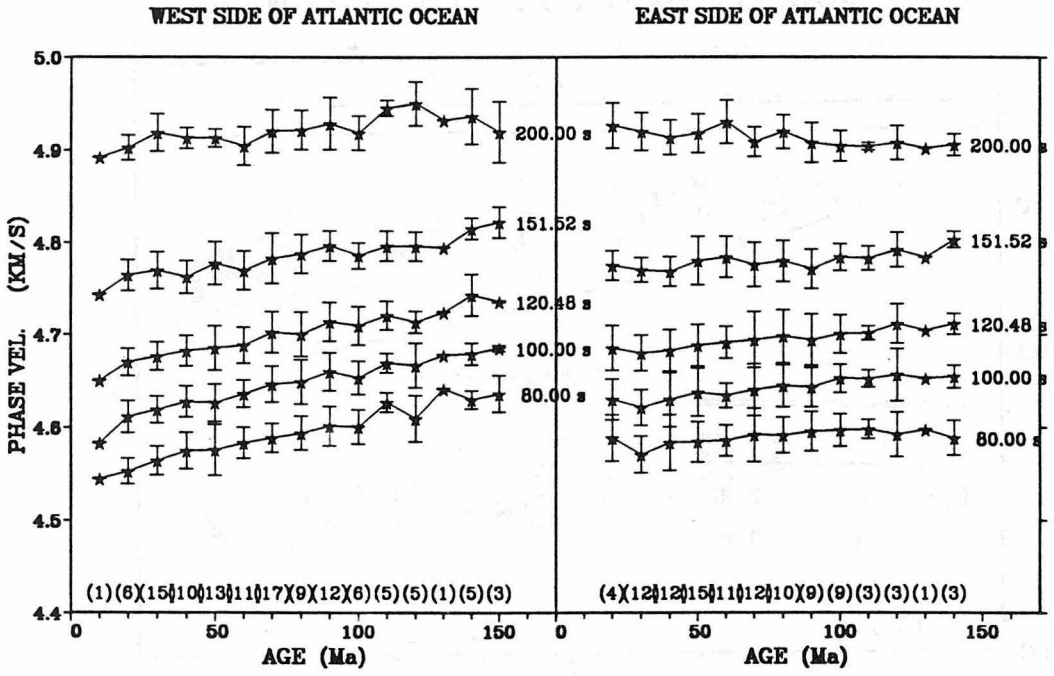

Fig. 5 Age-phase velocity curves on both sides of Mid-Atlantic Ridge. The velocity gradients are different on each side.